

Distributions and Sources of Dissolved Iron in the Polar Oceans

Maarten Bartholomeus Klunder

Colofon

Funding source, project number:

This research was funded by several grants to the NIOZ and by the GEOTRACES component of the Polarstern expeditions ARK XXII/2 and ANT XXIV/3.

ISBN:

978-90-367-5756-0

Graphic design cover and inside:

Rachel van Esschoten (www.divingduck.nl)

Photography:

Photography cover: copyright Florian Breier

Photography inside: Charles-Edouard Thuróczy, Maarten Klunder

Printed by:

Ipskamp Drukkers, Enschede (www.ipskampdrukkers.nl)

RIJKSUNIVERSITEIT GRONINGEN

Distributions and Sources of Dissolved Iron in the Polar Oceans

Proefschrift

ter verkrijging van het doctoraat in de
Wiskunde en Natuurwetenschappen
aan de Rijksuniversiteit Groningen
op gezag van de
Rector Magnificus, dr. E. Sterken,
in het openbaar te verdedigen op
vrijdag 5 oktober 2012
om 11.00 uur

door

Maarten Bartholomeus Klunder

geboren op 19 augustus 1980
te Oss

Promotor: Prof. dr. ir. H.J.W. De Baar

Beoordelingscommissie: Prof. dr. ir. E.P. Achterberg
Prof. dr. K.W. Bruland
Prof. dr. P.N. Sedwick

*"In the end,
we will conserve only what we love,
we will love only what we understand,
and we will understand only what we are taught."*

Baba Dioum

Voor mijn ouders
en dochter Mila

Contents

Chapter 1	11
Introduction	
Chapter 2	33
Dissolved iron in the Arctic shelf seas and surface waters of the Central Arctic Ocean: Impact of Arctic river water and ice-melt	
<i>Journal of Geophysical Research: Oceans, 117, C01027, 2012</i>	
Chapter 3	67
Dissolved iron in the deep waters of the Arctic Ocean: important role of hydrothermal sources, shelf input and scavenging removal	
<i>Journal of Geophysical Research: Oceans, 117, C04014, 2012</i>	
Chapter 4	101
Dissolved iron in the Atlantic Sector of the Southern Ocean	
<i>Deep-Sea Research II, 58 (25-26), 2678-2694, 2011</i>	
Chapter 5	143
Dissolved iron across the Weddell Sea and Drake Passage: impact of dissolved iron on nutrients uptake in the Weddell Sea	
<i>Submitted to Biogeosciences, September 2012</i>	
Chapter 6	179
Distribution of dissolved iron in the Southern Ocean: a compilation of high quality data in four depth layers	
Chapter 7	225
Summary and recommendations	
Chapter 8	237
Database	
Samenvatting	280
Acknowledgements	290
Biography	293
Publications	294



Chapter 1



Introduction

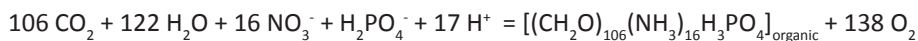
1.1 Iron in the Ocean

Iron (Fe) is the fourth most abundant element in the earth's crust (3.5% by mass) and is mostly present as ^{56}Fe . There are five other isotopic forms (^{54}Fe to ^{59}Fe), resulting in a relative atomic mass of 55.847 atomic mass unit (amu) [Taylor and McLennan, 1985; Turner *et al.*, 2001].

1.1.1 Evolution in relation to iron in the ocean

Photosynthesis, the process where carbon dioxide and water with the energy of sunlight (photons), are converted to organic compounds (notably sugars) and oxygen, is the key process for photo-autotrophic organisms. Within the oceans, these photo-autotrophic organisms comprise the unicellular algae or phytoplankton, including both prokaryotes (without cell nucleus) and eukaryotes (with cell nucleus). These algae in the open waters, together with macrophyte plants and zooxanthellae symbionts of coral reefs that are generally living on the seafloor, comprise the basis of marine ecosystems. Therefore all species in the higher trophic levels in the ocean depend on these autotrophs. The only exception to this life form are the subgroup of, mostly hydrothermal, chemo-autotrophs that derive their energy source chemically, and thus do not need the presence of sunlight.

In the present ocean, the dependence on sunlight forces the photo-autotrophic organisms to live near the surface, the euphotic zone, defined as the depth range where light penetrates until reaching less than 1% of the incoming solar irradiance at the sea surface [Steele, 1960]. To enable the process of photosynthesis and other essential processes in the cell, many chemical elements are needed [De Baar and La Roche, 2003]. During the development of life in the ocean, the most abundant and available nutrients were of vital importance for growth of the organism. For algae, nitrogen (N) and phosphorous (P) are vital for cell growth, and thus referred to as the major nutrients. The ideal stoichiometric uptake ratio of these nutrients was defined by Redfield, Ketchum and Richards [1963] as follows:



Not shown in this classical equation are the 6 bio-essential transition metal elements Mn, Fe, Co, Ni, Cu, Zn that are required by every organism, and among which Fe is arguably the most important. One subgroup of marine algae, the diatoms, also needs the element silicon (Si) because they build external skeletons of silicon-dioxide (SiO_2), called "frustules" around the cell. These diatoms represent a large part of the algae in the world oceans, particularly the Southern Ocean [Nelson *et al.*, 1995; Sarthou *et al.*, 2005 and references therein].

Besides the major nutrients, at least six other (trace) nutrients, iron (Fe), zinc (Zn), copper (Cu), manganese (Mn), nickel (Ni), cobalt (Co) are required for key

metabolic processes [Bruland *et al.*, 1991; Morel and Morel-Laurens, 1983]. Moreover, recent lines of evidence have shown that cadmium (Cd) is essential for several diatom species investigated thus far [Xu *et al.*, 2008; Abouchami *et al.*, 2011]. Most notably iron (Fe), along with the other metals from the first transition series, is well suited for storage, transport and transfer of energy within the cell [Frausto da Silva and Williams, 1994; De Baar and La Roche, 2003]. During the evolutionary development of life, both the intrinsic chemistry and the relative availability of each of these transition metal elements determined their biochemical function within the cell [De Baar and De Jong, 2001; De Baar and La Roche, 2003; Frausto da Silva and Williams, 1994]. Among these elements, iron (Fe) is not only essential for energy transfer within the cell, but also plays an important role in nitrate reduction, N₂-fixation and many other biochemical processes, being present in catalase and in superoxide dismutases [Sunda, 2001; Morel and Price, 2003]. In the primordial suboxic Archean ocean (3.8-2.5 Gy before present), iron (and several other metals) would have been highly soluble, and therefore present at high concentration as Fe²⁺ dissolved in seawater. However, with the ongoing process of photosynthesis (eq. 1), more and more free oxygen was produced and released in the ocean. Around 1 Gy this free oxygen was reduced and removed by the Fe (II), the latter becoming oxidized to solid Fe(III) oxides, precipitating out into massive iron oxide formations, until eventually little Fe (II) remained in seawater. From then on the oxygen was no longer being captured as iron-oxides, leading to a steady increase of oxygen in the atmosphere and ocean. This also led to a shift in the oceans, from the readily soluble abundant dissolved Fe (II) to the sparingly soluble Fe (III), and thus a dramatic decrease in the concentration of available Fe in the oceans. The resulting extremely low concentration of dissolved Fe in the modern ocean is a central topic in this thesis.

Other biologically essential transition metals also have very low concentrations in the modern ocean, yet it is only for Fe that there is strong evidence, both from field studies and laboratory experiments, of the limitation of growth of marine phytoplankton due to sub optimal availability [De Baar *et al.*, 1990, 1995, 2005; Martin and Fitzwater, 1988; Hunter and Turner, 2001]. However, some reports are made of the necessity of (dissolved) zinc for phytoplankton growth [Jakuba *et al.*, 2012 and reference therein]. Moreover, recently, Middag *et al.* [2010] also reported trends of dissolved manganese (Mn) in upper waters of the Southern Ocean, in support of the notion of Mn as a co-limiting factor for phytoplankton growth.

1.1.2 The “iron hypothesis”

As early as 1934, Hart noted that the phytoplankton concentrations around South Georgia Island were ten times higher than in other Southern Ocean regions. Hart [1934] mentioned: “ Among the ... chemical constituents of sea water ... possibly limiting phytoplankton production, iron may be mentioned (..) the land being regarded as a source of iron.” [Hart, 1934]. The very low (subnanomolar) concentration of Fe

in the seawater led to analytical limitations that prevented testing this hypothesis. It was not until 1988 that *John Martin* and coworkers reported an increase in chlorophyll *a* in shipboard experiments in August 1987, after adding Fe to High Nutrient Low Chlorophyll (HNLC) seawater from the Sub Arctic Pacific Ocean. These findings were the basis of the “glacial iron hypothesis” as proposed by *John Martin* and coworkers in 1988. In the “glacial Fe-hypothesis” it is proposed that enhanced aeolian iron supply during the last glacial maximum relieved phytoplankton from iron stress. This would have resulted in enhanced productivity and subsequent drawdown of atmospheric carbon dioxide [*Martin*, 1990]. In the following decades, clean sampling and analytical techniques allowed for a much better understanding of the distribution and sources of iron in the ocean [*Johnson et al.*, 1997; *De Baar and De Jong*, 2001; *Moore and Braucher*, 2008] and its relation with phytoplankton [*Timmermans et al.*, 2001; *Boyd et al.*, 2000; *De Baar et al.*, 2005]. *Morel et al.* [1991] hypothesized that the HNLC regions in the world oceans are dominated by small phytoplankton, adapted to low iron, and that grazing also controls the phytoplankton abundance in these regions. Small phytoplankton cells have a scale advantage; their higher surface to volume ratio allows diffusive transport and cellular uptake at lower ambient Fe concentrations [*Timmermans et al.*, 2001]. Moreover, smaller cells have a smaller boundary layer thickness, which enhances the concentration gradients between the outside and the inside of the cells [*Marchetti and Cassar*, 2009]. Multiplication of these factors causes the advantage for cells to increase quadratically with smaller radius. The shipboard Fe addition experiments in bottles [*De Baar et al.*, 1990; *Buma et al.*, 1991] were consistent also with the first lines of evidence for natural iron fertilization of the spring diatom bloom at the Polar Front in the Southern Ocean [*De Baar et al.*, 1995]. Another approach to demonstrate Fe limitation, was taken by adding dissolved Fe directly *in situ* to the surface ocean. Moreover, the notion of anthropogenic induced climate change led to an interest in CO₂ drawdown from the atmosphere into the ocean and possible sequestration of carbon into the deep ocean [*Martin*, 1990; *Raven and Falkowski*, 1999; *Takahashi et al.*, 2002]. Perhaps by Fe addition, this CO₂ drawdown might be stimulated; “The iron hypothesis”. These considerations have led to several mesoscale *in situ* Fe-enrichment experiments, synthesized first by [*De Baar et al.*, 2005] and next summarized by [*Boyd et al.*, 2007]. For all the *in situ* fertilization experiments, the chlorophyll levels and biomass increased upon Fe addition, but the amount of net uptake of carbon in the surface waters, and the ensuing export into the deep ocean were found to be quite modest [*De Baar et al.*, 2005; 2008]. In general, a strong ecosystem shift in favor of large size class of diatoms was always observed [*De Baar et al.*, 2005]. One drawback of these experiments is the pulsed addition(s) of Fe that might more resemble episodic dust supply, but not Fe supply by long term processes such as advection, upwelling and recycling [*Boyd et al.*, 2007]. Therefore, several natural iron “fertilization” studies were conducted downstream of islands in the Southern Ocean [*Blain et al.*, 2007; *Pollard et al.*, 2009]. The rationale behind this is that advection of iron from the sediments around these

islands will relieve the phytoplankton community downstream from iron stress. Natural fertilization studies [De Baar et al, 1995; Blain et al., 2007, Pollard et al., 2009] in general have shown enhanced carbon uptake and export due to iron input. Summarizing, the Fe additions in shipboard, in *in situ* 'artificial' fertilizations, and in the natural fertilization studies all have shown convincing evidence of the strong link of iron (availability) to primary production, and thus to the global carbon cycle.

1.1.3 Input sources and cycling of Fe

In the last few decades, many efforts were made to identify sources of Fe to the global ocean [De Baar and De Jong, 2001]. Several sources are known for Fe supply to the global ocean. The main pathways for the entrance of trace metals (including Fe) to the global ocean are shown in Figure 1.1 (after [Frank, 2011]). For the surface waters, the main sources are dust deposition, river water, emanation of reduced Fe from suboxic shelf sediments, and supply from below by upward mixing and advection of deeper waters that tend to have higher dissolved Fe concentrations. However, it should be noted that the Fe concentration in these waters is deficient relative to major nutrients (N,P) because Fe is removed from subsurface waters by scavenging. This explains the importance of sources other than vertical resupply. For the deep waters, there is additional supply from hydrothermal vent sources.

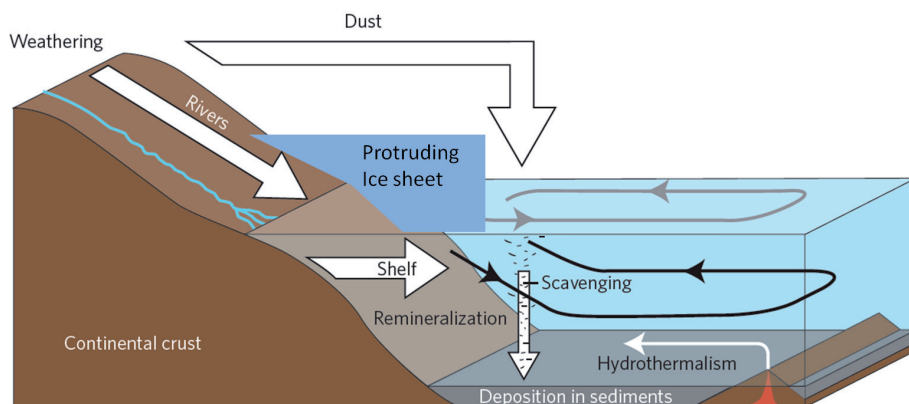


Fig. 1.1 External sources of trace metals (amongst which iron (Fe)) to the ocean (drafted after [Frank et al., 2011]). Also shown is the situation as found close to the Antarctic continent, where the ice-sheet extends far into the ocean, largely preventing shelf input of Fe.

An important input source to some regions of the upper ocean is atmospheric dust transported from continental desert sources via the atmosphere towards the sea surface. The earth's crust consists for ~3.5% by mass of Fe [Taylor, 1964], resulting in a significant (temporary) input source of aeolian Fe dust upon rain and/or dry deposition. Although this supply is most important in the low latitude region of the North Atlantic Ocean [Jickells and Spokes, 2001] it has also been identified as input source

to the southern South Atlantic Ocean [Cassar *et al.*, 2007; Chever *et al.*, 2010; Jickells *et al.*, 2005] and the SubAntarctic region south of Australia [Bowie *et al.*, 2009; Sedwick *et al.*, 2008], and the North Pacific [Measures and Brown, 2005] .

Another important source of DFe to the upper ocean are shelf sediments; Fe can be mobilized after reductive dissolution of iron oxides and organic moieties from the sediment [De Baar and De Jong, 2001; Elrod *et al.*, 2004]. Moreover, sediment resuspension and near- seabed mixing can cause a dissolution of Fe from suspended particles in shelf regions [Laës *et al.*, 2007 and references therein; Nédélec *et al.*, 2007, Homoky *et al.*, 2012]. Recently, Homoky *et al.*, [2012] have shown that these processes at the bottom interact; in some cases, after a benthic Fe flux, the Fe may be transported off shelf by suspended particles leading to a flux of Fe from the shelf sediments to the open ocean. For the Southern Ocean Islands and Antarctic Peninsula, shelf input sources have been shown to have a large downstream effect [Blain *et al.*, 2001; Blain *et al.*, 2007; Bucciarelli *et al.*, 2001; Pollard *et al.*, 2009; Ardelan *et al.*, 2010].

Rivers have been shown to be important sources of Fe to the ocean in many regions of the world [De Baar and De Jong, 2001]. However a large amount of the Fe delivered by rivers does not enter the coastal zone due to loss by flocculation and precipitation within the estuaries. Nevertheless the simultaneous delivery of DOM by rivers may enhance the formation of organic complexes with Fe, providing a mechanism to circumvent Fe loss in the estuary, enabling at least a small portion of the riverine Fe supply to reach the open ocean [Krachler *et al.*, 2005 and references therein].

When the Fe concentration within a certain ocean region, such as the Polar Oceans, is under study, also lateral advection of waters from different regions, could serve as an Fe source. For example, both [Sedwick *et al.*, 2008] and [Bowie *et al.*, 2009] mention advection of subtropical surface waters, enriched in Fe, to be an Fe input source to the Southern Ocean.

Although much attention has been given to lateral input sources and aeolian dust sources from above, perhaps the most important source of DFe to surface waters, comes from below, vertical upward net Fe transport either due to upwelling advection [Hoppema *et al.*, 2003], or vertical turbulent mixing, or deepening of the (winter) mixed layer. Although the relative importance of deep water sources differs between Ocean regions [Archer and Johnson, 2000; Fung *et al.*, 2000], it has been shown to be important in upwelling zones, such as the Southern Ocean [De Baar *et al.*, 1995; Watson *et al.*, 2000; Hoppema *et al.*, 2003].

The higher concentration of DFe in deep waters compared to surface waters have long been ascribed to the net effect of remineralization processes deeper in the water column [Johnson *et al.*, 1997; Martin *et al.*, 1989; De Baar and De Jong, 2001], and scavenging removal in interplay with organic complexation [Johnson *et al.*, 1997]. Boyd and Ellwood [2010] noted that the first process is most important in the 250m-1000m zone, whereas the latter process is dominant below 1000m depth.

With the ongoing discovery of hydrothermal vents at mid-ocean regions throughout the world oceans, also the hydrothermal input source term of DFe can be better constrained and in this thesis research has been shown [Klunder *et al.*, 2008, 2009] to be far more important and widespread than previously recognized, mainly in regions close to mid-ocean ridges [Boyle *et al.*, 2005; Tagliabue *et al.*, 2010; Wu *et al.*, 2011].

Removal of Fe from the surface waters of the water column is mediated by true biological uptake and non-biological adsorptive scavenging, albeit with mostly biogenic plankton particles as the scavenging agent. The particle reactive Fe is prone to scavenging removal from the water column [Whitfield and Turner, 1987; Johnson *et al.*, 1997], and thus the removal is probably directly dependent on the particle concentration [De Baar and de Jong, 2001]. Therefore, turbid waters, such as productive coastal zones and estuaries comprising both high abundances of plankton and suspended silt and clay, show a strong scavenging removal, although scavenging also plays a role in open oceans [Boyd and Ellwood, 2010].

Biological uptake of DFe from the surface waters by phytoplankton and subsequent export to the deeper waters is a key process in Fe cycling in the world oceans. The magnitude of this process is dependent on several factors, notably other growth limiting parameters (i.e. light energy, major nutrients, other trace nutrients), the C:Fe stoichiometric ratio of organisms and the settling velocity of biogenic debris out of the upper ocean into the deep waters. Nevertheless, the common Fe depth profile in the open oceans typically shows a minimum at the subsurface, corresponding to the chlorophyll a maximum [De Baar *et al.*, 2008; Sarthou *et al.*, 2007]. When this phytoplankton dies off or is consumed and sinks throughout the water column, there is net Fe transport into the deep ocean. Moreover adsorption of DFe onto organic surfaces may further enhance the Fe loss from the surface waters. On the other hand, the dissolved organic matter may form organic complexes with Fe, retarding scavenging removal [Bergquist *et al.*, 2007; Gledhill and van den Berg, 1994; Thuroczy *et al.*, thesis, 2011].

1.2 The Polar Oceans ...key to global climate

A major part of the world's ocean is defined as Polar. The Arctic Ocean is the ocean area around the geographic North Pole. It is a relatively small ocean surrounded by land, except for connections with the North Atlantic Ocean at the Davis Strait and Fram Strait, and with the North Pacific Ocean through the Bering Strait. Despite its relatively isolated location, the Arctic Ocean plays a crucial role in global ocean circulation. The intermediate and deep waters of the Arctic Ocean are strong contributors to the major southwards overflows: the Denmark Strait Overflow Water, the Iceland-Faröer Overflow Water, and the Faröer-Scotland Overflow Water. The Arctic intermediate waters cross the sills in a southwards direction, and provide dense waters to the overflow, eventually acting as a major driver of the the Meridional Overturning Circulation [Rudels, 2001] via the formation of North Atlantic Deep Water [Smethie and Fine, 2001; Swift, 1984].

The Arctic Ocean also plays an important role in the global nutrient cycles. The phosphate excess of the waters leaving the Arctic Ocean nicely complements hence enables a significant part of the nitrogen fixation in the North Atlantic, and thereby regulates the balance between nitrogen and phosphate limitation in the different oceans [Yamamoto-Kawai *et al.*, 2006]. It has long been assumed that the sea-ice in the Central Arctic Ocean prevents significant primary production. However, the Arctic shelf seas are recognized as very productive ocean regions. Moreover, decreasing sea-ice cover likely due to global warming of the Arctic region has led to an increase in primary production over the last few decades [Arrigo *et al.*, 2008; Pabi *et al.*, 2008]. As a consequence, there is an increase in the nitrate deficit relative to phosphate in the Arctic Ocean waters that contribute to the North Atlantic [Arrigo *et al.*, 2008]. Presumably, this has increased nitrogen fixation as a consequence, although because Fe is needed for the process of nitrogen fixation [Zehr *et al.*, 1993; Falkowski *et al.*, 1998], it is still unclear whether Fe concentration of the waters leaving the Arctic is sufficient to sustain this putative increased nitrogen fixation.

The Arctic is recognized for the strong contribution of freshwater by rivers to the total water column, leading to low salinity upper waters [Dittmar and Kattner, 2003; Rudels, 2001]. Almost everywhere in the Central Arctic, halocline waters are observed below the upper mixed layer. These halocline waters are advected from the shelves bringing freshwater; the ice-cover and relatively large salinity difference between these waters and lower Atlantic derived waters prevent mixing with deep waters [Aagaard *et al.*, 1981; Bauch *et al.*, 2009] and thereby block a major route for (trace) nutrients to the surface waters. This strong river input, the large amount of shelves, and the limited vertical mixing will together determine the trace metal inputs and cycling in the Arctic Ocean.

In the Southern Hemisphere, the Southern Ocean is defined as all waters south of the SubAntarctic Front, situated between about 40°S and 50°S. Further southwards the Polar Front meandering around the globe at about 50°S marks the northwards boundary of the Antarctic Ocean, comprising all waters south of the Polar Front. The Polar Front is defined as the surface expression of the 2 °C isotherm of seawater temperature, all surface waters south of the Polar Front are colder, to as low as about -1.85 °C, freezing point of seawater.

The Southern Ocean plays an important role in the global thermohaline circulation [Rintoul *et al.*, 2001]. Briefly, deep water masses from the Atlantic, Pacific and Indian Oceans flow southward towards the Antarctic continent. Here, they are transported eastward by the Antarctic circumpolar current (ACC), the wind driven current around Antarctica, which connects the Atlantic, Indian and Pacific Oceans [Rintoul *et al.*, 2001]. Amongst other oceans, in the Atlantic Sector, strong Ekman pumping causes upwelling of the Southwards flowing intermediate water (Central Deep Water, influenced by NADW) (Figure 1.2), bringing these nutrient rich waters to the surface. Upon their return flow Northwards, these waters subduct at the Polar

Front and form Antarctic Intermediate Waters (AAIW) spreading out into the three major oceans at a typical depth of around 1000 metres. Close to the Antarctic continent the waters lose sufficient buoyancy due to cooling and sea ice formation, to sink all the way down to become bottom waters [Orsi *et al.*, 1999]. These waters flow northwards close to the bottom as cold, nutrient rich, Antarctic Bottom Water (AABW), which still is recognizable far in the North Atlantic Ocean [Laës *et al.*, 2007; Sarmiento *et al.*, 2004; Middag, 2010].

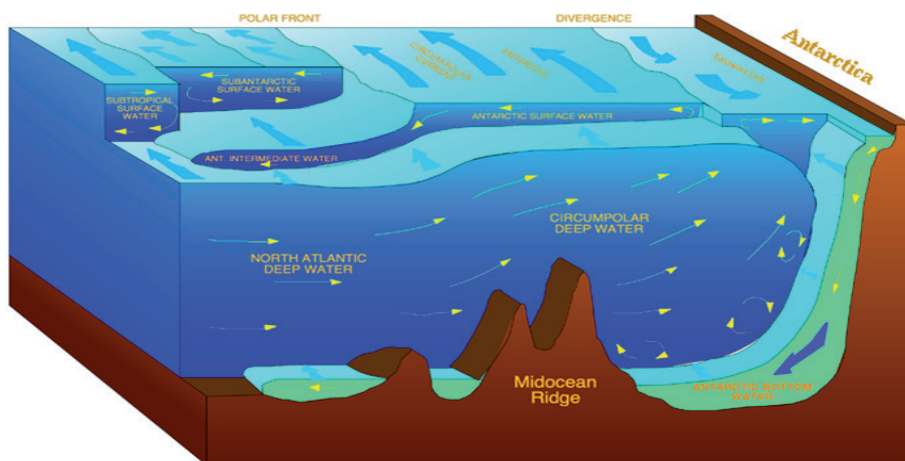


Fig. 1.2 Main water masses and currents in the Atlantic Sector of the Southern Ocean. North Atlantic Deep Water is (partly) formed from overflow waters originating from the Arctic Ocean (see text). (from H. Grobe, AWI).

The extensive upwelling of deep waters in the Southern Ocean delivers large amounts of nutrients (PO_4^{3-} , NO_3^- , Si(OH)_4) to the surface [Broecker and Peng, 1982; Sarmiento *et al.*, 2004]. Therefore this upwelling stimulates primary production, and the high abundance of silicate allows diatoms to make up for ~40% of total production in the Southern Ocean [De Master, 1981, 2002]. The availability of these major nutrients and the subsequent phytoplankton growth influences the CO_2 -drawdown reported to take place in summer in the Southern Ocean [Takahashi *et al.*, 2009]. Nevertheless, the present major nutrients are not (fully) used by phytoplankton, and this apparent growth limitation has been attributed to a lack of iron [Martin and Fitzwater, 1988]. Thus a large part of the Southern Ocean, in principle all surface waters of the Antarctic Ocean (i.e. south of the Polar Front) is a HNLC region (see section 1.1). Due to its great distance from land and continental shelves the Fe-input sources to most of the Southern Ocean are limited. Nevertheless, locally, major input sources of iron are aeolian deposition [Cassar *et al.*, 2007; Jickells *et al.*, 2005], melting of ice-bergs [Crook *et al.*, 2004; Lin *et al.*, 2011], Fe derived from shelves, Southern Ocean islands, or Peninsula [Sedwick *et al.*, 1997; Blain *et al.*, 2001; Bucciarelli *et al.*, 2001; Planquette *et al.* 2007; Ardelan *et al.*, 2010], and shallow remineralisation of phytoplank-

ton. Moreover, at the edge of the sea-ice Fe concentrations are fairly high [Lannuzel *et al.*, 2007; 2008, Sedwick and DiTullio, 1997], and have been shown to stimulate algal growth [Sedwick and DiTullio, 1997]. Sea-ice can be seen as a storage reservoir for iron; ice scavenges iron during formation in autumn/winter and releases it upon melting in spring, which is favorable for algal growth [Lannuzel *et al.*, 2008]. These input sources may enhance the Fe concentration locally, relieving phytoplankton from iron stress, and thereby stimulating phytoplankton growth.

More large scale delivery of Fe to the surface waters includes advection of subtropical waters from the North [Bowie *et al.*, 2009; Sedwick *et al.*, 2008] and vertical mixing and upwelling of deep waters [De Baar *et al.*, 1995; Löscher *et al.*, 1997; Measures and Vink, 2001; Croot *et al.*, 2004; Sedwick *et al.*, 2008] that are relatively rich in DFe.

1.3 GEOTRACES in the International Polar Year

This PhD thesis lies within the scope of the international GEOTRACES program. GEOTRACES is an international scientific program which aims to study biogeochemical cycles of trace metals in the world oceans (www.geotraces.org). The mission of the GEOTRACES program is the following:

“To identify processes and quantify fluxes that control the distributions of key trace elements and isotopes in the ocean, and to establish the sensitivity of these distributions to changing environmental conditions”

Although the GEOTRACES program aims to obtain a large dataset of element and isotope distributions from the research cruises executed, several elements have been designated ‘key parameters’. This is based on either the requirement for phytoplankton growth (Fe, Zn, Cu, Mn, [Peers and Price, 2004; Middag *et al.* thesis, 2010]), or the use as tracer for other elements such as Fe, (Al and Mn), paleotracer (Cd) and possible toxicity (Zn, Cu) (GEOTRACES Science plan and references therein)(www.geotraces.org). Also isotopes can be used as tracers for water mass circulation (^{14}C , ^{210}Pb , ^{226}Ra), for scavenging (^{231}Pa , ^{230}Th , ^{234}Th), and for submarine groundwater discharge (and thus shelf influence) by the relatively short lived ^{224}Ra and ^{228}Ra [Broecker and Peng, 1982; Cochran, 1992; Moore, 1996; Dulaiova *et al.*, 2009]. Through its important role in phytoplankton growth, Fe is strongly involved in both the carbon and the nitrogen cycle [Morel and Price, 2003; Morel *et al.*, 2003] in the world oceans and therefore is of importance for the world biogeochemical cycles.

The recent improvement in sampling, analysis and intercomparison of Fe measurements [Bruland and Lohan, 2003; De Baar *et al.*, 2008; Johnson *et al.*, 1997] have led to the possibility to sample, analyze and compare large numbers of seawater samples for Fe. Simultaneous measurement of several elements, isotopes of ele-

ments and physical and biological parameters can optimize the interpretation and understanding of global biochemical cycles. The work in this project therefore greatly benefits from comparison to and linkage with other data obtained within the same cruise and the Fe results served the other work.

Table 1.1 Listing of completed IPY-GEOTRACES research cruises [from Fahrbach et al., 2011]

Code and name of expedition	Research vessel	Chief scientist	GEOTRACES principal investigator	GEO-TRACES IPY number	Begin date	End date	Ocean or sea	Region
KH06 Sea of Okhotsk 1	Professor Khromov	Nakatsuka, Takeshi	Nishioka, Jun	IPY 9 section	2006-08-13	2006-09-12	Sea of Okhotsk (Arctic)	Western part
au0703 SAZ-SENSE	Aurora Australis	Griffiths, Brian	Bowie, Andrew	IPY 2 section	2007-01-17	2007-02-20	Sub-Antarctic & Polar Front	South off Tasmania
ATOS-1	Hesperides	Duarte, Carlos	Tovar-Sanchez, Antonio	IPY 10 section	2007-6-29	2007-07-27	Arctic	Iceland to Spitsbergen
ARK-XXII/2	Polarstern	Schauer, Ursula	Rutgers van der Loeff, Michiel	IPY 11 section	2007-07-29	2007-10-07	Arctic	Eurasian and central Arctic
KH07 Sea of Okhotsk 2	Professor Khromov	Nakatsuka, Takeshi	Nishioka, Jun	IPY 12 section	2007-08-05	2007-09-15	Sea of Okhotsk (Arctic)	Western part
au0701 SIPEX	Aurora Australis	Worby, Tony	Bowie, Andrew	IPY 3 section	2007-09-03	2007-10-17	Antarctica	East
MD166 Bonus GoodHope	Marion Dufresne	Speich, Sabrina	Boye, Marie	IPY 4 section	2008-02-08	2008-03-24	Southern Ocean	Atlantic sector
ANT-XXIV/3 Zero & Drake	Polarstern	Fahrbach, Eberhard	De Baar, Hein	IPY 5 section	2008-02-10	2008-04-10	Southern Ocean	Greenwich meridian, Weddell Sea, Drake Passage
au0806 SR3-GEOTRACES	Aurora Australis	Rintoul, Steve	Butler, Edward	IPY 6 section	2008-08-15	2008-09-28	Southern Ocean	Antarctica to Hobart
ISSS-08	Smirnitskiy	Semiletov, Igor	Andersson, Per	IPY 13 section	2008-08-15	2008-09-28	Arctic Siberian coast	Laptev Sea and East Siberian Sea
NBP0901 DynaLife	Nathaniel B. Palmer	Jacobs, Stan	De Baar, Hein	IPY 7 process study	2009-01-05	2009-02-28	Antarctica	Amundsen Sea; Pine Island Bay
Beaufort Sea	CCGS Amundsen	Francois, Roger	Francois, Roger	IPY 14 section	2009-08-27	2009-09-13	Arctic Ocean	Canada Basin

The work performed in this thesis was performed within the coordination of the 'International Polar Year' (IPY) Program 2007-2008 (www.ipy.org). This was an internationally coordinated program 'including research and observations in both the Arctic and Antarctic polar regions and exploring the strong links these regions have with the rest of the globe.' [*The scope of science in IPY*, 2007]. The IPY-GEOTRACES component comprised 6 Arctic cruises and 6 Antarctic cruises [*Fahrbach et al.*, 2011, see Table 1.1).

For this thesis, fieldwork was executed aboard the German Research Ice breaker *Polarstern*, during the cruises ARK XXII-2 and ANT XXIV-3, IPY Sections 11 and 5 respectively (see table 1.1).

1.4 Objective of this thesis

The objective of this thesis is to understand, and where possible quantify, the distribution, sources and sinks of Fe in the Polar Oceans. For the Arctic Ocean, the very limited data present previous to our expedition made our new transect a baseline for the Fe distribution in the (Eurasian) Arctic. Moreover, we aimed to constrain the role of the Arctic in the global cycling of Fe. For the Southern Ocean, some data was available previously, but the high resolution transects of this thesis enable a more thorough understanding of Fe input, cycling and removal in the Southern Ocean. Moreover, availability of other parameters (chemical and biological) does help us to determine and quantify the various sources of Fe to both Polar Oceans. The uptake of Fe by phytoplankton and subsequent sinking and remineralization is a process of major importance for the Fe cycle, and therefore also included in this thesis.

1.5 Thesis outline

Chapter 2 of the thesis describes the distribution of Fe in the Arctic shelf seas and surface waters of the Central Arctic Ocean. In the Barents Sea and Kara Sea, near surface Fe depletion by phytoplankton is observed, and lower concentrations in the Kara Sea possibly reflect scavenging removal and further distance from the Atlantic source. Very high DFe concentrations in the Laptev Sea are attributed to sediment resuspension, sinking of brine and regeneration of Fe. Mass balance equations using $\delta^{18}\text{O}$, salinity and nutrient data are used to distinguish between the different fresh-water sources; ice-melt, river water and the salinity deficit of Pacific derived water. The effect of Fe input from ice-melt is not very strong, and mostly restricted to the Nansen Basin. The Trans Polar Drift (TPD) carries river water to the surface waters in the Central Arctic (Amundsen and Makarov Basin), causing high (>2 nM) DFe concentrations. Two stations occupied were clearly situated on the North American side of the TPD; here the DFe was generally low and determined by the combined effects of

by ice-melt, biological uptake and remineralisation processes.

The DFe distribution in the Arctic Deep Waters is described in **Chapter 3**. The ice-sheet and strong halocline in the Arctic largely prevents vertical mixing with the upper waters, such that deep lateral input sources are more important for the distribution of DFe in the Deep Arctic Ocean. The DFe emanating from the slope and imported with the Atlantic Current are the most important sources in the Nansen Basin, at intermediate depth. A very strong effect of hydrothermal DFe input (DFe > 1.5 nM) is observed throughout most of the Nansen and Amundsen Basin, where the strongest signal is close to earlier observed vents [Edmunds *et al.*, 2003]. This indicates the strong importance of hydrothermalism for trace metal concentrations in Arctic Deep waters. The absence of DFe sources in the deepest (>3000m) Amundsen and Makarov Basins cannot be fully compensated by organic complexation [Thuroczy *et al.*, 2011] and leads to strong scavenging removal, that is reflected in very low DFe concentrations and a good linear correlation with dissolved Mn.

In the Southern Ocean, **Chapter 4** describes the distribution of DFe over the Greenwich meridian transect. The main sources to the surface waters are vertical mixing and upwelling. Locally, atmospheric deposition and ice-melt are also important Fe sources. Inverse correlation between Fe and fluorescence indicates biological depletion of Fe over part of the transect. The Fe concentration in the deep waters is determined by intrusion of Fe rich NADW from the North, hydrothermal Fe input from the Mid Ocean Ridge, and removal by settling particles. In the deep Weddell Gyre, the eastwards flow, close to the continent, contains significantly lower Fe than the westwards return flow, the latter likely due to the Fe enrichment at the Antarctic Peninsula region and/or at the Mid Ocean Ridge. The extremely low dissolved Fe concentrations adjacent to the ice-sheet covered continent are unique, the ice-sheet preventing the normal biogeochemical cycling that along other, non-ice-covered, continental margins causes a supply of dissolved Fe from the sediments.

The distribution of Fe in the Western Weddell Sea and Drake Passage is the subject of **Chapter 5**. In the Weddell Sea very low concentrations of DFe (0.01-0.1 nM) are reported, which can be partly explained with high POC export and/or primary production (indicated by chlorophyll fluorescence). The ratio of seasonal N:P removal in the Western Weddell Sea was constant (~11) with increasing DFe, whereas at the Greenwich meridian transect an increase in the N:P removal ratio with increasing DFe was observed. This is attributed to the smaller diatoms in the Western Weddell Sea, being less vulnerable to Fe limitation. The input of DFe from the Antarctic Peninsula shelf has the strongest influence in the Drake Passage, where it follows isopycnals far into the basin, consistent with higher manganese, aluminum and radium. An increase of DFe (~ 3 nM) and lower salinity towards the Tierra del Fuego shelf indicates fluvial/glacial DFe input. In the Deep Weddell Sea, formation of deep water (by downslope convection) causes relatively high Fe (0.6-0.8 nM) concentrations in the bottom waters relative to the water masses at mid depth (0.2-0.4 nM). Some of the bottom waters in the Weddell Sea cross the Scotia Ridge where it picks

up DFe and is observed as bottom water with high DFe (~ 1 nM) in the Deep Southern Drake Passage. Part of the Weddell Sea Deep Waters crosses the Scotia Ridge and spreads as AABW over the abyssal world Ocean. Most of the Deep Water flows along the ridge as the Eastwards limb of the Weddell Gyre and becomes enriched during this transit as seen from the increase in DFe of between the Antarctic Peninsula and the Greenwich meridian. Close to the South American continental shelf, at ~ 2000 m depth an increase in DFe (to >1.5 nM), corresponding to a Mn maximum and $\delta^3\text{He}$ anomaly is attributed to a hydrothermal source in the deep South Pacific Ocean.

In **Chapter 6** the Fe data obtained during ANT XXIV/3 is combined with the previously existing Fe data available from within the ACC, Weddell Gyre and Ross Gyre and next compiled and averaged over four different depth layers (ML, ML-300m, 300-1000m, >1000 m). The average concentration of dissolved iron increases with depth, from ~ 0.28 nM in the surface waters to ~ 0.56 nM below 1000 meters. Slightly higher concentrations south of the Polar Front region (PFR), compared to within the Polar Front region are attributed to upwelling of deep waters, mainly in the Atlantic sector. From Patagonia until 60°E , in the upper 1000m, relatively high DFe concentrations are observed. Within the Weddell Gyre, the dissolved iron is slightly higher in the eastward return flow than in the westward flow more to the south adjacent to the Antarctic continent and protruding ice-sheet, for all depths. Even higher concentrations are observed near to the Antarctic Peninsula, indicating the importance of sedimentary processes as a DFe source. This compilation of all DFe data available thus far in four depth ranges, gives insight in the DFe available to phytoplankton growth in the ACC and Southern Ocean Gyres, and therefore provides the best available data compilation of DFe for simulation modeling studies.

Finally the **Chapter 7** comprises a brief summary of the major findings and some recommendations for future research.

1.6 References

- Aagaard, K., L. K. Coachman, and E. Carmack (1981), On the halocline of the Arctic Ocean, *Deep Sea Research Part A. Oceanographic Research Papers*, 28(6), 529-545.
- Abouchami, W., Galer, S., De Baar, H., Alderkamp, A.-C., Middag, R., Laan, P. (2011), Modulation of the Southern Ocean cadmium isotope signature by ocean circulation and primary productivity. *Earth and Planetary Science Letters* 305, 83–91.
- Archer, D. E., and K. Johnson (2000), A model of the iron cycle in the ocean, *Global Biogeochem. Cycles*, 14(1), 269-279.
- Ardelan, M. V., O. Holm-Hansen, C. D. Hewes, C. S. Reiss, N. S. Silva, H. Dulaiova, E. Steinnes, and E. Sakshaug (2010), Natural iron enrichment around the Antarctic Peninsula in the Southern Ocean, *Biogeosciences*, 7(1), 11-25.
- Arrigo, K. R., G. van Dijken, and S. Pabi (2008), Impact of a shrinking Arctic ice cover on marine primary production, *Geophys. Res. Lett.*, 35(19), L19603.
- Bauch, D., I. A. Dmitrenko, C. Wegner, J. Hölemann, S. A. Kirillov, L. A. Timokhov, and H. Kassens (2009), Exchange of Laptev Sea and Arctic Ocean halocline waters in response to atmospheric forcing, *J. Geophys. Res.*, 114(C5), C05008.
- Bergquist, B. A., J. Wu, and E. A. Boyle (2007), Variability in oceanic dissolved iron is dominated by the colloidal fraction, *Geochimica et Cosmochimica Acta*, 71(12), 2960-2974.
- Blain, S., et al. (2001), A biogeochemical study of the island mass effect in the context of the iron hypothesis: Kerguelen Islands, Southern Ocean, *Deep Sea Research Part I: Oceanographic Research Papers*, 48(1), 163-187.
- Blain, S., et al. (2007), Effect of natural iron fertilization on carbon sequestration in the Southern Ocean, *Nature*, 446(7139), 1070-1074.
- Bowie, A. R., D. Lannuzel, T. A. Remenyi, T. Wagener, P. J. Lam, P. W. Boyd, C. Guieu, A. T. Townsend, and T. W. Trull (2009), Biogeochemical iron budgets of the Southern Ocean south of Australia: Decoupling of iron and nutrient cycles in the subantarctic zone by the summertime supply, *Global Biogeochem. Cycles*, 23(4), GB4034.
- Boyd, P., A. Watson, C. Law, E. Abraham, T. Trull, R. Murdoch, D. Bakker, A. Bowie, K. Bueseler, and H. Chang (2000), A mesoscale phytoplankton bloom in the polar Southern Ocean stimulated by iron fertilization, *Nature*, 407(6805), 695-702.
- Boyd, P. W., and M. J. Ellwood (2010), The biogeochemical cycle of iron in the ocean, *Nature Geosciences*, 3(10), 675-682.
- Boyd, P. W., et al. (2007), Mesoscale Iron Enrichment Experiments 1993-2005: Synthesis and Future Directions, *Science*, 315(5812), 612-617.
- Boyle, E. A., B. A. Bergquist, R. A. Kayser, and N. Mahowald (2005), Iron, manganese, and lead at Hawaii Ocean Time-series station ALOHA: Temporal variability and an intermediate water hydrothermal plume, *Geochimica et Cosmochimica Acta*, 69(4), 933-952.
- Broecker, W. and Peng, H. 1982. Tracers in the Sea, Eldigio Press, ISBN 096175110X
- Bruland, K. W., and M. C. Lohan (2003), Controls of Trace Metals in Seawater, in *Treatise on Geochemistry*, edited by D. H. Heinrich and K. T. Karl, pp. 23-47, Pergamon, Oxford.
- Bruland, K.W., Donat, J.R., Hutchins, D.A. (1991) Interactive influence of bioactive trace-metals on biological production in oceanic waters. *Limnol Oceanogr.* 36 (8), 1555-1577.

- Bucciarelli, E., S. Blain, and P. Tréguer (2001), Iron and manganese in the wake of the Kerguelen Islands (Southern Ocean), *Marine Chemistry*, 73(1), 21-36.
- Buma, A.G.J., H.J.W. de Baar, R.F. Nolting, A.J. van Bennekom, (1991), Metal enrichment experiments in the Weddell-Scotia Seas: Effects of iron and manganese on various plankton communities. *Limnol. Oceanogr.* 36(8): 1865-1878
- Cassar, N., M. L. Bender, B. A. Barnett, S. Fan, W. J. Moxim, H. Levy, and B. Tilbrook (2007), The Southern Ocean Biological Response to Aeolian Iron Deposition, *Science*, 317(5841), 1067-1070.
- Chever, F., E. Bucciarelli, G. Sarthou, S. Speich, M. Arhan, P. Penven, and A. Tagliabue (2010), Physical speciation of iron in the Atlantic sector of the Southern Ocean along a transect from the subtropical domain to the Weddell Sea Gyre, *J. Geophys. Res.*, 115(C10), C10059.
- Cochran, J.K., (1992), The oceanic chemistry of theuranium and thorium series nuclides. In *Uranium Series Disequilibrium—Application to Environmental Problems: Applications to Earth, Marine, and Environmental Sciences*, 2nd edition (ed. M. Ivanovich and R.S. Harmon) , pp. 334–395. Oxford University Press.
- Croot, P. L., K. Andersson, M. Öztürk, and D. R. Turner (2004), The distribution and speciation of iron along 6°E in the Southern Ocean, *Deep Sea Research Part II: Topical Studies in Oceanography*, 51(22-24), 2857-2879.
- De Baar, H. J. W., J. T. M. de Jong, D. C. E. Bakker, B. M. Loscher, C. Veth, U. Bathmann, and V. Smetacek (1995), Importance of iron for plankton blooms and carbon dioxide drawdown in the Southern Ocean, *Nature*, 373(6513), 412-415.
- De Baar, H.J.W., and De Jong, J.T.M. (2001), Distributions, Sources and Sinks of Iron in SeaWater, Chapter 5 in : *Biogeochemistry of iron in seawater*. (Eds. Hunter, D.R. and Turner, K.A), 123-253. IUPAC Book Series on Analytical and Physical Chemistry of Environmental Systems 7, John Wiley and Sons Ltd., Chichester, UK.
- De Baar, H.J.W. and J. La Roche (2003), Metals in the Oceans; Evolution, Biology and Global Change. In: F. Lamy and G. Wefer (eds.) *Marine Scientific Frontiers for Europe*, Springer Verlag, Berlin, pp. 79-105.
- De Baar, H. J. W., et al. (2005), Synthesis of iron fertilization experiments: From the Iron Age in the Age of Enlightenment, *J. Geophys. Res.*, 110(C9), C09S16.
- De Baar, H.J.W., Timmermans, K.R., Laan, P., de Porto, H.H., Ober, S., Blom, J.J., Bakker, M.C., Schilling, J., Sarthou, G., Smit, M.G., Klunder, M. (2008), Titan: A new facility for ultraclean sampling of trace elements and isotopes in the deep oceans in the international Geotraces program, *Marine Chemistry*, 111(1-2), 4-21.
- DeMaster, D.J. (1981). "The supply and accumulation of silica in the marine environment". *Geochimica et Cosmochimica Acta* 45: 1715-1732.
- DeMaster, D.J. (2002). The accumulation and cycling of biogenic silica in the Southern Ocean: revisiting the marine silica budget. *Deep-Sea Research II* 49: 3155-3167
- Dittmar, T., and G. Kattner (2003), The biogeochemistry of the river and shelf ecosystem of the Arctic Ocean: a review, *Marine Chemistry*, 83(3-4), 103-120.
- Dulaiova, H., M. V. Ardelan, P. B. Henderson, and M. A. Charette (2009), Shelf-derived iron inputs drive biological productivity in the Southern Drake Passage, *Global Biogeochemical Cycles*, doi:10.1029/2008GB003406.

- Edmonds, H. N., P. J. Michael, E. T. Baker, D. P. Connelly, J. E. Snow, C. H. Langmuir, H. J. B. Dick, R. Muhe, C. R. German, and D. W. Graham (2003), Discovery of abundant hydrothermal venting on the ultraslow-spreading Gakkel ridge in the Arctic Ocean, *Nature*, 421 (6920), 252-256.
- Elrod, V. A., W. M. Berelson, K. H. Coale, and K. S. Johnson (2004), The flux of iron from continental shelf sediments: A missing source for global budgets, *Geophys. Res. Lett.*, 31(12), L12307.
- Falkowski, P.G., Barber, R.T., Smetacek, V. (1998), Biogeochemical controls and feedbacks in Ocean Primary production. *Science*, 281 (200).
- Fahrbach, E., H.J.W. De Baar, V. Garçon and C. Provost (2011). Introduction to physics, carbon dioxide, trace elements and isotopes in the Southern Ocean: The *Polarstern* expeditions ANT-XXIV/3 (2008) and ANT-XXIII/3 (2006). *Deep-Sea Research II; Topical studies in Oceanography*, 58 (25-26) pp. 2501-2508.
- Frank, M. (2011), Oceanography: Chemical twins, separated, *Nature Geosciences*, 4(4), 220-221.
- Frausto da Silva, J.J.R., Williams, R.J.P. (1994) *The biological chemistry of the elements*, Clarendon Press, Oxford, UK, P.651.
- Fung, I. Y., S. K. Meyn, I. Tegen, S. C. Doney, J. G. John, and J. K. B. Bishop (2000), Iron supply and demand in the upper ocean, *Global Biogeochem. Cycles*, 14(1), 281-295.
- GEOTRACES Science Plan (www.geotraces.org)
- Gledhill, M., and C. M. G. van den Berg (1994), Determination of complexation of iron(III) with natural organic complexing ligands in seawater using cathodic stripping voltammetry. *Marine Chemistry*, 47(1), 41-54.
- Hart, T.J. (1934), On the phytoplankton of the Southwest Atlantic and the Bellingshausen Sea 1929-1931, *Discovery Reports*, 8, 1-268.
- Homoky, W.B., S. Severmann, J. McManus, W.M. Berelson, T.E. Riedel, P.J. Statham and R.A. Mills (2012), Dissolved oxygen and suspended particles regulate the benthic flux of iron from continental margins. *Marine Chemistry*, 134-135, 59-70
- Hoppema, M., H. J. W. de Baar, E. Fahrbach, H. H. Hellmer, and B. Klein (2003), Substantial advective iron loss diminishes phytoplankton production in the Antarctic Zone, *Global Biogeochem. Cycles*, 17(1), 1025.
- IPY Scope for Science (www.ipy.org)
- Jakuba, R. W., M. A. Saito, J. W. Moffett, and Y. Xu (2012), Dissolved zinc in the subarctic North Pacific and Bering Sea: Its distribution, speciation, and importance to primary producers, *Global Biogeochem. Cycles*, 26, GB2015, doi:10.1029/2010GB004004.
- Jickells, T. D., et al. (2005), Global Iron Connections Between Desert Dust, Ocean Biogeochemistry, and Climate, *Science*, 308(5718), 67-71.
- Jickells, T.D. and Spokes, L. J. (2001) Atmospheric Iron inputs to the oceans, Chapter 4 in: *Biogeochemistry of iron in seawater*. (Eds. Hunter, D.R. and Turner, K.A), 41-85. IUPAC Book Series on Analytical and Physical Chemistry of Environmental Systems 7, John Wiley and Sons Ltd., Chichester, UK.
- Johnson, K. S., R. M. Gordon, and K. H. Coale (1997), What controls dissolved iron concentrations in the world ocean?, *Marine Chemistry*, 57(3-4), 137-161.

- Johnson, K.S., Boyle, E., Bruland, K., Measures, C., Moffett, J., Aquilarislas, A., Barbeau, K., Cai, Y., Chase, Z., Cullen, J., Doi, T., Elrod, V., Fitzwater, S., Gordon, M., King, A., Laan, P., Laglera-Baquer, L., Landing, W., Lohan, M., Mendez, J., Milne, A., Obata, H., Osslander, L., Plant, J., Sarthou, G., Sedwick, P., Smith, G.J., Sohst, B., Tanner, S., Van Den Berg, S., Wu, J. (2007), Developing standards for dissolved iron in seawater. *Eos Transactions of the AGU* 88 (11), 131.
- Krachler, R., F. Jirsa, and S. Ayromlou (2005), Factors influencing the dissolved iron input by river water to the open ocean, *Biogeosciences*, 2(4), 311-315.
- Klunder, M.B., Middag, R.,Thuróczy, C.-E., Gerringa, L.J.A., De Baar, H.J.W. (2008), Distribution and sources of dissolved iron in the Arctic Ocean. In: SCAR-IACS IPY Conference, St. Petersburg, Russia, July 2008.
- Klunder, M.B., Laan, P., Bakker, K., Ober, S., De Baar, H.J.W.(2009), IPY-GEOTRACES: sources and distribution of dissolved iron in the Arctic and Southern oceans. In: ASLO Aquatic Sciences Meeting, Nice, January 2009.
- Laës, A., S. Blain, P. Laan, S. J. Ussher, E. P. Achterberg, P. Tréguer, and H. J. W. de Baar (2007), Sources and transport of dissolved iron and manganese along the continental margin of the Bay of Biscay, *Biogeosciences*, 4(2), 181-194.
- Lannuzel, D, V. Schoemann, J. de Jong, J, L. Chou, J.L. Tison (2007), Distribution and biogeochemical behaviour of iron in the East Antarctic sea-ice . *Marine Chemistry*, 106(1-2), 18-32
- Lannuzel, D, V. Schoemann, J. de Jong, J, L. Chou, B. Delille, S. Becquevort, J.L. Tison (2008). Iron study during a time series in the western Weddell pack ice, *Marine Chemistry*, 108 (1-2), 85-95
- Lin, H., S. Rauschenberg, C. R. Hexel, T. J. Shaw, and B. S. Twining (2011), Free-drifting icebergs as sources of iron to the Weddell Sea, *Deep Sea Research Part II: Topical Studies in Oceanography*, 58(11-12), 1392-1406.
- Loscher, B. M., H. J. W. De Baar, J. T. M. De Jong, C. Veth, and F. Dehairs (1997), The distribution of Fe in the antarctic circumpolar current, *Deep Sea Research Part II: Topical Studies in Oceanography*, 44(1-2), 143-187.
- Martin, J. H. (1990), Glacial-Interglacial CO₂ Change: The Iron Hypothesis, *Paleoceanography*, 5(1), 1-13.
- Martin, J. H., and S. E. Fitzwater (1988), Iron deficiency limits phytoplankton growth in the north-east Pacific subarctic, *Nature*, 331(6154), 341-343.
- Martin, J. H., R. M. Gordon, and S. E. Fitzwater (1990), Iron in Antarctic waters, *Nature*, 345(6271), 156-158.
- Martin, J. H., R. M. Gordon, S. Fitzwater, and W. W. Broenkow (1989), Vertex: phytoplankton/iron studies in the Gulf of Alaska, *Deep Sea Research Part A. Oceanographic Research Papers*, 36(5), 649-680.
- Marchetti, A. and N. Cassar (2009), Diatom elemental and morphological changes in response to iron limitation: a brief review with potential paleoceanographic applications, *Geobiology* 7, 419-431
- Measures, C. I., and S. Vink (2001), Dissolved Fe in the upper waters of the Pacific sector of the Southern Ocean, *Deep Sea Research Part II: Topical Studies in Oceanography*, 48(19-20), 3913-3941.

- Measures, C.I., M.T Brown and S. Vink (2005). Dust deposition to the surface waters of the western and central North Pacific inferred from surface water dissolved aluminum concentrations, *Geochemistry Geophysics Geosystems* 6(9) , 1-16.
- Middag, R. (2010), *Dissolved Aluminum and Manganese in the Polar Oceans*, PhD-thesis, University of Groningen, ISBN: 978-90-367-4513-0.
- Moore, W.S., 1996. Large groundwater inputs to coastal waters revealed by ^{226}Ra enrichments. *Nature*, 380: 612–614.
- Moore, J. K., and O. Braucher (2008), Sedimentary and mineral dust sources of dissolved iron to the world ocean, *Biogeosciences*, 5(3), 631-656.
- Morel, F.M.M. and Morel-Laurens, M.M.L. (1983), Trace metals and plankton in the oceans: facts and speculation. Chapter in: *Trace metals in sea water* (eds. C.S. Wong), 841-869, NATO conference series IV, marine sciences, v. 9, Plenum press, New York, USA.
- Morel, Francois M. M. Robert J. M. Hudson and Neil M. Price (1991), Limitation of Productivity by Trace Metals in the Sea. *Limnology and Oceanography* 36 (8), 1742-1755
- Morel, F. M. M., and N. M. Price (2003), The Biogeochemical Cycles of Trace Metals in the Oceans, *Science*, 300(5621), 944-947.
- Morel, F. M. M., A. J. Milligan, and M. A. Saito (2003), Marine Bioinorganic Chemistry: The Role of Trace Metals in the Oceanic Cycles of Major Nutrients, in *Treatise on Geochemistry*, edited by D. H. Heinrich and K. T. Karl, pp. 113-143, Pergamon, Oxford.
- Nédélec, F., P. J. Statham, and M. Mowlem (2007), Processes influencing dissolved iron distributions below the surface at the Atlantic Ocean-Celtic Sea shelf edge, *Marine Chemistry*, 104(3-4), 156-170.
- Nelson, D. M., P. Tréguer, M. A. Brzezinski, A. Leynaert, and B. Quéguiner (1995), Production and dissolution of biogenic silica in the ocean: Revised global estimates, comparison with regional data and relationship to biogenic sedimentation, *Global Biogeochem. Cycles*, 9(3), 359-372.
- Orsi, A. H., G. C. Johnson, and J. L. Bullister (1999), Circulation, mixing, and production of Antarctic Bottom Water, *Progress In Oceanography*, 43(1), 55-109.
- Pabi, S., G. L. van Dijken, and K. R. Arrigo (2008), Primary production in the Arctic Ocean, *J. Geophys. Res.*, 113(C8), C08005.
- Peers, G., and N. M. Price (2004), A role for manganese in superoxide dismutases and growth of iron-deficient diatoms, *Limnology and Oceanography*, 49(5), 1774-1783.
- Planquette, H., et al. Dissolved iron in the vicinity of the Crozet Islands, Southern Ocean (2007), *Deep Sea Research Part II: Topical Studies in Oceanography*, 54(18-20), 1999-2019.
- Pollard, R. T., et al. (2009), Southern Ocean deep-water carbon export enhanced by natural iron fertilization, *Nature*, 457(7229), 577-580.
- Raven, J. A.; P. G. Falkowski (1999). "Oceanic sinks for atmospheric CO_2 ". *Plant Cell & Environment* 22: 741–55
- Redfield, A.C., Ketchum, B.H., Richards, F.A. (1963), The influence of organisms on the composition of seawater. In: *The Sea* (ed. Hill, M.N), 2,26-27, Wiley Interscience, New York, USA.
- Rintoul, S. R., C. W. Hughes, and D. Olbers (2001), Chapter 4.6 The antarctic circumpolar current system, in *International Geophysics*, edited by J. C. Gerold Siedler and G. John, pp. 271-302, XXIX-XXXVI, Academic Press.

- Rudels, B. (2001), Arctic Basin Circulation, in *Encyclopedia of Ocean Sciences*, edited by H. S. John, pp. 177-187, Academic Press, Oxford.
- Sarmiento, J. L., N. Gruber, M. A. Brzezinski, and J. P. Dunne (2004), High-latitude controls of thermocline nutrients and low latitude biological productivity, *Nature*, 427(6969), 56-60.
- Sarthou, G., K. R. Timmermans, S. Blain, and P. Tréguer (2005), Growth physiology and fate of diatoms in the ocean: a review, *Journal of Sea Research*, 53(1-2), 25-42.
- Sarthou, G., A. R. Baker, J. Kramer, P. Laan, A. Laës, S. Ussher, E. P. Achterberg, H. J. W. de Baar, K. R. Timmermans, and S. Blain (2007), Influence of atmospheric inputs on the iron distribution in the subtropical North-East Atlantic Ocean, *Marine Chemistry*, 104(3-4), 186-202.
- Sedwick, P. N., A. R. Bowie, and T. W. Trull (2008), Dissolved iron in the Australian sector of the Southern Ocean (CLIVAR SR3 section): Meridional and seasonal trends, *Deep Sea Research Part I: Oceanographic Research Papers*, 55(8), 911-925.
- Sedwick, P. N., P. R. Edwards, D. J. Mackey, F. B. Griffiths, and J. S. Parslow (1997), Iron and manganese in surface waters of the Australian subantarctic region, *Deep Sea Research Part I: Oceanographic Research Papers*, 44(7), 1239-1253.
- Sedwick, P.N. and DiTullio, G.R. (1997), Regulation of algal blooms in Antarctic Shelf Waters by the release of iron from melting sea ice. *Geophys. Res. Lett.*, 24 (20), pp 2515, doi:10.1029/97GL02596.
- Smethie, W. M., and R. A. Fine (2001), Rates of North Atlantic Deep Water formation calculated from chlorofluorocarbon inventories, *Deep Sea Research Part I: Oceanographic Research Papers*, 48(1), 189-215.
- Sunda, W.G., 2001. Bioavailability and bioaccumulation of iron in the Sea, Chapter 3 in : *Biogeochemistry of iron in seawater*. (Eds. Hunter, D.R. and Turner, K.A), 41-85. IUPAC Book Series on Analytical and Physical Chemistry of Environmental Systems 7, John Wiley and Sons Ltd., Chichester, UK.
- Steele, J.H. (1960), Environmental control of photosynthesis in the Sea. *Limnology and Oceanography* Vol. 7, No. 2, pp. 137-150.
- Swift, J. H. (1984), The circulation of the Denmark Strait and Iceland-Scotland overflow waters in the North Atlantic, *Deep Sea Research Part A. Oceanographic Research Papers*, 31(11), 1339-1355.
- Tagliabue, A., et al. (2010), Hydrothermal contribution to the oceanic dissolved iron inventory, *Nature Geosciences*, 3(4), 252-256.
- Takahashi, T., S. C. Sutherland, R. Wanninkhof, C. Sweeney, R. A. Feely, D. W. Chipman, B. Hales, G. Friederich, F. Chavez, A. Watson, D. C. E. Bakker, U. Schuster, N. Metzl, H. Yoshikawa-Inoue, M. Ishii, T. Midorikawa, Y. Nojiri, C. Sabine, J. Olafsson, Th. S. Arnarson, B. Tilbrook, T. Johannessen, A. Olsen, Richard Bellerby, A. Körtzinger, T. Steinhoff, M. Hoppe, C. S. Wong, Bruno Delille, N. R. Bates and H. J. W. de Baar (2009). Climatological mean and decadal changes in surface ocean pCO₂, and net sea-air CO₂ flux over the global oceans. *Deep-Sea Res.* II, 56, 554-577
- Takahashi, T.; S. C. Sutherland, C. Sweeney, A. Poisson, N. Metzl, B. Tilbrook, N. Bates, R. Wanninkhof, R. A. Feely, C. Sabine, J. Olafsson and Y. C. Nojiri (2002), Global sea-air CO₂ flux based on climatological surface ocean pCO₂, and seasonal biological and temperature effects. *Deep Sea Res* II 49: 1601–22. doi:10.1016/S0967-0645(02)00003-6.

- Taylor, S.R., McLennan, S.M.(1985). *The Continental Crust: Its Composition and Evolution*. Blackwell.
- Thuroczy, C.E.T. (2011). *Physical and Chemical Speciation of Iron in the Polar Oceans*, PhD-Thesis, Rijks Universiteit Groningen.
- Timmermans, Klaas R., Loes J. A. Gerringa, Hein J. W. de Baar, Bas van der Wagt, Marcel J. W. Veldhuis, Jeroen T. M. de Jong, Peter L. Croot, Marie Boye (2001), Growth rates of large and small Southern Ocean diatoms in relation to availability of iron in natural seawater. *Limnol. Oceanogr.*, 46(2), 2001, 260-266 | DOI: 10.4319/lo.2001.46.2.0260
- Turner, D.R. and Hunter, K.A. (2001), *Biogeochemistry of iron in seawater*. IUPAC Book Series on Analytical and Physical Chemistry of Environmental Systems 7, John Wiley and Sons Ltd., Chichester, UK.
- Turner, D.R., Hunter, K.A. and De Baar, H.J.W. (2001), Introduction, Chapter 1 in : *Biogeochemistry of iron in seawater*. (Eds. Hunter, D.R. and Turner, K.A), 1-9. IUPAC Book Series on Analytical and Physical Chemistry of Environmental Systems 7, John Wiley and Sons Ltd., Chichester, UK.
- Watson, A. J., D. C. E. Bakker, A. J. Ridgwell, P. W. Boyd, and C. S. Law (2000), Effect of iron supply on Southern Ocean CO₂ uptake and implications for glacial atmospheric CO₂, *Nature*, 407(6805), 730-733.
- Wu, J., M. L. Wells, and R. Rember (2011), Dissolved iron anomaly in the deep tropical-subtropical Pacific: Evidence for long-range transport of hydrothermal iron, *Geochimica et Cosmochimica Acta*, 75(2), 460-468.
- Whitfield, M. and Turner, D.R. (1987). The role of particles in regulating the composition of seawater. In: *Aquatic surface chemistry; chemical processes at the particle-water interface*. Stumm, W. (Editors), Wiley, New York. 457-493.
- Xu, Y., Feng, L., Jeffrey, P.D., Shi, Y., Morel, F.M.M. (2008) Structure and metal exchange in the cadmium carbonic anhydrase of marine diatoms. *Nature* 452, 56–61.
- Yamamoto-Kawai, M., E. Carmack, and F. McLaughlin (2006), Nitrogen balance and Arctic throughflow, *Nature*, 443(7107), 43-43.
- Zehr, J. P., M. Wyman, V. Miller, L. Duguay, and D. G. Capone (1993), Modification of the Fe Protein of Nitrogenase in Natural Populations of *Trichodesmium thiebautii*, *Appl. Environ. Microbiol.*, 59(3), 669-676.



Chapter 2

Dissolved iron in the Arctic shelf seas and surface waters of the Central Arctic Ocean: Impact of Arctic river water and ice-melt

This chapter is based on:

Klunder, M. B., D. Bauch, P. Laan, H. J. W. de Baar, S. van Heuven, and S. Ober (2012), Dissolved iron in the Arctic shelf seas and surface waters of the central Arctic Ocean: Impact of Arctic river water and ice-melt, Journal of Geophysical Research: Oceans, 117, C01027 doi:10.1029/2011JC007133

Abstract

Concentrations of dissolved ($<0.2 \mu\text{m}$) Fe (DFe) in the Arctic shelf seas and in the surface waters of the Central Arctic Ocean are presented. In the Barents and Kara seas, near-surface DFe minima indicate depletion of DFe by phytoplankton growth. Below the surface, lower DFe concentrations in the Kara Sea ($\sim 0.4\text{--}0.6 \text{ nM}$) than in the Barents Sea ($\sim 0.6\text{--}0.8 \text{ nM}$) likely reflect scavenging removal or biological depletion of DFe. Very high DFe concentrations ($>10 \text{ nM}$) in the bottom waters of the Laptev Sea shelf may be attributed to either sediment resuspension, sinking of brine or regeneration of DFe in the lower layers. A significant correlation ($R^2 = 0.60$) between salinity and DFe is observed. Using $\delta^{18}\text{O}$, salinity, nutrients and total alkalinity data, the main source for the high ($>2 \text{ nM}$) DFe concentrations in the Amundsen and Makarov Basins is identified as (Eurasian) river water, transported with the Transpolar Drift (TPD). On the North American side of the TPD, the DFe concentrations are low ($< 0.8 \text{ nM}$) and variations are determined by the effects of sea-ice meltwater, biological depletion and remineralization and scavenging in halocline waters from the shelf. This distribution pattern of DFe is also supported by the ratio between unfiltered and dissolved Fe (high (> 4) above the shelf and low (< 4) off the shelf).

2.1 Introduction

The Arctic Ocean is linked to the global thermohaline circulation, mainly through a strong contribution of Arctic Ocean waters to North Atlantic Deep Water [Rudels, 2001]. Due to ice cover and harsh conditions, the Arctic Ocean is one of the least studied oceans, and knowledge of the trace metal distributions of the Arctic Ocean is very limited. In contrast to other world oceans, the Arctic Ocean is characterized by vast continental shelves (over 1/3 of the total Arctic Ocean area) and by a strong (seasonal) input of fresh water to surface waters from Siberian rivers (Ob, Yenisey, Lena) and Northamerican rivers (Mackenzie) and seasonal ice-melt [Aagaard *et al.*, 1981]. This freshwater causes a strong density difference between the mixed layer and deeper waters, which limits winter convection [Rudels, 2001]. These physical circumstances are expected to affect the distribution of dissolved iron (DFe) in the water column of the Arctic, resulting in a deviation from the vertical distribution common to open ocean profiles [Johnson *et al.*, 1997; Moore and Braucher, 2008]. Instead, in the Arctic Ocean, the strong lateral DFe supply into the stratified surface layers and relatively little vertical mixing are expected to result in high DFe concentrations in the surface layers, relative to lower concentrations at depth.

In other regions in the global ocean, Fe availability has been shown to be of vital importance to phytoplankton growth [Martin and Gordon, 1988; de Baar *et al.*, 1995; Boyd *et al.*, 2000]. In the Arctic, despite low temperatures and relatively low light levels, significant primary production is reported, most notably on the vast

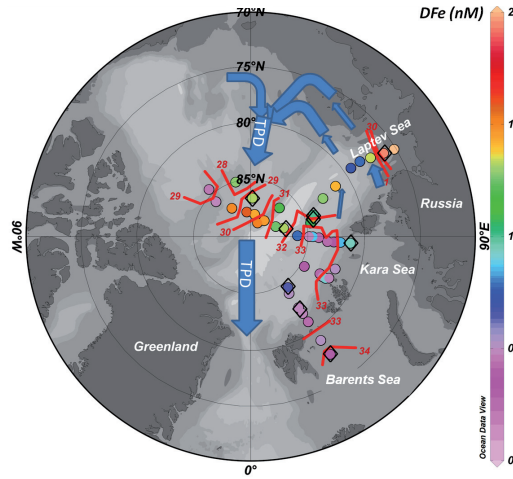


Fig. 2.1a Station map of all stations occupied during ARK XXII/2. Color scale indicates dissolved Fe averages of Surface Layer Waters (SLW). Stations measured for total Fe (TFE) are marked with an open diamond \diamond . Average salinity isolines of the Surface Layer Waters are shown in red. Blue arrows indicate the transpolar drift (schematically, after Rudels et al. [2001]).

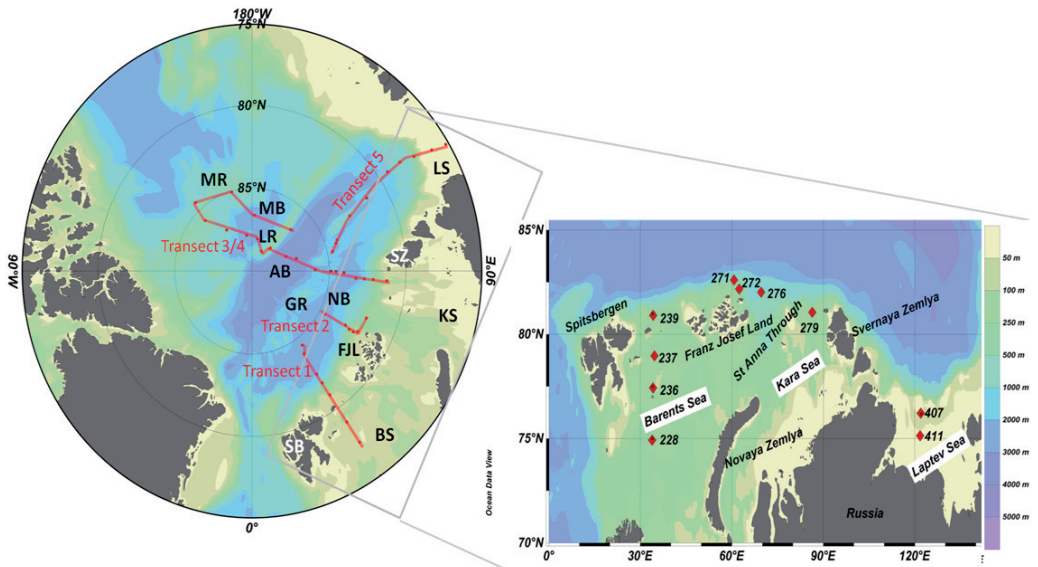


Fig. 2.1b Map of the Arctic Ocean, with the transects and shelf stations occupied during ARK XXII/2. The grey square in the overview marks the position of the enlargement (right panel) for the Arctic shelves. Abbreviations: BS: Barents Sea; FJL: Franz Josef Land; BS: Barents Sea; KS: Kara Sea; LS: Laptev Sea; NB: Nansen Basin; GR: Gakkel Ridge; AB: Amundsen Basin; LR: Lomonosov Ridge; MB: Makarov Basin; MR: Mendeleev Ridge.

Arctic shelves [Carmack and Wassmann, 2006; Arrigo *et al.*, 2008]. Recently more has become known about the role of light, temperature and nutrients in primary production in the Arctic Ocean [Gosselin *et al.*, 1997; Pabi *et al.*, 2008]. However, little is still known about the distribution of DFe and the role of DFe in Arctic primary production. A study by Measures [1999] showed reactive (unfiltered) Fe concentrations in the 1-4 nM range in the upper mixed layer over the central Arctic Ocean. They attributed these relatively high concentrations to melting of sea-ice with entrained sediments. Indeed, Nürnberg *et al.* [1994] have shown the importance of sediment entrainment in sea-ice for transport of sediment from Arctic rivers to the Central Arctic Ocean. Therefore the mechanism of melting of sediment laden sea-ice is a possible DFe source to the Central Arctic. Mass balance models using $\delta^{18}\text{O}$, salinity and nutrients showed that fluvial input sources significantly affect the surface waters of the Central Arctic, which comprises about 5-15% river water [Bauch *et al.*, 1995; Ekwurzel *et al.*, 2001]. Model calculations indicate that river water in the Eurasian Basin is of Siberian origin [Harms *et al.*, 2000]. Moreover, based on Ba concentrations from the same cruise as ours, Roeske *et al.* [2012] conclude that the observed river water is of Eurasian origin. Because DFe in the Siberian rivers is 2-3 orders of magnitude higher than common open ocean surface concentrations [Dai and Martin, 1995; Gebhardt *et al.*, 2005; Hölemann *et al.*, 2005; Moore and Braucher, 2008], even a small portion of the DFe in this water escaping the relatively high Arctic scavenging removal regime [Cai *et al.*, 2010] could strongly affect surface DFe concentrations in the Central Arctic Ocean.

In this paper we present the distribution of DFe on the Arctic shelves (Barents, Kara and Laptev seas) and in the surface waters (upper 250 m) of the Central Arctic, obtained during the ARK XXII/2 expedition of *RV Polarstern* in August-September 2007 (Fig. 2.1). The multi-component approach using $\delta^{18}\text{O}$, salinity and nutrients as well as total alkalinity (A_t) measurements taken during the same cruise (see also Bauch *et al.* [2011]) is used to study the influence of the different freshwater sources on the DFe distribution in the upper Arctic Ocean waters. The distribution of DFe in the deep waters of the Central Arctic Ocean is presented in a complementary manuscript by Klunder *et al.* [2012; This thesis, Ch. 3].

2.2 Material and methods

2.2.1 Sampling and analysis

Water samples were collected during the ARK XXII / 2 expedition of *RV Polarstern* between 1 August and 23 September, 2007 (Fig. 2.1). At discrete depths, samples were taken using 24 internally teflon coated PVC 12 liter GO-FLO samplers (General Oceanics Inc.) mounted on a Titanium frame, which was connected to a Kevlar hydrowire [De Baar *et al.*, 2008]. Inside a class 100 clean room environment samples

for DFe analysis were collected from the GO-FLO bottles [De Baar *et al.*, 2008]. Seawater was filtered using a 0.2 μm filter cartridge (Sartrobran-300, Sartorius) under nitrogen pressure. For each depth replicate samples of DFe were taken in 60 ml High Density Polyethylene (HDPE) sample bottles and acidified to $\text{pH} = 1.8$ with 12 M HCl (Baseline, Seastar Chemicals). Previously, all bottles, used for storage of reagents and samples, were acid cleaned according to a three step cleaning procedure, as described by Middag *et al.* [2009].

The DFe was measured using flow injection analysis with luminol chemiluminescence, where samples were buffered in-line to $\text{pH} = 4$, using a 0.12 M ammonium acetate buffer ($\text{pH} = 6.5$). The DFe was pre-concentrated on an IDA Toyopearl AF-Chelate resin [Klunder *et al.*, 2011]. After pre-concentration, the column was rinsed (60 sec.) with ultrapure type 1 water and subsequently Fe was eluted from the column (120 sec.) using 0.4 M HCl (Merck Suprapur). Pre-concentration time was usually 120 seconds, except for the Laptev Sea stations, where a short loading time (15 sec) enabled determination of the very high concentrations present at this location.

2.2.2 Calibration and validation

The system was calibrated using standard additions of Fe to low DFe seawater. If an outlying value for DFe was observed, the profiles of the other trace metals (dissolved aluminium (DAI) and manganese (DMn)) and other nutrients (silicic acid, nitrate and nitrite, phosphate) were evaluated for consistency with the regarded data point. In the case that no deviations were observed in the other parameters and both the initial and duplicate sample showed an exceptional value, the exceptional data point was considered as erroneous if the value deviated more than +25 % from the expected profile based linear interpolation between the DFe-concentration above and below the data point (after Middag *et al.* [2009] and Klunder *et al.* [2011]). The total number of data points for DFe during ARK XXII/2 was 785. In total 5 data points were rejected, of which only 2 data points were situated in Arctic surface waters. A table including stations positions, date, depth and DFe data is available as a separate chapter within this thesis. An electronic supplement including nutrient and total alkalinity data is available with the related manuscript [Klunder *et al.*, 2012]. The blank is the background concentration of DFe in ultrapure type 1 water and chemicals and is defined as the concentration measured at 0 seconds loading time; the blank was 0.02 ± 0.02 nM ($n = 41$) on average and did not exceed 0.075 nM. The detection limit (3σ of the blank) was 0.07 nM or 70 pM. The amount of Fe added to sample by addition of 12 M HCl (Baseline, Seastar) is < 0.4 pM per sample and is considered negligible [Klunder *et al.* 2011].

The accuracy of the Fe flow injection analysis system was verified by regularly analyzing SFe D2 standard seawater. The results agreed well with the community consensus values: 0.92 ± 0.057 nM, $n=24$. (Certified consensus values are: 0.92 ± 0.03 ; www.geotraces.org).

2.2.3 Other variables

Samples for dissolved Mn (DMn) and dissolved Al (DAI) were simultaneously sampled with those for DFe [Middag *et al.*, 2011; Middag *et al.*, 2009]. At some stations, besides the Fe in the dissolved fraction presented here, Fe was also measured in a smaller size fraction (<1000kDa) and a “total dissolvable” fraction (unfiltered) [Thuroczy *et al.*, 2011]. Salinity and potential temperature data were taken from the CTD profile.

Total Alkalinity (A_T) was determined by potentiometric titration in an open cell, according to the procedures outlined by Dickson *et al.* [2007]. Samples were collected in 250 ml borosilicate bottles and poisoned with 100 μ l of a 50% saturated solution of $HgCl_2$ (i.e., to a concentration of 0.02%) and stored dark and cool, but without freezing, until analysis. All samples were analyzed during the expedition, most within 24 hours after sampling, with only a few stations within 72 hours of sampling. A correction factor of 1.0002 was applied to the results to compensate for the diluting effect of adding the $HgCl_2$ solution. Precision of the analysis, defined as the standard deviation of differences between duplicate analyses of certified reference material (CRM, batch 76, distributed by the Scripps Institution of Oceanography; [Dickson 2001]) is 1.5 μ mol kg^{-1} ($n=68$). Analyses of CRM showed an initial bias of the instrument of about +0.3% (i.e., about 6 μ mol kg^{-1}), which over the course of the cruise decreased to about +0.1% (i.e., about 2 μ mol kg^{-1}). This minor inaccuracy and the gradual drift therein are corrected for in the results. The final dataset of A_T is accurate to ± 4 μ mol kg^{-1} , this being approximately twice the standard deviation of the CRM measurements after the correction for bias and drift is performed.

Oxygen isotopes were analyzed at the Leibniz Laboratory (Kiel, Germany) applying the CO_2 -water isotope equilibration technique on a Finnigan gas bench II unit coupled to a Finnigan DeltaPlusXL. At least 2 sub-samples were analyzed to reach an overall measurement precision for all $\delta^{18}O$ analysis of at least $\pm 0.03\text{‰}$ or smaller. For further details see Bauch *et al.* [2011]. The $^{18}O/^{16}O$ ratio is given versus VSMOW in the usual δ -notation [Craig, 1961].

2.2.4 Calculation of river water and sea-ice meltwater fractions

Stable oxygen isotopes of the water in conjunction with salinity have proven to be a useful and reliable tracer to identify and distinguish freshwater sources [Östlund and Hut, 1984]. Moreover, Atlantic and Pacific-derived waters within the marine fraction can be distinguished and quantified based on nutrient concentrations [Ekwurzel *et al.*, 2001; Jones *et al.*, 1998, 2008; Yamamoto-Kawai *et al.*, 2008]. The water mass fractions are calculated using either a three component or a four-component system of mass balance equations based on salinity, $\delta^{18}O$, and PO_4^* . The latter PO_4^* represents the initial phosphate concentration that accounts for organic respiration of dissolved oxygen and is defined as $PO_4^* = PO_4^{3-} + O_2 / 175 - 1.95 \cdot \mu$ mol kg^{-1} [Broecker *et al.*, 1985]. In deep waters and below a closed sea-ice cover at reduced O_2 air/sea

exchanges, the PO_4^* is a quasi-conservative tracer [Ekwurzel *et al.*, 2001]. The overall mass balance is governed by the following equations [Ekwurzel *et al.*, 2001]:

$$f_a + f_p + f_i + f_r = 1 \quad (1)$$

$$f_a S_a + f_p S_p + f_i S_i + f_r S_r = S_{\text{meas}} \quad (2)$$

$$f_a \delta^{18}\text{O}_a + f_p \delta^{18}\text{O}_p + f_i \delta^{18}\text{O}_i + f_r \delta^{18}\text{O}_r = \delta^{18}\text{O}_{\text{meas}} \quad (3)$$

$$f_a \text{PO}_4^*_a + f_p \text{PO}_4^*_p + f_i \text{PO}_4^*_i + f_r \text{PO}_4^*_r = \text{PO}_4^*_{\text{meas}} \quad (4)$$

where f_a is the fraction of Atlantic water, f_p the fraction of Pacific-derived water, f_i the fraction of sea-ice meltwater (or brine influence if f_i is negative), and f_r is the fraction of meteoric water for which the $\delta^{18}\text{O}$ signal is a suitable indicator. Meteoric water is all water ultimately due to precipitation. In the Arctic Ocean, this can be supplied as river water or as local net precipitation. River water and local precipitation are isotopically identical but river water exceeds net precipitation [Serreze *et al.*, 2006], therefore we refer to this fraction as river water. The S , O and PO_4^* with the corresponding subscripts are the endmember values and measured values of salinity, $\delta^{18}\text{O}$ and PO_4^* [see Bauch *et al.*, 2011]. In the Atlantic regime calculated fractions of Pacific-derived waters may be strongly negative, because of endmember uncertainties and also due to a non-conservative behavior of dissolved oxygen near the surface. In these cases, Pacific-derived water can be assumed to be absent and a 3-component system of equations is solved (equations 1-3 with f_p set to zero). An alternative calculation (similar to equations 1-4) using nitrate to phosphate ratios (N/P) facilitates the differences in nitrate levels between Atlantic and Pacific-derived waters [Jones *et al.*, 1998, 2008; Yamamoto-Kawai *et al.*, 2008]. Comparison of Pacific-derived fractions from PO_4^* and N/P-based calculations are especially important for the interpretation of station data on the Canadian Side of the Transpolar Drift (st. 338, 342, 345; Fig. 2.5). While the PO_4^* approach generally tends to underestimate Pacific-derived waters due to non-conservative behavior O_2 near the surface, the N/P approach in the Transpolar Drift contains a seemingly Pacific signal that in fact is originating from denitrification processes along the Siberian shelves [Bauch *et al.*, 2011].

A negative sea-ice meltwater fraction reflects the amount of water removed by sea-ice formation and the absolute value is proportional to the subsequent addition of brines to the remaining water column. All fractions are net values reconstructed from the $\delta^{18}\text{O}$ and salinity signature of each sample and are the result of time integrated effects on the sample volume over the residence time of the water. Uncertainties based on analytical errors are considerably smaller than systematic and conceptual errors arising from limited knowledge of endmember values. Systematic errors based on uncertainties in endmember salinity and $\delta^{18}\text{O}$ data remain mostly

within $\pm 1\%$ for river water and sea-ice meltwater fractions and uncertainties for Pacific water fraction are up to about 10% for the PO_4^* -based calculation [Ekwurzel *et al.* 2001] and up to 10% for the N/P-based method [Yamamoto-Kawai *et al.*, 2008]. For a detailed discussion see Bauch *et al.* [2011]

2.3 Hydrographic background

The largest inflow into the Arctic Ocean is Atlantic water, marked by high potential temperatures (θ) ($\sim 3\text{--}5^\circ\text{C}$) and high salinity (~ 35) [Rudels, 2001]. This Atlantic water enters the Arctic Ocean in two branches. One branch flows through the Fram Strait and then eastwards along the Siberian continental margin at a depth of $\sim 200\text{--}600$ m [Rudels, 2001]. The other branch flows over the Barents Sea and Kara Sea and joins the Fram Strait Branch at St Anna Trough [Rudels, 2001]. The dominant surface current across the Central Arctic Ocean is the Transpolar Drift (TPD), fed by surface waters from the Laptev and East Siberian seas. The TPD crosses the Central Arctic Ocean, and leaves the basin southward through Fram Strait and there constitutes forms the East Greenland Current [Rudels, 2001; Fig 2.1a].

Throughout the Arctic, the upper surface waters are strongly influenced by a major freshwater input from the Siberian and North American rivers, by Pacific inflow through Bering Strait and by melting of sea-ice [Aagaard and Carmack, 1989]. This results in a surface mixed layer (SML) marked by minima of salinity and potential temperature. During ARK XXII/2, the mixed layer (defined as the shallowest depth deeper than 10m where $\sigma - \sigma_{10\text{m}} < 0.05$ (after Rintoul *et al.* [2001]) varies between 11-25 m over the study area. During the Ultraclean CTD casts, in many cases the shallowest sample measured was situated below the SML. Below the SML, upper halocline waters (UHW) are marked by a nutrient maximum and are most pronounced in the Makarov basin at salinities of about 32.5-33.5 (e.g. [Guay and Kenison Falkner, 1997]). The lower halocline waters (LHW), observed in all Arctic basins, are originally formed by winter convection in the Nansen Basin [Rudels *et al.*, 2004] and intrusions of saline shelf water [Steele and Boyd, 1998], causing higher salinities 34-34.5 (e.g. [Guay and Kenison Falkner, 1997]) compared to the UHW. Steele and Boyd [1998] mention the formation of halocline waters in the Makarov Basin as a result of large amounts of freshwater leaving the Laptev Shelf Continental Margin. Below the halocline, Atlantic derived waters are observed, marked by a temperature maximum and higher salinity of about 34.92 in the south western Nansen Basin [Aagaard *et al.*, 1981]. In this study, the Surface Layer Waters (SLW) comprise the SML, UHW and LHW and are defined as waters with salinity < 34.5 (after [Guay and Kenison Falkner, 1997]).

2.4 Results

For all stations occupied during ARK XXII/2, the average DFe concentrations in the SLW together with isohalines are shown in Fig. 2.1a. Positions of transects are depicted in Fig. 2.1b. Since there is a clear correlation between DFe and salinity in the upper Arctic Ocean, the fractions of the different freshwater sources are displayed together with DFe (Figures 2.3-2.6) as they may give information about the different sources of Fe in the Arctic Ocean.

2.4.1 Shelf Seas

For the shelf seas, depth profiles of DFe, together with light transmission and salinity, are depicted in Fig. 2.2. In the Barents Sea (Fig. 2.2a; Fig. 2.3) high Fe (>1 nM) and salinity (>35.1) was found in the upper layer (25-50 m) southernmost station (228). Below a DFe enrichment in surface waters, stations 236 and 239 showed a subsurface minimum at ~ 50 m water depth (also at station 237), which corresponded to a maximum of fluorescence. Below 50 m, the DFe concentrations were relatively constant with depth (0.6-0.8 nM). The fractions of river water were relatively low in the Barents Sea and some sea-ice meltwater was observed in the upper water around station 239 (Fig. 2.3).

Four stations were occupied north-east of Franz Josef Land, over the St. Anna Trough and at the Kara Sea slope (Fig. 2.1b and profiles in 2.2b). All stations showed a surface depletion of DFe in the upper 10 m and a pronounced subsurface maximum at 25 m depth. At all stations this layer was marked by reduced temperature θ (not shown), relatively low salinity (<33.5), higher fluorescence (Fig. 2.2b) and some river water (up to 3%) as well as sea-ice meltwater (2-5%) was observed (Fig. 2.4). Below the DFe minimum at 25 m depth there was an enrichment at 75 m and below that a relatively low (0.4-0.5 nM) DFe concentrations (st 271/272) or a depletion at 75 m (st 276) and below that a relatively higher DFe (0.5-0.6 nM) (st 276/279).

Two stations (407 and 411) were occupied in the shallow Laptev Sea (Fig 2.2c). In the upper 10 m the DFe concentrations of ~ 3 nM coincided with low salinity and correspondingly high fractions of river water (12–14%) and some sea-ice meltwater ($\sim 3\%$). Below the low salinity layer low DFe concentrations (<2 nM), sea-ice meltwater and river water contributions were found at station 407. At station 411, closer to the shelf edge, high DFe concentrations (>10 nM) corresponded to higher salinity and lower light transmission (Fig. 2.2c), and a strong influence of brine waters (negative sea-ice meltwater fraction; $fi \sim -9\%$). Relatively high river water fractions ($\sim 15\%$) were observed.

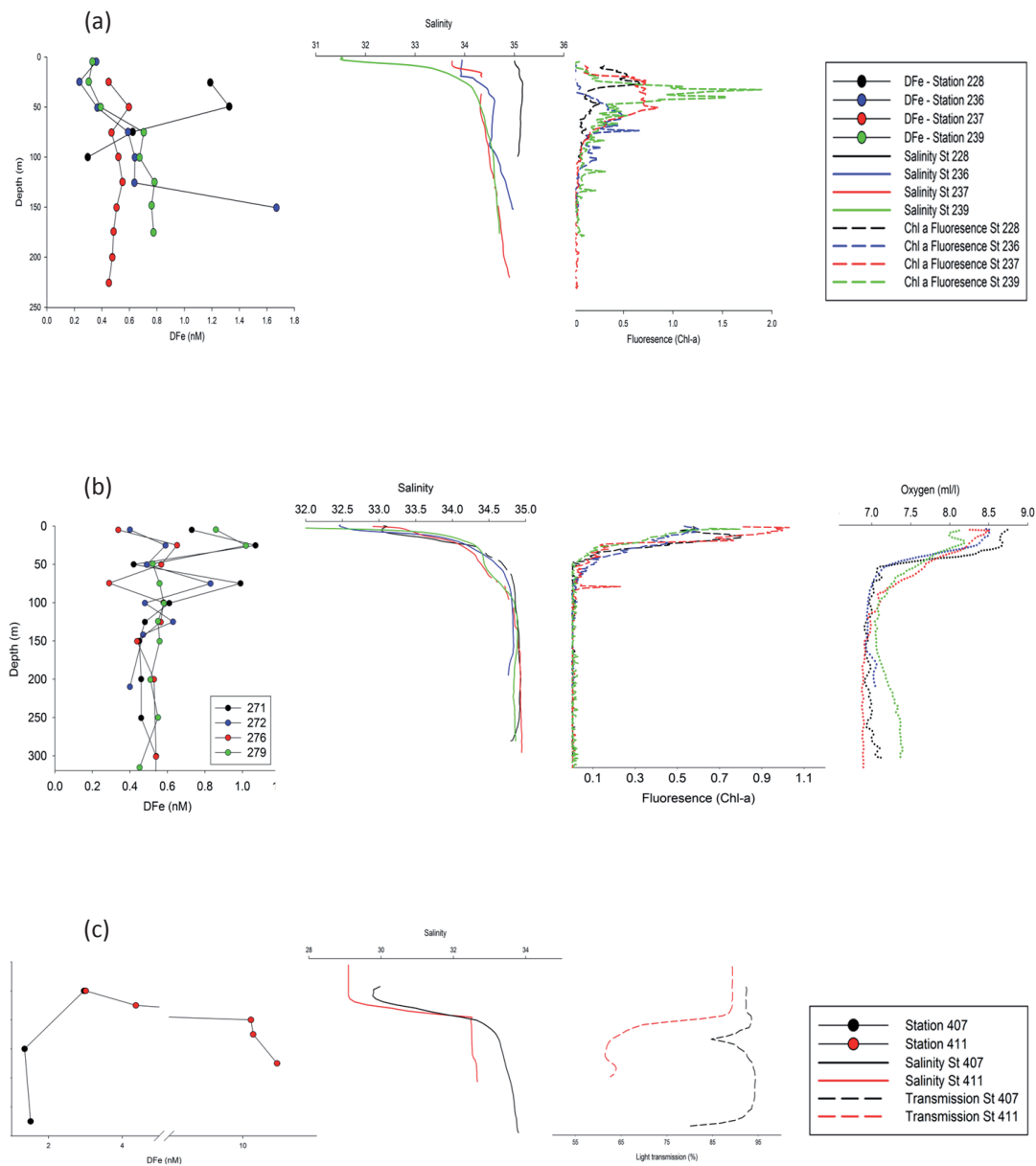


Fig 2.2 Depth profiles of DFe, salinity and fluoescence (indicative of Chl-a; arbitrary units) for the stations on (a) the Barents Sea Shelf, (b) Kara Sea Shelf and (c) the Laptev Sea Shelf (see Fig. 2.1b). For clarification of the discussion, for the Kara Sea shelf, also oxygen profiles are shown (see text) and for the Laptev Sea shelf also light transmission data is shown (see text). Station profiles for salinity, fluorescence, light transmission and oxygen follow the same colors as indicated in the DFe profile for each region.

2.4.2 Surface waters in the Central Arctic Basin

There was a strong relation between high DFe and low salinity in the Eurasian Basin and Central Arctic (Fig. 2.1a), where in the south western Nansen Basin low concentrations of DFe corresponded to high salinity and in the Amundsen and Makarov Basins increasing DFe corresponded to decreasing salinity. An exception to this inverse correlation pattern between salinity and DFe was the region above the Alpha Ridge: here at stations 338 and 342 (Fig. 2.1a), which we assume to be just outside the influence of the Transpolar Drift, salinity further decreased but also DFe concentrations were low. The position of the Transpolar Drift is inferred from the distribution

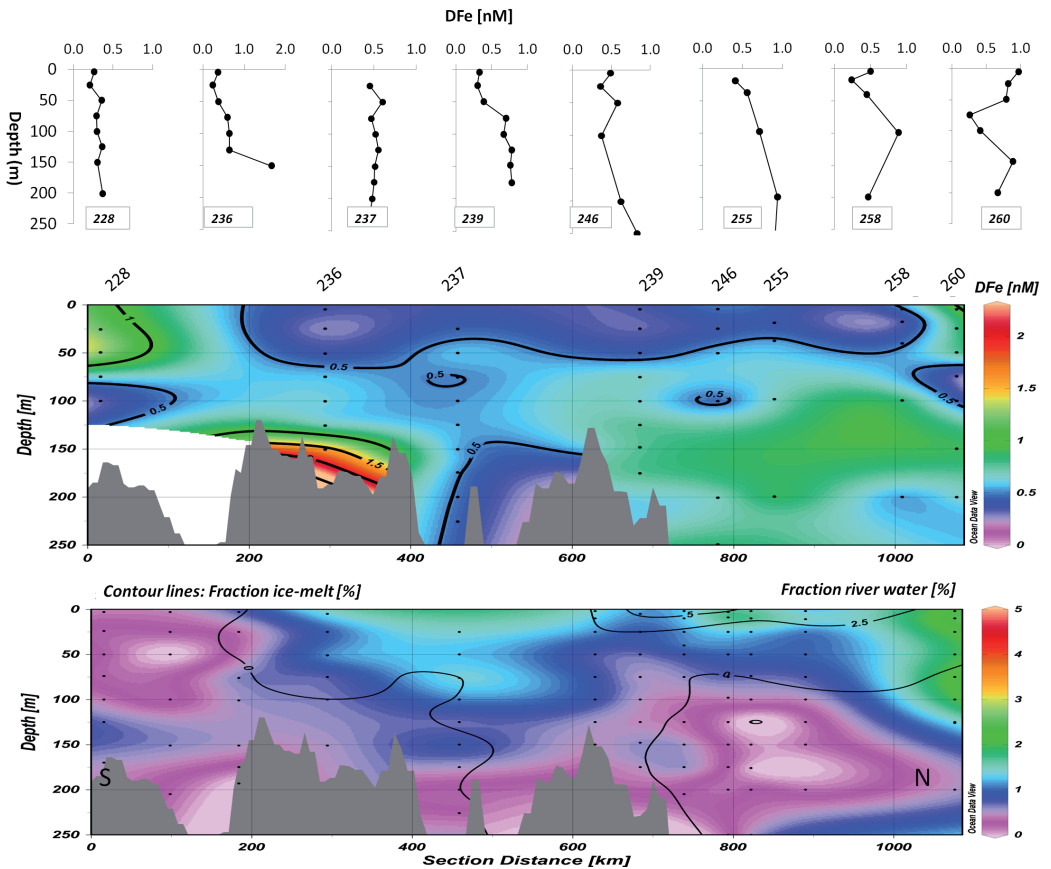


Fig. 2.3 Dissolved Fe depth profiles, dissolved Fe transect plot (upper panel) and transect plot of river water fractions (color) and sea-ice meltwater fractions (contours) (lower panel) in the upper 250 m of the water column at transect 1 (see Fig. 2.1b). Station numbers of transects are indicated above upper panel and South (S) and North (N) orientation within lower panel. Note the different scale for the DFe depth profiles. [Gridding: DIVA gridding (ODV) ; 72*72 (upper panel)& 60*60 (lower panel)]

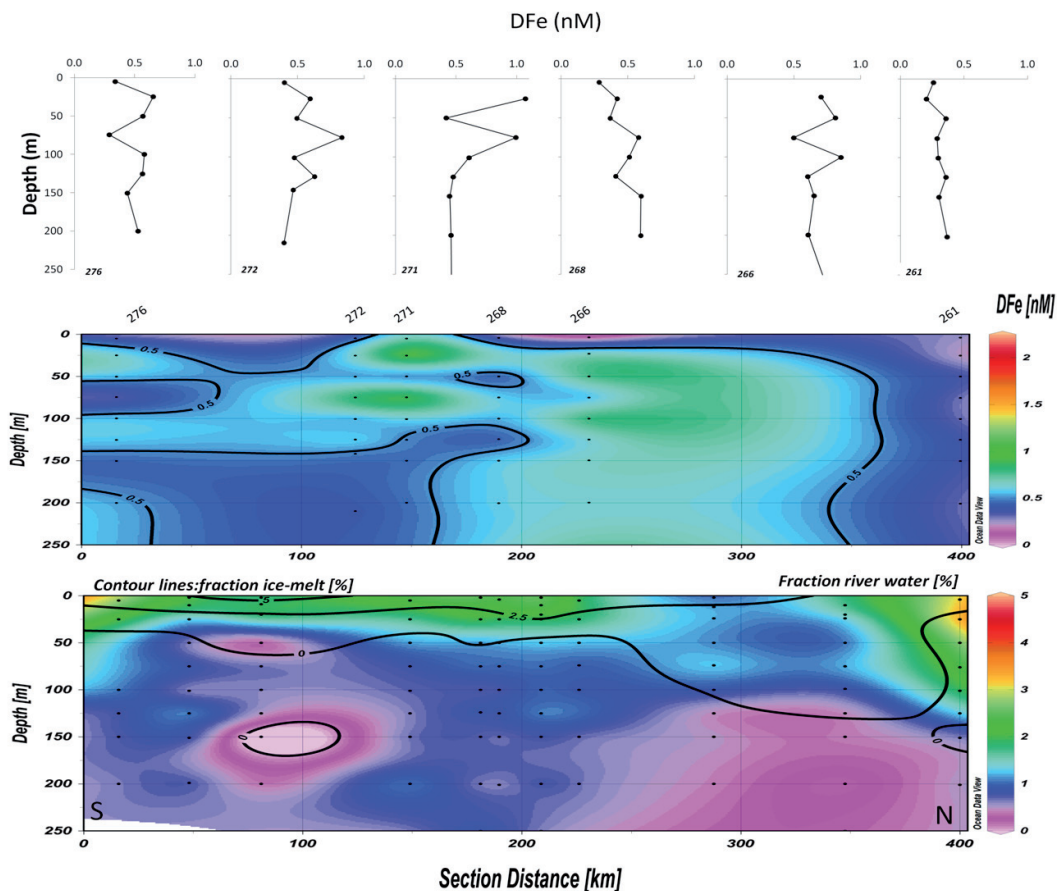


Fig 2.4 Dissolved Fe depth profiles, dissolved Fe transect plot (upper panel) and transect plot of river water fractions (color) and sea-ice meltwater fractions (contours) (lower panel) in the upper 250 m of the water column at transect 2 (see Fig. 2.1b). Station numbers of transects are indicated above upper panel and South (S) and North (N) orientation within lower panel. Note the different scale for the DFe depth profiles. [Gridding: DIVA gridding (ODV); 90*90 (upper panel)& 60*60 (lower panel)]

Fig. 2.5 See next page: Dissolved Fe depth profiles, dissolved Fe transect plot (upper panel) and transect plot of river water fractions (color) and sea-ice meltwater fractions (contours) and pacific water fraction (white contours) (lower panel) in the upper 250 m of the water column at transect 3/4 (see Fig. 2.1b). Station numbers of transects are indicated above upper panel and South (S) and North (N) orientation within lower panel. The different Basins are indicated by arrows below the transect plots. Note the different scale for the DFe depth profiles. The red bar in the lower panel indicates the region where water mass fractions are calculated using N/P ratio. [Gridding: DIVA gridding (ODV); 72*72 (upper panel)& 60*60 (lower panel)]

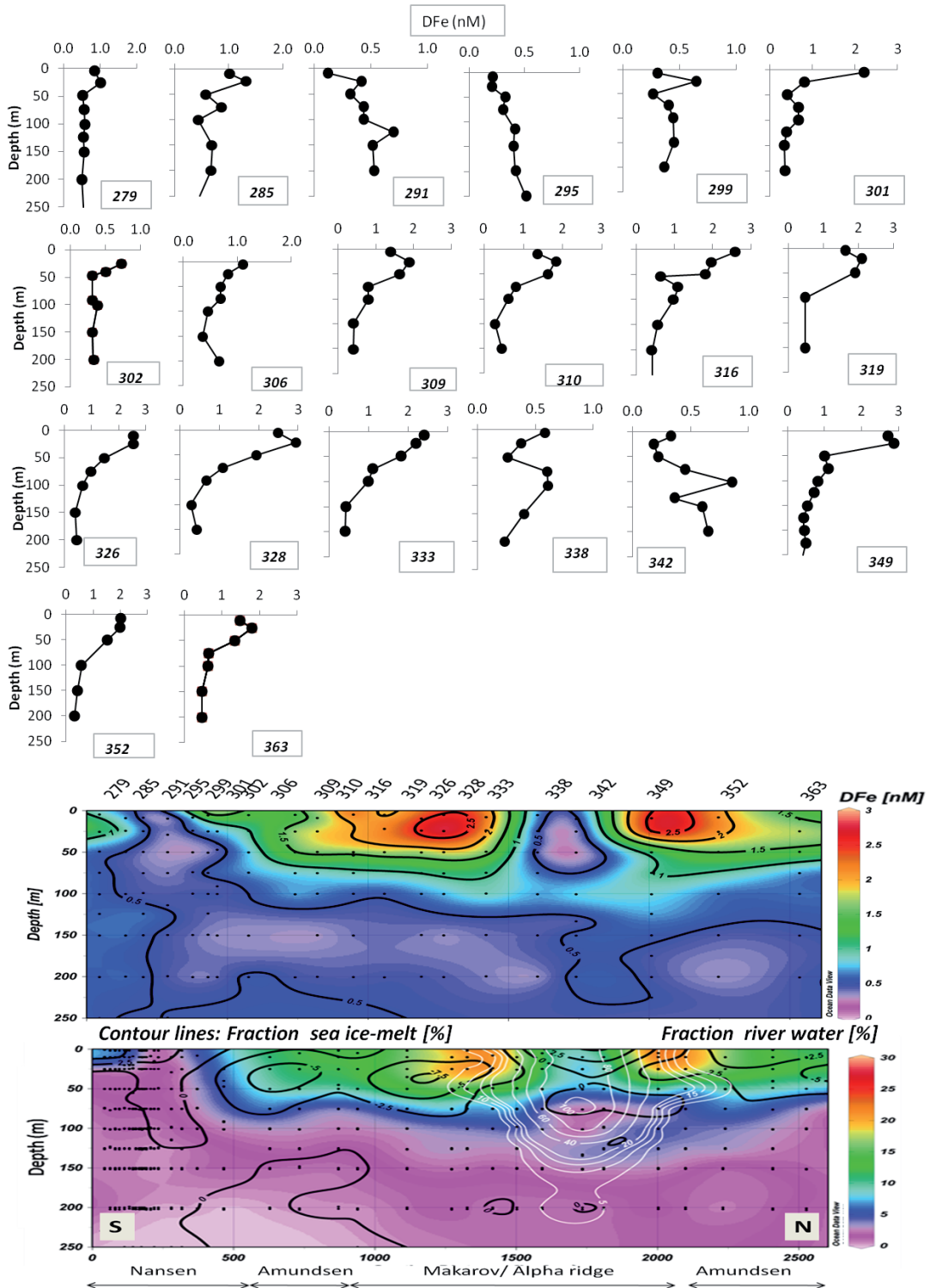


Figure 2.5

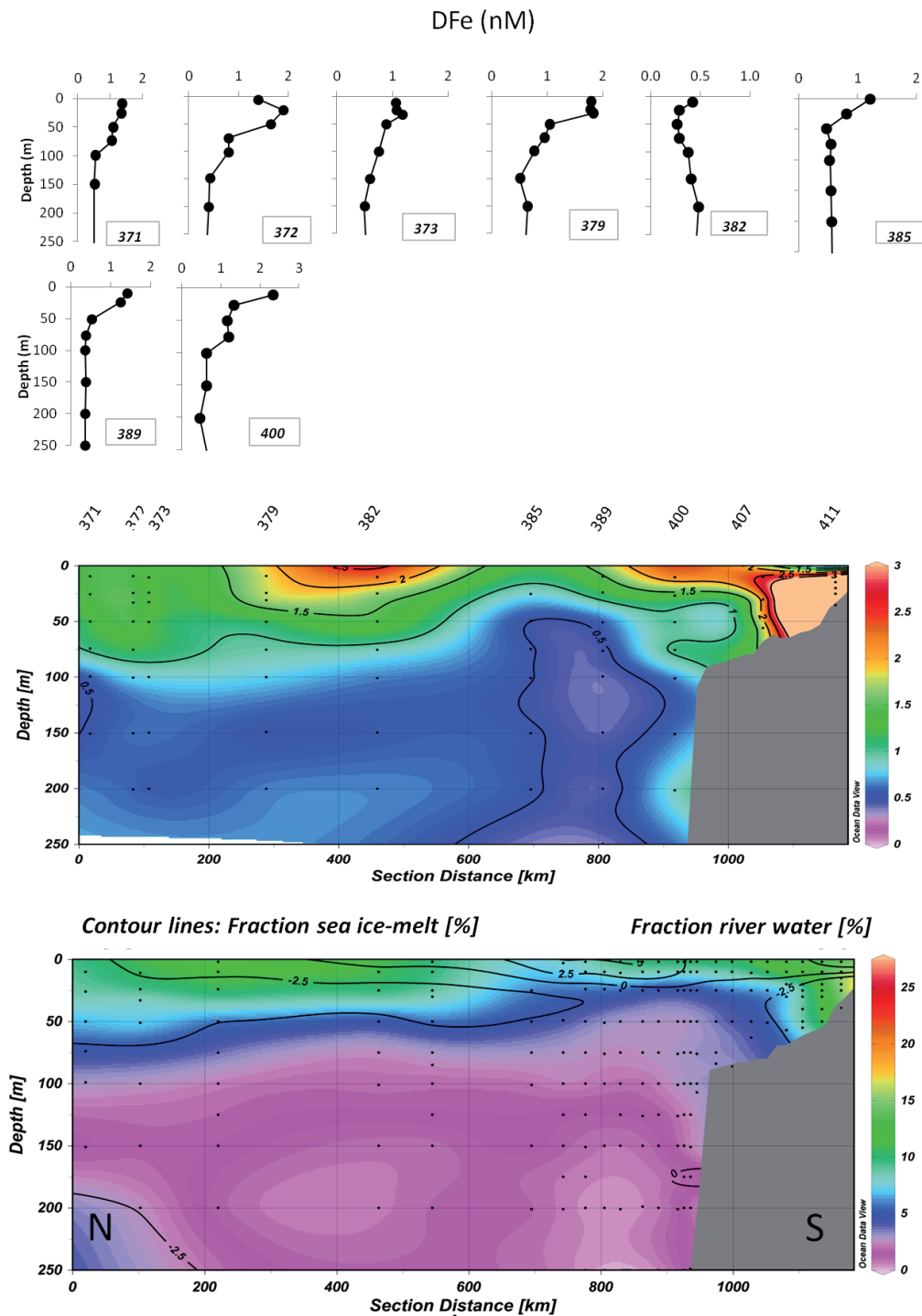


Figure 2.6

of Pacific-derived waters and extrema of river water and negative sea-ice meltwater fractions (see discussion in *Bauch et al.* [2011]). Moreover, the enhanced transport rates inferred from transient tracer evidence support this position of the TPD [*van der Loeff et al.*, 2012].

In the western part of the Nansen Basin (Transects 1 and 2), the concentrations of DFe were generally low in the upper surface, despite some freshwater from sea-ice meltwater and river water (Fig. 2.3, 2.4). In the northernmost station of transect 1, the DFe increased with increasing river water (Fig. 2.3), whereas further east, at the northernmost station of transect 2, high river water and low DFe was found (Fig. 2.4). The western part of the Nansen Basin had relatively low fractions of river water and sea-ice meltwater (with a total always <6%) in the upper surface. Sea-ice meltwater was mostly restricted to the upper 25 m where DFe was generally low (<0.5 nM). Although river water was present (2-3%) over most of the western Nansen Basin, the river influence was very low (<1%) at the shelf break just north of Franz Josef Land (Fig. 2.4).

Further east at the Kara Sea slope, increasing river water fractions and about constant sea-ice meltwater fractions coincided with relatively higher DFe (Fig. 2.4; ~0-150 km of section). In the central Nansen Basin both the DFe concentrations (~0.5 nM) and the river water fractions were relatively low (Fig. 2.5; see section at ~150-400 km).

Relatively high surface DFe concentrations were observed above the Gakkel Ridge together with large fractions of river water and some influence of brine waters (i.e. negative sea ice-meltwater fractions) (Fig. 2.6). In the Nansen Basin near the Laptev Sea margin, the surface DFe concentrations decreased as well as the fractions of river water and sea-ice meltwater (Fig. 2.6; ~600-800 km of section). Towards and onto the Laptev Sea shelf (see section 2.4.1 and Fig. 2.7) both the DFe concentrations and river water fractions increased again.

Towards the Amundsen Basin an increase was observed in the DFe concentrations that coincides with high river water fractions (>10%) and sea-ice formation (negative sea-ice meltwater fraction) (Fig. 2.5; see section at ~600-1000 km and at ~2500 km). This pattern was observed somewhat more pronounced, in the Makarov Basin further west (Fig. 2.5, see section at ~1100-1500 km and 2000-2400 km). A considerable influence of Pacific water (>20%) was observed in the entire Makarov Basin. On the North American side of the Transpolar Drift, Pacific-derived waters comprised a major fraction of the upper water column seen most pronounced at

Fig. 2.6 See former page: Dissolved Fe depth profiles, dissolved Fe transect plot (upper panel) and transect plot of river water fractions (color) and sea-ice meltwater fractions (contours) (lower panel) in the upper 250 m of the water column at transect 5 (see Fig. 2.1b). Station numbers of transects are indicated above upper panel and South (S) and North (N) orientation within lower panel. Note the different scale for the DFe depth profiles. [Gridding: DIVA gridding (ODV); 72°72 (upper panel) & 60°60 (lower panel)]

station 342 with $f_p \sim 90\%$ (Fig. 2.5). The maximum in Pacific fractions coincides with a strong DFe minimum, observed for all stations on the North American side of the TPD.

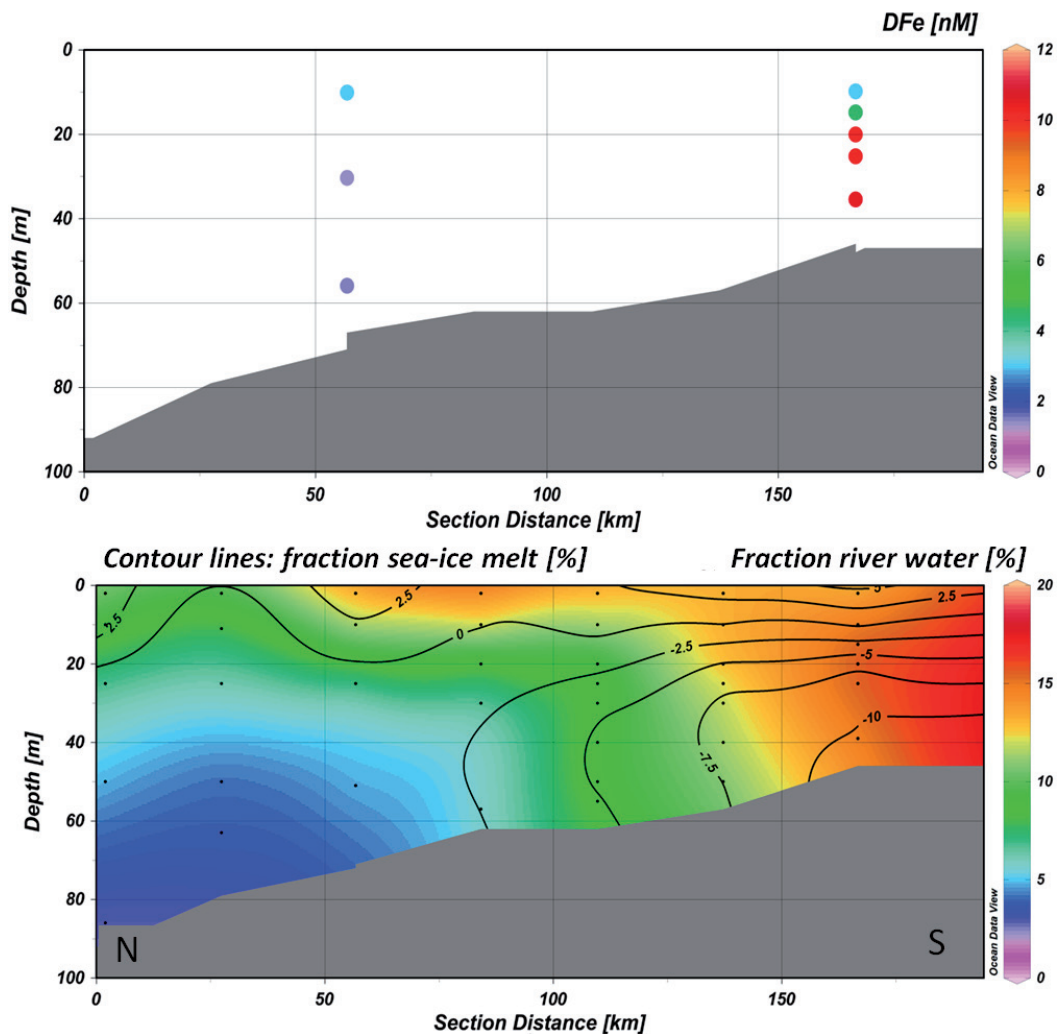


Fig. 2.7 Dissolved Fe datapoints plot (upper panel) and transect plot of of river water fractions (color) and sea-ice meltwater fractions (contours) (lower panel) in the upper 250 m of the water column of the stations on the Laptev Shelf (see Fig. 2.1b). Station numbers of transects are indicated above upper panel and South (S) and North (N) orientation within lower panel. [Gridding: DIVA gridding (ODV); 60*60 (lower panel)]

2.5 Discussion

The inverse linear relationship between DFe and salinity (Fig. 2.8a) demonstrates the important role of Arctic rivers in the delivery of DFe to the Arctic Ocean. Nevertheless, significant deviations from the linear trend indicate that there are also other important sources and processes. In the following discussion we first compare our results with existing (D)Fe data from the Arctic (2.5.1) and discuss the processes on the shelf seas (2.5.2). Then we discuss the concentration of DFe in freshwater sources (2.5.3) and compare the distribution of DFe in the central Arctic Ocean with the distribution of freshwater (2.5.4). Processes involved in sea-ice formation and transport will alter the ratio of total Fe (TFe) and the dissolved fraction (DFe). Therefore, in order to understand the impact of these sea-ice processes on the Fe distribution the ratio TFe/DFe is discussed (2.5.5).

2.5.1 Comparison with previously published data

Our study shows that concentrations of DFe in Siberian shelf seas are relatively low (<1 nM), except for the Laptev Sea where rather high concentrations (> 10 nM) are observed. In the Central Arctic, concentrations vary from ~ 0.5 nM in the Nansen Basin, to > 2 nM in the Amundsen and Makarov basins. To our knowledge no other data has been previously reported for dissolved ($0.2 \mu\text{m}$ filtered) DFe in the Arctic Ocean, but there are some studies reporting unfiltered Fe concentrations. Our observations are consistent with data of *Moore et al.* [1983], who reported a profile with ~ 1.5 nM of reactive iron in the surface waters above the Lomonosov Ridge. *Measures* [1999] reported generally higher concentrations in the range of 0.67–20 nM for reactive Fe on a transect across the Arctic Ocean, with 1.55–3.5 nM over the Lomonosov Ridge and the Makarov Basin and 0.67–1.31 nM for the western Nansen Basin. These ranges of unfiltered samples are slightly higher than the data presented here for filtered samples, but agree well with the values for unfiltered samples from our same casts [*Thuroczy et al.*, 2011]. *Tovar-Sanchez et al.* [2009] reported Fe concentrations of 10 ± 1.8 nM ($n=10$) in upper surface waters (1 m depth) just north of Spitsbergen and values are thereby roughly an order of magnitude higher than our data sampled slightly to the east at $\sim 15\text{--}20^\circ$ (see Figs. 2.2 and 2.3). However, the difference may be at least partly explained by the fact that *Tovar-Sanchez et al.* [2009] reported unfiltered Fe and sampled at ~ 1 m water depth to specifically capture the influence of melting of sea-ice. In contrast filtered (dissolved) Fe concentrations reported here are from > 10 m water depth.

2.5.2 Shelf seas

In the Barents Sea, all stations show a subsurface DFe minimum, often coinciding with a maximum in fluorescence (Fig. 2.2a). This fluorescence is due to presence of chl a, and may indicate uptake of DFe by phytoplankton. *Cai et al.* [2010] report a relatively high POC export in the Barents Sea from measurements collected on the same expedition, indicating significant primary production in the months before the expedition. Indeed, NASA SEAWifs images show high concentrations of chlorophyll ($\sim 5 \text{ mg m}^{-3}$) in the Barents Sea in the months before our cruise (May-June) [*Feldman and McClain*, 2011]. During our expedition concentrations had already decreased to ($< 1 \text{ mg m}^{-3}$) (NASA SEAWifs images [*Feldman and McClain*, 2011]; (see related publication [*Klunder et al.*, 2012])). Moreover, the chl a distribution in the Barents Sea shows variations of one order of magnitude in the region southeast of Spitsbergen in June-July 2007. Also satellite derived annual primary production data of the calendar year 2007 from the Arctic Ocean, show variations between $50\text{--}150 \text{ g C m}^{-2} \text{ yr}^{-1}$ over the Barents Sea Shelf [*Arrigo et al.*, 2008]. Therefore, it is likely that biological uptake and depletion of DFe in the months prior to the expedition has led to the observed low concentrations. Of the four Barents Sea stations, station 237 has the lowest POC export [*Cai et al.*, 2010] and relatively higher DFe, suggesting little DFe depletion by phytoplankton at this station, consistent with spatial variation within the Barents Sea (Fig. 2.3). The very high DFe concentration ($\sim 1.67 \text{ nM}$) close to bottom depth at station 236 is consistent with a similar high concentration observed in DMn distribution and is attributed to benthic efflux [*Middag et al.*, 2011]. The Kara Sea stations differ from the Barents Sea and Laptev Sea shelf sea stations as they are situated all on the outer shelf, close to the slope, rather than on the central shelf (Fig. 2.1b, inset). All Kara Sea stations show an upper surface biological depletion in DFe, consistent with the maximum chl a fluorescence signal in the upper 20 m surface water (Fig. 2.2b). Station 271, situated furthest from the shelf, shows a small intrusion of cold, fresher, slightly less oxygenated waters (Fig. 2.2b), likely from the shelf, below a stable mixed layer (upper 15 m). Higher DFe in these advected shelf waters may explain the higher DFe in the upper 25 m at station 271. Similarly, an even stronger decrease in salinity and oxygen may indicate intruding waters from the shelf at station 279, and thus explain the high DFe concentrations, although this is not confirmed in the θ profile (Fig. 2.2b). Below the upper 50 m the Atlantic core is recognized by higher θ and salinity; at station 271 and station 279 at ~ 75 to 175 m water depth. At stations, 272 and 276, situated further from the shelf, a deeper Atlantic water layer is observed. Below 100 m , the slightly lower DFe at station 271 and 272 ($\sim 0.4\text{--}0.45 \text{ nM}$) may be due to influence of Fram Strait Branch Waters, whereas the DFe at station 276 and 279 ($\sim 0.5\text{--}0.55 \text{ nM}$) may be influenced by Barents Sea Branch Waters (Fig. 2.4). In general, the DFe concentrations are slightly lower in the Kara Sea than in the Barents Sea; DFe may be removed during transport from the Atlantic source to the Kara Sea both by adsorptive scavenging removal and/or biological uptake. Remarkably, the

profile of dissolved Barium (Ba) as measured at station 276 follows a reverse pattern as DFe at this depth, with a small decrease at ~100-125 m. [Roeske *et al.*, 2012, their Fig. 2.4]. It may be possible that some small influence of advected shelf waters with a (small) sea-ice meltwater signal at ~100-125 m depth causes the lower Ba [Roeske *et al.*, 2012] yet higher DFe concentrations. Although these data do not provide a definitive conclusion, our suggestion of advected water with elevated sea-ice meltwater influence is consistent with the deviations observed in the salinity profile (Fig. 2.2b), high dissolved Al at a depth of 125 m [Middag *et al.*, 2009] and the higher $\delta^{18}\text{O}$ (not shown) at these depths. The DFe concentrations gradually decrease at station 276 below 300 m to ~0.45 nM at 620 m depth.

In the Laptev Sea (station 411; see Fig. 2.7) a very low light transmission signal is found below 20 m, corresponding to extremely high DFe. Because low light transmission indicates presence of particles, local resuspension from bottom sediment may be an input source for DFe (Fig 2.2c). Moreover, these enhanced DFe concentrations in the bottom waters may come from the rapid regeneration at depth of organic material exported from the upper waters. This mechanism has been reported for dissolved Barium (Ba) that shows a similar distribution with high concentrations in Laptev Sea bottom waters [Abrahamsen *et al.*, 2009; Roeske *et al.*, 2012]. Organic matter in this part of the Laptev Sea is mainly of terrestrial origin [Anderson *et al.*, 2009] and the dissolution of this organic matter may explain the observed high concentrations of DFe. Additionally, bottom waters on the Laptev Sea shelf are known to contain some river water and are also influenced by sea-ice formation (Fig. 2.7) [Bauch *et al.*, 2009]. Since river water fractions do not differ as much between surface and bottom layer (Fig. 2.7) the extremely enhanced DFe concentrations in the bottom layer are not primarily determined by river contribution. Brine rejection from sea-ice formation may be of importance in distributing DFe over the water column. For the Weddell Sea, Lannuzel *et al.* [2008] reported DFe enrichment upon brine drainage. Close to the shelf edge, the station 407 shows relatively lower DFe and higher salinity, than station 411 on the shelf (Fig. 2.2c), due to the Atlantic Boundary Current flowing along the Arctic shelf seas [Rudels *et al.*, 2004] transporting saline water with relatively low DFe [Klunder *et al.*, 2012] onto the outer Laptev Sea shelf.

2.5.3 Fe in freshwater sources

The inflow of river water is a major source of DFe to surface waters. The DFe concentrations in Arctic rivers vary considerably. Dai and Martin [1995] reported 250 -650 nM for the Ob and Yenisey rivers and Hölemann *et al.* [2005] reported a range of 410-7132 nM for the Lena river. Concentrations of DFe in river water are seasonally variable: both the North American and Eurasian rivers show a strong seasonal summer peak in their discharge volume with higher DFe concentration during the peak discharge [Rember and Trefry, 2004; Hölemann *et al.*, 2005]. These concentrations are orders of magnitude higher than common ocean seawater concentrations, ho-

wever a large amount of DFe is expected to be removed by precipitation/flocculation and sinking in the estuaries [Boyle *et al.*, 1977].

The melting of seasonal sea-ice is another possible input source of DFe [Measures, 1999]. In the Southern Ocean, melting of seasonal sea-ice has been shown to cause enrichment of DFe [Klunder *et al.*, 2010; Lannuzel *et al.*, 2008]. It is important to note that the DFe concentration in sea-ice can be modified by biological processes (uptake by phytoplankton and bacterial remineralisation) [van der Merwe *et al.*, 2009]. Also Arctic sea-ice may receive Fe from atmospheric sources [Darby *et al.*, 1974]. However, because the Arctic sea-ice is largely formed on the Arctic shelves, the entrainment of sediments, either from rivers or suspension at the shelf can be assumed to be a more significant process [Nürnberg *et al.*, 1994]. Hölemann *et al.* [2005] reported very high (281-10585 nM) DFe concentrations in sea-ice in the Laptev Sea, where the concentrations near the Lena River Delta exceeded the concentrations further on the shelf by two orders of magnitude. Tovar-Sanchez *et al.* [2009] reported concentrations of 532-864 nM total dissolvable Fe in Arctic sea-ice for stations north of Spitsbergen. This wide range of Fe enrichment in samples taken relatively close to each other illustrates the strong spatial variability of the input of sea-ice derived particulate and dissolved Fe, that will lead to patchiness in the distribution of DFe in Arctic sea-ice meltwater and consequently in the water below.

Moreover, the contribution of dissolved Fe to the total Fe in sea-ice cores has been shown to vary between less than 1% to 33% in the Subarctic Bering Sea [Aguilar-Islas *et al.*, 2008]. This stresses the role of release mechanisms and dissolution processes in delivery of dissolved Fe from sea ice sediments to the water column [Cámara-Mor *et al.*, 2010; Nürnberg *et al.*, 1994]. The Transpolar Drift (TPD) carries sediment laden sea-ice to the Central Arctic where it can be released upon melting [Cámara-Mor *et al.*, 2010; Nürnberg *et al.*, 1994]. It is important to note that the mass balance equations used in this study yield a net value of the sea-ice contribution over the residence time of the water and melting as well as formation may have taken place before the time of measurement. Therefore water with a negative value for the fraction sea-ice meltwater (reflecting net sea-ice formation) may still contain some recent addition of sea-ice meltwater, i.e. may still have a sea-ice related DFe source.

In the Makarov Basin, a large part of the freshwater component is due to waters of Pacific origin. This water may contain a different DFe signature compared to the marine waters in the Eurasian Basin that consist primarily of Atlantic-derived waters [Bauch *et al.*, 2011]. The DFe concentrations in the surface waters of the North Pacific vary widely (0.1 nM - 3 nM) [Takata *et al.*, 2004; Moore and Braucher, 2008; Aguilar-Islas *et al.*, 2008]. Besides this wide range in concentration of DFe in the North Pacific Ocean, there is significant biogeochemical modification of Pacific Waters during transit over the shallow shelves from the Bering Sea to the central Arctic [Codispoti *et al.*, 2005] (transit time in the order of 1-6 months [Woodgate *et al.*, 2005]). Therefore, the DFe endmember concentration in Pacific-derived waters

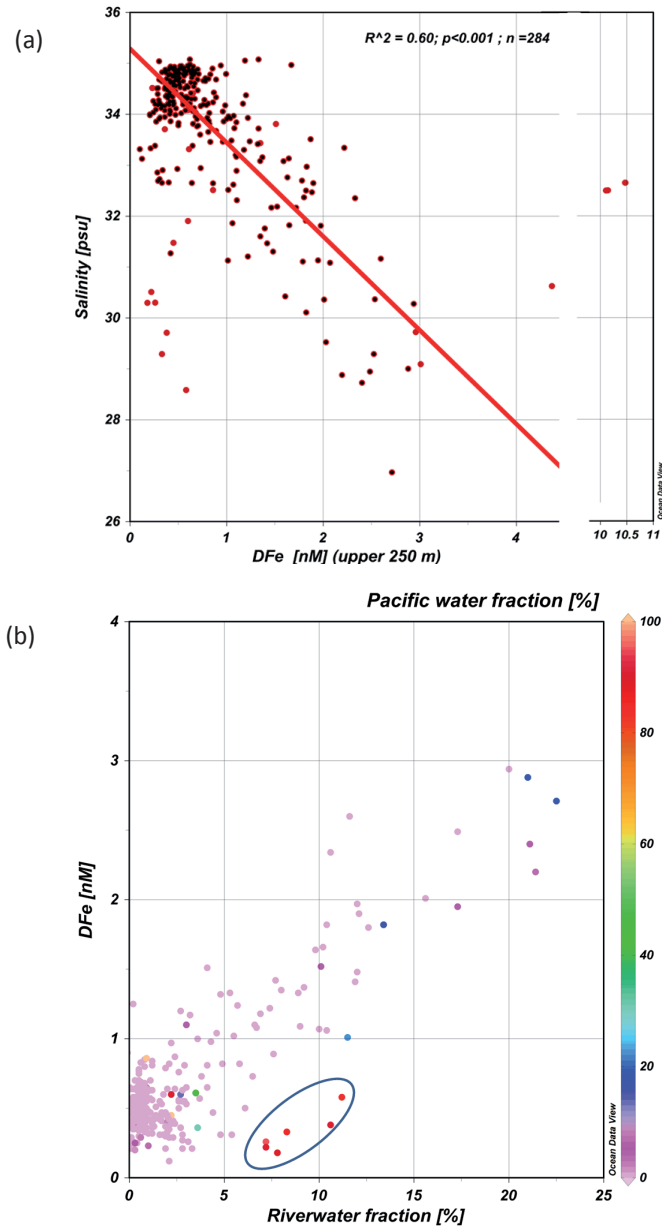


Fig. 2.8a Relation between DFe and Salinity in the upper 250 m. Red dots show all data, (smaller) black dots show all data points excluding stations 338/342 (see text section 5.4) and 407/411 (see text section 5.2). Correlation coefficient, p -value and N are given for the reduced dataset (black dots). Note the break within the DFe axis.

Fig. 2.8b Relation between the concentration of DFe (nM) and fraction of river water (%) for the whole water column in the Central Arctic Ocean (Shelf stations are excluded (see fig. 1.2b)). Fraction of Pacific-derived water (%) is shown in color scale. The blue ellipse indicates the data points >50 m at stations 338 and 342 (see text for discussion).

in the Arctic Ocean halocline has a wide range and cannot be defined as one single end-member value.

2.5.4 DFe concentration in correlation to freshwater distribution

The strong linear relationship between DFe and river water in the surface layer of the Central Arctic (Fig. 2.8b) indicates that river water is the most important DFe source in the Central Arctic Ocean. The DFe concentration does not exceed 1.5 nM in regions with river water fractions <10 %, whereas in regions with >15% river water fraction, DFe concentrations of up to 3 nM are found.

The small portion of total freshwater (river water and sea-ice meltwater <~6%) present in the Eastern Nansen Basin and over the Barents Sea and Kara Sea shelves does not show a clear correlation with the distribution of DFe. Sea-ice meltwater contributes about half of this freshwater but no related increase in DFe is observed (Figs. 2.3, 2.4). Thus sea-ice meltwater is generally not a significant source of DFe in this region. At the northernmost station of transect 1 (Fig. 2.3) and east of the St. Anna Trough (Fig. 2.4) small but significant input of river water correlated with high DFe. This river water originates from shelf regions further east where it becomes frozen and next transported as ice together with sea-ice [Bauch et al., 2011], and it melts again in the Barents Sea and eastern Nansen Basin. The DFe present in this river water transported as ice may be subject to biological Fe-depletion during transport causing strong spatial variation in concentrations of DFe (see section 2.5.3). Also, both the strong surface depletion in phosphate (see related publication [Klunder et al., 2012, *J. Geophys. Res.*]) and the relatively high POC-export fluxes ($1.7\text{--}5.5 \text{ mmol m}^{-2} \text{ d}^{-1}$) [Cai et al., 2010] indicate phytoplankton growth and subsequent export in the months prior to our expedition (see section 2.5.2). If this production would take up the DFe from sea-ice meltwater it would not be observed in the DFe concentrations despite considerable river water and sea-ice meltwater fractions. The facts that melting of sea-ice in the Barents Sea commenced in mid-May 2007 [Spreen and Kaleschke, 2008] and our sampling in the Barents Sea took place at the end of July 2007 are in favor of such a mechanism, which was also observed in the Ross Sea [Sedwick and DiTullio, 1997].

The two stations at the North American side of the TPD (station 338 and 342, Fig. 2.1a) significantly deviate from the correlation between DFe and river water fractions seen in the Eurasian Basin and in the TPD (Fig. 2.9). While river water fractions are lower compared to values found in the TPD, still significant river water fractions are observed which are not reflected in the actually low DFe concentrations (Fig. 2.5). At stations 338 and 342 an enrichment of DFe is observed at the surface, lower DFe concentration at the subsurface and another DFe-enrichment at 75-100 m depth (Fig. 2.9). Salinity at these stations is low at the surface, but increases in the upper 30 m, remains relatively constant between ~30-60 m depth and continues to increase below (Fig. 2.9). Compared to salinity values found at ~60 m an additional input of

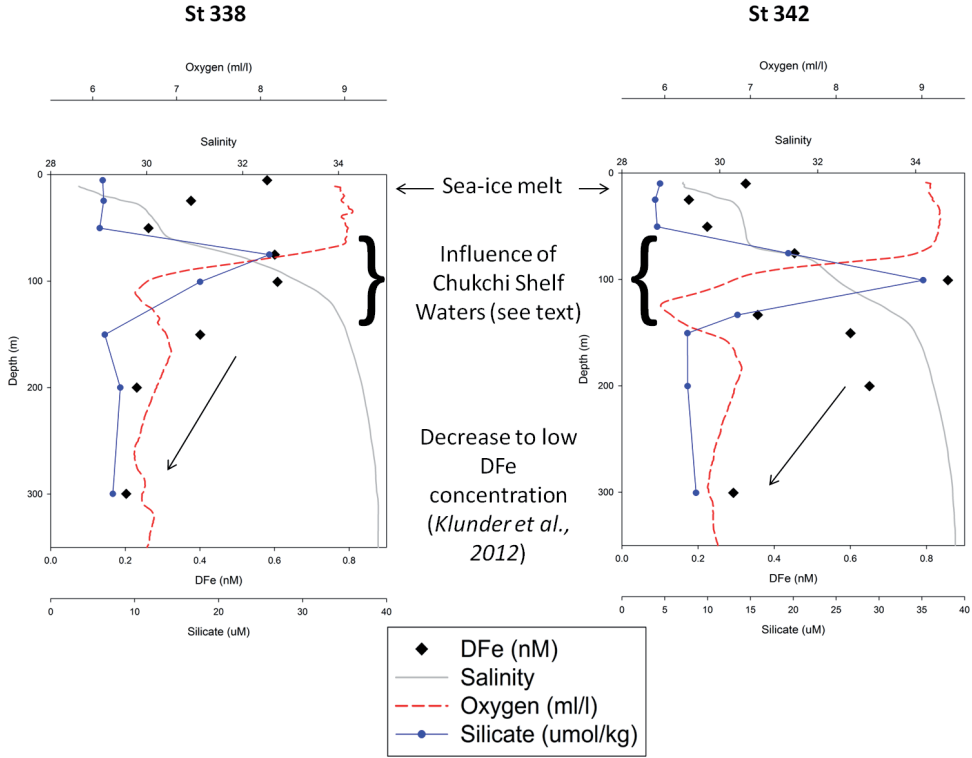


Fig. 2.9 Depth profiles in upper 300 m of DFe (nM), oxygen, salinity and salinity for stations 338 and 342 located on the North American side of the Transpolar Drift. Processes influencing the concentration of DFe are indicated (see text for explanation)

1-2% freshwater ($S=0$) is needed to obtain the low salinity values found in the upper 30 m. Moreover, there is a DFe decrease of 0.32 nM from 10 to 50 m and of 0.15 nM from 10 to 25 m for station 338 and 342 respectively. Although the fraction of (Eurasian) river water is high compared to that of sea-ice meltwater (8-10%), the river water fractions are relatively constant over the upper 50 m, whereas positive sea-ice meltwater fractions (~3%) are only observed in the shallowest sample (~10 m) and are consistent with the high DFe concentrations. From the lower salinity in the upper ~10 m, relative to the winter mixed layer salinity and the observed relation of high DFe with sea-ice meltwater it is suggested that the low salinity, high DFe input comes from the surface. Assuming DFe enrichment is caused solely by sea ice meltwater, the DFe endmember concentration is calculated using the extra sea-ice meltwater input of 2% and 1.5 % and the DFe decrease of 0.32 and 0.15 nM respectively. The DFe-concentration for the sea-ice meltwater endmember should thereby be ~16 nM and ~10 nM DFe, for stations 338 and 342 respectively. This calculated DFe concen-

tration for the sea-ice endmember is low compared to the reported DFe in Arctic sea-ice (see section 2.5.3). However, we may expect strong spatial variations in the amount of DFe released from melting of sediment laden sea-ice as it is dependent on the amount of sediment contained in the ice and on the dissolution mechanisms. The presence of chlorophyll *a* in the upper 50 m [Cai *et al.*, 2010], may point to biological depletion causing the lower DFe concentrations at ~25-50m depth. Instead of North American river water, Roeske *et al.*, [2012] attributed the waters at 50-100 m depth to halocline waters from the Chukchi Shelf, carrying the properties of mineralization processes between bottom waters and sediment. This is reflected in high Ba concentrations [Roeske *et al.*, 2012] and low O₂ and high silicate concentrations (Fig. 2.9). These mineralization processes could cause the DFe increase from 50m to ~100 m at station 338 and 342. The strongest influence of these waters from the Chukchi Sea is found at 100 m depth at station 342 as reflected in the Si maximum (Fig. 2.9) and may explain the high DFe concentrations here. In contrast, lower DFe concentrations (Fig. 2.9) at station 338 may be caused by mixing with Atlantic waters, which comprise already >60% of the water mass at 100 m. Below ~125 m, the DFe decreases (Fig. 2.9), consistent with the DFe concentration observed in the deep waters of the Makarov Basin [Klunder *et al.*, manuscript submitted].

An alternative explanation for the relatively low DFe values on the North American side of the TPD is the longer transit time of waters from the shelf seas to the Central Arctic in the Beaufort Gyre compared to the fast transport of river derived waters from the shelf to the Central Arctic by the TPD. This longer transit time would allow more Fe to be removed by scavenging processes. In addition, DFe may be taken up by phytoplankton in the preceding months, enhanced by the largely ice-free conditions in 2007 in this part of the Canadian Basin [Arrigo *et al.*, 2008].

A small subset of stations were also sampled for total alkalinity (A_T). The A_T data supports the finding that the low salinity (and high DFe input) within the TPD is caused by (mixing with) Eurasian river water, whereas the stations on the North American side of the TPD have a different freshwater signature. In Fig. 2.10 the A_T vs salinity relationship is depicted, including the mixing lines between Atlantic, Pacific, North American river water and Eurasian river water endmembers (see caption for endmember values). The DFe concentrations are shown in color. The high A_T , high salinity waters with low/moderate DFe, are mainly Nansen Basin waters. As aforementioned, some stations in this region are influenced by sea-ice meltwater (following grey arrow, Fig. 2.10). A decrease in A_T and salinity is seen at ~50 m (shallowest sampling depth for A_T) in the stations within the TPD (green ellipse), where also DFe concentrations increase. Remarkably, these datapoints lie between the Atlantic Water/Eurasian river water and Atlantic Water/Northamerican river water mixing lines. Substantial ice formation, as has been observed in the TPD (Fig.2.5), would result in the observed deviation from the Atlantic Water/Eurasian river water mixing line. Nevertheless, influence of Northamerican rivers to the TPD cannot be ruled out. There are two data points at ~50 m depth on the North American side of the TPD, showing

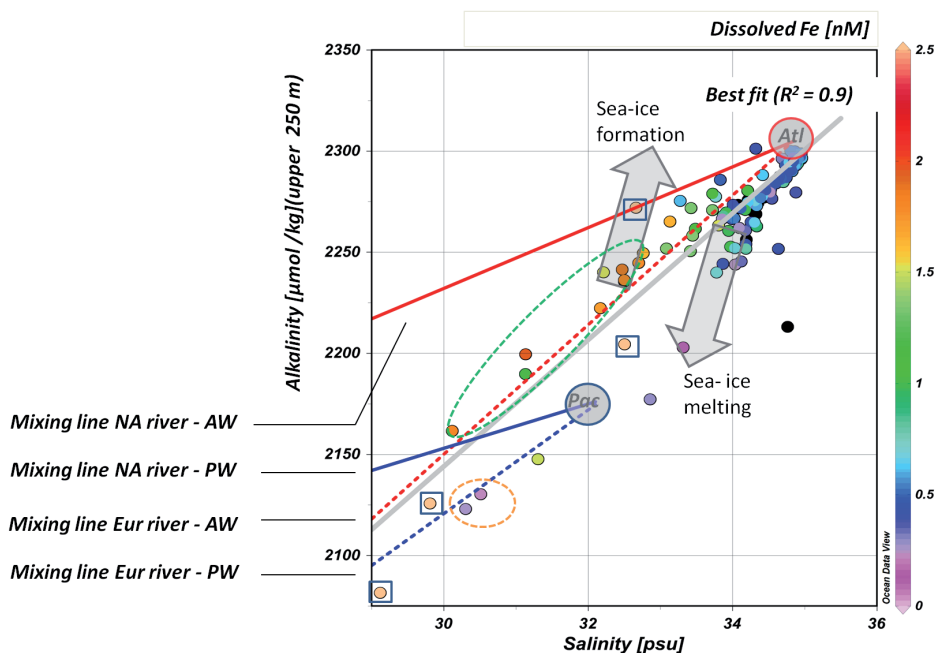


Fig. 2.10 Relation between Total Alkalinity and Salinity for the stations in the upper 250 m. DFe concentrations are shown in color. Mixing lines between Atlantic water and Eurasian (red dotted) and North American river water (red solid) and Pacific water and Eurasian (blue dotted) and North American river water (blue solid).

Endmember concentrations are following Yamamoto-Kawai et al. [2005]; Salinity: Atlantic water: 34.87; Pacific Water 32.1 (mean of 32.7 [Ekwurzel et al, 2001] and 31.5 [Anderson et al., 1994]). Total Alkalinity: Atlantic water: 2306 $\mu\text{mol/kg}$ and Pacific water: 2173 $\mu\text{mol/kg}$ [Anderson et al., 1994]. The river endmembers are calculated using $\text{Sal}=0$ and alkalinity values of 1181, 845, 788, 1707, and 1540 $\mu\text{mol/kg}$ for the Ob, Yenisey, Lena, Yukon, and Mackenzie Rivers, respectively [Cooper et al., 2008] multiplied with the partial distribution of these rivers to the total endmember [Holmes et al, 2002].

Gray arrows indicate sea-ice melting and sea-ice formation, relative to the Atlantic – Eurasian river water mixing line. Green ellipse includes the data points at ~50 m in the TPD (stations 309 – 333 and 349 – 352) and orange ellipse indicates the waters at ~50 m north of the TPD. Laptev Sea data points (stat. 407 and 411) are surrounded by a blue square and are consistent with mixing with river water and a strong sea-ice formation/ brine input signal in the deepest layer of stat. 411 (see text section 2.5.2).

a lower A_T relative to their salinity than within the TPD (orange ellipse). These data points are on the mixing line of Eurasian river water and Pacific Water (Fig. 2.10). This is consistent with the observed river water fractions of ~6-8 (Fig. 2.5) and influence of Pacific water flowing over the Chukchi Shelf (see section 2.5.3 and Roeske et al., [2012]). Anderson et al. [2004] noted that biological processes little affect the A_T in the Arctic Ocean which is in line with little change observed in A_T concentrations during transit over the Chukchi shelf.

2.5.5 Dissolved vs. total dissolvable Fe: implications for Fe delivery to the Arctic

Recent melt of sediment laden sea-ice or influx of riverine sediments from the shelves would result in a high concentration of Fe in the particulate phase and thus a relatively high unfiltered (total dissolvable) Fe concentration (TDFe). During transit from the shelves to the Central Arctic, dissolution processes, sinking and particle scavenging will lower the ratio of TDFe relative to DFe. Thus the ratio TDFe/DFe may give insight in these processes. For instance a rapid removal of TDFe compared to DFe with offshore distance from the Antarctic Peninsula was observed [Ardelan *et al.*, 2010] indicating strong settling loss of TDFe relative to DFe in surface waters. Fig. 2.11 shows the TDFe/DFe ratios versus salinity in the upper 100 m for stations on the Siberian shelves and for open ocean stations. Generally, the TDFe/DFe ratios are lower for open ocean stations than for shelf stations (closed and open dots in Fig. 2.11, respectively). The higher ratio at shelf stations indicates a strong and recent input of sediments, released during local melting of sea-ice or from rivers and causing very high Fe concentrations in the size fraction $>0.2 \mu\text{m}$. We suggest that recent local sea-ice meltwater was not present in the Central Arctic Ocean and that during

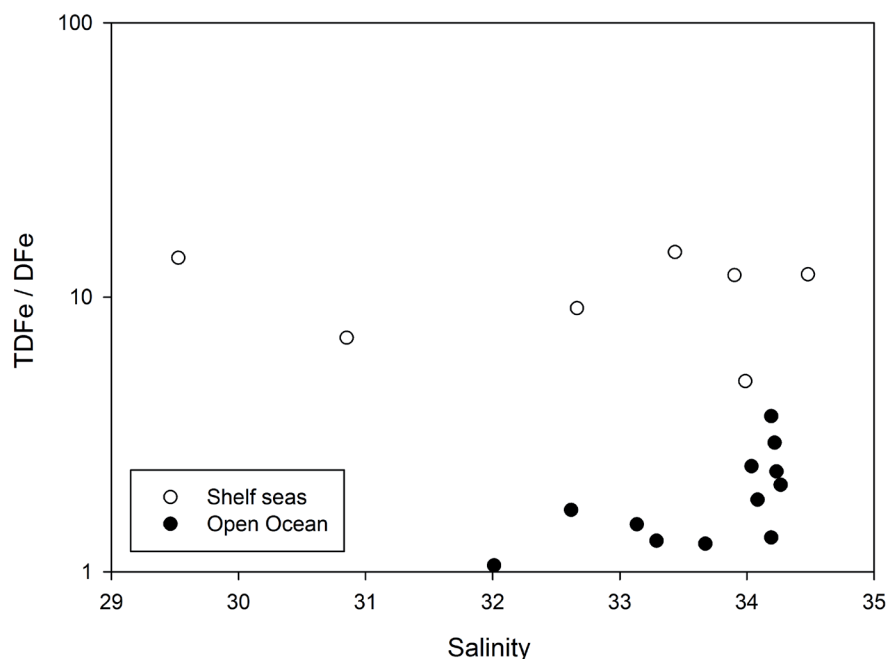


Fig. 2.11 Ratio total iron (TFe) over dissolved iron (DFe) for all points in the upper 100 m at shelf stations (open circles) and open ocean stations (closed circles). Shelf Sea Stations are indicated in Fig. 2.1b.

transit from the shelf seas to the central Arctic Ocean most of the Fe in the particulate fraction is removed, resulting in TDFe/DFe ratios close to 1 at these stations (Fig.2.11). In sea-ice cores from the Bering Sea the TDFe/TFe ratio is between 2.6-1800 (median 42) [Aguilar-Islas *et al.*, 2008], close to the TDFe/DFe ratios observed for shelf stations rather than to those observed in the Central Arctic (Fig.2.11). This strengthens our concept that river water rather than meltwater of sediment laden sea-ice is the dominant DFe input source in the central Arctic Ocean. In principle the melting of possibly sediment laden sea-ice at stations 338 and 342 should be visible in high TDFe/DFe ratios. Unfortunately this remains speculative because no TDFe measurements are available from stations 338 and 342.

2.6 Summary and conclusion

The data reveal that the DFe distribution throughout the surface waters of the central Arctic Ocean is largely correlated with freshwater input sources, which is predominantly Eurasian river water. On the shelves other factors influence the Fe distribution. In the Barents Sea and Kara Sea, DFe minima at high chl *a* concentrations indicate DFe depletion by phytoplankton growth. Strong carbon export and high chlorophyll abundance from satellite images indicate that it is likely that DFe input enabled primary production in the months prior to our cruise. This input likely comes from sea-ice meltwater and ice transported river water in the Barents Sea. Biological depletion of DFe could then explain the relatively low DFe concentrations despite significant sea-ice meltwater and river water signals. Very high DFe concentrations near the bottom of the Laptev Sea are attributed to either sediment resuspension, sinking of brine, or regeneration of Fe in the bottom layer.

In the central Arctic, both the Atlantic boundary current and the Transpolar Drift transport DFe within Arctic surface waters. The DFe concentration in the western part of the Eurasian Basin reflects mainly the concentrations of Atlantic surface water. The influence of Atlantic water can still be recognized at the Laptev Sea continental margin, in high salinities and relatively low DFe. Freshwater from the Eurasian rivers mainly transported by the TPD is the main contributor to DFe in the Amundsen and Makarov basins, where DFe concentrations > 2nM are observed. Here, the ratios of dissolved relative to “total dissolvable” Fe are low, likely due to dissolution of DFe and scavenging/sinking of DFe in the “total dissolvable” fraction. Above the Mendeleev-Alpha Ridge, on the North American side of the Transpolar Drift, two stations deviate from the pattern of river transported DFe. Here the DFe concentrations are generally lower than those within Surface Layer Water of the TPD. This may be caused by the presence of Pacific-derived waters having lower DFe concentrations due to biological depletion during transit, but also by (Eurasian) river water with longer residence times compared to river water in the Eurasian Basin and the TPD. Scavenging and uptake by phytoplankton during transport from the shelves may lo-

wer DFe concentrations. Mixing of river water with Atlantic- and Pacific-derived waters within the TPD and on the North American side of the TPD, respectively is also observed from the distribution of Total Alkalinity. More specifically, the DFe concentrations on the North American side of the Transpolar Drift are strongly determined by sea-ice meltwater in the upper 50 m. A significant influence of remineralisation is seen DFe enrichment at ~ 100 m depth. However, generally biological depletion of these waters during transit over the shelves results in a overall low DFe concentration.

The results suggest that shifts in delivery of DFe to the Arctic Ocean with regard to the regional change in climate may primarily depend on shifts in Arctic currents (e.g. shift in the position of the TPD) and on the amount of river runoff rather than on an expected further increase in sea-ice meltwater. However, loss of Arctic sea-ice cover also alters an important transport mechanism of river derived DFe within the Arctic Ocean and specially the Arctic shelf seas, which are the most productive areas [Pabi *et al.*, 2008]. Recently Arrigo *et al.* [2008] suggested an increase in denitrification in the Arctic Ocean, resulting in a further depletion of the already low nitrogen concentrations in the waters leaving the Arctic to the North Atlantic, this likely enhancing N_2 fixation in the North Atlantic [Arrigo *et al.*, 2008; Yamamoto-Kawai *et al.*, 2006]. This raises the question whether the Fe concentrations in the waters transported from the Arctic to the North Atlantic would contain enough Fe, which is reported to be a control factor for N_2 fixation [Falkowski *et al.*, 1998], to sustain such enhanced N_2 -fixation. Based on the results of this study, we may carefully confirm the relatively high concentration of DFe in the waters exiting the Arctic relative to the lower DFe in common North Atlantic surface waters [Moore and Braucher, 2008].

2.8 References

- Aagaard, K., L. K. Coachman, and E. Carmack (1981), On the halocline of the Arctic Ocean, *Deep Sea Research Part A. Oceanographic Research Papers*, 28(6), 529-545.
- Aagaard, K. and Carmack, E.C. (1989), The role of Sea Ice and Other freshwater in the Arctic Circulation. *Journal of Geophysical Research – Oceans*, 94(C10):14485-14498.
- Abrahamsen, E. P., et al. (2009), Tracer $\delta^{18}\text{O}$ derived freshwater composition of the Siberian continental shelf and slope following the extreme Arctic summer of 2007, *Geophys. Res. Lett.*, 36(7), L07602.
- Aguilar-Islas, A. M., R. D. Rember, C. W. Mordy, and J. Wu (2008), Sea ice-derived dissolved iron and its potential influence on the spring algal bloom in the Bering Sea, *Geophys. Res. Lett.*, 35(24), L24601.
- Anderson, L., G. Björk, O. Holby, E. Jones, G. Kattner, K. Koltermann, B. Liljeblad, R. Lindgren, B. Rudels, and J. Swift (1994), Water masses and circulation in the Eurasian Basin: Results from the Oden 91 expedition, *J. Geophys. Res.*, 99, 3273– 3283.
- Anderson, L. G., S. Jutterström, S. Kaltin, E. P. Jones, and G. Björk (2004), Variability in river runoff distribution in the Eurasian Basin of the Arctic Ocean, *J. Geophys. Res.*, 109(C1), C01016.
- Anderson, L. G., S. Jutterström, S. Hjalmarsson, I. Wåhlström, and I. P. Semiletov (2009), Out-gassing of CO₂ from Siberian Shelf seas by terrestrial organic matter decomposition, *Geophys. Res. Lett.*, 36(20), L20601.
- Ardelan, M. V., O. Holm-Hansen, C. D. Hewes, C. S. Reiss, N. S. Silva, H. Dulaiova, E. Steinnes, and E. Sakshaug (2010), Natural iron enrichment around the Antarctic Peninsula in the Southern Ocean, *Biogeosciences*, 7(1), 11-25.
- Arrigo, K. R., G. van Dijken, and S. Pabi (2008), Impact of a shrinking Arctic ice cover on marine primary production, *Geophys. Res. Lett.*, 35(19), L19603.
- Bauch, D., P. Schlosser, and R. G. Fairbanks (1995), Freshwater balance and the sources of deep and bottom waters in the Arctic Ocean inferred from the distribution of H₂¹⁸O, *Progress In Oceanography*, 35(1), 53-80.
- Bauch, D., I. A. Dmitrenko, C. Wegner, J. Hölemann, S. A. Kirillov, L. A. Timokhov, and H. Kassens (2009), Exchange of Laptev Sea and Arctic Ocean halocline waters in response to atmospheric forcing, *J. Geophys. Res.*, 114(C5), C05008.
- Bauch, D., M. Rutgers van der Loeff, N. Andersen, S. Torres-Valdes, K. Bakker, E. P. Abrahamsen (2011), Origin of freshwater and polynya water in the Arctic Ocean halocline in summer 2007. *Progress in Oceanography*, 91(4), 482-495.
- Boyd, P., A. Watson, C. Law, E. Abraham, T. Trull, R. Murdoch, D. Bakker, A. Bowie, K. Bueseler, and H. Chang (2000), A mesoscale phytoplankton bloom in the polar Southern Ocean stimulated by iron fertilization, *Nature*, 407(6805), 695-702.
- Boyle, E.A., J.M. Edmund, E.R. Sholkovitz (1977), The mechanism of iron removal in estuaries. *Geochimica et Cosmochimica Acta* 41(9), 1313-1324.
- Broecker, W. S., T. Takahashi, and T. Takahashi (1985), Sources and Flow Patterns of Deep-Ocean Waters as Deduced From Potential Temperature, Salinity, and Initial Phosphate Concentration, *J. Geophys. Res.*, 90(C4), 6925-6939.

- Cai, P., M. Rutgers van der Loeff, I. Stimac, E. M. Nöthig, K. Lepore, and S. B. Moran (2010), Low export flux of particulate organic carbon in the central Arctic Ocean as revealed by ^{234}Th : ^{238}U disequilibrium, *J. Geophys. Res.*, 115(C10), C10037.
- Cámara-Mor, P., P. Masqué, J. García-Orellana, J. K. Cochran, J. L. Mas, E. Chamizo, and C. Hanfland (2010), Arctic Ocean sea ice drift origin derived from artificial radionuclides, *Science of The Total Environment*, 408(16), 3349-3358.
- Carmack, E., and P. Wassmann (2006), Food webs and physical-biological coupling on pan-Arctic shelves: Unifying concepts and comprehensive perspectives, *Progress In Oceanography*, 71(2-4), 446-477.
- Codispoti, L. A., C. Flagg, V. Kelly, and J. H. Swift (2005), Hydrographic conditions during the 2002 SBI process experiments, *Deep Sea Research Part II: Topical Studies in Oceanography*, 52(24-26), 3199-3226.
- Cooper, L.W., J.W. McClelland, R.M. Holmes, P.A. Raymond, J.J. Gibson, C.K. Guay, B.J. Peterson (2008), Flow-weighted values of runoff tracers (d^{18}O , DOC, Ba, alkalinity) from the six largest Arctic rivers, *Geophysical Research Letters* 35, doi:10.1029/2008GL035007
- Craig, H. (1961), Isotopic variations in meteoric waters, *Science* (133), 1702-1703.
- Dai, M.-H., and J.-M. Martin (1995), First data on trace metal level and behaviour in two major Arctic river-estuarine systems (Ob and Yenisey) and in the adjacent Kara Sea, Russia, *Earth and Planetary Science Letters*, 131(3-4), 127-141.
- Dickson, A., 2001. Reference material for oceanic CO_2 measurements. *Oceanography* 14, 21-22.
- Dickson, A.G., C.L. Sabine, J. Christian (2007), Guide to best practices for ocean CO_2 measurements. PICES Special Publication 3, 191 pp.
- Darby, D. A., L. H. Burckle, and D. L. Clark (1974), Airborne dust on the Arctic pack ice, its composition and fallout rate, *Earth and Planetary Science Letters*, 24(2), 166-172.
- De Baar, H. J. W., J. T. M. de Jong, D. C. E. Bakker, B. M. Loscher, C. Veth, U. Bathmann, and V. Smetacek (1995), Importance of iron for plankton blooms and carbon dioxide drawdown in the Southern Ocean, *Nature*, 373(6513), 412-415.
- De Baar, H.J.W, K.R. Timmermans, P. Laan, P., H. H. De Porto, Ober, S., J.J. Blom, M. C. Bakker, J. Schilling, G. Sarthou, M.G. Smit and M. Klunder (2008), Titan: a new facility for ultraclean sampling of trace elements and isotopes in the interantional Geotraces program, *Marine Chemistry*, 111(1-2), 4-21
- Ekwurzel, B., P. Schlosser, R. A. Mortlock, R. G. Fairbanks, and J. H. Swift (2001), River runoff, sea-ice meltwater, and Pacific water distribution and mean residence times in the Arctic Ocean, *J. Geophys. Res.*, 106(C5), 9075-9092.
- Feldman, G. C., C. R. McClain, Ocean Color Web, SEAWifs 4, NASA Goddard Space Flight Center. Eds. N. Kuring, S.W. Bailey, 27-01-2011. <http://oceancolor.gsfc.nasa.gov/>
- Falkowski, P.G., Barber, R.T., Smetacek, V., 1998. Biogeochemical controls and feedbacks in Ocean Primary production. *Science*, 281 (200).
- Gebhardt, A. C., F. Schoster, B. Gaye-Haake, B. Beeskow, V. Rachold, D. Unger, and V. Ittekkot (2005), The turbidity maximum zone of the Yenisei River (Siberia) and its impact on organic and inorganic proxies, *Estuarine, Coastal and Shelf Science*, 65(1-2), 61-73.

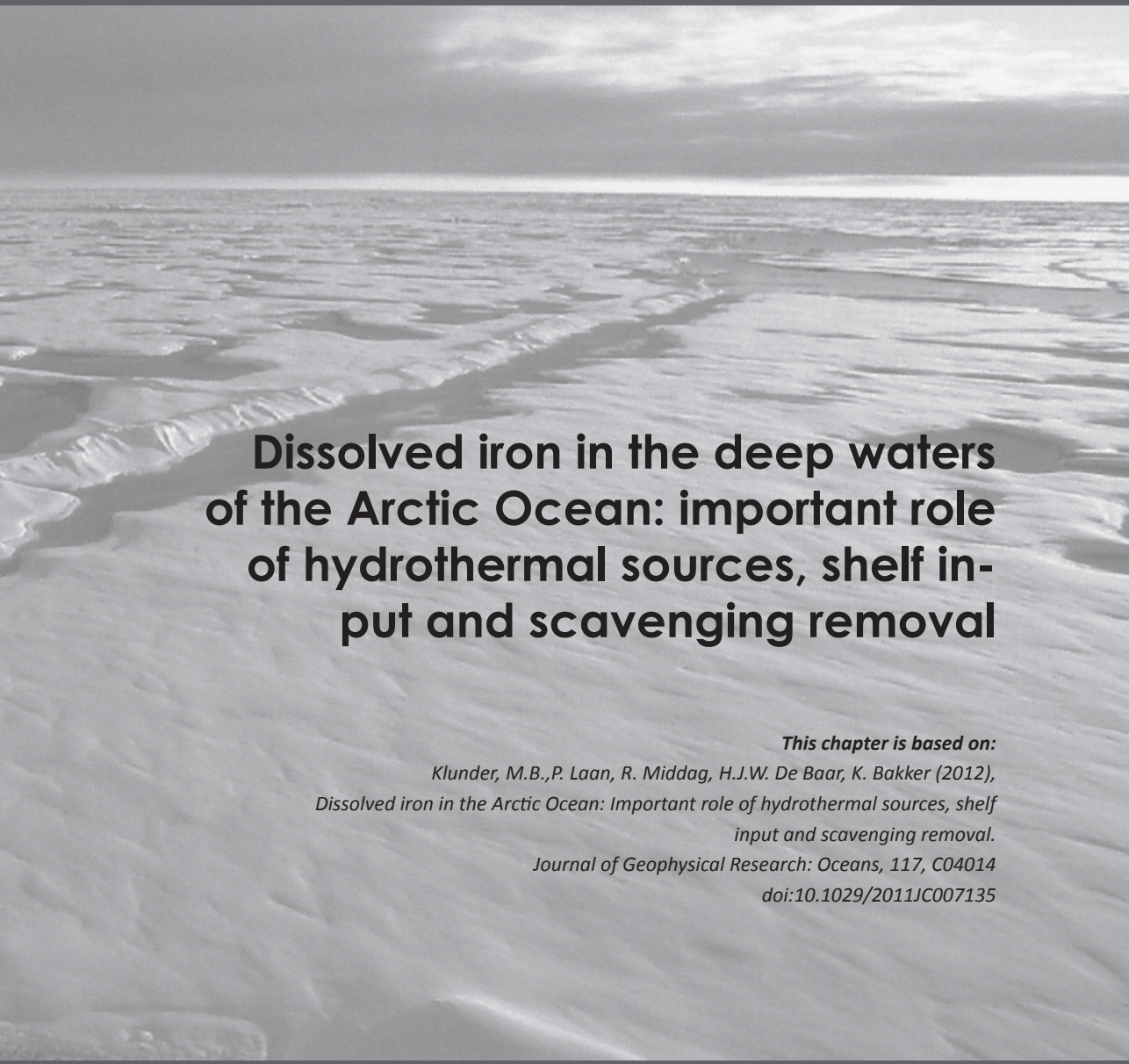
- Gosselin, M., M. Levasseur, P. A. Wheeler, R. A. Horner, and B. C. Booth (1997), New measurements of phytoplankton and ice algal production in the Arctic Ocean, *Deep Sea Research Part II: Topical Studies in Oceanography*, 44(8), 1623-1644.
- Guay, C. K., and K. Kenison Falkner (1997), Barium as a tracer of Arctic halocline and river waters, *Deep Sea Research Part II: Topical Studies in Oceanography*, 44(8), 1543-1569.
- Guay, C. K. H., F. A. McLaughlin, and M. Yamamoto-Kawai (2009), Differentiating fluvial components of upper Canada Basin waters on the basis of measurements of dissolved barium combined with other physical and chemical tracers, *J. Geophys. Res.*, 114(C1), C00A09.
- Harms, I. H., M. J. Karcher, and D. Dethleff (2000), Modelling Siberian river runoff -- implications for contaminant transport in the Arctic Ocean, *Journal of Marine Systems*, 27(1-3), 95-115.
- Hölemann, J. A., M. Schirmacher, and A. Prange (2005), Seasonal variability of trace metals in the Lena River and the southeastern Laptev Sea: Impact of the spring freshet, *Global and Planetary Change*, 48(1-3), 112-125.
- Holmes, R.M., J.W. McClelland, B.J. Peterson, I.A. Shiklomanov, A.I. Shiklomanov, A. V. Zhulidov, V.V. Gordeev, N. N. Bobrovitskaya (2002), A circumpolar perspective on fluvial sediment flux to the Arctic Ocean. *Glob. Biogeochem. Cycl.* 16 (4) 1098, doi:10.1029/2001GB001849
- Johnson, K. S., R. M. Gordon, and K. H. Coale (1997), What controls dissolved iron concentrations in the world ocean?, *Marine Chemistry*, 57(3-4), 137-161.
- Jones, E.P., L.G. Anderson and J.H. Swift, (1998) Distribution of Atlantic and Pacific waters in the upper Arctic Ocean: Implications for circulation. *Geophys. Res. Lett.*, 25(6), 765-768.
- Jones, E.P., L. G. Anderson, S. Jutterström, L. Mintrop, and J. H. Swift (2008), Pacific freshwater, river water and sea ice meltwater across Arctic Ocean basins: Results from the 2005 Beringia Expedition , *J. Geophys. Res.* , 113 , C08012, doi:10.1029/2007JC004124.
- Klunder, M.B, P.Laan, R. Middag, H.J.W. De Baar, J. v. Ooijen (2011). Dissolved Fe in the Southern Ocean (Atlantic Sector), *Deep-Sea Research II*, 58 (25-26), 2678-2694
- Klunder, M. B., P. Laan, R. Middag, H.J.W. de Baar, K. Bakker (2012), Dissolved iron in the Arctic Ocean: Important role of hydrothermal sources, shelf input and scavenging removal. *J. Geophys. Res.*, 117, C04014
- Lannuzel, D., V. Schoemann, J. de Jong, L. Chou, B. Delille, S. Becquevort, and J.-L. Tison (2008), Iron study during a time series in the western Weddell pack ice, *Marine Chemistry*, 108(1-2), 85-95.
- Martin, J. H. and R. M. Gordon (1988), Northeast Pacific iron distributions in relation to phytoplankton productivity, *Deep Sea Research Part A. Oceanographic Research Papers*, 35(2), 177-196.
- Measures, C. I. (1999), The role of entrained sediments in sea ice in the distribution of aluminium and iron in the surface waters of the Arctic Ocean, *Marine Chemistry*, 68(1-2), 59-70.
- Middag, R., P. Laan, H.J.W. De Baar and M.B. Klunder (2011), Fluvial and hydrothermal input of manganese into the Arctic Ocean, *Geochimica et Cosmochimica Acta*, 75(9, 2393-2408
- Middag, R., H. J. W. de Baar, P. Laan, and K. Bakker (2009), Dissolved aluminium and the silicon cycle in the Arctic Ocean, *Marine Chemistry*, 115(3-4), 176-195.

- Moore, R.M. (1983), The relationship between distributions of dissolved cadmium, iron and aluminium and hydrography in the central Arctic Ocean. In C.S. Wong, E. Boyle, K.W. Bruland, J.S. Burton and E.D. Goldberg (Eds.), *Trace metals in Sea Water*, Plenum Press, New York, pp. 131-142.
- Moore, J. K., and O. Braucher (2008), Sedimentary and mineral dust sources of dissolved iron to the world ocean, *Biogeosciences*, 5(3), 631-656.
- Nürnberg, D., I. Wollenburg, D. Dethleff, H. Eicken, H. Kassens, T. Letzig, E. Reimnitz, and J. Thiede (1994), Sediments in Arctic sea ice: implications for entrainment, transport and release, *Marine Geology*, 119(3-4), 185-214.
- Östlund, H. G., and G. Hut (1984), Arctic Ocean Water Mass Balance From Isotope Data, *J. Geophys. Res.*, 89(C4), 6373-6381.
- Pabi, S., G. L. van Dijken, and K. R. Arrigo (2008), Primary production in the Arctic Ocean, 1998-2006, *J. Geophys. Res.*, 113(C8), C08005.
- Rintoul, S., C. W. Hughes, and D. Olbers (2001), Chapter 4.6 The antarctic circumpolar current system, in *International Geophysics*, edited by J. C. Gerold Siedler and G. John, pp. 271-302, XXIX-XXXVI, Academic Press.
- Rember, R. D., and J. H. Trefry (2004), Increased concentrations of dissolved trace metals and organic carbon during snowmelt in rivers of the alaskan arctic, *Geochimica et Cosmochimica Acta*, 68(3), 477-489.
- Roeske, T., Rutgers van der Loeff, M., D. Bauch (2012), Utility of dissolved Ba in distinguishing North American from Eurasian runoff and in the light of its part in biogeochemical cycling of the Arctic Ocean, *Marine Chemistry*, 132-133, 1-14.
- Rudels, B., E. P. Jones, U. Schauer, and P. Eriksson (2004), Atlantic sources of the Arctic Ocean surface and halocline waters, *Polar Research*, 23(2), 181-208.
- Rudels, B. (2001), Ocean Current: Arctic Basin Circulation. In "Encyclopedia of Ocean Sciences" Eds J. Steele, S. Thorpe and K. Turekian. Academic Press, 177-187.
- Rutgers van der Loeff, M., O. Cai, I. Stimac, D. Bauch, C. Hanfland, T. Roeske and B. Moran (2012), Shelf-basin exchange times of Arctic surface waters estimated from ²²⁸Th/²²⁸Ra disequilibrium, *J. Geophys. Res.*, 117 (C3).
- Serreze, M.P, A. P. Barrett, A. G. Slater, R.A. Woodgate, K. Aagaard, R.B. Lammers, M. Steele, R. M., M. Meredith, and C.M. Lee (2006), The large-scale freshwater cycle of the Arctic. *J. Geophys. Res.*, 111 (C11), C11010.
- Sedwick and DiTullio (1997), Regulation of algal blooms in Antarctic Shelf waters by the release of iron from melting sea ice. *Geophys. Res. Letters* 24 (20), 2515-2518.
- Spreen, G. and L. Kaleschke (2008), AMSR-E ASI 6.25 km Sea-Ice Concentration Data V5.4. Institute of Oceanography, University of Hamburg, Germany, digital media (<ftp.projects.zmaw.de/sea-ice>)
- Steele, M., T. Boyd (1998), retreat of the cold halocline layer in the Arctic Ocean. *J. Geophys. Res.*, 103 (C5).
- Takata, H., K. Kuma, S. Iwade, Y. Yamajyoh, A. Yamaguchi., S. Takagi., K. Sakaoka, Y. Yasahit, E. Tanoue, T. Midorikawa, K. Kimura and J. Nishioka (2004), Spatial variability of iron in the surface water of the northwestern North Pacific Ocean, *Marine Chemistry*, 86(3-4), 139-157.

- Thuroczy, C.E.T, L.J.A. Gerringa, M.B. Klunder, P.Laan, H.J.W. De Baar (2011), Distinct trends in the iron speciation between the shallow shelf seas and the deep basins of the Arctic Ocean. *J. Geophys. Res.* , 116, C10009.
- Tovar-Sanchez, A., C. M. Duarte, S. Hernández-León, and S. A. Sañudo-Wilhelmy (2009), Impact of submarine hydrothermal vents on the metal composition of krill and its excretion products, *Marine Chemistry*, 113(1-2), 129-136.
- van der Merwe, P., D. Lannuzel, C. A. M. Nichols, K. Meiners, P. Heil, L. Norman, D. N. Thomas, and A. R. Bowie (2009), Biogeochemical observations during the winter-spring transition in East Antarctic sea ice: Evidence of iron and exopolysaccharide controls, *Marine Chemistry*, 115(3-4), 163-175.
- Woodgate, R. A., K. Aagaard, and T. J. Weingartner (2005), A year in the physical oceanography of the Chukchi Sea: Moored measurements from autumn 1990-1991, *Deep Sea Research Part II: Topical Studies in Oceanography*, 52(24-26), 3116-3149.
- Yamamoto-Kawai, M., N. Tanaka, and S. Pivovarov (2005), Freshwater and brine behaviors in the Arctic Ocean deduced from historical data of $\delta^{18}\text{O}$ and alkalinity (1929-2002 A.D.), *J. Geophys. Res.*, 110(C10), C10003.
- Yamamoto-Kawai, M., E. Carmack, and F. McLaughlin (2006), Nitrogen balance and Arctic throughflow, *Nature*, 443(7107), 43-43.
- Yamamoto-Kawai, M., F. A. McLaughlin, E. C. Carmack, S. Nishino, and K. Shimada (2008), Freshwater budget of the Canada Basin, Arctic Ocean, from salinity, $\delta^{18}\text{O}$, and nutrients, *J. Geophys. Res.* , 113 , C01007, doi:10.1029/2006JC003858.



Chapter 3



Dissolved iron in the deep waters of the Arctic Ocean: important role of hydrothermal sources, shelf input and scavenging removal

This chapter is based on:

*Klunder, M.B., P. Laan, R. Middag, H.J.W. De Baar, K. Bakker (2012),
Dissolved iron in the Arctic Ocean: Important role of hydrothermal sources, shelf
input and scavenging removal.
Journal of Geophysical Research: Oceans, 117, C04014
doi:10.1029/2011JC007135*

Abstract

Arctic Ocean waters exchange with the North Atlantic, and thus dissolved iron (DFe) in the Arctic has implications for the global Fe cycle. We present deep water (>250 m) DFe concentrations of the Central Arctic Ocean (Nansen, Amundsen and Makarov Basins). The DFe concentration in the deep waters varies considerably between these basins, with the lowest DFe concentrations (0.2-0.4 nM) in the Makarov Basin, higher concentrations (~ 0.45 nM) in the Amundsen Basin and highest concentrations (~0.6-0.7 nM) in the Nansen Basin. Atlantic input from the shelf seas and slopes enhances the DFe concentration in the Nansen Basin. Moreover, hydrothermal activity at the Gakkel Ridge causes a significant and widespread enrichment of DFe in the Eurasian Basins, at a depth of 2000-3000 m. Below this maximum, the important role of scavenging and absence of input sources are reflected in a strong relation with dissolved Mn (DMn) and in very low (<0.25 nM) DFe concentrations in the deepest (>3000 m) Amundsen and Makarov Basins. The depth profiles of DFe in the Arctic Ocean, notably in the Makarov Basin, deviate from the DFe distribution pattern observed in other parts of the world ocean.

3.1 Introduction

The trace metal iron (Fe) is an important factor in biogeochemical cycles of the world ocean via its control of phytoplankton growth [Martin and Gordon, 1988; De Baar *et al.*, 1995; Bruland *et al.*, 1995; Boyd *et al.*, 2000; Hunter and Turner, 2001] and is therefore of major importance for marine ecosystems. In recent decades, major advances have been made in understanding the role of Fe in global marine biogeochemical cycles [De Baar and De Jong, 2001; Gregg *et al.*, 2003; Parekh *et al.*, 2004]. However, due to harsh conditions, data on trace metal concentrations in the Arctic Ocean are scarce [e.g. Measures *et al.*, 1999; Middag *et al.*, 2009], in particular for deep waters. To the best of our knowledge, it is restricted to one vertical profile of DFe (<0.4 μM) concentrations in Baffin Bay, west of our study area, with DFe concentrations in the 4.5-11 nM range [Campbell and Yeats, 1982] and recently Nakayama *et al.* [2011] reported DFe data from the Canada Basin and Chukchi shelf. However, the Arctic region is of importance in understanding the global distribution of trace metals, such as Fe. The deep waters of the Arctic Ocean are linked with the North Atlantic Ocean, renewing North Atlantic Deep Water (NADW) [Rudels *et al.*, 2005], which has been shown to play an important role in the Fe cycle in the Atlantic Ocean [Laës *et al.*, 2003; Sarthou *et al.*, 2007] and Southern Ocean [Klunder *et al.*, 2010; Chever *et al.*, 2010]. Moreover, the major role of iron in nitrogen fixation raises the question whether the iron flux from the Arctic provides the increase in DFe in the Atlantic which is necessary for nitrogen fixation rates [Arrigo *et al.*, 2008].

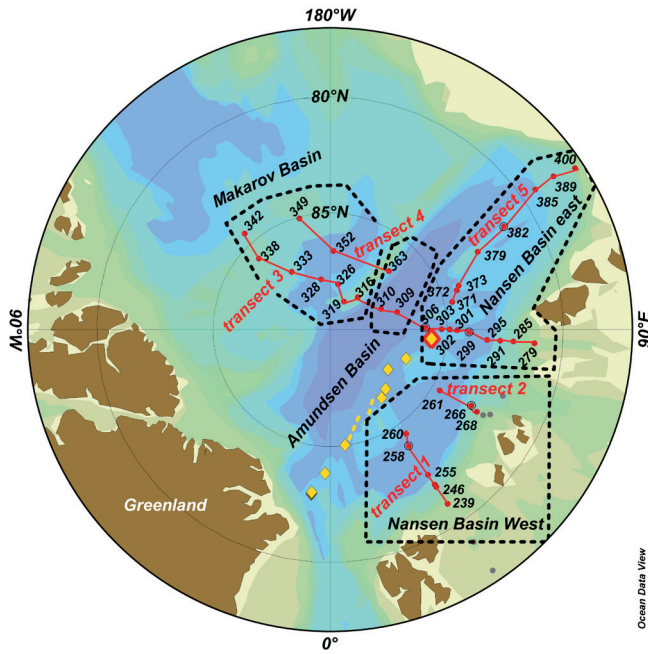


Fig. 3.1a

Chart of the Central Arctic Ocean, including the stations occupied during ARK XXII/2. Sampling stations for DFe are indicated (red dots) and station number is annotated. Grey dots represent stations which are described in [Klunder et al., 2012]. Four different regions are indicated by a black dotted line. Hydrothermal vents as reported by Edmonds et al. [2003] are shown as yellow diamonds. Largest diamond (red-yellow) shows the vent used for calculation in (Fig. 3.10).

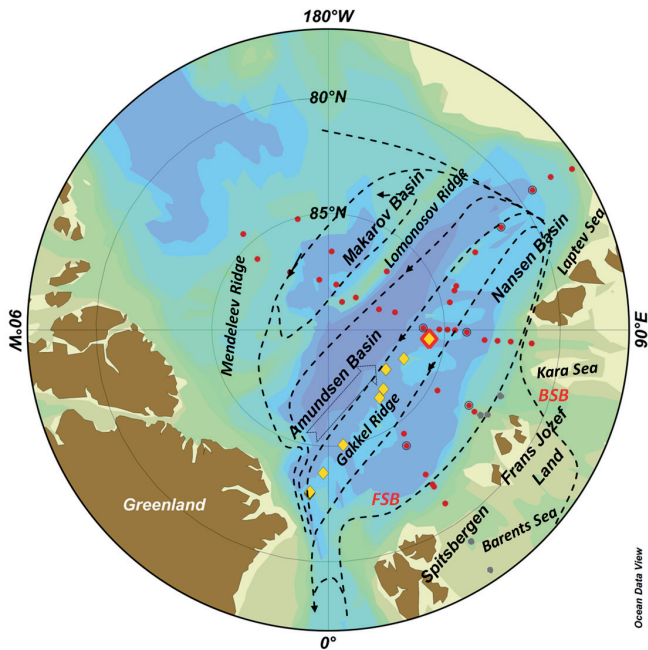


Fig. 3.1b

Chart of the Central Arctic Ocean, including the stations occupied during ARK XXII/2. Sampling stations for DFe are indicated (red dots). Grey dots represent stations which are described in [Klunder et al., 2012]. Flow directions (after Jones et al. [1995]) are indicated. Dotted arrow indicates deep (>2000 m) currents as proposed by Jones et al. [1995]. Indicated in red are the different branches of Atlantic water (FSB: Fram Strait Branch BSB: Barents Sea Branch).

Hydrothermal vents have been shown to be an important source of (dissolved) Fe in the deep world ocean [Klinkhammer *et al.*, 2001; Tagliabue *et al.*, 2010; Klunder *et al.*, 2011; Wu *et al.*, 2011]. Active vents have been identified above the Gakkel Ridge [Edmonds *et al.*, 2003]. These vents could be an important input source for DFe in the deep Arctic Ocean. Another possible input source of DFe is dissolution of resuspended particles originated from continental shelves. The transport of DFe from shelf regions to deep waters has been reported in the North Atlantic Ocean [Laës *et al.*, 2007], North Pacific Ocean [Elrod *et al.*, 2004, Lam and Bishop, 2008] and around islands in the Southern Ocean [Ardelan *et al.*, 2010; Bucciarelli *et al.*, 2001]. The DFe input by shelf sediments may be even more important in the Arctic as shallow shelf seas comprise roughly one third of the Arctic Ocean. The relatively large number of particles transported from rivers and shelf seas to the deep basins may shift the balance between organic complexation and scavenging removal [Wu *et al.*, 2001] and allow DFe to be scavenged out of the deep waters, resulting in relatively low concentrations for deep water.

Within the framework of the international IPY-GEOTRACES program trace metals were measured during a cruise in the Arctic Ocean. This paper describes the cycle of DFe in the deep Arctic Ocean. The distribution of DFe in the Arctic Shelf seas and surface waters can be found in the complementary manuscript [Klunder *et al.*, 2012].

3.2 Materials and Methods

3.2.1 Sampling and analysis

Seawater samples were collected during the ARK XXII / 2 expedition of the *RV Polarstern* between 1 August and 23 September 2007. Sampling stations were located in the Eurasian and Canada Basins; the cruise track is depicted in Fig. 3.1. At discrete depths, samples were collected using 24 internal teflon coated PVC GO-FLO Samplers (12 liter; General Oceanics Inc.) mounted on a Titanium frame (Ultraclean frame) which was connected to a Kevlar hydrowire with internal signal cables and controlled from aboard [De Baar *et al.*, 2008]. The samples for iron analysis were collected from the GO-FLO bottles in a class 100 clean room environment [De Baar *et al.*, 2008]. Seawater was filtered through a 0.2 μm filter cartridge (Sartrobran-300, Sartorius) under nitrogen pressure (1.5 atm.). For each depth replicate samples of dissolved iron were taken in 60 ml LDPE sample bottles and acidified to pH = 1.8 with 12 M HCl (Baseline, Seastar Chemicals). All bottles, used for storage of reagents and samples, were previously acid cleaned according to a three step cleaning procedure as described by [Middag *et al.*, 2009].

Dissolved Fe was measured using flow injection analysis with luminol chemiluminescence, where samples were buffered in-line to pH = 4, using a 0.12 M ammo-

nium acetate buffer (pH = 6.5). The Fe was pre-concentrated on an IDA Toyopearl AF-Chelate resin [Klunder *et al.*, 2011]. After pre-concentration, the column was rinsed (60 s) with de-ionized ultrapure (DI) water (18.2 MΩ) and Fe was eluted from the column (120 s) using 0.4 M HCl (Merck Suprapur) [Klunder *et al.*, 2010]. Subsequently, this mixture was mixed (in a 1m mixing coil at 35 °C) with 0.96 M NH₄OH and 0.5 M H₂O₂ (Merck Suprapur) and 0.3 mM luminol (with 0.7 mM TETA) (Sigma chemicals). Pre-concentration time was usually 120 s, except for the Laptev Sea stations, where a short loading time (15 s) enabled detection of the very high concentrations present.

3.2.2 Calibration and validation

The system was calibrated by standard additions of DFe (range 0.15-3 nM) to low DFe seawater. Initially filtered seawater from an earlier cruise (North Atlantic Ocean, water depth of chl a maximum) was used as calibration water, during the cruise new seawater from the depth of the chl a maximum was used. Generally, calibration water contained < 0.2 nM DFe. When an outlying value was suspected for DFe, profiles of Al, Mn and nutrients were considered to evaluate the consistency of the data point in question. In case no deviations were observed in the other parameters and both the initial and duplicate sample showed an exceptional value, the deviation in Fe-concentration was calculated, based on the values below and above. Briefly, the suspected outlying datapoint was considered as erroneous (likely due to contamination of the sample) in case the value positively deviated more than +25 % from this calculated “expected” profile based on the Fe-concentration above and below the data point (after Middag *et al.* [2009]). The total number of data points for Fe during ARK XXII/2 was 785. In total 5 datapoints were rejected, of which 3 were situated in the deeper waters discussed in this chapter. A table including stations positions, date, depth and DFe data is available as a separate chapter within this thesis. An electronic supplement including nutrient and total alkalinity data is available with the related manuscript [Klunder *et al.*, 2012]. The blank, the background concentration of DFe in DI water and chemicals, defined as the amount of photons measured when not loading any seawater onto the column, was 0.02 +/- 0.02 nM (n= 41) on average and did not exceed 0.075 nM. The detection limit (3σ of the blank) was 0.07 nmol l⁻¹. The amount of DFe added to the sample by addition of the equivalent of 2 ml 12 M HCl (Baseline, Seastar) per liter is < 3 pmol per sample; this is deemed negligible [Klunder *et al.*, 2011]. The accuracy of the Fe Flow injection analysis system was verified by regularly analyzing SAFe D2 standard seawater. The results agreed well with the community consensus values: 0.92 +/- 0.057 nM, n=24. (Reported values are: 0.92 +/- 0.03; www.geotraces.org).

3.2.3 Other parameters

Dissolved manganese (DMn) and aluminium (DAI) were simultaneously sampled with DFe [Middag *et al.*, 2009; Middag *et al.*, 2011]. Moreover, at selected stations Fe was measured in different size fractions; a non filtered fraction giving the total dissolvable Fe (TDFe) concentration (measured after 1 year dark storage [Thuróczy *et al.*, 2012]), and an ultra-filtrated fraction, giving the Fe fraction smaller than 1000kDa. These results as well as the organic complexation of Fe in the three size fractions are reported by Thuróczy *et al.* [2012]. Data of salinity and potential temperature were taken from the Ultraclean CTD. As an indication of particle concentration and presence, mostly light transmission data from the regular CTD is used, this CTD is deployed (by Alfred Wegener Institute) at the same stations just after the Ultraclean CTD deployment. At stations where no light transmission data were available, turbidity, from the turbidity sensor on the Ultraclean-CTD, is presented. Nutrient data was measured from hydrocasts with the Ultraclean frame and regular hydrocasts, as described by Middag *et al.* [2009].

3.3 Hydrography

Several transects were sampled from the extensive shelf waters into the Arctic Ocean's interior, of which the third and fourth transect extended as far east as the Mendeleev Ridge (Fig. 3.1a). The main source of water in the Arctic Ocean interior is surface and intermediate water flowing in from the North Atlantic Ocean (Fig. 3.1b). In the Arctic Ocean, the surface waters consist of the upper Polar Mixed Layer, freshened by ice-melt and outflow from the shelves. A strong, well defined halocline is found below the upper Polar Mixed Layer [Rudels, 2001]. The close to freezing temperatures yet strong salinity gradient with depth in the halocline prevents vertical mixing, which implies advective sources for the halocline waters above the Atlantic Waters [Rudels, 2001].

Below the halocline waters, Atlantic and intermediate waters are observed. These Atlantic waters form a boundary current, along the continental shelves in the Arctic Ocean [Rudels *et al.*, 2000]. This inflowing Atlantic water has two branches; the first one, almost unmodified warm, saline Atlantic water flows through Fram Strait (Fram Strait Branch (FSB)) following the Eurasian Basin slope. The second branch flows over the extended shelves of the Barents Sea (Barents Sea Branch (BSB)), where it is modified by brine-enriched shelf water (Fig. 3.1b). Incorporation of freshwater from ice melt and terrestrial runoff to the Barents Sea causes the Barents Sea branch end-member to be colder and less saline than the Fram Strait branch. Schauer *et al.* [1997] reported the inflow of BSB to the basin at depths between 200-1300 m and that this water is slightly less saline than the overlying Fram Strait Branch Water. Ekwurzel *et al.* [2001] defined Atlantic Water as water with salinity > 34.9 and po-

tential temperature (θ) $> 3^{\circ}\text{C}$, although it gets colder and fresher during the transit through Fram Strait or over the Barents Sea shelf. During our cruise only very few data points showed a $\theta > 3^{\circ}\text{C}$ [Middag *et al.*, 2009] but a salinity maximum of >34.95 was observed at transect 1, 2 and 3 (Fig. 3.2). Due to mixing with low salinity waters this maximum was not observed at transect 5. Upon mixing, the boundary current follows a counterclockwise circulation, with a branch flowing along the Gakkel Ridge back to Fram Strait, a branch following the Lomonosov Ridge, and a branch crossing the Lomonosov Ridge and entering the Makarov basin (Fig. 3.1b). The latter branch is largely influenced by sea-ice formation, brine rejection (i.e. increasing salinity) and subsequent formation and convection of dense water along the slopes, causing the Canada Basin to be strongly influenced by shelf waters. This influence of slope convection causes the Canada Basin Deep Water (CBDW) to be less cold and relatively saline compared to Eurasian Basin Deep Water (EBDW) [Rudels, 2001]. During this study the EBDW was observed in the Nansen and Amundsen Basins and defined as the deep ($S > 34.8$) waters with $\theta < -0.8^{\circ}\text{C}$ and the CBDW as the deep waters with $\theta < -0.4^{\circ}\text{C}$ (after Middag *et al.* [2009]). In this study, the CBDW observed in the Makarov Basin is named Makarov Basin Deep Water (MBDW). Finally, Atlantic and intermediate waters are defined as those waters with $\theta > -0.8^{\circ}\text{C}$ which are not part of the surface waters (after Middag *et al.* [2009]).

3.4 Results

3.4.1 Transect 1 and 2

This paper focuses on the concentrations of DFe in the deep waters of the Arctic Ocean, and does not include shelf stations along transect 1 and 2 (Fig. 3.1). For shelf and upper water column DFe values see the companion manuscript Klunder *et al.* [2012].

Above the continental slope of the Barents Sea, in general relatively high DFe values of $\sim 0.9 - 1.0$ nM were observed from ~ 200 m downwards, with very high values at ~ 400 m, at ~ 1000 m and close to the bottom (~ 2000 m) (Fig. 3.2, 3.3a and 3.4). The inflow of the Atlantic boundary layer was identified in the salinity, consistent with anomalies in the potential temperature (θ) (not shown) and turbidity profiles at ~ 500 - 800 m depth (Fig. 3.3a). Here, the DFe concentration decreased to ~ 0.7 nM, a typical concentration for (unmodified) Atlantic waters [Moore and Braucher, 2008].

Three stations were sampled in the Nansen Basin at transect 2. These three stations are not sufficient to make a contour plot and the DFe distribution is thus depicted as a depth profile in Fig. 3.5. Concentrations of DFe were relatively constant at 0.4 - 0.5 nM at ~ 500 m. From 700 m to the bottom, concentrations increased to 0.6 - 0.8 nM. In the upper 1000 m in the center of the Basin, there was a difference between the two transects; higher DFe (~ 0.7 nM) was observed in the western part (transect 1), whereas lower DFe concentrations (< 0.5 nM) were observed further ea-

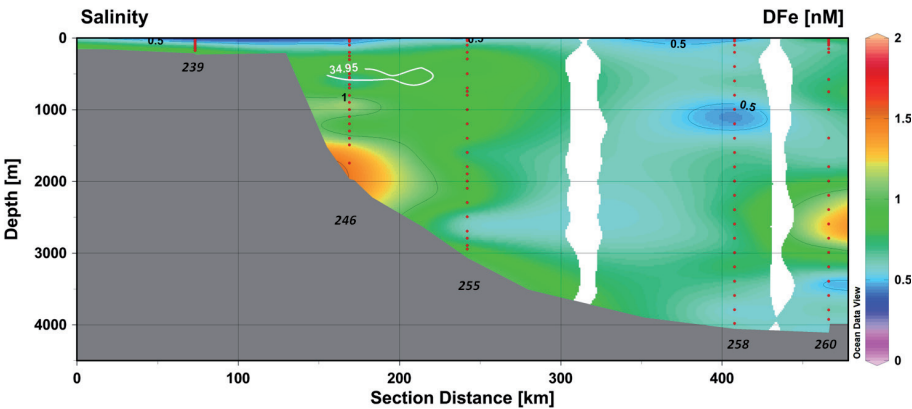


Fig. 3.2 Colour plot of concentrations of dissolved Fe (nM) for transect 1 (See Fig. 3.1a). Red dots indicate sample points. Station numbers are mentioned below the transect. White contourlines indicate a salinity of 34.95.

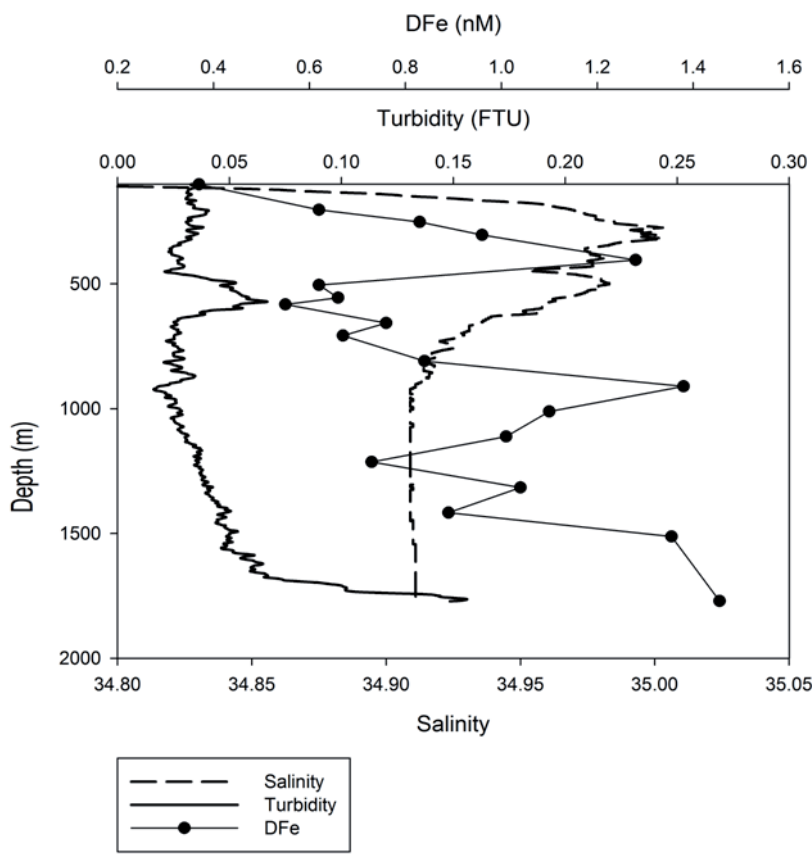


Fig. 3.3a Concentration of DFe (nM) and salinity profile of station 246 (Barents Sea Slope). Turbidity is also indicated in arbitrary units, indicative of particle concentration in the water.

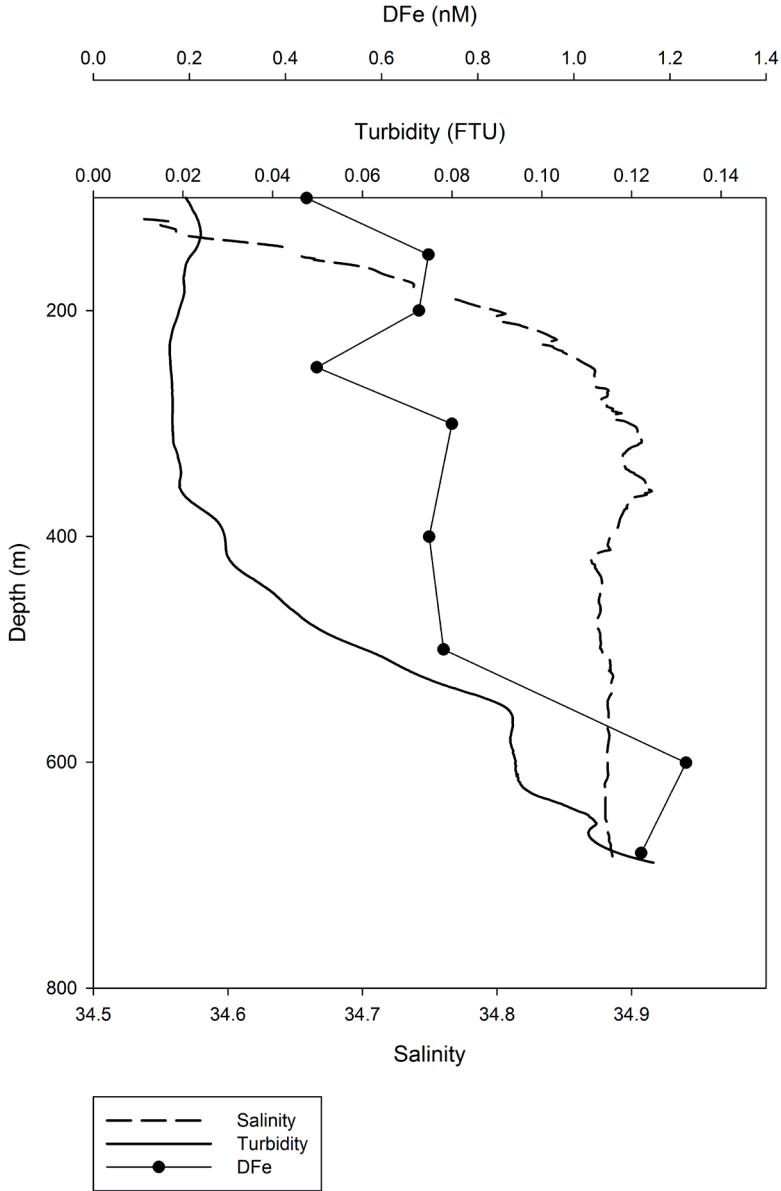


Fig. 3.3b Concentration of DFe (nM) and salinity profile of station 285 (Kara Sea Slope). Turbidity is also indicated in arbitrary units, indicative of particle concentration in the water.

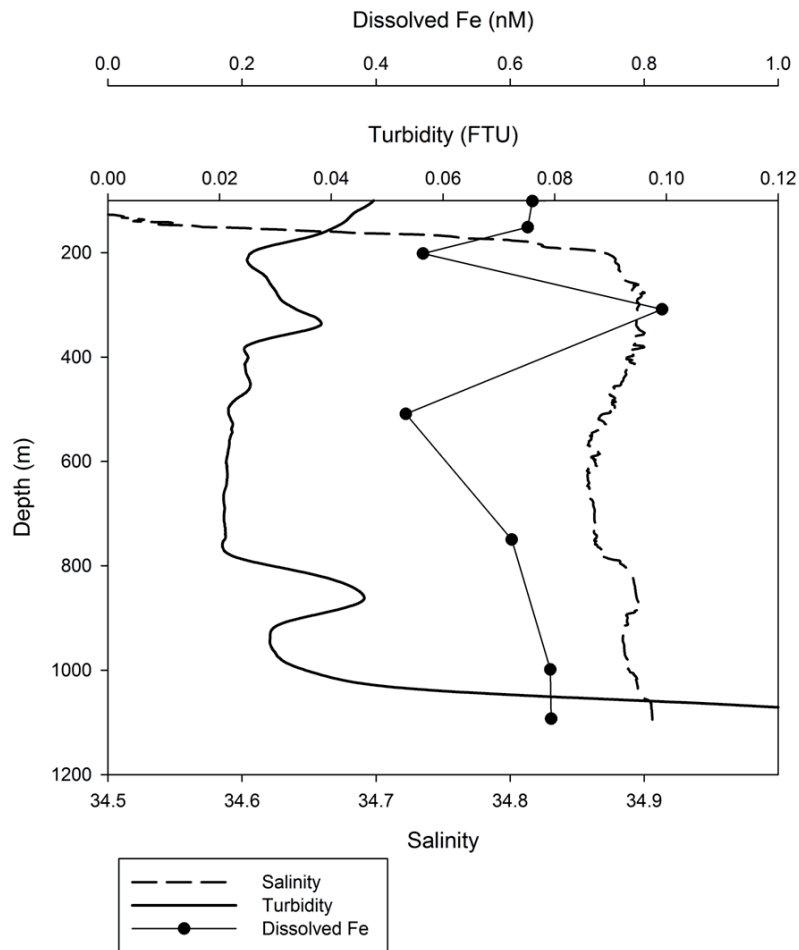


Fig. 3.3c Concentration of DFe (nM) of station 400 (Laptev Sea Slope). Turbidity is also indicated in arbitrary units, indicative of particle concentration in the water.

stwards (transect 2) (Fig. 3.2 and 3.5). Below 1000 m, concentrations increased to a very pronounced maximum with DFe concentrations ~1.3 nM at transect 1 and ~0.8 nM at transect 2. Moreover, at transect 2, two separate maxima were observed at ~2250 and 3200 m. At both transects, concentrations decreased towards the bottom below the maxima.

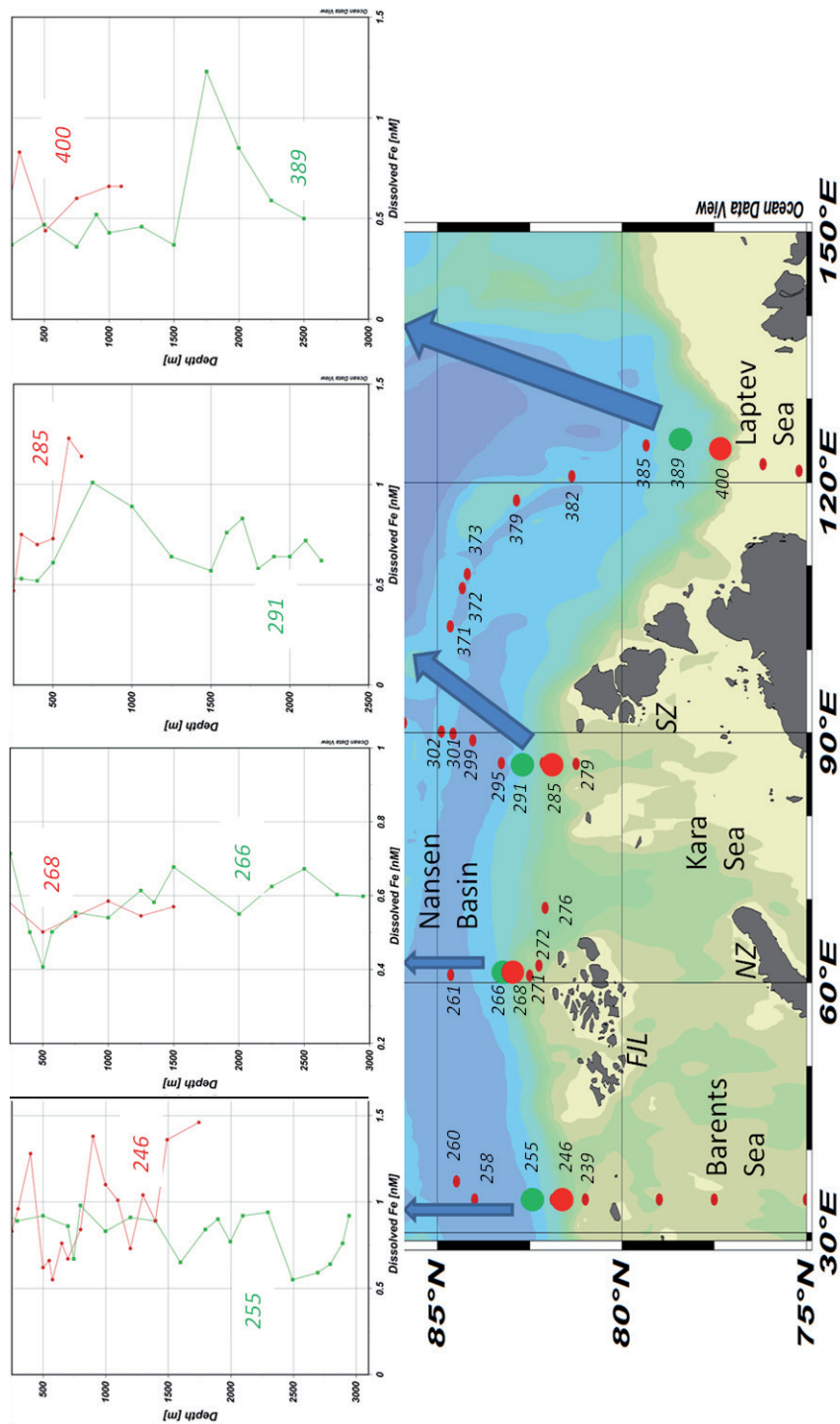


Fig. 3.4 Dissolved Fe depth profiles of slope stations (bottom depth < 3000m). Station numbers are indicated. FJL: Frans Jozef Land, NZ: Nova Zemlya, SZ: Svernaya Zemlya.

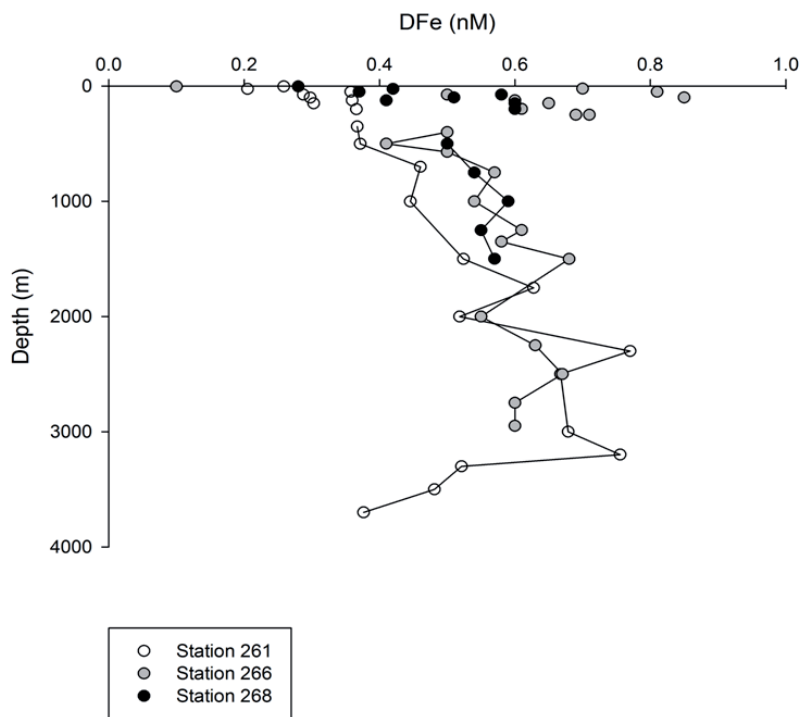


Fig. 3.5 Depth profiles of concentrations of dissolved Fe (nM) for all open ocean stations of transect 2. For clarity, connector line of the upper 1000 m is excluded.

3.4.2 Transect 3

Concentrations <0.5 nM were observed in the upper 1000 m of transect 3, throughout all basins (Fig. 3.6). Slightly higher (0.5–1 nM) concentrations were found above the shelf and slope of the Nansen Basin. An intrusion of high DFe (>1 nM) concentrations was observed from the Kara Sea shelf into the Basin just below the Atlantic water, at 750 m depth, consistent with a lower light transmission signal observed between 400–800 m (Fig. 3.3b) indicating a relatively high particle concentration.

A similar intrusion was observed slightly deeper below 1200 m depth with a small peak in DFe at ~ 1700 m, which shifts to ~ 1500 m depth further into the basin. This peak in the concentration of DFe is highest (from 0.61 to 0.84 nM) at the station closest to the shelf (station 291), where a similar maximum was observed in the depth profile of DMn concentrations [Middag *et al.*, 2011]. At station 299 this maximum was much less pronounced for the concentration of DFe and disappeared fully for DMn [Middag *et al.*, 2011]. A very pronounced DFe maximum of 1.71 nM was situated around 2500–3000 m depth above the Gakkel Ridge (Fig. 3.6, St. 306). This maximum in DFe influenced the deepest waters (>2000 m) of the Nansen Basin

and – although less pronounced – the waters at 2000-3000 m in the Amundsen and Makarov Basins (Fig. 3.6).

In the Amundsen Basin, the background concentrations of DFe were in general <0.5 nM, but concentrations reaching ~ 0.7 nM were observed at 2000-2500 m depth. Slightly higher DFe concentrations were found above the Lomonosov Ridge, and the concentrations of DFe decreased again to very low concentrations <0.3 nM in the deep Makarov Basin waters (Fig. 3.6).

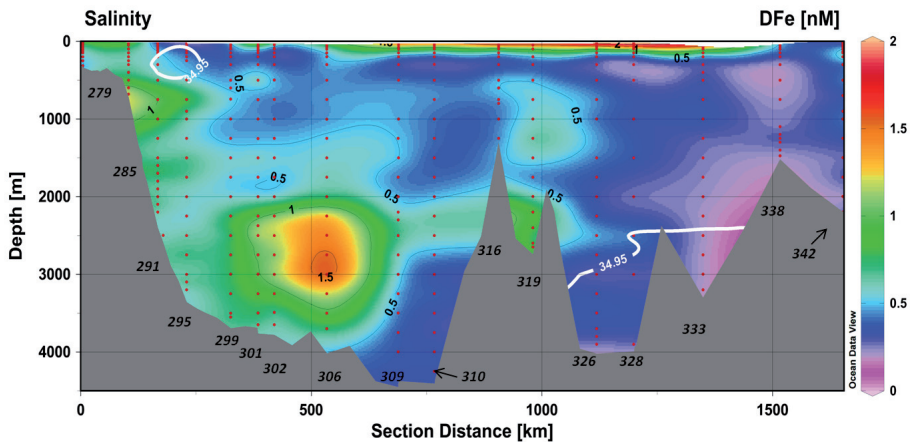


Fig. 3.6 Colour plot of concentrations of dissolved Fe (nM) for transect 3 (See Fig. 1a). Red dots indicate sample points. Station numbers are mentioned below the transect. White contour lines indicate a salinity of 34.95. Basins: Nansen Basin at 100-500 km, Amundsen Basin at 500-800 km and Makarov Basin at 1100 – 1500 km. Ridges: Gakkel Ridge at ~ 500 km, Lomonosov Ridge at ~ 800 -1100 km and Alpha Ridge at ~ 1500 km.

3.4.3 Transect 4

The fourth transect comprises three stations situated on the Mendeleev Ridge (349), in the Makarov Basin (352) and over the Lomonosov Ridge (363), respectively. These stations are too far apart to show in a contour plot; therefore the vertical profiles are shown (Fig. 3.7). At all stations the high DFe concentrations in the surface decreased to relatively constant concentrations (0.3-0.5 nM) between 200-500 m depth. Enhanced DFe concentrations (~ 0.8 nM) were observed at 1000 m and 1750 m above the Lomonosov Ridge. In the Makarov Basin, a maximum in the DFe concentration was observed at 1000 m, changing the trend of decreasing DFe with depth. In contrast, the Amundsen Basin stations showed a (slightly) increasing trend with depth between 1000-2000 m. Below 2000 m, a maximum at 2250 m and a very low concentration at 2750 m were observed at both stations. Below 1500 m depth, the station in the Makarov Basin showed a constant ~ 0.1 -0.15 nM lower concentration compared to the Amundsen Basin.

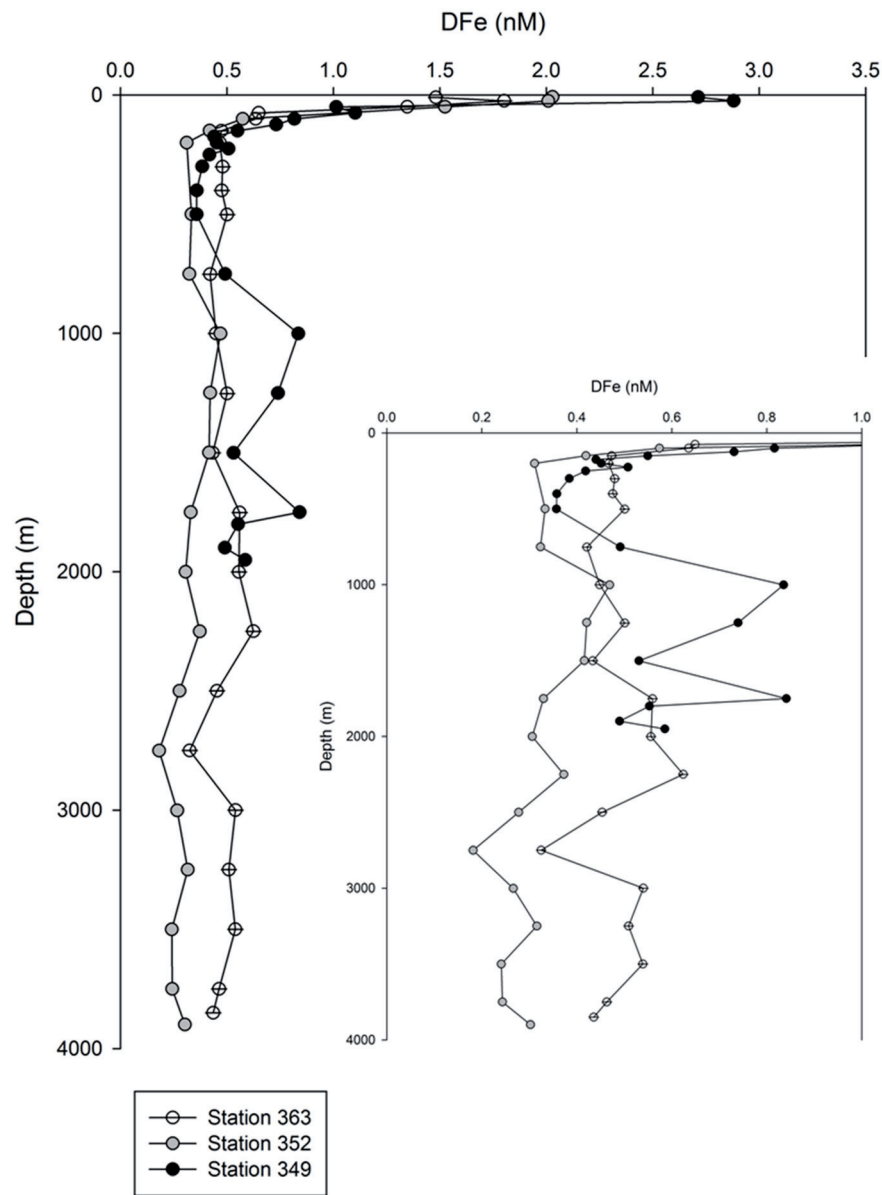


Fig. 3.7 Depth profiles of dissolved Fe for all open ocean stations of transect 4. The inset shows DFe at a 1 nM scale.

3.4.4 Transect 5

The fifth and last transect starts above the Nansen Gakkel Ridge approximately 0.6° Southwards and 12° Eastwards from the crossing of the Gakkel Ridge of transect 3 (Fig. 3.1). From here it follows a southeastward direction, along the Gakkel Ridge, Nansen Basin, Laptev Sea slope and the final station was located above the shelf of the Laptev Sea (<100 m depth). Figure 3.8 shows the DFe concentrations over transect 5. In general, the DFe concentration in the Deep Nansen Basin above the Gakkel Ridge was ~ 0.6 nM. The elevated concentrations, as determined at 2000-2500 m depth within transect 3, were hardly visible in transect 5. However, deeper in the water column, at 3000-3500 m depth, concentrations of DFe were elevated, accompanied by elevated DMn concentrations [Middag *et al.*, 2011] and potential temperature anomalies and transmission anomalies. In the middle of the water column (1000-3000 m depth) concentrations of 0.7-1 nM were observed, whereas above and below these depths, concentrations decrease (Fig. 3.7). An increase of the DFe concentration from the slope into the basin was observed at ~ 300 and at 1750-2000 m depth (Figures 3.3c, 3.4).

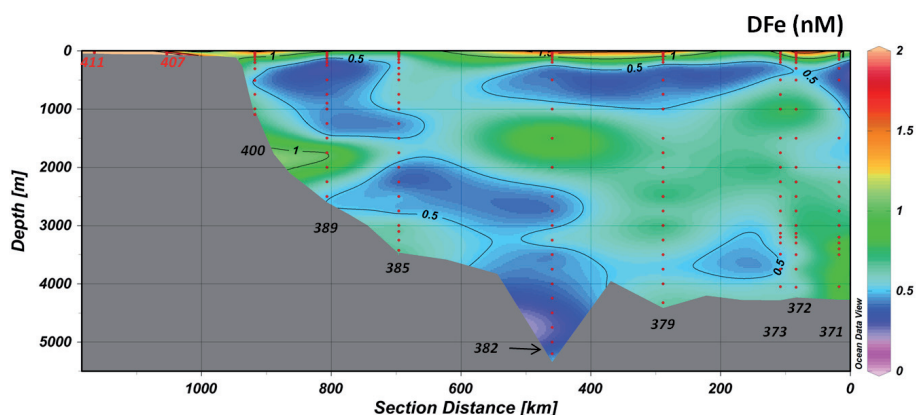


Fig. 3.8. Colour plot of concentrations of dissolved Fe (DFe, nM) for transect 5 (See Fig. 3.1a). Red dots indicate sample points. Station numbers are mentioned below the transect. White contourlines indicate a salinity of 34.95.

3.5 Discussion

3.5.1 Sources and sinks of Fe in the Arctic Basin

The here observed data for the Nansen, Amundsen and Makarov Basins can be compared with DFe data from the Canada Basin and Chukchi Slope [Nakayama *et al.*, 2011]. Deep waters in the Canada Basin show relatively constant DFe concentrations (~ 0.5 - 0.6 nM) similar to deep water concentrations in the Amundsen and Nansen Basins. The stations above the Chukchi slope show higher DFe concentrations (~ 0.9 - 1 nM) [Nakayama *et al.*, 2011], similar to shelf influenced DFe concentrations here observed on the Eurasian side of the Arctic Ocean. In this section we discuss the different factors influencing the the distribution of DFe in the Deep Waters of the Arctic Ocean. and give a comparison with DFe distribution in other ocean regions (Fig. 3.9). The concentration of DFe in the Arctic Ocean is determined by the DFe concentration of its contributories (Atlantic and Pacific Water) (see text section 3.5.1.1), *in situ* mineralization (3.5.1.2), input sources within the Arctic Ocean (advection of shelf derived water, re-suspended sediment (5.1.3), hydrothermal sources (3.5.1.4), and export processes (scavenging) and ligand binding and complexation capacity (3.5.1.5).

3.5.1.1 Interaction with the North Atlantic and North Pacific Oceans

The main contribution of the Arctic Ocean Waters is the inflow of water from the North Atlantic via Fram Strait (FSB) or the Barents Sea (BSB) [Rudels, 2001] (Fig. 3.1b; section 3.3). Slightly higher DFe concentrations (~ 0.8 - 0.95 nM) at the depth of the FSB inflow (high θ and salinity 200-400 m; Fig. 3.2 and 3.3a) observed at transect 1 indicate high DFe in the Atlantic source waters. Strong geostrophic velocities as reported above the Yarmuk Plateau just North of Spitsbergen [D'Asaro and Morison, 1992], may cause particle resuspension. However, because no significant turbidity increase is observed (Fig. 3.3a), this is not very likely, unless dissolution and fast sinking of possible resuspended particles have taken place. In general, the closer proximity to Fram Strait (thus Atlantic source) would explain the slightly higher DFe concentrations in the West part of the Nansen Basin compared to the East part (Figs. 3.2, 3.5 and 3.9).

Both the intermediate depth layers and the Polar Surface Waters (PSW) exit the Arctic through Fram Strait, west of the Greenwich Meridian [Rudels *et al.*, 2005; Tanhua *et al.*, 2005]. At intermediate depth, this return current is situated close to the Gakkel Ridge (Fig. 3.1b; [Jones *et al.*, 1995]) where relatively high Fe was observed. Also DFe-concentrations in PSW were relatively high [Klunder *et al.*, 2012]. These observations indicate that relatively high DFe concentrations are likely present in the Arctic contribution to the Iceland Scotland and Denmark Strait Overflow Waters, and would eventually augment DFe in North Atlantic Deep Water.

In the Makarov Basin, at 2700-3000 m depth, low DFe concentrations were observed as well as distinct phosphate and silicate maxima and a slight salinity mini-

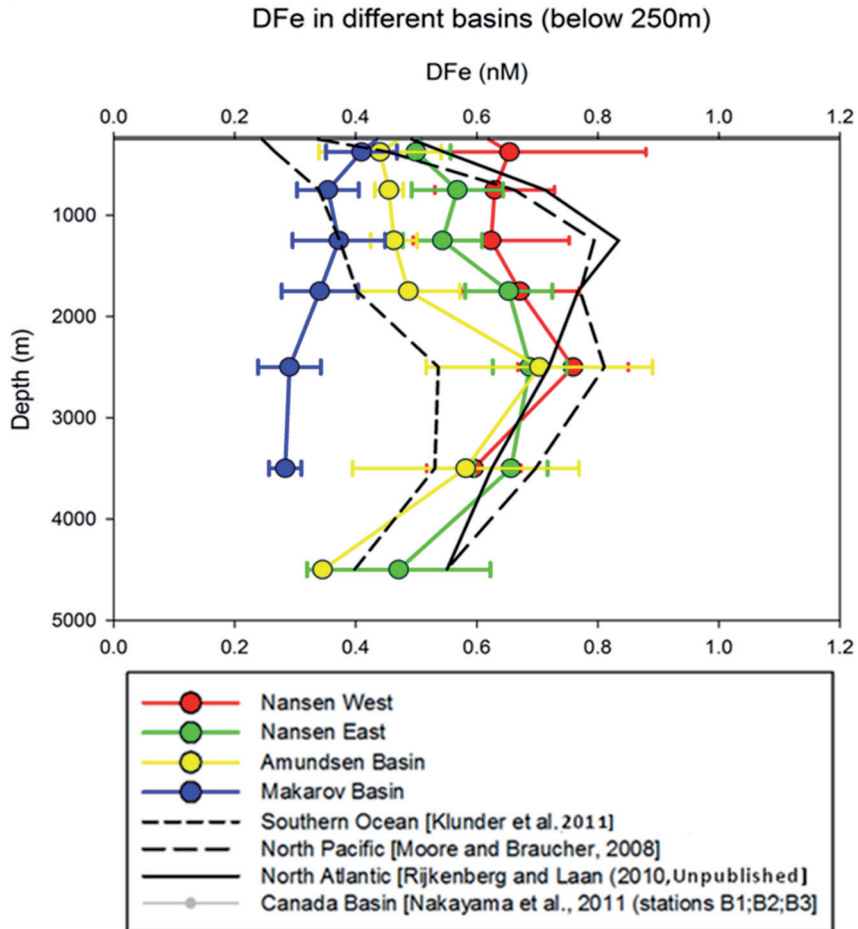


Fig. 3.9 Concentrations of DFe (nM) over the different regions in the Arctic Ocean (Fig. 3.1), averaged over depth intervals (250-500m, 500-1000m, 1000-2000m, 2000-3000m, 3000-4000m, 4000-5000m and 5000-6000m). Error bars indicate 95% confidence interval. For comparison, similar average values of vertical profiles are shown for the Southern Ocean, North Atlantic and North Pacific.

mum. This may reflect downslope convection of waters from the surface, entraining in the deeper waters of the Laptev and Chukchi slopes [Rudels, 2001]. Therefore the low DFe concentrations may be caused by either a low Pacific endmember concentration or biological depletion or enhanced scavenging of DFe during transit from the Pacific to the Arctic shelves [Klunder et al., 2012]. As [Aguilar-Islas et al., 2008] reported DFe-concentrations of 1.21-3.14 nM for North Pacific shelf stations, close to Bering Strait, we do not expect the Pacific source water to be low in DFe. Moreover,

the North Pacific water must flow over the Bering Sea Shelf, before reaching Bering Strait. *Aguilar et al.* [2007] has shown that DFe increases to ~4 nM at the shelf domain. Therefore, biological depletion and/or loss due to scavenging seems to be the more likely cause for the low DFe concentrations. See also *Klunder et al.*, 2012 and references therein.

3.5.1.2. Remineralization of exported biogenic particles

Remineralization of biogenic particles exported from the mixed layer would theoretically be reflected in a significant (positive) correlation between DFe and major nutrients (silicate(Si), phosphate (PO_4) and nitrate and nitrite ($\text{NO}_3 + \text{NO}_2$). Such a correlation is reported for DFe and ($\text{NO}_3 + \text{NO}_2$) and for DFe and Si in the North Atlantic Ocean [*Middag*, 2010, *PhD- thesis*]. Based on the relationship between Al and Si in the Arctic, *Middag et al.*[2009] concluded that dissolution of biogenic particles (mainly diatoms) must occur in the Atlantic and intermediate layers in the Arctic Ocean. For DFe and Si (or DFe and $\text{NO}_3 + \text{NO}_2$) however, such a significant (positive) correlation is not observed in the Atlantic and Intermediate waters or in the deep waters of the Arctic Ocean. Moreover, $^{234}\text{Th}/^{238}\text{U}$ - data from the same cruise showed that there was very little export of organic carbon from the upper 100 m to deeper waters in the Arctic Basins [*Cai et al.*, 2010].

This was confirmed by low organic carbon export as determined from PO_4 deficit [*Anderson et al.*, 2003] and sediment traps [*Fahl and Nöthig*, 2007]. The $^{234}\text{Th}/^{238}\text{U}$ ratios integrate the POC export over the preceding 1-2 months, whereas the Al-Si relation reflects processes at longer timescales. Therefore, based on the $^{234}\text{Th}/^{238}\text{U}$ data and the absence of the relationship between DFe and Si (and DFe and $\text{NO}_3 + \text{NO}_2$), we expect a relatively low influence of remineralization of organic particles on the DFe input in the intermediate waters of the Arctic Ocean. Also, in the deep waters (MBDW and EBDW), we did not observe a significant positive correlation between DFe and Si (or ($\text{NO}_3 + \text{NO}_2$)). However, these waters display a strong input of terrestrial material [*Middag et al.*, 2009; *Roeske*, unpublished data], diminishing a possible biogenic particle remineralisation signal.

3.5.1.3 Fe input from adjacent shelf seas and slopes

Although TDFe concentrations above the Barents and Kara Sea shelves are high (6-60 nM) [*Thuróczy et al.* 2012], the concentration of dissolved iron does not exceed that of the slope and open ocean region (0.4-0.54 nM) [*Klunder et al.* 2012]. The station at transect 1, close to the shelf (station 246) shows a complex pattern of different layers. High potential temperature (θ) and salinity indicate an Atlantic influence at ~200-300 m depth (see section 3.5.1.1; Fig. 3.2a). There is a thin layer at ~400 m, with low θ and salinity, where also an enrichment in $\delta^{18}\text{O}$ is observed (not shown), all indicative of ice-melt influence [*Ekwurzel et al.*, 2001; *Klunder et al.*, submitted]. Thus, meltwater influenced waters from the shelf may possibly explain the high DFe (1.22 nM) around this depth. Remarkably, the turbidity increase at ~500 m depth, indica-

tive of advective transport from the shelves, does not cause high DFe concentrations but higher DFe concentrations are observed at a smaller turbidity maximum at 900 m depth (Figure 3.5a). Towards the bottom, elevated DFe, consistent with turbidity (Fig. 3.3a) and elevated Mn [Middag *et al.*, 2011] indicates local resuspension at the slope. There is no sign of advective DFe transport far into the basin, as station 255 does not show enrichment in DFe (Fig. 3.4). Also no advective transport is observed from the shelves into the Basin at transect 2 (Figure 3.4 and 3.5). Further east (station 279-302), in the east part of the Nansen Basin, enrichment with DFe was observed close to the bottom of the Kara Sea slope (Figure 3.4 and 3.6). We suggest that the relatively low salinity and high turbidity corresponding to the DFe maximum (Fig. 3.2b) are the result of inflow of BSB water, which picks up particles from the shelf, and then enters the Nansen Basin at a depth of between 500 and 700 m (see section 3.3.1). Dissolution of Fe from these particles will then be the principal source of DFe. This process has been shown to enhance DFe levels in regions with strong geostrophic velocities, such as the Northeast Atlantic [Laës *et al.*, 2007] and above the New Zealand continental shelf [Croot and Hunter, 1998]. D'Asaro and Morison [1992] and Schauer *et al.* [1997] reported internal wave mixing and eddies in the Eastern Nansen Basin, which may have strong enough velocities to cause near-bed mixing and resuspension of sediments.

Dissolution from these particles ($>0.2 \mu\text{m}$) during transport from the shelf seas to the slope regions, could cause the maximum in DFe concentration observed in the entire Nansen Basin at ~ 750 m depth. The natural logarithm of this maximum concentration of DFe (750 m depth) versus the distance into the Nansen basin (St. 285-302), results in the following equation:

$$\ln [\text{DFe}] = -0.0038 * \text{distance (km)} + 0.27 \text{ (Eq. 1)}$$

$$(R^2=0.97, n=6, P<0.01)$$

Beyond station 302, no elevated values were observed at 750 m depth. From Eq. 1, we can calculate a scale length (defined as the distance to reduce the dissolved iron to 37% ($1/e$) of the initial concentration [Johnson *et al.*, 1997]) of 263 km. Johnson *et al.* [1997] reported a scale length of 5000 km at 1000 m depth in the East Pacific, off the coast of California. However, the strong scavenging regime and the fact that the currents in the Nansen Basin are along rather than perpendicular to the shelf (Fig. 3.1b) can explain the order of magnitude difference in off shore transport of shelf derived DFe between the Nansen Basin and the East Pacific, where conditions for advective transport are more favorable [Johnson *et al.*, 1997]. Laës *et al.*, [2007] observed that elevated Fe concentrations above the shelf, were not present ~ 147 km into the North Atlantic Ocean, confirming that the long distance transport of sediment derived DFe is strongly dependent on scavenging and advective transport by currents [Laës *et al.*, 2003, 2007].

More to the east, towards the Laptev Sea shelf, a maximum in DFe concentration was observed at 300 m, together with a turbidity maximum (Fig. 3.3c). Because of the correspondance of DFe with particle load and the fact that this maximum is ~ 700 m above the sea floor we suggest that the elevated DFe at this station is caused by advective transport from the Laptev Sea shelf. The shallow (~50 m) Laptev Sea contains a large amount of particles and a high DFe (1.5-10 nM) [Klunder *et al.*, 2012] and TDFe (~20-40 nM) concentrations [unpublished data]. Lower in the water column, at ~850 m, a turbidity and salinity maximum indicates the inflow of Atlantic water, possibly explained by the small fraction of Atlantic water coming through the Vilkitskij Strait, as reported by Aksenov *et al.* [2010]. Unfortunately, no DFe data is available for this depth, however, it is visible as a small enrichment at 900 m depth at station 389 (Fig. 3.4).

3.5.1.4 Fe input from hydrothermal origin

Hydrothermal vents are known to be an important source for iron in deep waters in the world ocean [Klinkhammer *et al.*, 2001; Tagliabue *et al.*, 2010]. Edmonds *et al.*, [2003] reported active hydrothermal vents in the Arctic; the most eastern vent was located at (85°39'N, 84°50'E), approximately 60 km from our station 306 (Fig. 3.1a). Indeed, elevated DFe concentrations were observed at a depth of 2000-3000 m in a large part of the Nansen and Amundsen Basins, and less pronounced, in the Makarov Basin (Fig. 3.6). The highest DFe concentrations were observed at station 306, suggesting that this station is located closest to the hydrothermal input source. Moreover, at this station between 2000-3000 m depth, Middag *et al.* [2011] observed over ten-fold higher DMn compared to background concentrations and anomalies in light transmission and temperature confirming the presence of a hydrothermal vent source. Consistent with observations from the Southern Ocean [Klunder *et al.*, 2011], hydrothermal enrichment in DMn and DFe but no enrichment in dissolved Aluminium (DAI) was observed in the Arctic Deep Waters [Middag *et al.*, 2009; 2011].

Based on a one dimensional scavenging model of Craig [1974], Weiss [1977] proposed an equation for removal of DMn with distance from a hydrothermal vent source. Applying this idea to DFe, for the special case where the currents are neglected ($v=0$) this equation is:

$$C = C_0 * e^{-Ax} \text{ (Eq. 2)}$$

Where:

C is the concentration of DFe from the (hydrothermal) source (nM)

C_0 is the initial concentration of DFe close the source (nM)

x is the distance to the source (cm)

$A = \sqrt{K_h^{-1} \times \tau^{-1}}$; $K_h = 5 \times 10^6 \text{ cm}^2/\text{s}$ [Weiss, 1977] and τ = residence time (s)

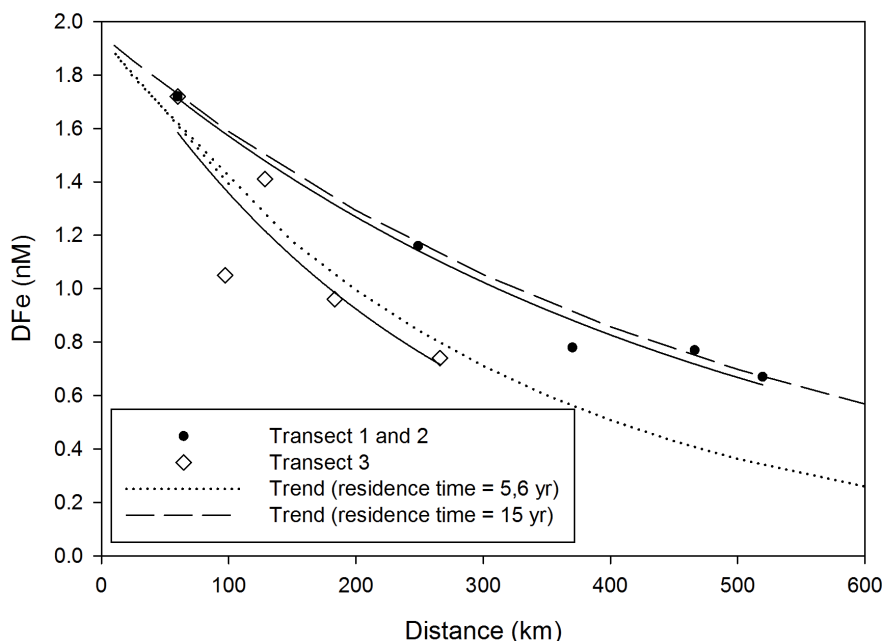


Fig. 3.10 Trend of DFe (nM) with distance at the 2000-3000 hydrothermal maximum in the Nansen Basin. Also shown is the calculated trend with distance using Eq. 2 (see text) and the residence time of 5,6 year (after Moore and Braucher [2008]) and 15 year (after De Baar and De Jong [2001]).

Shown in Fig. 3.10 are the DFe maxima at ~2250-2750 m versus the distance, for the stations, of transect 3 and transect 1 and 2 combined (only Nansen Basin stations). Also shown in Fig. 3.10 are the calculated DFe concentrations with distance, based on a residence time of 5.6 yr (reported for deep waters with strong scavenging regime by [Moore and Braucher, 2008]) and on a residence time of 15 yr (lower end of range in [De Baar and De Jong, 2001]). The value for $C_0 = 1.95$ nM (calculated from the fit of transect 3 and transect 1 and 2) (Eq. 2).

For transect 1 and 2, a higher DFe-concentration relative to distance is observed. The best fit of these stations gives a residence time of 14.4 yr, close to the model for a residence time of 15 yr. For the parallel decreasing trend of dissolved Mn a much shorter residence time of 2 yr was reported [Middag et al, 2011]. In contrast the stations of transect 3 show a lower DFe with distance, and the best fit gives a shorter 4.7 yr residence time. For the parallel decreasing trend of dissolved Mn again a shorter residence time of 0.4 yr was reported [Middag et al., 2011].

The relatively more rapid loss of Mn versus Fe is in contrast with previous observations, for much higher concentrations, very close to the hydrothermal source. For the Juan de Fuca Ridge, Field and Sherrell [2000] report a trend of DFe from 319 nM to 20 nM over the short distance of 3.7 km from the vent source, versus an apparent trend of DMn from 193 nM to 27 nM. By implicitly assuming that the latter

Mn trend is merely due to dilution, for DFe an apparent oxidation half-life of ~ 3.33 hours was derived. Latter more rapid loss of Fe versus Mn is in keeping with the generally more rapid inorganic oxidation of Fe versus Mn [Cowen *et al.*, 1990].

The key difference between our observations at low concentrations and long distances, and the high concentrations and short distances over the Juan de Fuca ridge, is in the natural organic complexation of Fe in ocean waters. Briefly there is a general background level of organic Fe-binding ligand of 1.98-2.05 nM observed in the same samples over Gakkel Ridge [Thuróczy *et al.*, 2011]. Such Fe-binding ligand concentrations are typical throughout the world oceans. When the DFe concentration is near this ligand concentration, most of the DFe is stabilized in solution thus preventing scavenging loss. In contrast dissolved Mn is not organically complexed, hence will be scavenged more rapidly. At the very high DFe in the

20-319 nM range over Juan de Fuca ridge, the low ~ 2 nM ligand concentration is inadequate, the large majority of dissolved Fe is inorganic, hence will be rapidly scavenged.

The difference in residence time observed for transect 1-2, and transect 3 is not expected within a uniform basin. The difference in DFe decrease may also be caused by the flow direction in the deep Arctic Ocean. Weiss [1977] showed a strong effect of velocity in removal with distance; a positively directed flow ($v > 0$; from the vent towards the location of the stations) would cause a higher concentration for the same distance compared to the modeled fit (where $v = 0$ is assumed). Based on the flow patterns (Fig. 3.1b), a positive flow is expected towards transect 1 and 2, whereas towards transect 3, more perpendicular to the currents, the direction is 0 or even slightly negative (Fig. 3.1b). Although the data does not provide a definite conclusion, it seems likely that the different decrease patterns of DFe with depth are related rather to flow patterns than to a (large) difference in residence time. To the best of our knowledge, there is no data on specific residence times of DFe with respect to hydrothermal input. Nevertheless, the fact that the residence time is between the range of 15-41 yr published by De Baar and De Jong [2001] for the deep oceans worldwide and the 5.6 yr published for deep oceans with a high scavenging regime by Moore and Braucher [2008] supports a strong scavenging regime in the deep Nansen Basin.

Hydrothermal vents are also reported at $\sim 37^\circ$ (~ 3200 m) and $\sim 43^\circ$ E (depth unknown) Edmonds *et al.* [2003] (Fig. 3.1b). With the general Northwest flow direction, transect 1 was situated downstream of the flow direction whereas transect 2 was further away and upstream of the flow direction (Fig. 3.1b; [Rudels, 2001]). In the Northwestern Nansen Basin, station 260 showed the strongest concentration increase of > 1 nM DFe at 2000-3000 m depth, whereas stations more to the east (st. 261) (Fig. 3.5) and south (st. 258) (Fig. 3.2) show separate DFe maxima (of ~ 0.1 nM above background) at ~ 2200 - 2600 m and ~ 3200 m. However, the strong DFe maximum at station 260 may also be caused by two separate DFe-enrichments, as was observed in the Mn signal [Middag *et al.*, 2011]. The fact that this is the strongest

signal, indicates that the hydrothermal plume which causes the DFe enrichment at 3200 m likely came from the North(-east) direction. Therefore we suggest that the elevated DFe concentration at ~3200 m originates from the hydrothermal vents at 37° and/or ~43° E as reported by *Edmonds et al. [2003]*.

Above the east part of the Gakkel Ridge, from ~103° E (station 371-373), the hydrothermal signal at ~2500 m was not very pronounced in the DFe (Fig. 3.8). However, a signal was observed in the light transmission, temperature and DFe profiles at ~3000-3500 m (Fig. 3.11). At station 372 (and 373) also total dissolvable Fe (TDFe) was measured at high resolution below 2000 m depth as shown in Figure 3.11. Although there are elevated concentrations of dissolved Fe over a broad depth range from 2200-3600 m depth, there is a local, stronger, maximum of total Fe (TDFe) at 3200-3360 m depth (Fig. 3.11). The stronger increase in TDFe relative to DFe in hydrothermal influenced

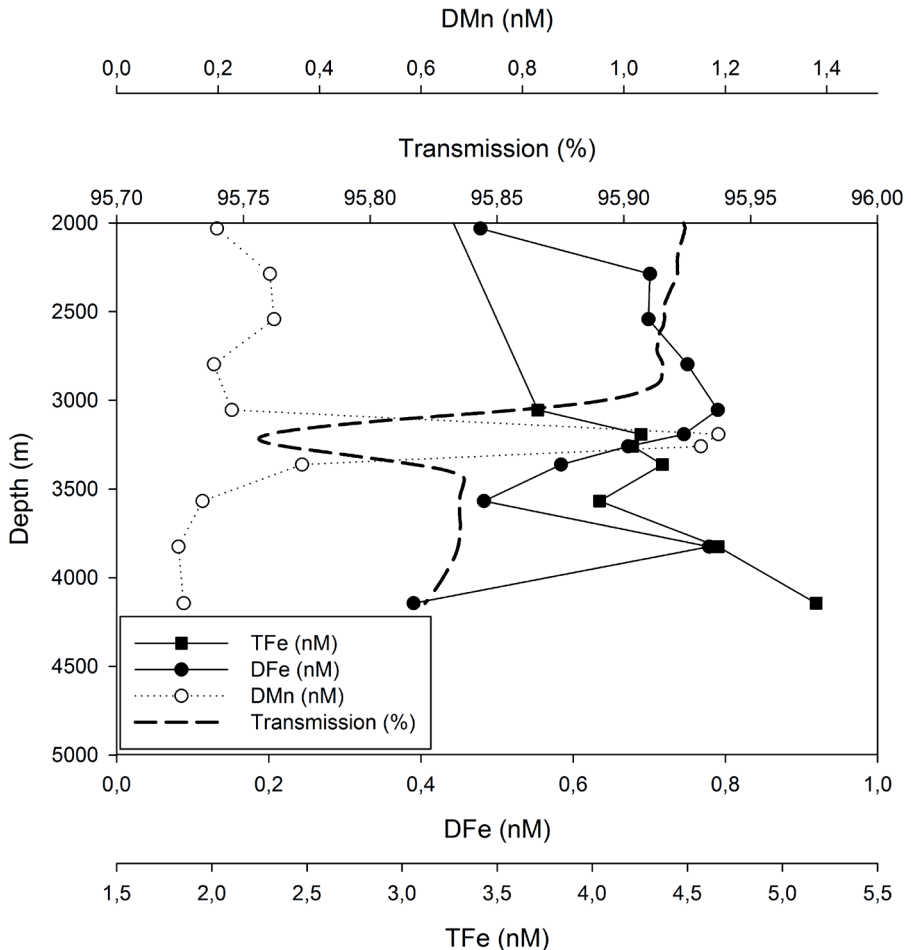


Fig. 3.11 Dissolved Fe (DFe, nM), Total Fe (TFe, nM), Dissolved Mn (DMn, nM) and transmission signal (%) (smoothed) for station 372, indicative of an hydrothermal plume.

waters is also reported by *Boyle et al.* [2005]. These findings are coincident with increase in dissolved manganese and a local increase in θ are observed at station 372, at a depth of 3100-3300 m [*Middag et al.*, 2011].

At station 372, a geostrophic velocity (relative to 3000 m depth) of close to 0 is observed, possibly preventing mixing of a hydrothermal source with waters above and below. In contrast, at station 371 and 373 stronger velocities are observed (data not shown), possibly causing mixing of a hydrothermal source with surrounding waters.

The increase in concentration in the hydrothermal plume is relatively low at station 372 compared to that at station 306 both for DFe and DMn [*Middag et al.*, 2011]. The vents described by *Edmonds et al.* [2003] are all situated west of 84°E (Fig. 3.1) and to the best of our knowledge there is no vent discovered east of 85°E. The fact that the signal is only observed at station 372, may imply that the source of the hydrothermal signal observed at station 372 comes from a thus far undiscovered vent in this region. Alternatively, the signal could be transported to the region of station 372 from further east. A strong hydrothermal source is observed at ~3200 m depth at 37°E ([*Edmonds et al.*, 2003]; Fig. 3.1a), which is situated slightly north of the rift valley, i.e. on the Amundsen Basin side of the ridge. Although the flow direction for water in the deep Amundsen Basin is westward [*Rudels*, 2001], an eastward return flow was proposed by *Jones et al.* [1995] for waters below 2000 m water in the Amundsen basin, which may explain the observation of the elevated DFe signal so far from the source.

3.5.1.5 *Fe in the deep waters; deep remineralization, scavenging and organic complexation*

Generally, in the deep waters of the world ocean the distribution of DFe is determined by an interplay of (passive) particle scavenging of iron from the dissolved phase [*Johnson et al.*, 1997] and organic complexation [*Wu and Luther*, 1995; *Wu et al.*, 2001]. The DFe distribution is also affected by the remineralization of biogenic particles [*Martin and Gordon*, 1988; *Sunda and Huntsman*, 1995]. The distribution of nitrate (NO_3^-) throughout the water column is determined by the process of biological uptake and remineralization and not by scavenging [*Murray*, 1992]. Therefore, the DFe / NO_3^- ratio can give an indication of the relative importance of the scavenging regime (and complexation). For example, *Sarthou et al.* [2007] showed lower values of the DFe / NO_3^- ratio were consistent with a stronger scavenging regime in the North Atlantic Ocean. In Table 3.1 the average DFe / NO_3^- ratios and DFe concentrations are shown for the deep waters (EBDW, MBDW) in the Nansen, Amundsen and Makarov Basin respectively. There is a significant difference in DFe / NO_3^- between the Nansen and Amundsen Basins (~33 %). *Parekh et al.* [2005] showed in a model study that decreasing the scavenging ratio by 40% results in a ~0.1 nM increase in DFe in the deep global oceans. Scavenging removal of DFe is reported for all Arctic Basins [*Thuroczy et al.* 2011]. The difference in DFe between the Nansen and Amund-

Table 3.1 $D\text{Fe}/\text{NO}_3^-$ ratio's and $D\text{Fe}$ concentrations in the deep waters (DMBW and DEBW) in the different Basins.

Basin		Nansen	Amundsen	Makarov
Water mass		DEBW	DEBW	DMBW
$D\text{Fe}/\text{NO}_3^-$	Average	0.047	0.031	0.026
	Standard deviation	0.017	0.007	0.013
	n*	154	28	52
	p**		<0.05	<0.05
	Decrease (%)		33%	16%
$D\text{Fe}$ (nM)	Average	0.70	0.47	0.39
	Standard deviation	0.25	0.11	0.19
	n*	157	28	52
	p**		<0.05	<0.05

* For 3 stations in the Nansen Basin there is no NO_3^- data available

** 2-sided heteroscedastic T-test

sen Basins is 0.23 nM (Table 3.1), significantly larger than the difference in scavenging removal that would be expected on the basis of the $D\text{Fe}/\text{NO}_3^-$ ratio and the model results of *Parekh et al.* [2005]. Possible explanations for this discrepancy are (i) larger input flux of $D\text{Fe}$ in the EBDW in the Nansen Basin or (ii) lower or less strong organic complexation (resulting in more scavenging removal) in the Amundsen Basin compared to the Nansen Basin or a combination of both factors.

As discussed above (sections 3.5.1.2; 3.5.1.4), there are strong input sources in the Nansen Basin, i.e. $D\text{Fe}$ input from the slope and hydrothermal $D\text{Fe}$ input. We argue that the difference in $D\text{Fe}$ between the Nansen Basin and Amundsen Basin can be attributed mainly to the larger Fe input flux in the deep Nansen Basin, which is also consistent with the Al and Ba data (see section 3.5.1.2), rather than to differences in organic complexation. The organic complexation and size fractionation of Fe is described in [Thuróczy et al., 2011]. Briefly, for the size fraction $<0.2\ \mu\text{m}$, ranges of ligand concentrations (Eq of nM), binding strengths (-) and ligand saturation (Excess L / Fe) are 1.82 ± 0.33 , 22.01 ± 0.15 and 1.46 ± 0.44 for the EBDW in the Nansen Basin. The values for the Amundsen Basin are 1.57 ± 0.50 , 21.59 ± 0.37 and 3.41 ± 0.6 respectively. In general, the fact that there is a higher reactivity yet lower saturation state of the ligands in the Nansen compared to the Amundsen Basin make that the difference in organic complexation is difficult to quantify [Thuróczy et al., 2011]. We argue that the difference in $D\text{Fe}$ between the Nansen Basin and Amundsen Basin can be attributed mainly to the larger Fe input flux in the deep Nansen Basin, which is also consistent with the Al and Ba data (see section 3.5.1.2), rather than to differences in organic complexation.

Between the Amundsen and Makarov Basin there is only a small decrease in the DFe / NO_3^- ratio, which is consistent with the small decrease in DFe between both Basins (Table 1). Canada Basin Deep Water is relatively old compared to Eurasian Basin Deep Water as the latter water mass is stronger affected by downslope convection [Rudels, 2001]. Therefore, the scavenging removal may have been going on for a longer time in the Makarov Basin. Moreover, in the Amundsen Basin hydrothermally originated DFe is present (Fig. 3.6), whereas this input source is very small for the Makarov Basin. The DFe scavenging removal as a consequence of lower reactivity of ligands in the Makarov Basin will lead to a little saturated ligands. Ligand characteristics (ligand concentration, binding strength and saturation) are 1.35 ± 39 , 21.64 ± 0.13 and 4.66 ± 0.45 respectively [Thuróczy *et al.*, 2011]. Therefore, we suggest that the difference in DFe input and in age between these water masses are the main factors controlling the DFe concentration.

To take a closer look at the importance of input fluxes relative to scavenging removal in the distribution of DFe we look at the relationship between DFe and DMn in the deep water masses. The formula for scavenging removal is:

$$S_c = k * [\text{Me}] * C_p \text{ (Eq. 3)}$$

With:

S_c = the scavenging rate removal (nM d^{-1})

k = the scavenging rate (d^{-1})

$[\text{Me}]$ = the concentration of the metal (nM)

C_p = the concentration of particles (-)

The behavior of DMn is similar to that of DFe. Therefore if the dominant process in the deep Arctic Ocean is scavenging, the relation of both metals is to be expected to be of the form $\text{DMn} = (a * \text{DFe}) / b$ with $a = S_{c, \text{Mn}} * k_{\text{Fe}}$ and $b = S_{c, \text{Fe}} * k_{\text{Mn}}$ (derived from Eq.3). In the deeper waters (>3000 m) of the Amundsen and Makarov Basins (Fig. 3.12), such a relation was observed, with $R^2 = 0.74$ ($n = 27$). Here, the “external” Fe-input was very low, and therefore scavenging removal likely is the dominant process. Higher in the water column, and in the Nansen Basin, there are more factors, such as hydrothermal and slope input, influencing the DFe and DMn distribution in all Arctic Basins, leading to a disappearance of the DFe, DMn - relationship (Fig. 3.12). Enrichment in DMn compared to DFe is observed in the stations qualified as “hydrothermal”. However, some data points in the Nansen Basin show relatively higher DFe compared to DMn (Fig. 3.12). A possible explanation may be that these waters are part of a deep counter current as proposed by Jones *et al.* [1995]. The long transit time from the vents (situated more to the East) would then remove DMn relatively fast compared to DFe, resulting in the observed a relatively low DMn compared to

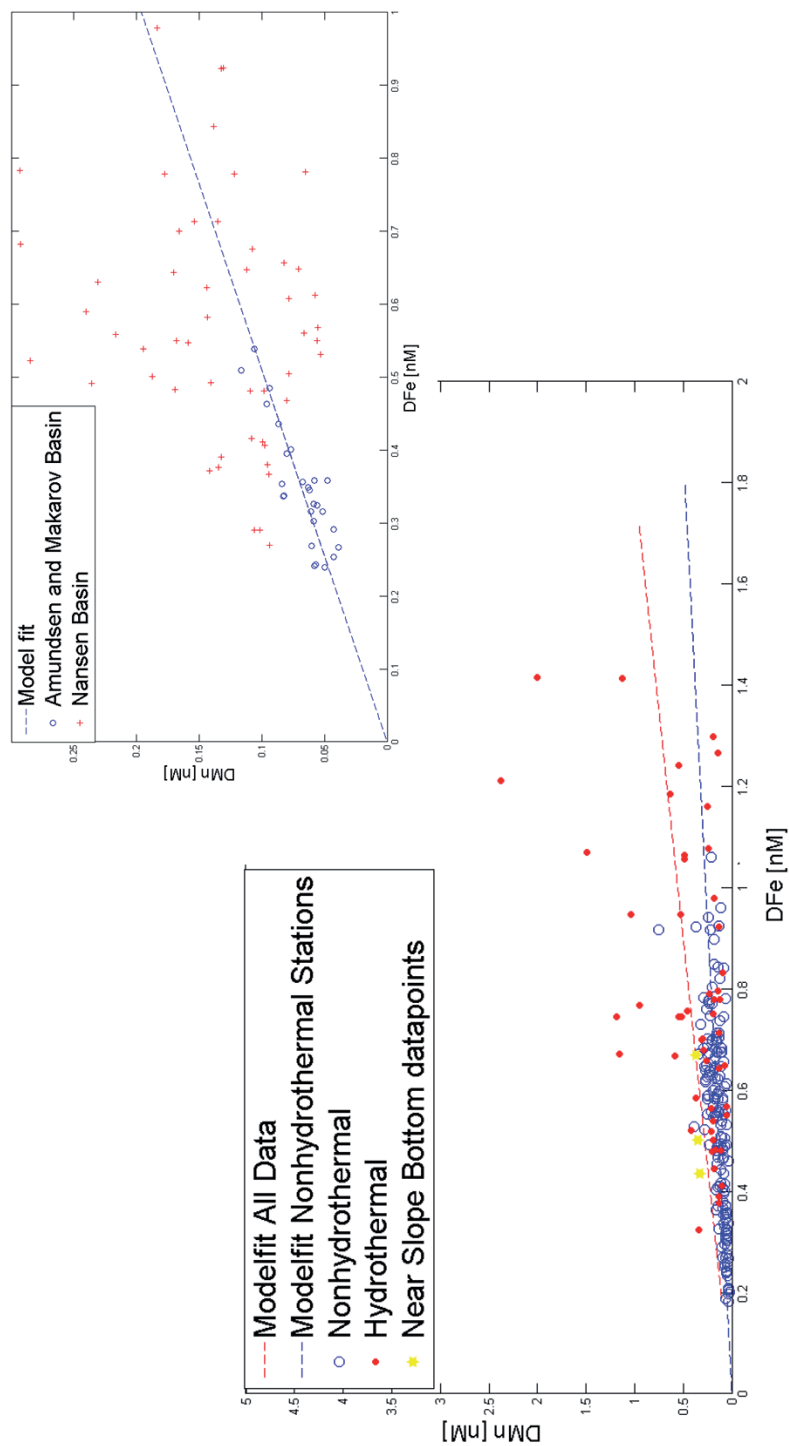


Fig. 3.12 Relationship between DFe (nM) and DMn (nM) for all datapoints within the DBMW and DEBW (see text). Stations indicated with “hydrothermal” are stations 260, 261, 301-306 and 372. Inset of Figure 12 at expanded scale: Relationship between DFe (nM) and DMn (nM) for all datapoints > 3000 m. Makarov and Amundsen datapoints show a correlation: $[DMn] \text{ (nM)} = (0.15 * [DFe] \text{ (nM)}) / 0.75$ with $R^2 = 0.74$, $n = 27$.

DFe. The deepest, near-bottom data points of the stations 255, 363, 389 situated above continental and Mendeleev Ridge slope regions appear to be enriched in DMn, which may be derived from recent resuspension of slope sediment [Middag *et al.*, 2011].

3.5.2 Implications for the DFe cycle in the deep Arctic Ocean

Recently, *Moore and Braucher* [2008] compiled the available data and presented (averaged) depth profiles of DFe concentration in three world ocean regions (North Atlantic, North Pacific and Southern Ocean). In Figure 3.9 similar plots for the Arctic Basins are shown (in the Nansen Basin discrimination is made between the East and West part of the Basin) along with the profiles of *Moore and Braucher* [2008], updated with recent DFe data [*Rijkenberg and Laan*, unpublished]. There are clear interbasin deviations in the DFe concentrations; a relatively high (~ 0.7 nM) concentration of DFe at 500-1500 m depth in the west part of the Nansen Basin compared to the East part and an even greater difference compared to the Amundsen and Makarov Basins, is likely caused by inflow of North Atlantic Water (see section 3.5.1.1). In general, in the upper 2000 m the concentrations decrease from the Siberian shelf to the Canadian side, with highest concentrations in the Nansen Basin and lowest in the Makarov Basin. Also shown are recent DFe concentrations from the Canada Basin (only Slope and Basin stations included (B1-B3)), close to the Chuckchi plateau ($150\text{--}160^\circ\text{W}$, $\sim 75^\circ\text{N}$) [*Nakayama et al.*, 2011]. The high concentrations in the upper depth interval (250-500) may be caused by intense remineralisation (as also confirmed by AOU and nutrients) [*Nakayama et al.*, 2011]. Below, DFe gradually declines and deep water concentrations are ~ 0.1 nM higher than those in the Makarov Basin, which could be attributed to slope influence (stations located nearby the slope) and to strong remineralisation, causing higher DFe at depth. No enrichment at ~ 2000 m depth is observed in this part of the Canada Basin. Moreover, the DFe distribution in the Arctic Ocean, particularly in the Makarov Basin, shows some deviation from the distribution in other regions of the world Ocean (Fig. 3.9). First of all, although dissolved Fe concentrations in the upper layers in the Arctic can be high (>2 nM) [*Klunder et al.*, 2012] the concentrations decrease readily with depth. The strong stratification largely prevents mixing between the deep waters and the surface waters [*Rudels*, 2001]. Secondly, the hydrothermal input is clearly visible in the Nansen and Amundsen Basins, resulting in a pronounced maximum in DFe at ~ 2500 m, which is not present in the North Atlantic (maximum at 1000-1500 m) and North Pacific (broad maximum (1000-3000m)). The hydrothermal maximum is absent in the Makarov Basin. Below this maximum, scavenging is the controlling factor and DFe concentrations decrease with depth, as also observed in other world oceans (Fig. 3.9).

Third, in the Makarov Basin, the absence of input sources and the fact that the water is relatively old, cannot be (fully) compensated by organic complexation leading to a strong scavenging removal and very low DFe concentrations (~ 0.25 nM).

3.6 Summary and Conclusions

The distribution of dissolved Fe in the deep waters of the Arctic Ocean deviates from that in all other regions of the world ocean. Moreover, there are strong differences between the different Arctic Ocean Basins. Over the whole Arctic Ocean, strong stratification largely prevents mixing between the deep water concentrations and the surface waters in the Arctic Ocean. However, DFe is transported from the shelf seas to the Arctic Deep waters, mainly by down slope convection and re-suspension of sediment from the slopes. The Atlantic Ocean is the main source of water to the Arctic, which is reflected in the higher Fe concentrations in the (western) Nansen Basin at intermediate depths. Remineralization of Fe from biogenic particles appears to have a relatively low impact on deep water DFe concentrations. This may be due to a low POC export from the surface, in combination with a strong scavenging regime, which enhances fast settling. The hydrothermal input source above the Gakkel ridge causes DFe enrichment at a depth of 2000-3000 m depth in most of the central Arctic Ocean. Below this depth layer, scavenging plays an important role in the deep waters, whereas the effect of organic complexation is relatively weak; concentrations decrease rapidly and reach very low values in the deep Makarov and Amundsen Basins. The high DFe concentration in the shelf waters flowing in the Central Arctic, ((mainly) river derived [Klunder *et al.*, 2012]), and hydrothermal enrichment of DFe to the Arctic Ocean will give a net addition of DFe to the marine environment. Upwelling of these waters [Yang, 2009] may cause relatively high DFe concentrations in the PSW and intermediate waters, and eventually in the return flow to the North Atlantic Ocean.

3.8 References

- Aguilar-Islas, A.M., R.D. Rember, C.W. Mordy and J. Wu (2008), Sea ice-derived dissolved iron and its potential influence on the spring algal bloom in the Bering Sea, *J. Geophys. Res.* 35, L24601
- Aguilar-Islas, A.M., M. P. Hurst, K.N. Buck, B. Sohst, G.J. Smith, M.C. Lohan, K. W. Bruland (2007). Micro- and macronutrients in the southeastern Bering Sea: Insight into iron-replete and iron-depleted regimes. *Progress in Oceanography* 73, 99–126.
- Aksenov, Y., S. Bacon, A.C. Coward, A.J.G. Nurser (2010), The North Atlantic Inflow to the Arctic Ocean, *J. Marine Systems* 79 (1-2), pp. 1-22
- Anderson, L. G., E. P. Jones, and J. H. Swift (2003), Export production in the central Arctic Ocean evaluated from phosphate deficits, *J. Geophys. Res.*, 108(C6), 3199.
- Ardelan, M. V., O. Holm-Hansen, C. D. Hewes, C. S. Reiss, N. S. Silva, H. Dulaiova, E. Steinnes, and E. Sakshaug (2010), Natural iron enrichment around the Antarctic Peninsula in the Southern Ocean, *Biogeosciences*, 7(1), 11-25.
- Arrigo, K. R., G. van Dijken, and S. Pabi (2008), Impact of a shrinking Arctic ice cover on marine primary production, *Geophys. Res. Lett.*, 35(19), L19603.
- Boyle, E. A., B. A. Bergquist, R. A. Kayser, and N. Mahowald (2005), Iron, manganese, and lead at Hawaii Ocean Time-series station ALOHA: Temporal variability and an intermediate water hydrothermal plume, *Geochimica et Cosmochimica Acta*, 69(4), 933-952.
- Boyd, P. W., et al. (2000), A mesoscale phytoplankton bloom in the polar Southern Ocean stimulated by iron fertilization, *Nature*, 407, 695–702, 2000
- Bruland, K.W., N.M. Price, M.L. Wells (1995), Iron chemistry in seawater and its relationship to phytoplankton: a workshop report, *Marine Chemistry*, 48(1), 157-182
- Bucciarelli, E., S. Blain, and P. Tréguer (2001), Iron and manganese in the wake of the Kerguelen Islands (Southern Ocean), *Marine Chemistry*, 73(1), 21-36.
- Cai, P., M. Rutgers van der Loeff, I. Stimac, E. M. Nöthig, K. Lepore, and S. B. Moran (2010), Low export flux of particulate organic carbon in the central Arctic Ocean as revealed by ²³⁴Th:²³⁸U disequilibrium, *J. Geophys. Res.*, 115(C10), C10037.
- Campbell, J.A., Yeats, P.A., 1982. The Distribution of Manganese, Iron, Nickel, Copper and Cadmium in the Waters of Baffin-Bay and the Canadian Arctic Archipelago. *Oceanologica Acta* 5 (2), 161-168.
- Chever, F., E. Bucciarelli, G. Sarthou, S. Speich, M. Arhan, P. Penven, and A. Tagliabue (2010), Physical speciation of iron in the Atlantic sector of the Southern Ocean along a transect from the subtropical domain to the Weddell Sea Gyre, *J. Geophys. Res.*, 115, C10059, doi:10.1029/2009JC005880.
- Cowen, J.P, G.P. Massoth and R.A. Feely (1990), scavenging rates of dissolved manganese in a hydrothermal vent plume, *Deep Sea Research Part A. Oceanographic Research Papers*, 37 (10), 1619-1637. *scavenging rates of dissolved manganese in a hydrothermal vent plume, Deep Sea Research A.* 37(10),p.161
- Craig, H. (1974), A scavenging model for trace elements in the deep sea, *Earth and Planetary Science Letters*, 23(1), 149-159.
- Croot, P. L., and K. A. Hunter (1998), Trace metal distributions across the continental shelf near Otago Peninsula, New Zealand, *Marine Chemistry*, 62(3-4), 185-201.

- D'Asaro, E. A., and J. H. Morison (1992), Internal waves and mixing in the Arctic Ocean, *Deep Sea Research Part A: Oceanographic Research Papers*, 39(2, Part 1), S459-S484.
- De Baar, H.J.W., J.T.M. De Jong, D.C.E. Bakker, B.M. Löscher, C. Veth, U. Bathmann and V. Smetacek (1995), Importance of Iron for Phytoplankton Spring Blooms and CO₂ Draw-down in the Southern Ocean. *Nature*, 373: 412-415.
- De Baar, H.J.W., J.T.M. De Jong (2001), Distributions, sources and sinks of iron in seawater. In: Turner, D., Hunter, K.A. (Eds.), *Biogeochemistry of iron in seawater*, IUPAC Book series on analytical and physical chemistry of environmental systems, vol.7; 2001, pp.123-254 (Chapter 5).
- De Baar, H. J. W., et al. (2008), Titan: A new facility for ultraclean sampling of trace elements and isotopes in the deep oceans in the international Geotraces program, *Marine Chemistry*, 111(1-2), 4-21.
- De Jong J.T.M, den Das J., Bathmann U., Stoll M.H.C., Kattner G., Nolting R.F., de Baar H.J.W. Dissolved iron at subnanomolar levels in the Southern Ocean as determined by ship-board analysis. *Anal. Chim. Acta*. 1998; 377: 113-124.
- Edmonds, H. N., P. J. Michael, E. T. Baker, D. P. Connelly, J. E. Snow, C. H. Langmuir, H. J. B. Dick, R. Muhe, C. R. German, and D. W. Graham (2003), Discovery of abundant hydrothermal venting on the ultraslow-spreading Gakkel ridge in the Arctic Ocean, *Nature*, 421(6920), 252-256.
- Ekwurzel, B., P. Schlosser, R. A. Mortlock, R. G. Fairbanks, and J. H. Swift (2001), River runoff, sea ice meltwater, and Pacific water distribution and mean residence times in the Arctic Ocean, *J. Geophys. Res.*, 106(C5), 9075-9092.
- Elrod, V.A., W.H. Berelson, K.H. Coale, K.S. Johnson (2004), The flux of iron from continental shelf sediments: a missing source for global budgets. *Geophys. Res. Lett.*, 31, 12307.
- Fahl, K., and E.-M. Nöthig (2007), Lithogenic and biogenic particle fluxes on the Lomonosov Ridge (central Arctic Ocean) and their relevance for sediment accumulation: Vertical vs. lateral transport, *Deep Sea Research Part I: Oceanographic Research Papers*, 54(8), 1256-1272.
- Field, M.P. and R.M. Sherrell (1999), Dissolved and particulate Fe in a hydrothermal plume at 90°45'N, East Pacific Rise: Slow Fe(II) oxidation kinetics in Pacific plumes. *Anal. Cosmo. Acta*, 64 (4), pp. 619-628
- Gregg, W. W., M. E. Conkright, P. Ginoux, J. E. O'Reilly, and N. W. Casey (2003), Ocean primary production and climate: Global decadal changes, *Geophys. Res. Lett.*, 30(15), 1809.
- Hunter, K.A., D. Turner (Eds.) (2001), *Biogeochemistry of iron in seawater*, IUPAC Book series on analytical and physical chemistry of environmental systems, vol.7; 2001, pp.123-254.
- Johnson, K. S., R. M. Gordon, and K. H. Coale (1997), What controls dissolved iron concentrations in the world ocean?, *Marine Chemistry*, 57(3-4), 137-161.
- Johnson K.S., Boyle E., Bruland K., Measures C., Moffett J., Aquilarislas A., Barbeau K., Cai Y., Chase Z., Cullen J., Doi. T., Elrod V., Fitzwater S., Gordon M., King A., Laan P., Laglera-Baquero L., Landing W., Lohan M., Mendez J., Milne A., Obata H., Osslander L., Plant J., Sarthou G., Sedwick P., Smith G.J., Sohst B., Tanner S., van den Berg S., Wu J. (2007), Developing Standards for Dissolved Iron in Seawater. *Eos, Transactions Am. Geoph. Union* (88) 131-132
- Jones, E. P., B. Rudels, and L. G. Anderson (1995), Deep waters of the Arctic Ocean: origins and circulation, *Deep Sea Research Part I: Oceanographic Research Papers*, 42(5), 737-760.

- Klinkhammer, G. P., C. S. Chin, R. A. Keller, A. Dählmann, H. Sahling, G. Sarthou, S. Petersen, F. Smith, and C. Wilson (2001), Discovery of new hydrothermal vent sites in Bransfield Strait, Antarctica, *Earth and Planetary Science Letters*, 193(3-4), 395-407.
- Klunder, M.B., D. Bauch, P. Laan, H.J.W. De Baar, S. v. Heuven, S. Ober (2012), Dissolved iron in the Arctic shelf seas and surface waters of the Central Arctic Ocean: Impact of Arctic river water and ice-melt. *Journal of Geophysical Research: Oceans*, 117, C01027, doi:10.1029/2011JC007133
- Klunder, M. B., P. Laan, R. Middag, H. J. W. De Baar, and J. v. Ooijen (2011), Dissolved iron in the Southern Ocean (Atlantic sector), *Deep-Sea Research II*, 58 (25-26), 2678-2694, doi:10.1016/j.dsr2.2010.10.042.
- Laës, A., S. Blain, P. Laan, E. P. Achterberg, G. Sarthou, and H. J. W. de Baar (2003), Deep dissolved iron profiles in the eastern North Atlantic in relation to water masses, *Geophys. Res. Lett.*, 30(17), 1902.
- Laës, A., S. Blain, P. Laan, S. J. Ussher, E. P. Achterberg, P. Tréguer, and H. J. W. de Baar (2007), Sources and transport of dissolved iron and manganese along the continental margin of the Bay of Biscay, *Biogeosciences*, 4(2), 181-194.
- Lam, P. J., and J. K. B. Bishop (2008), The continental margin is a key source of iron to the HNLC North Pacific Ocean, *Geophys. Res. Lett.*, 35(7), L07608.
- Martin, J. H., and R. Michael Gordon (1988), Northeast Pacific iron distributions in relation to phytoplankton productivity, *Deep Sea Research Part A. Oceanographic Research Papers*, 35(2), 177-196.
- Middag, R., H. J. W. de Baar, P. Laan, and K. Bakker (2009), Dissolved aluminium and the silicon cycle in the Arctic Ocean, *Marine Chemistry*, 115(3-4), 176-195.
- Middag, R. (2010), *Dissolved Aluminium and Manganese in the Polar Oceans*, PhD-thesis, Rijksuniversiteit Groningen, The Netherlands.
- Middag, R., H.J.W. de Baar, P. Laan and M.B. Klunder (2011), Fluvial and hydrothermal input of Manganese into the Arctic Ocean. *Geochimica et Cosmochimica Acta* 75 (9), 2393-2408
- Moore, J. K., and O. Braucher (2008), Sedimentary and mineral dust sources of dissolved iron to the world ocean, *Biogeosciences*, 5(3), 631-656.
- Murray J.W, Chapter 4: The Oceans (1992). In: *Global Biogeochemical Cycles*, eds. Butcher S.S., Charlson, R.J., Orians, G.H., Wolfe, G.V., pp. 175-213.
- Nakayama, Y., Fujita, S., Kuma, K. & Shimada, K.(2011). Iron and humic-type fluorescent dissolved organic matter in the Chukchi Sea and Canada Basin of the western Arctic Ocean. *J. Geophys. Res.*, 116, 1-16
- Parekh, P., M. J. Follows, and E. Boyle (2004), Modeling the global ocean iron cycle, *Global Biogeochem. Cycles*, 18(1), GB1002.
- Parekh, P., M. J. Follows, and E. A. Boyle (2005), Decoupling of iron and phosphate in the global ocean, *Global Biogeochem. Cycles*, 19(2), GB2020.
- Rudels, B., R. D. Muench, J. Gunn, U. Schauer, and H. J. Friedrich (2000), Evolution of the Arctic Ocean boundary current north of the Siberian shelves, *Journal of Marine Systems*, 25(1), 77-99.
- Rudels, B. (2001), Arctic Basin Circulation, in *Encyclopedia of Ocean Sciences*, edited by H. S. John, pp. 177-187, Academic Press, Oxford.

- Rudels, B., G. Björk, J. Nilsson, P. Winsor, I. Lake, and C. Nohr (2005), The interaction between waters from the Arctic Ocean and the Nordic Seas north of Fram Strait and along the East Greenland Current: results from the Arctic Ocean-02 Oden expedition, *Journal of Marine Systems*, 55(1-2), 1-30.
- Sarthou, G., A. R. Baker, J. Kramer, P. Laan, A. Laës, S. Ussher, E. P. Achterberg, H. J. W. de Baar, K. R. Timmermans, and S. Blain (2007), Influence of atmospheric inputs on the iron distribution in the subtropical North-East Atlantic Ocean, *Marine Chemistry*, 104(3-4), 186-202.
- Schauer, U., R. D. Muench, B. Rudels, and L. Timokhov (1997), Impact of eastern Arctic shelf waters on the Nansen Basin intermediate layers, *J. Geophys. Res.*, 102(C2), 3371-3382.
- Schauer, U., Loeng, H., Rudels, B., Ozhigin, V.K., Dieck, W.: Atlantic water flow through the Barents and Kara Seas. *Deep-Sea Res. I*, 49, 2281-2298, 2002.
- Schlitzer, R. Ocean Data View, <https://awi-bremerhaven.de/GEO/ODV,2002>.
- Sunda, W. G., and S. A. Huntsman (1995), Iron uptake and growth limitation in oceanic and coastal phytoplankton, *Marine Chemistry*, 50(1-4), 189-206.
- Tagliabue, A., et al. (2010), Hydrothermal contribution to the oceanic dissolved iron inventory, *Nature Geosciences*, 3(4), 252-256.
- Tanhua, T., K. A. Olsson, and E. Jeansson (2005), Formation of Denmark Strait overflow water and its hydro-chemical composition, *Journal of Marine Systems*, 57(3-4), 264-288.
- Thuróczy, C.-E., L.J.A. Gerringa, M. Klunder, P. Laan, H.J.W. de Baar (2011), Distinct trends in the iron speciation between the shallow shelf seas and the deep basins of the Arctic Ocean. *J. Geophys. Res.*, 116, C10009, doi:10.1029/2010JC006835
- Weiss, R. F. (1977), Hydrothermal manganese in the deep sea: Scavenging residence time and Mn/3He relationships, *Earth and Planetary Science Letters*, 37(2), 257-262.
- Wu, J., and G. W. Luther (1995), Complexation of Fe(III) by natural organic ligands in the Northwest Atlantic Ocean by a competitive ligand equilibration method and a kinetic approach, *Marine Chemistry*, 50(1-4), 159-177.
- Wu, J., E. Boyle, W. Sunda, and L.-S. Wen (2001), Soluble and Colloidal Iron in the Oligotrophic North Atlantic and North Pacific, *Science*, 293(5531), 847-849.
- Wu, J., M.L., Wells, R. Rember (2011), Dissolved iron anomaly in the deep tropical-subtropical Pacific: Evidence for long-range transport of hydrothermal iron. *Geochimica et Cosmochimica Acta* 75 (2), 460 -468
- Yang, J. (2009), Seasonal and interannual variability of downwelling in the Beaufort Sea, *J. Geophys. Res.*, 114, C00A14, doi:10.1029/2008JC005084



Chapter 4

Dissolved iron in the Atlantic Sector of the Southern Ocean

This chapter is based on:

*Klunder, M.B, P.Laan, R. Middag, H.J.W. De Baar, J. v. Ooijen (2011). Dissolved Fe in
the Southern Ocean (Atlantic Sector),
Deep-Sea Research II, 58 (25-26), 2678-2694*

Abstract

We report a comprehensive dataset of dissolved iron (Fe) comprising 482 values at 22 complete vertical profiles along a 1° latitudinal section at the Zero meridian. In addition a shorter high resolution (~00°09') surface section of the southernmost part of the transect (66°00'–69°35'S) is presented. Within the upper surface mixed layer the concentrations of dissolved Fe vary between 0.1 nM and 0.3 nM. An inverse trend versus fluorescence suggests significant Fe removal by plankton blooms. Vertical mixing and upwelling are the most important supply mechanisms of iron from below to the upper surface mixed layer. At lower latitude (42°S) there is a distinct maximum of 0.6–0.7 nM in the 2000–3000m depth range due to inflow of North Atlantic Deep Water. In one region (55°S) elevated dissolved Fe in the surface mixed layer is ascribed to recent deposition of aeolian dust originating from South America. Close to the Antarctic continent there is an indication of Fe supply in surface waters from icebergs. In the deep waters there is a strong indication of a hydrothermal plume of dissolved Fe and Mn over the ridge in the Bouvet region (52–56°S). In the Weddell Gyre basin the dissolved Fe in the deep water is 0.47 ± 0.16 nM in the eastward flow at ~56–62°S, and lower 0.34 ± 0.14 nM in the westward flow at high ~62–69°S latitude. At the edge of the continental ice-sheet on the prime meridian, the continental margin of the Antarctic continent appears to be less a source of dissolved Fe than everywhere else in the world, likely because it is unique in being overlain by the extending continental ice-sheet which largely prevents biogeochemical cycling.

4.1 Introduction

Dissolved Fe has been recognized as a key element for phytoplankton growth in the world oceans [Coale *et al.*, 1996]. It is needed for important biological processes such as photosynthesis and is used in several enzymes [Sunda, 2001]. Although Fe is the fourth most abundant element in the earth crust, it is only available in trace concentrations (generally <1 nM) in the oxygenated water of the world oceans [De Baar and De Jong, 2001]. In the Southern Ocean, the presence of ample major nutrients (N,P,Si) yet low phytoplankton abundance has been hypothesized to be due to lack of this essential trace nutrient [Gran, 1931; Hart, 1934, 1942; Martin, 1998] in combination with low light conditions [Sunda and Huntsman, 1997]. This was first confirmed in bottle incubations by De Baar *et al.* [1990] and Buma *et al.* [1991], and since then by others see review by De Baar and Boyd [2000]. During *in situ* Fe fertilization experiments the effect of extra Fe was shown repeatedly, however the light limitation effect of deep Surface Mixed Layers due to high wind velocity also plays a key role (see reviews by De Baar *et al.*, 2005 and Boyd *et al.*, 2007). More recently natural Fe fertilization was reported over shallow plateau regions around subantarctic islands [Blain *et al.*, 2007; Pollard *et al.*, 2009].

Due to the low concentration of dissolved Fe in open ocean waters, the sampling, filtration and analysis are very sensitive to contamination. As a result the world ocean dataset of dissolved Fe in the published literature is quite small both in number of data points and in geographical and vertical distribution, notably in the Southern Ocean.

Recently, more ocean datasets of dissolved Fe have become available in the Southern Ocean [Sedwick *et al.*, 1997;2008; Sohrin *et al.*, 2000; Boye *et al.*, 2001; Measures and Vink, 2001; Croot *et al.*, 2004; Nishioka *et al.*, 2005; Planquette *et al.*, 2007; Blain *et al.*, 2008a; Lai *et al.*, 2008], and elsewhere [Bell *et al.*, 2002; Laës *et al.*, 2003;2007; Sarthou *et al.*, 2003; Boyle *et al.*, 2005; Measures *et al.*, 2008]. Also more recent world ocean data compilations have been made [Gregg *et al.*, 2003; Parekh *et al.*, 2004; Moore and Braucher, 2008] and include Fe values in the Southern Ocean. Nevertheless, determining the concentration and basin wide gradients of dissolved iron in the deep ocean basins remains a challenge in oceanography, mainly in the (less studied) deep Southern Ocean.

Towards addressing this issue, two new developments allowed major progress in sampling trace metals over the recent years. Firstly, a new ultra clean sampling system has been developed and successfully tested [De Baar *et al.*, 2008] (see text section 4.2), allowing faster and more reliable clean sampling at higher resolution of notably the deep waters. Secondly, international exercises [Bowie *et al.*, 2003; Bowie *et al.*, 2006; Johnson *et al.*, 2007] have eventually led to the availability of certified reference samples of dissolved Fe in seawater.

Several sources of dissolved Fe to the Southern Ocean can be envisioned. The Fe in surface waters may come from above by dust input originating from adjacent continental source regions, notably Patagonia (South-America), South Africa and Australia [Jickells and Spokes, 2001; Sedwick *et al.*, 2008]. Alternatively Fe may come from below by upwelling and upward mixing of deeper waters containing higher dissolved Fe than the surface waters [Löscher *et al.* 1997; Croot *et al.*, 2004; Lai *et al.*, 2008]. Obviously the deep waters would in turn need a source as well, where reductive dissolution within sub-oxic marine sediments and remineralization of particles are known sources of Fe [De Baar and De Jong, 2001] and Mn [Froelich *et al.*, 1979]. Hydrothermal vents at active mid-ocean ridges are another known source of dissolved Fe and Mn [Klinkhammer *et al.*, 2001]. Parallel determination of dissolved Mn [Middag *et al.*, 2012] may provide clues to these source terms. Finally in the polar oceans, meltwater from the continental Antarctic ice sheet continuously flows into the sea where some of its Fe contents may become dissolved. Moreover, icebergs broken off from the ice-sheet often become temporarily grounded on the shelf and entrain dirt hence Fe from the shelf sediments [Löscher *et al.*, 1997]. Finally, the seasonal sea-ice also comprises some Fe [Lannuzel *et al.*, 2008] which upon melting may contribute to the Fe content of the surface waters.

Here we present the distribution of dissolved Fe in a high resolution (1°latitude) transect (Fig. 4.1) over the complete 4-5 km depth of the water column, overall

482 dissolved Fe values at 22 stations with 20-24 sample depths. This section is designed across the Antarctic Circumpolar Current (ACC) as to be representative of the ACC flowing all around Antarctica. Moreover the southernmost part of the section represents the eastern extent of Weddell Gyre. Within the Weddell Gyre, an additional small set of 24 samples for dissolved Fe was collected in the very surface waters from 66°02.18'S-69°35.15'S by deployment of a towed fish to obtain high (~00°09') resolution surface water concentrations. This sampling scheme allowed us to accurately determine the distribution of dissolved iron, and establish its sources in the Atlantic sector of the Southern Ocean.

4.2 Materials and Methods

4.2.1 Sampling

4.2.1.1 Vertical profile sampling

Seawater samples were collected during the ANT XXIV/3 expedition of the RV Polarstern (Capetown to Punta Arenas: 10 February until 14 April 2008) on its first transect from Cape Town to the Antarctic ice-sheet of Antarctica (Fig. 4.1). Here, in total 22 stations were sampled for analyses of dissolved Fe and other trace metals (see section 4.2.7). On the prime meridian transect, the resolution is typically 1°, except for a station at 66°30.06'S instead of ~66° S and the southernmost station at 69°24.03'S close to the approximately 200 m thick ice-sheet extending beyond the Antarctic continent over the shelf seas.

All bottles used for storage of reagents and samples were cleaned according to an intensive three step cleaning protocol extensively described by *Middag et al.* [2009]. Samples were taken using 24 internally teflon-coated PVC 12 liter GO-FLO Samplers (General Oceanics Inc.) mounted on a Titanium frame which was connected to a Kevlar hydrowire with internal signal cables for data transfer and control from the ship. Directly upon recovery the complete frame with samplers was placed inside a class 100 clean container [De Baar et al., 2008]. Seawater was filtered in line over

Fig. 4.1 Research area with station positions. Presented are all stations sampled for trace metals during the ZERO meridian transect of ANT XXIV/3, including station numbers for sampling with the ultraclean Titanium frame. Not shown are other stations in between (i.e. the missing numbers) where additional data of major nutrients and other variables was collected with a regular CTD/Rosette. Also, the ~66-69.30°S region where the towed fish is deployed for Surface Water Sampling is shown. Depth isolines are shown as well as fronts (normal, black), zones (italic, red) and major currents (arrows). Abbreviations in alphabetical order: AAZ: Antarctic Zone; ACCn: Antarctic Circumpolar Current northern branch; ACCs, Antarctic Circumpolar Current southern branch; ACoC: Antarctic Coastal Current; PF: Polar Front; PFZ: Polar Front Zone; SAF: Subantarctic Front; SAZ: Subantarctic Zone; SB-ACC: Southern Boundary of the ACC; STF: SubTropical Front (dotted line, its position not sampled nor defined in our cruise); WG: Weddell Gyre. The inset shows the sampling transect (red) in a regional context, also the Weddell Gyre is indicated. This figure is made using Ocean Data View (Schlitzer, 2009).

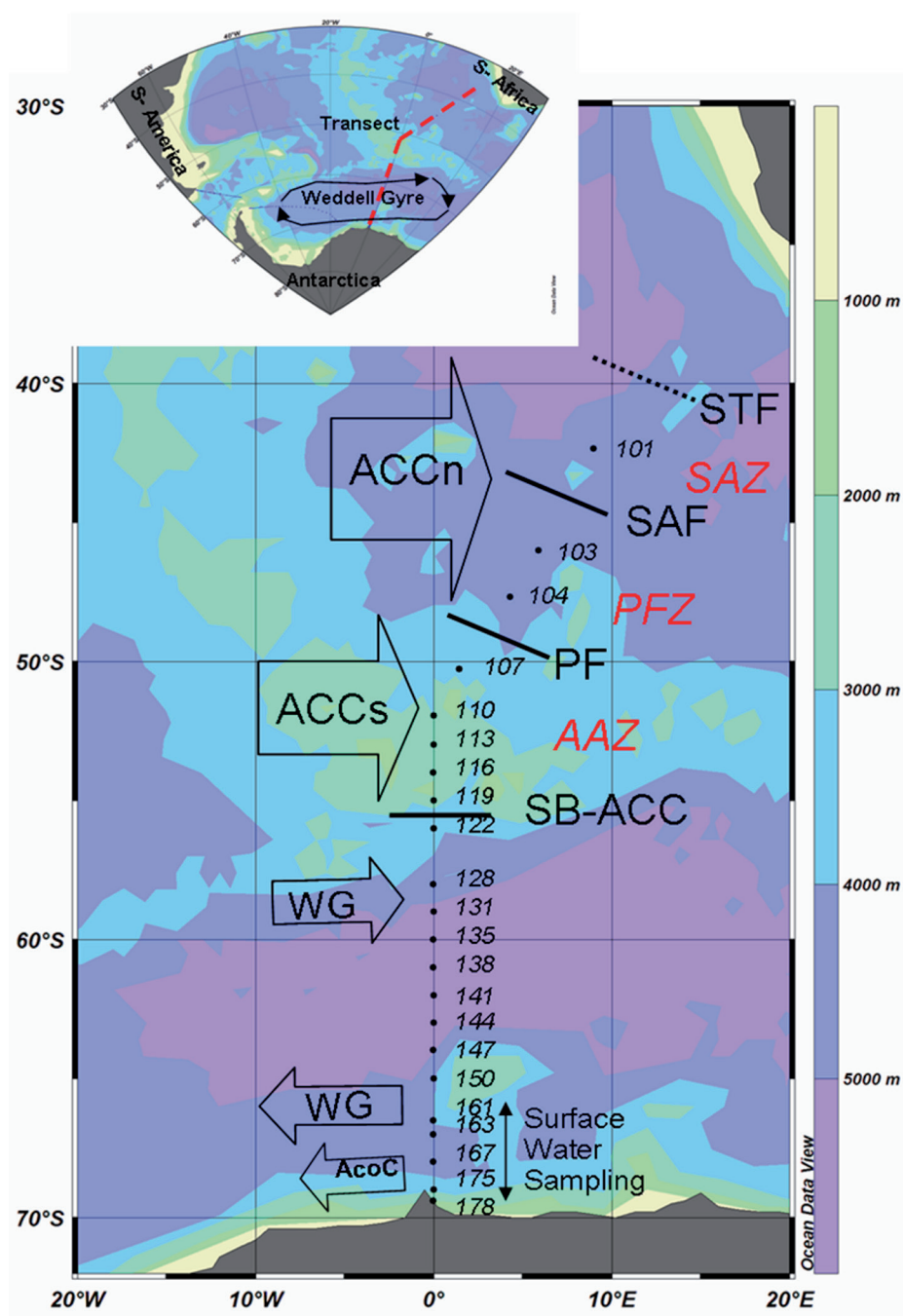


Figure 4.1

a 0.2 μm filter cartridge (Sartrobran-300, Sartorius) under 1.5 bar nitrogen pressure. Before seawater collection, the first 0.5 l. of seawater was filtered and disposed for rinsing purposes. Two (one for measuring, one for back-up) LDPE sample containers (NALGENE, 60 ml) were filled from each GO-FLO sampler for analyses of dissolved Fe.

4.2.1.2 Surface water sampling

In the Weddell Gyre, close to the Antarctic continent 24 additional samples were collected along the southernmost part of the transect ($66^{\circ}02.18'S$ - $69^{\circ}35.15'S$) using a towed epoxy-coated stainless steel torpedo deployed off a crane arm on the starboard side of the ship, after De Jong et al. (1998). In between vertical sampling stations, every hour a seawater sample was collected, and analyzed as described in section 4.2.5. Due to differences in ship speed this resulted in a slightly unequal resolution of $00^{\circ}09'$ on average.

4.2.2 Analysis of Fe

4.2.2.1 Chemicals

A solution of 0.4 M hydrochloric acid was made by diluting 30% concentrated HCl (Merck, suprapur, 10M), 0.35 M H_2O_2 solution by dilution of 30% H_2O_2 (Merck, suprapur) and the 0.96 M NH_4 solution was made from 25% NH_4OH (Merck, suprapur). Luminol stock solution was prepared by dissolving 270 mg luminol (3-aminophthalhydrazide, Aldrich) and 500 mg potassium hydroxide in 15 ml Milli-Q (MQ) water (MQ water is defined as ultrapure water with resistance $\geq 18.2 \text{ M}\Omega$). To prepare the final reagent used in this system 3 ml of luminol stock solution and 60 μl triethylenetetramine (TETA) (Merck) was diluted in 1 l of MQ. The 0.12 M ammonium acetate buffer (pH = 6.5) was made by diluting a 2.0 M buffer solution. This 2.0 M buffer solution was obtained by tenfold dilution of a saturated solution of ammonium acetate crystals after Aguilar-Islas et al. (2006).

4.2.2.2 Method

The shipboard analysis method used is by Flow Injection - Chemiluminescence method with preconcentration on iminodiacetic acid (IDA) resin as described by De Baar et al. [2008], with some minor modifications. One modification is the initial acidification of the samples; here the samples were acidified to pH = 1.8 by adding 120 μl per 60 ml sample (2‰) of ultraclean HCl (12M) (Seastar Baseline[®]Hydrochloric Acid, Seastar Chemicals) and left for at least 12 hours before analyzing.

The method detects Fe (III). Here, we ensured all the Fe was in the Fe (III) form, by adding 60 μl of a 1 ‰ hydrogen peroxide (Merck suprapur 30%) solution at least one hour before measuring as recommended by Johnson et al. [2007].

All samples of one station were measured within one run, from surface to deep and each sample analyzed in triplicate as follows. Each sample was buffered in-line to pH = 4.0 by mixing with a 0.12 M acetate buffer (pH = 6.5). After buffering,

the sample passed over a chelating iminodiacetic acid (IDA, Toyopearl, AFChelate 650 M)) column during 120 seconds. The column was rinsed by flow-through of MQ for 1 minute before the Fe was eluted with 0.4 M HCl (Merck suprapur). A four port selection valve (VICI, Switzerland) was used for switching between buffer/sample and MQ passing over the IDA- preconcentration column.

The eluent was mixed with the 0.96 M ammonia, 0.35 M hydrogen peroxide and the luminol solution. The mixture passed through a 5 meter length mixing coil in a constant 35°C water bath, before injection in a Hamamatsu (HC 135) photon counter. This injection step took 180 seconds.

A six port injection valve (VICI, Switzerland) was used to switch between inflow of sample and rinsing MQ over the column and elution by HCl. The autosampler valve, both switching valves and the detector were controlled by an interface developed in LabView™.

The system was calibrated for every run using standard additions (0.1-1.5 nM range) of an 895.5 nM Fe stock solution to filtered seawater obtained from the subsurface minimum, with lowest Fe concentrations. This calibration seawater was taken for each station at the depth of the chlorophyll maximum. Concentrations varied between 0.05 nM (station 163) and 0.25 nM (station 138). The stock solution was obtained by dilution of a 1000 ppm ICP-MS standard (Fluka Chemicals)

4.2.3 Blank, limit of detection and validation

Regularly the combined blank of the 1 minute MQ-column wash and the 0.4 M HCl for elution of the column was calculated from the amount of counts measured upon zero (0) seconds loading time. The average value for this blank was 32 ± 14 pM Fe ($n=19$) and this blank did not exceed 60 pM. By double versus single addition of the H_2O_2 it was found that this did not cause a blank. The contribution of the Seastar Baseline®Hydrochloric Acid is deemed negligible (<0.04 pM per sample).

The detection limit was determined regularly and defined as the standard deviation of 5 peaks of 10 seconds loading of low-Fe seawater (subsurface minimum), multiplied by 3. Average detection limit was typically 5.7 ± 2.9 pM Fe ($n=4$), and the detection limit did not exceed 8.5 pM Fe.

In order to validate the accuracy of the system, standard reference seawater was measured regularly, also in triplicate. This water was obtained during the preceding SAFe-cruise in 2004 and has since then proven to be of great value for validation of on-board Fe measurements (*Johnson et al.*, 2007). There is SAFe surface (S) water and SAFe deep (D2) water available to validate against different ranges of Fe concentration. The average value of the SAFe S waters we found was 0.13 ± 0.021 nM Fe ($n=11$) for our analysis, compared to the community consensus value of 0.097 ± 0.43 nM. However, a small difference between different SAFe S bottles appears to influence the results. Concentrations of 0.16 ± 0.01 nM Fe ($n=3$) for bottle S-391

and 0.172 nM for bottle S-135 (n=1) elevate our results for SAFe S calibration water. When excluding latter bottles S-391 and S-135 the average value of SAFe-S waters we found was 0.11 ± 0.012 (n=7). For the SAFe deep (D2) inter calibration waters we found an average value of 0.96 ± 0.06 nM Fe (n=10), consistent with the community consensus value of 0.91 ± 0.17 nM (*Johnson et al.*, 2007).

4.2.4 Other parameters

Samples for dissolved manganese (Mn) and aluminium (Al) and Zinc (Zn) were taken from the same Titan system, and results reported by *Middag et al.* (2011a,b) and *Croot et al.* [2011] respectively. Also major nutrients (silicate, nitrate and phosphate) were measured from samples from the Titan system, as well as at in-between stations from a standard CTD/Rosette system. Salinity (conductivity), temperature and pressure (depth) were measured using the CTD system (Seabird SBE 911+) mounted in the titanium frame. This CTD-system also included a Chelsea MK-III fluorometer, for measurements of fluorescence (arbitrary units). Another CTD/Rosette with regular samplers was deployed at in-between stations and did provide vertical light transmissometry records indicative of abundance of suspended particles.

The meteorological parameters, including precipitation, were measured regularly by the shipboard staff of the German Meteorological Service. Underway salinity and temperature were measured every ten seconds at a depth of 5 meter by an instrument operated by the company FIELAX. Synoptic sea-ice and ice-berg data were registered on board by dedicated ice-watch person on the bridge.

4.2.5 Database

The complete database of dissolved Fe is available as a separate chapter within this thesis. The complete relational database will be available at the international GEO-TRACES datacentre (<http://www.bodc.ac.uk/geotraces/>).

4.3 Hydrography

The hydrography of this region is extensively described [Klatt *et al.*, 2005; Gladyshev *et al.*, 2008] Here we give a short overview of the hydrography. The Southern Ocean is defined as all waters south of the Polar Front (the surface expression of the 2°C isotherm generally positioned at about 50°S), and the subantarctic zone between the Polar Front (~50°S) and the subantarctic Front typically situated at about 45°S.

As indicated on Fig. 5.1, we passed several fronts in the Southwards direction. The northern part of the transect lies within the SubAntarctic Zone, crossing the Meteor Ridge. Further South we crossed the region where three major ocean ridges meet at a latitude of about 52°S to 56°S; the region where the southernmost segment of the Mid-Atlantic Ridge, the westernmost segment of the Southwest Indian Ridge and the easternmost segment of the American-Antarctic Ridge meet. This so called Bouvet region separates the South Atlantic Basin and the Weddell Basin, to the south. This transect crossed this Weddell Basin towards the Antarctic continent.

Using the physical parameters obtained during the cruise and definitions as described by Orsi *et al.* [1995] and Klatt *et al.* [2005] one can discriminate the different water masses of the transect. In the north part of the transect, Subantarctic Surface Water (SSW) was recognized as far south as 50°S. Here it reached the Polar Front where it meets the Antarctic Surface Water (AASW). Below, Antarctic Intermediate Water (AAIW) flowed downward and northwards until ~1250 meter depth. Within the ACC, Upper Circumpolar Deep Water (UCDW) with slightly higher temperatures was found below the AAIW. Further North, there is the core of southwards flowing North Atlantic Deep Water (NADW) overlying the northwards flowing Antarctic Bottom Water (AABW). Progressing southwards, the characteristics of this NADW intrusion (high salinity, low temperature) were found relatively shallower in the water column and became less pronounced due to mixing with surrounding less saline water of Antarctic origin, mainly LCDW. The lower part of the LCDW is influenced by northwards flowing Weddell Sea Deep Water (WSDW). Southward of the Bouvet region, in the Weddell Basin, different water masses were found. Below the AASW, the Winter Water (WW) is the even colder water layer that shows as a temperature minimum at the bottom of the AASW. The WW is a remnant from the last winter before the overlying water was warmed by the summer. Below the WW, a relatively stable layer of WDW (Warm Deep Water) is observed until about 1000-1500 meter depth. Downwards, there was a layer of Weddell Sea Deep Water WSDW. Below that, Weddell Sea Bottom Water (WSBW), defined as water with a potential temperature lower than -0.7°C, was recognized. This was mainly found at depths below 4000 meter.

4.4 Results

4.4.1 Hydrography and major nutrients

The hydrography with major fronts, zones and currents (as described in the online electronic supplement) is summarized in Fig. 4.1. Along the complete vertical section the different water masses and the depth of the Surface Mixed Layer are shown in Fig. 4.2. Throughout the section the distinct surface layer with uniform potential density represents the Surface Mixed Layer (SML). The depth of this Surface Mixed Layer (Table 4.1) varied between 28 and 124 meter and was typically ~100 meter deep from station 101 (~42°20'S) to station 128 (~58°S), and 25-50 meter deep from station 131-175 (~59° – 69°S). On average the SML depth was ~65 meter.

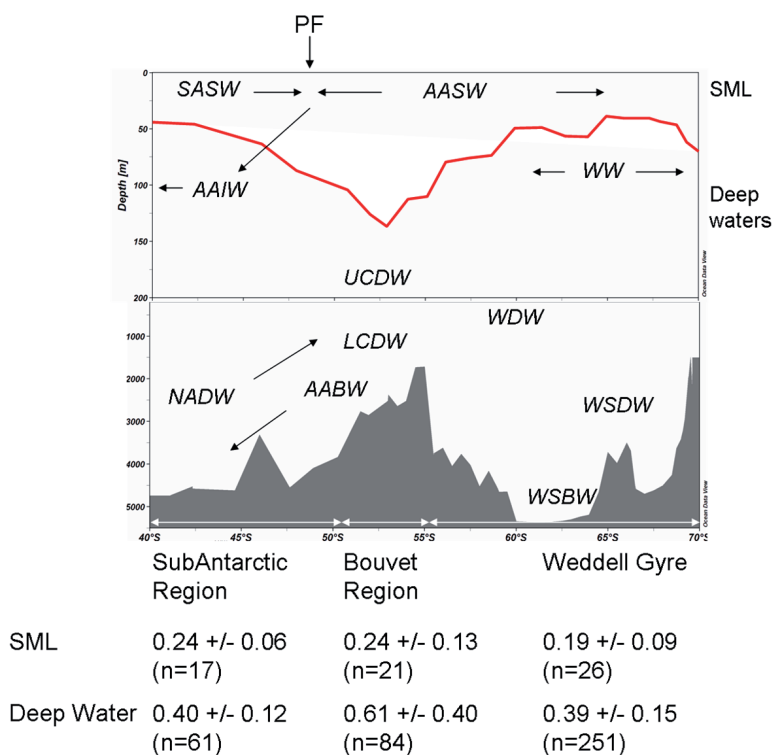


Fig. 4.2 Schematic overview of the transect with above the upper 200 meters and below the 200-5500 m depth range. The red line indicates the depth of the Surface Mixed Layer (SML). Water masses as further described in the online supplement are as follows: SASW: SubAntarctic Surface Water; AASW: Antarctic Surface Water; WW: Winter Water; AAIW: Antarctic Intermediate Water; UCDW: Upper Circumpolar Deep Water; NADW: North Atlantic Deep Water; LCDW: Lower Circumpolar Deep Water; WDW: Warm Deep Water; AABW: Antarctic Bottom Water; WSDW: Weddell Sea Deep Water; WSBW: Weddell Sea Bottom Water. Below the graph the average Fe concentration (average, standard deviation, n) is reported for both the SML and the Deep Water in the three distinct regions of the transect. This figure is made using Ocean Data View (Schlitzer, 2009).

Table 4.1 Mixed layer depths, SML average values for Fe and fluorescence and 25 meter average values for Fe and Al.

Station	Latitude (°S)	SML depth (m)	DFe (nM)	Fluorescence	DFe (nM)	Al (nM)
PS 71-			Surface Mixed Layer average		Upper 25 m average	
101	42.34	46	0.28	0.41	0.30	0.85
103	46.00	65	0.22	0.65	0.26	1.33
104	47.66	80	0.19	0.42	0.17	0.62
107	50.27	95	0.21	0.29	0.18	0.62
110	51.95	124	0.11	0.32	0.18	0.61
113	53.00	133	0.18	0.31	0.15	0.56
116	54.00	102	0.29	0.14	0.33	1.14
119	55.00	95	0.33	0.10	0.47	1.78
122	56.00	77	0.34	0.14	0.41	0.75
128	58.00	73	0.18	0.23	0.18	0.53
131	59.00	67	0.13	0.11	0.17	0.61
135	60.01	40	0.24	0.16	0.27	0.35
138	61.00	42	0.25	0.19	0.25	0.32
141	62.00	47	0.27	0.31	0.27	0.52
144	63.00	47	0.23	0.30	0.23	0.82
147	63.97	28	0.32	0.26	0.32	1.46
150	65.00	33	0.16	0.70	0.16	0.57
161	66.50	32	0.23	0.63	0.23	1.40
163	67.00	39	0.15	1.16	0.15	0.36
167	68.00	42	0.10	1.29	0.08	0.35
175	69.00	45	0.13	1.68	0.13	0.20
178	69.40	67	0.32	1.60	0.34	0.64

The distributions of nitrate and silicate along the section are displayed in Fig. 4.3. The distribution of phosphate is similar to that of nitrate (here not shown, see the online electronic supplement with the related manuscript [Klunder *et al.*, 2011, *DSR Part II*]).

In the surface waters of the Subantarctic Zone at the northernmost station 101 (Fig. 4.4) there is ample nitrate at ~15 μM . Going further southward the nitrate in surface waters further increases (Fig. 4.3) to about 26 μM (Fig. 4.4 stations 113, 167) which is the typical summer value in the Southern Ocean, due to seasonal depletion by biological uptake with about 6 μM versus the winter water at typical 32 μM . The trends for phosphate (not shown) are similar as for nitrate, increasing from

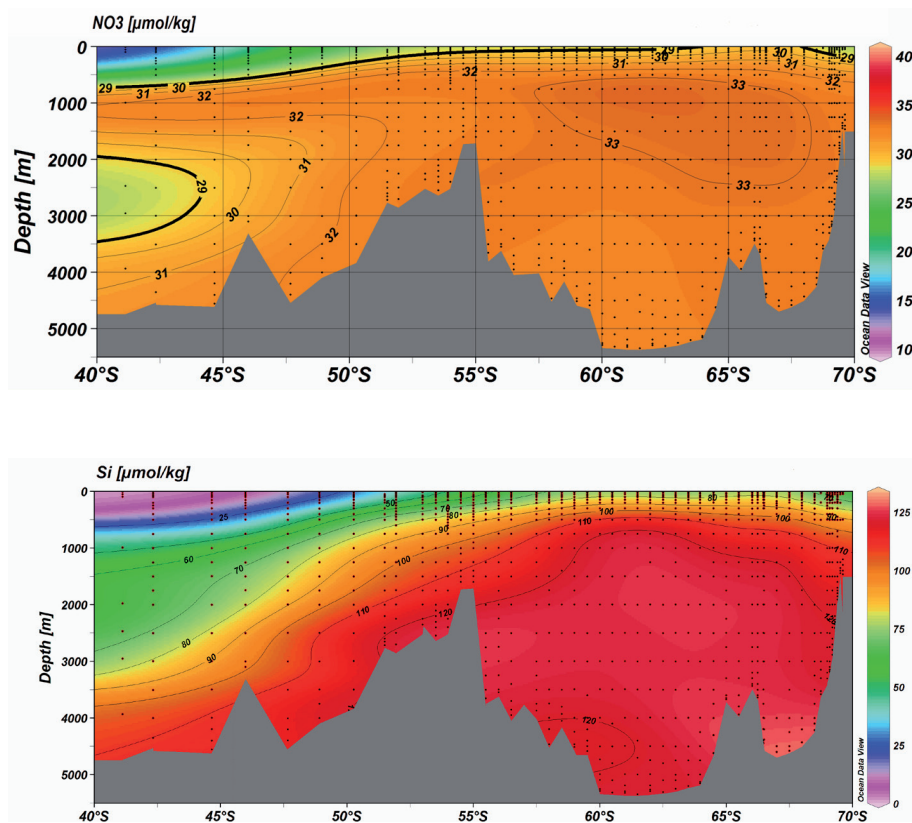


Fig. 4.3 Color and contour plots of the concentration [$\mu\text{mol/kg}$] of nitrate (upper graph) and silicate of the transect. Due to extra hydrocasts with regular CTD/Rosette there are more individual data-points (dots) than in the below Fig. 5 for dissolved Fe. This figure is made using Ocean Data View (Schlitzer, 2009).

1.04 μM (St. 101) to the typical summer value of about 1.7 μM (St. 113, 167). Thus at all stations phosphate and nitrate conditions were non-limiting for phytoplankton growth. The silicate is depleted at 0.5 μM at St. 101 (Fig. 4.4a), then slowly increases southward (Fig. 4.3) to 0.9 μM (St. 103), 1.9 μM (St. 104), thus less than the common 1 μM criterion for conceivable limitation of large diatoms. Across the Polar Front the silicate shows the well-known steep rise to the maximum surface value of 68 μM (St. 130, not shown) and then slightly decreases again to 51 μM (not shown) at southernmost station 178 near the continental ice-sheet. These surface waters show low summer values of silicate and nitrate coinciding with temperature stratification (Fig. 4.4, see insert graphs of St. 113 and St. 167). An improved more stable light climate due to summer stratification has most likely favored diatom growth [De Baar *et al.*, 2005] in the preceding months before our sampling, however there still is ample nitrate and silicate available. Here the combination of limitation by light with Fe deficiency is

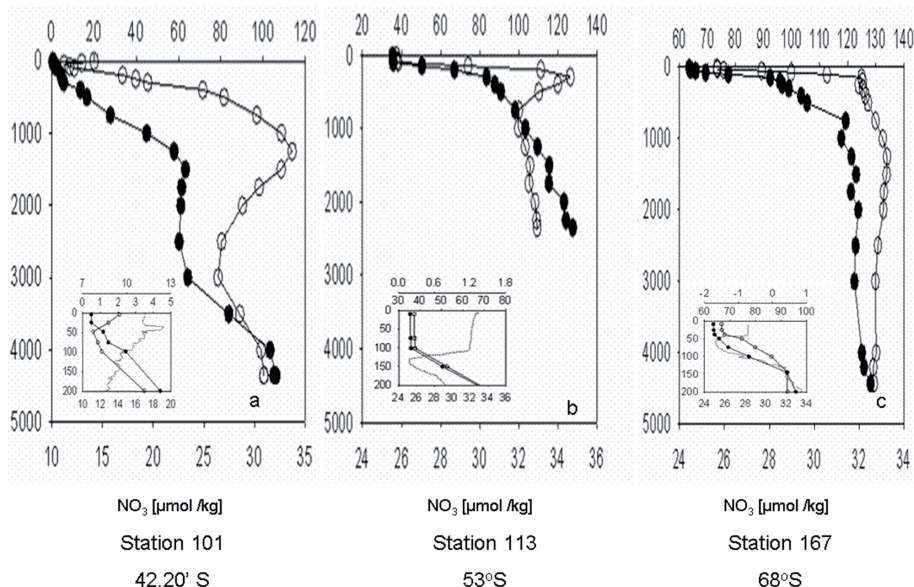


Fig. 4.4 Depth profiles of silicate (full circle) and nitrate (empty circle) of station 101 (a), station 113 (b) and station 167 (c) as indicative of three distinct regions (see text). Inserts in each graph show upper 200 meters at expanded scales of silicate and nitrate (horizontal; μM) and depth (vertical), as well as potential temperature (dotted line) with additional scales (ranging from 7 to 13 $^{\circ}\text{C}$, 0–1.8 $^{\circ}\text{C}$; and –2 to 1 $^{\circ}\text{C}$) along horizontal axis.

deemed limiting for phytoplankton growth [DeBaar *et al.*, 1990; 1995; 2005].

In the deep waters the more saline NADW coming from the north and rising southwards is easily recognized by the relatively low nitrate in the 2000–3000m depth range as marked by the black contour drafted at 29 μM (Fig. 4.3). This nitrate minimum is also visible in the vertical profiles of nitrate at St. 101 (Fig. 4.4a) where in the same 2000–3000m depth interval the silicate is uniform (and actually shows a slight minimum), as opposed to its typical steady increase with depth (St. 113) elsewhere along the section and in the world oceans.

4.4.2 General Distribution of Dissolved Fe throughout the Water Column

Along the complete section (Fig. 4.5) the dissolved Fe is depleted in the surface waters (upper graph) in two regions at 46–52 $^{\circ}\text{S}$ and 66–69 $^{\circ}\text{S}$, respectively. In between there is the station 119 at 55 $^{\circ}\text{S}$ with elevated Fe in surface waters attributed to a recent aeolian dust input (see below text section 4.4.1.1.2.).

The deep waters (Fig. 4.5, lower graph) clearly show the elevated dissolved Fe in the NADW, where the Fe = 0.55 nM contour (bold black line) more or less overlaps with the $\text{NO}_3 = 29 \mu\text{M}$ contour (bold black line, Fig. 4.3). More southwards there

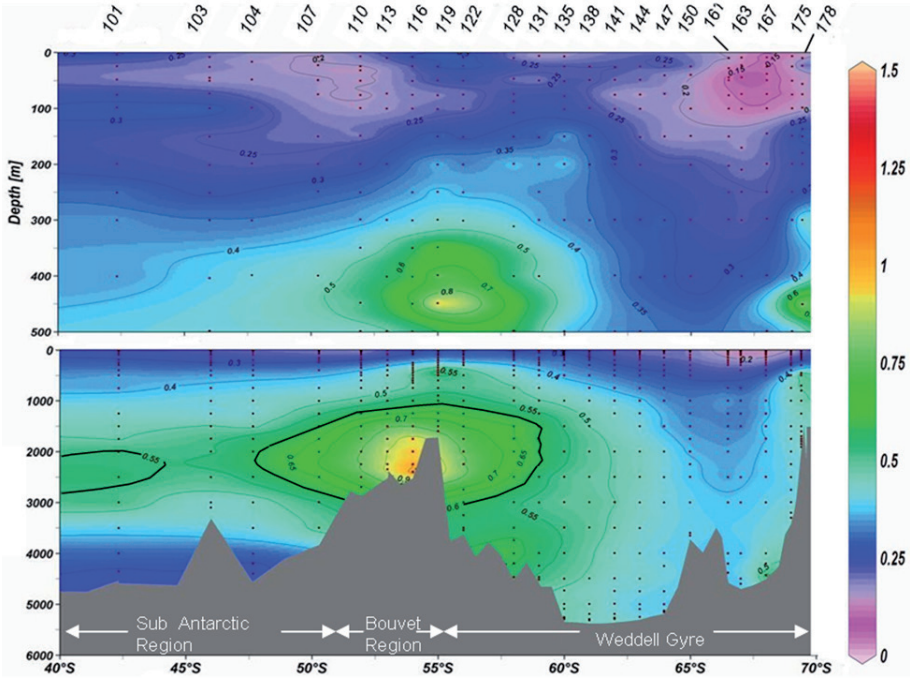


Fig. 4.5 Color and contour plot of the concentration of dissolved Fe [nM] of the transect in the upper 500 meter (upper graph) at expanded vertical depth scale, and over the complete ~5000 m depth (lower graph). Dots indicate Fe datapoints, trace metal station numbers are indicated. This figure is made using Ocean Data View (Schlitzer, 2009).

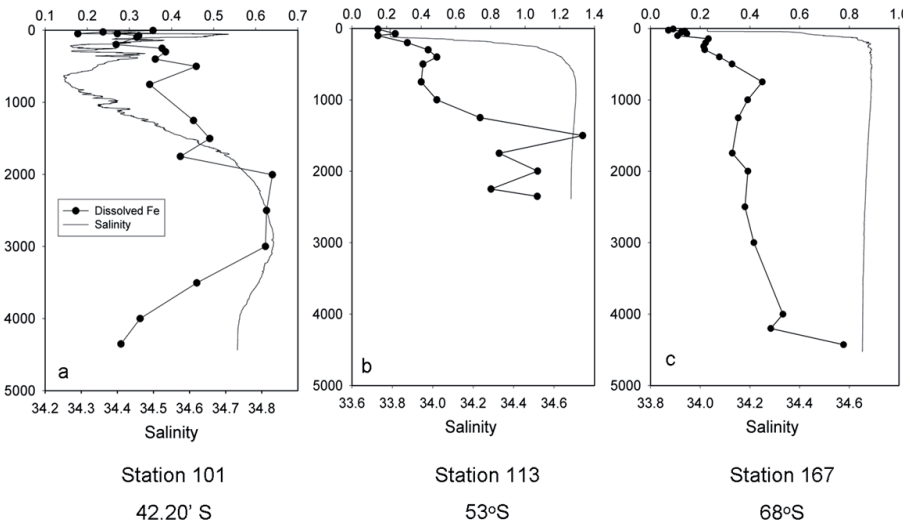


Fig. 4.6 Depth profiles of dissolved Fe (filled dots) and salinity (thin line) of station 101 (a), station 113 (b) and station 167 (c) as indicative of three distinct regions (see text).

is a strong Fe maximum over the Bouvet region attributed to hydrothermal input (see below text sections 4.3.4.2 and 4.4.2.1.2) where the Fe = 0.6 nM contour (bold black line) nicely overlaps with a similar Mn = 0.3 nM contour also delineating the hydrothermal plume (*Middag et al.*, 2011a). In contrast in the further southward Weddell Gyre the dissolved Fe becomes extremely low, with values decreasing from the eastward flowing branch (~60°S) to the westward flow (~66°S).

For the three distinct regions vertical profiles of dissolved Fe are shown in Fig. 4.6. All vertical profiles (Fig. 4.6) show a slight elevation in the surface (less clear at station 167), a subsurface minimum, and then low, slightly varying but increasing concentrations (<0.45 nM in the SubAntarctic region and Weddell Gyre, maximum 0.68 nM at 1000 m above the Bouvet region) until around 750-1000 meter depth. In the SubAntarctic region, higher concentrations of ~0.5 nM to 0.6 nM occurred from 2000-3000 meter, below which concentrations decreased until >0.4 nM (St. 101, Fig. 4.6a). The stations over the ridge crest in the Bouvet region showed a different vertical profile, with deep values > 1 nM from 1200 m downwards and a maximum of 2.2 nM at 1750 meter depth (St. 116). In the Weddell Gyre the Fe concentrations were relatively constant at about 0.5 nM until the bottom (Fig. 4.6c, St. 167).

For the three regions, the average dissolved Fe in the Surface Mixed Layer was 0.25 nM and 0.24 nM in the subAntarctic region and Bouvet region, respectively (Fig. 4.2), but significantly lower at 0.20 nM in the remote Weddell Gyre region, most notably in the westward flow at 66-69°S (Fig. 4.5, upper graph). In the deep waters the average dissolved Fe was significantly higher at 0.60 nM over the Bouvet region (Fig. 4.2) due to hydrothermal input as compared to 0.41 nM and 0.42 nM in the adjacent deep subAntarctic and deep Weddell Gyre regions, respectively.

4.4.3 Fe in the surface waters

4.4.3.1 Fe in the upper surface mixed layer

The surface waters were sampled in February and therefore represent the end of austral summer conditions. The upper surface concentration was measured at 10-25 meter and was generally below 0.3 nM, except for the stations 116 and 119 (54 and 55°S), where Fe concentrations were >0.4 nM.

The depth profiles of the Fe concentration showed a subsurface minimum at depths varying from 25 to 200 meters. A significant decrease of this subsurface minimum was found from station 138 (61°S) (0.25 +/- 0.01 nM) to station 175 (69°S) (0.05 +/- 0.001 nM), with the strongest decline from station 161 (66°30'S) (0.16 +/- 0.008 nM) southwards. Moreover the depth of the subsurface minimum followed the latitude: deeper minima were found at the higher latitudes.

4.4.3.2 Underway Sampling of the Southernmost Surface Waters

The samples with the towed torpedo were taken from the very upper water column (2-3 meter depth), thus represent the upper surface waters. Fig. 4.7 shows the con-

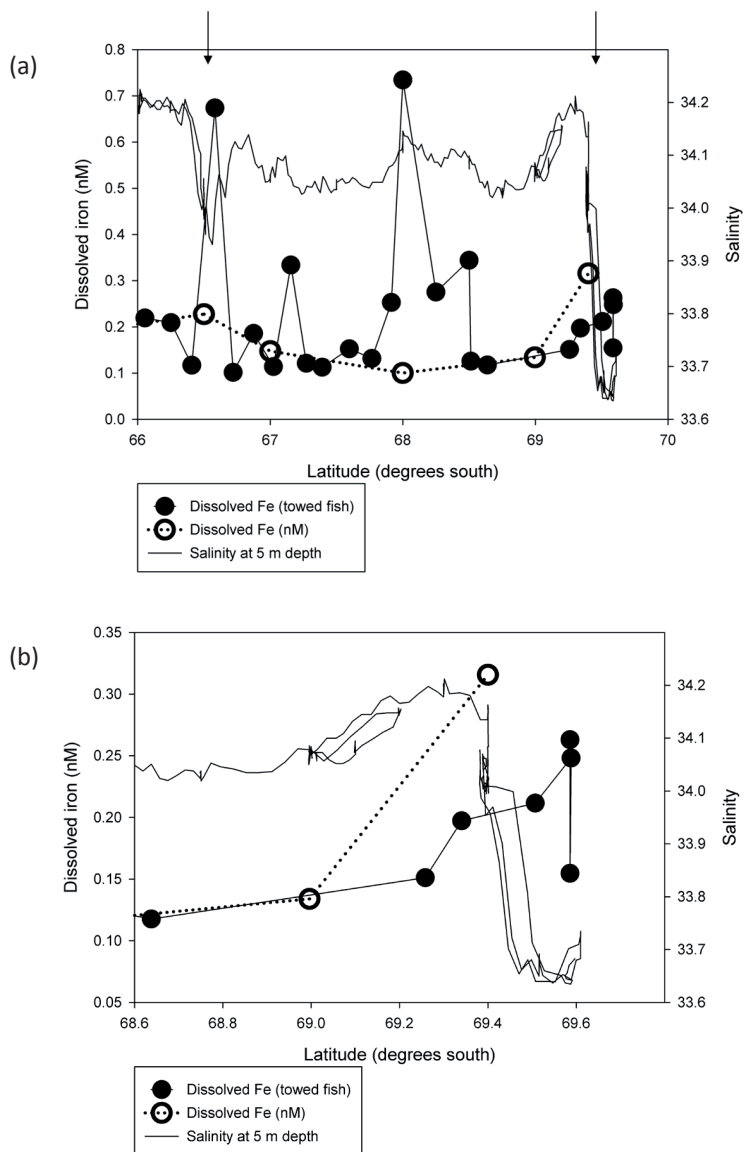


Fig. 4.7a Transect plot of the concentration of dissolved Fe in the upper 1-2 meter of the water column, as obtained by the towed fish (see text) (filled circles). Also plotted are surface mixed layer average Fe concentration collected with GO-FLO samplers (open circles) and the salinity at 5 meter depth from the ships inlet (Fielax) (solid line with dots). Despite some mismatch in sampling inlets and their sampling depth as well, and patchiness of filaments of mixing (melt)waters, distinct Fe maxima tend to coincide with salinity minima due to meltwater. Observed melting of icebergs and the ice-sheet is indicated.

Fig. 4.7b Same as Fig. 7a, but at expanded scales (region adjacent to the ice-sheet). Notice increasing dissolved Fe coinciding with decreasing salinity due to meltwater. The three Fe samples at 69°36' S were collected when the ship travelled straight westward in an open polynia, the different Fe values (0.26 nM, 0.25 nM, 0.15 nM) illustrative of patchiness of meltwater.

centrations obtained with the torpedo together with the averaged surface mixed layer concentration of dissolved Fe. From 66°S to 67°S (0.1-0.2 nM) dissolved Fe in the upper meters tended to be lower than the averaged surface mixed layer concentration. From 67°S southwards the concentration in the upper meters nicely followed the surface mixed layer average, with exception of concentrations at 67°16.34'S (~0.3 nM) and 67°45.57'S until 68°30.52'S (~0.3 nM). Very high (~0.7 nM) concentrations were observed at 66°33.82'S and 68°00.00'S. At the 66°33.82'S position this coincides with a strong salinity minimum (Fig. 4.7a) and the local observation of many icebergs. From 69°S southwards towards the continental ice sheet, both the Fe in the upper 2-3 meters and its averaged surface mixed layer concentration increased. The salinity at 5 meter depth was relatively constant at a value of around 34.2, until ~66°20'S (Fig. 4.7a). From there, the salinity values fluctuated from 34.03 to 34.13 with an exceptional depression to 33.93 at ~66°30'S. A strong increase was observed ($S = 34.2$) at 69°00'S, followed by a decline of salinity towards the ice-sheet; the southernmost station at ~69°36'S had a salinity of 33.7. This is immediately adjacent to the massive ice-sheet extending from the continent, and also many icebergs were present.

4.4.4 Fe in the Deep Waters

Here, we follow the subdivision in three distinct regions (Fig. 4.6).

4.3.4.1 Sub Antarctic region

The properties of these waters are largely influenced by the intrusion at 2000-3000 m depth of the North Atlantic Deep Water (NADW) [Gladyshev *et al.*, 2008]. The core of the NADW was located at ~3000 meter depth at station 101 (42°20'S) (Fig. 4.6a) and gradually rising to 2000 meter depth at station 104 (47°40'S), although at latter latitude the Fe rich NADW has been diluted strongly by mixing and was less pronounced (Fig. 4.5). The concentration of dissolved Fe was slightly elevated from 2000-3000 (~0.6 nM), compared to the overlying and underlying waters (~0.4 nM) (Figs 4.5, 4.6a).

4.4.4.2 Bouvet region

The deep waters above the ridge contained high concentrations of dissolved Fe compared to the waters South and North of the ridge. This high concentration was most prominent in the deeper waters and separated by a subsurface Fe minimum (0.05 - 0.20 nM) from the surface waters.

At stations 110 and 113 (52-53°S), the concentration steadily increased with depth from ~0.3-0.4 to ~0.55 nM at 1250 meter depth. This general increase in dissolved Fe with increasing depth coincided with the layer of relatively high salinity and potential temperature, which indicates mixing of LCDW with the NADW [Veth *et al.*, 1997]. At station 119 (~55°S), a maximum in dissolved Fe concentration of 1.2-1.8 nM

was followed by decrease to ~ 0.8 nM Fe at 1250 meter depth.

Below, in the LCDW, the concentration of Fe varied with latitude; concentrations were about ~ 0.5 nM interrupted by elevated concentration (maximum 2.2 nM).

4.4.4.3 Deep Weddell Gyre

Also in the Weddell Gyre a subsurface minimum is observed. Below this minimum the concentration gradually increased until a relatively constant concentration of ~ 0.45 nM was observed at 750-1000 meter (Fig. 4.5, Fig. 4.6c). Below the AASW the Fe concentrations gradually increased with depth. The downward increase was less pronounced and was observed only at shallower depths in the Northern part of the Weddell Gyre (stations 128-141; $\sim 57^\circ\text{S}$ - 62°S), compared to the Southern part (stations 141- 175: $\sim 62^\circ\text{S}$ - 69°S). At station 163 ($\sim 67^\circ\text{S}$) relatively low concentrations of ~ 0.4 nM Fe were found as deep as 2500 meter, and these concentrations did not change towards the bottom (Fig. 4.6c). This region of relatively low (< 0.4 nM) Fe concentration appears to coincide with a slight increase in salinity and potential temperature, which indicates the presence of WDW. Moreover, in the centre of the Weddell Gyre, out of the influence of the Bouvet Region, from station 131 to 175 (59°S - 69°S), dissolved Fe showed a negative relationship with potential temperature for waters with $\theta > -0.7^\circ\text{C}$ and salinity > 34.6 (comprising WDW and WSDW according to [Klatt *et al.*, 2005]), as follows:

$$[\text{Fe}] = -0.13 * \theta + 0.40 \quad (R^2 = 0.45, P < 0.01, n = 145) \text{ (Eq. 1)}$$

as depicted in Fig. 4.8 and discussed in below text section 4.2.1.3.

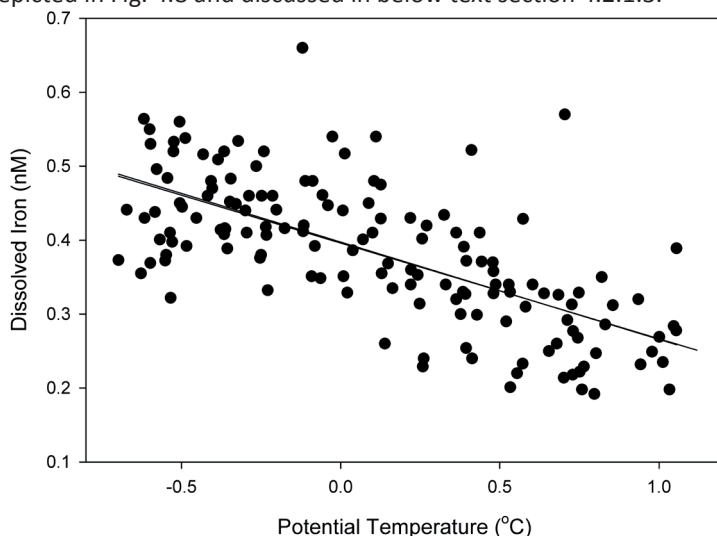


Fig. 4.8 Relation between dissolved Fe (nM) and potential temperature (θ) ($^\circ\text{C}$) within the Weddell Basin, for all waters with $\theta > -0.7$ and salinity > 34.6 . (Deep waters: WDW, WSDW). $[\text{Fe}] = -0.13 * \theta + 0.40$. ($R^2 = 0.45$, $P < 0.01$, $n = 145$).

4.5 Discussion

4.5.1 The Fe Cycle in the Surface Waters

4.5.1.1 Sources of Dissolved Fe in the surface waters

The origin of the dissolved Fe in surface waters may be (i) from below by upwelling and vertical mixing of deeper Fe-rich waters, or (ii) from above by partial dissolution of aerosol deposition, or (iii) from seasonal melting of the seasonal sea-ice cover of the Southern Ocean, or from partial dissolution of sediment carried along from (iv) the Antarctic ice-sheet with calving and melting ice-bergs, or (v) from the (Antarctic) continental margin sediments.

4.5.1.1.1 Upwelling and vertical mixing of deep waters with higher Fe concentration

Fe can be delivered in the surface waters from below, by both advective transport and turbulent diffusive fluxes (eddy-diffusion) [De Baar *et al.*, 1995; Löscher *et al.*, 1997; Croot *et al.*, 2004]. Here, we estimated the contribution of both processes, by using the same approach as De Baar *et al.* [1995] for all stations. For each station, we take the average value of all datapoints deeper than 1000 meter as an estimate of the deep water concentration. The average value for all stations is 0.55 ± 0.19 nM ($n=222$). By multiplying with a typical annual average upwelling velocity of about $15 * 10^{-5}$ cm s⁻¹ [Gordon *et al.*, 1977], we obtain a typical annual average advective Fe flux of the order of 0.82 pmol m⁻² s⁻¹. Due to the now established lower deep Fe concentrations than previously reported [Löscher *et al.*, 1997] this advective upwelling transport is about half the advective flux (1.7 pmol m⁻² s⁻¹) previously reported by De Baar *et al.* [1995] and Löscher *et al.* [1997], yet higher than the advective upwelling transport of 0.41 pmol m⁻² s⁻¹ reported by Croot *et al.* [2004]. Large regional differences appear in the average annual advective fluxes; our average value within the ACC is 1.05 pmol m⁻² s⁻¹, compared to 0.66 pmol m⁻² s⁻¹ in the Weddell Gyre. Moreover seasonality in upwelling velocity is well known to occur but cannot be taken into account due to lack of seasonal observations thus far. Although the advective upwelling flux here is calculated per station, some uncertainties may arise by using the average Fe concentration > 1000 m. There are some variations in deep Fe concentrations (Fig. 4.2). The standard deviation of all deep water concentrations, being 0.19 nM or 30%, affects the derived annual average upwelling flux accordingly.

We also calculated the vertical mixing or eddy-diffusive flux defined as the product of the typical annual average vertical turbulent diffusivity coefficient (K_z) ($3.0 * 10^{-5}$ m²s⁻¹) and $\delta[\text{Fe}]/\delta z$ [De Baar *et al.*, 1995; Löscher *et al.*, 1997]. Here, $\delta[\text{Fe}]/\delta z$ is defined as the concentration difference in dissolved iron between the deepest value within the surface mixed layer and the shallowest value directly below the surface mixed layer. However, difference in vertical distance to the base of the surface mixed layer varies between the different stations, introducing some small errors to the eddy-diffusive flux calculation. At 62-65°S an Fe minimum is observed directly

below the surface mixed layer, at the depth of the fluorescence maximum. In these stations the dissolved iron concentration directly below the pycnocline is used as the deepest concentration, here taking pycnocline depth values after *Middag et al.* (2012a, their Fig. 4.8). Due to a slight elevation of dissolved iron concentration within the very shallow surface mixed layer a negative (downward) eddy-diffusive flux is calculated at one station (St. 150, $\sim 65^\circ\text{S}$). Nevertheless, the annual average upward eddy-diffusive flux equals $0.034 \text{ pmol m}^{-2} \text{ s}^{-1}$ for the complete transect, which is comparable to the estimation of $0.048 \text{ pmol m}^{-2} \text{ s}^{-1}$ by *Croot et al.* [2004]. On an annual basis, our reported total upward transport equals $27.07 \text{ } \mu\text{mol m}^{-2} \text{ yr}^{-1}$ ($26.01 \text{ } \mu\text{mol m}^{-2} \text{ yr}^{-1}$ plus $1.06 \text{ } \mu\text{mol m}^{-2} \text{ yr}^{-1}$) representing the average of somewhat higher upward transport of $34.0 \text{ } \mu\text{mol m}^{-2} \text{ yr}^{-1}$ in the ACC and somewhat lower upward transport of $31.6 \text{ } \mu\text{mol m}^{-2} \text{ yr}^{-1}$ in the Weddell Gyre. *Measures and Vink* [2001] reported $30\text{--}33 \text{ } \mu\text{mol m}^{-2} \text{ yr}^{-1}$ transported by upwelling, and $0.47 \text{ } \mu\text{mol m}^{-2} \text{ yr}^{-1}$ by vertical mixing in the Pacific sector of the Antarctic Circumpolar Current at 170°W , similar to our estimates. For the Australian sector of the Southern Ocean, at 140°W *Sedwick et al.* [2008] reported a vertical resupply of $\sim 0.01\text{--}0.1 \text{ nM}$ over a four month summer period due to eddy-diffusion. Our upward transport of $34.0 \text{ } \mu\text{mol m}^{-2} \text{ yr}^{-1}$ in the ACC (SML depth $\sim 100 \text{ m}$) and $31.6 \text{ } \mu\text{mol m}^{-2} \text{ yr}^{-1}$ in the Weddell Basin (SML depth $\sim 50 \text{ m}$) leads to an estimate of $\sim 0.11\text{--}0.14 \text{ nM}$ increase for the same period, and thus 0.33--

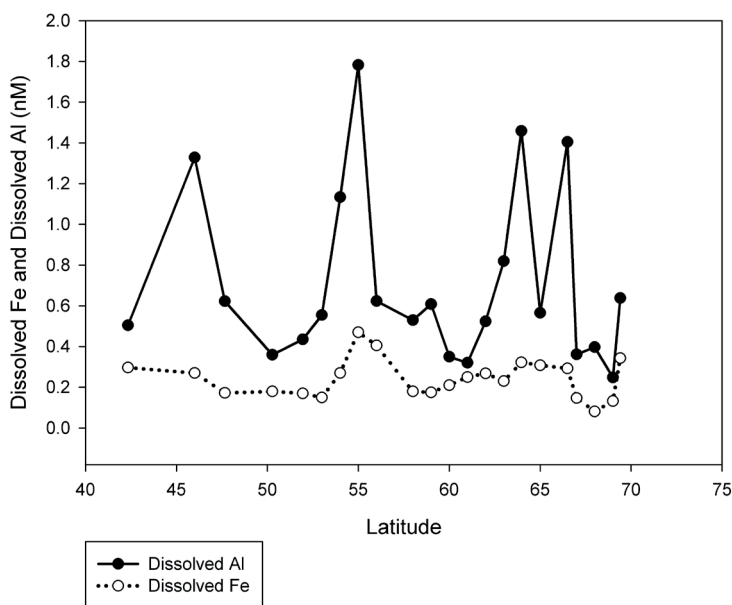


Fig. 4.9 Transect plot of concentrations of dissolved Fe (open circles) and dissolved Al (filled circles) in the upper 25 meters of the water column. For deriving a correlation between Al and Fe, the southernmost station near the ice-sheet has been excluded (Eq. 2, see text section 4.4.1.13).

0.42 nM per year. Overall the rates of advective upwelling transport are virtually the same in the Pacific and Atlantic sectors, but the Fe supply rate of vertical mixing appears to be larger in the Atlantic part of the Southern Ocean (this study; *Croot et al.* [2004]). In the Australian sector of the Southern Ocean, *Lai et al.* [2008] also ascribed higher Fe concentrations in surface waters to upwelling deep waters, as confirmed by high salinity, temperature and silicate concentrations.

4.5.1.1.2 Fe Sources from Atmospheric Deposition

Input of dissolved Fe by dissolution of aeolian transported particles (dust) originating from land is a well recognized mechanism [*Martin and Fitzwater*, 1988; *Fung et al.*, 2000; *Jickells et al.*, 2005; *Cassar et al.*, 2007; *Planquette et al.*, 2007]. Dissolved Al is deemed a suitable tracer for dust deposition [*Measures et al.*, 2008; *Han et al.*, 2008]. We here calculated dissolved Fe and Al averaged over the upper 25 meter from the vertical sampling (Fig. 4.9, Table 4.1). Surface Al and Fe show a weak similarity along the transect (Fig. 4.9). When we exclude station 178, nearest to the ice sheet (where surface water Fe is influenced by ice-melt, section 4.1.1.4), we observe a weak but significant correlation between the upper 25 meter averaged dissolved Fe and Al, as follows:

$$[\text{Fe}] = 0.15 * [\text{Al}] + 0.12 \quad (R^2=0.46, P<0.01, n=21) \quad (\text{Eq. 2})$$

The here observed Fe:Al ratio of 0.15 is lower than the ratio 0.26 for the continental crust reported by *Wedepohl et al.* [1995], but is not very different from the ratio of 0.19 reported by *Mackie et al.* [2006] for precipitated dust. Removal of dissolved Fe due to uptake by phytoplankton can lower the Fe concentration compared to Al, leading to a slightly lower Fe:Al ratio. Although estimations of the share of wet deposition to the total worldwide deposition vary from 23% to 73% [*Jickells and Spokes*, 2001], the importance of wet deposition is confirmed by *Hand et al.* [1999], and *Wolff et al.*, [1998] (summarized by *Hand et al.*, [1999]). During the transect we encountered a strong rain event with 0.3 mm hr⁻¹ on average at 53°48'S and another rain event with average of 0.18 mm hr⁻¹ at 55°40'S (data not shown). Therefore the local elevated concentrations of dissolved Fe and Al observed in the upper 25 meter (Fig. 4.9) around 54-56°S are ascribed to recent wet deposition. This is consistent with previous findings of *Croot et al.* [2004] in the region. Air mass back-trajectories (Fig. 4.10a) are consistent with dust input originating from Patagonia causing elevated dissolved Fe and Al at about 55°S (Fig. 4.10b), in contrast to the adjacent regions (Fig. 4.10a and c).

Dust deposition model studies show a gradual decrease in dust deposition towards the south [*Mahowald et al.*, 1999; *Duce and Tindale*, 1991; *Cassar et al.*, 2007] and recognize the relatively high contributions of dust coming from Patagonia, reaching almost as far east as the zero meridian at ~55°S. Using such model results, the transect here occupied lies completely within the 0 to 0.2 g m⁻² y⁻¹ deposition

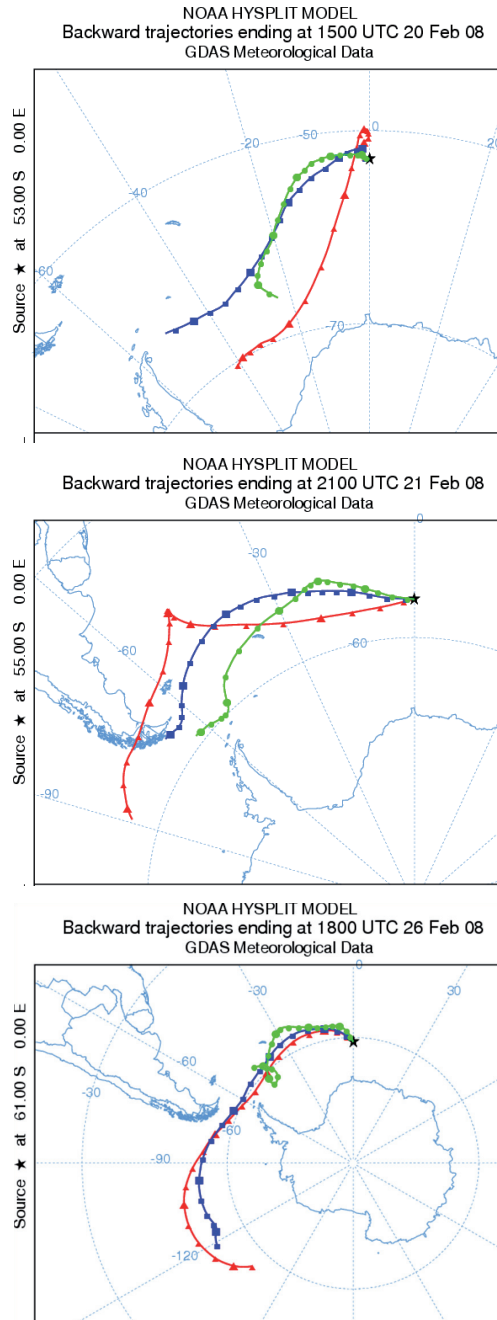


Fig. 4.10 Five day (120 hours) back-trajectory analyses for air parcels at elevations of 10 (green), 500 (blue) and 1000 (red) meter, as calculated using the NOAA HYSPLIT model (Draxler and Rolph, 2003; Rolph, 2003). The back trajectories start from (a) $53^{\circ}00.00\text{ S}$ at 15:00 UTC on February 20, 2008, (b) $55^{\circ}00.00\text{ S}$ at 21:00 UTC on February 21, 2008 and (c) $61^{\circ}00.00\text{ S}$ at 16:00 UTC on February 26, 2008 respectively.

range [Jickells *et al.*, 2005; Mahowald *et al.*, 2005]. According to Duce and Tindale [1991] the dust deposition range over the transect varies from $>0.1 \text{ g m}^{-2} \text{ y}^{-1}$ in the north part of our transect to $<0.01 \text{ g m}^{-2} \text{ y}^{-1}$ towards the Antarctic continent. Recently, an increase of solubility with decreasing dust concentrations was reported [Baker and Croot, 2008]. Baker *et al.* [2006] report a median value of 8.3 % solubility for the remote South Atlantic and Edwards and Sedwick [2001] reported a median value of 32% solubility for samples of snow from Antarctica. Hence, we take the 8.3% solubility for the remote South Atlantic (and $0.1 \text{ g m}^{-2} \text{ y}^{-1}$ dust deposition [Duce and Tindale, 1991] as a lower limit and the 32% solubility for Antarctic snow (and $0.01 \text{ g m}^{-2} \text{ y}^{-1}$ dust deposition [Duce and Tindale, 1991] as an upper limit. Using an Fe content of dust of $\sim 3.5\%$ as reported by Taylor and McLennan [1985] and used by Mahowald *et al.* [2005], this results in an influx rate of Fe dissolved from dust between 2 and $5.2 \cdot 10^{-6} \text{ mol m}^{-2} \text{ yr}^{-1}$. In terms of the concentration of dissolved Fe over an average 65 m deep SML, this would represent an annual increase of 0.03-0.08 nM due to dust input alone. This is an order of magnitude lower than the atmospheric Fe influx reported by Sedwick *et al.* [2008] north of the Polar Front, in the Australian Sector of the Southern Ocean. This difference may partly be explained by differences in the dust deposition; Jickells *et al.* [2005] and Mahowald *et al.* [1999] estimated the dust deposition directly South of Australia between $0.2\text{-}2.0 \text{ g m}^{-2} \text{ y}^{-1}$, roughly an order of magnitude higher than the flux over the zero meridian. Lancelot *et al.* [2009] suggest a modeled dust deposited Fe flux of $0.02 - 0.1 \text{ pmol m}^{-2} \text{ s}^{-1}$ over the zero meridian, which is in close agreement with our findings.

4.5.1.1.3 Melting of seasonal sea-ice

Several studies discuss the seasonal melting of sea-ice as a possible mechanism for dissolved Fe input in the Surface Mixed Layer (SML) [Löscher *et al.*, 1997; Measures *et al.*, 2001; Croot *et al.*, 2004; Lannuzel *et al.*, 2008]. Simulations of the Antarctic sea-ice extent by the University of Bremen (<http://iup.physik.uni-bremen.de:8084/amsr/amsre.html>) show that our study region is virtually sea-ice free throughout February 2008 until the end of March 2008. The freshwater released by sea-ice melt earlier in the season causes a relatively fresh layer on top of the more saline, colder winter water (WW) [Park *et al.*, 1998, their Fig. 4.4). From 60°S to $69^{\circ}24'\text{S}$ (stations 135-178), we can clearly distinguish the latter more saline colder winter water (WW) with potential temperature of $\sim -1.65^{\circ}\text{C}$ and salinity of ~ 34.34 , using data from the CTD profiles in our stations. If we assume that the salinity deficit between the surface and the winter water is caused *solely* by sea ice melt, and sea-ice salinity is 5 (ice plus brine; Eicken, [1992]) we can calculate the apparent winter sea-ice thickness by integrating the salinity deficit at each depth from surface to winter water. This is a similar approach as used by Hoppema *et al.* [2007] for nutrient depletion. Using this approach we find the reconstructed apparent winter sea-ice thicknesses in the range of 33-163 cm, with an average of $58 \pm 30 \text{ cm}$ ($n=11$). There is a clear distinction between the stations 135-167 from 60°S to 68°S with an average of $47 \pm 13 \text{ cm}$ ($n=9$) and the

final two stations 175 and 178 near the ice sheet (69°S and 69°24'S) with highest estimates of 67 cm and 163 cm, respectively. *Worby et al.* [2008] find, in the period with maximum sea-ice extent, (spring; September-October-November) an average sea ice thickness of 89 cm and an ice coverage of 82% in the East Weddell Gyre (45°W-20°E). This would correspond to an overall 73 cm thickness for a presumed 100% coverage.

Lannuzel et al. [2008] studied temporal changes in dissolved Fe concentration of Weddell Sea pack ice. They found vertical integrated dissolved Fe concentrations of 1.1 -13.3 $\mu\text{mol m}^{-2}$ and total dissolvable (dissolved plus particulate) concentrations of 6.1-59.4 $\mu\text{mol m}^{-2}$ in the ISPOL station in the Weddell Sea. This vertical integrated value comprises brine, sea-ice and snow for a 90 cm deep ice-core. For our reconstructed average sea ice thickness of 58+/-30 cm this would correspond to a range with the lower value of 0.34 $\mu\text{mol m}^{-2}$ (the dissolved Fe in the sea-ice) and a higher value of 57.5 $\mu\text{mol m}^{-2}$ as upper limit in the case all the particulate Fe in the sea-ice would also dissolve. Over a ~40 m SML (average 60-69.24°S) this equals 0.01 – 1.43 nM Fe supply from ice-melt. Nevertheless, the here used sea-ice thickness and Fe concentrations vary widely between different regions [*Lannuzel et al.*, 2008], which results in major uncertainties in the Fe flux from the sea-ice to the ocean, beyond our estimated range. It should be noted that seasonal sea ice can be seen as a storage of both Fe captured from the surface waters during autumn sea-ice formation and external Fe supply of dust deposition accumulated in snow on top of the sea-ice [*Lannuzel et al.*, 2008]. During melting season this Fe will be released in a relatively short period of time leading to temporary increased Fe supply.

4.4.1.1.4 Fe Sources from the Antarctic continental ice-sheet and free drifting icebergs

The melting of the Antarctic ice sheet or free-ranging icebergs are alternative input sources of dissolved Fe to the surface waters [*Croot et al.*, 2004]. This Fe originates either from dust blown from Patagonia, or from contact of the ice-sheet with the underlying continent or from grounding of ice-bergs over the shelf. Obviously these processes result in a very heterogeneous distribution of Fe in the ice, as indeed shown in the very wide natural range of Fe concentrations between 0.52-120 nM in land-ice [*Edwards et al.*, 1998] or 10.8-99.3 nM [*Löscher et al.*, 1997] in meltwater from ice-bergs. In two regions (~69°24'S, ~66°30'S) higher dissolved iron coincides with extreme salinity minima (Fig 4.7a). In above section 4.1.1.3. all salinity minima in the surface water had been ascribed *solely* to melting of seasonal sea-ice. Here alternatively, we assess implications when one would ascribe the two extreme salinity minima *solely* to the melting of the continental ice-sheet and/or free drifting ice-bergs. When comparing the background salinity 34.084 along 66-69°S with the minimum 33.653 at 66°36'S we derive a local 1.3% ice-sheet meltwater contribution. Now taking [Fe] of 0.15 nM of 69°15' S as background value and the highest 0.26 nM as enhanced due to this 1.3 % ice-sheet meltwater one may derive:

$$\text{Fe}_{\text{mixture}} = 0.26 \text{ nM} = (0.987 \times \text{Fe}_{\text{seawater}}) + (0.013 \times \text{Fe}_{\text{ice-sheet}}) = (0.15 \text{ nM}) + (0.11 \text{ nM}) \text{ (Eq. 3)}$$

from which we derive an apparent Fe concentration in the ice-sheet end member of 8.6 nM. Similarly, for the salinity minimum region at $\sim 66^{\circ}30'S$, where a high abundance of ice-bergs was observed, one may derive 0.86% ice berg meltwater, hence the observed Fe concentration difference of 0.56 nM would be consistent with an Fe content of 66.4 nM in the iceberg end-member. The apparent ice-sheet end-member of 8.6 nM and apparent ice-berg end-member of 66.4 nM fall within the above mentioned wide and variable natural range previously reported. Thus melting of ice-sheet or ice-bergs may, in principle, account for the Fe maxima coinciding with the extreme salinity minima, but likely several other processes, such as sea-ice melting or biological interactions also play a role. Finally due to the very wide natural variability of Fe content of ice-sheet and icebergs, in combination with major uncertainty in the percentage of total Fe that will dissolve in meltwater or seawater, we reckon that an accurate assessment of Fe supply by ice-sheet and ice-bergs will always remain very difficult. At best one may realize that these may, or may not, be significant sources of dissolved Fe to the surface waters of the Southern Ocean.

4.5.1.1.5 *Continental ice-sheet of Antarctica prevents Fe supply to surface waters from continental shelf sediments.*

The continental shelves surrounding the islands in the Southern Ocean, such as Bouvet, Kerguelen and Crozet are known to bring significant elevated Fe concentrations to the deep oceans [Croot *et al.*, 2004; Planquette *et al.*, 2007; Blain *et al.*, 2007; 2008a; 2008b]. In addition, Sohrin *et al.* [2000] reported patches of elevated iron south of the Polar Front at $140^{\circ} E$, which was (partly) attributed to organic rich sediments from the slope.

During ANT XXIV/3 however, no indication of significant input from organic rich sediments from the continental shelf of the Antarctic continent was observed. This is likely due to the extension of the continental ice-sheet quite far into the ocean basin. Our southernmost station (178) at $69^{\circ}24.03'S$ was located very close to the 200 m thick ice-sheet, but was still >2000 m deep. The common occurrence of plankton blooms in this region directly adjacent to the ice-sheet may well yield significant export of organic carbon to the underlying slope sediments, and upon its oxidative bacterial degradation in the surface sediments the ensuing suboxic conditions may well yield reductive dissolution of Fe (see section 4.2.1.3, Elrod *et al.* [2004]). However such reducing sediments here are far too deep (>2000 m) for any significant input into the local surface waters. Below the extended ice-sheet itself (Middag *et al.*, 2011a, their Fig. 4.13) there is deemed to be no biological production, thus the only and presumably very insignificant export of organic matter to the seafloor is by lateral input from biological production in waters outside the ice-sheet extent. Rutgers Van der Loeff *et al.* [2011]) reported a C export flux of $9.9 \text{ mmol C m}^{-2} \text{ d}^{-1}$ at 100 m depth at the station (178) nearest to the ice-edge. However, they mention that this is most likely an overestimation due to advective fluxes. The C export at

stations further in the basin was low; 3.1-4.5 mmol C m⁻² d⁻¹ (Rutgers Van der Loeff *et al.* [2011]). Hence the seafloor of the continental shelf under the extended ice sheet likely comprises very low organic carbon. Such low organic supply is unlikely to lead to suboxic let alone anoxic conditions. Therefore these local sediments are unlikely to be a reductive source for dissolved Fe (or Mn) to the overlying bottom waters and in turn to the surface waters. In contrast to continental shelf sediments throughout the world, the unique permanent ice-sheet extending off the Antarctic continent at the zero meridian largely prevents the normal biogeochemical mechanisms for mobilization of Fe and Mn [Middag *et al.* 2011] from the underlying shelf sediments. Thus Antarctica is unique because when approaching from the open ocean the dissolved Fe and Mn tend to decrease, as opposed to the always increasing trend towards all other continents [De Baar and De Jong, 2001].

The Fe measured in acidified unfiltered samples during the ANT XXIV/3 cruise provides information about the labile fraction of the particulate Fe. However, no unfiltered samples were collected at stations near the ice-sheet, precluding additional information.

4.5.1.2 Removal of Fe from surface waters

Dissolved Fe predominantly exists in the trivalent Fe(III) oxidation state in seawater, of which the large majority is bound by organic Fe-complexing moieties [Thuróczy *et al.*, 2011]. In general the Fe(III) state is very 'particle-reactive' and tends to adsorb to small colloids within larger (> 0.2 µm) size classes, causing a sinking loss term of Fe from surface waters. Moreover Fe is taken up directly by phytoplankton and bacteria [De Baar and De La Roche, 2003], and upon predation of these by micro- and mesozooplankton and krill, part of the intracellular Fe may become dissolved again [Sarhou *et al.*, 2008]. Yet another part may end up in large fecal pellets which tend to settle down into deeper waters [Tovar-Sanchez *et al.*, 2007; Hutchins and Bruland, 1994].

Below an effort is made to distinguish between (i) the biological uptake inside the living plankton cell, and (ii) scavenging and sinking loss.

4.5.1.2.1 Fe Removal by Biological Uptake

Uptake by phytoplankton and subsequent export from the surface mixed layer is an important mechanism for iron removal from the mixed layer [Coale *et al.*, 2005]. Mixed layer average concentrations of dissolved Fe and chlorophyll fluorescence (Table 1) are shown in Fig. 4.11. North of the Polar Front (41-46 °S) southward decreasing Fe (~0.3 to ~0.2 nM) coincides with relatively high fluorescence. South of the Polar Front within the AAZ (50°S-55°S), a weak but significant negative correlation was found:

$$\text{Fluorescence} = -0.67 * [\text{DFe}] + 0.37 \quad (R^2=0.39, P < 0.01, n=19) \quad (\text{Eq. 4})$$

Further southwards in the Weddell Gyre (56°S-69.24°S) a similar trend was found:

$$\text{Fluorescence} = -3.99 * [\text{DFe}] + 1.45 \quad (R^2=0.41, P < 0.01, n=25) \quad (\text{Eq. 5})$$

The southernmost station (178) at 69°24'S, is strongly influenced by the Antarctic ice sheet, hence is excluded from the relationship in (Eq. 5). The slope of the relationship (Eq. 5) between dissolved Fe and fluorescence within the Weddell Gyre is significantly steeper than the preceding relationship (Eq. 4) within the AAZ ($P < 0.05$, 2-sided t-test).

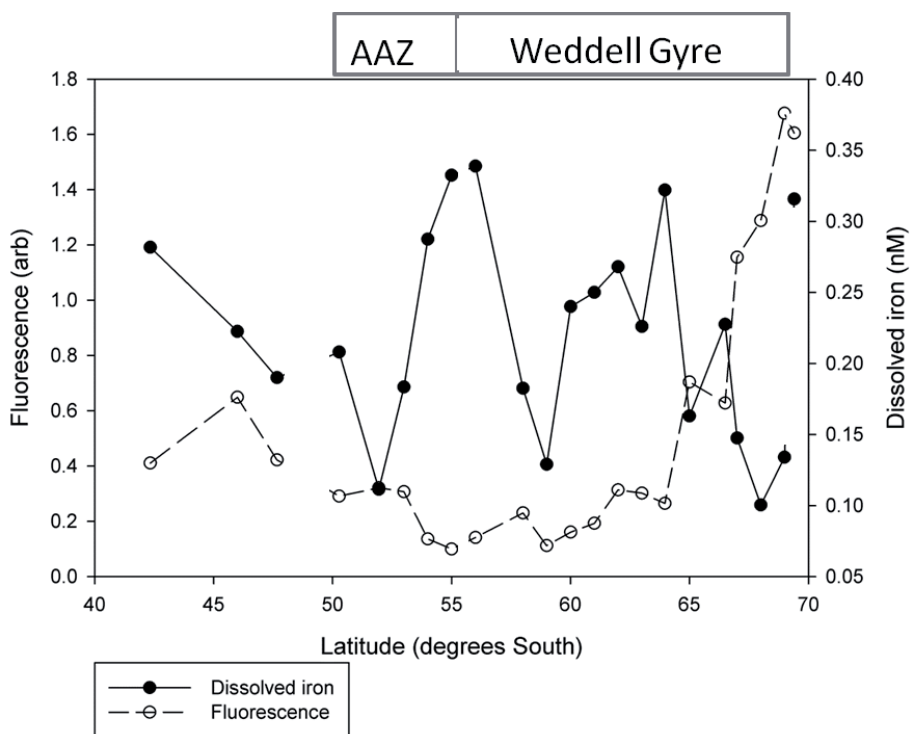


Fig. 4.11 Transect plot of the average concentration (nM) of dissolved Fe (filled circles) and fluorescence (open circles) in the upper Surface Mixed Layer (SML). Each datapoint is the average of 2 to 4 independent datapoints for shallow and deep SML respectively. The five datapoints for the AAZ (50°S-55°S; stations 107, 110, 113, 116, 119) represent 21 independent datapoints as used for Eq. 4 (see text section 4.2.1.2)); the thirteen datapoints for the Weddell Gyre (56°S-69°24'S, St. 122 to 175) represent 25 independent datapoints as used for Eq. 5.

While realizing that other factors also affect the Fe concentration in the surface water, the significant negative relations (Eqs. 4 and 5) between fluorescence and dissolved Fe here suggest that removal of dissolved Fe by phytoplankton primary production has occurred in the time preceding our study. This is supported by findings of *Middag et al.* [2011a], who also report uptake of the biological essential trace metal Mn by phytoplankton in the SML along the same transect.

We can calculate the removal of Fe from the upper waters over the complete transect until the ice-edge (section 4.1.1.5). Using the average carbon export ($5.3 \pm 2.4 \text{ mmol C m}^{-2} \text{ d}^{-1}$; [Rutgers Van der Loeff *et al.*, 2011] and a C:Fe ratio of $\sim 10^5$ [Twining *et al.* 2004], we obtain an estimation of the Fe removal of $0.06 \pm 0.03 \cdot 10^{-6} \text{ mol m}^{-2}$ over the preceding four months (summer). Using a typical sinking velocity of 40 m d^{-1} [Garritty *et al.*, 2005] leads to a seasonal export of $0.16 \pm 0.07 \text{ nM}$. However, it should be noted that our cruise took place in late austral summer, conceivably leading to a relative high estimation of the carbon export, perhaps resulting in an overestimation of the biological drawdown. Nevertheless, in another region, at about 140°E south of the PF, and with another approach based on spring Fe data and seasonal nitrate drawdown, *Sedwick et al.* [2008] calculated a very similar value of seasonal biological drawdown of Fe of $\sim 0.14\text{--}0.18 \text{ nM}$. An Fe drawdown of the same magnitude ($\sim 0.24 \text{ nM}$) was derived by *Measures et al.* [2001] at 170°W . Chlorophyll a can be ascribed largely to diatoms, as they are a very important phytoplankton group within the Southern Ocean, where diatoms tend to dominate under high silicate conditions [Sarhou *et al.*, 2005. At our transect, in the northernmost (station 101-107), haptophytes and chlorophytes dominated the phytoplankton community. All other stations from station 107 to the ice-sheet had a diatoms dominated community (except at station 141, $\sim 62^\circ\text{S}$). [Alderkamp *et al.*, 2010; Neven *et al.*, 2011].

4.5.1.2.2 Fe Removal by Adsorptive Scavenging

In addition to true biological uptake, adsorptive scavenging on settling particles (both biogenic and lithogenic) is a mechanism of Fe removal from the upper ocean [Wu *et al.*, 2001]. However, dissolved Fe is strongly protected from scavenging by binding to dissolved organic ligands ([Wu *et al.*, 2001; De Baar and de Jong, 2001] and for this transect assessed by *Thuróczy et al.* [2011].

4.5.2 The Fe Cycle in Deep Waters

4.4.2.1 Sources of Fe to Deep Waters

The distribution of dissolved Fe in the deep waters of this part of the Southern Ocean is largely influenced by (i) the inflow of different water masses, (ii) the input by hydrothermal vents and (iii) the input from reductive sediments.

4.5.2.1.1 Inflow of NADW rich in dissolved Fe

The vertical profiles of salinity and nutrients make clear that the deep waters in the North East part of the transect were largely influenced by NADW. Higher dust input at the surface [Moore and Braucher, 2007], a closer proximity to the continent and mixing of water masses with enriched iron (Labrador Sea, Mediterranean Sea) [Laës *et al.*, 2003] cause elevated concentrations of Fe in the NADW in the Atlantic Basin. The intrusion of NADW into the Southern Ocean is clearly marked by higher Fe and lower NO_3 concentrations progressing southwards at 2000-3000 m depth (Figs 4.3, 4.4a, 4.5, 4.6a). This NADW affects the Fe concentration in the circumpolar waters north of the Bouvet region. The concentrations found in the NADW (~ 0.6 nM) are consistent with the lower range of the values of 0.6-1.0 nM reported previously by Löscher *et al.* [1997] for a station at 50°S, 6°W. Based on the northernmost profile (Fig. 4.6a) we make an estimation of the net input of NADW (~ 0.61 nM) to the Southern Ocean (~ 0.41 nM) by the difference of ~ 0.2 nM. We can multiply this concentration difference with the total volume transport of $930 \cdot 10^{12} \text{ m}^3 \text{ yr}^{-1}$ of NADW into the Atlantic Sector (20°E to 65°W) of the Southern Ocean [De Baar *et al.*, 1997] and dividing by the total surface area of $2.05 \cdot 10^{13} \text{ m}^2$ of latter Atlantic sector [Losch, AWI, pers. communication, 2010] would yield in an influx of $9.1 \cdot 10^{-6} \text{ m}^{-2} \text{ yr}^{-1}$.

4.5.2.1.2 Hydrothermal vent input at the ridge crest in the Bouvet region

At the Bouvet region, hydrothermal activity is deemed to be the cause of the above mentioned (3.4.2) elevated Fe and Mn concentrations within the shown contour (fig. 4.5). For a similar, but stronger hydrothermal anomaly in the Arctic Ocean, this was accompanied by significant anomalies of temperature and suspended particles (lower light transmission), as well as anomalies in calculated $[\text{Al}/(\text{Al}+\text{Mn}+\text{Fe})] \cdot 100$ ratio values [Klunder *et al.*, 2012]. Briefly, Boström and Peterson [1969] have shown that hydrothermal (metalliferous) sediments are enriched in Fe and Mn and relatively depleted in lithogenous elements such as Al, and were able to demonstrate this hydrothermal component with the $[\text{Al}/(\text{Al}+\text{Mn}+\text{Fe})] \cdot 100$ ratio concept. Here over the Bouvet region a temperature anomaly was not discernible, but lower light transmission was found from 1600 depth to the seafloor at $\sim 53^\circ 31' \text{ S}$ (not shown) and accompanied by anomalous element ratio values indicative of hydrothermal Fe input (Fig. 4.12).

4.5.2.1.3 Input into subsurface waters from sediment sources elsewhere

Within the upper 500 meters of the water column (Fig. 4.5, upper graph) two distinct subsurface maxima were found, just south of the Bouvet region and adjacent to the Antarctic continent, respectively.

At the stations over (St. 119) or just south (St. 122, 128) of the ridge a maximum of dissolved Fe was observed at intermediate depth range (Fig. 4.5; 400-700 meter depth). At station 128 this is confirmed by a maximum of labile particulate Fe at 500 meter depth [Thuroczy, 2009, pers. comm.]. These Fe maxima might have

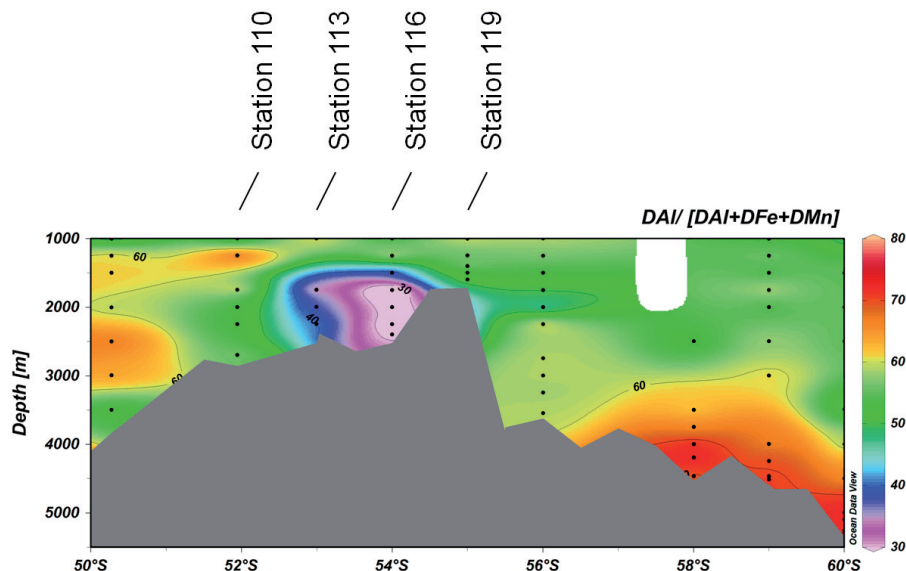


Fig. 4.12 Color plot of $[DAI]/([DAI]+DFe+DMn)]*100$ ratio for the zero meridian transect; stations 110, 113, 116 and 119 are indicated. This figure is made using Ocean Data View (Schlitzer, 2009).

originated from the shelf sediments of the Bouvet region. However, the maxima are located relatively high above the deep seafloor and there is a layer with lower dissolved Fe in between the maxima and the seafloor. Therefore, we suggest these Fe maxima to derive from the continental shelf of the Antarctic peninsula which is situated upstream of both the ACC and Weddell Gyre passing our zero meridian section. As shown in Fig. 4.1, the ocean topography along the flow path is relatively shallow, and geostrophic velocities are strong [Klatt *et al.* 2005], enabling Fe to be transported far from the peninsula towards the zero meridian. Moreover on the second transect crossing the Weddell Sea, and the third transect across Drake Passage, we indeed found elevated dissolved Fe over the shelf of the Antarctic peninsula [see Chapter 5]). Moreover, Lam *et al.* [2006] showed that sediment transport from continental margins can indeed be a source of Fe over distances of 900 km.

At station 178, the high concentrations of >1 nM at 450-500 m correspond with maxima of salinity and potential temperature (data not shown). Klatt *et al.* [2005] show that these are features of the westward flowing Antarctic Coastal Current. Therefore we state that these elevated Fe concentrations are to be explained by transport of Fe with the Antarctic Coastal Current. Here we also find an oxygen minimum and from 300-450 m depth, lower light transmission, i.e. higher abundance of suspended particles. Thus re-suspension of particles from the more eastward shelves and subsequent dissolution could be a possible Fe source here. The sedimentary flux as suggested by Lancelot *et al.* [2009] in a modeling study is >0.5 $\text{pmol m}^{-2} \text{s}^{-1}$ close to the continent and <0.02 $\text{pmol m}^{-2} \text{s}^{-1}$ above the open ocean. Another model

exercised by *Tagliabue et al.* [2009] suggests a stronger impact of sedimentary Fe input compared to dust Fe input. In both model simulation studies sedimentary Fe input is a function of bottom topography and neither the now observed Fe fluxes from hydrothermal input, nor northerly watermasses (NADW) brought to the surface by upwelling, nor the adverse effect of the ice-sheet on Fe fluxes, had been taken into consideration in preceding model simulation studies.

4.5.2.1.4 Fe supply into deep waters of the Weddell Gyre

The dissolved Fe concentration varies between the different water masses within the Weddell Gyre. The water transport in the Weddell Gyre is well described by *Klatt et al.* [2005]. The deep water masses (WDW, WSDW and WSBW) (see hydrography section) are defined as waters with salinity > 34.6. Between ~56°S and 62°S (St. 122 to 141), where the Weddell Gyre flows eastward, the concentration of dissolved Fe in these deep waters is significantly ($P < 0.01$, 2-tailed homoscedastic students t-test) higher ($0.47 \text{ nM} \pm 0.16$, $n=98$) than the concentrations (0.33 ± 0.14 , $n=126$) in the westward flow, between ~62°S - 69°24'S (St. 144 to 178). From the relationship between potential temperature (θ) and dissolved Fe (Fig. 4.8) we conclude that the distribution of dissolved Fe is strongly dependent on ocean circulation and mixing. The Fe concentrations in the WDW ($\theta > 0$) are lower than in the WSDW ($-0.7 < \theta < 0$) [*Klatt et al.*, 2005]. Dissolved Fe, Mn and light transmission data suggest that the westward flow of the Weddell Gyre, coming from the remote Indian sector of the Southern Ocean, at high latitudes (station 141-178; 62°S-69°24'S) contains slightly clearer water (higher light transmission values due to less particles) and lower trace metal concentrations, compared to the more northerly, eastward flowing waters of the Weddell Gyre (122-141; 56°S-69°S). Latter waters have been flowing along the North Weddell Ridge, where presumably there has been entrainment of particles coming from the slope sediments of the ridge. Also hydrothermal inputs from Bransfield Strait [*Klinkhammer et al.*, 2001] may have contributed Fe to these eastward flowing waters. Another important input source for Fe in deep waters is reductive dissolution. Locally, some stations show slightly elevated (by ~0.2 nM) concentrations towards the bottom (178, 167 (Figs. 4.5, 4.6c)).

4.5.2.2 Removal of Dissolved Fe from Deep Waters

4.5.2.2.1 Upward advective upwelling supply and vertical mixing

The supply of Fe by upwelling and vertical mixing is extensively described in section 4.1.1.1. Supply to the upper oceans implicates removal of dissolved Fe from the deep waters by the water replacing the upper ocean waters, because the concentrations of dissolved iron in the upper waters are lower (~0.2 nM) than the concentrations in the deep (~0.4 nM) (Figs. 4.2, 4.5, 4.6). Thus we suggest a removal rate of $0.85 \text{ pmol m}^{-2} \text{ s}^{-1}$ (as calculated in 4.4.1.1.1) by hydrography of advective upwelling and vertical mixing.

4.5.2.2.2 Competition between stabilization by organic complexes and removal by scavenging onto settling particles

Dissolved Fe can be removed from the deep waters by scavenging onto sinking biogenic particles (see 4.1.2.2). Although lower than in the surface waters, also in the deep waters there still is an excess of organic ligands over dissolved Fe [Thuróczy *et al.*, 2011], counteracting the adsorptive scavenging removal of dissolved Fe. However, ~42% of the dissolved Fe is within the “colloidal” fraction (here operationally defined as 1000 kDa - <0.2 μm) in the waters below 1000 m [Thuróczy, pers. communication, 2009]. Thus coagulation, aggregation and subsequent settling of these particles will remove a part of the dissolved iron from the deep waters. This mechanism is suggested also in the Pacific and Atlantic Oceans by Wu *et al.* [2001]. Walter *et al.* [2000] also observed scavenging in the Weddell Sea, although in relatively low quantity due to the low particle fluxes. Because this mechanism will create aggregates with sizes

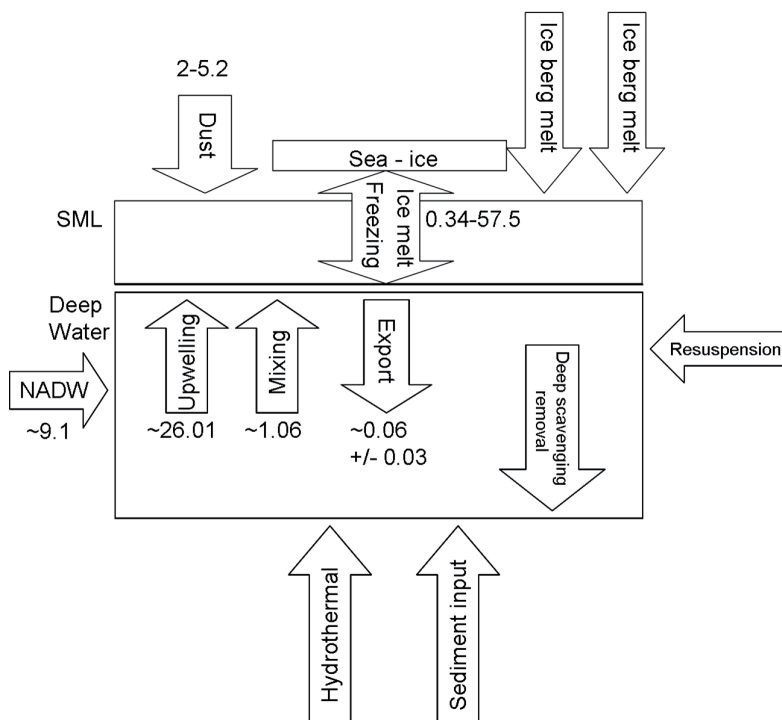


Fig. 4.13 Schematic of Fe fluxes towards an eventual Fe budget of the Atlantic Sector of the Southern Ocean. For several fluxes an estimate [$10^6 \text{ mol m}^{-2} \text{ yr}^{-1}$] is given in the graph, see main text for derivation of estimates. For other fluxes a basinwide estimate in $10^6 \text{ mol m}^{-2} \text{ yr}^{-1}$ units is not feasible. Melting of the continental ice-sheet would account for a local influx of 0.11 nM. Similarly at ~66 °S, melting of free-drifting icebergs may account for a local increase of 0.56 nM. However, latter numbers are subject to large deviations and are therefore not in the graph. Moreover there are strong indications of local Fe supply from hydrothermal activity, reducing sediments and sediment re-suspension, see main text, but extrapolation to a basinwide estimate is as yet not feasible either.

larger than 0.2 μm , an increase with depth may be conceivable for the “labile particulate Fe” in the water column [Thuróczy *et al.*, 2011]. Indeed, an increase with depth was observed from <1 nM in the upper 1000 m to 2.77 – 8.31 nM for the deepest samples, at the five measured stations (103, 107, 128, 131, 163) along the zero meridian [Thuróczy *et al.*, pers. communication, 2009].

Finally, the figure 4.13 provides a schematic overview of the processes causing in- and output fluxes of Fe to the SML and deep waters as discussed above, and where possible an estimate [10^{-6} mol m^{-2} yr^{-1}] of the flux is given in the graph. For some other fluxes we cannot yet give such a value.

4.6 Conclusions

The average dissolved Fe in the upper surface mixed layer of the Atlantic sector of the Southern Ocean varies between 0.1 – 0.3 nM. The most important source of dissolved Fe to the upper surface mixed layer is advective upwelling, which tends to be one order of magnitude higher than the upward Fe supply by vertical mixing. We conclude that the contribution of dust deposition as predicted using dust deposition models and our data is 5-10 times smaller than advective upwelling. Nevertheless, this study also shows that local and temporal input events as dust deposition and ice melt can cause considerable (presumably short term) elevations in the concentration of dissolved Fe. Supply by aeolian wet deposition events may be of local significance but cannot yet be accurately quantified in the context of a basinwide annual Fe budget of the overall surface waters. Iron uptake by phytoplankton and scavenging can decrease dissolved Fe concentrations in the upper layer.

In the deep waters, elevated Fe concentrations in the SubAntarctic region are caused by intrusion of NADW to these SubAntarctic waters. The presence of elevated dissolved Fe over the ridge crest in the Bouvet region suggests a far more significant role than hitherto realized of hydrothermal vents as a major source term of Fe and Mn for deep waters of ocean basins. Furthermore, dissolved Fe in the eastward extent of the Weddell Gyre is significantly higher than in deep waters of the westward deep return flow. The slightly higher concentrations in the eastward flowing part of the Weddell Gyre are tentatively ascribed to hydrothermal iron inputs from Bransfield Strait and/or dissolution processes from the slope sediments of the North Weddell Ridge. The Antarctic continental ice-sheet extends well beyond its grounding line and therefore also covers the water column over the Antarctic shelf and slope. This largely prevents biological production, hence strongly minimizes the biogeochemical cycling over and within the shelf and slope. And subsequently minimizes lateral supply of Fe (and Mn) from the shelf and slope into adjacent open ocean waters. Thus in contrast to all other continental margins of the world, the dissolved Fe around Antarctica is lower towards the continent.

4.7 References

- Alderkamp, A.-C., De Baar, H.J.W., Visser, R.J.W., Arrigo, K.R.(2010), Can photoinhibition control phytoplankton abundance in deeply mixed water columns of the Southern Ocean? *Limnology and Oceanography*, 55 (3), 1248-1264.
- Aguilar-Islas, A.M., Resing, J.A., Bruland, K.W.(2006), Catalytically enhanced spectrophotometric determination of manganese in seawater by flow-injection analysis with a commercially available resin for on-line preconcentration. *Limnology and Oceanography: Methods* 4, 105-113
- Baker, A.R., Croot, P.L.(2008). Atmospheric and marine controls on aerosol iron solubility in seawater, *Mar. Chem.*. doi:10.1016/j.marchem.2008.09.003
- Baker, A.R., Jickells, T.D., Witt, M. and Linge, K.L. (2006), Trends in the solubility of iron, aluminium, manganese and phosphorus in aerosol collected over the Atlantic Ocean. *Mar. Chem.* , 98 (1), 43-58.
- Bell, J., Betts, J. and Boyle, E.(2002), MITES: a moored in situ trace element serial sampler for deep-sea moorings. *Deep Sea Res. earch Part I* 49 (11), 2103-2118.
- Blain S., Quéguiner, B., Armand, L., Belviso, Bombled, B. Bopp, L., Bowie, A. Brunet, C. , Brussaard, C., Carlotti, F. Christaki, U. Corbière, A., Durand, I.Ebersbach, F., Fuda, J.-L., Garcia, N., Gerringa, L., Griffiths, B., Guigue, C., Guillermin, C., Jacquet, S., Jeandel, C., Laan, P., Lefèvre, D., Lo Monaco, C.,Malits, A., Mosseri, J.,Obernosterer, I., Park, Y-H., Picheral, M., Pondaven, P., Remenyi, T., Sandroni, V., Sarthou, G., Savoye, N., Scouarnec, N.,Souhaut, M., Thuiller, D., Timmermans, K.R., Trull, T., Uitz, J., van Beek, P., Veldhuis, M., Vincent, D., Viollier, D., Vong L., Wagener, T. (2007), Effect of natural iron fertilization on carbon sequestration in the Southern Ocean. *Nature*, 446 (7139),1070-1074.
- Blain, S., Sarthou, G. and Laan, P.(2008a), Distribution of dissolved iron during the natural iron-fertilization experiment KEOPS (Kerguelen Plateau, Southern Ocean). *Deep Sea Research Part II* 55 (5-7), 594-605.
- Blain, S., Quéguiner, B., Trull, T. (2008b), The natural iron fertilization experiment KEOPS (Kerguelen Ocean and Plateau compared Study): An overview. *Deep Sea Research Part II*. 55 (5-7), 559-565.
- Boström, K. and Peterson, M.N.A. (1969), The origin of aluminum-poor ferromanganoan sediments in areas of high heat flow on the East Pacific Rise. *Marine Geology*, 7 (5), 427-447.
- Bowie, A.R, Achterberg, E.P., Blain, S., Boye, M.,Croot, P.L., De Baar, H.J.W., Laan, P., Sarthou, G., Worsfold, P.J. (2003), Shipboard analytical intercomparison of dissolved iron in surface waters along a north-south transect of the Atlantic Ocean. *Marine Chemistry* 84 (1-2), 19-34.
- Bowie, A.R, Achterberg, E.P., Croot, P.L., De Baar, H.J.W., Laan, P., Moffett, J.W., Ussher, S., Worsfold, P.J. (2006), A community-wide intercomparison exercise for the determination of dissolved iron in seawater. *Marine Chemistry* 98 (1): 81-99.
- Boyd, P.W., Jickells, T., Law, C.S., Blain, S., Boyle, E.A., Buesseler, K.O. Coale, K.H.,
- Cullen, J.J., De Baar, H.J.W., Follows, M., Harvey, M., Lancelot, C., Levasseur, M., Owens, N.J.P., Pollard, R. Rivkin, R.B. Sarmiento, J., Schoemann, V., Smetacek, V., Takeda, V. Tsuda, A. Turner, S.,Watson, A. (2007), Mesoscale Iron Enrichment Experiments 1993–2005: Synthesis and Future Directions. *Science* 315, 612-617.

- Boye, M., van den Berg, C.M.G., De Jong, J.T.M., Leach, H., Croot, P., De Baar, H.J.W. De Baar (2001), Organic complexation of iron in the Southern Ocean. *Deep Sea Research Part I* 48 (6), 1477-1497.
- Boyle, E.A., Bergquist, B.A., Kayser, R.A. and Mahowald, N. (2005), Iron, manganese, and lead at Hawaii Ocean Time-series station ALOHA: Temporal variability and an intermediate water hydrothermal plume. *Geochimica et Cosmochimica Acta* 69 (4), 933-952.
- Buma, A.G.J., H.J.W. de Baar, R.F. Nolting, A.J. van Bennekom (1991), Metal enrichment experiments in the Weddell-Scotia Seas: Effects of iron and manganese on various plankton communities. *Limnol. Oceanogr.* 36(8): 1865-1878
- Cassar, N, Bender, M.L., Barnett, B.A., Fan, S., Moxim, W.J., Levy II, H., Tilbrook, B.(2007), The Southern Ocean Biological Response to Aeolian Iron Deposition, *Science* 317 (1067-1070).
- Coale, K.H., Johnson, K.S., Fitzwater, S.E., Gordon, R.M., Tanner, S., Chavez, F.P., et al. (1996), A massive phytoplankton bloom induced by an ecosystem-scale iron fertilization experiment in the equatorial Pacific Ocean. *Nature* 383, 495-501.
- Coale, K.H., Gordon, R.M., Wang, X. (2005), The distribution and behavior of dissolved and particulate iron and zinc in the Ross Sea and Antarctic Circumpolar current along 170°W. *Deep Sea Research I* 52, 295-318.
- Croot, P.L., Andersson, K., Öztürk, M. and Turner, D.R. (2004), The distribution and speciation of iron along 6°E in the Southern Ocean. *Deep Sea Research Part II* 51 (22-24), 2857-2879.
- Croot, P.L, Baars, O., Streu, P. (2011), The distribution of dissolved zinc in the Atlantic sector of the Southern Ocean. *Deep Sea Research Part II*, 58 (25-26), 2707-2719
- De Baar, H.J.W., A.G.J. Buma, R.F. Nolting, G.C. Cadée, G. Jacques and P.J. Tréguer (1990), On iron limitation of the Southern Ocean: experimental observations in the Weddell and Scotia Seas. *Mar. Ecol. Prog. Ser.*, 65, 105-122
- De Baar, H.J.W., De Jong, J.T.M., Bakker, D.C.E., Löscher, B., Veth, C., Bathman, U., Smetacek, V. (1995), Importance of iron for plankton blooms and carbon dioxide drawdown in the Southern Ocean. *Nature*, 373 (6513): 412-415.
- De Baar, H.J.W., M.A. van Leeuwe, R.A. Scharek, L. Goeyens, K. Bakker and P. Fritsche (1997) Nutrient anomalies in *Fragilariopsis kerguelensis* blooms, iron deficiency and the nitrate/phosphate ratio (A.C. Redfield) of the Antarctic Ocean. *Deep-Sea Research II*, 44 (1/2), 229-260.
- De Baar, H.J.W., P.M. Boyd (2000), The Role of Iron in Plankton Ecology and Carbon Dioxide Transfer of the Global Oceans. Chapter 4 in: Hanson, R.B., Ducklow, H.W. and Field, J.G. (Eds.), *The Dynamic Ocean Carbon Cycle: A Midterm Synthesis of the Joint Global Ocean Flux Study*, International Geosphere Biosphere Programme Book Series, Vol. 5, Cambridge University Press, (ISBN 0 521 65603 6), 61-140.
- De Baar, H.J.W., de Jong, J.T.M.(2001), Distributions, Sources and Sinks of Iron in Seawater. Chapter 5 in: Turner, D. and Hunter, K.A. (eds.) *Biogeochemistry of Iron in Seawater*, IUPAC Book Series on Analytical and Physical Chemistry of Environmental Systems, Volume 7, pp. 123-254.
- De Baar, H.J.W., De La Roche, J.(2003), Metals in the Oceans; Evolution, Biology and Global change. In F. Lamy and G. Wefer (eds.) *Marine Scientific Frontiers for Europe*, Springer Verlag, Berlin, pp79-105.

- De Baar, H.J.W., Boyd, P.W., Coale, K.H., Landry, M.R., Tsuda, A.K., Assmy, P., Bakker, D.C.E., Bozec, Y., Barber, R.T., Brzezinski, M.A., Buesseler, K.O., Boyé, M., Croot, P.L., Gervais, R.F., Gorbunov, M.Y., Harrison, P.J., Hiscock, W.T., Laan, P., Lancelot, C., Law, C., Levasseur, M., Marchetti, A., Millero, F. J., Nishioka, J., Nojiri, Y., van Oijen, T., Riebesell, U., Rijkenberg, M.J.A., Saito, H., Takeda, S., Timmermans, K.R., Veldhuis M.J.W., Waite, A.M. (2005), Synthesis of iron fertilization experiments: From the Iron Age in the Age of Enlightenment. *Journal of Geophysical Research* 110, C09S16, doi1029/2004JC002601
- De Baar, H.J.W., Timmermans, K.R., Laan, P., De Porto, H.H., Ober, S., Blom, J.J., Bakker, M.C., Schilling, J., Sarthou, G., Smit, M.G., Klunder, M. (2008), Titan: A new facility for ultraclean sampling of trace elements and isotopes in the deep oceans in the international Geotraces program. *Marine Chemistry* 111(1-2), 4-21.
- De Jong, J.T.M., Den Das, J., Bathmann, U., Stoll, M.H.C., Kattner, G., Nolting, R.F., De Baar, H.J.W. (1998), Dissolved iron at subnanomolar levels in the Southern Ocean as determined by ship-board analysis. *Analytica Chimica Acta* 377, 113-124.
- Duce, R.A. and Tindale, N.W. (1991), Atmospheric transport of iron and its deposition in the ocean. *Limnology and Oceanography* 36, 1715-1726
- Draxler, R.R., Rolph, G.D., 2003. HYSPLIT (HYbrid Single-Particle
- Lagrangian Integrated Trajectory) model access via NOAA ARL READY
- website /<http://www.arl.noaa.gov/ready/hysplit4.htSMLS>. NOAA Air
- Resources Laboratory, Silver Spring, MD.
- Edwards, R., Sedwick, P., Morgan, V., Boutron, C.F., Hong, R. (1998), Iron in ice cores from Law Dome, East Antarctica: implications for past deposition of aerosol iron. *Annals of Glaciology* 27, 365-370.
- Edwards, R. and Sedwick, P. (2001), Iron in East Antarctic snow; Implication for atmospheric iron deposition and algal production in Antarctic waters. *Geophysical Research Letters*, 28 (20), 3907-3910.
- Eicken, H., Salinity Profiles of Antarctic Sea Ice: Field Data and Model Results (1992), *J. Geophys. Res.* 97 (10), 15545-15557.
- Elrod, V.A., Berelson, W.M., Coale, K.H., Johnson, K.S. (2004), The flux of iron from continental shelf sediments: A missing source for global budgets. *Geophys. Res. Lett.* 31, L12307, doi: 10.1029/2004GL020216
- Froelich, P.N., Klinkhammer, G.P., Bender, M.L., Luedtke, N.A., Heath, G.R.,
- Cullen, D., Dauphin, P., Hammond, D., Hartman, B., Maynard, V. (1979), Early
- oxidation of organic matter in pelagic sediments of the eastern equatorial Atlantic:
- suboxic diagenesis. *Geochimica et Cosmochimica Acta* 43 (7), 1075-1090.
- Fung, I.Y., Meyn, S.K., Tegen, I., Doney, S.C., John, S.G., Bisshop, J.K.G. (2000), Iron Supply and Demand in the Upper Ocean. *Global Biogeochemical Cycles* 14 (1), 281-295.
- Garrity, C., Romseier, R.O., Peinert, R., Kern, S., Fisher, G. (2005), Water-column particulated organic carbon modeled fluxes in the ice-frequented Southern Ocean. *Journal of Marine Systems* 56, 133-149.
- Gladyshev, S., Arhan, M., Sokov, A. and Speich, S. (2008), A hydrographic section from South Africa to the southern limit of the Antarctic Circumpolar Current at the Greenwich meridian. *Deep Sea Research Part I* 55(10), 1284-1303.

- Gordon, A.L., Taylor, H.W., Georgi, D.T. (1977), Antarctic oceanography zonation. In: M.J. Dunbar (eds.), *Polar Oceans*. Arct. Inst. N. America (McGill University Montreal).
- Gran, H.H. (1931), On the conditions for the production of plankton in the sea. *Rapports et Proces-verbaux Conseil Permanent d'Exploration de la Mer* 75, 37-46.
- Gregg, W.W., Ginoux, P., Schopf, P.S. and Casey, N.W. (2003), Phytoplankton and iron: validation of a global three-dimensional ocean biogeochemical model. *Deep Sea Research Part II* 50 (22-26), 3143-3169.
- Han, Q., Moore, J.K., Zender, C., Measures, C. and Hydes, D. (2008), Constraining oceanic dust deposition using surface ocean dissolved Al. *Global Biogeochemical Cycles* 22, GB2003, doi:10.1029/2007GB002975.
- Hand, J. L., Mahowald, N. M., Chen, Y., Siefert, R. L., Luo, C., Subramaniam, A., Fung, I. (1999), Estimates of atmospheric-processed soluble iron from observations and a global mineral aerosol model: Biogeochemical implications. *Journal of Geophysical Research* 109, D17205, doi:10.1029/2004JD004574.
- Hart, T.J. (1934), On the phytoplankton of the Southwest Atlantic and the Bellingshausen Sea, 1929-1931. *Discovery Reports* 8, 1-68.
- Hart, T.J. (1942), Phytoplankton periodicity in Antarctic surface waters. *Discovery Reports* 21, 261-365.
- Hoppema, M., Middag, R., De Baar, H.J.W., Fahrbach, E., van Weerlee, E., Thomas, H. (2007), Whole season net community production in the Weddell Sea. *Polar Biology* 31, 101-111.
- Hutchins, D.A., Bruland, K.W. (1994), Grazer mediated regeneration and assimilation of Fe, Zn and Mn from planktonic prey. *Marine Ecology Progress Series* 110, 259-269
- Jickells T. D and Spokes, L.J. (2001). Atmospheric Iron Inputs to the Oceans. Chapter 4 in: Turner, D. and Hunter, K.A. (eds.) *Biogeochemistry of Iron in Seawater*, IUPAC Book Series on Analytical and Physical Chemistry of Environmental Systems, Volume 7, pp.123-254.
- Jickells, T.D., An, T.S., Andersen, K.K., Baker, A.R., Bergametti, G., Brooks, N., Cao, J.J., Boyd, P.W., Duce, R.A., Hunter, K.A., Kawahata, H., Kubilay, N., laRoche, J., Liss, P.S., Mahowald, N., Prospero, J.M., Ridgwell, A.J., Tegen, I., Torres, R. (2005), Global Iron Connections Between Desert Dust, Ocean Biogeochemistry, and Climate, *Science* 308 (67), 67-71.
- Johnson, K.S., Boyle, E., Bruland, K., Measures, C., Moffett, J., Aquilarislas, A., Barbeau, K., Cai, Y., Chase, Z., Cullen, J., Doi, T., Elrod, V., Fitzwater, S., Gordon, M., King, A., Laan, P., Laglera-Baquer, L., Landing, W., Lohan, M., Mendez, J., Milne, A., Obata, H., Osslander, L., Plant, J., Sarthou, G., Sedwick, P., Smith G.J., Sohst, B., Tanner, S., Van Den Berg, S., Wu, J. (2007), Developing Standards for Dissolved Iron in Seawater, *Eos Transactions of the AGU* 88 (11), 131.
- Klatt, O., Fahrbach, E., Hoppema, M. and Rohardt, G. (2005), The transport of the Weddell Gyre across the Prime Meridian. *Deep Sea Research Part II* 52 (3-4), 513-528.
- Klinkhammer, G.P., Chin C.S., Keller, R.A., Dählman, A., Sahling, H., Sarthou, G., Petersen, S., Smith, F., Wilson, C. (2001), Discovery of new hydrothermal vent sites in Bransfield Strait, Antarctica. *Earth and Planetary Science Letters* 193 (3-4), 395-407.
- Laës, A., Blain, S., Laan, P., Achterberg, E.P., Sarthou, G., De Baar, H.J.W., (2003), Deep dissolved iron profiles in the eastern North Atlantic in relation to water masses. *Geophys. Res. Lett.* 30 (17), 1-3.

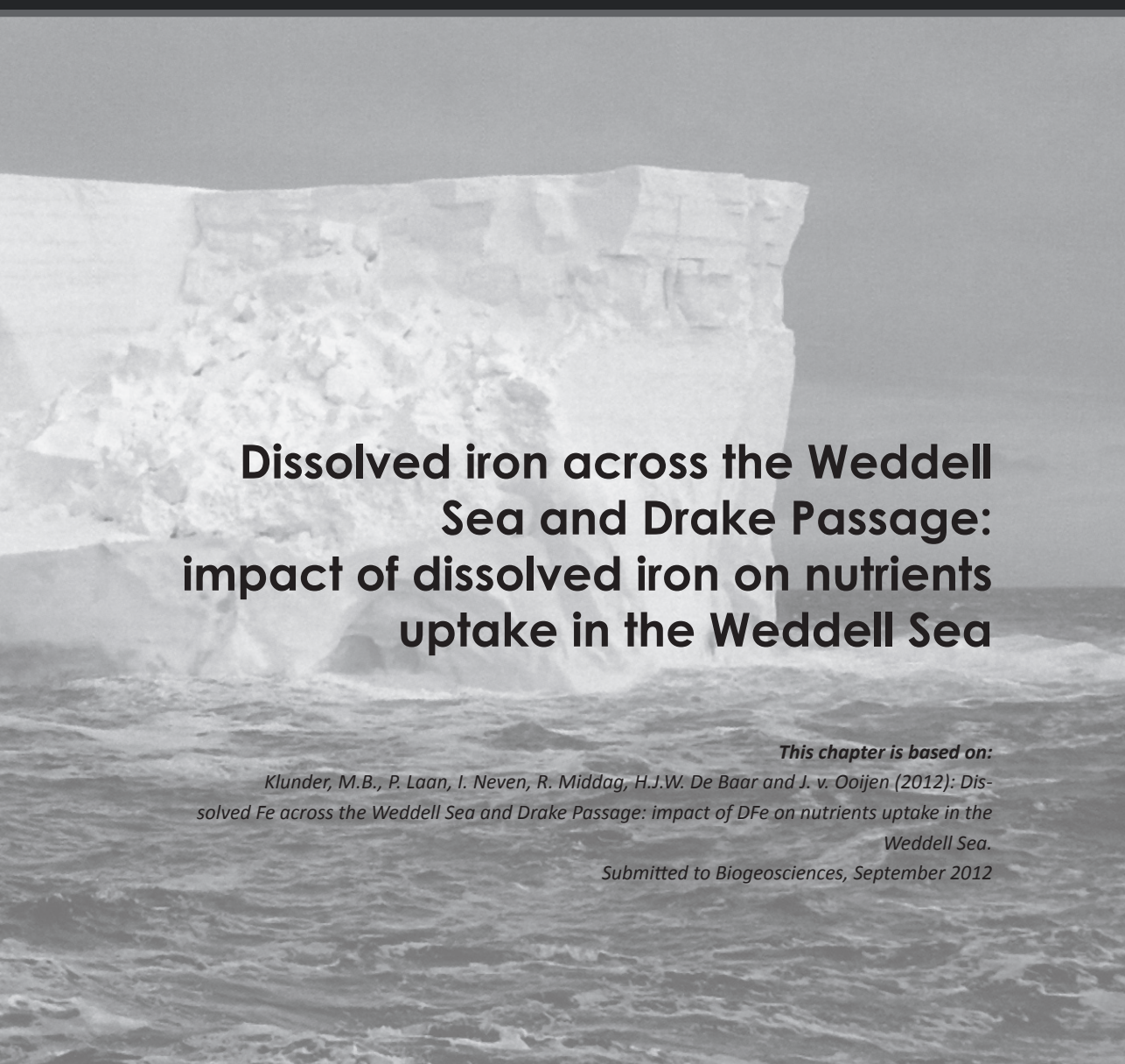
- Laës, A., Baker, A.R., Kramer, J., Laan, P., Ussher, S., Achterberg, E.P., De Baar, H.J.W., Timmermans, K.R., Blain, S. (2007), Sources and transport of dissolved iron and manganese along the continental margin of the Bay of Biscay. *Biogeosciences* 4, 181-194.
- Lai, X., Norisuye, K., Mikata, M., Minami, T., Bowie A.R., Sohrin, Y. (2008), Spatial and temporal distribution of Fe, Ni, Cu and Pb along 140°E in the Southern Ocean during austral summer 2001/02. *Mar. Chem.* 111, 171-183.
- Lam, P.J., Bishop, J.K.B., Henning, C.C., Marcus, M.A., Waychunas, G.A., Fung, I. (2006), Wintertime phytoplankton bloom in the subarctic Pacific supported by continental margin iron. *Global biogeochemical Cycles* 20, GB1006, doi:10.1029/2005GB002557
- Lancelot, C., de Montety, A., Goosse, H., Becquevort, Schoemann, V., Pasquer, B., Vancoppenolle, M. (2009), Spatial distribution of the iron supply to phytoplankton in the Southern Ocean: a model study. *Biogeosciences Discussions* 6, 4919-4962.
- Lannuzel, D., V. Schoemann, J.T.M. De Jong, L. Chou, B. Delille, S. Becquevort, J.-L. Tison (2008), Iron study during a time series in the western Weddell pack ice. *Marine Chemistry* 108(1-2), 85-95.
- Löscher, B.M., De Baar, H.J.W., De Jong, J.T.M., Veth, C. and Dehairs, F. (1997), The distribution of Fe in the antarctic circumpolar current. *Deep Sea Research Part II* 44 (1-2), 143-187.
- Mackie D.S., Peat, J.M., McTainsh, G.H., Boyd, P.W., Hunter, K.A. (2006), Soil abrasion and eolian dust production: implications for iron partitioning and solubility. *Geochemistry Geophysics Geosystems* 7, 12, doi: 10.1029/2006GL026557,
- Mahowald, N., Kohfeld, K., Hansson, M., Balkanski, Y., Harrison, S.P., Prentice, I.C., Schulz, M., and Rodhe H. (1999), Dust sources and deposition during the last glacial maximum and current climate: A comparison of model results with paleodata from ice cores and marine sediments. *Journal of Geophysical Research* 104 (D13), 15,895–15,916.
- Mahowald, N.M., Baker, A.R., Bergametti, G., Brooks, N., Duce, R.A., Jickells, T.D., Kubilay, N., Prospero, J.M., Tegen, I., 2005. Atmospheric global dust cycle and iron inputs to the ocean. *Global Biogeochemical Cycles* 19 (4025). doi:10.1029/2004GB002402
- Martin, J.H. and Fitzwater, S.E. (1988), Iron deficiency limits phytoplankton growth in the north-east Pacific subarctic. *Nature*, 331 (6154), 341-343.
- Measures, C.I. and Vink, S. (2001), Dissolved Fe in the upper waters of the Pacific sector of the Southern Ocean. *Deep Sea Research Part II* 48 (19-20), 3913-3941.
- Measures, C.I., Landing W.M., Brown, M.T., Buck, C.S. (2008), High-resolution Al and Fe data from the Atlantic Ocean CLIVAR-CO2 Repeat Hydrography A16N transect; Extensive linkages between atmospheric dust and upper ocean geochemistry. *Global Biogeochemical Cycles* 22, GB 1005, doi: 10.1029/2007GB003042
- Middag R., De Baar, H.J.W., Laan, P., Bakker, K. (2009), Dissolved Aluminium and the silicon cycle in the Arctic Ocean. *Marine Chemistry* 115, 176-195.
- Middag, R., De Baar, H.J.W., Laan, P., Cai, P., van Ooijen, J.C. (2011a), Dissolved Manganese in the Southern Ocean. *Deep-Sea Research II*, 58 (25-26), 2661-2677.
- Middag, R., van Slooten, C., De Baar, H.J.W., Laan, P. (2011b), Dissolved Aluminium in the Southern Ocean. *Deep-Sea Research II*, 58 (25-26), 2647-2660.
- Moore, J.K. and Braucher, O. (2008), Sedimentary and mineral dust sources of dissolved iron to the world ocean. *Biogeosciences* 5 (3), 631-656.

- Neven, I., Stefels, J., De Baar, H.J.W., Elzenga, T. (2011), High adaptability in inorganic carbon uptake by Southern Ocean phytoplankton in response to ambient CO₂. *Deep-Sea Research II*, 58 (25-26), 2636-2646.
- Nishioka, J., S. Takeda, H.J.W. De Baar, P.L. Croot, M. Boye, P. Laan, K.R. Timmermans (2005), Changes in the concentration of iron in different size fractions during an iron enrichment experiment in the open Southern Ocean. *Marine Chemistry* 95 (1-2), 51-63.
- Orsi, A.H., Whitworth, T. and Nowlin, W.D.(1995), On the meridional extent and fronts of the Antarctic Circumpolar Current. *Deep Sea Research Part I: Oceanographic Research Papers*, 42(5), 641-673.
- Parekh, P., Follows, M.J. and Boyle, E. (2004), Modeling the global ocean iron cycle. *Global Biogeochemical Cycles* 19, GB 2020, doi:10.1029/2004GB002280.
- Park, Y.H., Charriaud, E. and Fieux, M. (1998), Thermohaline structure of the Antarctic Surface Water/Winter Water in the Indian sector of the Southern Ocean. *Journal of Marine Systems* 17(1-4): 5-23.
- Planquette, H., P.J. Statham, G.J. Fones, M.A. Charette, C.M. Moore, I. Salter, F. H. Nédélec, S.L. Taylor, M. French, A.R. Baker, N. Mahowald, T. M. Jickells (2007), Dissolved iron in the vicinity of the Crozet Islands, Southern Ocean. *Deep Sea Research Part II: Topical Studies in Oceanography* 54(18-20): 1999-2019.
- Pollard, R.T. et al.(2009), Southern Ocean deep-water carbon export enhanced by natural iron fertilization. *Nature*, 457(7229): 577-580.
- Rutgers van der Loeff, M., Cai, P., Stimac, I., Bracher, A., Middag, R., Klunder, M.B., van Heuven, S. (2011), ²³⁴Th in surface waters: distribution of particle export flux across the Antarctic Circumpolar Current and in the Weddell Sea during the GEOTRACES expedition ZERO and DRAKE. *Deep-Sea Research II*, 58 (25-26), 2749-2766.
- Sarthou, G., Baker, A.R., Blain, S., Achterberg, E.P., Boye, M., Bowie, A., Croot., P.L., Laan, P., De Baar, H.J.W., Jickells, T.M., Worsfold, P.F. (2003), Atmospheric iron deposition and sea-surface dissolved iron concentrations in the eastern Atlantic Ocean. *Deep Sea Research I*, 50 (10-11), 1339-1352.
- Sarthou, G., Timmermans, K.R., Blain, S. and Tréguer, P. (2005), Growth physiology and fate of diatoms in the ocean: a review. *Journal of Sea Research* 53 (1-2), 25-42.
- Sarthou, G., Vincent, D., Christaki, U., Obernosterer, I., Timmermans, K.R., Brussaard, C.P.D. (2008), The fate of biogenic iron during a phytoplankton bloom induced by natural fertilisation: Impact of copepod grazing. *Deep Sea Research Part II: Topical Studies in Oceanography* 55 (5-7), 734-751.
- Schlitzer R., Ocean Data View, <http://odv.awi.de>, 2009.
- Sedwick, P.N., Edwards, P.R., Mackey, D.J., Griffiths, F.B., Parslow, J.S.(1997), Iron and manganese in surface waters of the Australian subantarctic region. *Deep-Sea Research I* 44, 1239-1253.
- Sedwick, P.N., Bowie, A.R., Trull, T.W. (2008), Dissolved iron in the Australian sector of the Southern Ocean (CLIVAR SR3 section); Meridional and seasonal trends. *Deep Sea Research I* 55, 911-925.
- Sohrin, Y., Iwamoto, S., Matsui, M., Obata, H., Nakayama, E., Suzuki, K., Handa, N., Ishii, H. (2000), The distribution of Fe in the Australian Section of the Southern Ocean. *Deep-Sea Research Part I* 47 (1), 55-84

- Sunda, W.G. and Huntsman, S.A.(1997), Interrelated influence of iron, light and cell size on marine phytoplankton growth. *Nature* 390, 389-392, doi: 10.1038/37093
- Sunda, W.G. (2001), Bioavailability and Bioaccumulation of iron in the sea. Review chapter 3 in: Turner, D. and Hunter, K.A. (eds.) *Biogeochemistry of Iron in Seawater*, IUPAC Book Series on Analytical and Physical Chemistry of Environmental Systems, Volume 7, 123-254.
- Tagliabue, A., Bopp, L., Aumont, O. (2009), Evaluating the importance of atmospheric and sedimentary iron sources to Southern Ocean biogeochemistry. *Geophys. Res. Lett.* , 36, L13601, doi:10.1029/2009GL038914.
- Taylor S. R. and McLennan S. M. , 1985 *The Continental Crust: Its Composition and Evolution*. Blackwell.
- Thuróczy, C.-E., Gerringa, L.J.A, Klunder, M.B., Laan, P., De Baar H.J.W. (2011), . Observation of consistent trends in the organic complexation of dissolved iron in the Atlantic Sector of the Southern Ocean, 2011. *Deep-Sea Research II*, 58 (25-26), 2678-2694.
- Tovar-Sanchez, A., Duarte, C.M.,Hernández-Léon S.,Sañudo-Wilhelmy, S.A. (2007), Krill as a central node for iron cycling in the Southern Ocean. *Geophys. J Res. Lett.* 34: L61101.
- Twining, B. S., Baines, S.B., Fisher, N.S., Landry, M.R. (2004), Cellular iron contents of plankton during the Southern Ocean Iron Experiment (SOFEX). *Deep-Sea Research part I* 51, 1827-1850.
- Veth, C., Peeken, I. and Scharek, R. (1997), Physical anatomy of fronts and surface waters in the ACC near the 6°W meridian during austral spring 1992. *Deep Sea Research Part II* 44 (1-2), 23-49.
- Walter, H.J., Rutgers van der Loeff, M.M., Höltnen, H. and Bathmann, U. (2000), Reduced scavenging of ²³⁰Th in the Weddell Sea: implications for paleoceanographic reconstructions in the South Atlantic. *Deep Sea Research Part I* 47(7), 1369-1387.
- Wedepohl, K.H. The composition of the continental crust (1995), *Geochimica et Cosmochimica Acta* 59 (7), 1217-1232.
- Wolff, E. W., Hall, E.J., Mulvaney, R., Pasteur, E.C., Wagenbush, D., Legrand, M. (1998), Relationship between chemistry of air, fresh snow and firn cores for aerosol species in coastal Antarctica. *J. Geophys. Res.* 103, (11), 057–11,070.
- Worby, A. P., Geiger, C.A., Paget, M.J., Van Woert, M.L., Ackley, S.F., DeLiberty, T.L. (2008), Thickness distribution of Antarctic sea ice. *J. Geophys. Res.* 113, C05S92, doi:10.1029/2007JC004254.
- Wu, J., Boyle, E., Sunda, W. and Wen, L.-S. (2001), Soluble and Colloidal Iron in the Oligotrophic North Atlantic and North Pacific. *Science* 293, 847-849.



Chapter 5



Dissolved iron across the Weddell Sea and Drake Passage: impact of dissolved iron on nutrients uptake in the Weddell Sea

This chapter is based on:

Klunder, M.B., P. Laan, I. Neven, R. Middag, H.J.W. De Baar and J. v. Ooijen (2012): Dissolved Fe across the Weddell Sea and Drake Passage: impact of DFe on nutrients uptake in the Weddell Sea.

Submitted to Biogeosciences, September 2012

Abstract

This chapter reports the first full depth distributions of dissolved iron (DFe) over a high resolution Weddell Sea transect and Drake Passage transect. Very low dissolved DFe concentrations (0.01-0.1 nM range) are observed in the surface waters in the Weddell Sea, and within the Polar regime in the Drake Passage. Locally, enrichment in surface DFe is observed, likely due to recent ice melt (Weddell Sea) or dust deposition (Drake Passage). In the Weddell Sea, the low DFe concentrations can be partly explained with high POC export and/or primary production (indicated by chlorophyll fluorescence). As expected, in high DFe regions a strong silicate drawdown compared to nitrate drawdown is observed, although this appears not to be caused by the Peninsula shelf. In the Western Weddell Sea transect, with relatively small diatoms, no relationship between N:P and N:Si removal ratios and DFe is observed, whereas in the at the Greenwich Meridian, where diatoms are significantly larger, the N:P and N:Si removal ratio increased with increasing DFe. These findings confirm the important role of DFe in Southern Ocean (biologically mediated) nutrient cycles. Higher DFe concentrations of > 1.5 nM over the shelf around the Antarctic Peninsula. These are a source of Fe by lateral transport along isopycnal surfaces into the Drake Passage. At the South American continent, high (>2 nM) DFe concentrations is caused by fluvial/glacial input of DFe. On the Weddell Sea side of the Peninsula region, formation of deep water (by downslope convection) causes relatively high Fe (0.6-0.8 nM) concentrations in the bottom waters relative to the water masses at mid depth (0.2-0.4 nM). During transit of Weddell Sea Bottom Water to Drake Passage, through the Scotia Sea, extra DFe is taken up from seafloor sources, resulting in highest bottom water concentrations in the southernmost part of the Drake Passage of >1 nM. The Weddell Sea Deep Water concentrations (~0.32 nM) are consistent with the (lowest) DFe concentrations observed in Atlantic AABW.

5.1 Introduction

5.1.1 Rationale

It is now well established that phytoplankton growth in the High-Nutrient Low-Chlorophyll (HNLC) Southern Ocean is severely limited as a result of low Fe concentrations [De Baar *et al.*, 1990; Buma *et al.*, 1991; De Baar *et al.*, 1995] in combination with light limitation due to deep mixing [Mitchell *et al.*, 1991; Lancelot *et al.*, 2000; De Baar *et al.*, 2005] as well as photo-inhibition [Alderkamp *et al.*, 2010, 2011]. Although there have been very little deep water values of dissolved Fe (DFe) in the Weddell Sea reported in the literature [De Jong *et al.*, 2012], several studies have reported dissolved Fe values in the upper waters [Sanudo-Wilhelmy *et al.* 2002; Lannuzel *et al.*, 2008; Lin *et al.*, 2011].

North of the Antarctic Peninsula, the ~800 km wide Drake Passage is the narrowest opening between Antarctica and the South American continent. The eastward flowing Antarctic Circumpolar Current (ACC) is forced through the narrow Drake Passage, resulting in strong velocities [Sokolov and Rintoul, 2007]. Thus far no data did exist for dissolved Fe in the complete deep water column of the Drake Passage. However in the upper water column the distribution of (dissolved) iron (DFe) in the region around the Antarctic Peninsula is relatively well studied in recent years [Sanudo-Wilhelmy *et al.*, 2002; Lin *et al.*, 2011]. Some studies focus specifically on the peninsula region because of the important role that Fe plays in the phytoplankton blooms observed close to the Peninsula and further east, following the main currents [Dulaiova *et al.*, 2009; Ardelan *et al.*, 2010].

The GEOTRACES program of the International Polar Year 2007-2008 was designed to produce the first-ever deep ocean sections of dissolved Fe and other (bio-essential) trace metals in the polar oceans. The expedition ANT/XXIV/3 aboard ice-breaker R.V. Polarstern in 2008 [Fahrbach *et al.*, 2011] comprises the two first deep sections of dissolved Fe across the Weddell Sea and Drake Passage, respectively, reported here together with a complete deep section of dissolved Fe along the Greenwich meridian [Klunder *et al.*, 2011].

5.1.2 Sources of Fe to the Southern Ocean

There are several input sources of Fe to the surface waters of the Southern Ocean. Possibly the most important is the supply from below of (Fe rich) deep waters [De Baar *et al.*, 1995, their Table 1; Löscher *et al.*, 1997; Hoppema *et al.*, 2003; Croot *et al.*, 2004; Klunder *et al.*, 2011]. Estimates of input of DFe by upwelling range from ~53.6 $\mu\text{mol m}^{-2} \text{y}^{-1}$ in the ACC [Löscher *et al.*, 1997] to 34 $\mu\text{mol m}^{-2} \text{y}^{-1}$ (ACC) and 31.6 $\mu\text{mol m}^{-2} \text{y}^{-1}$ (Weddell Gyre) [Klunder *et al.*, 2011]. Atmospheric dust deposition is deemed to be very low [Jickells *et al.*, 2005] and melting of free floating icebergs, that previously were grounded on shelves and carry , sediment supplies Fe to surrounding waters [Löscher *et al.*, 1997; Lin *et al.*, 2011]. Both atmospheric dust input and iceberg melting are episodic, and a challenge to assess in a basin wide or annual supply estimate. Nevertheless, the modelling results from Raiswell [2011], indicated that input of bio available Fe to the Weddell Sea by icebergs may be as large as total dust input ($5.6 \times 10^5 - 1.8 \times 10^7 \text{ mol Fe/100 days melting}$). Rare events of dust deposition were observed along the Greenwich Meridian [Klunder *et al.*, 2011; Middag *et al.*, 2011; 2012]. Anoxia in pore waters of shelf sediments causes dissolution of reduced Fe [Elrod *et al.*, 2004], some of which by either sediment resuspension [Luther and Wu, 1997] and/or eddy diffusion enters overlying waters. Upon entrainment and mixing these Fe enriched shelf waters are found around and beyond the Antarctic Peninsula [Dulaiova *et al.*, 2009] and in the island archipelago's like the Kerguelen plateau [Bucciarelli *et al.*, 2001; Blain *et al.*, 2007; Chever *et al.*, 2010] and Crozet islands [Planquette *et al.*, 2007]. In the Drake Passage, eddy activity may involve both

upwelling and downwelling and thereby influence the distribution of DFe [Kahru *et al.*, 2007]. Phytoplankton blooms observed at and close to the Antarctic Peninsula shelf regions may be explained by the delivery of shelf derived DFe. There are several lines of evidence that limited availability of DFe for phytoplankton may influence the uptake ratio of nutrients in the Southern Ocean [De Baar *et al.*, 1997; Takeda, 1998; Marchetti and Cassar, 2009]. Upon Fe deficiency the cellular N content decreases, leading to lower N/P ratio of plankton. For diatoms, that generally continue to produce the opaline (SiO₂) frustules, this implies a lowering of their overall N/Si content [Takeda *et al.*, 1998 and overview by Marchetti and Cassar, 2009]. Moreover, Hoppema *et al.* [2007] have shown less Si removal relative to C removal and more Si relative to N removal in the surface waters approaching the Peninsula region, which they attributed to better DFe availability.

In the deep waters, the North Atlantic Deep Water (NADW) enters the ACC at ~2000-3000 m depth [Klunder *et al.*, 2011]. This iron-rich water mass (Fe~0.7 nM) eventually flows into the Weddell Sea as Warm Deep Water. In the Weddell Sea, this water becomes incorporated in the Weddell Gyre System. The return flow to the ACC is largely Weddell Sea Deep Water, which leaves the Weddell Gyre northwards over the Scotia Ridge, into the Scotia Sea and further north into the worlds abyssal oceans as Antarctic Bottom Water (AABW) [Naveira Garabato *et al.*, 2002]. The deep Drake Passage is dominated by Circumpolar Deep Waters which contain generally ~0.4-0.5 nM DFe [Klunder *et al.*, 2011]. However, at the ~2000 m depth at the Patagonian Continental Shelf, an additional water mass derived from the East Pacific Ocean, carrying hydrothermal properties (Well *et al.* [2003]; Sudre *et al.* [2011]).

In this study we present the distribution of dissolved (<0.2 μ m fraction) iron (DFe) over two transects, one crossing the Weddell Sea and one crossing the Drake Passage. The first transect comprises 8 stations in the Weddell Sea, from the Central Weddell Sea (17°E) towards onto the Antarctic Peninsula shelf close to Joinville Island (Figure 5.1a). The other transect goes from Elephant Island (Figure 5.1b), situated on the shelf to the Northeast of the Antarctic Peninsula.

The simultaneous sampling for trace metals [Middag *et al.*, 2010; 2011; 2012], major nutrients (Si, NO₃, PO₄), biological parameters [Rutgers van der Loeff *et al.*, 2011; Neven *et al.*, 2011] and physical parameters [Fahrbach *et al.*, 2011] allows us to investigate the input of DFe from the Antarctic Peninsula to the surrounding waters in the Weddell Sea and in Drake Passage and to give an estimation of the relative nutrient removals in relation to DFe concentrations. Moreover, other sources and sinks of DFe in the Weddell Sea and Drake Passage are discussed. The DFe data presented here were collected in March 2008, thus towards the end of the vegetative season, when DFe may be depleted and limiting for phytoplankton growth [Sedwick *et al.*, 2000]. This would be reflected in nutrient removal in the months prior to our occupation of the transect. Using the deficit between the remnant winter water and the surface waters an estimation of this nutrient removal can be made [Hoppema *et al.*, 2007]. Here we present estimates for such removal and investigate their relation with DFe availability.

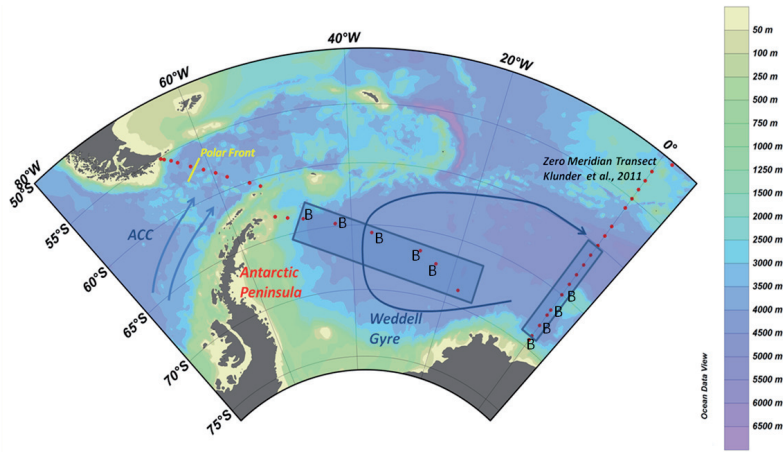


Fig. 1a Sampling region including Weddell Sea and Drake Passage stations (red marked). Also shown are the Weddell Gyre and Antarctic Circumpolar Current (ACC) and Polar Front (schematically). The blue shade shows the stations for which removal is calculated (see text; Fig. 5.6 and 5.7). Stations for which biological (phytoplankton) data is available are marked with a 'B' (see text).

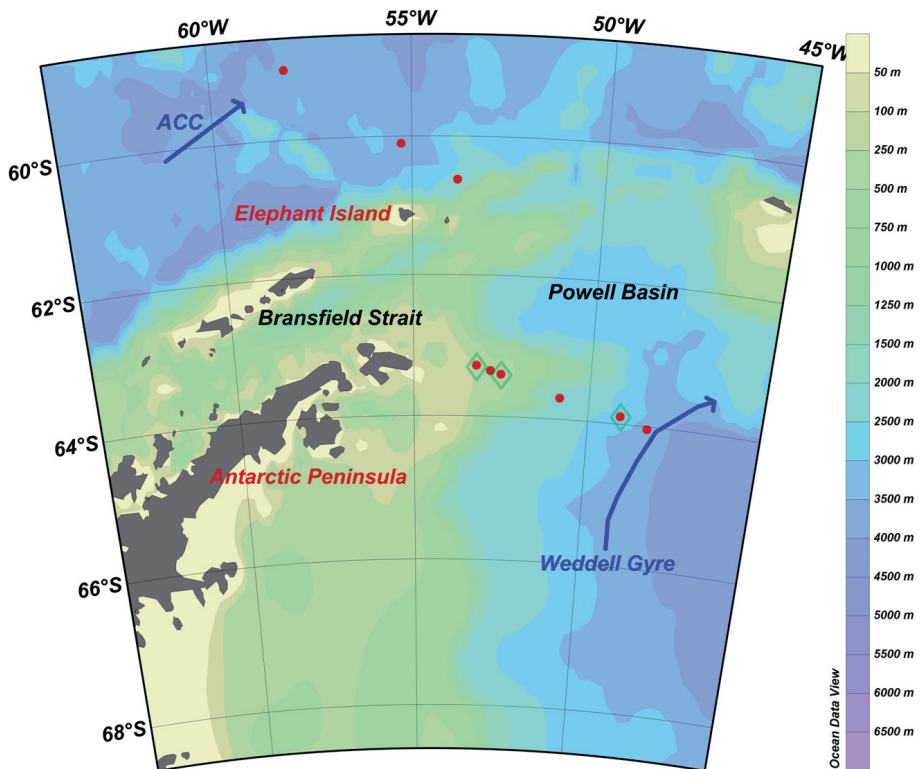


Fig 1b Large scale overview of Peninsula region at expanded regional scale. Sample stations are indicated with red dots; green diamond marks stations with a few (<5) samples. Weddell Gyre and ACC are indicated (schematically).

5.2 Methods

5.2.1 Sampling and analysis

Water samples were collected during the ANT XXIV/3 expedition of *RV Polarstern* between March 15 and April 12, 2008 (Fig. 5.1a). Samples were taken and analysed under clean conditions extensively described in *De Baar et al.* [2008] and Chapters 1, 3 and 4 of this thesis. Seawater was filtered over a 0.2 μm filter cartridge (Sartobran-300, Sartorius) under nitrogen pressure. For each depth replicate samples of DFe were taken in 60 ml HDPE sample bottles and acidified to pH = 1.8 with 12 M HCl (Baseline, Seastar Chemicals) and left overnight. All bottles, used for storage of reagents and samples, were acid cleaned according to a three step cleaning procedure, as described by *Middag et al.* [2010]. We ensured all the Fe was in the Fe (III) form, by adding 60 μl of a 1 % hydrogen peroxide (Merck suprapur 30%), at least one hour before measurement. The DFe was measured using flow injection analysis with luminol chemiluminescence, where DFe was pre-concentrated on an IDA Toyopearl AF-Chelate resin [*Klunder et al.*, 2011]. After pre-concentration, the column was rinsed (60 sec.) with de-ionized ultrapure (DI) water (18.2 M Ω) and subsequently Fe was eluted from the column (120 sec.) using 0.4 M HCl (Merck Suprapur). Pre-concentration time was usually 120 seconds.

5.2.2 Calibration and validation

The system was calibrated using standard additions of Fe to low DFe seawater. For all samples a duplicate sample was taken. For outlying values, profiles of the other trace metals dissolved aluminium (DAI) and manganese (DMn) as well as nutrients were evaluated for consistency. In case no deviations were observed in the other parameters and both the initial and duplicate sample showed an exceptional value, the exceptional data point was considered as erroneous if the value deviated more than +25 % from the expected profile based on linear interpolation between the DFe-concentration in the seawater samples above and below the data point (after *Middag et al.* [2010] and *Klunder et al.* [2010]). Each sample was analysed three times (three peaks) and standard deviation was generally below 5%.

Regularly the combined blank of the 1 min MQ-column wash and the 0.4 M HCl for elution of the column was calculated from the amount of counts measured upon zero (0) seconds loading time. The average value for this blank was 14 \pm 11 pmol (n=18) and this blank did not exceed 40 pM. By double versus single addition of the H₂O₂ it was found that this did not cause a quantifiable blank. The contribution of the Seastar Baselines Hydrochloric Acid is deemed to be negligible (0.04 pM/sample; see *Klunder et al.* [2011]). The detection limit was determined regularly and defined as the standard deviation of 5 peaks of 10 s loading of low-Fe seawater (subsurface minimum), multiplied by 3. Average detection limit was typically 9 \pm 5 pM Fe (n=7),

and the detection limit did not exceed 17 pM Fe. Therefore, in this study, all values < 0.01 nM are presented as 0.01 nM.

In order to validate the accuracy of the system, standard reference seawater was measured regularly, in triplicate. There is SAFe surface (S) water and SAFe deep (D2) water available to validate against different ranges of Fe concentration [Johnson et al. 2007]. The average concentrations we found were 0.085 +/- 0.023 nM (n=16) and 0.958 +/- 0.039 (n=13) for SAFe S and SAFe D2 respectively. These results are fairly consistent with the community consensus values 0.094 +/- 0.008 for SAFe S and 0.923 +/- 0.029 nM for SAFe D2 (www.geotraces.org, datasheet version November 2011).

In order to investigate the relationship between DFe and net nutrient removal in the Weddell Sea, the seasonal nutrient uptake in the upper layer above the Winter Water is calculated. This method and the assumptions needed are described in more detail by *Hoppema et al.* [2002;2007]. Briefly, the difference in nutrient concentration between the Winter Water (subsurface θ minimum <-1.6 °C) and the overlying surface water was calculated. Upon vertical integration, the net seasonal nutrient removal is obtained. To correct for spatial variations in diluting meltwater, concentrations are normalized to a salinity of 34.5. For comparison, also the net removal for the stations situated within the Weddell Gyre at the Greenwich Meridian at 0°W [*Klunder et al.*, 2011] were included. The stations with a Winter Water layer, allowing nutrient removal calculation are situated between 59 - 69°S at the Greenwich meridian and between 17-48.5°W in the west Weddell Sea transect and are marked by the two shaded area's in Fig. 5.1a. Moreover, for discussion of the relation between DFe and nutrients, also the phytoplankton community in our stations is studied. Stations for which phytoplankton data is available are marked with a 'B' in Figure 5.1a. More details about phytoplankton data can be found in [*Neven et al.*, 2011].

5.2.3 Hydrography

Transport of water masses in the Weddell Sea is dominated by the Weddell Gyre, a cyclonic current, with its westward component near the Antarctic continent and an eastward component along Bouvet Ridge (fig. 5.1a; [*Klatt et al.*, 2005; *Fahrbach*, 2004]). Although the whole Weddell Sea is influenced by the gyre, the strongest velocities are observed close to the continental shelves [*Fahrbach et al.*, 1994]. The Weddell Sea is dominated by five water masses distinguished on the basis of potential temperature (θ) and salinity (after *Klatt et al.* [2005]). In the upper surface, the low salinity (<34.6) Antarctic Surface Water (AASW) is found. As remnant of the preceding winter, a θ minimum, marks the Winter Water layer at ~100 m depth (Fig. 5.2a). Below the Winter Water, warm Deep Water is found. This water enters the Weddell Gyre from the Antarctic Circumpolar Current in the North, and carries the Lower Circumpolar Deep Water properties ($\theta > 0$; Sal >34.6) (Fig. 5.2a). The most

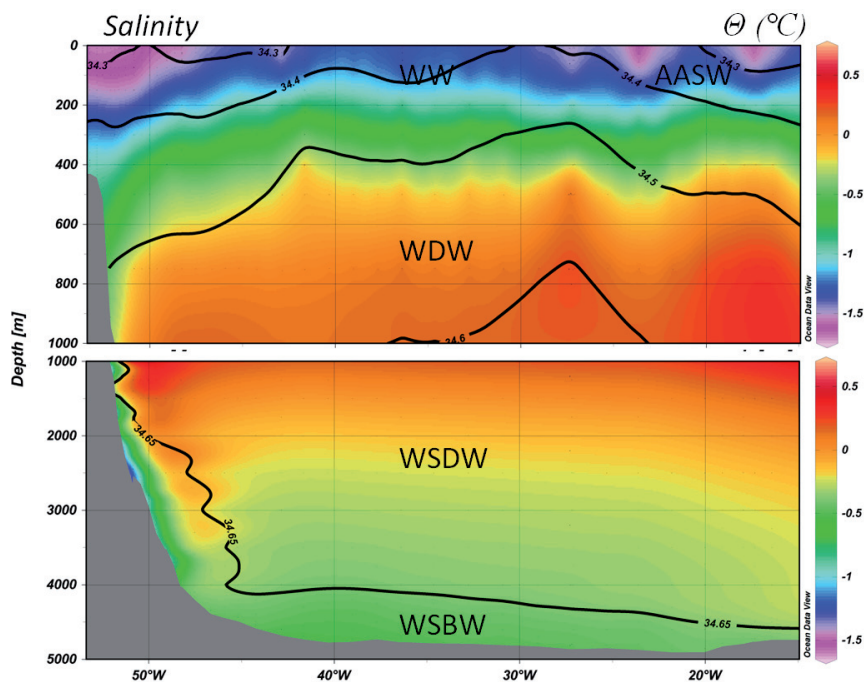


Fig. 5.2a Potential temperature (color) and salinity (contour) section of the Weddell Sea transect. Approximate location of water masses is indicated.

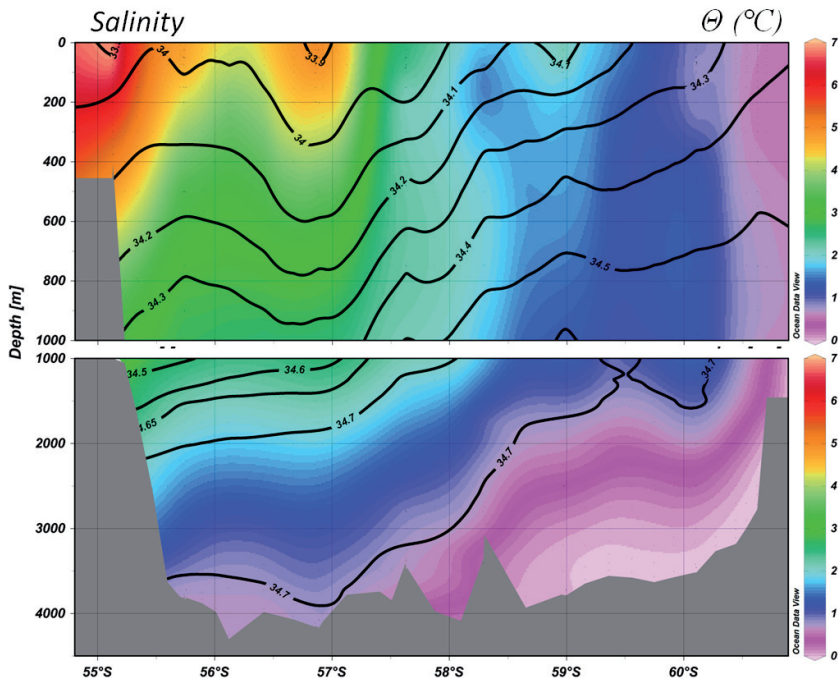


Fig. 5.2b Potential temperature (color) and salinity (contour) section of the Drake Passage transect.

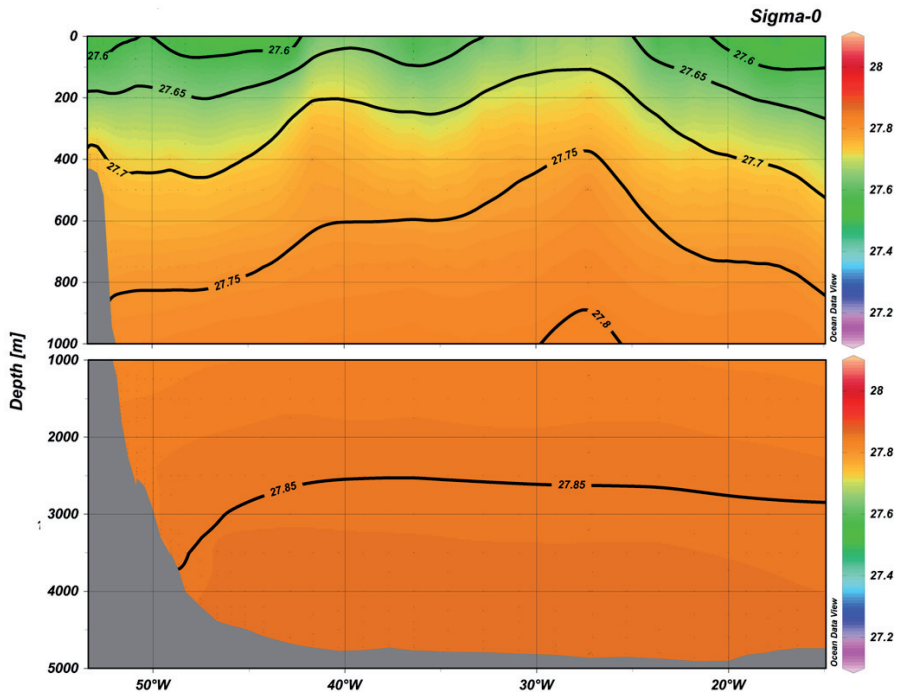


Fig. 5.3a Sigma-theta section of the of the Weddell Sea transect

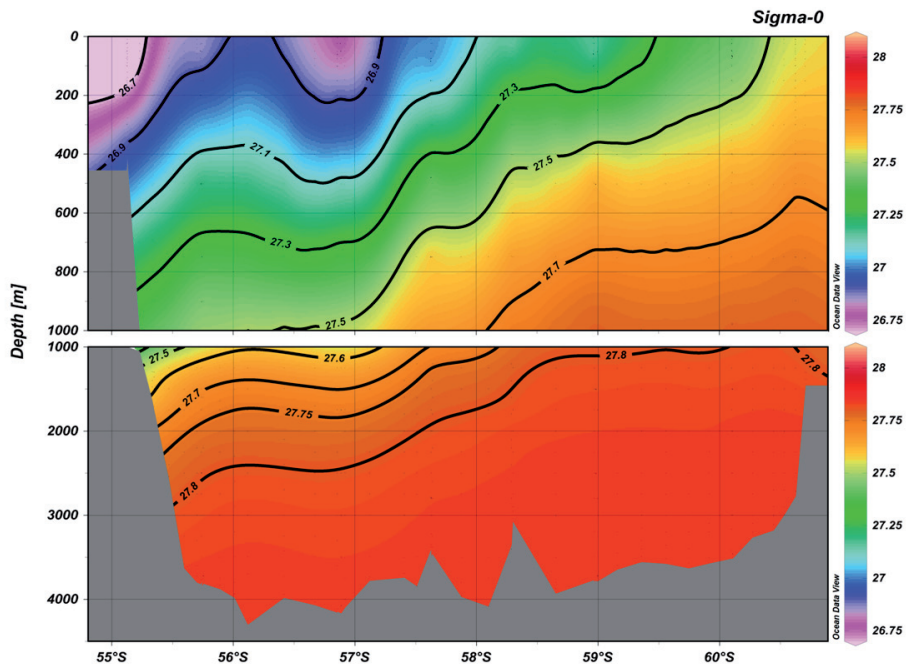


Fig. 5.3b Sigma-theta section of the of the Drake Passage transect

voluminous water mass in the Weddell Sea is the slightly colder Weddell Sea Deep Water ($-0.7 < \theta < 0$) which is observed from ~1500 m to ~4000 m depth. The western part of the Weddell Sea is known as an important region for bottom water formation. Intense cooling of surface waters causes loss of buoyancy and subsequent sinking along the Peninsula slope [Huhn *et al.*, 2008], resulting in the formation of Weddell Sea Bottom Water (WSBW) ($\theta < -0.7$) (Fig. 5.2a). Both the latter WSBW and the WDW influence the WSDW through mixing. Eventually, the Weddell Basin Deep Water leaves the Weddell Sea at the Scotia Ridge and extends further Northwards as AABW [Orsi *et al.*, [1993]; Naveiro Garabato *et al.*, [2002]]. The magnitude of these processes is considerable; estimations are from 8-9 to 11 Sv (1Sv is $10^6 \text{ m}^3\text{s}^{-1}$; Orsi *et al.* [1993]; Naveiro Garabato *et al.*, [2002]; Klatt *et al.* [2005]). Not all inflowing Warm Deep Water ends up as WSDW and leaves the Weddell Gyre as AABW; upwelling of deep waters and subsequent Ekman transport causes a loss of water at intermediate depths that eventually flows equatorwards as (Antarctic Intermediate Water) AAIW; a process with important consequences for the biogeochemical composition of the surface waters in the Atlantic Ocean [Hoppema *et al.*, 2003]. The σ_θ - plot shows slightly denser water in Central Gyre, and somewhat less dense water closer to the ridges. Also relatively lighter water is seen along the slope (Fig. 5.3a).

The Drake Passage is marked as the passage where all Southern Ocean fronts are very near to each other because of its narrow extent. At the Drake Passage, the Antarctic Circumpolar Current (ACC) approaches the continental shelves, bounded by the Subantarctic front at 55.6°S in the North and the Southern Boundary of the ACC (SBACC) at 60.4°S in the South. Within the ACC, the Polar Front (PF) is found at 57.3°S (defined as the northernmost extent of the 2°C subsurface θ minimum [Pollard *et al.*, 2002]). Here, it is clearly visible that the colder, more saline water subducts as AAIW under warmer waters (fig. 5.2b). Southwards of the SB ACC, near the Antarctic Peninsula, the Weddell Scotia Confluence Zone is found. Sudre *et al.* [2011] distinguished the different water masses in the Drake Passage using multiparametric analysis. Briefly, in the surface waters in the south part of the transect (south of 58.5°S), the Antarctic Surface Water (AASW) was observed to a maximum depth of ~100 m. North of 58.5°S , the Subantarctic Surface Water (SASW) reach from the surface to a maximum of 700 m depth at the Patagonian side. Winter Water (WW) was observed over most of the transect, at a depth of 200-300 at 56°S to ~100m at 60°S (Fig. 5.2b). AAIW followed a downward path; from 300-600 m at the Polar Front, to 800-1200 m depth at the Patagonian shelf (Fig. 5.2b). This pattern of water masses shoaling towards the south is also observed in the Circumpolar Waters below; Upper Circumpolar Water (UCDW) and Lower Circumpolar Water (LCDW) were observed from ~1200-2200 m and ~2200-4000 m respectively at the Patagonian Shelf, and found up to ~150-700 m and ~700-3000 m, respectively, south of the Polar Front. South of 58°S , the Weddell Sea Deep Water (WSDW) was observed as a 500 m thick bottom layer (Fig. 5.2b). Close to the Patagonian shelf (55 - 56.5°S), at ~2000-3000 m depth, an additional deep water mass is identified by high $\delta^3\text{He}$ concentrations.

This water mass, named Southeast Pacific Deep Slope Water (SPDSW) was earlier reported by *Well et al.*, [2003] and for this cruise by [*Sudre et al.*, 2011] and [*Middag et al.*, 2011]. It originates from the South Pacific. The Drake Passage is known for the occurrence of mesoscale eddies. Locally, these eddies may be of major importance for the transport of trace elements; as reported for dissolved Zn [*Croot et al.*, 2011] and iodate [*Bluhm et al.*, 2011]. The position of the fronts as well as the pattern of water masses, shoaling to the South, are clearly visible from the sigma-theta plot (Fig. 5.3b).

5.3 Results

The distribution of DFe in the Weddell Sea is depicted in figure 5.4 and the depth profiles are given in figure 5.5. Generally, the DFe concentrations within the Weddell Sea surface waters are very low, ranging from <0.01 nM (Lowest Limit of Detection; LLoD) to 0.1 nM. Exceptions to this pattern are slightly higher concentrations (0.12 - 0.17 nM) at the upper surface (10 m depth) at 27°W, and in the upper 50m at 48°W. Although there is little increase in DFe in the upper 100 m towards the Peninsula, concentrations show a sudden increase between 200 and 600 m, near the shelf break. In the south and north part of the Weddell Sea transect, concentrations in the WDW are 0.2-0.3 nM, whereas in the Central Weddell Sea, even lower concentrations (0.1-0.2 nM) were observed. Below the WDW, in the Weddell Sea Deep Water, concentrations start to increase, to values of 0.2-0.4 nM, where the lowest concentrations are observed in the centre of the Gyre, and slightly higher values in the direction of the shelves. These concentrations are relatively low for deep water concentrations in the Southern Ocean [*Tagliabue et al.*, 2012; This thesis, Chapter 6]. Below 4000 m, at most stations WSBW is observed, with slightly higher DFe concentrations, likely as a result of deep water formation along the shelf.

The distribution of DFe in the Drake Passage is depicted in figure 5.6 and the depth profiles are given in figure 5.7. In the Drake Passage, strong fluctuations are observed in the DFe concentration in the surface waters. Close to the Peninsula the DFe concentrations reach 1-2 nM, with a maximum in the subsurface, 100-200 m, depth. Further north, surface concentrations are low (<0.2 nM), but an enrichment in DFe is observed at 58.3°S (station 238), corresponding to high Al concentrations [*Middag et al.*, 2011]. At the Northern end of the transect, close to Tierra de Fuego, DFe enrichment corresponds with enrichment of DMn and DAI and low salinities [*Middag et al.* 2011]. In the Drake passage, the DFe increase with depth is stronger than that in the Weddell Sea; concentrations > 0.25 nM are observed from 25 – 200 m in the Southern Drake Passage, and from > 400 m in the Northern Drake Passage (WW and AAIW, see section 5.4.3). Below this, the DFe concentrations follow the southwards ascending pattern also observed in DMn and typical for the water mass distribution in the Drake Passage [*Middag et al.*, 2011; *Sudre et al.*, 2011]. The most

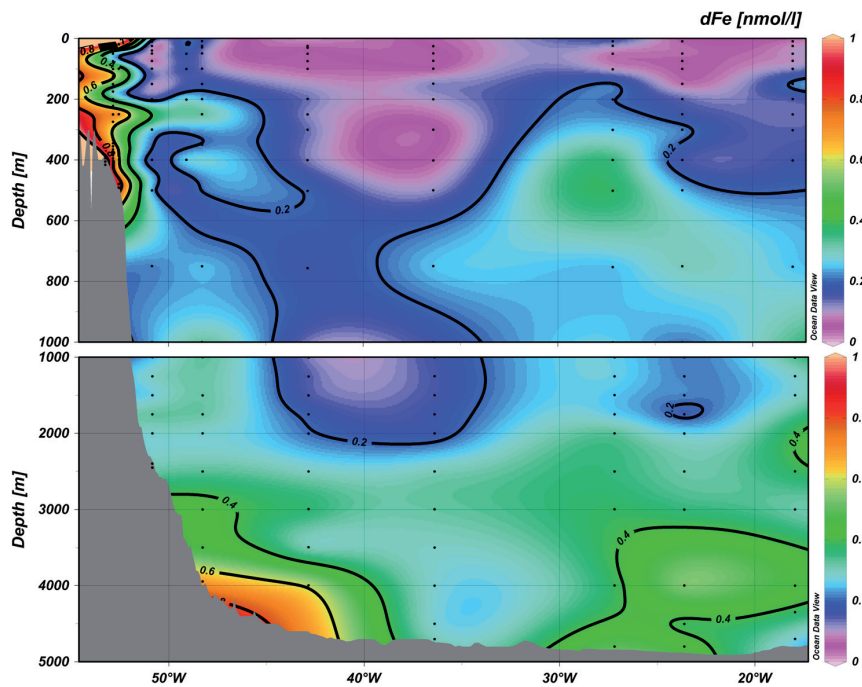


Fig. 5.4 Section plot of *dFe* concentrations in the Weddell Sea transect.

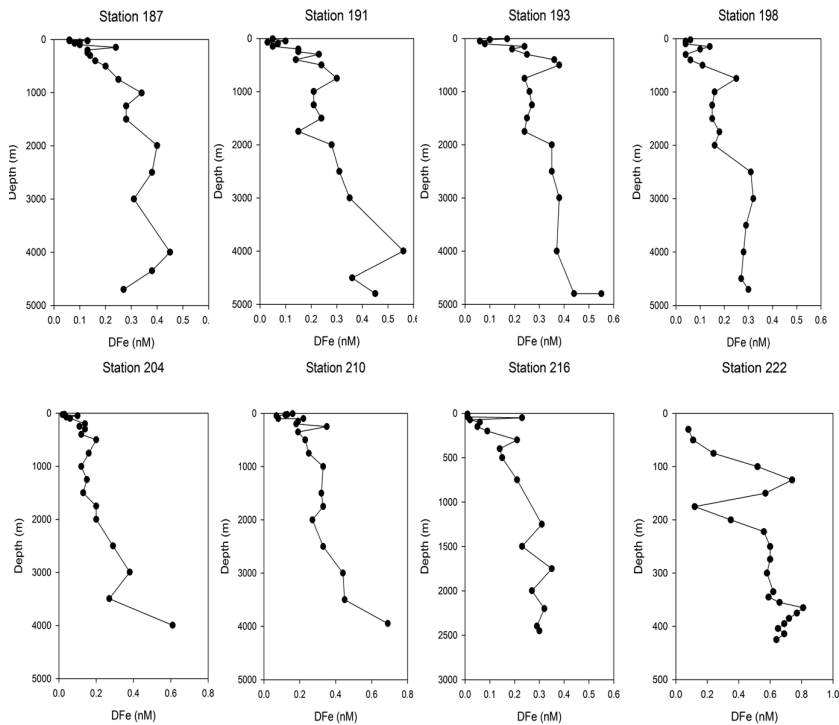


Fig. 5.5 Depth profiles of *dFe* from the Weddell Sea transect.

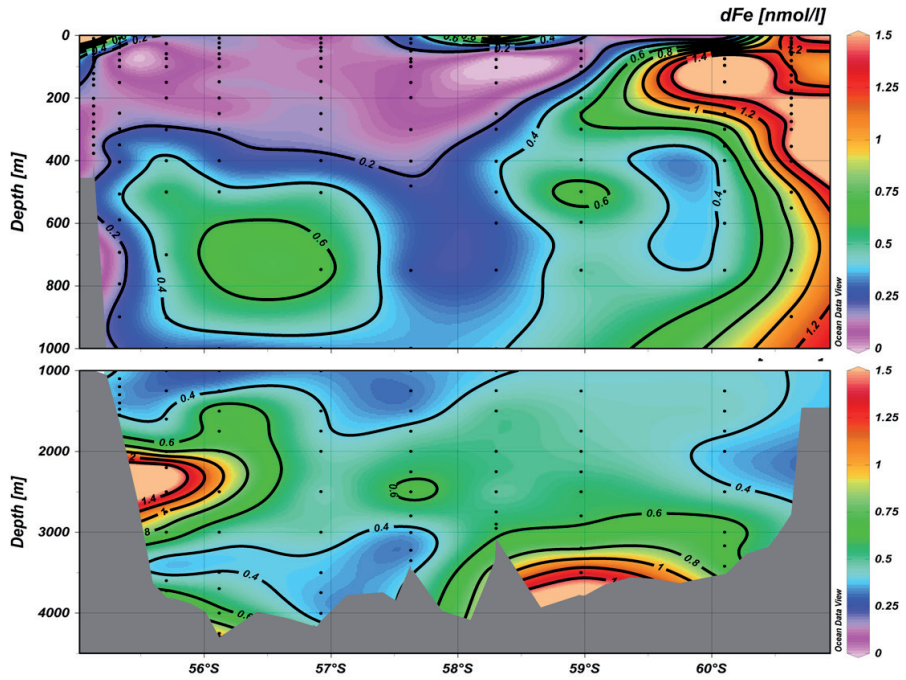


Fig. 5.6 Section plot of DFe concentrations in the Drake Passage transect.

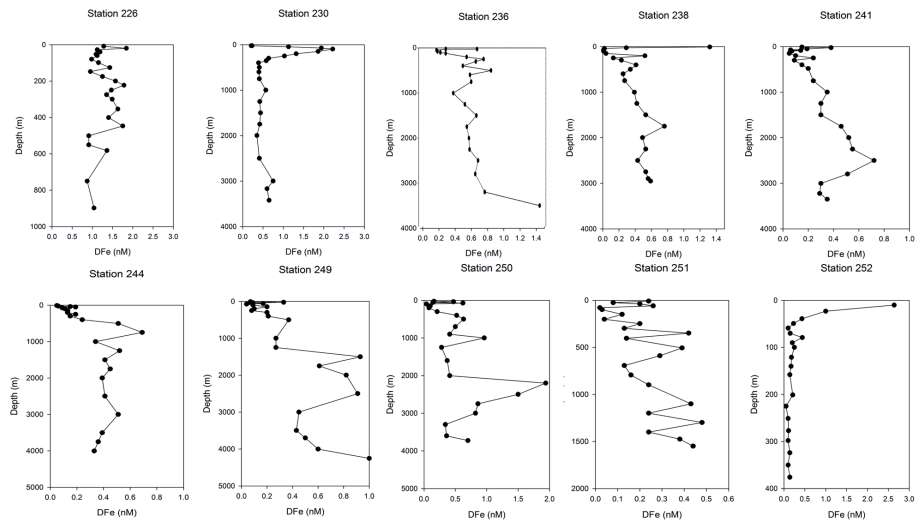


Fig. 5.7 Depth profiles of DFe from the Drake Passage transect

northerly station, situated above the Patagonian shelf has very high DFe concentrations (2.64 nM at 25m) in the upper surface sample. Deeper in the water column, onto the continental slope and shelf, a strong, local, maximum in DFe (>1.5 nM) is observed at ~ 2500 m depth. This maximum is consistent with the presence of South Pacific Deep Slope Water (SPDSW), originating from the Central South Pacific, carrying a hydrothermal signal (see section 5.4.3) [Middag *et al.*, 2011; Sudre *et al.*, 2011]. The DFe data, along with physical and station information is available as a separate chapter in this thesis.

The nutrient removals for the Weddell Sea Stations are shown in Fig. 5.9. There is a strong variation in the nutrient removals for both transects; nevertheless removal of nutrients decreases towards the continent is at the Greenwich meridian transect. Fig 5.9d shows the weighted average DFe concentration in the upper layer above the Winter Water –the layer from where nutrients are removed- and also shows a less nutrient removal, when going southward along this transect. In the Weddell Sea, more of a trend is observed; removal of nutrients increase northwards until ~ 64.5 °S and then followed by a sudden drop. For the Weddell Sea, removal of nutrients are consistent with findings of Hoppema *et al.* [2007] for data from the same transect in March 2005, who also observed the sudden decrease in removal around ~ 64.5 °S, for none of the stations in the Weddell Sea transect is a removal of DFe observed; DFe values are uniform with depth until the Winter Water.

5.4 Discussion

5.4.1 Comparison with other data in the region

Dissolved Fe data of the central Weddell Gyre is scarce and mainly available for the surface waters of the near margin region. Here the recently reported DFe data are discussed. Sanudo-Wilhelmy *et al.* [2002] occupied a transect as far west as 46 °W, and reported surface DFe (< 1 m depth) concentrations in the range of 0.5-2 nM for off-shelf stations. These reported values are significantly higher than the concentrations reported here, possibly due to the difference in depth; biological depletion may be less at 1 m, whereas input of atmospheric dust may increase DFe concentrations. The higher DFe concentrations could also reflect the difference in sampling time; Sanudo-Wilhelmy report data from February and early March, whereas our occupation of the same region was end March, early April. Recently, De Jong *et al.* [2011] reported an DFe data from in two stations; first station was an ISPOL station above the slope in the Weddell Sea. DFe concentration range from 0.6-0.9 nM (upper 200m) to 1-3 nM (200-1000m) and 5-20 nM below 1200m to bottom (1376m) The other station was situated upstream of the Patagonian continent, on the Scotia Ridge and showed relatively high DFe concentrations (~3 nM in upper ML; 8-13 nM in 100-750m depth; 2-4 nM in 1000-3000m depth and 8-10 nM at 3500m to bottom

(4200m.) More DFe data in this region is primarily related to sea-ice/iceberg studies. *Lannuzel et al.* [2008] reported concentrations of 0.9 – 2 nM in the upper 30 m in the Western Weddell Sea, for a large part as a result of ice-melt. *Lin et al.* [2011] reported DFe concentrations in the 1-2 nM range for a cruise in the Powell Basin, in March 2009. The relatively higher concentration may be due to the fact that this cruise track was designed to study the effect of icebergs on DFe, and therefore may be biased towards areas with high concentrations. Moreover, the Powell Basin is situated downstream of the Peninsula, therefore shelf derived higher concentrations may be expected. Indeed, the 1-2 nM range is consistent with our stations 222 and 226. In the Drake Passage, *Martin et al.* 1990 reported surface concentration of 0.16 nM, a minimum of ~0.1 nM at 100m depth, and increase to 0.4 nM at 500m depth. *Ardelan et al.* [2010] reported ~0.2 nM for ACC surface waters and ~0.6 nM (on average) for shelf-derived waters, North of King George Island (data also used in *Dulaiova et al.* [2009]). In an incubation study, *Hopkinson et al.* [2007] reported concentrations ~0.1-0.14 nM in the open ACC waters to ~1.6-1.7 nM for shelf waters.

5.4.2. Distributions of DFe in the Weddell Sea

5.4.2.1. Surface waters in the Weddell Sea

The very low surface DFe (<LLOD (10pM) to 100pM) concentration over most of the Weddell Sea transect indicates a strong depletion of Fe and/or lack of input sources. The significant vertical advection reported for the Weddell Sea ([*Weppernig et al.*, 1996]; *Haine et al.* [2008]; *De Jong et al.* [2012]) indicates that upwelling from deeper waters is an important source of DFe to the Weddell Sea surface. Moreover, in our study region, melting of floating icebergs (mainly in the Weddell Sea) and sediment derived Fe are important sources, as confirmed by modelling studies [*Lancelot et al.*, 2009] and fieldwork [*Dulaiova et al.*, 2009; *Ardelan et al.*, 2010; *Lin et al.*, 2010], mainly along the Antarctic Peninsula. The Weddell Sea and Scotia Sea are accumulation regions for icebergs [*Stuart and Long*, 2011] and DFe enrichment due to icebergs is reported [*Lin et al.*, 2011]. *Lannuzel et al.* [2008] reported high (~ 1 nM) DFe concentrations upon the melting of seasonal sea-ice in the Weddell Sea. However, these concentrations were reported in November–December, at the time of significant sea-ice melt. During our occupation of the transect, in March 2008, any DFe derived from sea-ice earlier in the season, would likely already have been taken up by phytoplankton. Possible effect of melting sea-ice or icebergs on the distribution of DFe would be reflected in low salinity. Almost all of the upper 25 m DFe values are below <0.1 nM, and salinities are high (>34). However, at station 210 a small enrichment is observed (DFe = 0.16 nM) at 10 m depth corresponding to a slightly lower salinity (33.8) (Fig. 5.2a, 5.4). This could be caused by a small amount of sea-ice meltwater, as this station is situated at the ice edge.

A significant relationship of dissolved Mn with nutrients (PO_4 , NO_3 and Si) and (inverse) with fluorescence indicates biological depletion of Mn from the surface

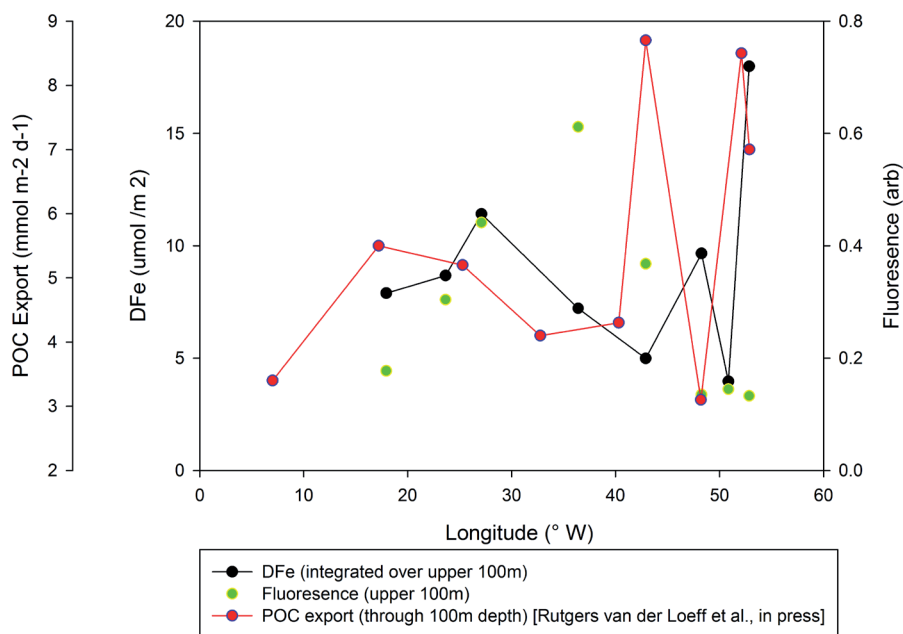


Fig. 5.8 DFe (integrated over upper 100 m), fluorescence signal (average over upper 100m) and POC export (through 100 m depth) over the Weddell Sea transect.

waters of this transect [Middag *et al.*, 2011; 2012]. No correlation was found for DFe and major nutrients; $R^2 < 0.1$ in the upper 100 meter of the Weddell Sea. This may be caused by the complex pattern and seasonality in sources and biological uptake and other sinks of DFe. However, to discuss the role of (biological) DFe removal during and prior to our cruise, the export of organic carbon and fluorescence are good indicators. Rutgers van der Loeff *et al.* [2011] reported POC export estimates, based on $^{234}\text{Th}/^{238}\text{U}$ disequilibrium, for the same transect. Unfortunately, the POC export data was not always from the same stations as the trace metal data of the Weddell Sea transect. Nevertheless, we can discuss the pattern of DFe, fluorescence and POC export. Figure 8 shows the integrated DFe over the upper 100 m, the average fluorescence and the POC export at 100 m depth [Rutgers van der Loeff *et al.*, 2011]. We take the good agreement between the average fluorescence over the upper 100m and the chlorophyll data for the same transect [Neven *et al.*, 2011] as a confirmation that average fluorescence roughly represents the phytoplankton abundance. In the west part of the Weddell Gyre ($\sim 17\text{--}24^\circ\text{W}$), the depth-integrated DFe is around an average of $\sim 8 \mu\text{mol m}^{-2}$. Here, recent uptake of DFe is probably low as the fluorescence signal is low and POC export is somewhat higher. Further west, in the Central Gyre, DFe can maintain some higher inventories, despite the increase in chlorophyll a; this could be explained by the low POC export, thus low removal earlier in the season. However between the stations at $\sim 27^\circ\text{W}$ and $\sim 36^\circ\text{W}$, the strong increase in

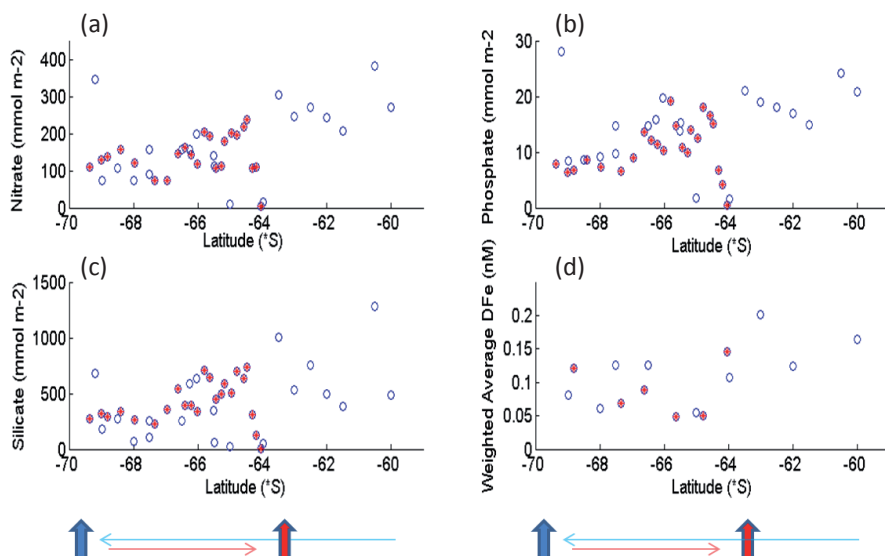


Fig. 5.9 Removal of nitrate (a), phosphate (b), silicate (c) and weighted average DFe (d) against latitude for the Weddell Sea transect (red filled circles), and the Greenwich meridian transect (blue circles) [Klunder et al., 2011]. Location of the shelf (500 m depth isobaths) is marked for the Greenwich Meridian transect (blue arrow) and the Weddell Sea transect (red arrow). Light arrows (blue and red) indicate the direction of the transect.

chlorophyll a may be visible in the strong decrease of the DFe inventory. The lowest DFe surface concentrations were observed where relatively high C export was found, especially at station 204 ($\sim 43^\circ\text{W}$). Here, very low integrated DFe ($\sim 5 \text{ nmol m}^{-2}$) was observed and POC export reaches $8.7 \text{ mmol m}^{-2} \text{ d}^{-1}$ (through 100m depth; Rutgers van der Loeff et al., [2011]) (Fig. 5.8). Moreover, also removal of PO_4 , NO_3 , Si (not shown) and low Mn [Middag et al., 2011a; 2011b] are observed, indicating biological removal of nutrients and trace metals in the time prior to our cruise. This is confirmed by satellite chlorophyll a data (monthly mean chl-a data; GlobColour Archive) showing an ice edge bloom in this region in February 2008 [Rutgers van der Loeff et al., 2011]. Further West, at 48°W , there has been an ice cover in the months prior to our cruise [monthly mean chl-a satellite data; Rutgers van der Loeff et al., 2011], and very little C export has been observed, enabling DFe, as well as PO_4 , NO_3 , Si and Mn [Middag et al., 2011; 2012] to maintain higher concentrations, likely in combination with input due to surface ice-melt (see above). Towards the shelf, POC export is high, likely as a result of (another) strong bloom in January 2008 [Rutgers van der Loeff et al., 2011]. This bloom may have caused some DFe removal, leading to lower concentrations of DFe, despite the closer proximity to the shelf source of Fe (Fig. 6). Above the shelf, the shelf-derived DFe sources ensure continuously high DFe in this region, although there is large POC export [Rutgers van der Loeff et al., 2011]. In this region, little recent biological uptake is expected; fluorescence data indicates

very little phytoplankton abundance in the shelf region (Fig. 5.8), in line with findings of *Neven et al.* [2011] and satellite derived chlorophyll [*Rutgers van der Loeff et al.*, 2011] and with the depleted nutrients above the shelf.

The nutrient removal values in the Central Weddell Sea (fig. 5.9) are consistent with findings of *Hoppema et al.* [2007] for data from the same transect in March 2005, who also observed suddenly less removal around $\sim 64.5^\circ\text{S}$. There is no trend in DFe removal in the Central Weddell Sea. However, a continuous input of DFe from the Antarctic shelf region stimulating production and thus nutrient removal in the near margin region, as supposed by *Hoppema et al.* [2007], would be reflected in the relationship between DFe and the nutrient removal values, unless there is a major excess of iron. Fig. 5.10 (a-f) shows the relationship between the amount of DFe present in the water above the Winter Water layer (weighted average) and nutrient removals for both transects. It is important to note however, that the nutrient removal estimates represent a difference, emerged over spring and summer, whereas DFe value represents the DFe concentration at the moment of sampling. It appears that the regions with a strong nutrient removal do indeed have high Fe concentrations, although this is mainly seen in the stations at the prime meridian. Two stations in the west Weddell Sea transect (st 198 and 204) show a nutrient removal in accordance with the Greenwich Meridian transect and with earlier findings in this region [*Hoppema et al.*, 2007], despite low DFe concentrations. Although there may be some difference in Fe supply to the Weddell Gyre and to the Zero Meridian, this may be explained by earlier growth and export of phytoplankton, which would cause a depletion of nutrients still present, whereas the momentary DFe concentration would be lower, due to uptake earlier in time. For the region of station 204, a very high POC is observed indeed. Around station 198, no sample for POC export has been taken, but the fluorescence signal is high (fig. 5.8). Likely, concentrations of DFe

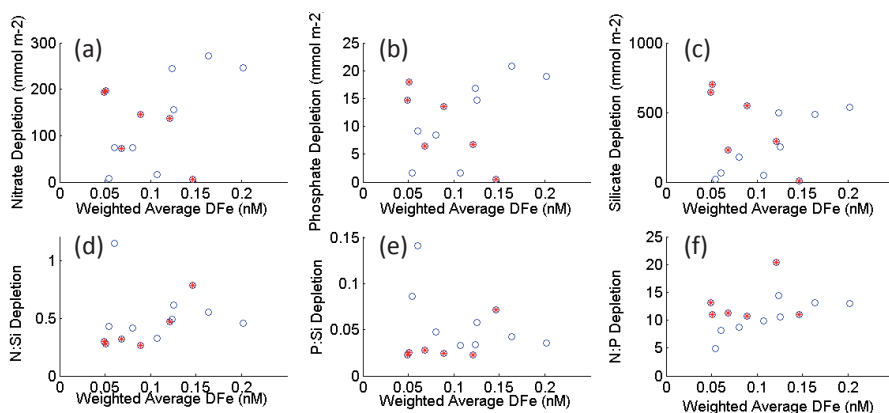


Fig. 5.10 Removal of nitrate (a), phosphate (b), silicate (c) and the removal ratios of N:Si (d), P:Si (e) and N:P (f) vs the weighted average DFe concentrations for the Weddell Sea transect (red filled circles), and the Greenwich Meridian transect (blue circles) [Klunder et al., 2011].

are not low enough to limit primary production. The scatter in the DFe, nutrient-plots may well be explained by two interacting processes in the Southern Ocean; continuous supply of Fe during the growing season may result in high DFe despite large nutrient removal and the resupply at the start of the season will lead to removal of DFe and nutrients over the season. The high DFe despite low nutrient removal that is observed in station 210 may be attributed to the recent dust deposition (see above), which would not be reflected in the nutrient drawdown.

Diatoms are the most abundant phytoplankton species in the Weddell Sea. For blooms of the diatom *Fragilariopsis kerguelensis* at the Polar Front, it has been shown that uptake of nitrate can be severely impaired under Fe-limited conditions [De Baar et al., 1997], overview in Marchetti and Cassar, [2009]). Briefly Fe is essential in the enzymes nitrate reductase and nitrite reductase for reductive conversion of nitrate into ammonia for synthesis of amino acids of proteins [Geider and La Roche, 1994; De Baar et al., 1997]. Under Fe-stress, this conversion is hampered, while the uptake and incorporation of phosphate and silicate is not directly affected. As a result the biomass of Fe-limited diatoms has anomalously low N:P and N:Si element ratio, while on the other hand the seawater left behind shows anomalously high N:P ratios [De Baar et al., 1997] and N:Si ratio [Takeda et al., 1998]. Fig. 5.9d. shows the nutrient removal relative to the weighted average DFe, and generally shows the lowest (<0.4) N:Si removal ratio at lower DFe (<0.1 nM) concentrations and the highest N:Si removal ratios (>0.4) at DFe > 0.1 nM concentrations. For the worldwide biological cycling of Si and N by diatoms, the global average element ratio is close to N:Si = ~1 [De Baar et al., 1997]. However *Fragilariopsis kerguelensis* and other major bloom-forming Antarctic diatoms are heavily silicified and a ratio N:Si = ~0.4 is normal under Fe replete conditions [De Baar et al., 1997].

Regarding P:Si (Fig. 5.10e) and N:P (Fig. 5.10f) removal ratios, the results are not so straightforward. There is a tendency of increasing N:P removal ratio (from ~5 to ~15) with increasing DFe, but this is only visible in the Greenwich meridian stations. The Weddell Sea stations show a relatively constant N:P removal ratio (~13) with DFe. This difference in N:P removal ratio between the two regions could be explained by a upwelling of waters from below with different nutrient signature (such as NADW with a relatively high N:P [De Baar et al., 1997]). To test this hypothesis, the surface (0-150 m) concentrations of major nutrients (N, P, Si) were subtracted from the subsurface (150-250 m) and intermediate (250-1000m) nutrient concentrations; no differences were observed between the regions. Thus this hypothesis can be excluded.

The difference in nutrient uptake ratios might then be explained by a different species composition. Both regions are dominated by diatoms [Alderkamp et al., 2010]; however, in the Central Weddell Sea stations the size of the diatoms is generally somewhat smaller [Neven et al., 2011]. From the same expedition, specific counts and measurements of the phytoplankton community are available for stations at the ZERO meridian (150, 161, 167 and 178) and for stations in the Eastern Weddell Gyre (191, 193, 198, 204 and 210), see fig. 5.1a. Here we use estimations of the size of

Table 5.1 Size and volume of diatom species at the Greenwich Meridian and Eastern Weddell Sea stations.

	Station	Average Bio volume/cell (μm^3)	Percentage of species	
			Large ($>5000 \mu\text{m}^3$) (%)	Small ($< 1000 \mu\text{m}^3$) (%)
Greenwich Meridian	150	3408	78	5
	167	8436	87	2
	161	8272	88	2
	178	7810	82	2
	Average	6981	84	3
	St deviation	2397	5	1
Eastern Weddell Sea	191	7420	94	5
	193	4506	74	5
	198	2735	49	7
	204	3390	75	7
	210	3240	57	12
	Average	4258	70	7
	St deviation	1882	18	3
Difference*		0.048	0.084	0.018

(* *p*-value (1 sided *t*-test)).

the diatoms present in both regions. The diatoms were significantly smaller in terms of biovolume (T-test, $p < 0.1$) on average in the Eastern Weddell Sea region (average $4258 \pm 1883 \mu\text{m}^3$) than at the Greenwich Meridian (average $6981 \pm 2397 \mu\text{m}^3$) (Table 5.1). This pattern is confirmed by the larger number of smaller ($< 1000 \mu\text{m}^3$) diatoms in the Eastern Weddell region compared to the Greenwich Meridian (7% and 3% respectively) and the lower number of large diatoms ($> 5000 \mu\text{m}^3$) (7% and 84% respectively) (Table 5.1). *Marchetti and Cassar* [2009] summarized several studies of the effect of iron deficiency on nutrient uptake and reported stronger Si relative to N uptake in Fe limited diatoms, dependent on diatom size. There are two mechanisms via which the N:P uptake ratio of diatoms is influenced by their size. First, the specific growth rate of diatoms with regard to Fe is dependent on their surface to volume (S/V) ratio [Sarhou et al., 2005; De Baar et al., 2005]; smaller diatoms generally have a smaller S/V ratio which is beneficial in their Fe uptake [see also Timmermans et al., 2004]. This benefit is because a smaller S/V ratio allows more uptake relative to the intracellular needs, but also because smaller cells have a smaller boundary layer thickness, enhancing the concentration gradients [Marchetti and Cassar, 2009]. Therefore, impairment of N uptake as a result of Fe limitation [De Baar et al., 1997] is more likely to occur in larger species, as observed in the Greenwich Meridian stations. Moreover, also the uptake kinetics of nitrogen depends on the S/V ratio, whereas such a relation is not found for P uptake [Sarhou et al., 2005]. Our findings

for the N:P removal ratios are in line with culture experiments of *Timmermans et al.* [2004]. They reported that the largest species (small S/V ratio) showed the strongest effect of Fe depletion in their N:P uptake; and this effect became lower with smaller species. The fact that larger species take up N less efficiently relative to P could contribute to the low N:P removal ratios found at low DFe in the Greenwich Meridian stations, while these are not found at similar DFe in the Central Weddell Sea.

During the EIFEX in situ iron fertilization experiment, *Hoffmann et al.* [2006] found for the large ($>20\ \mu\text{m}$) size class of phytoplankton, comprising large diatoms, that at low ambient dissolved Fe had cellular N:P ratio ~ 5 , which increased to ~ 15 – 16 upon Fe enrichment. Such differences were absent for the smaller ($<20\ \mu\text{m}$) size classes. These diatom size classes are comparable to the here observed classes, with a median size of 20 – $25\ \mu\text{m}$. We conclude that the low N:Si and N:P uptake ratio's indicate the important, and possibly limiting, role for DFe for phytoplankton abundance and for the uptake and cycling of nutrients in the Weddell Sea. However, many other factors are involved, amongst which are species composition and form. The authors note here that the DFe concentrations in the surface waters along the transect are low ($< 0.25\ \text{nM}$) compared to the concentrations in the enrichment experiments mentioned above [*Takeda*, 1998; *Timmermans et al.*, 2004 and *Hoffman et al.*, 2006] and therefore the relative effects of DFe availability as shown in the abovementioned studies are expected to be lower in our field situation.

5.4.2.2 Deep waters in the Weddell Sea

In the deep waters in the Weddell Sea the dissolved Fe concentrations are very low, and increase with depth. Following the properties derived by *Klatt et al.* [2005] (See Section 5.3), we can calculate the DFe in the different water masses in the Weddell Sea; in the WDW the concentrations are 0.21 ± 0.08 ($n=52$); in the WSDW 0.32 ± 0.12 ($n=42$) and in the WSBW 0.35 ± 0.10 ($n=11$). For comparison, *Klunder et al.* [2011] reported concentrations of deep waters of the Weddell Gyre at the Greenwich meridian; a DFe concentration of $0.33 \pm 0.14\ \text{nM}$ in deep waters (WDW, WSDW, WSBW) in the westward flowing southernmost limb of the Weddell Gyre, and $0.47\ \text{nM} \pm 0.16\ \text{nM}$ in the, more northern, eastward flowing limb. As expected, the concentrations here observed are similar, but slightly lower than those observed in the westward flowing component at the Greenwich Meridian. This is the same water mass, and apparently some DFe may be lost due to scavenging removal during transit from 0°W to the Weddell Sea. However, there is a large difference in DFe concentration between the Weddell Sea transect deep waters and the eastward limb of the Weddell Gyre at the Greenwich Meridian. This indicates that on its way eastwards, there must be significant input of DFe to the deep waters at the South Scotia Ridge. These sources could be either sediment resuspension or DFe flux from the sediment at the South Scotia Ridge ridge and/or inflow of Circumpolar Deep Waters in the 45 – 55°S region as observed by *Matano et al.* [2002]. Moreover, also hydrothermal input from the South Scotia Ridge may be an important Fe input source

[German *et al.*, 2000; Klinkhammer *et al.*, 2001; Tagliabue *et al.*, 2010].

The deep water masses leave the Weddell Sea and form the AABW flowing into the ACC and the abyssal world oceans [Naviera Garabato *et al.*, 2002; Hoppema *et al.*, 2010]. The here reported DFe concentrations of ~0.3–0.35 nM for WSDW, thus eventually for the AABW, are on the lower end of the large range of DFe concentrations observed in AABW throughout the Atlantic Ocean; ~0.3 nM [Klunder *et al.*, 2011], 0.38–0.8 nM [Chever *et al.*, 2010] and 0.28–0.93 nM [Rijkenberg *et al.*, 2011] for the South Atlantic and 0.7–0.8 nM [Laës *et al.*, 2003], 0.5 nM [Middag, 2010, Chapter 5], [~0.36–0.92 nM] [Rijkenberg *et al.*, 2011] for the North Atlantic. This supports the idea of DFe enrichment of AABW, by mixing with overlying NADW as well as supply from underlying sediment on its way northwards as proposed by Klunder *et al.* [2011].

Downslope subduction of surface waters close to the Peninsula, along the slope, renewing WSBW, has been observed in the Weddell Sea. This is also seen in the θ sections of our cruise (Fig. 5.3). Moreover, recently observed maxima in dissolved barium [Hoppema *et al.*, 2010], iodate, CFC-12 [Bluhm *et al.*, 2011] and DMn [Middag *et al.*, 2010] in the WSBW, indicate such downslope movement of dense shelf waters. The distribution of DFe is not conclusive regarding this downslope convection of WSBW; little enrichment is observed at ~51°W, 2500 m depth, despite indications of shelf water input (low θ (not shown) and higher DMn) [Middag *et al.*, 2010]. However, in the deeper waters, some enrichment of DFe is observed, corresponding to lower θ , thus indicating DFe enrichment of WSBW due to downslope convection. Unlike for DMn [Middag *et al.*, 2010] and dissolved Ba [Hoppema *et al.*, 2010], the DFe delivered by this process to the WSBW appears to be not sufficient to significantly enhance the DFe concentration in the WSDW by mixing.

5.4.3 Distribution of Fe in Drake Passage

5.4.3.1 Surface and sub-surface waters in Drake Passage

During our cruise, we observed an input of DFe from the shelves around Elephant Island into the Drake Passage, consistent with earlier findings of DFe [e.g. [Dulaiova *et al.*, 2009] and concentrations of DMn and DAi from the same sample points (Fig. 11; [Middag *et al.*, 2011a]). Above the shelf, high DFe concentrations are observed at the σ_θ isopycnal levels of 27.5 (1.87 nM), 27.55 (1.5 nM) and ~27.64 (2 nM). The first two peaks are observed as a broad peak further into the Drake Passage at station 230. Unfortunately there are no samples at this σ_θ level at station 236 (Fig. 5.11). Remarkably, the peak at σ_θ is 27.64 is observed as a small peak at station 236 but not the further offshore at station 230. This illustrates the many dynamic small gyre like structures, or eddies, observed to the north of Elephant Island [Ardelan *et al.* 2010 (their figure 5.10); Hewes *et al.*, 2009] causing a complex pattern of off-shelf currents in this region. The input of DFe from the Antarctic Peninsula shelf north of Elephant Island is in line with findings Ardelan *et al.* [2010], who observed DFe enrichment at

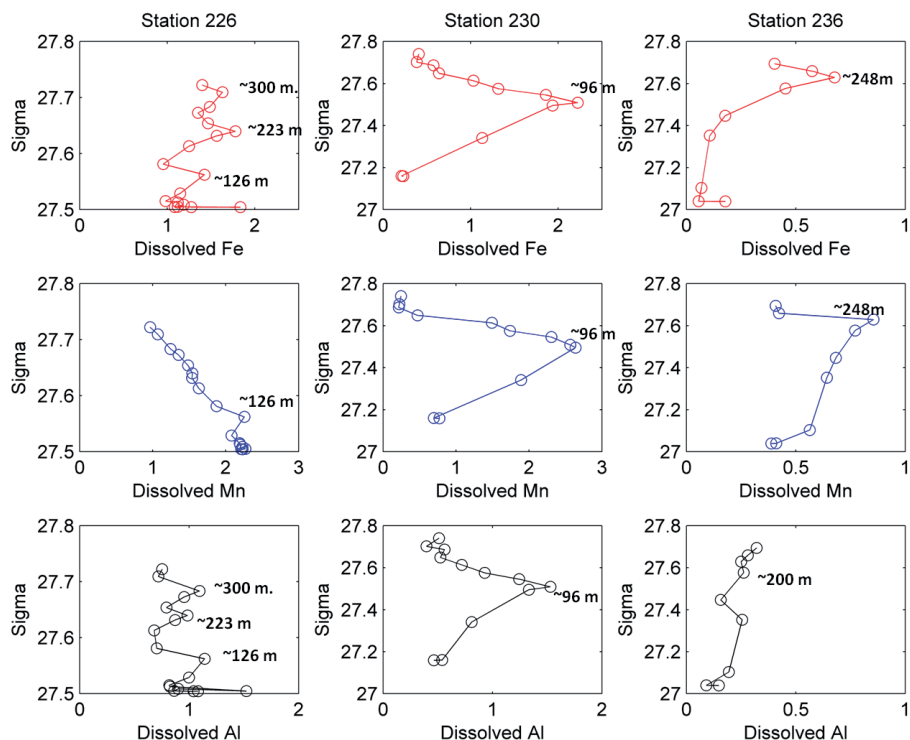


Fig. 5.11 Sigma theta versus Dissolved Fe, Dissolved Mn [Middag et al., 2011] and Dissolved Al [Middag et al., 2011] (nM) for the stations adjacent to Elephant Island (see Fig. 5.1b). Note the different metal concentration scales for different stations. Also corresponding depths of peak values are shown.

$\sigma_\theta = 27.5$ - 27.6 . Moreover, Charette et al. [2011] reports maximum concentration of radium (Ra) values at σ_θ is 27.5 - 27.6 for this region, indicating shelf-derived waters. Despite the low number of stations, we estimated the scale length (distance where the DFe concentration is $1/e$ of the initial concentration) at ~ 200 km. This is reasonably similar to the scale length for DFe observed for shelf input in the Nansen Basin (Arctic Ocean) (~ 263 km). As in the Drake Passage [Renault et al., 2011], also in the Nansen Basin the direction of the shelf current is perpendicular to the shelf [Klunder et al., 2011] resulting in a relatively short scale length as compared to other oceans [Johnson et al., 1997]. In our study region, Nielsdottir et al. [2012] reported a scale length in the same order, ~ 102 km, for transects at South Georgia island and Bird Island. The here reported scale length of ~ 200 km is considerably higher than the ~ 25 km reported by Ardelan et al. [2010] for the same region; partly this may be explained by the fact that latter scale length is calculated for the upper ~ 50 m, not for the subsurface maximum thus that there is more rapid DFe removal from the surface layer.

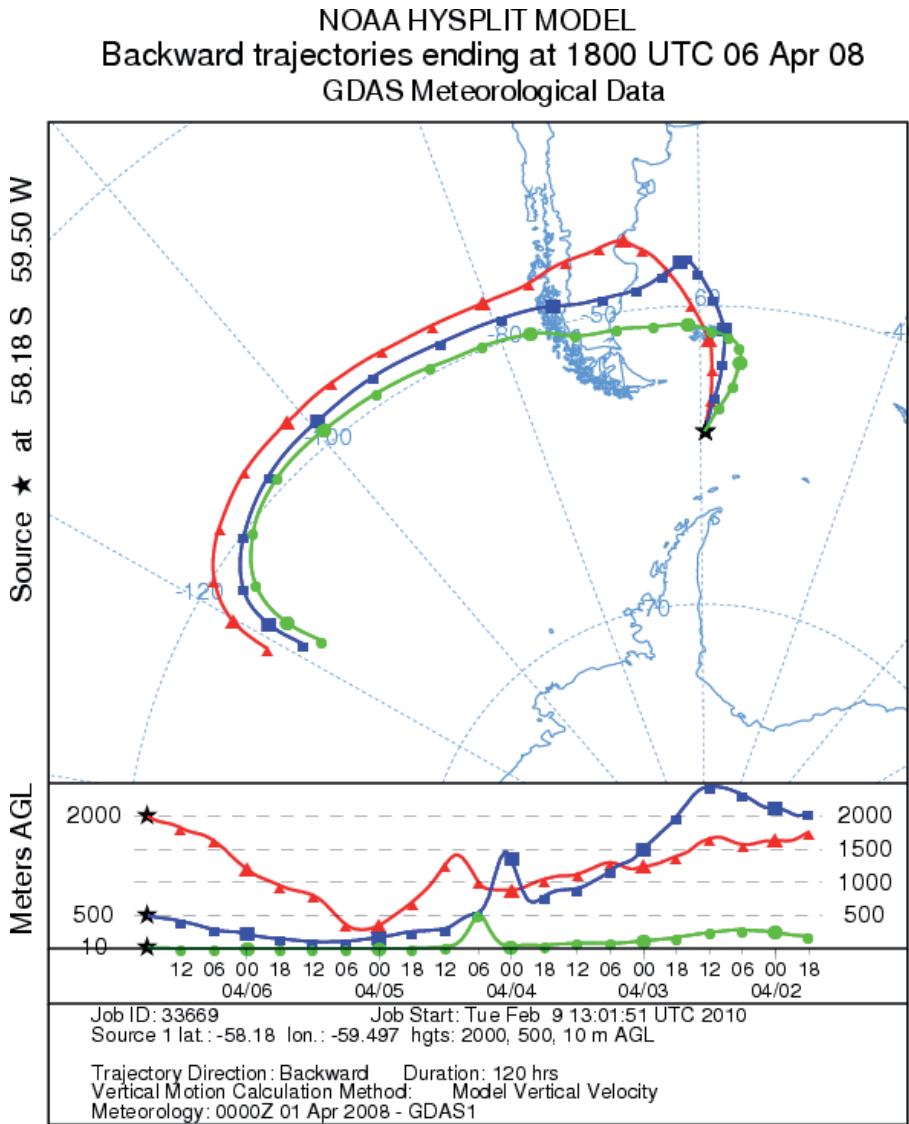


Fig. 5.12 Five day backwards air-trajectory from station 238 during ANT XXIV-3.

Further into the Drake Passage, at ~350 km from the shelf, the shelf waters carrying high DFe are found in the subsurface, below a low DFe upper layer of 150 m. In the North part of the Drake Passage, this low DFe layer extends to ~ 500 m depth (Fig. 5.2b). The DFe = 0.2 nM contour does coincide roughly with the 34.2 isohaline and with the surface and subsurface water masses (SASW, AASW and WW) as classified by *Sudre et al.*, [2011] for this transect. Maximum primary production in the Drake Passage is observed in the December – February period (*Moore and Abbott* [2001]). Biological removal of DFe from the surface waters and subsequent downwards trans-

Table 5.2 Shipboard precipitation data during ANT XXIV/3 (Bordwetterwarte, www.awi.de/polarstern).

Date/time	Weatherstation precipitation (mm)	
06-04-08 07:00	0.02	
06-04-08 08:00	0.03	
06-04-08 09:00	0.03	
06-04-08 10:00	0.05	
06-04-08 11:00	0.04	
06-04-08 12:00	0.01	
06-04-08 13:00	0.02	
06-04-08 14:00	0.01	
06-04-08 15:00	0.01	
06-04-08 16:00	0.01	
06-04-08 17:00	0.02	
06-04-08 18:00	0.01	
06-04-08 19:00	0.02	
06-04-08 20:00	0.04	
06-04-08 21:00	0.04	Start of Station 238
06-04-08 22:00	0.02	
06-04-08 23:00	0.01	
07-04-08 00:00	0	
07-04-08 01:00	0	
07-04-08 02:00	0	
07-04-08 03:00	0.02	
07-04-08 04:00	0.05	
07-04-08 05:00	0.03	
07-04-08 06:00	0	
07-04-08 07:00	0	
07-04-08 08:00	0	
07-04-08 09:00	0	
07-04-08 10:00	0	
07-04-08 11:00	0	
07-04-08 12:00	0	
07-04-08 13:00	0	
07-04-08 14:00	0	
07-04-08 15:00	0	
07-04-08 16:00	0	
07-04-08 17:00	0	
07-04-08 18:00	0	Start of Station 241
07-04-08 19:00	0.03	
07-04-08 20:00	0	
07-04-08 21:00	0.02	
07-04-08 22:00	0.02	
07-04-08 23:00	0.05	

port (see Fig. 5.2b) may cause the sharp difference in DFe concentrations between these subsurface waters and the deeper Circumpolar Deep Waters (Fig. 5.6), even at ~1000m depth. However, given the strong geostrophic velocities for the surface waters of our transect (0.1-0.4 m/s at 100 m depth; [Renault *et al.*, 2011]) these (sub) surface waters originate (mostly) from the South Pacific Ocean. These waters from the Pacific Sector of the Southern Ocean are low in DFe (~0.05 nM in the 100 - 120 °W region in Januari/Februari [Gerringa *et al.*, 2012] and ~0.2 nM at 120°W in March/April [De Baar *et al.*, 1999]), due to biological removal or lack of input sources [De Baar *et al.*, 1999; Hiscock *et al.*, 2001].

An exception to this pattern are the relatively high DFe concentrations observed in the uppermost water column at station 238. A concentration of 1.35 nM and 0.32 nM at 10 and 25 m depth, respectively, is followed by DFe depleted waters (<0.06 nM) in the upper 200 m. This surface maximum shows good correspondence with high dissolved Al concentrations at the same depths [Middag *et al.*, 2011]. Five day NOAA HYSPLIT backwards trajectory (figure 5.12) confirm that the air above this region originates from the Patagonia, The nearby station 241 does not show an upper surface maximum despite air originating from Patagonia, which may be explained by shipboard precipitation (rain) data shows that the 24 hours prior to occupation of station 238 there has been significant precipitation, whereas during the hours before occupation of station 241 no precipitation is reported (Table 5.2).

The 400 m deep station above the Patagonian shelf, close to Tierra del Fuego, shows high dissolved Fe concentrations in the upper 150m, where salinity is low (Fig. 5.2b, 5.6). There is a strong inverse correlation between DFe and salinity ($R^2=0.85$, $P<0.001$, $n=11$), pointing towards fluvial input of DFe. Similar high concentrations and correlations were observed for DMn and DAi [Middag *et al.*, 2011]. This DFe maximum is only observed in the most northern station, above the shelf (Fig. 5.6), but does not extend far into the Drake Passage. The latter may be explained by the very strong eastward velocity in this region (>40 cm/s; [Renault *et al.*, 2011]) bringing the elevated Fe signal more eastward than the other stations of our section. Although the amount of freshwater flowing into the Drake Passage is relatively small, the order of magnitude higher DFe in these waters compared to the common Drake Passage surface waters, may cause substantial DFe enrichment to the surface waters.

5.4.3.2 Deep Waters of Drake Passage

In the Southern Drake Passage, around 59-60°S, a strong enrichment in DFe is observed in the bottom waters (>3000m) (Fig. 6). This enrichment is also observed in the concentrations of DMn and DAi [Middag *et al.*, 2011]. These enrichments could be caused by downslope convection of dense water along the slope. Meredith *et al.* [2003] reported a direct ventilation of deep waters in the Drake Passage by dense shelf waters north of Elephant Island. This mechanism was only observed during and after austral winter, and strongest in ENSO years, although 2008 had a strong negative ENSO index [Jullion *et al.*, 2010]. Moreover, Sudre *et al.* [2011] have shown that

WSDW may follow a westward direction upon leaving the Weddell Sea through the gaps in the South Scotia Ridge. *Huhn et al.*, [2008] reported a similar pathway for WSBW formed along the Peninsula Slope in the Western Weddell Sea. Concentrations of DFe in the deep waters in the Southern Drake Passage are significantly higher than those in the WSDW and WSBW in the Weddell Sea (Fig. 5.2); parallel with higher DMn [*Middag et al.*, 2010;2011]). Thus there was likely a source during transport from the Weddell Sea to Drake Passage. Although in this region, hydrothermal vents are present [*Klinkhammer et al.*, 2001], DFe enrichment by mixing with hydrothermally influenced waters is unlikely, because this would be reflected in enhanced $\delta^3\text{He}$ concentrations, which are not observed [*Sudre et al.*, 2011]. The lowered light transmission [*Middag et al.*, 2012] in these water masses is an indication of resuspended particles, likely picked up during transport from the Weddell Sea to the location of our Drake Passage transect. Thereafter, high DFe concentrations could occur upon dissolution of these particles or by mixing with DFe rich pore waters during this resuspension, as also has been shown to cause enrichment of DMn [*Middag et al.* 2011].

Circumpolar Deep Waters are enriched relative to the lower SPDW and upper AAIW. From 2000 – 3000 meter depth ascending Southwards, the Circumpolar Deep Waters (LCDW/UCDW) bring slightly more DFe (>0.5 nM) to the surface waters. Above the UCDW, relatively low DFe waters >0.25 nM are transported northwards as AAIW. However, these waters do not reach deeper than 500 m, as there is a water layer with high DFe at $55.5 - 57^\circ\text{S}$ from 500-1000m.

A layer with an anomalously high DFe concentration is observed towards the South American flank of the Drake Passage, at $\sim 2000\text{-}3000$ m depth. This relatively small water mass has earlier been classified by *Well et al.* [2003] and *Sudre et al.* [2011] as South Pacific Deep Slope Water, originating from the East Pacific Rise (EPR), carrying a significant $\delta^3\text{He}$ signal as a result of the hydrothermal activity at the EPR [*Well et al.*, 2003]. *Middag et al.* [2012] reported a clear trend between $\delta^3\text{He}$ and manganese, both good indicators for hydrothermal vents, in this water mass. We assume the high DFe in the SPDSW water also to be of hydrothermal origin, and although this water mass is small, the large difference in DFe (1.5-2 nM) relative to its surrounding deep water masses (~ 0.5 nM) causes the SPDSW to be a considerable source of DFe to the deep waters in the Drake Passage, and eventually to the deep South Atlantic Ocean.

5.5 Summary and Conclusions

Surface dissolved Fe concentrations can reach very low values (~ 0.01 nM) in the Central Weddell Sea. Generally, concentrations are <0.1 nM in the upper 100 m. The DFe concentrations in the upper 100m can be (partly) explained by phytoplankton uptake and POC export in the surface waters, stressing the important role of biological

processes in the DFe distribution. The only DFe input from the Antarctic Peninsula shelf is observed above the shelf, with little sign of advection of these waters into the Weddell Basin. Dissolved Fe in the deep water masses of the Weddell Sea is low compared to deep water concentrations observed worldwide [Moore and Braucher, 2008]. In the Weddell Sea, no clear influence of the shelf is observed in the seasonal nutrient or DFe drawdown. However, the Si:N removal ratio is stronger in low DFe regions, indicating DFe control on the algal nutrient uptake kinetics and eventually on algal growth. In the Eastern Weddell Gyre, no effect of DFe on the N:P removal ratio (~ 13) was observed. At the Greenwich Meridian, however, the N:P removal ratio increased with increasing DFe. This difference between regions is likely caused by differences in diatom size; the diatoms at the Greenwich meridian are significantly larger. Our results indicate that DFe enrichments due to shelf sources are restricted to the Antarctic Peninsula shelf, and do not have a large scale effect on the DFe concentration, and the related nutrient removal, in the Weddell Gyre. Nevertheless, the concentration of DFe appears to influence the diatom growth in the Weddell Sea, although this effect is related with the diatom size. The difference in deep water DFe concentrations between the transect here presented and the 0° W transect indicates significant enrichment of deep waters with DFe during eastward transit along the Scotia Ridge. There is an indication of some DFe enrichment with formation of WSBW by downslope convection of shelf waters. However, the small difference from WSDW suggests that this is not a significant DFe source to the WSDW. In the Drake Passage, just North of Elephant Island, strong (~ 2 nM) DFe input from the shelf is observed, following the same isopycnals as earlier observed for shelf water input in this region. The relatively low scale length indicates that DFe enrichment does not reach far north into the Drake Passage, due to the strong eastward velocities of the ACC. However, this makes the shelf region a source of DFe for regions further East, in the Scotia Sea. Generally, surface waters in the Drake Passage have low DFe concentrations (< 0.2 nM), as a result of biological removal, both in Drake Passage and further west, in the remote South Pacific, where DFe concentrations are very low in surface waters. Locally, DFe enrichment is observed caused by atmospheric (58.3° S) or fluvial input sources (55.1° S; above Patagonian shelf). Dissolved Fe concentrations of > 1 nM are observed in the deep waters in the South of the Drake Passage, likely coming from Weddell Sea Deep Waters, enriched with DFe by sediment resuspension or flux from the porewaters during transit over the Scotia Ridge. Further into the Drake Passage, the distribution of DFe generally follows the water masses, with highest DFe in the Circumpolar Deep Waters. Towards the shelf of Tierra del Fuego, strong DFe enrichment is observed in the South Pacific Deep Slope Water, a water mass coming from the Pacific carrying hydrothermal properties, notably elevated Mn and $\delta^3\text{He}$ [Middag *et al.*, 2012 and Sudre *et al.*, 2011].

5.6 References

- Alderkamp, A-C, de Baar, H. J. W., Visser, R.J. W. and Arrigo, K.R. (2010), Can photo inhibition control phytoplankton abundance in deeply mixed water columns of the Southern Ocean? *Limnol. Oceanogr.*, 55(3), 1248–1264 . DOI: 10.4319/lo.2010.55.3.1248
- Alderkamp, A-C, Garcon, V. , De Baar, H.J.W. and Arrigo, K.R. (2011), Short-term photoacclimation effects on photoinhibition of phytoplankton in the Drake Passage (Southern Ocean), *Deep Sea Research Part I: Oceanographic Research Papers*, 58 (9), 943-95
- Ardelan, M.V., Holm-Hansen, O. , Hewes, C.D. , Reiss, C.S., Silva, N.S. , Dulaiova, H. , Steinnes, H. and Sakshaug, E. (2010), Natural iron enrichment around the Antarctic Peninsula in the Southern Ocean, *Biogeosciences*, 7, 11–25, 2010.
- Baars, O. , P.Croot (2011), The speciation of dissolved zinc in the Atlantic Sector of the Southern Ocean, *Deep-Sea Research II*, 58 (25-26) pp. 2720-2732
- Bluhm, K., P.Croot, O.Huhn, G.Rohardt and K.Lochte, (2011), Distribution of Iodide and iodate in the Atlantic sector of the southern ocean during austral summer, *Deep-Sea Research II*, 58 (25-26) pp. 2733-2748
- Blain et al.(2007), Effect of natural iron fertilization on carbon sequestration in the Southern Ocean, *Nature* 44, doi:10.1038/nature05700
- Boyd, P.W., Jickells, T., Law, C.S., Blain, S., Boyle, E.A., Buesseler, K.O., Coale, K.H., Cullen, J.J., De Baar, H.J.W., Follows, M., Harvey, M., Lancelot, C., Levasseur, M., Owens, N.J.P., Pollard, R., Rivkin, R.B., Sarmiento, J., Schoemann, V., Smetacek, V., Takeda, V., Tsuda, A., Turner, S., Watson, A. (2007), Mesoscale iron enrichment experiments 1993–2005: synthesis and future directions. *Science* 315, 612–617.
- Bucciarelli, E., S. Blain, P. Tréguer (2001), Iron and manganese in the wake of the Kerguelen Islands Southern Ocean. *Marine Chemistry* 73 pp.21–36.
- Buma, A.G.J., H.J.W. de Baar, R.F. Nolting, A.J. van Bennekom (1991), Metal enrichment experiments in the Weddell-Scotia Seas: Effects of iron and manganese on various plankton communities. *Limnol. Oceanogr.* 36(8): 1865-1878
- Cassar, N., M.L. Bender, B.A. Barnett, S. Fan, W.J. Moxim, H. Levy II, B. Tilbrook (2007), The Southern Ocean biological response to aeolian iron deposition. *Science* 317, 1067–1070.
- Charrette, M. (2011), The Role of Ocean Mixing in Southern Ocean Iron-fueled Phytoplankton Blooms: Insight from Radium Isotopes.. Presentation at the The Modeling and Synthesis of Southern Ocean Natural Iron Fertilization Workshop. Woods Hole, Monday June 27.
- Chever, F., E. Bucciarelli, G., Sarthou, S. Blain, A.R. Bowie (2010), An iron budget during the natural iron fertilization experiment KEOPS (Kerguelen Islands, Southern Ocean). *Biogeosciences*, 7, 455–468, 2010
- Chever, F., E. Bucciarelli, G., Sarthou, S. Speich, M. Arhan, P. Penven, A. Tagliabue. (2010), Physical speciation of iron in the Atlantic sector of the Southern Ocean along a transect from the subtropical domain to the Weddell Sea Gyre. *Journal of Geophysical Research*, Vol. 115, C10059, doi:10.1029/2009JC005880.
- Croot, P., K. Andersson, M. Öztürk and D. R. Turner (2004), The distribution and speciation of iron along 6°E in the Southern Ocean. *Deep Sea Research Part II* 51 (22-24), 2857-2879.

- Croot, P., O. Baars, P. Streu (2011), The distribution of dissolved zinc in the Atlantic Sector of the Southern Ocean. *Deep-Sea Research II*, 58 (25-26) pp. 2707-2719
- De Baar, H.J.W., A.G.J. Buma, R.F. Nolting, G.C. Cadée, G. Jacques and P.J. Tréguer (1990), On iron limitation of the Southern Ocean: experimental observations in the Weddell and Scotia Seas. *Mar. Ecol. Prog. Ser.*, 65, 105-122
- De Baar, H.J.W., De Jong, J.T.M., Bakker, D.C.E., Löscher, B., Veth, C., Bathman, U., Smetacek, V. (1995), Importance of iron for plankton blooms and carbondioxide drawdown in the Southern Ocean. *Nature* 373 (6513), 412-415.
- De Baar, H.J.W., M.A. van Leeuwe, R. Scharek, L. Goeyens, K.M.J. Bakker, P. Fritsche (1997), Nutrient anomalies in *Fragilariopsis Kerguelensis* blooms, iron deficiency and the nitrate/phosphate ratio (A.C. Redfield) of the Antarctic Ocean. *Deep Sea Research II* 44 (1-2), pp. 229-260
- De Baar, H.J.W., J.T.M. de Jong a, R.F. Nolting, K.R. Timmermans, M.A. van Leeuwe, U. Bathmann, M. Rutgers van der Loeff, J. Sildam (1999), Low dissolved Fe and the absence of diatom blooms in the remote South Pacific Ocean. *Marine Chemistry* (66) pp. 1-34
- De Baar, H.J.W., de Jong, J.T.M. (2001), Distributions, sources and sinks of iron in seawater. In: Turner, D., Hunter, K.A. (Eds.), *Biogeochemistry of Iron in Seawater*, IUPAC Book Series on Analytical and Physical Chemistry of Environmental Systems, vol. 7; 2001, pp. 123-254 (Chapter 5).
- De Baar, H.J.W., P.W. Boyd, K.H. Coale, M.R. Landry, A. Tsuda, P. Assmy, D.C.E. Bakker, Y. Bozec, R.T. Barber, M.A. Brzezinski, K.O. Buesseler, M. Boyé, P.L. Croot, F. Gervais, M.Y. Gorbunov, P.J. Harrison, W.T. Hiscock, P. Laan, C. Lancelot, C. Law, M. Levasseur, A. Marchetti, F.J. Millero, J. Nishioka, Y. Nojiri, T. V. Oijen, U. Riebesell, M.J.A. Rijkenberg, H. Saito, S. Takeda, K.R. Timmermans, M.J.W. Veldhuis, A. Waite, C.S. Wong (2005), Synthesis of Iron Fertilization Experiments: From the Iron Age in the Age of Enlightenment. In: Orr, J. C., S. Pantoja, and H.-O. Pörtner (eds.) *The Oceans in a High-CO2 World. Special Issue of Journal of Geophysical Research C (Oceans)* 110: 1-24.
- Duce, R.A., N.W. Tindale, N.W. (1991), Atmospheric transport of iron and its deposition in the ocean. *Limnology and Oceanography* 36, 1715-1726.
- Dulaiova, H. , Ardelan, M.V., Henderson, P.B., Charette M.A. (2009), Shelf-derived iron inputs drive biological productivity in the southern Drake Passage. *Global Biogeochemical Cycles*, vol. 23, gb4014, doi:10.1029/2008GB003406
- Elrod, V.A., Berelson, W.M., Coale, K.H., Johnson, K.S. (2004), The flux of iron from continental shelf sediments: a missing source for global budgets. *Geophys. Res. Lett.* 31, L12307. doi:10.1029/2004GL020216
- Fahrbach, E., G. Rohardt, M. Schroder, V. Strass (1994), Transport and structure of the Weddell Gyre. *Ann. Geophysicae* 12, pp. 840-855.
- Geider, R.J., J. La Roche (1994), The role of iron in phytoplankton photosynthesis, and the potential for iron-limitation of primary productivity in the sea. *Photosynthesis Research* 39 pp. 275-301
- German, C.R., Livermore, R.A, E.T. Baker, N.I. Bruguir, D.P. Connelly, A.P. Cunningham, P. Morris, I.P. Rouse, P.J. Statham, P.A. Tyler (2000), Hydrothermal plumes above the East Scotia Ridge: an isolated high-latitude back-arc spreading centre. *Earth and Planetary Science Letters* 184(1), 241-250

- Gerringa, L.J.A., A-C Alderkamp, P Laan, C-E Thuróczy, H.J.W. De Baar, M.M. Mills, G.L. van Dijken, H. van Haren, K.R. Arrigo (2011), Fe from melting glacier fuels the algal bloom in Pine Island Bay (Amundsen Sea, Southern Ocean). *Deep-Sea Research Part II*, 71–76, 32–48
- Haine, T.W.N., A.J. Watson, M.I. Liddicoat, R.R. Dickson (1998), The flow of Antarctic Bottom Water the Southwestern Indian Ocean estimated using CFC's. *Journal of Geophysical Research* 103, 27637–27653.
- Hewes, C.D., C.S. Reiss, O. Holm-Hansen (2009), A quantitative analysis of sources for summertime phytoplankton variability over 18 years in the South Shetland Islands (Antarctica) region. *Deep Sea Research Part I* 56(8), 1230–1241
- Hiscock M.R., J. Marra, W.O. Smith Jr., R. Goericke, C. Measures, S. Vink, R. J. Olson, H. M. Sosik, R. T. Barber (2003), Primary productivity and its regulation in the Pacific Sector of the Southern Ocean. *Deep-Sea Research II* 50 533–558.
- Hoffman, L.J., I. Peeken, K. Lochte, P., Assmy, M. Veldhuis (2006), Different reactions of Southern Ocean phytoplankton size classes to iron fertilization. *Limnol. Oceanogr.*, 51(3), 1217–1229
- Hopkinson B.M. Mitchell, G., Reynolds, R.A. Wang, H. Selph, K.E., Measures, C.I., Hewes, C.D., Holm-Hansen, O. Barbeau, K.A. (2007), Iron limitation across chlorophyll gradients in the southern Drake Passage: Phytoplankton responses to iron addition and photosynthetic indicators of iron stress. *Limnol. Oceanogr.*, 52(6), 2540–2554
- Hoppema, M H.J.W. De Baar, E. Fahrbach, H. Hellmer, B. Klein (2003), Substantial advective iron loss diminishes phytoplankton production in the Antarctic Zone. *Global Biogeochemical Cycles*, 17(1), 25 , pp. 1–9.
- Hoppema M., R. Middag, H.J.W. De Baar, E. Fahrbach, E.M. van Weerlee, H. Thomas (2007), Whole season net community production in the Weddell Sea. *Polar Biology* 31, pp.101–111.
- Hoppema, M., F. Dehairs, J. Navez, C. Monnin, C. Jeandel, E. Fahrbach, H.J.W. De Baar (2010), Distribution of barium in the Weddell Gyre: Impact of circulation and biogeochemical processes. *Marine Chemistry* 122, 118–129.
- Huhn, O., H.H. Hellmer, M. Rhein, C. Rodehacke, W. Roether, M.P. Schodlok, M. Schröder (2008), Evidence of deep- and bottom-water formation in the western Weddell Sea. *Deep-Sea Research II* 55, 1098–1116
- Jickells, T.D., L.J. Spokes (2001), Atmospheric iron inputs to the oceans. In: Turner, D., Hunter, K.A. (Eds.), *Biogeochemistry of Iron in Seawater*, IUPAC Book Series on Analytical and Physical Chemistry of Environmental Systems, vol.7 ; 2001, pp. 123–254 (Chapter 4).
- Jullion, L., S. C. Jones, A. C. Naveira Garabato, and M. P. Meredith (2010), Wind-controlled export of Antarctic Bottom Water from the Weddell Sea. *Geophys. Res. Lett.* 37, L09609, doi:10.1029/2010GL042822
- Kahru, M., B. G. Mitchell, S. T. Gille, C. D. Hewes, and O. Holm-Hansen (2007), Eddies enhance biological production in the Weddell-Scotia Confluence of the Southern Ocean. *Geophys. Res. Lett.* 34, L14603, doi:10.1029/2007GL030430
- Klatt, O., E. Fahrbach, M. Hoppema, G. Rohardt (2005), The transport of the Weddell Gyre across the Prime Meridian. *Deep Sea Research Part II* 52 (3–4), 513–528.

- Klinkhammer, G.P., C.S. Chin, R.A. Keller, A. Dählman, H. Sahling, G. Sarthou, S. Petersen, F. Smith, C. Wilson (2001), Discovery of new hydrothermal vent sites in Bransfield Strait, Antarctica. *Earth and Planetary Science Letters* 193 (3–4), 395–407.
- Klunder, M.B., Laan, P., Middag, R., de Baar, H.J.W., van Ooijen, J.C. (2011), Dissolved Fe in the Southern Ocean (Atlantic sector). *Deep-Sea Research II*, 58 (25–26) pp. 2678–2694.
- Lancelot, C., E. Hannon, S. Becquevort, C. Veth, H.J.W. De Baar (2000), Modelling phytoplankton blooms and carbon export production in the Southern Ocean: dominant controls by light and iron in the Atlantic sector in Austral spring 1992 *Deep Sea Research Part I: Oceanographic Research Papers*, 47 (9), pp. 1621–1662.
- Lancelot, C., A. deMontety, H. Goosse, S. Becquevort, V. Schoemann, B. Pasquer, M. Vancoppenolle (2009), Spatial distribution of the iron supply to phytoplankton in the Southern Ocean: a model study. *Biogeosciences Discussions* 6, 4919–4962.
- Laës, A., S. Blain, P. Laan, E.P. Achterberg, G. Sarthou, H.J.W. De Baar (2003), Deep dissolved iron profiles in the eastern North Atlantic in relation to water masses. *Geophys. Res. Lett.* 30 (17), 1–3.
- Lannuzel, D., Schoemann, V., De Jong, J.T.M., Chou, L., Delille, B., Becquevort, S., Tison, J.-L. (2008), Iron study during a time series in the western Weddell pack ice. *Marine Chemistry* 108 (1–2), 85–95.
- Lösscher, B., H.J.W. De Baar, J.T.M. De Jong, C. Veth, F. Dehairs (1997), The distribution of Fe in the Antarctic Circumpolar Current. *Deep-Sea Research Part II* 44 (1–2) pp. 143–187
- Lin, H., S. Rauschenberg, C.R. Hexel, T.J. Shaw, B.S. Twining (2011), Free drifting icebergs as sources of iron to the Weddell Sea. *Deep Sea Research Part II* 58, 1392–1406.
- Luther, III. G.W., and J. Wu (1997), What controls dissolved iron concentrations in the world ocean? - a comment. *Marine Chemistry* 57, pp. 174–181
- Marchetti, A., Cassar, N. (2009), Diatom elemental and morphological changes in response to iron limitation: a brief review with potential paleoceanographic applications. *Geobiology* 7, pp. 419–431
- Martin, J.H., Fitzwater, S.E. (1988), Iron deficiency limits phytoplankton growth in the north-east Pacific subarctic. *Nature* 331 (6154), 341–343.
- Martin, J. H., Gordon, R. M., and Fitzwater, S. E. (1990), Iron in Antarctic waters, *Nature*, 345, 156–158,
- Matano, R.P., A.L. Gordon, R.D. Muench, E.D. Palma (2002), A numerical study of the circulation in the northwestern Weddell Sea. *Deep-Sea Research Part II* 49, 4827–4841
- Meredith, M.P., C.W. Hughes, P. R. Foden (2003), Downslope convection north of Elephant Island, Antarctica: Influence on deep waters and dependence on ENSO. *Geophys. Res. Lett.* 30 (9), 1462, doi:10.1029/2003GL017074.
- Middag R. (2010), Dissolved Aluminium and Manganese in the Polar Oceans. PhD thesis, Rijks University of Groningen, The Netherlands
- Middag, R., H.J.W. de Baar, P. Laan and O. Huhn (2012), The effects of continental margins and water mass circulation on the distribution of dissolved aluminium and manganese in Drake Passage. *J. Geophys. Res.* 117, C01029
- Middag, R., H.J.W. de Baar, P. Laan, P.H. Cai, J.C. van Ooijen (2011), Dissolved manganese in the Atlantic sector of the Southern Ocean. *Deep-Sea Research Part II*, 58 (25–26), 2661–2677.

- Mitchell, G.B., O. Holm-Hansen (1991), Observations of modelling of the Antarctic phytoplankton crop in relation to mixing depth. *Deep Sea Research Part A. Oceanographic Research Papers*, 38 (8-9) pp. 981-1007
- Moore, J. K., M.R. Abbott (2002), Surface chlorophyll concentrations in relation to the Antarctic Polar Front: seasonal and spatial patterns from satellite observations. *Journal of Marine Systems* 37, 69– 86
- Neven, I., J. Stefels, S. van Heuven, H.J.W. De Baar, J.T.M., Elzinga (2011), High plasticity in inorganic carbon uptake by Southern Ocean phytoplankton in response to ambient CO₂. *Deep-Sea Research II*, 58 (25-26), 2636-2646
- Naveira Garabato, A.C., E.L., McDonagh, D.P., Stevens, K.J. Heywood, R.J. Sanders (2002), On the export of Antarctic Bottom Water from the Weddell Sea. *Deep-Sea Research Part II* 49, 4715–4742
- Nielsdottir, M.C., T.S. Bibby, C. Mark Moore, D.J. Hinz, R. Sanders, M. Whitehouse, R. Korb, E.P. Achterberg (2012), *Marine Chemistry* 130-131, 62-72
- Orsi, A.H., W.D. Nowlin Jr, T. Whitworth III (1993), On the circulation and stratification of the Weddell Gyre. *Deep Sea Research Part I* 40, 169-203.
- Planquette, H., P.J. Statham, G.R. Fones, M.A. Charette, C. Mark Moore, I. Salter, F.H. Nedelec, S.L. Taylor, M. French, A.R. Baker, N. Mahowald, T.D. Jickells (2007), Dissolved iron in the vicinity of the Crozet Islands, Southern Ocean. *Deep-Sea Research Part II* 54, 1999–2019
- Pollard, R.T., M.I. Lucas, J.F. Read (2002), Physical controls on biogeochemical zonation in Southern Ocean. *Deep Sea Research Part II* 49 (18) 3931-3950.
- Raiswell, R. (2011), Iceberg-hosted nanoparticulate Fe in the Southern Ocean: Mineralogy, origin, dissolution kinetics and source of bioavailable Fe. *Deep-Sea Research Part II*, 58 (11-12), 1364-1375
- Renault, A., C. Provost, N. Sennechael, N. Barré, A. Kartavtseff (2011), Two full-depth velocity sections in the Drake Passage in 2006—Transport estimates, *Deep-Sea Research Part II*, 58 (25-26) 2572-2591
- Rijkenberg, M., L.J.A, Gerringa, P. Laan, V. Schoemann, R. Middag, S.M.A.C. van Heuven, L. Salt, H.M. van Aken, J.T.M. De Jong and H.J.W. De Baar (2011), Dissolved Fe in the Western Atlantic Ocean: Distribution, sources, sinks and cycling. Abstracts Goldschmidt Conference, Prague 2011.
- Rutgers vanderLoeff, M., P. Cai, I. Stimač, A. Bracher, R. Middag, M.B. Klunder, van Heuven, S. (2011), ²³⁴Th in surface waters: distribution of particle export flux across the Antarctic Circumpolar Current and in the Weddell Sea during the GEOTRACES expedition ZERO and DRAKE. *Deep-Sea Research Part II*, 58 (25-26) pp. 2749-2766
- Sañudo-Wilhelmy, S.A., K.A. Olsen, J.M. Scelfo, T.D. Foster, A.R. Flegal (2002), Trace metal distributions off the Antarctic Peninsula in the Weddell Sea. *Marine Chemistry* 77, 157-170.
- Sarthou, G., K.R. Timmermans, S. Blain, P. Tréguer (2005), Growth physiology and fate of diatoms in the ocean: a review. *Journal of Sea Research* 53, 25-42
- Sokolov, S. and Rintoul, S.R. (2007), On the relationship between fronts of the Antarctic Circumpolar Current and surface chlorophyll concentrations in the Southern Ocean. *J. Geophys. Res.* 112, C07030.

- Stuart, K.M, D.G. Long (2011), Tracking large tabular icebergs using the SeaWinds Ku-band microwave scatterometer. *Deep Sea Research Part II: Topical Studies in Oceanography*, 58 (11-12), 1285-1300.
- Sudre, J., Garçon, V., Provost, C., Sennechaël, Huhn, O., Lacombe, M. (2011), Multiparametric analysis of water masses across Drake Passage during ANT-XXIII/3. *Deep-Sea Research Part II*, 58 (25-26), 2592-2612
- Tagliabue, A., L. Bopp, J-C. Dutay, A.R. Bowie, F.Chever, P.Jean-Baptiste, E. Bucciarelli, D. Lannuzel, T.Remenyi, G.Sarthou, O.Aumont, M.Gehlen, C.Jeandel (2010), Hydrothermal contribution to the oceanic dissolved iron inventory. *Nature Geosciences* 3, 252 – 256.
- Tagliabue, A., T. Mtshali, O. Aumont, A. R. Bowie, M. B. Klunder, A.N. Roychoudhury, S. Swart (2012), A global compilation of dissolved iron measurements: focus on distributions and processes in the Southern Ocean. *Biogeosciences*, 9, 2333-2349
- Takeda, S. (1998), Influence of iron availability on nutrient composition ratio of diatoms in oceanic waters. *Nature* 393:774-777.
- Timmermans K.R., B. v.d Wagt, H.J.W. De Baar (2004), Growth rates, half-saturation constants, and silicate, nitrate, and phosphate depletion in relation to iron availability of four large, open-ocean diatoms from the Southern Ocean. *Limnol. Oceanogr.*, 49(6), 2141–2151
- Well, R., W. Roether, D.P., Stevens (2003) An additional deep water mass in Drake Passage as revealed by ³He data. *Deep-Sea Research Part I* 50 (9), 1079-1098.
- Weppernig R., P. Schlosser, S. Khatiwala, R.G. Fairbanks (1996), Isotope data from ice Station Weddell: implications for deep water formation in the Weddell Sea. *J. Geophys. I Res.* 101, 25723-25739.



Chapter 6

**Distribution of dissolved iron in the
Southern Ocean:
a compilation of high quality data
in four depth layers**



Abstract

The Southern Ocean is known as a region within the world oceans, where iron (Fe) can be the limiting factor for phytoplankton growth. Within the Southern Ocean, the ACC (Antarctic Circumpolar Current) is the eastward flowing current extended uninterrupted around the Antarctic continent. In this study, all available dissolved iron ($< 0.4 \mu\text{m}$) concentrations within the ACC, Weddell Gyre and Ross Gyre are compiled and averaged over four different depth layers: (i) upper mixed layer (UML), (ii) subsurface (UML<subsurface<300 m.), (iii) intermediate (300 < intermediate <1000 m), and (iv) deep (>1000 m) waters. The average concentration of dissolved iron increases with depth, from 0.28 nM in the upper mixed layer waters to 0.56 nM below 1000 meters. Slightly higher concentrations south of the Polar Front region (PFR), compared to within the PFR are attributed to upwelling of deep waters, mainly in the Atlantic sector. For the upper mixed layer, subsurface and intermediate waters, values are high just east of Patagonia, and in eastward general flow direction tend to stabilize in the Indian and Pacific sectors. Surface DFe in the Atlantic and Indian Sectors is higher than in the Pacific Sector. DFe increases and stabilizes with depth; the relative standard deviation is lower, but differences between the Atlantic, Indian and Pacific basins remain.

For the Weddell Gyre, the dissolved iron is similar in the eastward flow compared to the westward flow more to the south, for all depths. However, there is more variability in the DFe concentrations in the latter westward flow. Much higher concentrations are observed near to the Antarctic Peninsula, indicating the importance of sedimentary processes as an Fe source.

In the Ross Sea, the average DFe concentrations are ~ 0.2 nM in the upper 300 m, possibly reflecting both removal by biological uptake, but also input from sedimentary sources. Deep in the water column DFe increases to ~ 0.4 nM, as a result of regeneration of DFe and inflow of waters further North.

This compilation study addresses and quantifies the mechanisms accounting for the dissolved iron concentration available to phytoplankton growth in the Southern Ocean. Moreover, this study does provide high quality ground-truthed data for modeling studies.

6.1 Introduction

Dissolved iron is well known to be of major importance for primary production in the world oceans; it is needed for vital processes, amongst which are photosynthesis and respiratory electron transport [Sunda, 2001]. Therefore, a deficit of iron can diminish phytoplankton growth, even when sufficient amounts of major nutrients are present [Martin et al, 1988]. Large regions in the world Ocean, primarily the subArctic North Pacific, the Equatorial Pacific and the Southern Ocean are known to be such High Nu-

trient Low Chlorophyll (HNLC) regions. [Martin *et al.*, 1988, De Baar and Boyd, 2000; Boyd *et al.* 2001, De Baar *et al.*, 1990, 2005].

The northern boundary of the Antarctic Circumpolar Current is the Subtropical Front [Orsi *et al.*, 1995] situated at about 40 °S (Figure 6.1), and here we take 40 °S as the northern limit of the here presented dataset of dissolved Fe. The continuous eastward flow of the ACC is driven by the mighty westerly winds around ~45-55 °S [Trenberth [1990], and continues around the Antarctic continent without being interrupted. Due to its undisturbed, fast flowing nature, the ACC is considered a connection between the Atlantic, Indian and Pacific Oceans [Rintoul *et al.*, 2001]. The ACC extends the entire span from the sea surface to the deep seafloor, and as such is by far the largest ocean current in the world, with an estimated transport rate of about 150 Sv [Mazloff *et al.*, 2010].

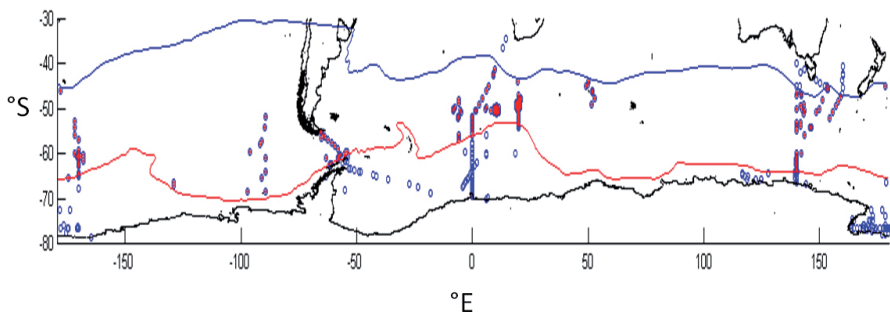


Fig. 6.1 Schematic overview of the Southern Ocean with coastline in black, the Subtropical Front (Blue) and the Southern Boundary of the ACC (Red). Stations with DFe data are given in blue, data used for the ACC Compilation is marked in red within the blue circle. Other data for the Weddell Gyre and Ross Sea Gyre are open symbols south of the ACC. Open symbols north of the Subtropical Front are excluded from this study.

In general, the Southern Boundary of the ACC (SB-ACC) is located very near to the Antarctic Continent. At Drake Passage, however, this pattern changes; the narrow passage causes the ACC to accelerate, and the bottom topography of the Scotia Ridge (<2000 m), causes the ACC to shift northward. This relatively northern location of the Southern Boundary of the ACC enables the Weddell Gyre to extend as far north as 50 °S [Orsi *et al.* 1995] (Fig. 6.1). The Weddell Gyre (WG) is the large scale cyclonic circulation pattern in (and eastward beyond) the Weddell Sea. In the south, the WG extends almost as far as the Antarctic continent, following a westwards flow pattern, towards the Antarctic Peninsula, where it follows bottom topography to the north along the Antarctic Peninsula, and then flows eastwards following the ridge system of the South Scotia, North Weddell and Southwest Indian ridges (Figure 6.1, [Klatt *et al.* 2005]). A similar shift northwards of the SB-ACC is observed at ~ 160 °E – 140 °W, where the Ross Gyre extends northward from the Antarctic continent (Fig. 6.1).

Further southwards there is still the permanently ice-covered part of the Weddell Sea proper, for which thus far no DFe data exists. On the other hand, for the Ross Sea that is mostly open waters in most austral summers, there is a relatively small set of DFe values available in the literature.

The important role of Fe for primary production has led to several expeditions over the past decades to determine the distribution and sources and sinks of (dissolved) iron (Fe) in the Southern Ocean. Nevertheless, because of the vast area (14% of the surface of the planet), the harsh conditions and the difficulty of the very contamination-sensitive iron sampling and analysis, the Southern Ocean is still relatively sparsely studied (both spatially and temporally). Most studies were conducted in spring-summer, and thus far mostly restricted to the upper 300-800 metres. Some studies have focused on the open ACC and its fronts [De Baar *et al.*, 1995; Löscher *et al.*, 1997; De Baar *et al.*, 1999; De Jong *et al.*, 1998; Boye *et al.*, 2001]. Other studies were mostly situated around the Southern Ocean Islands [Bucciarelli *et al.*, 2001; Planquette *et al.* 2007; Blain *et al.*, 2008]. Moreover, many studies were aimed at the effects of Fe addition as to relieve Fe limitation of the plankton ecosystem and the ensuing mechanism of drawdown of atmospheric CO₂, and amended mostly the artificial Fe concentrations.

The preceding studies have provided insight into the distribution and input sources of dissolved iron (DFe) to the Southern Ocean. In the surface waters dissolved Fe input is caused by dissolution from dust deposition, upwelling of deep waters, melt of sea-ice and icebergs, input of DFe from continental margins and plateaus and from Subtropical surface waters [Sedwick *et al.* 1999, 2008; Measures *et al.*, 2001; Croot *et al.*, 2004; Blain *et al.*, 2008; Lannuzel *et al.*, 2008; Klunder *et al.*, 2011, Bowie *et al.*, 2009, This thesis, Chapter 5]. Mixing with deep water masses flowing in from higher latitudes (NADW, Klunder *et al.*, 2011), sedimentary input [Tagliabue *et al.*, 2009] and hydrothermal vents [Klinkhammer *et al.* 2001; Klunder *et al.*, 2011, 2012] are known to be important sources of Fe to the deep waters. Progress has been made recently in modeling studies determining and quantifying processes which affect the concentration of DFe in the Southern Ocean. These studies indicate that the input sources are not evenly distributed between the three different Southern Ocean Sectors, and that there are large spatial and temporal differences between input sources [Parekh *et al.*, 2005; Moore and Braucher, 2008, Tagliabue *et al.*, 2009; Lancelot *et al.*, 2009; Tagliabue *et al.*, 2010]. None of these studies exclusively focuses on the differences within the Southern Ocean, notably the between ACC and the Weddell Gyre and Ross Sea Gyre and between the different Antarctic regions.

The fast flowing, circular nature of the ACC will, partly, determine the distribution of nutrients and trace elements within the ACC, e.g. the concentration of these elements in a certain region will depend both on the input and concentration “upstream” as well as local processes and fluxes [Green and Sambrotto, 2006]. The same holds, to a lesser extent, for the slower moving cyclonic Weddell Gyre and Ross Sea Gyre.

Upon a first limited compilation of oceanic data of dissolved Fe, restricted to data of mostly one laboratory [Johnson *et al.*, 1997], it became apparent that in previous articles data had been omitted without reporting such. Next a detailed comprehensive compilation of all world ocean data was produced as a worldwide community effort, with special attention also to including and appropriate reporting of rejected data values [De Baar and De Jong, 2001]. This was succeeded by data compilations of Parekh *et al.* (2005) and Moore and Braucher (2008), respectively. In general, in all these global ocean Fe databases, the vast Southern Ocean was underrepresented compared to the other Oceans.

Very recently improved ultraclean deep water sampling systems [De Baar *et al.*, 2008] have been deployed in the GEOTRACES program in the context of the 2007-2008 International Polar Year (www.geotraces.org). The far more intensive sampling at higher spatial resolution has resulted in a large number of new data in the Southern Ocean [Lai *et al.*, 2008 ; Sedwick *et al.*, 2008; Klunder *et al.*, 2011; Lannuzel *et al.*, 2012]. This is particularly true in the deeper (>500m) waters, where almost four times as much data is available since 2008. Moreover by the regular measurement of reference samples provided by the SFe and GEOTRACES programs (www.geotraces.org), for the first time an independent quality assurance has been achieved for these recently produced large data sets. This has also provided a more objective benchmark for assessing the accuracy, or not, of previously published data.

Here, we compile all Fe data within the ACC, Weddell Gyre and Ross Gyre, and group this data by defining four different depth layers: (i) the upper mixed layer (UML), (ii) the subsurface layer (UML<subsurface<300 m.), (iii) the intermediate layer (300 < intermediate <1000 m.) and (iv) the deep (>1000 m) waters. For each station the upper mixed layer is defined as it was found at time of sampling, i.e. for each station there is the individual UML depth that serves for grouping the data. For all four depths intervals, we look at spatial (latitudinal, longitudinal) and temporal trends, to better establish regional dissolved iron distribution and different Fe sources within the Southern Ocean. We attempt to constrain, if present, the “upstream” effect of the ACC and Weddell Gyre. The Polar Front (PF) is often mentioned as a region of enhanced Fe input, because of its frontal dynamics [De Baar *et al.*, 1995; Löscher *et al.*, 1997; De Jong *et al.*, 1998; Boye *et al.*, 2001; Croot *et al.*, 2004]. Moreover, the Polar Front region is known to contain elevated concentrations of chlorophyll-a. This study presents a differentiation between the waters within, north of and south of the Polar Front (PF) [Orsi *et al.*, 1995].

The depth-differentiated compilation enables us to better constrain the distribution of Fe within the ACC and the sources of DFe to the ACC. This study gives insight in the role of Fe in the biological pump within the ACC and Weddell Gyre regions. Moreover, this compilation enables a large step forward in the merging of model and field studies of Southern Ocean iron biogeochemistry.

6.2 Data and Method

The starting point of our data set is the dissolved iron concentrations in the ACC and the Weddell Gyre, as recently obtained by the authors during the ANT XXIV/3 expedition in 2008 of RV Polarstern along the Greenwich Meridian, and next crossing the Weddell Sea and Drake Passage [Klunder *et al.*, 2011], and the 2009 Amundsen Sea expedition NPB01 aboard RV IB. Nathaniel B. Palmer [Gerringa *et al.*, 2012]. During the ANT XXIV/3-cruise, the sampling was performed using the trace metal clean sampling system Titan as described by De Baar *et al.* [2008]. During NPB01, independent GOFLO samplers were mounted one by one on a simple 6 mm diameter Dyneema hydrowire and tripped with all-plastic messengers. Analysis of dissolved iron concentrations was done with an automated flow injection system as described in De Jong *et al.* [1998]. This method was slightly modified as described in Klunder *et al.* [2011]. During the ANT XXIV/3 and NPB01 cruises 0.2 μm filters were used to define 'dissolved' Fe. However, during several other studies for DFe in the Southern Ocean 0.4 μm filters have been used. Bruland and Rue [2001] mention 0.2 – 0.4 μm pore size filters as the “widely accepted way of operationally defining dissolved metal forms in seawater” We therefore define “dissolved” iron as all iron in the fraction $<0.4 \mu\text{m}$. The GEOTRACES community researchers have agreed on using 0.2 μm filters in the future.

The DFe concentrations of the ANT XXIV/3 cruise [Klunder *et al.*, 2011] This thesis, Chapter 5] are the basis of the data compilation. For this, and the other data sets mentioned below, the outliers that had been rejected in the original articles and data sets were excluded. Secondly other recently published datasets by others were added [Sedwick *et al.*, 2008; Lannuzel *et al.*, 2008]. Next from the original articles and datasets, data was selected and included. Several articles and data were also mentioned in preceding data compilations [Johnson *et al.*, 1997; De Baar and De Jong, 2001; Parekh *et al.*, 2005; Moore and Braucher, 2008]. On the other hand some original data was excluded by the following criteria. Briefly high dissolved Fe values reported very near to the coast, in a study aimed to investigate the DFe coming from ocean islands (and their surrounding shelves [Blain *et al.*, 2001 (DFe 0.52 -12 nM); Bucciarelli *et al.*, 2001 (DFe 0.26 – 1.94 nM) and (coastal stations of) Planquette *et al.*, 2007 (DFe 0.4-2.16 nM)], and very high dissolved Fe due to very nearby hydrothermal vents [Klinkhammer *et al.*, 2001 (DFe 2.16 – 12.56 nM)] were excluded. Moreover, two ISPOL stations reported by De Jong *et al.* [2011] (DFe 0.6- 23.4 nM) are not included due to their anomalous high concentration as a result of shelf processes. Also some historical datasets that appear to have very high Fe concentrations compared to very recently obtained values in the same region, are excluded. For each excluded dataset a specified account is given in the online, the appendix provides the reference citations of such not-used data sets.

For all stations, the average DFe was calculated for different depth intervals. The first depth interval was the upper mixed layer as defined by homogenous seawater

ter density (i.e. salinity and temperature) until the depth where a significant gradient of density was observed. Depth of the upper mixed layer in this compilation varied from 10 to 400 meter depth, averaging at 80 ± 47 m depth. The UML interval included 477 data points averaged over 195 stations. Below the UML the concentrations were averaged over the depth interval between UML depth and 300 m. We named these subsurface waters, and they comprised 539 data points averaged over 191 stations. Below the subsurface waters, the intermediate waters are from 300 to 1000 meter depth. This interval has 320 data points over 109 stations. Finally 428 data points are found in the deep waters >1000 meter, averaged over 58 stations. The source publications of all the included data sets are listed in the references. The complete data set, including Fe values, date, latitude, longitude, Fe analysis method, filter size, UML depth and references are available in the online supplement. Here also the excluded data sets and their underlying source articles are summarized.

6.3 Results

Figures 6.2-6.5 show chart plots of the dissolved Fe concentrations in the 4 different depth layers. Per station, values are averaged over the depth interval. It is very clear that the dissolved iron concentration increases with depth, from 300m downwards. Since most historical data is measured in the upper surface waters, the highest number of samples is found in the UML and subsurface waters. On the other hand, the deep waters include the lowest number of samples, and therefore display a lower spatial resolution around the Southern Ocean. Similar figures are shown for the Weddell Sea stations in the four different depth layers in figures 6.6-6.9 and for the Ross Sea in figures 6.10-6.13. The low number of DFe data > 1000m in the Ross Sea can be explained by the fact that the Ross Sea for a large part has a continental shelf > 1000m.

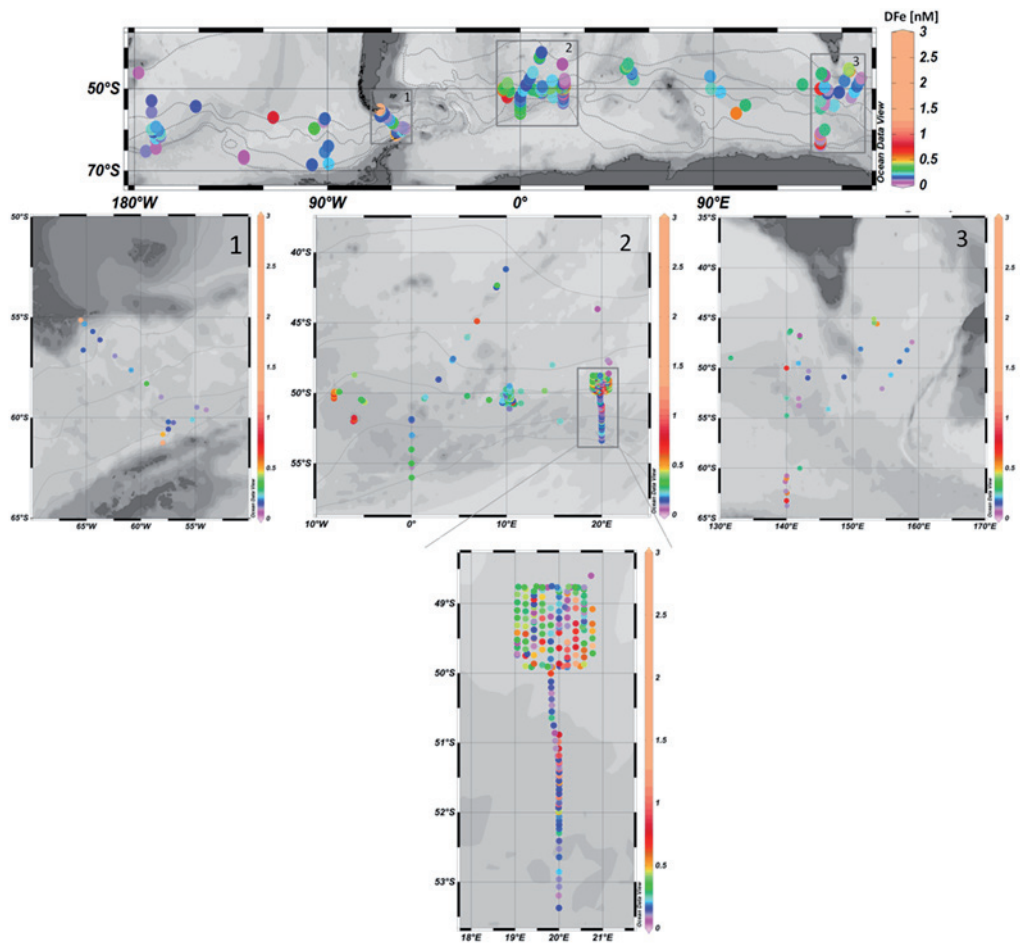


Fig. 6.2 Dissolved Fe averaged over the UML per station. Regions with dense sampling are shown enlarged. Grey lines represent fronts (STF, SAF, PF, SACCF, SB-ACC).

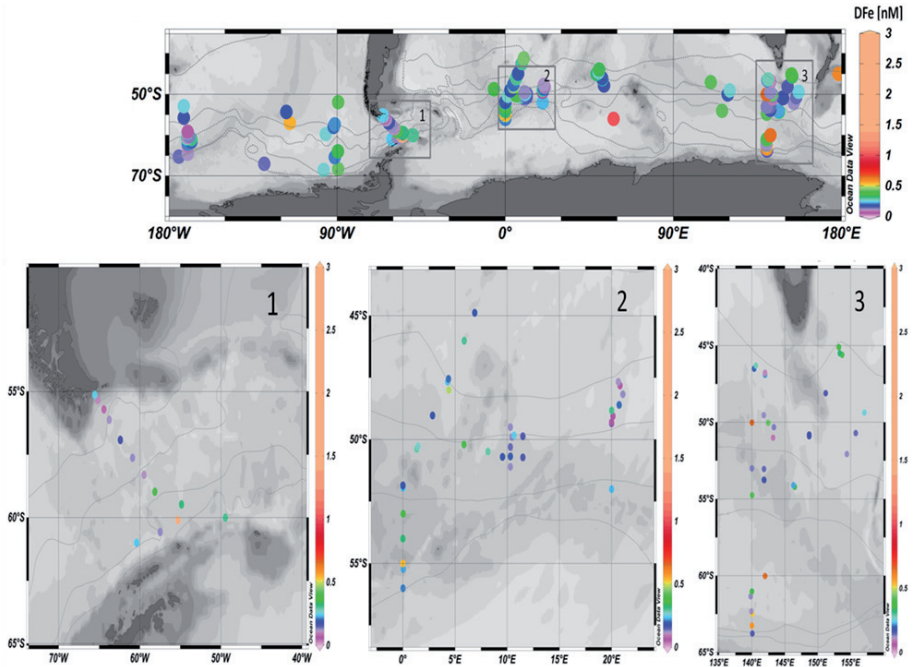


Fig. 6.3 Dissolved Fe averaged over the Subsurface Layer (UML-300m) per station. Regions with dense sampling are shown enlarged. Grey lines represent fronts (STF, SAF, PF, SACCF, SB-ACC).

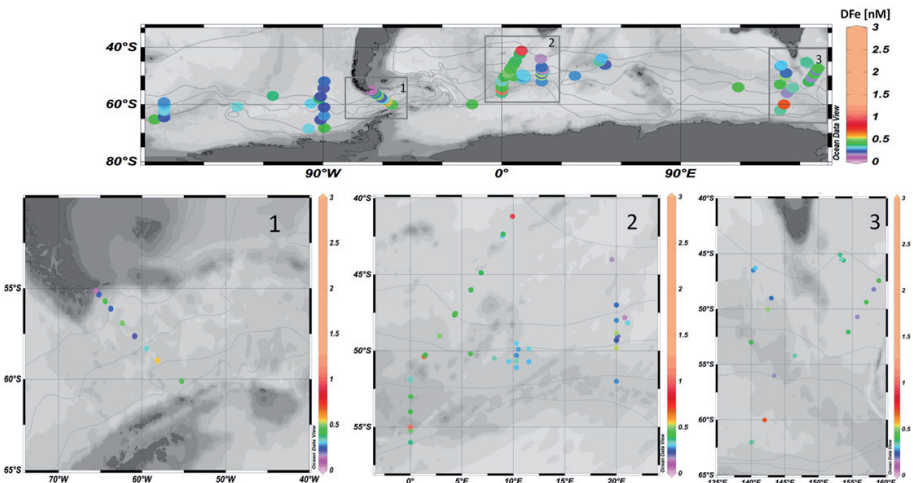


Fig. 6.4 Dissolved Fe averaged over the Intermediate Layer (300-1000m) per station. Regions with dense sampling are shown enlarged. Grey lines represent fronts (STF, SAF, PF, SACCF, SB-ACC).

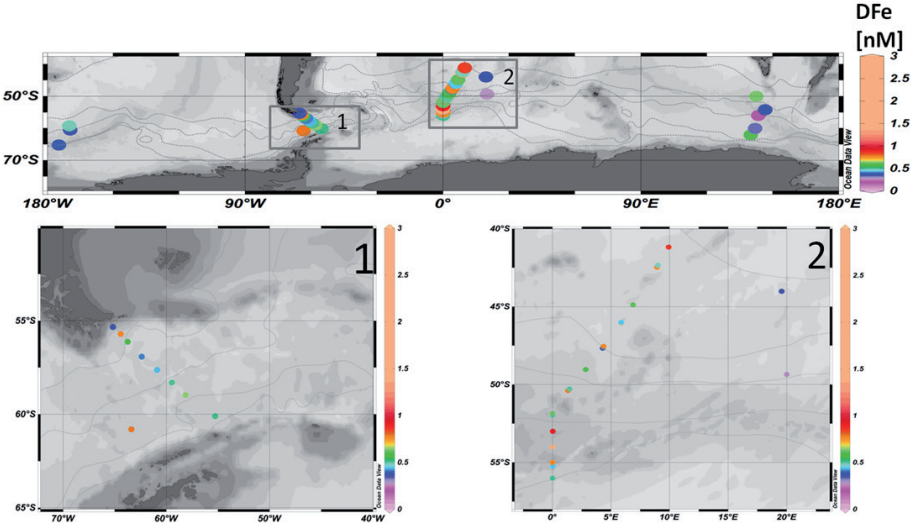


Fig. 6.5 Dissolved Fe averaged over the Deep Layer (>1000m) per station. Regions with dense sampling are shown enlarged. Grey lines represent fronts (STF, SAF, PF, SACCf,SB-ACC).

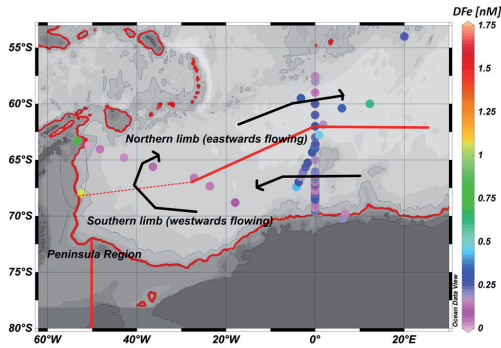


Fig. 6.6

Dissolved Fe in the Weddell Sea averaged over the Upper Mixed Layer per station. Three different regions are marked (see text). The flow of the Weddell Gyre is indicated.

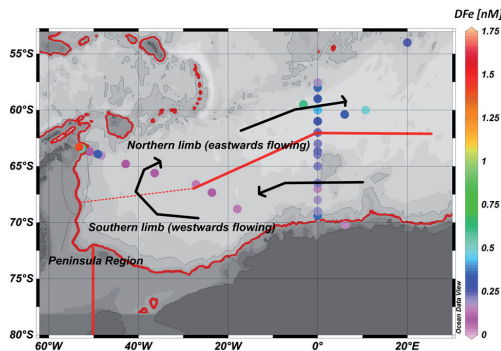


Fig. 6.7

Dissolved Fe in the Weddell Sea averaged over the Subsurface Layer (UML-300m) per station. Three different regions are marked (see text). The flow of the Weddell Gyre is indicated.

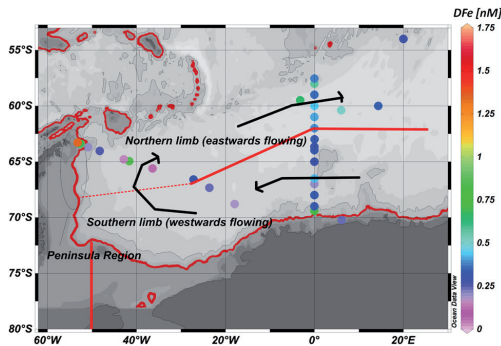


Fig. 6.8

Dissolved Fe in the Weddell Sea averaged over the Intermediate Layer (300-1000m) per station. Three different regions are marked (see text). The flow of the Weddell Gyre is indicated.

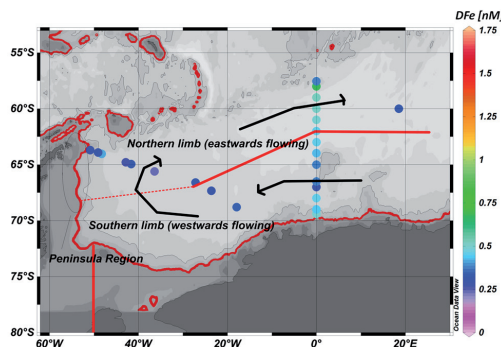


Fig. 6.9

Dissolved Fe in the Weddell Sea averaged over the Deep Layer (>1000m) per station. Three different regions are marked (see text). The flow of the Weddell Gyre is indicated.

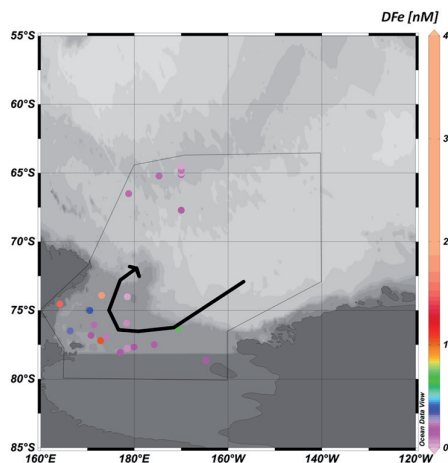


Fig. 6.10

Dissolved Fe in the Ross Sea averaged over the Upper Mixed Layer per station. The region of the Ross Sea Gyre is depicted (schematically). The flow of the Ross Sea Gyre is indicated.

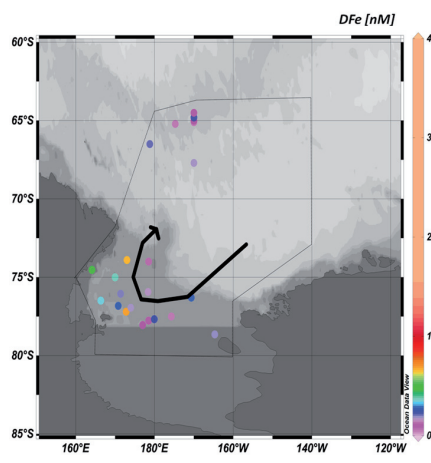


Fig. 6.11

Dissolved Fe in the Ross Sea averaged over the Subsurface Layer (UML-300m) per station. The region of the Ross Sea Gyre is depicted (schematically). The flow of the Ross Sea Gyre is indicated.

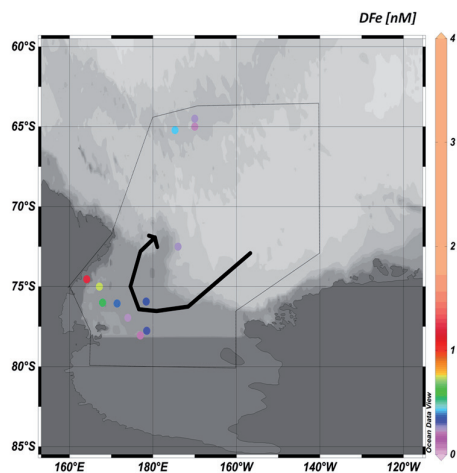


Fig. 6.12

Dissolved Fe in the Ross Sea averaged over the Intermediate Layer (300-1000m) per station. The region of the Ross Sea Gyre is depicted (schematically). The flow of the Ross Sea Gyre is indicated.

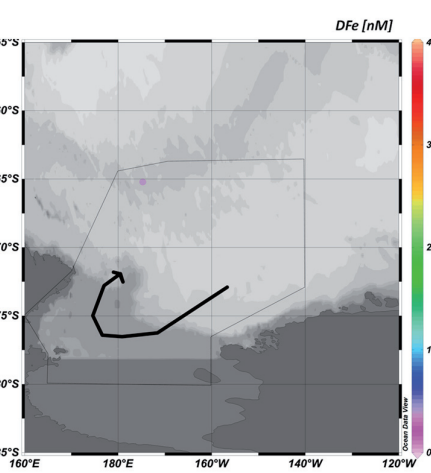


Fig. 6.13

To the best of our knowledge, there is only 1 Deep (>1000m) station in the Ross Sea Gyre. To be systematic, this graph is shown. Dissolved Fe in the Ross Sea averaged over the Deep Layer (>1000m) per station. The region of the Ross Sea Gyre is depicted (schematically). The flow of the Ross Sea Gyre is indicated.

6.3.1 Upper Mixed Layer

6.3.1.1 Antarctic Circumpolar Current

Figure 6.1 shows the DFe concentration averaged over the upper mixed layer for all stations situated within the ACC. Because of relatively intensive sampling south of the South-American, African and Australian continents, we zoomed in on these regions (Fig. 6.1). Figures 6.1-6.13 show that the Southern Ocean has vast areas that have yet to be investigated; there are no data points from 60~120 °E, and one data-point between 100 and 160 °W. Nevertheless, in the studied areas the dissolved Fe concentration in the surface waters around the ACC are low, generally <0.3 nM, with a few exceptions (around Tasmania, New Zealand, above the Bouvet Ridge at 6°W, and close to land/shelf regions). This is reflected in the average DFe concentrations in the UML of 0.28 ± 0.29 nM ($n=791$). Average DFe concentrations of the different sectors of the Southern Ocean and the difference between sectors are summarized in Table 6.1. Significantly ($p<0.05$) higher concentrations are found in the Atlantic sector and Indian Sector, compared to the the Pacific Sector. However, the DFe data in the Indian sector may be influenced by some very high DFe concentrations measured, resulting in a much larger standard deviation than the Atlantic Sector (see boxplots in figure 6.14).

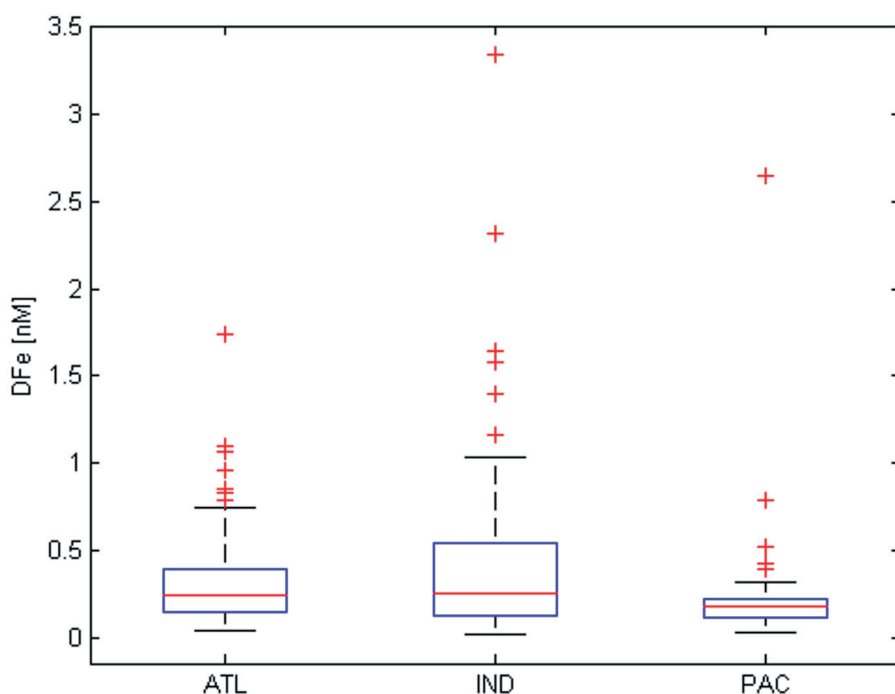


Fig. 6.14 Boxplots of DFe data in the Upper Mixed Layer, divided by sector.

Table 6.1 Dissolved Fe per sector. Properties and statistical differences are given. See text for division of the sectors.

	ATL	PAC	IND
Mixed Layer (ML)			
Average DFe	0.30	0.20	0.32
Stdev	0.27	0.21	0.34
Geometric mean	0.23	0.15	0.22
Min	0.01	0.03	0.02
Max	2.50	2.64	3.34
p-value*	1.23E-05**	2.47E-06***	3.39E-01***
# samples	305	206	279
Subsurface Layer (ML-300m)			
Average DFe	0.34	0.20	0.28
Stdev	0.51	0.14	0.19
Geometric mean	0.22	0.16	0.22
Min	0.01	0.02	0.03
Max	3.75	1.00	1.06
p-value*	0.001	0.000	0.113
# samples	156	235	279
Intermediate Layer (300-1000m)			
Average DFe	0.43	0.31	0.32
Stdev	0.22	0.12	0.14
Geometric mean	0.38	0.29	0.29
Min	0.10	0.09	0.09
Max	1.82	0.69	0.79
p-value*	0.000	0.711	0.000
# samples	115	120	87
Deep Layer (> 1000m)			
Average DFe	0.62	0.52	0.43
Stdev	0.31	0.31	0.30
Geometric mean	0.57	0.47	0.36
Min	0.21	0.24	0.15
Max	2.21	1.94	1.44
p-value*	0.046	0.170	0.001
# samples	133	52	42

* p-value of 2 sided t-test, bold if $p < 0.05$ (= significant difference) **Atlantic Sector → Indian Sector; *** Indian Sector → Pacific Sector; **** Pacific Sector → Atlantic Sector

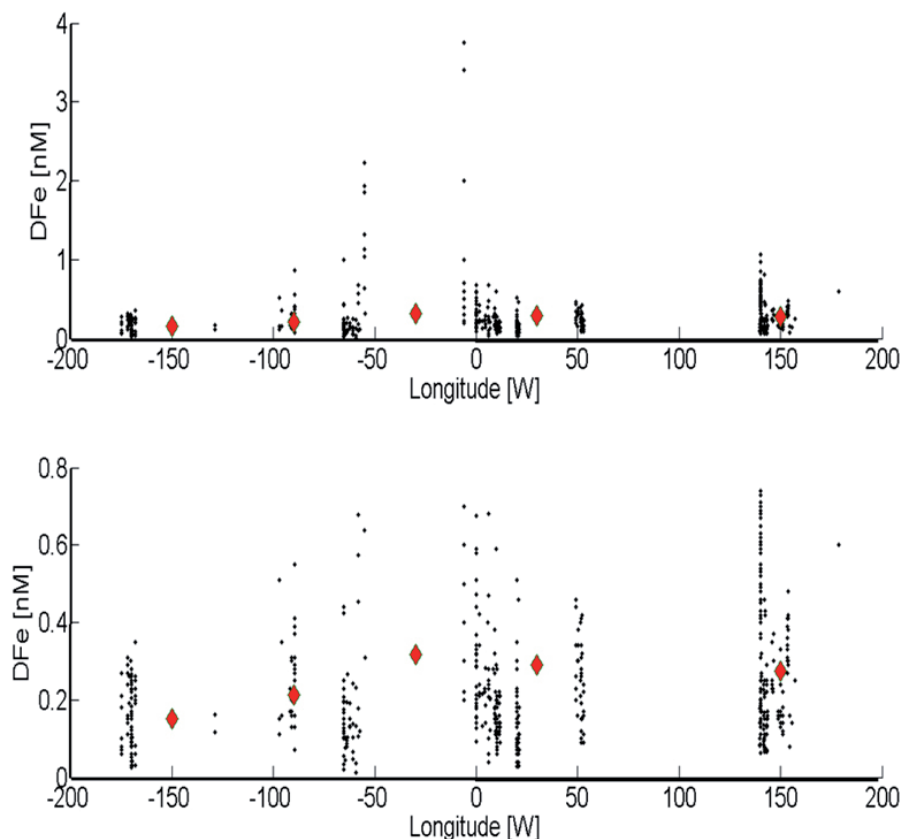


Fig. 6.15 DFe concentrations vs. longitude for individual datapoints in the Mixed Layer in large scale (upper graph) and smaller scale (lower graph); red dots indicated averages over 60° longitude

Figure 6.15 shows all available data points averaged over bins of 60° longitude. There is a trend of DFe enrichment in the 60°W-0°W regions compared to the other regions. This region comprising the Atlantic Sector just east of Patagonia shows the largest increase of Fe in the surface waters, indicating a strong input source. Further towards the East, average concentrations decrease to a lowest value in the region 180-120°W, in the remote Pacific sector.

The latitudinal differences within the UML are shown in figure 6.16. There is no significant trend in DFe values with latitude. However, when averaging the DFe datapoints over 5° latitude intervals, there appears to be a (very) weak trend with higher values in the North changing to lower values approaching the Antarctic continent. This is interrupted by a slight increase in the region (55-60°S) (fig. 6.16), just south of the Polar Front.

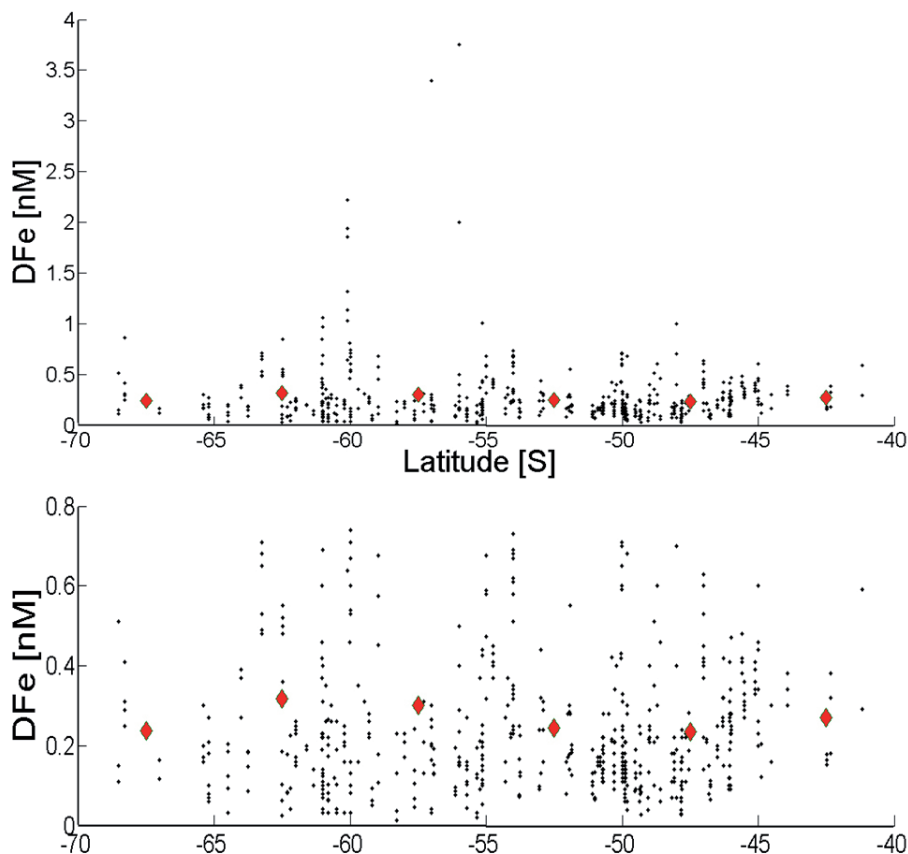


Fig. 6.16 DFe concentrations versus latitude for individual datapoints in the Mixed Layer in large scale (upper graph) and smaller scale (lower graph); red dots indicated averages over 5° latitude

6.3.1.2 Weddell Gyre

In this work we compare DFe in three different regions of the Weddell Gyre, defined by its hydrography based on work of Klatt *et al.*, 2005 and Fahrbach *et al.*, 1994 (see appendix). Briefly, the Weddell Gyre is divided in a westwards flowing limb (WFL) close to the Antarctic continent, and an eastwards return flow limb (EFL), close to Bouvet ridge. Data from the stations where bottom depth was less than 1000m (west of 40°W) are grouped as the “Peninsula region (Pr)” (Fig. 6.6). Figure 6.6 displays the concentration of DFe averaged over the UML in the Weddell Gyre. The DFe varies widely over the Weddell Gyre region. Generally low concentrations are observed in the Westwards Flowing Limb in the south of the Gyre and central Weddell Sea, although there were also some higher concentrations (range 0.02-1.57 nM) (Fig 6.6). Similar concentrations are seen in the eastwards flowing, northeast part of the Weddell Gyre (0.12-1.46 nM). There is a gap in data for the lower latitudes, close to the North Weddell - South Indian Ridge system from ~45°W to ~6°W. The dissolved iron

concentrations close to the Antarctic Peninsula (west of $\sim 50^\circ\text{W}$) are high in general but have strong variability (<0.010 (below detection limit) - 2.64 nM)

Table 6.3 gives the average DFe in the UML, with standard deviations in statistical differences (T-test) between the three different parts of the Weddell Gyre. The Peninsula region has a significantly higher concentration of DFe compared to the eastward and westward flow. The westward flow and eastward return flow have a similar average concentration. However, the number of samples is relatively low; for the combined UML and UML-300m depth intervals, we obtain 109, 117 and 37 samples in the westwards, eastwards limb and Peninsula region respectively. These results show that the westward flow has a significantly lower concentrations of DFe, compared to the eastward return flow, in the upper 300 meters.

6.3.1.3 Ross Gyre

The concentration of DFe in the upper mixed layer in the Ross Sea is marked by a very high standard deviation (figure 6.10). There is a total of 189 samples, varying from $0.02\text{--}4.1\text{ nM}$. The average DFe is $\sim 0.68\text{ nM}$ (table 6.4), whereas the median is $\sim 0.2\text{ nM}$ (boxplot, fig 6.17). This indicates that there is a large number of very low DFe concentrations and some samples having very high concentrations causing a large variation (see fig. 6.17).

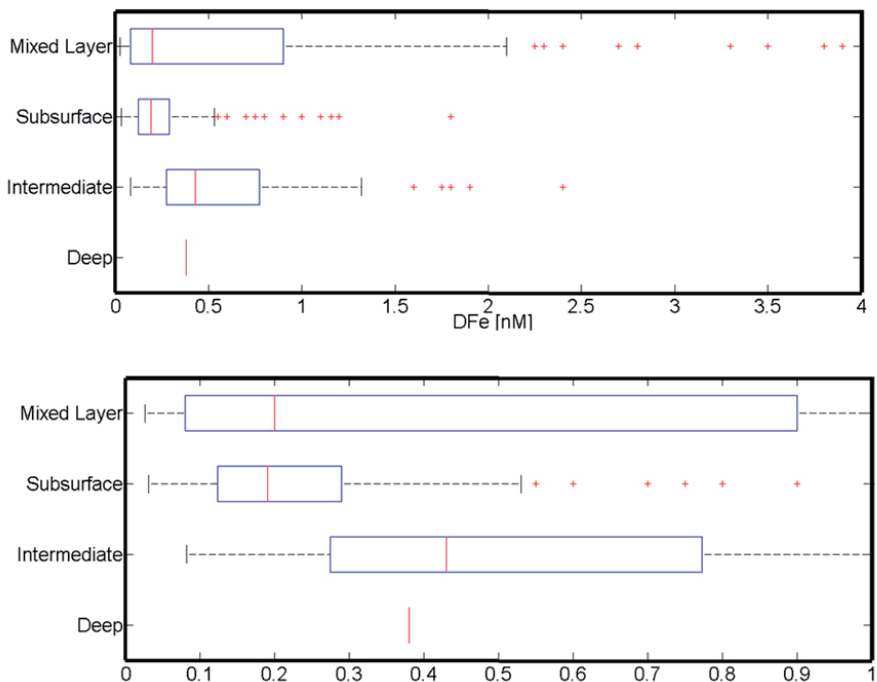


Fig. 6.17 Boxplot of DFe measurements in different layers the Ross Sea in large scale (upper panel) and smaller scale (lower panel)

6.3.2 Subsurface Waters

6.3.2.1 Antarctic Circumpolar Current

There are strong differences in dissolved iron concentration per region in the ACC (Fig 6.3). The waters from the base of the UML to 300 meter depth show, on average, similar concentrations as the UML values (0.26 ± 0.29 nM, $n=677$). In some stations a clear subsurface minimum is observed, situated directly under the mixed layer, whereas in many stations the layer until 300 meter depth reflects the higher concentrations (0.4-0.5 nM) of the waters below. High concentrations are observed close to the Patagonian continental shelf and the Antarctic Peninsula [This thesis, Chapter 5], around the Kerguelen Islands ([Bucciarelli *et al.* 2001], see section 6.2.2; not shown) and by Löscher *et al.* [1995] close to the Bouvet Junction. Also for these values in the UML-300m range, we calculated the DFe per sector (Table 6.1). Similar to the UML averages, in the subsurface, significantly ($p < 0.05$) higher concentrations are found in the Atlantic and Indian sector, compared to Pacific Sector. On a longitudinal scale, the concentration of DFe in the UML-300m interval roughly follows the trend of the overlying Upper Mixed Layer (Fig.6.18). The higher concentration at 180-120°W may be attributed to the absence of very high DFe concentrations observed in the UML, reflecting biological DFe-uptake in the UML and regeneration in the subsurface as determining factors for the DFe distribution (Table 6.1). Contrary to the UML, there is not a decreasing trend southwards in the DFe concentrations in both all the data and in the 5° latitude averaged data (see figure 6.S1).

6.3.2.2 Weddell Gyre

As shown in Fig. 6.3b, in the Weddell Gyre, there is less spatial coverage of DFe data in the layer UML-300 compared to within the UML (Fig. 6.6, Table 6.2). In the northern limb, the concentrations of DFe in the UML-300 meter depth layer in the Weddell Gyre are somewhat higher than those observed in the UML. However, as described above, the DFe concentration in the southern westward flowing limb is significantly lower than that in the northern eastward flowing limb, and both have significantly lower DFe than the Peninsula region.

6.3.2.3 Ross Gyre

In the ML-300m layer, there is a total of 279 samples, varying from 0.03-1.8 nM. Here, the variation is much lower (fig. 6.11), as shown from the lower standard deviation (Table 6.4) and the fact that the average DFe (0.28 nM; table 6.4) and the median are close to each other (see figures 6.11 and 6.17).

6.3.3 Intermediate Waters (300-1000 meter depth)

6.3.3.1 Antarctic Circumpolar Current

In the intermediate layer, from 300 to 1000 m. depth, only a few values <0.2 nM are observed. Concentrations of ~ 0.45 nM are observed at and near the Greenwich meridian, at Drake Passage, in the Australian Sector, south of Tasmania and close to the Antarctic Continent at 90° W. Lower concentrations of ~ 0.3 nM are reported for 20° E, 170° W and 90° W regions (Fig. 6.8). The average DFe concentration is higher than that in the UML and UML-300 depths and the DFe concentrations in the intermediate layer are more consistent: 0.37 ± 0.17 nM, $n=322$. Therefore it is more difficult to see differences between the different sectors. However, from Table 6.1 and Figure 6.18 it is clear that the Atlantic Sector, mainly the region around the Zero Meridian, has a higher concentration compared to the other regions. In the Atlantic Sector the difference between the concentrations in the intermediate layer relative to those in the upper 300 m is less than that in the Indian and Pacific Sectors. On a latitudinal scale, there is a slight increase in the 55 - 60° S region, which is just south of the PF in most regions and known as a region of major upwelling (Antarctic Divergence [Tomczak and Godfrey, 2003]). (see Figure 6.S1).

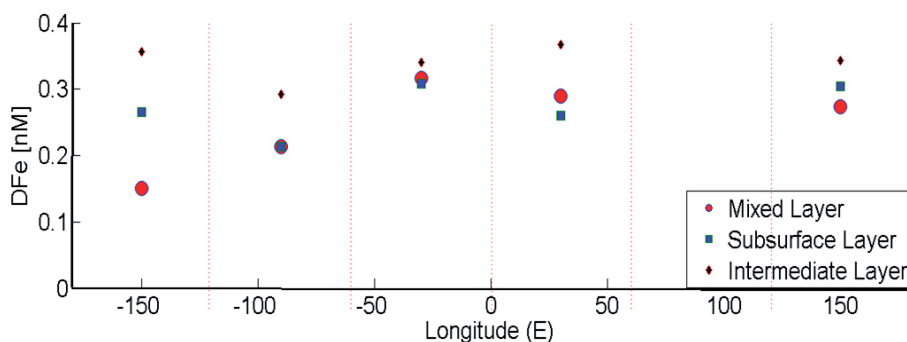


Fig. 6.18 DFe concentrations versus longitude for the Upper Mixed Layer, Subsurface (UML-300m) Layer and Intermediate (300-1000m) Layer averaged over 60° longitude

6.3.3.2 Weddell Gyre

There is a low number of data points for the west part of the Weddell Gyre; only 1 station above the sediments, in the Peninsula region (Fig. 6.8). Nevertheless, there is little difference in DFe between the southern limb and the northern limb and both differ significantly from the Peninsula region.

6.3.3.3 Ross Gyre

There is a total of 63 samples, varying from 0.08-2.4 nM. Also here, the deviation is larger and there is a clear difference between the average DFe and the median (Table 6.4 en fig. 6.17). However, in general, concentrations are much higher than in the upper 300m (fig. 6.12).

6.3.4 Deep Waters

6.3.4.1 Antarctic Circumpolar Current

The number of stations with deep water data points for DFe is relatively low. The DFe concentrations in the deep Southern Ocean are ~ 0.45 nM around the globe and somewhat higher concentrations (> 0.6 nM) are observed at the Bouvet region, close to the Antarctic continent, closest to Tasmania, and in the Drake Passage.

The dissolved Fe concentrations in the waters below 1000 meter depth are on average 0.56 ± 0.31 nM ($n=227$). The Indian and Pacific sectors both have a significantly lower DFe concentration than the Atlantic Sector. In the Indian sector the deep DFe concentration is lowest with 0.43 ± 0.30 nM. In all sectors, there is a relatively large difference (> 0.1 nM) between the concentrations in the upper 1000m and those below 1000m. A relatively clear trend of decreasing DFe with latitude is observed for the deep layer, interrupted with high values at $50-55^\circ\text{S}$ (figure 6.S1). At the zero meridian, this region is close to the Bouvet Ridge, where hydrothermal activity has been identified as a DFe source [Klunder *et al.*, 2011].

6.3.4.2 Weddell Gyre

Overall the deep DFe concentrations in the WG are relatively constant, (0.41 ± 0.13 nM ($n=218$)). There are by definition no data points for the Peninsula region (fig. 6.4d). The northern and southern limb both show similar concentrations (0.42 and 0.40 respectively), below the upper 1000 m.

6.3.4.3 Ross Gyre

There is only one station with Ross Sea data below 1000m, where DFe is ~ 0.4 nM, comparable to the intermediate waters (fig. 6.13).

6.4 Discussion

6.4.1 Fe in the Upper Mixed Layer and the ML-300m layer

6.4.1.1 Fe differentiated per sector; is the Atlantic sector a source of Fe for the ACC?

In this text section both the upper mixed layer and the Subsurface Layer (UML-300m depth) will be discussed together, representing the upper waters. From Figures 6.2 and 6.3 and Table 6.1 it appears that the Atlantic sector and (less so) the Indian sector have relatively high concentration of DFe in the upper 300 m, as compared to the Pacific sector. Because the average of the data points in this compilation of are largely influenced by the high DFe input processes, it will be good to also calculate the geometric mean (Table 6.1). Although the geometric mean values are $0.04-0.12$ nM lower than those from the arithmetic mean, in general, the trend between the

different sectors and different depths is similar. The only exception is the fact that the geometric mean of DFe in the Subsurface is equal in the Atlantic and Indian sectors. From the individual data points plotted on a longitude scale a maximum is shown east of Patagonia, in the 60 °W-0 °E and 0 °E-60 °E regions (Fig. 6.16). There are several possible causes for the high DFe in these regions. One is the strong influence of atmospheric dust as a Fe source. Although all continental land masses around the Southern Ocean contain vast (semi) arid areas, enabling dust transport to the Southern Ocean, mean wind stress shows clearly stronger winds over Southern Patagonia, compared to Africa, Australia and New Zealand [Tomczak, 2001]. Dust deposition models show the largest impact of dust in the Southern Ocean to be observed east of the South American continent, in the Atlantic Sector of the Southern Ocean, both in area and in intensity [Mahowald *et al.*, 1999; Jickells *et al.*, 2005; Fan *et al.*, 2006]. Also, in this region, the bottom topography east of the Drake Passage causes the ACC to flow northwards, i.e. east of Patagonia (Fig. 6.1, Orsi and Whitworth [1995]). As shown in the dust deposition model of Jickells *et al.* [2005] (their Figure 2), the ACC coincides with the zones with deposition up to $2.0 \text{ g m}^{-2} \text{ y}^{-1}$ compared to $<0.5 \text{ g m}^{-2} \text{ y}^{-1}$ in the plumes in the other sectors. Recently, Cassar *et al.* [2007] showed the largest deposition fluxes of dust derived dissolved Fe to the ocean east of Patagonia. The region south(east) of Australia, shows lower, yet still significant deposition fluxes of Fe, reaching the ACC. The deposition fluxes caused by dust from the African continent are mostly restricted to the area north of 40°S and thus do hardly reach the ACC. From 70°W- 180°W (Pacific Sector), the deposition fluxes are very low. Similar findings are shown by Lancelot *et al.* [2009] in a model study. Both studies recognize a southwards decrease in the dust derived Fe fluxes. For example, slightly higher DFe in the UML in the 60 °W-120 °W region is observed, partly due to very high ($>2\text{nM}$) upper surface values, consistent with very high surface DAI concentrations, derived from dust deposition events during the occupation of the Drake Passage transect [This thesis, Chapter 5; Middag *et al.*, 2012a]. Summarizing, both the high deposition load off Patagonia as well as the locally northwards flow pattern of the ACC make dust deposition likely a stronger source in the Atlantic Sector compared to the Indian, and especially the Pacific sector. However, constraining the Fe input from dust deposition data is still limited by a lack of direct measurements in the Southern ocean.

Another major input source of Fe to the Southern surface Ocean waters is dissolved Fe supply from sediments [De Baar and De Jong, 2001; Tagliabue *et al.*, 2009]. This iron may be delivered to the ACC either from the Southern Ocean Islands or the Antarctic Peninsula region [Ardelan *et al.*, 2009]. For several regions, both the distance of Fe transport and the initial DFe concentration originating from these land masses is reported. For the Antarctic Peninsula the “scale length” (decrease of the DFe to $1/e$ (~37%) of the ‘initial’ value near the land mass) [Johnson *et al.*, 1997] is 25 km suggesting a (theoretical) original concentration of $\sim 2.65 \text{ nM}$ [Ardelan *et al.*, 2009]. For Kerguelen these values are 150 km and 12.58 nM, respectively [Bucciarelli *et al.*, 2001], and for the Crozet Islands, 25 km and 2 nM, respectively [Planquette *et*

al., 2007]. *Nielsdottir et al.* [2012] reported a scale length of ~102 km around South Georgia and Bird Island. Also an important influence of sediment derived Fe is observed off the westcoast of New-Zealand, although this influence is strongest north of the ACC at 45°S [Croot *et al.*, 2005]. These findings show that lateral Fe supply by land masses is variable both spatially and in quantity, but can be substantial. On a larger scale, *Tagliabue et al.* [2009] modeled the relative influx of dust derived and sediment derived Fe in the Southern Ocean, and showed a relatively strong effect of both sediment input and dust input in Atlantic Sector. In our compilation study, also a strong (sediment derived) Fe-input was reported in those regions where the SB-ACC approaches the Antarctic Shelf (south of 65°S) (Fig. 6.1-6.3). The dust deposition pathway would (directly) affect only the upper surface waters, whereas the Fe derived from the sediment is often also visible in the subsurface waters. The fact that the UML and the UML-300 intervals resemble each other quite well (Fig. 6.14), in all regions except 120-180°W would indicate a substantial contribution of sediment derived Fe in the DFe concentration in this region. Also other input sources such as upwelling of deep waters and ice-melt are not uniformly divided over the different sectors. *Sokolov and Rintoul* [2007] have shown for the ACC that vertical velocity (at chosen 288 m depth) is strongly dependent on local bottom topography. This implies that there are several regions in the ACC (Kerguelen Plateau, Mid Ocean Ridge, Pacific Antarctic Ridge, Drake Passage) with enhanced upwelling e.i. enhanced contribution of Fe-rich deeper waters to the upper water layers. Although strong upwelling occurs over the complete ACC, the strongest vertical velocity is found around the Drake Passage, thus influencing the downstream Atlantic Sector.

The melting of seasonal sea-ice is also an important source of Fe to the Southern Ocean [Smith and Comiso, 2008; Lannuzel *et al.*, 2008]. Sea-ice extension maps (University of Hamburg, Gunnar Spreen and Lars Kaleschke; Smith and Comiso, 2008), show that the extent of the seasonal ice edge is, in some regions, always within the ACC. The regions, where the seasonal ice edge is situated within the ACC, are situated in all three Sectors of the ACC. Therefore we cannot constrain any difference in the sea-ice melt derived Fe-input between the sectors. In general, dust-derived Fe, sediment-derived Fe, and Fe from upwelled deep water appear to impact the DFe concentration in the 60°W- 60°E region most, but any significant “upstream” effect cannot be constrained from available data. From the similar geometric mean between the Indian and Atlantic sector in the subsurface (and surface) it appears that the differences are mainly caused by a few, very high DFe data points in the Atlantic sector. These differences should be considered carefully; the differences between the Atlantic and Indian and the Pacific sector are still considerable.

6.4.1.2 Latitudinal trends in Fe in the upper 300 meter in the ACC

On average, the UML and UML-300 m depth data in the ACC do not indicate any meridional trend (Fig.6.15). However, from individual studies, such a trend is observed: *Sedwick et al.* [1997; 2008] reported such a trend for the region west of Tasmania,

although for the spring cruise an increase was observed again southernmost station at 66 °S. *Measures et al.* [2001] reports southwards decreasing DFe concentrations in the UML for their late summer transect at 170 °W, but this trend was interrupted by higher concentrations measured in the south part of the Polar Front Region. *Cassar et al.* [2007] reported a southwards decrease in modeled Fe deposition from the STF to the Southern Boundary of the ACC. However, important input sources such as upwelling, ice-melt and lateral advection [*Croot et al.*, 2004; *Klunder et al.*, 2011] are not mentioned in the latter study. *Klunder et al.* [2011] and *Croot et al.* [2006] report upwelling of relatively iron rich Upper Circumpolar Deep Waters (UCDW) which reaches the (sub)surface south of the Polar Front. This may explain the relative Fe enrichment in the 55 °S-60 °S region, a mechanism which will be discussed in section 6.4.1.3. Moreover, it should be mentioned that these data are only for the ACC, which has its southernmost extension not further south than 55 °S in some places, thus low DFe regions may occur south of the ACC.

6.4.1.3 DFe north and south of the Polar Front

Figure 6.19 shows the DFe concentrations averaged over the regions North and South of the Polar Front, and within the Polar Front region (N-PF, S-PF and PFr respectively), where the PFr is defined as a 2° latitude band around the PF after *Moore et al.* [2002], their Fig 6.1. The data are differentiated in spring-early summer (Oct-Dec) values and late summer-autumn values (Jan-Apr). Also Fe supply and output processes are shown. In spring-early summer there is little variation between DFe in the North of PF and PF regions; DFe south of the PF is much higher. In late summer-autumn however, the DFe in the PFr increases, whereas in the S-PF the DFe decreases. This indicates that (some of) the processes depicted in Fig. 6.19 show seasonal variability. Three major processes determining the biogeochemical cycles in this region are upwelling of UCDW, sea-ice melt and Fe uptake by phytoplankton and subsequent export from the UML. For all regions that we report data from, the maximum sea-ice extent is situated south of the Polar Front [*Kaleschke and Spreen*, see section 6.5.1.1; *Smith and Comiso*, 2008]. As a consequence, Fe input from melting sea-ice will affect the waters south of the PF but not the waters within the PF. *Lannuzel et al.* [2008] show that melting sea-ice can lead to significant DFe input in the upper layers. It is also partly responsible for a seasonal shift in DFe i.e. iron “stored” in sea-ice during formation (April-September) will be released during ice-melt (November-March). This iron released from seasonal sea-ice melt will thus be observed only in the south part of the ACC. Based on the model of *Lancelot et al.* [2009] a $\sim 0.1 \mu\text{mol Fe m}^{-3}$ release into the ocean in the South part of the ACC from summer ice-melt can be calculated. This would lead to a 0.02 nM contribution to a 50m ML over this period. Also *Measures et al.* [2001] report high increasing concentrations of DFe from the PF southwards during an early summer cruise where the sea-ice retreated. However, it should be noted that this is close to the detection limit of DFe measurements,

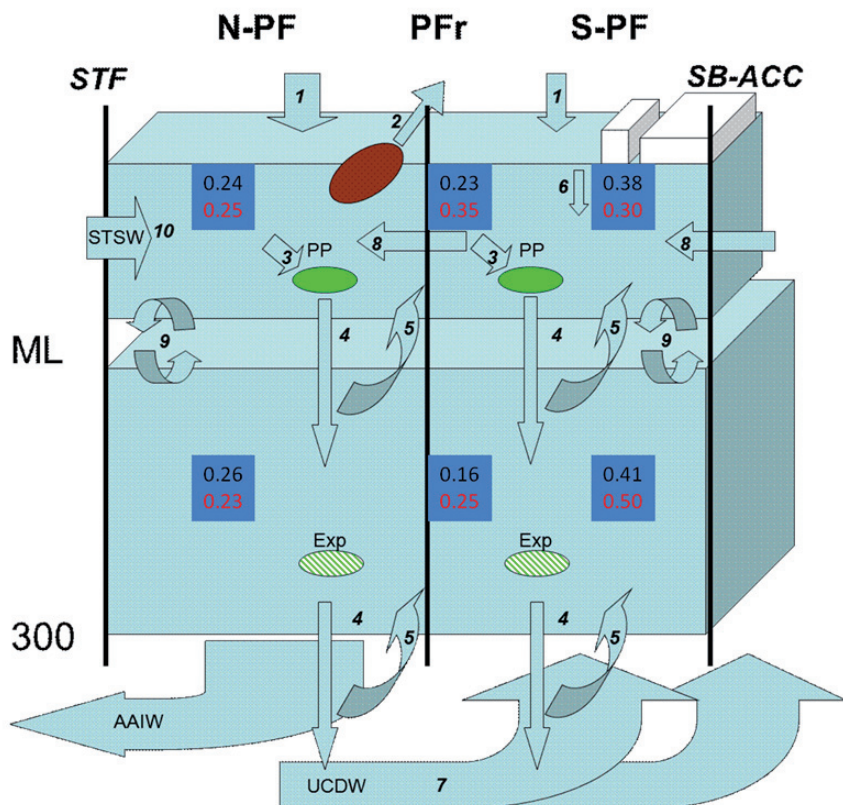


Fig. 6.19 Schematic depiction of the ACC, including Polar Frontal Region and processes involved North and South of the Polar Front. Mean DFe concentrations are given for each region for (blue) spring/early summer and (red) late summer/autumn. Processes are: 1: Dust input. 2: Lateral advection from sediments 3: Primary productivity (Fe depletion) 4: Export 5: Remineralization/regeneration of Fe 6: Seasonal sea-ice melt 7: Upwelling of deep waters 8: Ekman transport 9: Vertical mixing 10: Inflow of Subtropical waters

whereas the DFe content of melting sea-ice is highly variable [Lannuzel *et al.*, 2008]. Another important process is the upwelling of UCDW, south of the Polar Front [Speer *et al.* 2001; Sloyan and Rintoul, 2001; Hoppema *et al.* 2003] (see section 6.5.1.1). South of the PF, the UCDW reaches the surface, and subsequently this water is driven northwards and southwards by Ekman transport. However, on the way northwards it is depleted in DFe by phytoplankton uptake [Hoppema *et al.*, 2003].

Highest chlorophyll concentrations in the ACC are observed in December [Moore and Abbott, 2002; Smith and Comiso, 2008; Sokolov and Rintoul, 2008] and the chlorophyll levels decrease strongly from January onwards. Therefore, most of the Fe-depletion due to primary production and subsequent export will take place in December, leading to the lowest UML concentration of Fe in the following months, notably south of the PF. The presence of algal blooms near the edge of the retreating ice in summer has been reported [Klunder *et al.*, 2011; Rutgers van der Loeff *et al.*,

Table 6.2 DFe and standard deviation for the Polar Frontal Region and the region North and South of the Polar Front. Statistical differences are given. See text for explanation.

	Polar Front		
	North PF	PF	South PF
Mixed layer			
DFe	0.23	0.29	0.32
Stdev	0.21	0.30	0.36
Number of samples	228	420	142
p*	0.00**	NaN	0.34***
Subsurface Layer			
DFe	0.24	0.18	0.46
Stdev	0.13	0.16	0.55
Number of samples	316	225	129
p*	0.00**	NaN	0.00***
Intermediate Layer			
DFe	0.33	0.32	0.46
Stdev	0.13	0.14	0.26
Number of samples	153	99	70
p*	0.50**	NaN	0.00***
Deep Layer			
DFe	0.58	0.46	0.63
Stdev	0.30	0.21	0.38
Number of samples	92	67	68
p*	0.00**	NaN	0.00***

*p-value; 2 sided t-test, 95% confidence interval; bold: $p < 0.05$ (=significant difference); **between region North of PF and PF; *** between region South of PF and PF.

2011]. The region north of the PF is strongly influenced by Subtropical Waters, carrying relatively higher Fe-concentrations, as shown for the Atlantic Sector [Klunder *et al.*, 2011] and Indian Sector [Bowie *et al.*, 2009]. These waters influence the surface and subsurface waters north of the Polar Front and have more constant Fe contents throughout the year and therefore this route of DFe input is less episodic and more constant as is dust deposition. Nevertheless, concentrations in the region north of the PF are still lowest of all concentrations.

In the layer UML-300 m, concentrations in the N-PF region are comparable to the UML, not surprising as the influence of subtropical waters may reach deeper than the mixed layer [Bowie *et al.*, 2009; Klunder *et al.*, 2011] and deep winter mixing is common in the subantarctic zone [Rintoul *et al.*, 2001]. In the PFr, lower concentrations are observed in spring/early summer. Most likely this reflects the absence of UML input sources (dust, Ekman transport). In the S-PF region, concentrations are significantly higher in both seasons, consistent with the upwelling of deep (Atlantic) waters [Fe > 0.4 nM, Klunder *et al.*, 2011; Moore and Braucher, 2008] occurring south of the PF [Trull *et al.*, 2001; Hoppema *et al.*, 2003], delivering Fe to the subsurface

waters. For the S-PF, late summer/autumn concentrations are higher in the UML-300m interval, which most likely reflects (shallow) remineralization and regeneration of Fe [Tortell *et al.*, 1997; Aristegui *et al.*, 2002]. Löscher *et al.* [1997] and Coale *et al.* [2005] reported an important role (up to 50%) of vertical mixing and upwelling for Fe delivery from below to the surface waters.

6.4.1.4 Temporal differences in the DFe distribution

Moore *et al.* [2002] report phytoplankton growth to be light limited in the spring months, the highest phytoplankton growth is observed in December-January, leading to chronic DFe depleted conditions in the following late summer-autumn period. Hoppema *et al.* [2003] modeled the seasonal pattern of the concentration of DFe within the ACC, based on processes mentioned in section 6.4.1.1 (upwelling,

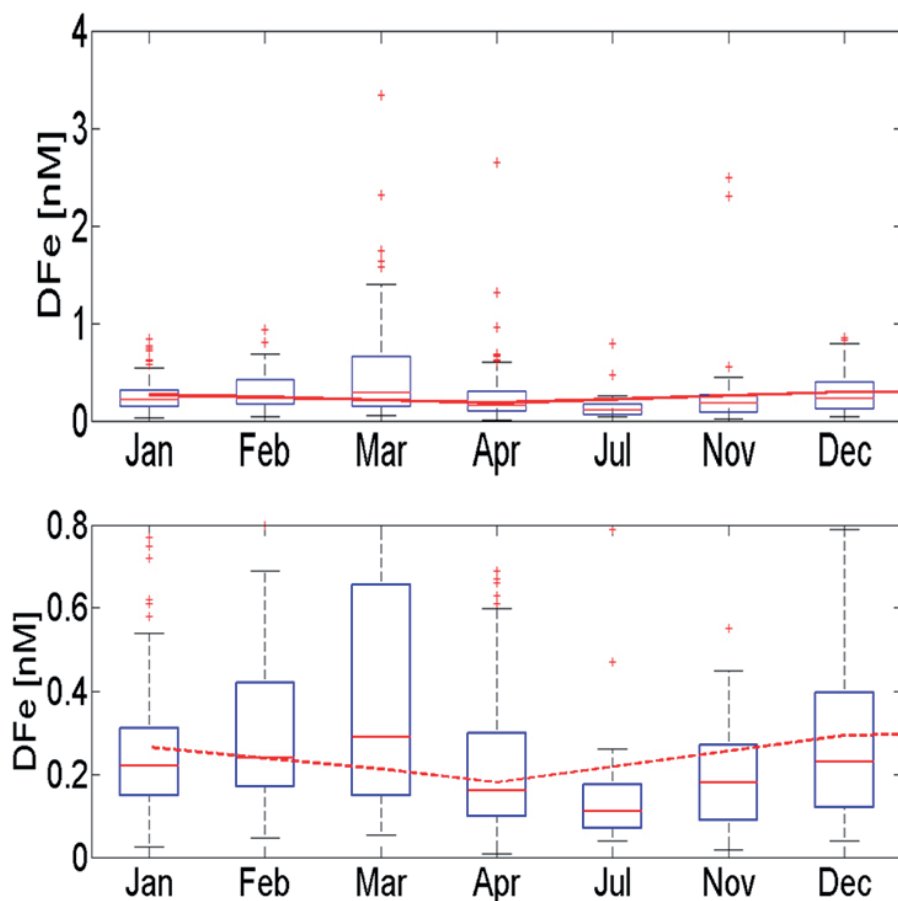


Fig. 6.20 Boxplots of dissolved Fe averaged per month in large scale (upper panel) and smaller scale (lower panel). Red line indicates the modeled DFe concentration from [Hoppema *et al.*, 2003]. Lower panel is upper panel on a larger scale.

Ekman transport, phytoplankton uptake) (Figure 6.19). Although there is some scatter, which may (partly) be explained by ice-melt, both our compilation and the model show a decreasing trend from January to April (although high values in March, cause a slightly higher average (Figure 6.20 (upper panel))). Due to stronger winds causing deepening of the UML i.e. mixing with relatively Fe rich subsurface layers, and absence of primary productivity, Fe in the UML is expected to increase during winter [Hoppema *et al.*, 2003]. However, relatively low (~ 0.2 nM) concentrations are observed in winter by Ellwood *et al.* [2008], southeast of Tasmania. It should be noted that to the best of our knowledge, this is the only study reporting wintertime concentrations. From the November onset of the austral spring blooming season, a decrease in DFe as modeled by Hoppema *et al.*, [2003] is indeed observed in the compilation. In general, the average DFe concentration appears to be mainly lower than that predicted by the Hoppema *et al.* [2003] model. The temporal changes in Fe in the ACC cannot be fully explained in a simplified model using primary production, vertical mixing and Ekman transport [Hoppema *et al.*, 2003], but also other processes (such as ice-melt) should be considered. Moreover, (the differences in) biological uptake and remineralization and recycling of Fe have a significant seasonal effect on the dissolved iron concentration.

6.4.2 Intermediate and deep waters in the ACC; a consistent Fe reservoir?

6.4.2.1 Intermediate waters

In the ACC, the 300-1000 meter depth layer consists mainly of northwards flowing AAIW, and the Circumpolar Deep Waters below. De Brauwere *et al.* [2007] show, for the Australian Sector of the Southern Ocean, that AAIW and SAMW constitute the largest part of this layer north of the Subantarctic front. Only in the deepest part, from the SAF northwards, the presence of UCDW rapidly increases. A similar water mass distribution is shown for the Atlantic Sector by Tomczak *et al.* [2001]. This important role of the waters from Antarctic origin (SAMW, AAIW, [Tomczak, 2001; Mc Cartney, 1977] north of the PF and that of upwelling of UCDW/NADW further south [De Brauwere *et al.*, 2001], results in a relatively low average concentration of DFe in the intermediate waters (0.36 ± 0.18 nM ($n=332$)) and significantly ($p < 0.05$) higher DFe south of the PF region compared to within and north of the PF. For a part, this may be caused by the fact that the intermediate waters in the north have been at the surface recently, where biological processes caused the depletion in DFe. Exceptionally high values are observed above and close to the Bouvet Region (fig. 6.1b). Also there are significant differences between the sectors. The Atlantic Sector shows significantly higher concentrations than the Pacific and Indian Sectors ($P < 0.05$, table 6.2). These trends are confirmed in the geometric mean (table 6.1). As described in section 6.3.2.1, the largest part of upwelling (of NADW) takes place in the western Atlantic Sector. During upwelling, water is transported from deeper than 1000m to

less than 300 meter depth and thus passes the intermediate water layer (300-1000 meter depth). The relatively high DFe of the NADW (~ 0.6 nM; *Klunder et al.*, 2011) can thus cause higher DFe in the intermediate waters. Moreover, these high values may reflect the input of DFe from continental margins to the intermediate waters [*Löscher et al.*, 1997] (see section 6.3.3.1), and from hydrothermal vent plumes. Vents are reported at intermediate depth (~ 1100 meter) in Bransfield Strait [*Klinkhammer et al.*, 2001] and above the Bouvet junction [*Klunder et al.*, 2011].

6.4.2.2 Deep Waters in the ACC

As expected [*Johnson et al.*, 1997; *Moore and Braucher*, 2008], the DFe in the deep waters of the Southern Ocean is higher than in the intermediate layer, and subject to a large variation. Although concentrations as low as 0.15 nM are observed in the Indian Sector, some very high concentrations (>2 nM) occur in the Atlantic Sector. *Klunder et al.* [2011] have suggested that the high concentrations at 53°S - 54°S are likely caused by hydrothermal activity. Indeed, hydrothermal influence may be reflected in the relatively high DFe in the deep waters from 50°S - 55°S (see figure 6.S1).

Hydrothermal input is expected to be an important input source of dissolved iron to the deep ocean [*Klinkhammer et al.* 2002; *Tagliabue et al.*, 2010]. Also, the higher concentrations at 140°E , more to the North and close to the Peninsula at Drake Passage are expected to be caused by hydrothermal input of Fe [*Sohrin et al.*, 2000; *Klinkhammer et al.*, 2001, This thesis, Chapter 5].

Elevated concentrations of up to >1 nM are found at 140°E , 65.3°S by *Sohrin et al.* [2000], which they attribute to formation of AABW. For the deep layer, averaging these bottom concentrations with the lower concentrations (0.36-0.55 nM) higher in the water column (2500-1000m.) levels out the average concentration as shown in figure 6.5. Despite the relatively large standard deviation (0.56 ± 0.31 nM), the DFe concentration is high compared to the upper 1000 meters and may be considered a DFe source.

6.4.3 DFe in the Weddell Gyre and Ross Sea

6.4.3.1 DFe in the upper 300 meter in the Weddell Gyre

In this text section both the Upper Mixed Layer and the Subsurface Layer (UML-300m depth) will be discussed together, representing the upper waters. Within the Weddell Gyre there is a pattern of relatively low DFe in the southern westwards flowing limb, slightly higher in the northern eastwards flowing limb and highest concentrations above the slope/shelf or Peninsula region (Table 6.3). We ascribe this difference to several factors. First, also in this region, there is upwelling of NADW-influenced UCDW as described in section 6.3.2.1. The upwelled deep water may furthermore be enriched in DFe due to hydrothermal iron input close to the Scotia Ridge, Bouvet Ridge [*Klunder et al.*, 2011] and further downstream, along the North Weddell Ridge or as far west as Bransfield Strait [*Klinkhammer et al.* 2001; *Tovar-Sanchez et*

Table 6.3 DFe in the Weddell Gyre, average's and statistical differences between the different sectors are given.

Region	DFe	Standard deviation	Geometric Mean	Number of samples	p-value*
Mixed Layer					
Peninsula	0.99	0.37	0.85	25	7.1E-11**
NL ^{\$}	0.23	0.25	0.15	33	8.8E-01***
SL [#]	0.22	0.13	0.19	58	1.5E-10****
Subsurface Layer					
Peninsula	0.61	0.34	0.52	12	5.8E-03**
NL ^{\$}	0.28	0.20	0.22	76	3.0E-03***
SL [#]	0.20	0.10	0.17	69	1.4E-03****
Intermediate Layer					
Peninsula	0.76	0.21	0.74	15	9.5E-07**
NL ^{\$}	0.34	0.18	0.29	52	9.5E-01***
SL [#]	0.35	0.19	0.31	38	9.1E-07****
Deep Layer					
Peninsula	no data	no data		no data	no data
NL ^{\$}	0.42	0.15	0.39	118	2.6E-01***
SL [#]	0.40	0.09	0.39	100	NaN

^{\$} Northern, Eastwards flowing limb; [#] Southern, Westwards flowing limb; *p-value; 2 sided t-test, 95% confidence interval; bold: $p < 0.05$ (=significant difference); **between Peninsula region and NL; *** between NL and SL; **** between SL and Peninsula region.

al 2009]. Moreover, the westwards flowing limb is situated further south, and therefore the upwelling waters will mix with Weddell Sea Deep Water (relatively low DFe). This would lead to relatively low DFe delivery in deep waters in the westwards flowing limb compared to the eastwards flowing limb where the stronger influence of WDW causes relatively high Fe delivery in westwards flowing limb, mainly to the UML-300m layer.

Secondly, the strong eastwards flowing limb flows along the Antarctic Peninsula shelf and then along slope of the North Weddell Ridge system. Here, the strong geostrophic velocities (> 4.0 m/s, *Fahrbach et al.*, 1994) enable the current to pick up particles and emanating Fe-rich benthic waters in this part of the flow. This could enrich the water in DFe derived from sediment pore waters or enhanced particle resuspension. During the Weddell Sea transect of the ANT XXIV/3 expedition (which provided most data for this region (Fig. 6.8 and 6.9)), lower light transmission values (i.e. more particles) were observed (data not shown) in the eastward, compared to the westward flowing limb. Unlike at the Greenwich Meridian transect, this transmission minimum was not correlated with fluorescence, but most likely caused by lithogenic sediment particles. These will be less common in the westward flowing limb, as the region of origin for the westwards flowing limb is the remote Indian Sector ($\sim 30^\circ$ E) where very low DFe-concentrations are expected, due to absence of external input sources.

Third, the low concentration of DFe (0.23 ± 0.10 nM, $n=33$) in the UML in the eastwards flowing limb is most likely due to depletion by phytoplankton. Parallel measurements of dissolved manganese, light transmission (lower) and DIC (lower) and fluorescence (higher) does indicate phytoplankton growth in eastwards flowing limb, at the Greenwich meridian [Rutgers Van der Loeff *et al.*, 2011]. The geometric mean DFe values of the different regions of the Weddell Sea do confirm this trend; they are generally lower than the average DFe values but with similar trends between regions and depth layers. However, clearly the region of the northernmost, eastwards flowing limb shows a lower geometric mean, indicating that the arithmetic mean is determined by some high DFe values, whereas overall DFe is low <0.14 nM. Possibly as a result of biological depletion as mentioned above.

Besides sediment input, Lannuzel *et al.* [2008] showed seasonal melting of sea ice to release DFe. This iron is incorporated in the sea-ice during winter, and released to the surface waters during spring. Sea-ice coverage maps (Kaleschke and Spreen (2011), see section 6.4.1.4) show that sea-ice covers the complete Weddell Gyre in austral winter, yet in summer retreats almost until the continent in the south and roughly to the borders of the Peninsula region in the Weddell Sea. Therefore, during one annual cycle, first the eastwards flowing limb and later the westwards flowing limb are influenced with melting ice, but the temporal coverage of the data here is too poor to reveal this input. Nevertheless, we do see that the southernmost station along the Greenwich meridian at the ANT XXIV/3 cruise showed higher concentrations of DFe. This was the station closest to the retreating sea-ice, melting of which may have caused the high DFe [Klunder *et al.*, 2011]. Also several stations reported by Lannuzel *et al.* [2008] at 68°S , 55°W appeared sea-ice influenced in terms of DFe concentration.

The concentration of DFe above the shelf of the Antarctic Peninsula is significantly higher ($P<0.01$) than in both Gyre limbs (see section 6.3.1.2). The high and variable concentrations close to the Antarctic Peninsula and Bransfield Strait, at 63 – 64°S , 50 – 55°W are expected to be caused by sediment input, or sea-ice melt. A source of DFe may well be the sediment from the slope or DFe rich benthic waters [Homoky *et al.*, 2012] brought to the surface waters by upwelling and vertical mixing. Both Lancelot *et al.* [2009] and Tagliabue *et al.* [2009] modeled a strong effect of sediments on the input of Fe to the Weddell Sea, decreasing from the shelf area to the central Weddell Sea.

6.4.3.2 Intermediate and deep waters in the Weddell Gyre

The intermediate 300–1000m depth waters of the Weddell Gyre are relatively homogenous in physical properties such as potential temperature, salinity and oxygen, and also in transmission. This is also reflected in the DFe concentrations, 0.34 – 0.35 nM in both the eastwards flowing limb and westwards flowing limb. Also here, higher concentrations above the shelf (Peninsula region) suggest sedimentary input from the shelf, although the number of data points is low and the standard deviation high (DFe

= 0.76 +/- 0.21 nM, n=15). The geometric mean values largely follow the same trend as the arithmetic mean DFe values. In the deep (>1000m) layers, formation of Weddell Sea Bottom Water causes surface waters to cascade down the slope [Klatt *et al.*, 2005], which is observed here in the waters of the eastwards flowing limb [Middag *et al.*, 2012b]. This water reflects the DFe concentration from the surface, and during rapid descending flow brings particles in resuspension and entrains DFe rich pore-water, resulting in a further increasing DFe concentration. The fact that subduction takes place mainly in winter, when surface DFe concentration is highest, enhances the DFe concentration. The effect of (lithogenic or hydrothermal) particles (lower transmission) is also seen close to the Bouvet Ridge, at the Greenwich meridian. Input of Fe from hydrothermal vents (see section 6.4.3.1) may have more influence on the northern limb, flowing along the Bouvet Ridge, compared to the southern limb [Klunder *et al.*, 2011]. Klinkhammer *et al.* [2001] reported elevated concentrations of dissolved and particulate Fe (0.7-12.6 nM and 5.4-128 nM respectively), due to hydrothermal vents, at intermediate depths (~1000-1500 m) in Bransfield Strait, which may affect the water in the Weddell Gyre. Given these input sources it is remarkable that, although slightly higher and with less variability, the concentrations in the eastwards flowing limb are similar to those in the westwards flowing limb. Over the whole water column in the central Weddell Sea, the DFe largely confirms the “common” profile as suggested previously by Moore and Braucher [2008], for the Southern Ocean.

6.4.3.4 DFe in the Ross Sea

The large deviation in the mixed layer in the Ross Sea likely reflects the important role of two input sources in the central Ross Sea; sediment derived DFe and DFe from sea-ice melt, either via deposition of snow, containing dust, or via uptake of colloidal particulate Fe from the sediment during ice-formation [Sedwick *et al.*, 2000]. Indeed, in the UML and the UML-300m layer, lowest concentrations are observed at around 180 °E or further east, and higher concentrations closer to the shelf. This is in line with the big difference between median and average DFe and the large standard deviation, and would indicate waters with relatively lower DFe, from the central Ross Sea, coming onto the shelf. The fact that the geometric mean value of the DFe concentrations of the ML is much lower than the arithmetic mean value and more consistent with the subsurface layer does indicate that the Mixed Layer data is largely influenced by a few high DFe data points (Table 6.4). They may be caused by the processes mentioned above, which are then overrepresented in this compilation. For the other layer in the Ross Sea, the geometric mean follows the arithmetic mean. The shelf influence and sea-ice melt, together with a large seasonal biological drawdown of DFe in the surface waters, will be reflected in the slightly higher concentrations further West, close to the continent. Due to these sources, the average DFe in the UML in the Ross Sea is high at ~0.7 nM. Sedwick *et al.* [2000, 2011] and De Baar and De Jong (2001) mention a (strong) biological removal of DFe from the surf-

ace waters in the Ross Sea. During spring, this removal can be sufficient to capture DFe inputs from the shelf [Sedwick *et al.*, 2011]. Therefore, the average value here presented should be looked at cautiously when interpreting DFe in the mixed layer in the Ross Sea.

Table 6.4 DFe in the Ross Sea Gyre, average's and statistical differences between the different sectors are given.

	Average DFe	St. Dev	Geometric Mean	Min	Max	# samples
Mixed layer	0.613	0.823	0.26	0.026	4.1	189
Subsurface Layer	0.252	0.227	0.25	0.031	1.8	279
Intermediate Layer	0.615	0.492	0.61	0.082	2.4	63
Deep Layer	0.38	0	0.38	0.38	0.38	1

The increase in average DFe in the 300-1000m zone, may be caused by sinking and regeneration of DFe from the mixed layer. Moreover, DFe concentrations in this region may be enriched by deep convective mixing, which occurs in the Southern Ross Sea during the winter months [Gordon *et al.*, 2000; Sedwick *et al.*, 2011]. Also input from the shelf may be important, given the highest concentrations being close to the shelf at ~75 °S, 170 °E. Moreover, in the shallow Ross Sea, the 300-1000 m layer is near the sea floor [Dinniman *et al.*, 2003], and thus influence of benthic DFe inputs is likely. The Deep Ross Sea waters reflect the deep waters from further north (upwelling UCDW) and thus carry a similar DFe concentration (~0.4 nM).

6.5 Conclusions

This compilation gives insight in the circumpolar distribution of DFe. The spatial and temporal resolution of the data is not sufficient to derive strong statistical trends on a longitudinal or latitudinal scale. Nevertheless, it shows the enhanced values of DFe in the 60 °W-10 °E region in the upper 300m, in other words a significantly higher Fe in the Atlantic and Indian Sectors, as compared to the Pacific Sector. We attributed this to enhanced dust input and sedimentary sources. Also stronger upwelling of Fe richer deep waters due to a strong NADW component may play a role. On a latitudinal transect, the average DFe concentrations appear to decrease towards the continent, with the exception of the 55-65 °S region, most likely due to enhanced upwelling in this region.

We report higher DFe both south and north of, compared to the values within the Polar Front. This is attributed to inflow of Subtropical Surface Waters in the north and enhanced upwelling and strong influence of ice-melt in the south. These input sources appear stronger than the removal via phytoplankton uptake and ex-

port. On the other hand the latter phytoplankton uptake and export are a stronger control in the Polar Front for removal of DFe, hence the ensuing lower DFe at the Polar Front.

The here compiled DFe concentrations are almost entirely restricted to the spring and autumn seasons (October-April). Observed differences with the simplified model of *Hoppema et al.* [2003] indicate an important role of ice-melt, sediment resuspension and influx from subtropical waters. Nevertheless, in general a decrease in Fe concentrations is observed as the growing season progresses. Remarkably, unexpectedly low concentrations in winter were observed in the Pacific Sector in July by *Ellwood et al.* [2008].

The concentrations of DFe in the Weddell Gyre are different between the two different limbs and the region close to the Antarctic Peninsula, where higher DFe values were observed. Here, the waters can pick up Fe from the sediments. The stronger deviation in the northern limb compared to the southern limb may also reflect this input. In the deeper waters, the waters in the northern part of the gyre show higher Fe and lower light transmission. This indicates sediment resuspension as important Fe source. However, also bottom water formation and hydrothermal vents may enhance DFe concentrations above the peninsula and in the northern limb over the Bouvet Ridge.

The strong standard deviation in concentrations of DFe in the mixed layer of the Ross Sea reflect the strong interaction of input sources and seasonal biological uptake. The low concentrations in the upper 300m show a sudden increase in the intermediate and deep layers, possibly as a result of regeneration of DFe, benthic inputs, and inflow of waters from further North.

This study has shown that the Atlantic and Indian sectors of the Southern Ocean have relatively higher Fe concentrations compared to the Pacific sector, and that deep waters show somewhat more constant Fe concentrations throughout the Southern Ocean. As scientific cruises are by definition limited to certain time and space, it will be difficult to constrain all factors affecting the biogeochemical cycle of Fe in the Southern Ocean. Therefore, modeling studies will be needed for further investigation of the role of Fe in the Southern Ocean (eco)system. By providing an extensive set of Fe measurements this study may aid modelers in constraining the processes controlling Fe sources and sinks of the ACC and Weddell and Ross Gyres. However, to better understand the processes it will be inevitable to gain more information from shipboard expeditions; where particularly the seasonal coverage (cruises in Antarctic winter) and specific process (e.g. ice-melt) as focus of expeditions will give better insight in the processes involved in Southern ocean DFe cycling.

6.6 References

- Aristegui, J.V., Denis, J. Almunia, M. F Montero (2002), Water-column remineralization in the Indian sector of the Southern Ocean during early spring *Deep Sea Research Part II: Topical Studies in Oceanography*, 49 (9-10) pp.1707-1720
- Ardelan, M.V., O. Holm-Hansen, C.D. Hewes, C.S. Reiss, N.S. Silva, H. Dulaiova, H. Steinnes and E. Sakshaug (2010), Natural iron enrichment around the Antarctic Peninsula in the Southern Ocean, *Biogeosciences*, 7, 11–25.
- Bruland, K. and E. Rue (2001), Analytical methods for the determination of concentrations and speciation of iron. In: Turner, D., Hunter, K.A.(Eds.), *Biogeochemistry of Iron in Seawater*, IUPAC Book Series on Analytical and Physical Chemistry of Environmental Systems, vol.7 ; 2001, pp. 123–254 (Chapter ?).
- Bowie, A.R., D. Lannuzel, T. A. Remenyi, T. Wagener, P. J. Lam, P. W. Boyd, C. Guieu, A. T. Townsend, and T. W. Trull (2009), Biogeochemical iron budgets of the Southern Ocean south of Australia: Decoupling of iron and nutrient cycles in the subantarctic zone by the summertime supply, 2009. *Global Biogeochem. Cycles*, 23, GB4034, doi:10.1029/
- Boyd, P., A. Watson, C. Law, E. Abraham, T. Trull, R. Murdoch, D. Bakker, A. Bowie, K. Bueseler, and H. Chang (2000), A mesoscale phytoplankton bloom in the polar Southern Ocean stimulated by iron fertilization, *Nature*, 407(6805), 695-702.
- Boye, M., C M G Van Den Berg, J T M De Jong, H Leach, P Croot, H J W De Baar (2001), Organic complexation of iron in the Southern Ocean. *Deep-Sea Research I* 48 (6), 1477–1497.
- Boye, M., J. Nishioka, P. L. Croot, P. Laan, K.R. Timmermans, H.J.W. de Baar, 2005. Major deviations of iron complexation during 22 days of a mesoscale iron enrichment in the open Southern Ocean *Marine Chemistry*, 96, (3-4), pp. 257-271
- Blain, S., Que'guiner, B., Trull, T. (2008b), The natural iron fertilization experiment KEOPS (KErguelen Ocean and Plateau compared Study): an overview. *Deep-Sea Research II* 55 (5–7), 559–565.
- Blain, S., P.Tréguer, S. Belviso, E. Bucciarelli, M.Denis, S. Desabre, M. Fiala, V. Martin Jézéquel, J. Le Fèvre, P. Mayzaud, J-C. Marty, S.Razouls (2001), A biogeochemical study of the island mass effect in the context of the iron hypothesis: Kerguelen Islands Southern Ocean. *Deep Sea Research Part I: Oceanographic Research Papers*, 48 (1) 163-187
- Bucciarelli, E., S. Blain, P. Tréguer (2001), Iron and manganese in the wake of the Kerguelen Islands Southern Ocean. *Marine Chemistry* 73 pp.21–36.
- Cassar, N.,M.L. Bender, B.A. Barnett, S. Fan, W.J. Moxim, H. Levy II, B. Tilbrook (2007), The Southern Ocean biological response to aeolian iron deposition. *Science* 317, 1067–1070.
- Coale, K.H., Gordon, R.M., Wang, X. (2005), The distribution and behavior of dissolved and particulate iron and zinc in the Ross Sea and Antarctic Circumpolar current along 170 °W. *Deep-Sea Research I* 52, 295–318.
- Croot, P.L., Andersson, K., Öztürk, M., Turner, D.R. (2004), The distribution and speciation of iron along 6 °E in the Southern Ocean. *Deep-Sea Research II* 51 (22–24),2857–2879.
- Croot, P.L., P.Laan, J. Nishioka, V. Strass, B. Cisewski, M. Boye, K. R. Timmermans, R. G. Belterby, L. Goldson, P. Nightingale, H. J.W. de Baar (2005), Spatial and temporal distribution of Fe(II) and H₂O₂ during EisenEx, an open ocean mesoscale iron enrichment. *Marine Chemistry*, 95 (1-2), 65-88.

- Croot, P.L., R.D. Frew, S. Sander, K.A. Hunter, M.J. Ellwood, E.R. Abraham, C.S. Law, M.J. Smith and P.W. Boyd (2007), The effects of physical forcing on iron chemistry and speciation during the FeCycle experiment in the South West Pacific. *Journal of Geophysical Research*, 112, C06015,
- De Baar, H.J.W., Timmermans, K.R., Laan, P., De Porto, H.H., Ober, S., Blom, J.J., Bakker, M.C., Schilling, J., Sarthou, G., Smit, M.G., Klunder, M. (2008), Titan: a new facility for ultraclean sampling of trace elements and isotopes in the deep oceans in the international Geotraces program. *Marine Chemistry* 111 (1–2), 4–21.
- De Baar, H.J.W., P.W. Boyd, K.H. Coale, M.R. Landry, A. Tsuda, P. Assmy, D.C.E. Bakker, Y. Bozec, R.T. Barber, M.A. Brzezinski, K.O. Buesseler, M. Boyé, P.L. Croot, F. Gervais, M.Y. Gorbunov, P.J. Harrison, W.T. Hiscock, P. Laan, C. Lancelot, C. Law, M. Levasseur, A. Marchetti, F.J. Millero, J. Nishioka, Y. Nojiri, T. V. Oijen, U. Riebesell, M.J.A. Rijkenberg, H. Saito, S. Takeda, K.R. Timmermans, M.J.W. Veldhuis, A. Waite, C.S. Wong (2005), Synthesis of Iron Fertilization Experiments: From the Iron Age in the Age of Enlightenment. In: Orr, J. C., S. Pantoja, and H.-O. Pörtner (eds.) *The Oceans in a High-CO₂ World. Special Issue of Journal of Geophysical Research C (Oceans)* 110: 1-24.
- De Baar, H.J.W., J.T.M. de Jong, R.F. Nolting, M.A. van Leeuwe, K.R. Timmermans M. Templin, M.M. Rutgers van der Loeff and J. Sildam (1999), Low dissolved Fe and the absence of diatom blooms in remote Pacific waters of the Southern Ocean. *Marine Chemistry*, 66, 1-34.
- De Baar, H. J. W., J. T. M. de Jong, D. C. E. Bakker, B. M. Loscher, C. Veth, U. Bathmann, and V. Smetacek (1995), Importance of iron for plankton blooms and carbon dioxide drawdown in the Southern Ocean, *Nature*, 373(6513), 412-415.
- De Brauwere, A., S. H. M. Jacquet, F. De Ridder, F. Dehairs, R. Pintelon, J. Schoukens, W. Baeyens (2007), Water mass distributions in the Southern Ocean derived from a parametric analysis of mixing water masses. *Journal of geophysical Research-Oceans*, 112 C02021, doi:10.1029/2006JC003742,
- De Jong, J.T.M., Den Das, J., Bathmann, U., Stoll, M.H.C., Kattner, G., Nolting, R.F., De Baar, H.J.W. (1998), Dissolved iron at subnanomolar levels in the Southern Ocean as determined by ship-board analysis. *Analytica Chimica Acta* 377, 113–124.
- Dinniman, M.S., J.M. Klinck, W.O. Smith Jr. (2003), Cross-shelf exchange in a model of the Ross Sea circulation and biogeochemistry. *Deep Sea Research Part II* 50 (22-26), 3103-3120.
- Ellwood, M, Boyd, P, Sutton, P. (2008), Winter-time dissolved iron and nutrient distribution in the Subantarctic Zone from 40-52 °S; 155-160 °E. *Geophysical Research Letters*, (35), L11604,
- Fahrbach, E., G. Rohardt, M. Schroder, V. Strass (1994), Transport and structure of the Weddell Gyre. *Ann. Geophysicae* 12, pp. 840-855.
- Fan, S.-M., W. J. Moxim, and H. Levy (2006), Aeolian input of bioavailable iron to the ocean. *Geophys. Res. Lett.*, 33, L07602, doi:10.1029/2005GL024852
- Gerringa, L.J.A. A-C Alderkamp, P. Laan, C.-E. Thuróczy, H.J.W. De Baar, M.M. Mills, G.L. van Dijken, H van Haren, K. R. Arrigo (2011), Iron from melting glaciers fuels the phytoplankton blooms in Amundsen Sea (Southern Ocean): Iron biogeochemistry. *Deep Sea Research Part II: Topical Studies in Oceanography* 71–76, 16-31

- Gordon, L. I., L. A. Codispoti, J. C. Jennings Jr., F. J. Millero, J. M. Morrison, and C. Sweeney (2000), Seasonal evolution of hydrographic properties in the Ross Sea, Antarctica, 1996–1997, *Deep Sea Res, Part II*, 47, 3095–3117
- Green, S.E., R.N. Sambrotto (2006), Net community production in terms of C, N, P and Si in the Antarctic Circumpolar Current and its influence on regional water mass characteristics. *Deep-Sea Research I* 53, pp111–135
- Hall, J.A. and K. Safi (2001), The impact of in situ Fe fertilisation on the microbial food web in the Southern Ocean. *Deep-Sea Res. II* 48 pp. 2591-2613.
- Homoky, W.B., S. Severmann, J. McManus, W.M. Berelson, T.E. Riedel, P.J. Statham and R.A. Mills (2012), Dissolved oxygen and suspended particles regulate the benthic flux of iron from continental margins. *Marine Chemistry*, 134-135, 59-70
- Hoppema, M H.J.W. De Baar, E. Fahrbach, H. Hellmer, B. Klein (2003), Substantial advective iron loss diminishes phytoplankton production in the Antarctic Zone. *Global Biogeochemical Cycles*, 17(1), 25, pp. 1-9.
- Jickells, T.D., An, T.S., Andersen, K.K., Baker, A.R., Bergametti, G., Brooks, N., Cao, J.J., Boyd, P.W., Duce, R.A., Hunter, K.A., Kawahata, H., Kubilay, N., laRoche, J., Liss, P.S., Mahowald, N., Prospero, J.M., Ridgwell, A.J., Tegen, I., Torres, R. (2005), Global iron connections between desert dust, ocean biogeochemistry and climate. *Science* 308(67), 67–71.
- Johnson, K. S., R. M. Gordon, and K. H. Coale (1997), What controls dissolved iron concentrations in the world ocean?, *Marine Chemistry*, 57(3-4), 137-161.
- Klatt, O., E. Fahrbach, M. Hoppema, G. Rohardt (2005), The transport of the Weddell Gyre across the Prime Meridian. *Deep Sea Research II* 52 (3-4), 513-528.
- Klinkhammer, G.P., Chin, C.S., Keller, R.A., Dahlman, A., Sahling, H., Sarthou, G., Petersen, S., Smith, F., Wilson, C. (2001), Discovery of new hydrothermal vent sites in Bransfield Strait, Antarctica. *Earth and Planetary Science Letters* 193 (3–4), 395–407.
- Klunder M.B., P. Laan, R. Middag, H.J.W. De Baar, J.C. van Ooijen (2011), Dissolved iron in the Southern Ocean (Atlantic sector) *Deep Sea Research Part II: Topical Studies in Oceanography*, 58, (25-26) pp. 2678-2694.
- Klunder, M.B., 2012, This thesis, chapter 5.
- Lannuzel, D., Schoemann, V., De Jong, J.T.M., Chou, L., Delille, B., Becquevort, S., Tison, J.-L. (2008), Iron study during a time series in the western Weddell pack ice. *Marine Chemistry* 108 (1–2), 85–95.
- Lancelot, C., de Montety, A., Goosse, H., Becquevort, S., Schoemann, V., Pasquer, B., Vancoppenolle, M. (2009), Spatial distribution of the iron supply to phytoplankton in the Southern Ocean: a model study. *Biogeosciences* 6, 4919–4962.
- Löscher, B.M., De Baar, H.J.W., De Jong, J.T.M., Veth, C., Dehairs, F. (1997), The distribution of Fe in the Antarctic circumpolar current. *Deep-Sea Research II* 44 (1–2), 143–187.
- Mahowald, N., Kohfeld, K., Hansson, M., Balkanski, Y., Harrison, S.P., Prentice, I.C., Schulz, M., Rodhe, H. (1999), Dust sources and deposition during the last glacial maximum and current climate: a comparison of model results with paleodata from ice cores and marine sediments. *Journal of Geophysical Research* 104, 15.895–15.916.
- Martin, J.H., Fitzwater, S.E. (1988), Iron deficiency limits phytoplankton growth in the north-east Pacific subarctic. *Nature* 331 (6154), 341–343.

- Martin, J.H., R.M. Gordon, and S.E. Fitzwater (1990), Iron in Antarctic waters. *Nature* 345: 156-158.
- Mazloff, Matthew R., Patrick Heimbach, Carl Wunsch (2010), An Eddy-Permitting Southern Ocean State Estimate. *J. Physical Oceanography*, 40, 880–899.
- McCartney, M. S. (1977), Subantarctic mode water. A voyage of discovery, *supplement to Deep-Sea Res.*, 24 (Suppl. to George Deacon 70th Anniversary Volume), 103–119.
- Measures, C.I., Vink, S. (2001), Dissolved Fe in the upper waters of the Pacific sector of the Southern Ocean. *Deep-Sea Research II* 48 (19–20), 3913–3941.
- Middag, R. H.J.W. de Baar, P. Laan (2012), The effects of continental margins and water mass circulation on the distribution of dissolved aluminium and manganese in Drake Passage. *Journal of Geophysical Research-Oceans*, 117 C01019
- Middag, R. H.J.W. de Baar, P. Laan (2012), Fluxes of dissolved aluminum and manganese to the Weddell Sea and indications for manganese co-limitation. Accepted for publication after revisions, *Limnology and Oceanography*, August 2012.
- Moore, J.K., Abbott, M.R. (2002) Surface chlorophyll concentrations in relation to the Antarctic Polar Front: Seasonal and Spatial Patterns from Satellite Observations. *J. Marine Systems*, (37), 69-86.
- Moore, J.K., Braucher, O. (2008), Sedimentary and mineral dust sources of dissolved iron to the world ocean. *Biogeosciences* 5 (3), 631–656.
- Nielsdottir, M.C., T.S. Bibby, C. Mark Moore, D.J. Hinz, R. Sanders, M. Whitehouse, R. Korb, E.P. Achterberg (2012), *Marine Chemistry* 130-131, 62-72
- Nishioka, J., S.Takeda, H.J.W. de Baar, P.L. Croot, M.Boye, P.Laan, K.R. Timmermans (2005), Changes in the concentration of iron in different size fractions during an iron enrichment experiment in the open Southern Ocean, *Marine Chemistry*, 95: 51-63
- Nolting R.F., H.J.W. De Baar, A.J. van Bennekom and A. Masson (1991), Cadmium, copper and iron in the Scotia Sea, Weddell Sea and Weddell/Scotia Confluence (Antarctica) *Marine Chemistry*, 35 (1-4) pp. 219-243
- Orsi, A. H., T. Whitworth III and W. D. Nowlin, Jr. (1995), On the meridional extent and fronts of the Antarctic Circumpolar Current, *Deep-Sea Research. I*, 42, 641-673
- Park, Y-H., Gamberoni, L., Charriaud, E. (1993), Frontal structure, water masses, and circulation in the Crozet Basin. *Journal of Geophysical Research* 98, 12361–12385.
- Parekh, P., Follows, M.J., Boyle, E. (2004), Modelling the global ocean iron cycle. *Global Biogeochemical Cycles* 19, GB 2020
- Planquette, H., Statham, P.J., Fones, G.J., Charette, M.A., Moore, C.M., Salter, I., Nede lec, F.H., Taylor, S.L., French, M., Baker, A.R., Mahowald, N., Jickells, T.M. (2007), Dissolved iron in the vicinity of the Crozet Islands, Southern Ocean. *Deep- Sea Research II* 54 (18–20), 1999–2019
- Pollard, R.T., M.I Lucas, J.F Read (2002), Physical controls on biogeochemical zonation in the Southern Ocean), *Deep Sea Research Part II* 49 (16), pp. 3289-3305
- Rintoul, S. R., C. Hughes and D. Olbers (2001), The Antarctic Circumpolar Current System. In: *Ocean Circulation and Climate*, G. Siedler, J. Church, and J. Gould, (Eds.), Academic Press, 271-302.
- Ribbe, J. and M. Tomczak (1997), On convection and the formation of Subantarctic Mode Water in the Fine Resolution Antarctic Model (FRAM) *J. Marine Systems* 13, 137-154.

- Rutgers van der Loeff, M., Cai, P., Stimac, I., Bracher, A., Middag, R., Klunder, M.B., van Heuven, S. (2011), ^{234}Th in surface waters: distribution of particle export flux across the Antarctic Circumpolar Current and in the Weddell Sea during the GEOTRACES expedition ZERO and DRAKE. *Deep-Sea Research II* 58, 2749–2766.
- Sañudo-Wilhelmy, S.A., K.A. Olsen, J.M. Scelfo, T.D. Foster, A.R. Flegal (2002), Trace metal distributions off the Antarctic Peninsula in the Weddell Sea. *Marine Chemistry* 77, 157–170.
- Sedwick, G. R. DiTullio, and D. J. Mackey (2000), Iron and manganese in the Ross Sea, Antarctica: Seasonal iron limitation in Antarctic shelf waters, *J. Geophys. Res.* 105 (C5), 11,321–11,336
- Sedwick, G. R. DiTullio, D. A. Hutchins, P. W. Boyd, F. B. Griffiths, A. C. Crossley, T. W. Trull, and B. Quéguiner (1999), Limitation of algal growth by iron deficiency in the Australian Subantarctic region, *Geophys. Res. Lett.* 26, 2865–2868.
- Sedwick, and G. R. DiTullio (1997), Regulation of algal blooms in Antarctic shelf waters by the release of iron from melting sea ice, *Geophys. Res. Lett.* 24, 2515–2518, 1997.
- Sedwick, P. R. Edwards, D. J. Mackey, F. B. Griffiths, and J. S. Parslow (1997), Iron and manganese in surface waters of the Australian subantarctic region, *Deep-Sea Research I* 44, 1239–1253,
- Sedwick, P.N., Bowie, A.R., Trull, T.W. (2008), Dissolved iron in the Australian sector of the Southern Ocean (CLIVAR SR3 section); Meridional and seasonal trends. *Deep-Sea Research I* 55, 911–925.
- Sedwick, P. N. Marsay, C.M., Sohst, B., A.M Aguilar-Islas, A.M., Lohan, M. C. Long, M.C. Arrigo, K.R. Dunbar, R.B., Saito, M.A. Smith, W.O. and G. R. DiTullio (2011), Early season depletion of dissolved iron in the Ross Sea polynya: Implications for iron dynamics on the Antarctic continental shelf, *J. Geophys. Res.*, 116, C12019
- Sloyan, B.M., S.R. Rintoul (2001), Circulation, Renewal, and Modification of Antarctic Mode and Intermediate Water. *J. Physical Oceanography*, 31, 1005–1030.
- Smith, W. O., Jr., and J. C. Comiso (2008), Influence of sea ice on primary production in the Southern Ocean: A satellite perspective, *J. Geophys. Res.*, 113, C05S93
- Sohrin, Y., S. Iwamoto, M. Matsui, H. Obata, E. Nakayama, K. Suzuki, N. Handa, M. Ishii (2000), The distribution of Fe in the Australian sector of the Southern Ocean *Deep Sea Research Part I: (47)* 1, pp. 55–84.
- Sokolov, S. and Rintoul, S.R. (2007), On the relationship between fronts of the Antarctic Circumpolar Current and surface chlorophyll concentrations in the Southern Ocean. *J. Geophys. Res.* (112), C07030.
- Speer, K., S. R. Rintoul, and B. Sloyan (2000), The Diabatic Deacon Cell. *J. Physical Oceanography* 30, 3212–3222.
- Sunda, W. (2001), Bioavailability and bioaccumulation of iron in the sea. In: Turner, D., Hunter, K.A. (Eds.), *Biogeochemistry of Iron in Seawater*, IUPAC Book Series on Analytical and Physical Chemistry of Environmental Systems, vol.7 ; 2001, pp. 123–254 (Chapter4).
- Tagliabue, A., Bopp, L., Aumont, O. (2009), Evaluating the importance of atmospheric and sedimentary iron sources to Southern Ocean biogeochemistry. *Geophys. Res. Lett.* 36, L13601.

- Tagliabue, A., L. Bopp, J-C. Dutay, A.R. Bowie, F.Chever, P.Jean-Baptiste, E. Bucciarelli, D. Lannuzel, T.Remenyi, G.Sarthou, O.Aumont, M.Gehlen, C. Jeandel (2010), Hydrothermal contribution to the oceanic dissolved iron inventory. *Nature Geosciences* 3, 252 – 256.
- Tomczak, M.(2000), An introduction to online physical oceanography. *Oceanography* 13, 104-105.
- Tomczak, M., S. Godfrey (2003), *Regional Oceanography: an Introduction*. Daya Publishing House, Delhi. Tortell, P. D., M.T. Maldonado, J. Granger, N. Price, N.(1999), Marine bacteria and biogeochemical cycling of iron in the oceans. *Fems Microbiology Ecology*, 29(1), 1-11.
- Tovar-Sanchez, A., C.M. Duarte, S. Hernández-León, S.A. Sañudo-Wilhelmy (2009), Impact of submarine hydrothermal vents on the metal composition of krill and its excretion products. *Marine Chemistry* 113, (1-2) pp. 129-136
- Timmermans, K.R., L.J.A. Gerringa, H.J.W. de Baar, B. van der Wagt, M.J.W. Veldhuis, J.T.M. de Jong, P.L. Croot, M. Boye (2001), Growth rates of large and small Southern Ocean diatoms in relation to availability of iron in natural seawater. *Limnol. Oceanogr.* 46: 260 – 266.
- Trull, T.W., Rintoul, S.R., Hadfield, M., Abraham, E.R. (2001), Circulation and seasonal evolution of polar waters south of Australia: Implications for iron fertilization of the Southern Ocean. *Deep-Sea Research II*, 48 pp. 2439-2466
- Twining, B.S., S.B. Baines, N.S. Fisher, M.R. Landry (2004), Cellular iron contents of plankton during the Southern Ocean Iron Experiment (SOFEX) *Deep Sea Research Part I: 51, (12), pp. 1827-1850*
- Van Aken, H. Ridderinkhof, W. P.M. de Ruijter (2004), North Atlantic deep water in the south-western Indian Ocean *Deep-Sea Research I* 51 (2004) 755–776
- Westerlund, S., P. Öhman (1991), iron in the water column of the Weddell Sea *Marine Chemistry*, 35 (1-4) pp 199-217
- Withworth III, T., Nowlin Jr., D.W. (1897), Water Masses and Currents of the Southern Ocean at the Greenwich Meridian *Journal of Geophysical Research*, 92, C6, pp.6462-6476

6.10 Appendix

6.10.1 Database values that were excluded

On the one hand there exist several data sets showing elevated Fe concentrations due to natural causes, for example Fe supply from island shelves, along with the Polar Frontal jet stream, near the sea-ice, and near hydrothermal vent fields. Dissolved Fe concentrations largely exceeding 1 nM in the surface waters are observed near the Kerguelen island shelves by *Blain et al.* [2001], *Bucciarelli et al.* [2001], and in the Polar Front sampled (<400 m) with kevlar hydrowire by *De Baar et al.* [1995]. The concentrations as presented by *Blain et al.* [2001] and *Bucciarelli et al.* [2001] receive considerable Fe-input from the Kerguelen Islands, as the aim of these studies is to give insight in natural Fe supply by the Kerguelen/ other islands. This causes local high concentrations of iron close to the shelf. *Bucciarelli et al.* [2001] show that the dissolved iron concentration strongly decreases with distance from the Kerguelen. Because the number of datapoints is low, these datapoints will bias the Indian Ocean Sector data towards high concentrations, which is not representative for the complete region. Similar for *Planquette et al.*, [2007] station M3 and M7. De Jong et al. (in press) reports several new datasets. For the ISPOL datasets in the special sea-ice environment of the western Weddell Sea and Scotia Sea, there were relatively high dissolved Fe values (3-20 nM) reported. *Klinkhammer et al.* [2001] report dissolved iron close to Hook ridge ~62°10' S and ~57° 17' W and ~62°40' S, 59°05' W. However, these dissolved iron data were in context of a study nearby hydrothermal vents, and thus specific depths and stations are chosen. To ensure representative concentrations for the different Southern Ocean regions for the statistical analysis, we excluded the datasets of *Bucciarelli et al.* [2001], *Blain et al.* [2001], *Planquette et al.* [2007], *De Baar et al.* [1995], ISPOL data of *De Jong et al.* [2011], and *Klinkhammer et al.* [2001].

On the other hand there exist several historical datasets that appear to represent quite high values that here are attributed to inadvertent contamination. For example *Löscher et al.* [1997] not only list the above mentioned upper water (<400m depth) dataset (De Baar et al., 1995) that was collected with single GO-FLO samplers mounted on a special kevlar wire, but also some 15 deep values (492-4828m range) that were collected with GO-FLO samplers fitted on an epoxy-coated stainless steel CTD frame deployed with a regular steel hydrowire. In retrospect the reported deep concentrations are in a high range (0.4-2.8 nM) and afterwards this is attributed to inadvertent contamination due to the steel hydrowire. The [Fe] dataset obtained during the ANT XXIV/3 cruise (2008) largely outnumbers the historically available datasets in the Weddell Gyre [*Klunder et al.*, 2011; *Klunder et al.*, This thesis, Chapter 5]. Pioneering studies to the dissolved iron concentration in the Weddell Gyre by *Nolting et al.* [1991], *Westerlund and Ohman* [1991] and *Sanudo-Wilhelmy et al.* [2002] tend to report much higher Fe values than the modern values [*Klunder et al.*,

2011]. Presumably the sampling methods, for example by hand from a zodiac, may have been inadequate to rigorously exclude inadvertent contamination. Therefore the older datasets *Löscher et al.* [1997; deep values >400m], *Nolting et al.* [1991], *Westerlund and Ohman* [1991] and *Sanudo-Wilhelmy et al.* [2002] now appear to be mostly of historical interest and are excluded from the statistical analysis.

The complete database including the values here excluded is to be found in the online supplement.

6.10.2 Determination of depth of Upper Mixed Layer

In some cases, the upper mixed layer depth was determined in the same study as the [Fe] values, or temperature, salinity or density profiles were reported, in which cases an UML depth could be estimated. For the ANT XXIV/3 and NPB01 cruises most stations showed a strong subsurface gradient in the density profile, which was chosen as the mixed layer depth. Where no UML depth could be determined, UML depth was estimated via the position and date to seek other studies nearby of which the UML depth was deducted.

6.10.3 Hydrography and differentiation of regions

6.10.3.1 ACC

First, the (STF) Subtropical Front separates the warm saline tropical water from the north and more southerly cold saline waters [*Sokolov and Rintoul*, 2001]. This front is located mainly around 40 °S, bordering the Southern Ocean from the north. In the Atlantic Sector it even reaches as far south as 30 °S [*Tomczak et al.*, 2001; *Cassar et al.*, 2007]. This front defines the northern border of the Antarctic Circumpolar Current (ACC) (Fig. 6.1). More to the south the strong Subantarctic Front (SAF) is found [*Sokolov and Rintoul*, 2001]. Further polewards, varying between 45 °S and 63 °S, the Polar Front (PF) is defined as the northernmost extend of the 2°C subsurface (200m.) minimum. *Moore and Abbott* [2002] showed the multi-year average of the PF, using Satellite Temperature data. This figure is here used to define the PF. More to the south, two different fronts can be distinguished, which are separated fronts, but occasionally coincide [*Orsi et al.* 1995]. The SACCF is defined as the southern boundary of waters with $\theta > 1.8$ in the θ_{\max} . [*Orsi et al.*, 1995; *Sokolov and Rintoul*, 2001]. More commonly described is the Southern Boundary of the ACC (SB-ACC), the southern boundary of low-oxygen UCDW [*Orsi et al.*, 1995; *Sokolov and Rintoul*, 2001]. The zone between the PF and the SB-ACC is defined as Antarctic Zone (AAZ) [*Pollard et al.* 2002].

The water masses within the ACC are, from south to north; from the SB-ACC northward, Ekman pumping causes the cold, dense and highly oxygenated Antarctic Surface Water (AASW) to flow northward where it meets Subantarctic Water at the Polar Front. Here, the AASW subducts and, upon mixing with upwelled water and

melted sea-ice (see below), forms Antarctic Intermediate Water (AAIW) but continues the northward flow [Whitworth and Nowlin, 1987; Orsi *et al.* 1995; Debrauwere *et al.*, 2007]. Debrauwere *et al.* [2007] also report a large amount of fresh ($S < 34$) Circumpolar surface water (CSW) in the Indian Sector.

The northernmost part of the ACC, generally comprises Subantarctic Surface Water (SASW). This water reflects the properties of the tropical waters to the north. This is relatively saline compared to the AASW, except for the Drake Passage, where the SASW reflects the relatively fresh waters of the Southeast Pacific [Whitworth and Nowlin, 1987]. North of the SAF, winter convection creates subsurface Subantarctic Mode Water (SAMW) [Ribbe and Tomczak [1997], Tomczak [2001]; Debrauwere [2007]]. Below the SAMW, the Circumpolar Deep Water (CDW) is found. These waters are divided in Upper (UCDW) and Lower (LCDW) Circumpolar Deep Water. The UCDW is characterized by low oxygen and high nutrient concentrations, reflecting influence from the Antarctic waters to the South. The LCDW contains high salinities, which indicates mixing with deep waters from the North, in particular North Atlantic Deep Water (NADW) [Orsi *et al.* 1998; Klunder *et al.* 2011; their fig. 6.2]. The upwelled water from the North Atlantic Ocean comes from depths around 2500-4000 meter and moves southward and upward, until as close to the surface as 200 m, south of the PF, where mixing with AASW and melted sea-ice takes place and AAIW is formed, following the AAIW circulation pattern [Tomczak, 2001; Hoppema *et al.*, 2003]. This upwelling of deep waters from the North takes place in all three ocean basins [Van Aken *et al.*, 2004], but Tomczak [2001] shows that this upwelling is most constrained and well described in the West Atlantic part of the Southern Ocean. The subsurface layers consist mainly of relatively warm and saline (SAMW) and the northwards flowing AAIW.

Here we separated the different Sectors by longitudinal borders; Atlantic Sector 65°W – 20°E; Indian Sector 20°E-140°E; Pacific Sector 140°E-65°W.

6.10.3.2 Weddell Gyre

The Weddell Gyre is a cyclonic Gyre border by the SB-ACC in the North, the Continent (or the Antarctic Coastal Current) in the South and the Antarctic Peninsula in the West. To the east, the WG does not come across any natural boundaries, and thus can extend as far as 30 °E, in the Enderby basin [Klatt *et al.*, 2005]. Outflow features over these ridges are observed just off the Peninsula, in the Weddell Scotia confluence [Nolting *et al.*, 1991] and at ~30 °W, where the Scotia ridge and the North Weddell Ridge meet [Klatt *et al.* 2005]. In the surface the northward flowing AASW is found, below which the Winter Water (WW) is identified [Park *et al.*, 1993; Klunder *et al.*, 2011, in preparation] formed during convective overturning during winter, and persistent during the season. In the Deep Weddell Sea, the saline Warm Deep Water (WDW), the slightly colder and very saline Weddell Sea Deep Water (WSDW) and the coldest Weddell Sea Bottom Water are distinguished.

Klatt et al. [2005] reported a westwards flowing current south of 62°S and an eastwards flowing current further north, over a zero meridian transect. Further to the West in the Weddell Sea, the structure of the Weddell Gyre was described by *Fahrbach et al.* [1994]. For the upper 1000 m the situation is relatively clear; southeast of 66.6 °S, 26.5°W the current are westward, north of this point the currents are eastward, except for a small region (34-37°S) where we have no datapoints. Therefore, for the upper three layers we interpolate the distinction of the east versus westward flowing current between these two positions 62°S, 0°W , 66.6 °S, 26.5°W (Fig. 6.3). To the best of our knowledge there is no information of the flow direction west of the transect presented in *Fahrbach et al.* [1994]. However, *Fahrbach et al.* [1994] reported an eastward flow at ~64.5 °S, 46 °W and 64 °S, 49 °W. The fact that the samples (from stations deeper then 3000m, will be discussed below) we grouped in the eastward current are all located relatively near to these locations (all north of 66 °S), gives us confidence that these samples are correctly contributed to the northern, eastwards flow.

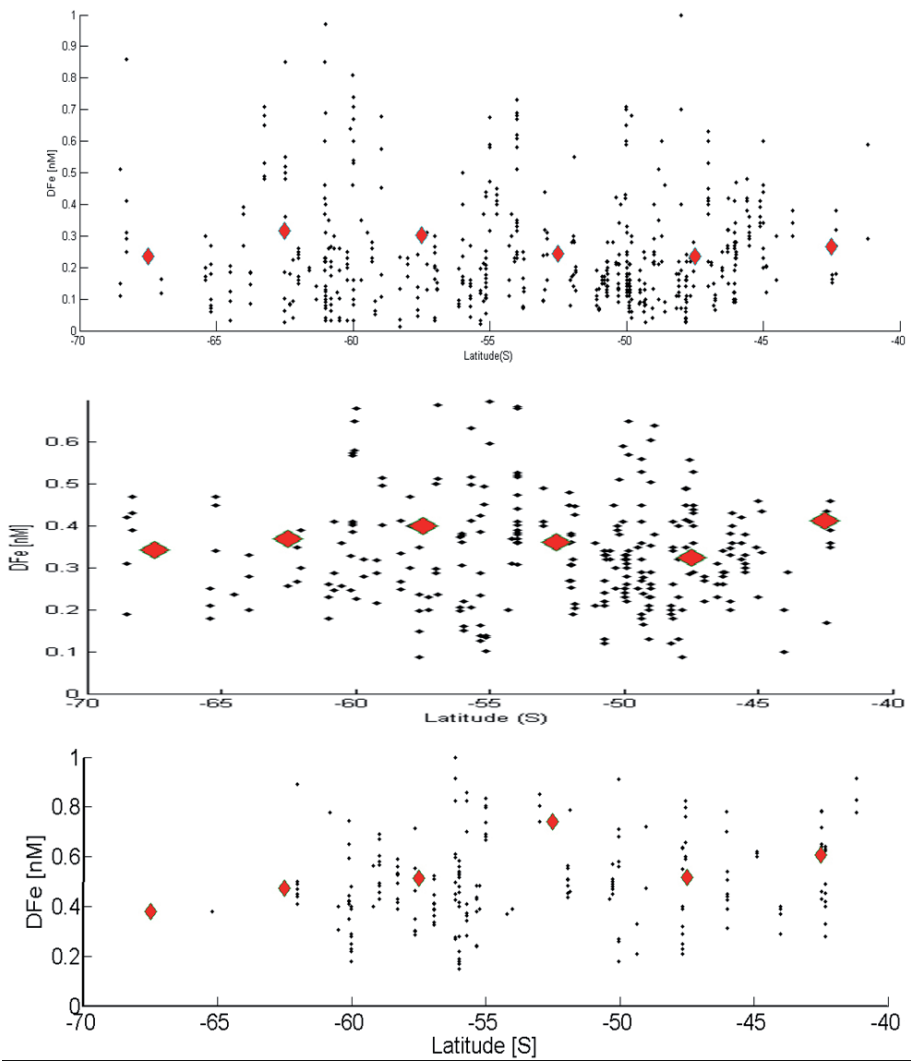


Fig. 6.S1 Dissolved Fe versus latitude for all samples in the (upper panel) Subsurface Layer (UML-300m), (middle panel) Intermediate Layer (300-1000m) and (lower panel) Deep Layer (>1000m). Red dots represent averages over 5° latitude.



Chapter 7

Summary and recommendations



7.1 Summary

In the course of this thesis in total 1656 sample values of dissolved iron (DFe) have been collected for DFe in the two Polar oceans. An additional 49 data values were rejected as outliers not used in the thesis, but still available in the database along with the criteria for rejection (see also in each research chapter and the database chapter). The large number of sample values, the high resolution and the simultaneous sampling of major nutrients, Fe-ligands and other trace metals as well as physical and biological parameters has led to new insights in the distribution of DFe in the Arctic Ocean and in the Southern Ocean.

In the Arctic Ocean, higher concentrations of DFe (~ 0.8 nM) are measured in the Barents Sea than in the Kara Sea (0.4 – 0.6 nM). Although the Kara Sea stations were situated more on the shelf break, closer to the basin, it is likely that scavenging removal and biological uptake of DFe in the waters caused a depletion of DFe during water mass transport from the North Atlantic to the Central Arctic Ocean (Barents Sea Branch). The highest DFe concentrations were observed in the Laptev Sea bottom waters, where concentrations exceeded 10 nM. This could be caused by sediment resuspension, as indicated by the high particle concentration and/or by regeneration of organic matter as also supported by the distribution of dissolved barium. Moreover, sinking of brine-enriched surface waters may (partly) explain the high DFe here observed.

In the surface waters of the Central Arctic Ocean a significant inverse correlation is observed between salinity and DFe, indicating freshwater source(s) for DFe. In this thesis, mass balance calculations, using $\delta^{18}\text{O}$, salinity and nutrient concentrations are used to estimate the contribution of different freshwater sources to the central Arctic Ocean. We conclude that the highest DFe concentrations are originating from Eurasian river waters, which are further transported with the Trans Polar Drift (TPD) into the centre of the Arctic basin. On the North American side of the TPD, lower DFe concentrations are attributed to biological depletion of Pacific waters flowing over the Chukchi Shelf. These interpretations of the results are strengthened by the distribution of – simultaneously measured - total alkalinity, and by the distribution of Total Fe, which was available for 8 stations from this expedition.

Deeper in the water column, below the Polar Surface Waters (PSW), the deep water concentrations differ between the Basins. The highest concentrations were observed in the Nansen Basin (~ 0.6 – 0.7 nM), lower in the Amundsen Basin (~ 0.45 nM) and lowest in the Makarov Basin (~ 0.25 nM). Moreover, at intermediate depth (250 – 1000 m) the highest DFe is observed in the west part of the Nansen Basin (closest to Fram Strait), likely reflecting inflow of Atlantic waters into the Nansen Basin. Most remarkably, at ~ 2500 m depth a distinct strong maximum in DFe is observed in the Nansen and Amundsen Basins. Good correspondence with dissolved manganese (DMn) maxima, particle concentration and slightly elevated temperature, indicate

hydrothermal activity as a DFe source. Indeed hydrothermal vents have previously been reported on the Gakkel Ridge, near our sampling station. These vents appear to cause significant enrichment with DFe in the Deep Arctic Ocean Basins, consistent with earlier reported flow directions of Arctic Deep Ocean currents. Moreover, significant input of DFe from the shelf slope has been observed in the Nansen Basin, both at the Kara Sea slope as at the Laptev Sea slope. In contrast, the absence of these sources and a strong scavenging removal apparently leads to very low DFe concentrations in the deepest (>3000 m) Makarov Basin.

In the Southern Ocean, the concentrations of DFe in the surface waters were generally low (0.1 -0.3 nM), and lowest concentrations (<0.010 nM) were observed in the Central Weddell Sea.

In the vicinity of continental shelves in other world oceans, an enrichment in DFe and DMn is always observed. The opposite is true near the Antarctic Continental Shelf at the Greenwich Meridian, where concentrations of DFe (and DMn [*Middag et al.* [2011]) are extremely low. The permanent ice sheet extending of the Antarctic continent is unique in that it largely prevents the, commonly observed, biogeochemical mechanisms that cause enrichment in DFe and DMn [*Middag et al.*, 2011]. Locally, occasionally higher DFe concentrations in the (upper) surface layer could be related to ice-melt (low salinity) or aeolian deposition, the latter also indicated by enriched dissolved Aluminium.

On the other hand the Antarctic Peninsula Shelf is, like in other oceans, a regular source of DFe and DMn [*Middag et al.*, 2011], and lateral advection along isopycnal surfaces is an important source of DFe to the adjacent and downstream surface waters in Drake Passage. Although above the shelf the DFe concentrations were high, the off shelf influence was not observed in surface waters on the Weddell Sea side of the Antarctic Peninsula shelf. The relationship of DFe and chlorophyll fluorescence and POC export were assessed and interpreted in context of the role of DFe in phytoplankton growth in the Southern Ocean. Moreover in most part of the Weddell Sea transect, the concentration and availability of DFe appears to affect the ratio of uptake of nitrate relative to silicate by diatoms, consistent with previously reported field and laboratory studies. Also the removal ratio of N:P is affected by the DFe concentration, although this effect is only observed at the Greenwich Meridian, where the average size of the diatoms present was much higher. We conclude that the concentration of DFe has implications for the nutrient drawdown ratios, and thus the nutrient cycle in the Southern Ocean.

There are several sources of DFe to the surface waters, the most important of which are upwelling and vertical mixing of the deep waters that are relatively rich in dissolved Fe. Melting of seasonal sea ice has been shown to be another important DFe source to the surface waters, but this source is highly variable hence difficult to quantify. Moreover, seasonal sea ice can be seen as a seasonal storage – capturing DFe in autumn, releasing it in spring - rather than a truly external source of “new”

DFe to the surface waters of a region. Locally, input of DFe by wet or dry deposition is seen occasionally and supported by precipitation data, air mass back trajectories and correlation with (elevated) dissolved Aluminium. However, in general there is only a minor role of dust deposition in the DFe cycle in our study region, as consistent with assessments of deposition rates in the Southern Ocean of global deposition models. In the Drake Passage, shelf-derived DFe from the Antarctic Peninsula shelves on the South side, and fluvial input from the Northern boundary (Tierra del Fuego) are important sources for DFe to the surface waters. However, due to the strong eastward flowing circumpolar current versus the South-North direction of our transect it was not possible to investigate the downstream full magnitude of these DFe inputs to the Southern Ocean.

In the deep waters of the Southern Ocean, the DFe was found to be lowest in the Antarctic Bottom Waters (AABW: $\sim 0.3 - 0.4$ nM). These waters are formed as Weddell Sea Deep Water in the Weddell Sea and constitute a cold, fresh, low DFe water mass flowing Northwards through the abyssal Atlantic Ocean. Higher concentrations were observed in overlying the Circumpolar Deep Waters, which were clearly distinguishable in both the Greenwich meridian and Drake Passage transects. These waters are slightly enriched in DFe, which is caused by the high DFe in their source, the North Atlantic Deep Water (NADW), the latter as observed in the NADW component in the northernmost stations of the transect along the Greenwich meridian. In its turn, these Circumpolar Deep Waters flow over the Bouvet Ridge to form the Warm Deep Water in the Weddell Sea, thereby acting as a DFe source to the Weddell Gyre.

The deep waters also show a strong hydrothermal source of DFe into the Southern Ocean. This is seen in two locations. Firstly close to the sampling region at the Bouvet Ridge, there is a dominant DFe plume visible over the Ridge crest, also accompanied by a distinct plume of DMn. Secondly in the Drake Passage, there is a relatively small volume water mass originating from the East Pacific, that carries a hydrothermal signal with very high (>1 nM) DFe concentrations.

When looking at DFe in the deep waters along the trajectory of the Weddell Gyre, the deep water concentrations decrease from the transect at the Greenwich meridian (0°W) towards the Central Weddell Sea and close to the Peninsula. This decrease is found when following the westward limb, which flows close to the Antarctic continent. However, in the eastward flowing limb, situated more to the north, the deep water DFe concentrations are relatively high. An input of extra Fe with Warm Deep Water over Bouvet Ridge is unlikely as most Warm Deep Water flows into the Weddell Gyre further to the East, at $0-20^\circ\text{E}$. Thus enrichment in DFe must occur on the way eastward, where the Weddell Gyre flows close to Bouvet Ridge, the extra Fe supply probably caused by particle resuspension from the Ridge or by hydrothermal activity.

The formation of Weddell Sea Bottom Water (WSBW) by downslope convection is a well known phenomenon of the Weddell Sea. For other elements, such as Mn and Ba this process has been shown to enrich the WSBW concentrations. Although there were indications of the formation of Bottom Water during our cruise, no significant enrichment of the WSBW with DFe is observed. However, on the North side of the Peninsula, deep waters enriched in DFe are observed. It is suggested that these are Deep Waters that originate from the Weddell Sea, following a pathway through Powell Basin. The strong velocity of this water mass may cause sediment re-suspension, reflected in the observed high turbidity due to high amount of particles. The input of seafloor derived DFe will then be the cause of the high DFe concentrations as also observed in the distribution of dissolved Manganese.

The large number of Southern Ocean data presented in this thesis, constitute the basis of a compilation of DFe concentrations in the Antarctic Circumpolar Current (ACC) and Weddell Gyre. This circumpolar compilation provides insight in the sources and possible downstream dilution of DFe within the ACC. Indeed from the compilation it shows that DFe in the upper 1000 m is higher in the region from 60°W to 60°E, compared to the other regions. These higher DFe concentrations in the Atlantic sector likely are caused by more dust deposition, sedimentary sources (Islands, Antarctic Peninsula and Patagonia at Drake Passage), and last but not least, the strong influence of upwelling deep waters carrying the high Fe signal of NADW origin.

7.2 Recommendations for future research

This thesis was designed as the first ever survey of both Polar Oceans of dissolved Fe, in 2 cruises comprising long sections with closely spaced stations of 24 samples each, distributed over the full water column depth. This now having been completed, one would like to return to the Polar oceans for more detailed studies of several interesting features.

One of the major findings of this thesis was the important role of hydrothermal vents in the distribution of dissolved Fe in the deep Polar Oceans, as first presented in conferences in 2008 and 2009. Although hydrothermal vents were acknowledged as sources of DFe to the ocean, until about a decade ago it was commonly understood that, due to the rapid oxidation, virtually all Fe precipitated out of the water column very close to the vent source location, mainly by rapid formation of oxyhydroxide deposits [De Baar and De Jong, 2001]. In the last decade, there have been reports of hydrothermal DFe input in the Pacific [Mackey *et al.*, 2002; Boyle *et al.*, 2005; Boyle and Jenkins, 2008] and Atlantic Oceans [Bennett *et al.*, 2008], sometimes far away from the hydrothermal source [Wu *et al.*, 2011]. We reckon that due to the improved ultraclean sampling and analyses of recent years and in this thesis, the true ambient

DFe in the deep ocean at large has now been found to be very low. That low baseline now established allows the hydrothermal vent plumes to stand out more distinctly, i.e. the extent of latter vent plumes now is seen to be much wider than previously realized. Nevertheless, for a long time, modeling studies have ignored contribution of hydrothermal vents to the deep Ocean DFe cycle, and focused on the role of sediments and remineralisation [Aumont and Bopp, 2006; Moore and Braucher, 2008] for deep sea Fe input. Recently, our findings of more basinwide impact of hydrothermal vents in deep DFe concentration has become incorporated in modeling and overview studies by Tagliabue *et al.* [2010] and Boyd and Ellwood [2010]. Most recently Sander and Koschinsky [2011] show that, in the presence of sufficient organic ligands, hydrothermal DFe can account for 9% of the deep ocean DFe budget.

During our expeditions, we reported several occasions of hydrothermal DFe input. The most important example was located in the Arctic Ocean. One or more hydrothermal vents over the Nansen-Gakkel Ridge, are not only reported to locally enrich the DFe concentrations, but these enrichments could be traced further everywhere in the Nansen Basin. The location of hydrothermal vents, at the Ocean ridges often far from land, remote regions usually with low dust and sediment inputs, makes them an important source of DFe. In a further study it should be noteworthy to look more specifically at the hydrothermal DFe enrichment. Ideally, one would locate a vent or vent field and gather more information about the iron chemistry (distribution of particulate, dissolved, soluble Fe) and then repeat these measurements on a high resolution section with increasing distance from the vent. In such study it is important to also gather more data about the organic complexation of DFe as it recently has been shown to largely influence the amount of Fe that can escape oxidation and precipitation and thus reaches the ambient deep ocean water [Thuróczy *et al.*, 2011b; Sander and Koschinsky, 2011]. Such an experiment, ideally repeated in several lateral directions (to capture the role of the currents in the advective Fe-transport), would give more insight in the quantitative contribution of hydrothermal vents to the deep ocean DFe budget. Moreover, for such an experiment, Fe-isotope fractionation is promising to discriminate between hydrothermal and other sources in the deep ocean [Bennett *et al.*, 2008]. When designing such an experiment, it should be noted that there is large difference in the type of vents, spreading ridges and amount and composition of fluid output.

The cycling of dissolved Fe in the upper ocean depends, as other nutrients and metals, largely on the seasonal cycle. Briefly, the paradigm is that in the Southern Ocean, DFe is consumed by spring time primary production, this process continues until Fe is depleted in summer, possibly causing Fe-limitation in phytoplankton growth. In autumn, when the Antarctic storms commence, the Upper Mixed Layer deepens, and upwelling occurs causing a 'winter replenishment' of DFe [De Baar and De Jong, 2001; Measures *et al.*, 2001; Hoppema *et al.*, 2003; Sedwick *et al.*, 2008]. Other important contributions to the Fe input, such as the melting of sea-ice to the surface

water (in spring) [Lannuzel *et al.*, 2008] and (wet) atmospheric deposition [Gaiero *et al.*, 2003] also depend on the seasons.

However, many expeditions in the Southern Ocean have a time frame of only 2-3 months, and thus cannot cover all of these processes. Several studies, reporting a compilation of DFe-data from different expeditions [De Baar and De Jong, 2001; Moore and Braucher, 2008; Tagliabue *et al.*, 2012; This thesis, Chapter 6] have shown that most of the regions have a DFe data coverage at least from early to late summer. The only study describing 'winter' DFe concentrations so far does not comply with the paradigm and shows relatively low DFe concentration (~ 0.15 nM, in July in the Indian Sector of the Southern Ocean; [Ellwood *et al.*, 2008]). Due to the different removal processes for Fe, such as biological uptake, scavenging, export and (shallow) remineralization, it is problematic to assume that the Winter Water concentrations at the θ_{\max} can be regarded as 'winter-reserve' as is done for major nutrients in this thesis (Chapter 5). Therefore, to better understand the seasonal cycle and supply mechanisms of DFe to the (surface) ocean it would be vital to also obtain data in the winter months. Ideally, a seasonal series of measurements in an open Southern Ocean region would be performed, including measurements of density and vertical and horizontal velocity, to constrain the processes of mixed layer deepening and mixing, upwelling and Ekman transport, processes which are important for biogeochemical cycling [Hoppema *et al.*, 2003] because of the large volumes of water involved. Admittedly, the major challenges for operating a research vessel in winter time in the Southern Ocean are realized.

The work in this thesis focused on high resolution transects of the whole 4-6 km deep water column. This is important for understanding of the cycling of Fe throughout the ocean. Moreover, there is a great interest in DFe as the primary biolimiting trace element for phytoplankton in the surface ocean. Indeed, several findings of the current thesis have shed more light on this issue. Nevertheless, it would be of great interest to return and do more high resolution sampling at much higher vertical resolution of 24 sampling depths within the upper 300-500 m. The upper 300 m covers the biologically most interesting layers and would allow a sample every 15 m. Such a high resolution would enable to determine the very likely small scale vertical gradients in DFe, as already indicated in temperature, salinity, particle concentration, chlorophyll a and oxygen of the CTD-sensor data. This would give a better insight in the relation between (D)Fe and biological processes even at small scale (sometimes significant differences in 10-20 m depth layers as observed in this thesis in the Arctic (Chapter 2).

Besides investigations of the (dissolved) Fe concentrations, Manganese (Mn) and Aluminium (Al) have been investigated in the companion GEOTRACES IPY PhD research thesis by Middag [2010] and Fe-complexation and size fractionation were studied in the companion GEOTRACES IPY thesis by Thuróczy [2011a]. As a pre-

sumption to this thesis it was noted that dissolved aluminium (DAI) is known as a good tracer for aeolian deposition of aerosols (and thus several metals) to the open ocean. Indeed, in some locations in the Southern Ocean elevated Fe concentrations in surface waters corresponded to elevated Al concentrations indicating aeolian deposition as a source. However, in some of our study regions also DMn showed an increase in the surface (at 55°S, Greenwich Meridian). On the other hand, dissolved manganese (DMn) was shown to be used as a source tracer of sedimentary and hydrothermal DFe input. In this thesis, in both Polar Oceans we observed shelf/sediment DFe-enrichment. However, at the Drake Passage, an increase in DAI is consistent with increased DFe and DMn from the shelf (Chapter 5). These findings imply that DAI cannot solely or simply be used as a distinctive tracer for DFe input from atmospheric dust and DMn should not solely or simply be taken as a distinctive tracer for shelf input of DFe.

Hydrothermal DFe enrichment did nicely correspond with Mn enrichment in all cases, and without any enhancement of DAI. However, this increase for Mn usually showed a high peak (relative to background) and relatively fast decrease with distance from the source, whereas DFe had a smaller peak, but longer visible. This is remarkable as the underlying classical **inorganic** kinetics of oxidation is known to show higher oxidation (i.e. precipitation) rate for Fe as compared to Mn [Landing and Bruland, 1987]. The difference is likely due to **organic** complexation of Fe largely preventing such oxidation, thus overall the removal rate of Fe actually is slower than for Mn. These findings are important for the use of Mn as a tracer for sedimentary or hydrothermal Fe-input, and are particularly interesting now that Mn has been suggested as a co-limiting element in the Southern Ocean [Middag, 2010]. For a next expedition, it would be beneficial to look specifically at the different behaviour of Fe and Mn upon input from the shelf sediment. Both with regard to the use of Mn as a source tracer for Fe as with regard to the possible co-limiting role of both metals for phytoplankton growth. In such a study, laboratory experiments where the Fe complexation could be regulated, by regulating amount and type of ligands, could be a useful addition to field data. For the deep sea, in order to constrain the difference in behaviour between Fe and Mn from sediment and hydrothermal sources, a useful contribution could be expected from (thermodynamic) modelling, in addition to field data.

In the companion PhD research thesis of Charles-Edouard Thuróczy [2011], some work has been done on size fractionation of dissolved Fe. The distribution of the available Fe over different size classes was studied as follows: (i) unfiltered, (ii) 0.2 μm filtered (the 'dissolved fraction as described in this thesis) and (iii) 1000kDa (an operationally defined class of approx. $\sim 0.1 \mu\text{m}$, representing soluble Fe [Thuróczy, 2011]). From Thuróczy [2011] and other work, the size fractionation of Fe has appeared to be of major importance for the bio-availability of Fe in the Southern Ocean [Hurst and Bruland, 2007; Chever *et al.*, 2010] and also in quantification of the Fe input from different sources [Planquette *et al.*, 2007]. Comparison of the 'unfiltered'

fraction versus the filtered fraction can, by difference, give an indication of the Fe in particles. Nevertheless, to better quantify the amount of Fe in the particulate phase, filtering of seawater and measurement of the particulates on the filter is indispensable [see *Hurst and Bruland, 2007*]. Therefore, when returning to the Polar Oceans a more detailed study of size classes would be of interest, including filtering of seawater for determination of the particulate fraction.

An important recent development in the ultra clean sampling of trace elements in the Oceans is the new Titan frame with new large PRISTINE samplers, which makes possible to sample 24 depths of 27 L clean seawater. This enables researchers to take clean seawater for seawater sampling (dissolved fraction, unfiltered fraction), as well as for methods where more seawater is needed due to filtering (soluble fraction, particulate fraction, stable isotopes). Also, new techniques in ICP-MS [*Milne et al., 2010*] make it possible to simultaneously measure many elements within one sample, which brings down the need for large amounts of seawater. Moreover at the same time, with such a method, it is reassured that the sample comes from the same bottle, ruling out some possible sampling inconsistency when comparing the metals. Last but not least, the new intercalibration program with intercalibration reference sea-water samples for most metals (www.geotraces.org) is a major step forward, and will in coming years further help to assure uniformity in different DFe measurement methods between different laboratories.

7.3 References

- Aumont, O., L. Bopp (2006), Globalizing results from ocean in situ iron fertilization studies, *Global Biogeochem. Cycles*, 20, GB2017, doi:10.1029/2005GB002591.
- Bennett, S.A., E.P. Achterberg, D.P. Connelly, P.J. Statham, G.R. Fones, C.R. German (2008), The distribution and stabilisation of dissolved Fe in deep-sea hydrothermal plumes. *Earth and Planetary Science Letters*, 270 (3-4) pp. 157-167.
- Boyle, E. A., B. A. Bergquist, R. A. Kayser, and N. Mahowald (2005), Iron, manganese, and lead at Hawaii Ocean Time-series station ALOHA: Temporal variability and an intermediate water hydrothermal plume, *Geochimica et Cosmochimica Acta*, 69(4), 933-952.
- Boyle E. A. and Jenkins W. (2008) *Goldschmidt abstracts. Geochim. Cosmochim. Acta* 72(12, Suppl. 1), A107.
- Chever, F., E. Bucciarelli, G. Sarthou, S. Speich, M. Arhan, P. Penven, A. Tagliabue (2010), Physical speciation of iron in the Atlantic Sector of the Southern Ocean along a transect from the subtropical domain to the Weddell Sea Gyre. *J. Geophys. Res.* 115, C10059, doi:10.1029/2009JC005880.
- De Baar, H.J.W., J.T.M. De Jong (2001), Distributions, sources and sinks of iron in seawater. In: Turner, D., Hunter, K.A. (Eds.), *Biogeochemistry of iron in seawater*, IUPAC Book series on analytical and physical chemistry of environmental systems, vol.7; 2001, 123-254 (Chapter 5).
- Ellwood, M., Boyd, P., Sutton, P. (2008), Winter-time dissolved iron and nutrient distribution in the Subantarctic Zone from 40-52S; 155-160E. *Geophys. Res. Lett.*, (35), L11604,
- Gaiero, D.M., J.-L. Probst, P.J. Depetris, S.M. Bidart, L. Leleyter (2003), Iron and other transition metals in Patagonian riverborne and windborne materials: geochemical control and transport to the southern South Atlantic Ocean. *Geochimica et Cosmochimica Acta* 67 (19), 3603-3623
- Hurst, M.P., K.W. Bruland (2007), An investigation into the exchange of iron and zinc between soluble, colloidal, and particulate size-fractions in shelf waters using low-abundance isotopes as tracers in shipboard incubation experiments. *Marine Chemistry* 103 (3-4) 211-226
- Lannuzel, D., V. Schoemann, J.T.M. De Jong, L. Chou, B. Delille, S. Becquevort, J.-L. Tison (2008), Iron study during a time series in the western Weddell pack ice. *Marine Chemistry* 108 (1-2), 85-95.
- Landing, W.M., K. Bruland (1987), The contrasting biogeochemistry of iron and manganese in the Pacific Ocean. *Geochimica et Cosmochimica Acta* 51, 29-43.
- Mackey, D.J., J.E., O'Sullivan, R.J. Watson (2002), Iron in the western Pacific: a riverine or hydrothermal source for iron in the Equatorial Undercurrent? *Deep Sea Research Part I*, 49 (5), pp 877-893
- Middag, R. (2010), Dissolved Aluminium and Manganese in the Polar Oceans. *PhD-Thesis*, University of Groningen, ISBN 978-90-367-4513-0.
- Milne, A., W. Landing, M. Bizimis, P. Morton (2010), Determination of Mn, Fe, Co, Ni, Cu, Zn, Cd and Pb in seawater using high resolution magnetic sector inductively coupled mass spectrometry (HR-ICP-MS). *Analytica Chimica Acta*, 665 (2) , 200-207

- Moore, J. K., and O. Braucher (2008), Sedimentary and mineral dust sources of dissolved iron to the world ocean, *Biogeosciences*, 5(3), 631-656.
- Planquette, H., G. R. Fones, P.J. Statham, P. J. Morris (2009), Origin of iron and aluminium in large particles (> 53 µm) in the Crozet region, Southern Ocean. *Marine Chemistry* 115 (1-2), 31-42
- Sander, S.G., A. Koschinsky (2011), Metal flux from hydrothermal vents increased by organic complexation. *Nature Geosci.* 20(2), 145-150.
- Sedwick, P.N., A.R. Bowie, T.W. Trull (2008), Dissolved iron in the Australian sector of the Southern Ocean: (CLIVAR SR3 section): Meridional and seasonal trends. *Deep-Sea Research* 55, 911– 925
- Tagliabue, A., L. Bopp, J-C. Dutay, A.R. Bowie, F.Chever, P.Jean-Baptiste, E. Bucciarelli, D. Lannuzel, T.Remenyi, G.Sarthou, O.Aumont, M.Gehlen, C.Jeandel (2010), Hydrothermal contribution to the oceanic dissolved iron inventory. *Nature Geosciences* 3, 252 – 256.
- Tagliabue, A., T. Mtshali, O. Aumont, A.R. Bowie, S. Swart, M.B. Klunder (2012), A global compilation of over 13,000 dissolved iron measurements: focus on distributions and processes in the Southern Ocean. *Biogeosciences* 9, 2333-2349
- Thuróczy, C.E.T. (2011a), Physical and Chemical Speciation of Iron in the Polar Oceans. *PhD-Thesis*, University of Groningen, ISBN 978-90-367-5140-7.
- Thuróczy, C.E.T., L.J.A. Gerringa, M.B. Klunder, P.Laan, M. Le Guitton, H.J.W. De Baar (2011b), Distinct trends in the speciation of iron between the shelf seas and the deep basins of the Arctic Ocean. *J. Geophys. Res.* 116, C10009, doi:10.1029/2010JC006835
- Wu, J., M.L., Wells, R. Rember (2011), Dissolved iron anomaly in the deep tropical-sub-tropical Pacific: Evidence for long-range transport of hydrothermal iron. *Geochimica et Cosmochimica Acta* 75 (2), 460 -468



Chapter 8

Database



Database

This appendix section comprises the data of the shipboard determination of dissolved Fe of the ARK XXII/2 and ANT XXIV/3 cruises together with the location, time and depth of each sample.

The accuracy of the shipboard Fe flow injection analysis system was verified by regularly analyzing SAFe S and SAFe D2 standard seawater. The results agreed well with the community consensus values: SAFe S: 0.101 ± 0.034 nM ($n=26$) and SAFe D2: 0.94 ± 0.07 ($n=44$). Consensus values (www.geotraces.org; November 2011) are 0.090 ± 0.007 and 0.90 ± 0.02 for SAFe S and SAFe D2 respectively.

The tables below show all datapoints, including some outliers that were rejected and given in between brackets. The procedure for identifying occasional outliers and criteria for rejection are comparable to the approach published by *Middag* [2010, thesis page 27] and *Middag et al.* [2011]. Suspected outliers were labelled as such based on three criteria. When for the sampled GO-FLO the nutrient data were anomalous for that depth, indicating closing at the wrong depth, the sample was marked as suspected outlier. In case the trace metal data (Al, Mn and Fe) were elevated for the same GO-FLO for more than one cast, indicating a contaminated GO-FLO the sample was also marked as suspected outlier. The third criterion was when one data point of Fe gave anomalous result for its depth considering the data points at shallower and greater depth. This was done by visual inspection of the depth profiles. Data points that would not fit the profile shape were compared with potential temperature, salinity, nutrients and the concentration of dissolved manganese and aluminium to see if those parameters showed a similar trend. If this was the case, the data point was left in. If there was no similar trend with other parameters, the following test was applied: a linear regression was determined between the concentrations of Fe below and above the suspect data point (two above and two below, where possible), versus depth. With the linear regression equation the 'theoretical' concentration was calculated for that depth. When this calculated value was more than 25% lower or higher than the measured value, it was marked as a suspected outlier and not further used in the calculations or graphs and final interpretation and ensuing thesis chapter and/or published article. During the ARK XXII/2 cruise 785 datapoints were obtained, of which 2 outliers that were too low most likely due to measurement failures and 3 were too high likely due to inadvertent contamination. During the ANT XXIV/3 cruise a total of 920 samples were obtained, of which 44 outliers that were too high and therefore rejected. In the below data tables the total 49 rejected outliers are given in between brackets.

The complete relational database including chemical, physical and biological parameters is available at www.geotraces.org.

Middag, R. (2010) Dissolved Aluminium and Manganese in the Polar Oceans. PhD thesis, University of Groningen; page 27.

Middag R., H.J.W. De Baar, P. Laan, P.H. Cai, J.C. van Ooijen (2011), Dissolved manganese in the Atlantic sector of the Southern Ocean. *Deep-Sea Research Part II* 58, 2661-2677

ARK XXII/2

A total of 785 DFe datapoints is available from downcast stations from ARK XXII/2. For methods, see Chapter 2.2 and 3.2. Outliers (see above) are marked with () brackets.

DATA TABLE ARK XXII/2

Station	Latitude [°N]	Longitude [°E]	Date	Depth [m]	θ (°C)	Salinity	dFe [nmol/l]
228	75.000	33.998	30-07-07	100	1.12	35.039	0.30
228	75.000	33.998	30-07-07	75	2.13	35.077	0.62
228	75.000	33.998	30-07-07	50	2.81	35.079	1.33
228	75.000	33.998	30-07-07	26	3.98	35.055	1.19
236	77.497	34.000	31-07-07	151	1.67	34.969	1.67
236	77.497	34.000	31-07-07	126	1.14	34.873	0.64
236	77.497	34.000	31-07-07	100	0.31	34.724	0.64
236	77.497	34.000	31-07-07	75	-1.47	34.556	0.59
236	77.497	34.000	31-07-07	51	-1.57	34.510	0.37
236	77.497	34.000	31-07-07	25	-0.12	34.261	0.24
236	77.497	34.000	31-07-07	5	2.66	33.946	0.36
237	78.991	33.999	31-07-07	226	1.47	34.883	0.45
237	78.991	33.999	31-07-07	200	1.58	34.852	0.48
237	78.991	33.999	31-07-07	174	1.02	34.758	0.50
237	78.991	33.999	31-07-07	150	0.79	34.715	0.51
237	78.991	33.999	31-07-07	125	0.27	34.650	0.55
237	78.991	33.999	31-07-07	100	-0.78	34.529	0.52
237	78.991	33.999	31-07-07	76	-1.27	34.445	0.47
237	78.991	33.999	31-07-07	50	-1.55	34.321	0.60
237	78.991	33.999	31-07-07	25	-1.52	34.223	0.45
239	80.993	33.984	01-08-07	175	0.88	34.711	0.78
239	80.993	33.984	01-08-07	148	0.83	34.659	0.76
239	80.993	33.984	01-08-07	125	0.81	34.653	0.78
239	80.993	33.984	01-08-07	100	0.54	34.615	0.67
239	80.993	33.984	01-08-07	75	-0.24	34.472	0.70
239	80.993	33.984	01-08-07	50	-0.71	34.346	0.39
239	80.993	33.984	01-08-07	25	-0.87	33.910	0.30
239	80.993	33.984	01-08-07	5	-0.97	32.656	0.33
246	81.868	34.013	02-08-07	1745	-0.74	34.911	1.46
246	81.868	34.013	02-08-07	1491	-0.70	34.910	1.36
246	81.868	34.013	02-08-07	1397	-0.68	34.909	0.89
246	81.868	34.013	02-08-07	1298	-0.64	34.909	1.04
246	81.868	34.013	02-08-07	1197	-0.58	34.908	0.73
246	81.868	34.013	02-08-07	1097	-0.50	34.908	1.01
246	81.868	34.013	02-08-07	998	-0.41	34.908	1.10
246	81.868	34.013	02-08-07	899	-0.24	34.909	1.38
246	81.868	34.013	02-08-07	799	0.09	34.917	0.84
246	81.868	34.013	02-08-07	698	0.56	34.924	0.67
246	81.868	34.013	02-08-07	649	0.76	34.926	0.76
246	81.868	34.013	02-08-07	576	1.18	34.944	0.55
246	81.868	34.013	02-08-07	549	1.31	34.951	0.66

DATA TABLE ARK XXII/2 Continued

Station	Latitude [°N]	Longitude [°E]	Date	Depth [m]	θ (°C)	Salinity	dFe [nmol/l]
246	81.868	34.013	02-08-07	499	1.64	34.971	0.62
246	81.868	34.013	02-08-07	399	1.79	34.954	1.28
246	81.868	34.013	02-08-07	300	2.36	34.979	0.96
246	81.868	34.013	02-08-07	249	2.58	34.983	0.83
246	81.868	34.013	02-08-07	201	2.75	34.982	0.62
246	81.868	34.013	02-08-07	100	2.02	34.820	0.37
246	81.868	34.013	02-08-07	50	-1.37	34.345	0.58
246	81.868	34.013	02-08-07	25	-1.60	34.076	0.36
246	81.868	34.013	02-08-07	4	-1.39	32.928	0.49
255	82.503	33.952	03-08-07	2944	-0.93	34.936	0.92
255	82.503	33.952	03-08-07	2893	-0.92	34.935	0.76
255	82.503	33.952	03-08-07	2794	-0.91	34.932	0.64
255	82.503	33.952	03-08-07	2694	-0.90	34.931	0.59
255	82.503	33.952	03-08-07	2495	-0.89	34.928	0.55
255	82.503	33.952	03-08-07	2295	-0.87	34.926	0.94
255	82.503	33.952	03-08-07	2096	-0.85	34.923	0.92
255	82.503	33.952	03-08-07	1996	-0.84	34.922	0.77
255	82.503	33.952	03-08-07	1896	-0.81	34.920	0.90
255	82.503	33.952	03-08-07	1796	-0.79	34.919	0.84
255	82.503	33.952	03-08-07	1597	-0.72	34.917	0.65
255	82.503	33.952	03-08-07	1397	-0.65	34.913	0.89
255	82.503	33.952	03-08-07	1198	-0.50	34.911	0.91
255	82.503	33.952	03-08-07	998	-0.24	34.912	0.83
255	82.503	33.952	03-08-07	798	0.31	34.923	0.98
255	82.503	33.952	03-08-07	745	0.58	34.929	0.67
255	82.503	33.952	03-08-07	698	0.80	34.936	0.86
255	82.503	33.952	03-08-07	499	1.63	34.952	0.92
255	82.503	33.952	03-08-07	292	2.37	34.959	0.89
255	82.503	33.952	03-08-07	200	2.68	34.958	0.94
255	82.503	33.952	03-08-07	98	1.95	34.792	0.71
255	82.503	33.952	03-08-07	37	-1.77	34.265	0.56
255	82.503	33.952	03-08-07	19	-1.67	34.083	0.41
258	83.999	34.014	06-08-07	3980	-0.93	34.942	0.61
258	83.999	34.014	06-08-07	3791	-0.93	34.943	0.50
258	83.999	34.014	06-08-07	3592	-0.93	34.943	0.66
258	83.999	34.014	06-08-07	3392	-0.93	34.942	0.62
258	83.999	34.014	06-08-07	3192	-0.94	34.940	0.84
258	83.999	34.014	06-08-07	2992	-0.94	34.937	0.68
258	83.999	34.014	06-08-07	2793	-0.94	34.934	0.68
258	83.999	34.014	06-08-07	2594	-0.93	34.932	0.70
258	83.999	34.014	06-08-07	2394	-0.91	34.929	0.78
258	83.999	34.014	06-08-07	2194	-0.89	34.926	0.69
258	83.999	34.014	06-08-07	1995	-0.85	34.924	0.71
258	83.999	34.014	06-08-07	1797	-0.81	34.921	0.67
258	83.999	34.014	06-08-07	1597	-0.74	34.920	0.68
258	83.999	34.014	06-08-07	1397	-0.65	34.918	0.58
258	83.999	34.014	06-08-07	1197	-0.50	34.914	0.43
258	83.999	34.014	06-08-07	997	-0.27	34.909	0.44

DATA TABLE ARK XXII/2 Continued

Station	Latitude [°N]	Longitude [°E]	Date	Depth [m]	θ (°C)	Salinity	dFe [nmol/l]
258	83.999	34.014	06-08-07	798	0.14	34.907	0.57
258	83.999	34.014	06-08-07	600	0.95	34.922	0.68
258	83.999	34.014	06-08-07	399	1.83	34.941	0.53
258	83.999	34.014	06-08-07	200	2.03	34.883	0.47
258	83.999	34.014	06-08-07	100	-1.21	34.335	0.89
258	83.999	34.014	06-08-07	40	-1.80	34.183	0.45
258	83.999	34.014	06-08-07	18	-1.70	34.037	0.24
258	83.999	34.014	06-08-07	5	-1.68	33.784	0.50
260	84.489	36.139	07-08-07	3925	-0.93	34.942	0.55
260	84.489	36.139	07-08-07	3791	-0.93	34.943	0.65
260	84.489	36.139	07-08-07	3592	-0.93	34.943	0.57
260	84.489	36.139	07-08-07	3392	-0.93	34.942	0.41
260	84.489	36.139	07-08-07	3192	-0.94	34.940	0.78
260	84.489	36.139	07-08-07	2992	-0.94	34.937	0.83
260	84.489	36.139	07-08-07	2793	-0.94	34.934	1.27
260	84.489	36.139	07-08-07	2593	-0.93	34.931	1.30
260	84.489	36.139	07-08-07	2394	-0.91	34.929	1.16
260	84.489	36.139	07-08-07	2194	-0.89	34.926	1.08
260	84.489	36.139	07-08-07	1995	-0.86	34.923	0.80
260	84.489	36.139	07-08-07	1796	-0.81	34.921	0.64
260	84.489	36.139	07-08-07	1397	-0.65	34.917	0.61
260	84.489	36.139	07-08-07	998	-0.28	34.910	0.65
260	84.489	36.139	07-08-07	749	0.27	34.907	0.78
260	84.489	36.139	07-08-07	579	1.00	34.927	0.69
260	84.489	36.139	07-08-07	200	2.02	34.864	0.67
260	84.489	36.139	07-08-07	150	1.29	34.685	0.89
260	84.489	36.139	07-08-07	100	-1.79	34.251	0.41
260	84.489	36.139	07-08-07	74	-1.83	34.203	0.26
260	84.489	36.139	07-08-07	50	-1.82	34.184	0.79
260	84.489	36.139	07-08-07	24	-1.71	34.027	0.82
260	84.489	36.139	07-08-07	5	-1.67	33.861	0.97
261	84.645	60.934	07-08-07	3700	-0.93	34.942	0.38
261	84.645	60.934	11-08-07	3501	-0.93	34.942	0.48
261	84.645	60.934	11-08-07	3300	-0.93	34.940	0.52
261	84.645	60.934	11-08-07	3199	-0.94	34.939	0.76
261	84.645	60.934	11-08-07	3000	-0.94	34.936	0.68
261	84.645	60.934	11-08-07	2750	-0.93	34.932	(0.32)
261	84.645	60.934	11-08-07	2500	-0.91	34.929	0.67
261	84.645	60.934	11-08-07	2301	-0.89	34.927	0.77
261	84.645	60.934	11-08-07	2001	-0.85	34.923	0.52
261	84.645	60.934	11-08-07	1751	-0.79	34.920	0.63
261	84.645	60.934	11-08-07	1501	-0.70	34.917	0.52
261	84.645	60.934	11-08-07	1002	-0.26	34.909	0.45
261	84.645	60.934	11-08-07	702	0.52	34.910	0.46
261	84.645	60.934	11-08-07	502	1.34	34.930	0.37
261	84.645	60.934	11-08-07	352	1.88	34.920	0.37
261	84.645	60.934	11-08-07	201	2.23	34.875	0.37
261	84.645	60.934	11-08-07	151	1.27	34.684	0.30

DATA TABLE ARK XXII/2 Continued

Station	Latitude [°N]	Longitude [°E]	Date	Depth [m]	θ (°C)	Salinity	dFe [nmol/l]
261	84.645	60.934	11-08-07	125	0.28	34.502	0.36
261	84.645	60.934	11-08-07	101	-1.15	34.279	0.30
261	84.645	60.934	11-08-07	76	-1.84	34.184	0.29
261	84.645	60.934	11-08-07	50	-1.82	34.162	0.36
261	84.645	60.934	11-08-07	25	-1.70	33.984	0.21
261	84.645	60.934	11-08-07	4	-1.59	33.382	0.26
266	83.138	61.741	13-08-07	2950	-0.92	34.936	0.60
266	83.138	61.741	13-08-07	2749	-0.90	34.930	0.60
266	83.138	61.741	13-08-07	2500	-0.87	34.926	0.67
266	83.138	61.741	13-08-07	2250	-0.84	34.922	0.63
266	83.138	61.741	13-08-07	2001	-0.79	34.919	0.55
266	83.138	61.741	13-08-07	1751	-0.73	34.917	(0.24)
266	83.138	61.741	13-08-07	1501	-0.66	34.915	0.68
266	83.138	61.741	13-08-07	1351	-0.58	34.914	0.58
266	83.138	61.741	13-08-07	1250	-0.50	34.913	0.61
266	83.138	61.741	13-08-07	1000	-0.13	34.914	0.54
266	83.138	61.741	13-08-07	751	0.70	34.929	0.57
266	83.138	61.741	13-08-07	571	0.94	34.917	0.50
266	83.138	61.741	13-08-07	501	1.23	34.923	0.41
266	83.138	61.741	13-08-07	401	1.61	34.926	0.50
266	83.138	61.741	13-08-07	300	2.26	34.954	0.69
266	83.138	61.741	13-08-07	251	2.51	34.961	0.71
266	83.138	61.741	13-08-07	200	2.64	34.957	0.61
266	83.138	61.741	13-08-07	150	2.72	34.939	0.65
266	83.138	61.741	13-08-07	125	2.70	34.922	0.60
266	83.138	61.741	13-08-07	100	2.66	34.900	0.85
266	83.138	61.741	13-08-07	75	2.48	34.859	0.50
266	83.138	61.741	13-08-07	50	1.33	34.702	0.81
266	83.138	61.741	13-08-07	23	-1.43	33.778	0.70
266	83.138	61.741	13-08-07	4	-1.64	33.314	0.10
268	82.806	60.797	14-08-07	1500	-0.62	34.914	0.57
268	82.806	60.797	14-08-07	1251	-0.50	34.912	0.55
268	82.806	60.797	14-08-07	1001	-0.20	34.913	0.59
268	82.806	60.797	14-08-07	751	0.57	34.927	0.54
268	82.806	60.797	14-08-07	501	1.07	34.923	0.50
268	82.806	60.797	14-08-07	301	2.12	34.946	(0.23)
268	82.806	60.797	14-08-07	201	2.49	34.953	0.60
268	82.806	60.797	14-08-07	150	2.58	34.936	0.60
268	82.806	60.797	14-08-07	125	2.54	34.914	0.41
268	82.806	60.797	14-08-07	100	2.42	34.886	0.51
268	82.806	60.797	14-08-07	75	1.98	34.824	0.58
268	82.806	60.797	14-08-07	50	0.18	34.545	0.37
268	82.806	60.797	14-08-07	25	-1.50	33.864	0.42
268	82.806	60.797	14-08-07	4	-1.61	32.856	0.28
271	82.503	60.795	15-08-07	301	-0.56	34.774	0.54
271	82.503	60.795	15-08-07	251	1.59	34.913	0.46
271	82.503	60.795	15-08-07	200	2.04	34.932	0.46
271	82.503	60.795	15-08-07	150	2.15	34.911	0.45

DATA TABLE ARK XXII/2 Continued

Station	Latitude [°N]	Longitude [°E]	Date	Depth [m]	θ (°C)	Salinity	dFe [nmol/l]
271	82.503	60.795	15-08-07	125	1.94	34.867	0.48
271	82.503	60.795	15-08-07	101	2.05	34.861	0.61
271	82.503	60.795	15-08-07	75	1.49	34.793	0.99
271	82.503	60.795	15-08-07	50	0.69	34.634	0.42
271	82.503	60.795	15-08-07	25	-1.56	33.971	1.07
271	82.503	60.795	15-08-07	5	-1.53	32.945	0.73
272	82.252	61.996	15-08-07	210	-0.34	34.762	0.40
272	82.252	61.996	15-08-07	142	0.96	34.818	0.47
272	82.252	61.996	15-08-07	125	1.08	34.814	0.63
272	82.252	61.996	15-08-07	101	1.25	34.808	0.48
272	82.252	61.996	15-08-07	75	1.30	34.782	0.83
272	82.252	61.996	15-08-07	50	0.85	34.666	0.49
272	82.252	61.996	15-08-07	25	-1.15	34.197	0.59
272	82.252	61.996	15-08-07	5	-1.64	32.661	0.40
276	82.084	68.960	17-08-07	650	-0.67	34.897	0.43
276	82.084	68.960	17-08-07	501	0.57	34.881	0.49
276	82.084	68.960	17-08-07	400	1.47	34.922	0.53
276	82.084	68.960	17-08-07	302	2.12	34.947	0.54
276	82.084	68.960	17-08-07	200	2.40	34.921	0.53
276	82.084	68.960	17-08-07	150	2.47	34.903	0.44
276	82.084	68.960	17-08-07	125	2.22	34.860	0.56
276	82.084	68.960	17-08-07	100	1.81	34.797	0.58
276	82.084	68.960	17-08-07	75	-0.47	34.514	0.29
276	82.084	68.960	17-08-07	50	-1.63	34.334	0.57
276	82.084	68.960	17-08-07	25	-1.58	33.814	0.65
276	82.084	68.960	17-08-07	5	-1.69	32.904	0.34
279	81.245	86.203	19-08-07	316	-0.71	34.864	0.45
279	81.245	86.203	19-08-07	250	-0.77	34.848	0.55
279	81.245	86.203	19-08-07	201	-0.67	34.806	0.51
279	81.245	86.203	19-08-07	150	0.89	34.880	0.56
279	81.245	86.203	19-08-07	124	1.13	34.875	0.55
279	81.245	86.203	19-08-07	101	1.22	34.846	0.58
279	81.245	86.203	19-08-07	75	0.85	34.757	0.56
279	81.245	86.203	19-08-07	49	-0.78	34.531	0.52
279	81.245	86.203	19-08-07	26	-1.63	33.959	1.02
279	81.245	86.203	19-08-07	5	-1.50	32.645	0.86
285	82.142	86.331	20-08-07	680	-0.50	34.887	1.14
285	82.142	86.331	20-08-07	601	-0.48	34.879	1.23
285	82.142	86.331	20-08-07	500	-0.27	34.880	0.73
285	82.142	86.331	20-08-07	400	0.24	34.868	0.70
285	82.142	86.331	20-08-07	300	1.27	34.897	0.75
285	82.142	86.331	20-08-07	250	1.35	34.870	0.47
285	82.142	86.331	20-08-07	200	1.10	34.815	0.68
285	82.142	86.331	20-08-07	150	0.16	34.683	0.70
285	82.142	86.331	20-08-07	100	-1.45	34.486	0.44
285	82.142	86.331	20-08-07	75	-1.75	34.429	(0.87)
285	82.142	86.331	20-08-07	50	-0.95	34.304	0.59
285	82.142	86.331	20-08-07	24	-1.58	33.415	1.32

DATA TABLE ARK XXII/2 Continued

Station	Latitude [°N]	Longitude [°E]	Date	Depth [m]	θ (°C)	Salinity	dFe [nmol/l]
285	82.142	86.331	20-08-07	9	-1.63	32.517	1.02
291	82.710	86.266	21-08-07	2200	-0.85	34.922	0.62
291	82.710	86.266	21-08-07	2100	-0.83	34.920	0.72
291	82.710	86.266	21-08-07	2000	-0.81	34.919	0.64
291	82.710	86.266	21-08-07	1900	-0.79	34.918	0.64
291	82.710	86.266	21-08-07	1800	-0.77	34.917	0.58
291	82.710	86.266	21-08-07	1700	-0.75	34.916	0.83
291	82.710	86.266	21-08-07	1600	-0.72	34.914	0.76
291	82.710	86.266	21-08-07	1500	-0.69	34.913	0.57
291	82.710	86.266	21-08-07	1500	-0.69	34.913	0.66
291	82.710	86.266	21-08-07	1250	-0.56	34.911	0.64
291	82.710	86.266	21-08-07	1000	-0.31	34.912	0.89
291	82.710	86.266	21-08-07	751	0.38	34.919	1.01
291	82.710	86.266	21-08-07	500	1.85	34.967	0.61
291	82.710	86.266	21-08-07	400	2.40	34.987	0.52
291	82.710	86.266	21-08-07	300	2.73	34.985	0.53
291	82.710	86.266	21-08-07	201	2.92	34.949	0.53
291	82.710	86.266	21-08-07	150	3.09	34.945	0.52
291	82.710	86.266	21-08-07	124	2.85	34.883	0.70
291	82.710	86.266	21-08-07	99	2.16	34.743	0.44
291	82.710	86.266	21-08-07	75	-0.25	34.337	0.44
291	82.710	86.266	21-08-07	50	-1.80	34.120	0.32
291	82.710	86.266	21-08-07	25	-1.74	34.058	0.42
291	82.710	86.266	21-08-07	9	-1.64	33.126	0.12
295	83.272	86.284	22-08-07	3200	-0.93	34.940	0.53
295	83.272	86.284	22-08-07	3100	-0.93	34.938	0.78
295	83.272	86.284	22-08-07	3000	-0.93	34.936	0.56
295	83.272	86.284	22-08-07	2750	-0.92	34.932	0.74
295	83.272	86.284	22-08-07	2500	-0.90	34.929	0.67
295	83.272	86.284	22-08-07	2250	-0.88	34.925	0.49
295	83.272	86.284	22-08-07	2000	-0.84	34.922	0.56
295	83.272	86.284	22-08-07	1750	-0.79	34.919	0.68
295	83.272	86.284	22-08-07	1500	-0.72	34.916	0.72
295	83.272	86.284	22-08-07	1251	-0.57	34.913	0.57
295	83.272	86.284	22-08-07	1000	-0.30	34.910	0.61
295	83.272	86.284	22-08-07	901	-0.10	34.912	0.62
295	83.272	86.284	22-08-07	750	0.41	34.918	0.94
295	83.272	86.284	22-08-07	500	1.76	34.958	0.54
295	83.272	86.284	22-08-07	250	2.74	34.957	0.51
295	83.272	86.284	22-08-07	200	2.86	34.939	0.42
295	83.272	86.284	22-08-07	150	2.70	34.872	0.40
295	83.272	86.284	22-08-07	114	0.81	34.543	0.41
295	83.272	86.284	22-08-07	75	-1.77	34.225	0.31
295	83.272	86.284	22-08-07	50	-1.76	34.180	0.33
295	83.272	86.284	22-08-07	29	-1.64	33.999	0.21
295	83.272	86.284	22-08-07	10	-1.65	33.332	0.21
299	84.051	89.043	23-08-07	3551	-0.93	34.942	0.74
299	84.051	89.043	23-08-07	3500	-0.93	34.942	0.63

DATA TABLE ARK XXII/2 Continued

Station	Latitude [°N]	Longitude [°E]	Date	Depth [m]	θ (°C)	Salinity	dFe [nmol/l]
299	84.051	89.043	23-08-07	3250	-0.93	34.941	0.71
299	84.051	89.043	23-08-07	3000	-0.94	34.936	0.70
299	84.051	89.043	23-08-07	2750	-0.93	34.933	0.67
299	84.051	89.043	23-08-07	2500	-0.91	34.929	0.67
299	84.051	89.043	23-08-07	2500	-0.91	34.929	0.65
299	84.051	89.043	23-08-07	2250	-0.89	34.926	0.77
299	84.051	89.043	23-08-07	2000	-0.85	34.923	0.56
299	84.051	89.043	23-08-07	1750	-0.78	34.920	0.49
299	84.051	89.043	23-08-07	1500	-0.70	34.917	0.51
299	84.051	89.043	23-08-07	1251	-0.55	34.912	0.46
299	84.051	89.043	23-08-07	1000	-0.31	34.905	0.44
299	84.051	89.043	23-08-07	746	0.34	34.913	0.54
299	84.051	89.043	23-08-07	601	0.81	34.915	0.42
299	84.051	89.043	23-08-07	501	1.14	34.916	0.41
299	84.051	89.043	23-08-07	300	1.56	34.892	0.35
299	84.051	89.043	23-08-07	201	1.65	34.827	0.37
299	84.051	89.043	23-08-07	150	0.62	34.568	0.45
299	84.051	89.043	23-08-07	100	-1.66	34.255	0.45
299	84.051	89.043	23-08-07	74	-1.68	34.190	0.41
299	84.051	89.043	23-08-07	50	-1.78	34.092	0.27
299	84.051	89.043	23-08-07	24	-1.63	33.382	0.65
299	84.051	89.043	23-08-07	8	-1.69	32.730	0.31
301	84.580	89.837	24-08-07	3650	-0.93	34.942	0.71
301	84.580	89.837	24-08-07	3500	-0.93	34.942	0.92
301	84.580	89.837	24-08-07	3250	-0.94	34.940	0.98
301	84.580	89.837	24-08-07	3000	-0.94	34.936	1.06
301	84.580	89.837	24-08-07	2750	-0.93	34.932	1.24
301	84.580	89.837	24-08-07	2501	-0.91	34.929	1.41
301	84.580	89.837	24-08-07	2375	-0.90	34.927	1.18
301	84.580	89.837	24-08-07	2251	-0.88	34.926	0.95
301	84.580	89.837	24-08-07	2001	-0.84	34.923	0.56
301	84.580	89.837	24-08-07	1751	-0.77	34.921	0.59
301	84.580	89.837	24-08-07	1501	-0.67	34.917	0.64
301	84.580	89.837	24-08-07	1252	-0.54	34.908	0.48
301	84.580	89.837	24-08-07	1002	-0.31	34.898	0.49
301	84.580	89.837	24-08-07	752	0.08	34.885	0.43
301	84.580	89.837	24-08-07	501	1.00	34.905	0.80
301	84.580	89.837	24-08-07	301	1.72	34.903	0.59
301	84.580	89.837	24-08-07	201	1.81	34.839	0.36
301	84.580	89.837	24-08-07	150	0.84	34.643	0.34
301	84.580	89.837	24-08-07	124	0.02	34.475	0.39
301	84.580	89.837	24-08-07	100	-0.86	34.305	0.67
301	84.580	89.837	24-08-07	75	-1.65	34.123	0.66
301	84.580	89.837	24-08-07	51	-1.81	34.007	0.41
301	84.580	89.837	24-08-07	25	-1.68	33.653	0.81
301	84.580	89.837	24-08-07	6	-1.65	33.343	2.22
302	84.892	90.058	25-08-07	3650	-0.93	34.942	0.54
302	84.892	90.058	25-08-07	3490	-0.93	34.942	0.50

DATA TABLE ARK XXII/2 Continued

Station	Latitude [°N]	Longitude [°E]	Date	Depth [m]	θ (°C)	Salinity	dFe [nmol/l]
302	84.892	90.058	25-08-07	3250	-0.94	34.940	0.75
302	84.892	90.058	25-08-07	3001	-0.94	34.936	1.06
302	84.892	90.058	25-08-07	2751	-0.93	34.932	0.85
302	84.892	90.058	25-08-07	2502	-0.91	34.929	0.95
302	84.892	90.058	25-08-07	2251	-0.88	34.925	1.10
302	84.892	90.058	25-08-07	2001	-0.83	34.922	0.45
302	84.892	90.058	25-08-07	1751	-0.77	34.919	0.45
302	84.892	90.058	25-08-07	1500	-0.67	34.916	0.50
302	84.892	90.058	25-08-07	1251	-0.52	34.910	0.48
302	84.892	90.058	25-08-07	1001	-0.28	34.899	0.38
302	84.892	90.058	25-08-07	751	0.04	34.880	0.41
302	84.892	90.058	25-08-07	499	0.87	34.894	0.36
302	84.892	90.058	25-08-07	300	1.48	34.884	0.39
302	84.892	90.058	25-08-07	201	1.43	34.826	0.33
302	84.892	90.058	25-08-07	150	0.98	34.665	0.32
302	84.892	90.058	25-08-07	101	-0.81	34.321	0.39
302	84.892	90.058	25-08-07	91	-1.45	34.206	0.31
302	84.892	90.058	25-08-07	47	-1.78	33.937	0.31
302	84.892	90.058	25-08-07	40	-1.77	33.831	0.50
302	84.892	90.058	25-08-07	25	-1.69	33.602	0.73
306	85.923	91.122	26-08-07	3701	-0.94	34.941	0.75
306	85.923	91.122	26-08-07	3500	-0.93	34.940	1.07
306	85.923	91.122	26-08-07	3250	-0.93	34.937	1.21
306	85.923	91.122	26-08-07	3000	-0.92	34.934	1.72
306	85.923	91.122	26-08-07	2750	-0.90	34.932	1.61
306	85.923	91.122	26-08-07	2500	-0.89	34.929	1.46
306	85.923	91.122	26-08-07	2251	-0.87	34.926	1.42
306	85.923	91.122	26-08-07	2001	-0.82	34.922	0.66
306	85.923	91.122	26-08-07	1749	-0.75	34.920	0.65
306	85.923	91.122	26-08-07	1501	-0.65	34.916	0.55
306	85.923	91.122	26-08-07	1249	-0.50	34.908	0.53
306	85.923	91.122	26-08-07	1003	-0.34	34.892	0.45
306	85.923	91.122	26-08-07	751	-0.02	34.878	0.47
306	85.923	91.122	26-08-07	501	0.70	34.886	0.44
306	85.923	91.122	26-08-07	301	1.20	34.864	0.55
306	85.923	91.122	26-08-07	201	1.03	34.777	0.66
306	85.923	91.122	26-08-07	151	0.04	34.529	0.36
306	85.923	91.122	26-08-07	101	-1.30	34.212	0.45
306	85.923	91.122	26-08-07	75	-1.73	33.905	0.69
306	85.923	91.122	26-08-07	50	-1.80	33.765	0.69
306	85.923	91.122	26-08-07	24	-1.69	33.458	0.83
306	85.923	91.122	26-08-07	5	-1.68	32.313	1.11
309	87.046	104.793	27-08-07	1500	-0.62	34.913	0.54
309	87.046	104.793	27-08-07	1002	-0.34	34.885	0.47
309	87.046	104.793	27-08-07	502	0.59	34.875	0.47
309	87.046	104.793	27-08-07	301	1.13	34.856	0.35
309	87.046	104.793	27-08-07	201	1.03	34.791	0.41
309	87.046	104.793	27-08-07	148	-0.02	34.528	0.42

DATA TABLE ARK XXII/2 Continued

Station	Latitude [°N]	Longitude [°E]	Date	Depth [m]	θ (°C)	Salinity	dFe [nmol/l]
309	87.046	104.793	27-08-07	101	-1.30	34.211	0.81
309	87.046	104.793	27-08-07	75	-1.63	33.873	0.81
309	87.046	104.793	27-08-07	50	-1.76	33.133	1.64
309	87.046	104.793	27-08-07	25	-1.69	32.650	1.90
309	87.046	104.793	27-08-07	5	-1.69	31.758	1.40
309	87.033	104.945	28-08-07	3998	-0.94	34.943	0.35
309	87.033	104.945	28-08-07	3749	-0.94	34.942	0.36
309	87.033	104.945	28-08-07	3499	-0.95	34.939	0.40
309	87.033	104.945	28-08-07	3250	-0.94	34.937	0.40
309	87.033	104.945	28-08-07	3000	-0.93	34.934	0.48
309	87.033	104.945	28-08-07	2750	-0.92	34.930	0.49
309	87.033	104.945	28-08-07	2500	-0.89	34.927	0.65
309	87.033	104.945	28-08-07	2300	-0.87	34.924	0.64
309	87.033	104.945	28-08-07	2201	-0.85	34.923	0.48
309	87.033	104.945	28-08-07	2001	-0.80	34.921	0.47
309	87.033	104.945	28-08-07	1751	-0.71	34.920	0.41
309	87.033	104.945	28-08-07	1251	-0.48	34.902	0.51
310	87.658	112.039	28-08-07	4251	-0.94	34.943	0.35
310	87.658	112.039	28-08-07	3999	-0.94	34.943	0.36
310	87.658	112.039	28-08-07	3750	-0.94	34.942	0.32
310	87.658	112.039	28-08-07	3501	-0.94	34.940	0.34
310	87.658	112.039	28-08-07	3251	-0.94	34.937	0.44
310	87.658	112.039	28-08-07	3001	-0.93	34.934	0.34
310	87.658	112.039	28-08-07	2750	-0.92	34.930	0.51
310	87.658	112.039	28-08-07	2500	-0.90	34.927	0.60
310	87.658	112.039	28-08-07	2251	-0.86	34.923	0.70
310	87.658	112.039	28-08-07	2000	-0.81	34.920	0.49
310	87.658	112.039	28-08-07	1750	-0.72	34.920	0.40
310	87.658	112.039	28-08-07	1501	-0.63	34.912	0.34
310	87.658	112.039	28-08-07	1251	-0.50	34.900	0.40
310	87.658	112.039	28-08-07	1001	-0.34	34.885	0.40
310	87.658	112.039	28-08-07	751	-0.07	34.871	0.44
310	87.658	112.039	28-08-07	500	0.61	34.875	0.45
310	87.658	112.039	28-08-07	298	1.10	34.854	0.35
310	87.658	112.039	28-08-07	200	0.86	34.768	0.45
310	87.658	112.039	28-08-07	150	-0.05	34.511	0.28
310	87.658	112.039	28-08-07	100	-1.31	34.212	0.62
310	87.658	112.039	28-08-07	75	-1.61	33.932	0.8
310	87.658	112.039	28-08-07	50	-1.74	32.763	1.63
310	87.658	112.039	28-08-07	25	-1.65	31.910	1.82
310	87.658	112.039	28-08-07	9	-1.67	31.604	1.35
316	88.177	139.616	30-08-07	1250	-0.44	34.900	0.39
316	88.177	139.616	30-08-07	1001	-0.29	34.882	0.39
316	88.177	139.616	30-08-07	801	-0.08	34.869	0.39
316	88.177	139.616	30-08-07	750	-0.00	34.868	0.46
316	88.177	139.616	30-08-07	601	0.35	34.869	0.49
316	88.177	139.616	30-08-07	501	0.58	34.867	0.57
316	88.177	139.616	30-08-07	301	1.29	34.864	0.46

DATA TABLE ARK XXII/2 Continued

Station	Latitude [°N]	Longitude [°E]	Date	Depth [m]	θ (°C)	Salinity	dFe [nmol/l]
316	88.177	139.616	30-08-07	250	1.21	34.828	0.42
316	88.177	139.616	30-08-07	201	1.06	34.783	0.42
316	88.177	139.616	30-08-07	150	-0.02	34.512	0.56
316	88.177	139.616	30-08-07	100	-1.32	34.177	0.98
316	88.177	139.616	30-08-07	75	-1.61	33.844	1.10
316	88.177	139.616	30-08-07	54	-1.71	32.653	(0.64)
316	88.177	139.616	30-08-07	50	-1.72	32.501	1.82
316	88.177	139.616	30-08-07	25	-1.64	31.811	1.97
316	88.177	139.616	30-08-07	5	-1.68	31.164	2.60
319	88.665	153.661	31-08-07	2650	-0.82	34.923	0.92
319	88.665	153.661	31-08-07	2600	-0.80	34.924	0.67
319	88.665	153.661	31-08-07	2401	-0.74	34.926	0.82
319	88.665	153.661	31-08-07	2200	-0.67	34.929	0.96
319	88.665	153.661	31-08-07	2000	-0.55	34.940	0.58
319	88.665	153.661	31-08-07	1750	-0.55	34.924	0.41
319	88.665	153.661	31-08-07	1501	-0.49	34.912	0.59
319	88.665	153.661	31-08-07	1250	-0.41	34.898	0.70
319	88.665	153.661	31-08-07	1001	-0.25	34.881	0.60
319	88.665	153.661	31-08-07	750	0.07	34.871	0.55
319	88.665	153.661	31-08-07	500	0.62	34.873	0.54
319	88.665	153.661	31-08-07	300	1.06	34.852	0.49
319	88.665	153.661	31-08-07	201	0.50	34.673	0.48
319	88.665	153.661	31-08-07	100	-1.37	34.116	0.48
319	88.665	153.661	31-08-07	50	-1.73	32.470	1.88
319	88.665	153.661	31-08-07	22	-1.60	31.084	2.07
319	88.665	153.661	31-08-07	5	-1.64	30.424	1.61
326	88.029	170.084	01-09-07	3900	-0.54	34.955	0.24
326	88.029	170.084	01-09-07	3800	-0.54	34.955	0.32
326	88.029	170.084	01-09-07	3700	-0.54	34.955	0.33
326	88.029	170.084	01-09-07	3500	-0.54	34.955	0.35
326	88.029	170.084	01-09-07	3251	-0.54	34.955	0.36
326	88.029	170.084	01-09-07	3001	-0.53	34.955	0.25
326	88.029	170.084	01-09-07	2750	-0.53	34.955	0.35
326	88.029	170.084	01-09-07	2500	-0.52	34.955	0.49
326	88.029	170.084	01-09-07	2249	-0.52	34.953	0.30
326	88.029	170.084	01-09-07	2000	-0.51	34.950	0.31
326	88.029	170.084	01-09-07	1750	-0.49	34.943	0.36
326	88.029	170.084	01-09-07	1500	-0.44	34.931	0.42
326	88.029	170.084	01-09-07	1001	-0.20	34.895	0.38
326	88.029	170.084	01-09-07	751	0.03	34.876	0.46
326	88.029	170.084	01-09-07	500	0.48	34.867	0.37
326	88.029	170.084	01-09-07	300	0.89	34.843	0.45
326	88.029	170.084	01-09-07	200	0.34	34.649	0.45
326	88.029	170.084	01-09-07	150	-0.51	34.410	0.41
326	88.029	170.084	01-09-07	100	-1.50	34.032	0.68
326	88.029	170.084	01-09-07	75	-1.61	33.461	0.96
326	88.029	170.084	01-09-07	50	-1.63	32.167	1.46
326	88.029	170.084	01-09-07	24	-1.53	30.369	2.54

DATA TABLE ARK XXII/2 Continued

Station	Latitude [°N]	Longitude [°E]	Date	Depth [m]	θ (°C)	Salinity	dFe [nmol/l]
326	88.029	170.084	01-09-07	10	-1.55	29.292	2.52
328	87.830	189.437	02-09-07	3900	-0.54	34.955	0.27
328	87.830	189.437	02-09-07	3001	-0.53	34.955	0.29
328	87.830	189.437	02-09-07	2501	-0.52	34.955	0.46
328	87.830	189.437	02-09-07	2001	-0.51	34.950	0.26
328	87.830	189.437	02-09-07	1501	-0.44	34.932	0.37
328	87.830	189.437	02-09-07	1001	-0.22	34.896	0.32
328	87.830	189.437	02-09-07	501	0.43	34.869	0.28
328	87.830	189.437	02-09-07	301	0.89	34.843	0.44
328	87.830	189.437	02-09-07	201	0.29	34.628	0.42
328	87.830	189.437	02-09-07	150	-0.54	34.397	0.29
328	87.830	189.437	02-09-07	101	-1.53	33.961	0.68
328	87.830	189.437	02-09-07	76	-1.61	33.200	1.09
328	87.830	189.437	02-09-07	50	-1.64	31.131	1.95
328	87.830	189.437	02-09-07	25	-1.53	30.279	2.94
328	87.830	189.437	02-09-07	5	-1.54	28.947	2.49
333	87.028	213.601	04-09-07	3201	-0.53	34.955	0.20
333	87.028	213.601	04-09-07	3000	-0.53	34.955	0.21
333	87.028	213.601	04-09-07	2750	-0.52	34.955	0.20
333	87.028	213.601	04-09-07	2501	-0.52	34.954	0.21
333	87.028	213.601	04-09-07	2250	-0.51	34.952	0.21
333	87.028	213.601	04-09-07	2000	-0.51	34.948	0.23
333	87.028	213.601	04-09-07	1751	-0.49	34.940	0.24
333	87.028	213.601	04-09-07	1501	-0.45	34.926	0.26
333	87.028	213.601	04-09-07	1250	-0.35	34.908	0.25
333	87.028	213.601	04-09-07	1000	-0.20	34.889	0.39
333	87.028	213.601	04-09-07	750	0.05	34.869	0.34
333	87.028	213.601	04-09-07	501	0.55	34.863	0.37
333	87.028	213.601	04-09-07	401	0.79	34.859	0.38
333	87.028	213.601	04-09-07	301	0.82	34.831	0.37
333	87.028	213.601	04-09-07	200	0.04	34.587	0.40
333	87.028	213.601	04-09-07	150	-0.80	34.358	0.43
333	87.028	213.601	04-09-07	100	-1.54	33.911	1.00
333	87.028	213.601	04-09-07	75	-1.61	33.166	1.10
333	87.028	213.601	04-09-07	49	-1.57	30.110	1.82
333	87.028	213.601	04-09-07	24	-1.54	28.880	2.20
333	87.028	213.601	04-09-07	8	-1.55	28.728	2.40
338	85.704	224.961	05-09-07	1476	-0.42	34.932	0.20
338	85.704	224.961	05-09-07	1400	-0.39	34.926	0.28
338	85.704	224.961	05-09-07	1301	-0.35	34.920	0.24
338	85.704	224.961	05-09-07	1250	-0.33	34.918	0.35
338	85.704	224.961	05-09-07	1201	-0.30	34.915	0.29
338	85.704	224.961	05-09-07	1100	-0.24	34.907	0.20
338	85.704	224.961	05-09-07	749	0.05	34.883	0.21
338	85.704	224.961	05-09-07	501	0.41	34.867	0.20
338	85.704	224.961	05-09-07	300	0.61	34.828	0.20
338	85.704	224.961	05-09-07	200	-0.13	34.518	0.23
338	85.704	224.961	05-09-07	150	-0.95	34.227	0.40

DATA TABLE ARK XXII/2 Continued

Station	Latitude [°N]	Longitude [°E]	Date	Depth [m]	θ (°C)	Salinity	dFe [nmol/l]
338	85.704	224.961	05-09-07	101	-1.50	33.315	0.61
338	85.704	224.961	05-09-07	75	-1.53	31.906	0.60
338	85.704	224.961	05-09-07	50	-1.59	30.300	0.26
338	85.704	224.961	05-09-07	25	-1.39	29.711	0.38
338	85.704	224.961	05-09-07	5	-1.54	28.586	0.58
342	84.500	221.581	07-09-07	2200	-0.50	34.952	0.26
342	84.500	221.581	07-09-07	2000	-0.50	34.947	0.20
342	84.500	221.581	07-09-07	1750	-0.48	34.940	0.30
342	84.500	221.581	07-09-07	1500	-0.42	34.928	0.25
342	84.500	221.581	07-09-07	1250	-0.30	34.915	0.33
342	84.500	221.581	07-09-07	1000	-0.13	34.900	0.41
342	84.500	221.581	07-09-07	901	-0.04	34.895	0.40
342	84.500	221.581	07-09-07	700	0.19	34.882	0.31
342	84.500	221.581	07-09-07	501	0.40	34.862	0.47
342	84.500	221.581	07-09-07	301	0.30	34.764	0.29
342	84.500	221.581	07-09-07	200	-0.42	34.413	0.65
342	84.500	221.581	07-09-07	151	-1.20	34.082	0.60
342	84.500	221.581	07-09-07	133	-1.46	33.708	0.36
342	84.500	221.581	07-09-07	101	-1.38	32.513	0.86
342	84.500	221.581	07-09-07	76	-1.51	31.476	0.45
342	84.500	221.581	07-09-07	51	-1.59	30.511	0.22
342	84.500	221.581	07-09-07	25	-1.44	30.297	0.18
342	84.500	221.581	07-09-07	10	-1.47	29.291	0.33
349	85.064	195.528	09-09-07	1951	-0.50	34.950	0.59
349	85.064	195.528	09-09-07	1900	-0.50	34.948	0.49
349	85.064	195.528	09-09-07	1800	-0.49	34.945	0.55
349	85.064	195.528	09-09-07	1751	-0.49	34.943	0.84
349	85.064	195.528	09-09-07	1501	-0.44	34.928	0.53
349	85.064	195.528	09-09-07	1251	-0.34	34.909	0.74
349	85.064	195.528	09-09-07	1001	-0.21	34.887	0.84
349	85.064	195.528	09-09-07	751	0.07	34.871	0.49
349	85.064	195.528	09-09-07	501	0.54	34.862	0.36
349	85.064	195.528	09-09-07	401	0.82	34.860	0.36
349	85.064	195.528	09-09-07	300	0.82	34.830	0.38
349	85.064	195.528	09-09-07	251	0.70	34.790	0.42
349	85.064	195.528	09-09-07	225	0.45	34.701	0.51
349	85.064	195.528	09-09-07	201	0.16	34.600	0.45
349	85.064	195.528	09-09-07	175	-0.25	34.472	0.44
349	85.064	195.528	09-09-07	150	-0.70	34.338	0.55
349	85.064	195.528	09-09-07	124	-1.15	34.162	0.73
349	85.064	195.528	09-09-07	101	-1.54	33.870	0.82
349	85.064	195.528	09-09-07	75	-1.55	32.891	1.10
349	85.064	195.528	09-09-07	50	-1.54	31.128	1.01
349	85.064	195.528	09-09-07	25	-1.48	29.004	2.88
349	85.064	195.528	09-09-07	9	-1.40	26.967	2.71
352	86.638	177.555	10-09-07	3900	-0.54	34.955	0.30
352	86.638	177.555	10-09-07	3750	-0.54	34.955	0.24
352	86.638	177.555	10-09-07	3500	-0.54	34.955	0.24

DATA TABLE ARK XXII/2 Continued

Station	Latitude [°N]	Longitude [°E]	Date	Depth [m]	θ (°C)	Salinity	dFe [nmol/l]
352	86.638	177.555	10-09-07	3250	-0.54	34.955	0.32
352	86.638	177.555	10-09-07	3001	-0.53	34.955	0.27
352	86.638	177.555	10-09-07	2751	-0.53	34.955	0.18
352	86.638	177.555	10-09-07	2500	-0.52	34.955	0.28
352	86.638	177.555	10-09-07	2251	-0.52	34.953	0.37
352	86.638	177.555	10-09-07	2001	-0.51	34.950	0.31
352	86.638	177.555	10-09-07	1751	-0.49	34.944	0.33
352	86.638	177.555	10-09-07	1500	-0.44	34.932	0.42
352	86.638	177.555	10-09-07	1250	-0.36	34.915	0.42
352	86.638	177.555	10-09-07	1001	-0.22	34.897	0.47
352	86.638	177.555	10-09-07	751	0.01	34.879	0.32
352	86.638	177.555	10-09-07	500	0.46	34.868	0.33
352	86.638	177.555	10-09-07	200	0.44	34.684	0.31
352	86.638	177.555	10-09-07	150	-0.31	34.460	0.42
352	86.638	177.555	10-09-07	100	-1.47	34.077	0.57
352	86.638	177.555	10-09-07	50	-1.66	32.186	1.52
352	86.638	177.555	10-09-07	26	-1.63	30.361	2.01
352	86.638	177.555	10-09-07	8	-1.59	29.525	2.03
363	86.459	135.017	13-09-07	3850	-0.94	34.943	0.44
363	86.459	135.017	13-09-07	3750	-0.94	34.943	0.46
363	86.459	135.017	13-09-07	3500	-0.94	34.941	0.54
363	86.459	135.017	13-09-07	3250	-0.93	34.938	0.51
363	86.459	135.017	13-09-07	3000	-0.92	34.934	0.54
363	86.459	135.017	13-09-07	2750	-0.91	34.930	0.33
363	86.459	135.017	13-09-07	2500	-0.89	34.925	0.45
363	86.459	135.017	13-09-07	2249	-0.85	34.922	0.62
363	86.459	135.017	13-09-07	2001	-0.79	34.919	0.56
363	86.459	135.017	13-09-07	1752	-0.71	34.915	0.56
363	86.459	135.017	13-09-07	1501	-0.57	34.911	0.43
363	86.459	135.017	13-09-07	1253	-0.38	34.901	0.50
363	86.459	135.017	13-09-07	1001	-0.12	34.890	0.45
363	86.459	135.017	13-09-07	752	0.16	34.872	0.42
363	86.459	135.017	13-09-07	502	0.91	34.880	0.50
363	86.459	135.017	13-09-07	400	1.25	34.878	0.48
363	86.459	135.017	13-09-07	301	1.27	34.831	0.48
363	86.459	135.017	13-09-07	201	0.74	34.732	0.47
363	86.459	135.017	13-09-07	151	-0.13	34.559	0.47
363	86.459	135.017	13-09-07	100	-1.09	34.303	0.64
363	86.459	135.017	13-09-07	75	-1.54	34.065	0.65
363	86.459	135.017	13-09-07	50	-1.70	33.082	1.35
363	86.459	135.017	13-09-07	25	-1.73	32.370	1.80
363	86.459	135.017	13-09-07	10	-1.68	31.303	1.48
371	84.653	102.736	16-09-07	4050	-0.94	34.942	0.92
371	84.653	102.736	16-09-07	3500	-0.94	34.941	0.71
371	84.653	102.736	16-09-07	3400	-0.93	34.941	1.06
371	84.653	102.736	16-09-07	3301	-0.94	34.940	0.78
371	84.653	102.736	16-09-07	3201	-0.94	34.938	0.73
371	84.653	102.736	16-09-07	2999	-0.94	34.935	0.70

DATA TABLE ARK XXII/2 Continued

Station	Latitude [°N]	Longitude [°E]	Date	Depth [m]	θ (°C)	Salinity	dFe [nmol/l]
371	84.653	102.736	16-09-07	2750	-0.92	34.931	0.68
371	84.653	102.736	16-09-07	2500	-0.90	34.928	0.62
371	84.653	102.736	16-09-07	2251	-0.87	34.924	0.63
371	84.653	102.736	16-09-07	2000	-0.81	34.922	0.56
371	84.653	102.736	16-09-07	1500	-0.62	34.913	0.54
371	84.653	102.736	16-09-07	1001	-0.32	34.881	0.50
371	84.653	102.736	16-09-07	501	0.60	34.871	0.35
371	84.653	102.736	16-09-07	301	1.03	34.849	0.50
371	84.653	102.736	16-09-07	151	0.16	34.583	0.51
371	84.653	102.736	16-09-07	100	-1.16	34.260	0.55
371	84.653	102.736	16-09-07	74	-1.68	33.923	1.04
371	84.653	102.736	16-09-07	50	-1.80	33.726	1.08
371	84.653	102.736	16-09-07	26	-1.76	33.422	1.33
371	84.653	102.736	16-09-07	10	-1.69	33.157	1.37
372	84.328	107.310	17-09-07	4061	-0.94	34.942	0.39
372	84.328	107.310	17-09-07	3750	-0.93	34.942	0.78
372	84.328	107.310	17-09-07	3500	-0.93	34.941	0.48
372	84.328	107.310	17-09-07	3301	-0.93	34.940	0.58
372	84.328	107.310	17-09-07	3200	-0.93	34.940	0.67
372	84.328	107.310	17-09-07	3134	-0.93	34.940	0.75
372	84.328	107.310	17-09-07	3000	-0.94	34.937	0.79
372	84.328	107.310	17-09-07	2750	-0.93	34.933	0.75
372	84.328	107.310	17-09-07	2501	-0.91	34.929	0.70
372	84.328	107.310	17-09-07	2251	-0.88	34.926	0.70
372	84.328	107.310	17-09-07	2001	-0.83	34.923	0.48
372	84.328	107.310	17-09-07	1502	-0.67	34.916	0.58
372	84.328	107.310	17-09-07	1003	-0.36	34.894	0.85
372	84.328	107.310	17-09-07	502	0.64	34.882	0.60
372	84.328	107.310	17-09-07	301	1.10	34.858	0.54
372	84.328	107.310	17-09-07	201	0.98	34.784	0.64
372	84.328	107.310	17-09-07	150	0.19	34.549	0.66
372	84.328	107.310	17-09-07	101	-1.25	34.236	0.86
372	84.328	107.310	17-09-07	75	-1.66	33.929	1.22
372	84.328	107.310	17-09-07	50	-1.76	33.511	1.87
372	84.328	107.310	17-09-07	33	-1.73	33.079	1.59
372	84.328	107.310	17-09-07	24	-1.67	32.168	1.72
372	84.328	107.310	17-09-07	9	-1.72	31.821	1.65
373	84.199	108.936	17-09-07	4049	-0.93	34.942	0.70
373	84.199	108.936	17-09-07	3749	-0.93	34.942	0.37
373	84.199	108.936	17-09-07	3492	-0.93	34.942	0.55
373	84.199	108.936	17-09-07	3300	-0.93	34.940	0.59
373	84.199	108.936	17-09-07	3201	-0.94	34.939	0.52
373	84.199	108.936	17-09-07	3131	-0.94	34.939	0.53
373	84.199	108.936	17-09-07	3001	-0.94	34.936	0.49
373	84.199	108.936	17-09-07	2749	-0.93	34.932	0.57
373	84.199	108.936	17-09-07	2500	-0.91	34.929	0.58
373	84.199	108.936	17-09-07	2249	-0.88	34.925	0.64
373	84.199	108.936	17-09-07	2000	-0.83	34.923	0.80

DATA TABLE ARK XXII/2 Continued

Station	Latitude [°N]	Longitude [°E]	Date	Depth [m]	θ (°C)	Salinity	dFe [nmol/l]
373	84.199	108.936	17-09-07	1750	-0.76	34.920	0.61
373	84.199	108.936	17-09-07	1500	-0.67	34.916	0.62
373	84.199	108.936	17-09-07	1001	-0.37	34.893	0.77
373	84.199	108.936	17-09-07	750	-0.08	34.875	0.64
373	84.199	108.936	17-09-07	500	0.63	34.879	0.64
373	84.199	108.936	17-09-07	200	0.95	34.783	0.50
373	84.199	108.936	17-09-07	150	0.07	34.534	0.60
373	84.199	108.936	17-09-07	100	-1.40	34.192	0.76
373	84.199	108.936	17-09-07	51	-1.79	33.674	0.89
373	84.199	108.936	17-09-07	33	-1.76	33.304	1.18
373	84.199	108.936	17-09-07	24	-1.67	32.618	1.07
373	84.199	108.936	17-09-07	11	-1.71	31.862	1.06
379	82.865	117.830	18-09-07	4325	-0.93	34.942	0.64
379	82.865	117.830	18-09-07	4000	-0.93	34.942	0.58
379	82.865	117.830	18-09-07	3750	-0.93	34.943	0.49
379	82.865	117.830	18-09-07	3500	-0.93	34.942	0.56
379	82.865	117.830	18-09-07	3249	-0.94	34.940	0.63
379	82.865	117.830	18-09-07	3000	-0.94	34.936	0.75
379	82.865	117.830	18-09-07	2751	-0.93	34.932	0.55
379	82.865	117.830	18-09-07	2501	-0.90	34.928	0.77
379	82.865	117.830	18-09-07	2251	-0.87	34.925	0.66
379	82.865	117.830	18-09-07	2002	-0.82	34.922	0.58
379	82.865	117.830	18-09-07	1751	-0.76	34.919	0.67
379	82.865	117.830	18-09-07	1501	-0.68	34.916	0.59
379	82.865	117.830	18-09-07	1001	-0.40	34.896	0.49
379	82.865	117.830	18-09-07	746	-0.12	34.880	0.47
379	82.865	117.830	18-09-07	502	0.61	34.886	0.48
379	82.865	117.830	18-09-07	200	1.16	34.828	0.65
379	82.865	117.830	18-09-07	149	0.50	34.634	0.51
379	82.865	117.830	18-09-07	100	-1.03	34.282	0.77
379	82.865	117.830	18-09-07	75	-1.59	34.057	0.96
379	82.865	117.830	18-09-07	50	-1.73	33.485	1.05
379	82.865	117.830	18-09-07	31	-1.74	32.970	1.83
379	82.865	117.830	18-09-07	24	-1.68	32.699	1.78
379	82.865	117.830	18-09-07	9	-1.66	31.107	1.79
382	81.358	120.719	19-09-07	5201	-0.92	34.942	2.34
382	81.358	120.719	19-09-07	5000	-0.93	34.942	1.66
382	81.358	120.719	19-09-07	4749	-0.93	34.942	1.51
382	81.358	120.719	19-09-07	4500	-0.93	34.943	0.87
382	81.358	120.719	19-09-07	4248	-0.93	34.943	0.64
382	81.358	120.719	19-09-07	4001	-0.93	34.943	0.55
382	81.358	120.719	19-09-07	3750	-0.93	34.943	0.65
382	81.358	120.719	19-09-07	3500	-0.93	34.943	0.53
382	81.358	120.719	19-09-07	3250	-0.93	34.942	0.55
382	81.358	120.719	19-09-07	3000	-0.93	34.940	1.00
382	81.358	120.719	19-09-07	2750	-0.94	34.935	0.68
382	81.358	120.719	19-09-07	2500	-0.93	34.931	0.44
382	81.358	120.719	19-09-07	2001	-0.86	34.924	0.40

DATA TABLE ARK XXII/2 Continued

Station	Latitude [°N]	Longitude [°E]	Date	Depth [m]	θ (°C)	Salinity	dFe [nmol/l]
382	81.358	120.719	19-09-07	1501	-0.73	34.918	0.47
382	81.358	120.719	19-09-07	1000	-0.43	34.902	0.61
382	81.358	120.719	19-09-07	500	0.51	34.887	0.37
382	81.358	120.719	19-09-07	200	1.19	34.833	0.48
382	81.358	120.719	19-09-07	150	0.63	34.670	0.41
382	81.358	120.719	19-09-07	101	-0.61	34.377	0.38
382	81.358	120.719	19-09-07	75	-1.36	34.195	0.29
382	81.358	120.719	19-09-07	50	-1.68	33.856	0.27
382	81.358	120.719	19-09-07	25	-1.67	32.693	0.29
382	81.358	120.719	19-09-07	10	-1.66	31.272	0.42
385	79.352	124.360	20-09-07	3426	-0.92	34.941	0.68
385	79.352	124.360	20-09-07	3251	-0.92	34.941	0.55
385	79.352	124.360	20-09-07	3101	-0.93	34.938	0.65
385	79.352	124.360	20-09-07	3001	-0.93	34.936	0.68
385	79.352	124.360	20-09-07	2751	-0.92	34.932	0.41
385	79.352	124.360	20-09-07	2500	-0.91	34.928	0.36
385	79.352	124.360	20-09-07	2251	-0.88	34.924	0.55
385	79.352	124.360	20-09-07	2000	-0.84	34.921	0.40
385	79.352	124.360	20-09-07	1751	-0.79	34.919	0.59
385	79.352	124.360	20-09-07	1501	-0.70	34.916	0.50
385	79.352	124.360	20-09-07	1251	-0.57	34.913	0.40
385	79.352	124.360	20-09-07	1000	-0.36	34.905	0.54
385	79.352	124.360	20-09-07	892	-0.25	34.902	0.58
385	79.352	124.360	20-09-07	750	0.10	34.907	0.56
385	79.352	124.360	20-09-07	500	1.08	34.919	0.58
385	79.352	124.360	20-09-07	400	1.36	34.910	0.63
385	79.352	124.360	20-09-07	301	1.89	34.920	0.57
385	79.352	124.360	20-09-07	201	2.23	34.912	0.56
385	79.352	124.360	20-09-07	150	1.70	34.793	0.55
385	79.352	124.360	20-09-07	101	-0.59	34.389	0.53
385	79.352	124.360	20-09-07	75	-1.44	34.192	0.55
385	79.352	124.360	20-09-07	50	-1.79	33.989	0.47
385	79.352	124.360	20-09-07	25	-1.68	33.815	0.82
385	79.352	124.360	20-09-07	-1	-0.97	31.207	1.22
389	78.355	124.515	21-09-07	2502	-0.92	34.935	0.5
389	78.355	124.515	21-09-07	2250	-0.87	34.924	0.59
389	78.355	124.515	21-09-07	2000	-0.82	34.920	0.85
389	78.355	124.515	21-09-07	1751	-0.77	34.914	1.23
389	78.355	124.515	21-09-07	1499	-0.66	34.912	0.37
389	78.355	124.515	21-09-07	1251	-0.51	34.906	0.46
389	78.355	124.515	21-09-07	1000	-0.32	34.896	0.43
389	78.355	124.515	21-09-07	901	-0.21	34.892	0.52
389	78.355	124.515	21-09-07	749	-0.05	34.883	0.36
389	78.355	124.515	21-09-07	500	0.81	34.900	0.47
389	78.355	124.515	21-09-07	250	1.91	34.886	0.37
389	78.355	124.515	21-09-07	200	1.85	34.847	0.36
389	78.355	124.515	21-09-07	150	1.05	34.696	0.38
389	78.355	124.515	21-09-07	100	-1.13	34.354	0.37

DATA TABLE ARK XXII/2 Continued

Station	Latitude [°N]	Longitude [°E]	Date	Depth [m]	θ (°C)	Salinity	dFe [nmol/l]
389	78.355	124.515	21-09-07	76	-1.63	34.203	0.39
389	78.355	124.515	21-09-07	51	-1.74	34.024	0.53
389	78.355	124.515	21-09-07	24	-1.62	33.469	1.24
389	78.355	124.515	21-09-07	10	-0.09	31.467	1.42
400	77.388	123.402	22-09-07	1093	-0.19	34.907	0.66
400	77.388	123.402	22-09-07	999	-0.09	34.895	0.66
400	77.388	123.402	22-09-07	750	-0.02	34.867	0.60
400	77.388	123.402	22-09-07	509	0.50	34.865	0.44
400	77.388	123.402	22-09-07	308	1.39	34.869	0.83
400	77.388	123.402	22-09-07	202	1.73	34.843	0.47
400	77.388	123.402	22-09-07	151	0.07	34.623	0.63
400	77.388	123.402	22-09-07	101	-1.63	34.418	0.63
400	77.388	123.402	22-09-07	76	-1.54	34.375	1.20
400	77.388	123.402	22-09-07	51	-1.35	34.209	1.17
400	77.388	123.402	22-09-07	27	-1.39	33.720	1.33
400	77.388	123.402	22-09-07	10	-1.51	32.353	2.33
407	76.181	122.129	23-09-07	56	-1.63	33.810	1.51
407	76.181	122.129	23-09-07	30	-1.58	33.434	1.35
407	76.181	122.129	23-09-07	10	-0.12	29.723	2.96
411	75.200	121.358	23-09-07	35	0.02	32.653	10.47
411	75.200	121.358	23-09-07	25	0.46	32.504	10.14
411	75.200	121.358	23-09-07	20	0.48	32.498	10.11
411	75.200	121.358	23-09-07	15	1.18	30.626	4.37
411	75.200	121.358	23-09-07	10	0.45	29.092	3.01

ANT XXIV/3

A total of 920 DFe datapoints is available from ANT XXIV/3; 896 samples from down-cast stations and 24 surface samples [See Chapter 4]. For methods see Chapter 5.2 and 6.2. Outliers are marked with () brackets.

DATA TABLE ANT XXIV/3

Station	Latitude [°N]	Longitude [°E]	Date	Depth [m]	θ (°C)	Salinity	dFe [nmol/l]
101	-42.338	8.995	13-02-08	4353	0.72	34.732	0.28
101	-42.338	8.995	13-02-08	4000	0.77	34.736	0.33
101	-42.338	8.995	13-02-08	3505	1.33	34.783	0.40
101	-42.338	8.995	13-02-08	3000	1.88	34.828	0.62
101	-42.338	8.995	13-02-08	2501	2.16	34.818	0.63
101	-42.338	8.995	13-02-08	2005	2.46	34.766	0.64
101	-42.338	8.995	13-02-08	1751	2.60	34.717	0.42
101	-42.338	8.995	13-02-08	1502	2.71	34.621	0.49
101	-42.338	8.995	13-02-08	1253	2.82	34.494	0.45
101	-42.338	8.995	13-02-08	753	3.86	34.274	0.35
101	-42.338	8.995	13-02-08	502	5.76	34.352	0.46
101	-42.338	8.995	13-02-08	401	6.91	34.449	0.36
101	-42.338	8.995	13-02-08	301	6.68	34.267	0.39
101	-42.338	8.995	13-02-08	251	7.07	34.273	0.38
101	-42.338	8.995	13-02-08	199	7.52	34.262	0.27
101	-42.338	8.995	13-02-08	98	9.38	34.453	0.32
101	-42.338	8.995	13-02-08	76	9.13	34.264	0.32
101	-42.338	8.995	13-02-08	48	10.36	34.246	0.27
101	-42.338	8.995	13-02-08	48	10.36	34.197	0.18
101	-42.338	8.995	13-02-08	25	10.87	34.075	0.24
101	-42.338	8.995	13-02-08	4	10.99	34.02	0.36
103	-46.000	5.881	16-02-08	3099	1.09	34.738	0.51
103	-46.000	5.881	16-02-08	3001	1.17	34.742	0.31
103	-46.000	5.881	16-02-08	2501	1.63	34.769	0.44
103	-46.000	5.881	16-02-08	2001	2.19	34.78	0.43
103	-46.000	5.881	16-02-08	1747	2.36	34.75	(0.77)
103	-46.000	5.881	16-02-08	1747	2.36	34.75	0.54
103	-46.000	5.881	16-02-08	1501	2.46	34.704	(0.61)
103	-46.000	5.881	16-02-08	1253	2.47	34.611	0.39
103	-46.000	5.881	16-02-08	1001	2.59	34.488	0.45
103	-46.000	5.881	16-02-08	751	2.80	34.327	0.40
103	-46.000	5.881	16-02-08	499	3.17	34.185	0.43
103	-46.000	5.881	16-02-08	404	3.42	34.161	0.40
103	-46.000	5.881	16-02-08	300	3.95	34.137	0.36
103	-46.000	5.881	16-02-08	251	4.21	34.125	0.24
103	-46.000	5.881	16-02-08	201	4.41	34.078	0.25
103	-46.000	5.881	16-02-08	151	4.82	33.984	0.23
103	-46.000	5.881	16-02-08	100	4.93	33.869	0.47
103	-46.000	5.881	16-02-08	73	6.84	33.807	0.28
103	-46.000	5.881	16-02-08	50	7.82	33.746	0.20

DATA TABLE ANT XXIV/3 Continued

Station	Latitude [°N]	Longitude [°E]	Date	Depth [m]	θ (°C)	Salinity	dFe [nmol/l]
103	-46.000	5.881	16-02-08	45	7.82	33.746	0.18
103	-46.000	5.881	16-02-08	26	7.83	33.746	0.27
103	-46.000	5.881	17-02-08	8	7.84	33.746	0.24
104	-47.664	4.289	17-02-08	4397	0.41	34.694	0.29
104	-47.664	4.289	17-02-08	4202	0.43	34.696	0.25
104	-47.664	4.289	17-02-08	4006	0.46	34.699	0.32
104	-47.664	4.289	17-02-08	3502	0.66	34.713	0.39
104	-47.664	4.289	17-02-08	3002	0.99	34.731	0.40
104	-47.664	4.289	17-02-08	2499	1.44	34.753	0.55
104	-47.664	4.289	17-02-08	1997	2.06	34.778	0.64
104	-47.664	4.289	17-02-08	1748	2.23	34.76	0.63
104	-47.664	4.289	17-02-08	1500	2.38	34.728	0.23
104	-47.664	4.289	17-02-08	1252	2.38	34.649	0.21
104	-47.664	4.289	17-02-08	998	2.51	34.547	0.49
104	-47.664	4.289	17-02-08	750	2.64	34.411	0.42
104	-47.664	4.289	17-02-08	502	2.77	34.239	0.49
104	-47.664	4.289	17-02-08	399	2.85	34.164	0.45
104	-47.664	4.289	17-02-08	301	3.22	34.118	0.35
104	-47.664	4.289	17-02-08	199	3.55	33.944	0.23
104	-47.664	4.289	17-02-08	99	4.51	33.811	0.22
104	-47.664	4.289	17-02-08	48	6.47	33.727	0.21
104	-47.664	4.289	18-02-08	17	6.47	33.727	0.17
107	-50.274	1.453	18-02-08	3500	0.31	34.688	(0.77)
107	-50.274	1.453	18-02-08	3500	0.31	34.688	0.57
107	-50.274	1.453	18-02-08	2993	0.46	34.695	0.51
107	-50.274	1.453	18-02-08	2500	0.71	34.704	0.5
107	-50.274	1.453	18-02-08	2002	1.06	34.719	0.47
107	-50.274	1.453	18-02-08	1749	1.44	34.745	0.48
107	-50.274	1.453	18-02-08	1500	1.61	34.743	0.45
107	-50.274	1.453	18-02-08	1250	1.94	34.745	0.49
107	-50.274	1.453	18-02-08	1001	2.03	34.71	0.45
107	-50.274	1.453	18-02-08	748	2.11	34.638	0.40
107	-50.274	1.453	18-02-08	499	2.15	34.524	(0.56)
107	-50.274	1.453	18-02-08	400	2.11	34.461	0.39
107	-50.274	1.453	18-02-08	301	1.88	34.322	(0.49)
107	-50.274	1.453	18-02-08	249	1.79	34.252	0.34
107	-50.274	1.453	18-02-08	199	1.46	34.13	0.21
107	-50.274	1.453	18-02-08	150	1.00	33.928	0.24
107	-50.274	1.453	18-02-08	100	3.17	33.761	(0.38)
107	-50.274	1.453	18-02-08	75	3.18	33.761	0.21
107	-50.274	1.453	18-02-08	50	3.18	33.761	0.27
107	-50.274	1.453	18-02-08	49	3.18	33.761	0.21
107	-50.274	1.453	19-02-08	23	3.18	33.762	0.20
107	-50.274	1.453	19-02-08	8	3.18	33.761	0.15
110	-51.945	0.013	19-02-08	2700	0.33	34.687	0.57
110	-51.945	0.013	19-02-08	2500	0.36	34.688	0.45
110	-51.945	0.013	19-02-08	2249	0.41	34.691	0.51
110	-51.945	0.013	19-02-08	2000	0.51	34.695	0.56

DATA TABLE ANT XXIV/3 Continued

Station	Latitude [°N]	Longitude [°E]	Date	Depth [m]	θ (°C)	Salinity	dFe [nmol/l]
110	-51.945	0.013	19-02-08	1748	0.71	34.705	0.48
110	-51.945	0.013	19-02-08	1499	0.91	34.712	0.51
110	-51.945	0.013	19-02-08	1248	1.23	34.723	0.44
110	-51.945	0.013	19-02-08	1000	1.51	34.724	0.38
110	-51.945	0.013	19-02-08	750	1.71	34.708	0.31
110	-51.945	0.013	19-02-08	601	1.80	34.673	0.31
110	-51.945	0.013	19-02-08	499	1.83	34.634	0.36
110	-51.945	0.013	19-02-08	448	1.82	34.613	0.38
110	-51.945	0.013	19-02-08	398	1.79	34.581	(0.51)
110	-51.945	0.013	19-02-08	350	1.74	34.546	0.25
110	-51.945	0.013	19-02-08	299	1.68	34.508	0.29
110	-51.945	0.013	19-02-08	250	1.41	34.403	0.30
110	-51.945	0.013	19-02-08	200	1.05	34.239	0.18
110	-51.945	0.013	19-02-08	149	0.89	33.922	0.14
110	-51.945	0.013	19-02-08	99	2.33	33.711	0.16
110	-51.945	0.013	19-02-08	76	2.33	33.711	0.06
110	-51.945	0.013	19-02-08	51	2.33	33.711	0.05
110	-51.945	0.013	19-02-08	32	2.34	33.711	0.05
110	-51.945	0.013	20-02-08	25	2.35	33.711	0.16
110	-51.945	0.013	20-02-08	7	2.36	33.711	0.20
113	-52.997	0.029	20-02-08	2351	0.30	34.684	1.07
113	-52.997	0.029	20-02-08	2249	0.31	34.684	0.80
113	-52.997	0.029	20-02-08	1997	0.36	34.686	1.07
113	-52.997	0.029	20-02-08	1749	0.45	34.689	0.85
113	-52.997	0.029	20-02-08	1501	0.59	34.694	1.33
113	-52.997	0.029	20-02-08	1250	0.81	34.7	0.74
113	-52.997	0.029	20-02-08	1000	1.06	34.706	0.49
113	-52.997	0.029	20-02-08	749	1.27	34.708	0.40
113	-52.997	0.029	20-02-08	499	1.55	34.669	0.41
113	-52.997	0.029	20-02-08	401	1.58	34.628	0.49
113	-52.997	0.029	20-02-08	300	1.41	34.546	0.44
113	-52.997	0.029	20-02-08	200	0.63	34.275	0.32
113	-52.997	0.029	20-02-08	150	0.32	33.923	(0.05)
113	-52.997	0.029	20-02-08	100	1.20	33.79	0.15
113	-52.997	0.029	21-02-08	74	1.22	33.79	0.25
113	-52.997	0.029	21-02-08	10	1.27	33.789	0.15
116	-54.000	-0.000	21-02-08	2398	0.23	34.681	1.92
116	-54.000	-0.000	21-02-08	2248	0.25	34.681	1.63
116	-54.000	-0.000	21-02-08	2000	0.32	34.684	1.55
116	-54.000	-0.000	21-02-08	1749	0.41	34.687	2.21
116	-54.000	-0.000	21-02-08	1499	0.56	34.691	1.20
116	-54.000	-0.000	21-02-08	1249	0.79	34.7	0.39
116	-54.000	-0.000	21-02-08	999	1.07	34.706	0.68
116	-54.000	-0.000	21-02-08	750	1.39	34.71	0.36
116	-54.000	-0.000	21-02-08	649	1.49	34.705	0.53
116	-54.000	-0.000	21-02-08	600	1.54	34.701	0.39
116	-54.000	-0.000	21-02-08	552	1.58	34.694	0.44
116	-54.000	-0.000	21-02-08	500	1.61	34.68	0.52

DATA TABLE ANT XXIV/3 Continued

Station	Latitude [°N]	Longitude [°E]	Date	Depth [m]	θ (°C)	Salinity	dFe [nmol/l]
116	-54.000	-0.000	21-02-08	450	1.63	34.669	0.40
116	-54.000	-0.000	21-02-08	401	1.67	34.649	0.38
116	-54.000	-0.000	21-02-08	350	1.68	34.628	0.47
116	-54.000	-0.000	21-02-08	301	1.69	34.602	0.31
116	-54.000	-0.000	21-02-08	301	1.69	34.601	0.36
116	-54.000	-0.000	21-02-08	251	1.64	34.56	0.32
116	-54.000	-0.000	21-02-08	152	0.40	34.197	(0.77)
116	-54.000	-0.000	21-02-08	101	0.99	33.851	0.26
116	-54.000	-0.000	21-02-08	76	1.02	33.85	0.27
116	-54.000	-0.000	21-02-08	51	1.03	33.848	0.26
116	-54.000	-0.000	21-02-08	25	1.05	33.846	0.14
116	-54.000	-0.000	21-02-08	8	1.05	33.846	0.52
119	-55.001	0.001	21-02-08	1598	0.53	34.689	0.83
119	-55.001	0.001	21-02-08	1500	0.60	34.692	0.74
119	-55.001	0.001	21-02-08	1499	0.61	34.692	0.68
119	-55.001	0.001	21-02-08	1400	0.71	34.695	0.67
119	-55.001	0.001	21-02-08	1248	0.90	34.7	0.80
119	-55.001	0.001	21-02-08	1247	0.90	34.701	0.80
119	-55.001	0.001	21-02-08	1000	1.17	34.709	0.69
119	-55.001	0.001	21-02-08	899	1.29	34.711	0.82
119	-55.001	0.001	21-02-08	750	1.45	34.707	0.76
119	-55.001	0.001	21-02-08	600	1.62	34.694	0.70
119	-55.001	0.001	21-02-08	502	1.68	34.683	0.60
119	-55.001	0.001	21-02-08	449	1.63	34.66	1.82
119	-55.001	0.001	21-02-08	399	1.65	34.641	1.21
119	-55.001	0.001	21-02-08	349	1.63	34.615	1.24
119	-55.001	0.001	21-02-08	299	1.58	34.572	0.68
119	-55.001	0.001	21-02-08	250	1.51	34.533	0.58
119	-55.001	0.001	21-02-08	201	1.09	34.403	0.59
119	-55.001	0.001	21-02-08	150	0.55	34.253	0.47
119	-55.001	0.001	21-02-08	101	0.84	33.869	0.32
119	-55.001	0.001	21-02-08	76	0.88	33.867	0.20
119	-55.001	0.001	22-02-08	50	0.91	33.862	0.33
119	-55.001	0.001	22-02-08	25	0.92	33.861	0.47
122	-56.005	0.009	22-02-08	3548	-0.53	34.655	0.53
122	-56.005	0.009	22-02-08	3496	-0.53	34.655	0.53
122	-56.005	0.009	22-02-08	3247	-0.51	34.656	0.59
122	-56.005	0.009	22-02-08	2996	-0.47	34.657	0.54
122	-56.005	0.009	22-02-08	2747	-0.40	34.659	0.56
122	-56.005	0.009	22-02-08	2499	-0.34	34.661	(0.12)
122	-56.005	0.009	22-02-08	2247	-0.24	34.664	0.52
122	-56.005	0.009	22-02-08	1998	-0.17	34.666	0.48
122	-56.005	0.009	22-02-08	1753	-0.05	34.67	0.46
122	-56.005	0.009	22-02-08	1500	0.07	34.674	0.40
122	-56.005	0.009	22-02-08	1251	0.18	34.678	0.42
122	-56.005	0.009	22-02-08	997	0.36	34.684	0.38
122	-56.005	0.009	22-02-08	745	0.51	34.685	0.31
122	-56.005	0.009	22-02-08	501	0.61	34.674	0.36

DATA TABLE ANT XXIV/3 Continued

Station	Latitude [°N]	Longitude [°E]	Date	Depth [m]	θ (°C)	Salinity	dFe [nmol/l]
122	-56.005	0.009	22-02-08	400	0.68	34.664	(1.87)
122	-56.005	0.009	22-02-08	301	0.69	34.646	0.38
122	-56.005	0.009	22-02-08	250	0.28	34.571	0.29
122	-56.005	0.009	22-02-08	201	-0.16	34.494	0.24
122	-56.005	0.009	22-02-08	151	-0.67	34.369	0.16
122	-56.005	0.009	22-02-08	100	-0.11	34.114	0.15
122	-56.005	0.009	22-02-08	75	0.60	34.009	0.19
122	-56.005	0.009	22-02-08	50	0.65	34.005	0.36
122	-56.005	0.009	23-02-08	24	0.68	34.005	0.42
122	-56.005	0.009	23-02-08	9	0.74	34.005	0.39
128	-58.004	-0.001	23-02-08	4466	-0.67	34.65	0.72
128	-58.004	-0.001	23-02-08	4194	-0.65	34.65	0.70
128	-58.004	-0.001	23-02-08	3998	-0.63	34.652	0.77
128	-58.004	-0.001	23-02-08	3747	-0.59	34.653	0.69
128	-58.004	-0.001	23-02-08	3497	-0.54	34.654	0.61
128	-58.004	-0.001	23-02-08	2996	-0.45	34.657	0.50
128	-58.004	-0.001	23-02-08	2498	-0.34	34.661	0.70
128	-58.004	-0.001	23-02-08	1997	-0.16	34.666	0.86
128	-58.004	-0.001	23-02-08	1744	-0.05	34.67	0.66
128	-58.004	-0.001	23-02-08	1500	0.05	34.673	0.81
128	-58.004	-0.001	23-02-08	1001	0.30	34.682	0.49
128	-58.004	-0.001	23-02-08	749	0.44	34.685	0.66
128	-58.004	-0.001	23-02-08	498	0.57	34.682	0.64
128	-58.004	-0.001	23-02-08	401	0.58	34.674	0.48
128	-58.004	-0.001	23-02-08	311	0.64	34.662	0.48
128	-58.004	-0.001	23-02-08	199	0.39	34.599	0.53
128	-58.004	-0.001	23-02-08	151	-0.30	34.479	0.32
128	-58.004	-0.001	23-02-08	108	-1.07	34.322	0.34
128	-58.004	-0.001	23-02-08	87	-0.28	34.144	0.29
128	-58.004	-0.001	23-02-08	74	0.31	34.074	0.31
128	-58.004	-0.001	24-02-08	47	0.37	34.062	0.18
128	-58.004	-0.001	24-02-08	10	0.37	34.061	0.18
131	-59.000	0.001	24-02-08	4513	-0.76	34.646	0.54
131	-59.000	0.001	24-02-08	4466	-0.76	34.646	0.53
131	-59.000	0.001	24-02-08	4245	-0.74	34.647	0.49
131	-59.000	0.001	24-02-08	3996	-0.72	34.648	0.53
131	-59.000	0.001	24-02-08	3495	-0.64	34.652	(0.77)
131	-59.000	0.001	24-02-08	2997	-0.53	34.655	0.52
131	-59.000	0.001	24-02-08	2496	-0.42	34.659	0.46
131	-59.000	0.001	24-02-08	1999	-0.30	34.662	0.44
131	-59.000	0.001	24-02-08	1750	-0.21	34.665	0.46
131	-59.000	0.001	24-02-08	1499	-0.12	34.668	0.66
131	-59.000	0.001	24-02-08	1250	-0.03	34.671	0.54
131	-59.000	0.001	24-02-08	1001	0.09	34.675	0.45
131	-59.000	0.001	24-02-08	749	0.22	34.68	0.36
131	-59.000	0.001	24-02-08	501	0.36	34.685	0.32
131	-59.000	0.001	24-02-08	401	0.44	34.686	0.41
131	-59.000	0.001	24-02-08	300	0.49	34.686	0.34

DATA TABLE ANT XXIV/3 Continued

Station	Latitude [°N]	Longitude [°E]	Date	Depth [m]	θ (°C)	Salinity	dFe [nmol/l]
131	-59.000	0.001	24-02-08	250	0.53	34.685	0.34
131	-59.000	0.001	24-02-08	200	0.52	34.677	0.29
131	-59.000	0.001	24-02-08	152	-0.20	34.576	0.19
131	-59.000	0.001	24-02-08	99	-1.18	34.392	(0.34)
131	-59.000	0.001	24-02-08	50	0.14	34.007	0.14
131	-59.000	0.001	26-02-08	24	0.14	34.008	(0.23)
131	-59.000	0.001	26-02-08	6	0.14	34.008	0.12
135	-60.005	-0.002	26-02-08	5291	-0.81	34.645	0.63
135	-60.005	-0.002	26-02-08	5287	-0.81	34.645	0.54
135	-60.005	-0.002	26-02-08	5254	-0.81	34.645	0.47
135	-60.005	-0.002	26-02-08	5094	-0.81	34.645	0.49
135	-60.005	-0.002	26-02-08	4994	-0.81	34.645	0.47
135	-60.005	-0.002	26-02-08	4733	-0.80	34.646	0.44
135	-60.005	-0.002	26-02-08	4500	-0.78	34.647	0.53
135	-60.005	-0.002	26-02-08	3998	-0.70	34.651	0.51
135	-60.005	-0.002	26-02-08	3491	-0.59	34.654	0.55
135	-60.005	-0.002	26-02-08	2996	-0.50	34.657	0.45
135	-60.005	-0.002	26-02-08	2497	-0.40	34.66	0.48
135	-60.005	-0.002	26-02-08	1999	-0.28	34.663	0.57
135	-60.005	-0.002	26-02-08	1501	-0.11	34.669	0.48
135	-60.005	-0.002	26-02-08	1000	0.11	34.677	0.54
135	-60.005	-0.002	26-02-08	499	0.38	34.686	0.33
135	-60.005	-0.002	26-02-08	300	0.53	34.687	0.33
135	-60.005	-0.002	26-02-08	200	0.70	34.689	0.57
135	-60.005	-0.002	26-02-08	150	0.26	34.63	0.63
135	-60.005	-0.002	26-02-08	102	-1.70	34.394	0.32
135	-60.005	-0.002	26-02-08	78	-1.71	34.316	0.34
135	-60.005	-0.002	26-02-08	51	-0.11	33.949	0.34
135	-60.005	-0.002	26-02-08	25	0.09	33.909	0.27
135	-60.005	-0.002	26-02-08	7	0.09	33.906	0.21
138	-61.001	-0.004	26-02-08	5321	-0.80	34.645	0.46
138	-61.001	-0.004	26-02-08	5294	-0.80	34.645	0.37
138	-61.001	-0.004	26-02-08	5192	-0.80	34.645	0.50
138	-61.001	-0.004	26-02-08	4994	-0.80	34.645	0.62
138	-61.001	-0.004	26-02-08	4495	-0.78	34.647	0.53
138	-61.001	-0.004	26-02-08	3995	-0.70	34.65	(0.40)
138	-61.001	-0.004	26-02-08	3495	-0.60	34.654	0.53
138	-61.001	-0.004	26-02-08	2997	-0.51	34.657	0.56
138	-61.001	-0.004	26-02-08	2497	-0.40	34.659	0.47
138	-61.001	-0.004	26-02-08	1998	-0.29	34.663	0.46
138	-61.001	-0.004	26-02-08	1498	-0.12	34.668	0.42
138	-61.001	-0.004	26-02-08	999	0.10	34.676	0.41
138	-61.001	-0.004	26-02-08	750	0.22	34.68	0.43
138	-61.001	-0.004	26-02-08	501	0.36	34.684	0.41
138	-61.001	-0.004	26-02-08	300	0.48	34.685	0.37
138	-61.001	-0.004	26-02-08	201	0.60	34.682	0.34
138	-61.001	-0.004	26-02-08	149	0.65	34.672	0.25
138	-61.001	-0.004	26-02-08	100	-1.17	34.466	0.26

DATA TABLE ANT XXIV/3 Continued

Station	Latitude [°N]	Longitude [°E]	Date	Depth [m]	θ (°C)	Salinity	dFe [nmol/l]
138	-61.001	-0.004	27-02-08	49	-1.64	34.234	0.28
138	-61.001	-0.004	27-02-08	25	0.18	33.911	0.25
141	-62.000	0.000	27-02-08	5294	-0.81	34.645	0.59
141	-62.000	0.000	27-02-08	5265	-0.81	34.645	0.45
141	-62.000	0.000	27-02-08	5192	-0.81	34.645	0.33
141	-62.000	0.000	27-02-08	4993	-0.81	34.645	0.39
141	-62.000	0.000	27-02-08	4744	-0.80	34.646	0.37
141	-62.000	0.000	27-02-08	4496	-0.78	34.647	0.37
141	-62.000	0.000	27-02-08	3995	-0.67	34.651	0.44
141	-62.000	0.000	27-02-08	3496	-0.58	34.654	0.50
141	-62.000	0.000	27-02-08	2997	-0.49	34.657	0.54
141	-62.000	0.000	27-02-08	2497	-0.39	34.66	0.51
141	-62.000	0.000	27-02-08	1998	-0.27	34.663	0.50
141	-62.000	0.000	27-02-08	1248	0.01	34.672	0.52
141	-62.000	0.000	27-02-08	998	0.13	34.677	0.43
141	-62.000	0.000	27-02-08	749	0.26	34.681	0.40
141	-62.000	0.000	27-02-08	500	0.40	34.684	0.37
141	-62.000	0.000	27-02-08	399	0.44	34.684	0.37
141	-62.000	0.000	27-02-08	300	0.48	34.68	0.33
141	-62.000	0.000	27-02-08	200	0.55	34.672	0.22
141	-62.000	0.000	27-02-08	151	0.37	34.622	(0.31)
141	-62.000	0.000	27-02-08	101	-1.61	34.346	0.219
141	-62.000	0.000	27-02-08	76	-1.81	34.281	0.13
141	-62.000	0.000	28-02-08	49	-0.84	34.115	0.23
141	-62.000	0.000	28-02-08	26	0.27	33.996	0.27
144	-63.000	0.004	28-02-08	5252	-0.80	34.645	0.44
144	-63.000	0.004	28-02-08	5099	-0.80	34.645	0.36
144	-63.000	0.004	28-02-08	5000	-0.79	34.646	0.36
144	-63.000	0.004	28-02-08	4750	-0.75	34.648	0.48
144	-63.000	0.004	28-02-08	4501	-0.70	34.649	0.52
144	-63.000	0.004	28-02-08	4001	-0.62	34.652	0.43
144	-63.000	0.004	28-02-08	3501	-0.54	34.656	0.41
144	-63.000	0.004	28-02-08	3001	-0.45	34.657	0.43
144	-63.000	0.004	28-02-08	2499	-0.37	34.66	0.52
144	-63.000	0.004	28-02-08	2000	-0.24	34.664	0.52
144	-63.000	0.004	28-02-08	1501	-0.09	34.669	0.48
144	-63.000	0.004	28-02-08	1250	0.01	34.672	0.43
144	-63.000	0.004	28-02-08	1001	0.11	34.676	0.48
144	-63.000	0.004	28-02-08	752	0.22	34.679	0.34
144	-63.000	0.004	28-02-08	500	0.33	34.683	0.34
144	-63.000	0.004	28-02-08	403	0.38	34.683	0.30
144	-63.000	0.004	28-02-08	299	0.41	34.682	0.24
144	-63.000	0.004	28-02-08	201	0.26	34.649	0.24
144	-63.000	0.004	28-02-08	152	-0.32	34.527	0.23
144	-63.000	0.004	28-02-08	101	-1.75	34.277	0.20
144	-63.000	0.004	28-02-08	75	-1.70	34.208	0.13
144	-63.000	0.004	28-02-08	49	-0.75	34.067	0.27
144	-63.000	0.004	28-02-08	25	0.52	33.938	0.23

DATA TABLE ANT XXIV/3 Continued

Station	Latitude [°N]	Longitude [°E]	Date	Depth [m]	θ (°C)	Salinity	dFe [nmol/l]
147	-63.967	-0.021	28-02-08	5155	-0.80	34.645	0.38
147	-63.967	-0.021	28-02-08	5127	-0.80	34.645	0.46
147	-63.967	-0.021	28-02-08	5000	-0.79	34.646	0.39
147	-63.967	-0.021	28-02-08	4750	-0.70	34.65	0.37
147	-63.967	-0.021	28-02-08	4500	-0.62	34.651	0.56
147	-63.967	-0.021	28-02-08	4250	-0.58	34.654	0.43
147	-63.967	-0.021	28-02-08	3998	-0.55	34.655	0.38
147	-63.967	-0.021	28-02-08	3499	-0.46	34.657	(0.98)
147	-63.967	-0.021	28-02-08	3001	-0.36	34.66	0.41
147	-63.967	-0.021	28-02-08	2500	-0.23	34.664	0.41
147	-63.967	-0.021	28-02-08	1999	-0.06	34.67	0.46
147	-63.967	-0.021	28-02-08	1499	0.16	34.677	0.34
147	-63.967	-0.021	28-02-08	998	0.43	34.688	0.30
147	-63.967	-0.021	28-02-08	751	0.58	34.692	0.31
147	-63.967	-0.021	28-02-08	503	0.82	34.699	0.35
147	-63.967	-0.021	28-02-08	401	0.94	34.7	0.32
147	-63.967	-0.021	28-02-08	300	1.06	34.696	0.39
147	-63.967	-0.021	28-02-08	202	1.12	34.681	(0.54)
147	-63.967	-0.021	28-02-08	151	1.04	34.658	0.17
147	-63.967	-0.021	28-02-08	100	-0.01	34.526	(0.55)
147	-63.967	-0.021	28-02-08	74	-1.57	34.343	0.28
147	-63.967	-0.021	29-02-08	41	0.16	34.045	0.18
147	-63.967	-0.021	29-02-08	24	0.44	34.001	0.32
150	-65.000	0.001	29-02-08	3673	-0.50	34.655	(0.72)
150	-65.000	0.001	29-02-08	3650	-0.50	34.655	0.45
150	-65.000	0.001	29-02-08	3600	-0.48	34.655	0.39
150	-65.000	0.001	29-02-08	3300	-0.43	34.657	(0.52)
150	-65.000	0.001	29-02-08	3000	-0.38	34.658	0.41
150	-65.000	0.001	29-02-08	2749	-0.32	34.66	(0.53)
150	-65.000	0.001	29-02-08	2500	-0.25	34.663	0.38
150	-65.000	0.001	29-02-08	2249	-0.18	34.666	0.42
150	-65.000	0.001	29-02-08	2000	-0.09	34.669	0.35
150	-65.000	0.001	29-02-08	1750	0.01	34.672	0.35
150	-65.000	0.001	29-02-08	1501	0.13	34.676	0.36
150	-65.000	0.001	29-02-08	1248	0.25	34.681	0.31
150	-65.000	0.001	29-02-08	999	0.39	34.687	0.33
150	-65.000	0.001	29-02-08	750	0.52	34.689	(0.51)
150	-65.000	0.001	29-02-08	501	0.71	34.695	0.29
150	-65.000	0.001	29-02-08	400	0.80	34.696	0.25
150	-65.000	0.001	29-02-08	300	0.76	34.685	0.23
150	-65.000	0.001	29-02-08	201	0.83	34.681	0.29
150	-65.000	0.001	29-02-08	149	0.76	34.672	0.20
150	-65.000	0.001	29-02-08	100	0.80	34.666	0.19
150	-65.000	0.001	09-03-08	40	-0.18	34.028	0.14
150	-65.000	0.001	09-03-08	25	-0.11	34.012	0.16
161	-66.501	-0.001	09-03-08	4381	-0.57	34.653	0.40
161	-66.501	-0.001	09-03-08	4204	-0.55	34.653	0.37
161	-66.501	-0.001	09-03-08	4000	-0.53	34.654	0.40

DATA TABLE ANT XXIV/3 Continued

Station	Latitude [°N]	Longitude [°E]	Date	Depth [m]	θ (°C)	Salinity	dFe [nmol/l]
161	-66.501	-0.001	09-03-08	3000	-0.36	34.66	0.39
161	-66.501	-0.001	09-03-08	2500	-0.23	34.664	0.33
161	-66.501	-0.001	09-03-08	1998	-0.06	34.67	0.35
161	-66.501	-0.001	09-03-08	1749	0.04	34.673	0.39
161	-66.501	-0.001	09-03-08	1501	0.15	34.677	0.37
161	-66.501	-0.001	09-03-08	1250	0.27	34.682	0.42
161	-66.501	-0.001	09-03-08	748	0.57	34.693	0.43
161	-66.501	-0.001	09-03-08	299	1.00	34.698	0.27
161	-66.501	-0.001	09-03-08	251	1.05	34.695	0.28
161	-66.501	-0.001	09-03-08	203	1.05	34.687	0.28
161	-66.501	-0.001	09-03-08	150	1.01	34.671	0.24
161	-66.501	-0.001	09-03-08	101	0.58	34.612	0.18
161	-66.501	-0.001	09-03-08	77	-0.97	34.433	0.19
161	-66.501	-0.001	09-03-08	50	-1.77	34.347	0.16
161	-66.501	-0.001	09-03-08	44	-1.74	34.334	0.17
161	-66.501	-0.001	09-03-08	28	-1.17	34.1	0.16
161	-66.501	-0.001	09-03-08	10	-0.76	33.91	0.29
163	-67.000	-0.000	09-03-08	4601	-0.63	34.652	0.36
163	-67.000	-0.000	09-03-08	4499	-0.60	34.653	0.37
163	-67.000	-0.000	09-03-08	4002	-0.53	34.654	0.32
163	-67.000	-0.000	09-03-08	3000	-0.37	34.659	0.41
163	-67.000	-0.000	09-03-08	2501	-0.24	34.664	0.42
163	-67.000	-0.000	09-03-08	2000	-0.07	34.669	(0.53)
163	-67.000	-0.000	09-03-08	1501	0.14	34.677	0.26
163	-67.000	-0.000	09-03-08	1251	0.26	34.682	0.23
163	-67.000	-0.000	09-03-08	1001	0.39	34.687	0.25
163	-67.000	-0.000	09-03-08	748	0.53	34.69	0.20
163	-67.000	-0.000	09-03-08	401	0.86	34.7	0.31
163	-67.000	-0.000	09-03-08	300	0.94	34.698	0.23
163	-67.000	-0.000	09-03-08	250	0.98	34.696	0.25
163	-67.000	-0.000	09-03-08	210	1.03	34.694	0.20
163	-67.000	-0.000	09-03-08	171	1.02	34.687	0.16
163	-67.000	-0.000	09-03-08	101	0.72	34.651	0.11
163	-67.000	-0.000	09-03-08	74	0.55	34.627	0.09
163	-67.000	-0.000	09-03-08	44	-0.87	34.036	0.05
163	-67.000	-0.000	09-03-08	45	-0.81	33.996	0.08
163	-67.000	-0.000	10-03-08	23	-0.75	33.972	0.16
163	-67.000	-0.000	10-03-08	9	-0.75	33.971	0.13
167	-68.000	-0.000	10-03-08	4429	-0.58	34.653	0.78
167	-68.000	-0.000	10-03-08	4201	-0.54	34.654	0.48
167	-68.000	-0.000	10-03-08	4002	-0.52	34.654	0.53
167	-68.000	-0.000	10-03-08	2999	-0.36	34.66	0.42
167	-68.000	-0.000	10-03-08	2499	-0.25	34.663	0.38
167	-68.000	-0.000	10-03-08	1999	-0.08	34.67	0.39
167	-68.000	-0.000	10-03-08	1746	0.02	34.673	0.33
167	-68.000	-0.000	10-03-08	1502	0.13	34.677	0.48
167	-68.000	-0.000	10-03-08	1252	0.24	34.681	0.35
167	-68.000	-0.000	10-03-08	1000	0.39	34.687	0.39

DATA TABLE ANT XXIV/3 Continued

Station	Latitude [°N]	Longitude [°E]	Date	Depth [m]	θ (°C)	Salinity	dFe [nmol/l]
167	-68.000	-0.000	10-03-08	749	0.51	34.689	(0.45)
167	-68.000	-0.000	10-03-08	499	0.64	34.689	0.33
167	-68.000	-0.000	10-03-08	399	0.73	34.691	0.28
167	-68.000	-0.000	10-03-08	298	0.73	34.682	0.22
167	-68.000	-0.000	10-03-08	250	0.70	34.675	0.21
167	-68.000	-0.000	10-03-08	199	0.75	34.672	0.22
167	-68.000	-0.000	10-03-08	145	0.57	34.65	0.23
167	-68.000	-0.000	10-03-08	100	-0.95	34.505	0.11
167	-68.000	-0.000	10-03-08	74	-1.58	34.43	0.15
167	-68.000	-0.000	10-03-08	50	-1.60	34.36	0.12
167	-68.000	-0.000	10-03-08	38	-0.74	34.031	0.14
167	-68.000	-0.000	11-03-08	25	-0.73	34.028	0.07
167	-68.000	-0.000	11-03-08	9	-0.73	34.027	0.09
175	-68.996	0.003	11-03-08	3301	-0.35	34.657	0.45
175	-68.996	0.003	11-03-08	3200	-0.35	34.657	0.48
175	-68.996	0.003	11-03-08	2996	-0.33	34.658	0.45
175	-68.996	0.003	11-03-08	2752	-0.30	34.658	0.41
175	-68.996	0.003	11-03-08	2500	-0.25	34.66	0.46
175	-68.996	0.003	11-03-08	2251	-0.20	34.661	0.44
175	-68.996	0.003	11-03-08	2000	-0.12	34.664	0.41
175	-68.996	0.003	11-03-08	1749	-0.04	34.667	0.45
175	-68.996	0.003	11-03-08	1500	0.07	34.67	0.40
175	-68.996	0.003	11-03-08	1251	0.17	34.674	(0.51)
175	-68.996	0.003	11-03-08	1001	0.33	34.678	0.43
175	-68.996	0.003	11-03-08	750	0.48	34.683	0.36
175	-68.996	0.003	11-03-08	499	0.68	34.686	0.33
175	-68.996	0.003	11-03-08	400	0.73	34.681	0.31
175	-68.996	0.003	11-03-08	300	0.75	34.672	0.33
175	-68.996	0.003	11-03-08	250	0.75	34.664	0.27
175	-68.996	0.003	11-03-08	199	0.68	34.654	0.26
175	-68.996	0.003	11-03-08	149	0.25	34.607	0.22
175	-68.996	0.003	11-03-08	100	-1.36	34.462	0.17
175	-68.996	0.003	11-03-08	75	-1.59	34.415	0.05
175	-68.996	0.003	11-03-08	50	-1.19	34.094	0.13
175	-68.996	0.003	11-03-08	25	-1.13	33.98	0.14
175	-68.996	0.003	12-03-08	25	-1.13	33.981	0.14
175	-68.996	0.003	12-03-08	6	-1.13	33.981	0.13
178	-69.400	-0.004	12-03-08	1910	0.05	34.669	0.49
178	-69.400	-0.004	12-03-08	1850	0.06	34.668	0.43
178	-69.400	-0.004	12-03-08	1800	0.07	34.669	0.48
178	-69.400	-0.004	12-03-08	1749	0.08	34.669	0.44
178	-69.400	-0.004	12-03-08	1699	0.10	34.67	0.48
178	-69.400	-0.004	12-03-08	1601	0.13	34.67	0.53
178	-69.400	-0.004	12-03-08	1500	0.16	34.671	0.51
178	-69.400	-0.004	12-03-08	1250	0.25	34.672	0.54
178	-69.400	-0.004	12-03-08	999	0.34	34.668	0.60
178	-69.400	-0.004	12-03-08	800	0.36	34.657	0.52
178	-69.400	-0.004	12-03-08	701	0.38	34.65	0.68

DATA TABLE ANT XXIV/3 Continued

Station	Latitude [°N]	Longitude [°E]	Date	Depth [m]	θ (°C)	Salinity	dFe [nmol/l]
178	-69.400	-0.004	12-03-08	502	0.64	34.655	0.97
178	-69.400	-0.004	12-03-08	451	0.67	34.651	1.05
178	-69.400	-0.004	12-03-08	300	-0.24	34.542	0.64
178	-69.400	-0.004	12-03-08	200	-1.56	34.422	0.30
178	-69.400	-0.004	12-03-08	180	-1.64	34.408	0.28
178	-69.400	-0.004	12-03-08	150	-1.67	34.396	0.44
178	-69.400	-0.004	12-03-08	137	-1.70	34.371	0.36
178	-69.400	-0.004	12-03-08	99	-1.36	34.127	0.19
178	-69.400	-0.004	12-03-08	75	-1.34	34.085	0.28
178	-69.400	-0.004	12-03-08	56	-1.33	34.081	0.26
178	-69.400	-0.004	15-03-08	24	-1.56	33.929	0.46
178	-69.400	-0.004	15-03-08	10	-1.58	33.912	0.22
187	-68.797	-17.947	15-03-08	4700	-0.77	34.647	0.27
187	-68.797	-17.947	15-03-08	4349	-0.63	34.653	0.38
187	-68.797	-17.947	15-03-08	3999	-0.58	34.654	0.45
187	-68.797	-17.947	15-03-08	2999	-0.41	34.659	0.31
187	-68.797	-17.947	15-03-08	2498	-0.31	34.662	0.38
187	-68.797	-17.947	15-03-08	1994	-0.15	34.667	0.40
187	-68.797	-17.947	15-03-08	1751	-0.06	34.67	(2.17)
187	-68.797	-17.947	15-03-08	1499	0.04	34.673	0.28
187	-68.797	-17.947	15-03-08	1250	0.15	34.678	0.28
187	-68.797	-17.947	15-03-08	1005	0.27	34.682	0.34
187	-68.797	-17.947	15-03-08	752	0.41	34.687	0.25
187	-68.797	-17.947	15-03-08	502	0.57	34.69	0.2
187	-68.797	-17.947	15-03-08	402	0.65	34.691	0.16
187	-68.797	-17.947	15-03-08	302	0.75	34.69	0.14
187	-68.797	-17.947	15-03-08	250	0.65	34.677	0.13
187	-68.797	-17.947	15-03-08	200	0.31	34.642	0.13
187	-68.797	-17.947	15-03-08	149	-0.69	34.543	0.24
187	-68.797	-17.947	15-03-08	100	-1.68	34.45	0.10
187	-68.797	-17.947	15-03-08	73	-1.77	34.427	0.08
187	-68.797	-17.947	15-03-08	50	-1.73	34.411	0.10
187	-68.797	-17.947	15-03-08	25	-1.84	33.812	0.06
187	-68.797	-17.947	17-03-08	25	-1.84	33.812	0.13
187	-68.797	-17.947	17-03-08	10	-1.84	33.812	0.06
191	-67.339	-23.621	17-03-08	4799	-0.82	34.645	0.45
191	-67.339	-23.621	17-03-08	4503	-0.77	34.648	0.36
191	-67.339	-23.621	17-03-08	3998	-0.63	34.653	0.56
191	-67.339	-23.621	17-03-08	3000	-0.46	34.658	0.35
191	-67.339	-23.621	17-03-08	2501	-0.36	34.661	0.31
191	-67.339	-23.621	17-03-08	2001	-0.23	34.664	0.28
191	-67.339	-23.621	17-03-08	1749	-0.15	34.667	0.15
191	-67.339	-23.621	17-03-08	1501	-0.05	34.67	0.24
191	-67.339	-23.621	17-03-08	1251	0.05	34.674	0.21
191	-67.339	-23.621	17-03-08	1000	0.17	34.678	0.21
191	-67.339	-23.621	17-03-08	750	0.30	34.683	0.3
191	-67.339	-23.621	17-03-08	500	0.45	34.687	0.24
191	-67.339	-23.621	17-03-08	400	0.51	34.688	0.14

DATA TABLE ANT XXIV/3 Continued

Station	Latitude [°N]	Longitude [°E]	Date	Depth [m]	θ (°C)	Salinity	dFe [nmol/l]
191	-67.339	-23.621	17-03-08	300	0.50	34.681	(0.23)
191	-67.339	-23.621	17-03-08	250	0.48	34.677	0.15
191	-67.339	-23.621	17-03-08	200	0.16	34.645	0.15
191	-67.339	-23.621	17-03-08	149	-0.84	34.554	0.05
191	-67.339	-23.621	17-03-08	100	-1.69	34.477	0.07
191	-67.339	-23.621	17-03-08	74	-1.72	34.463	0.03
191	-67.339	-23.621	18-03-08	50	-1.75	34.279	0.10
191	-67.339	-23.621	18-03-08	9	-1.85	34.135	0.05
193	-66.606	-27.185	18-03-08	4800	-0.83	34.644	(0.55)
193	-66.606	-27.185	18-03-08	4799	-0.83	34.644	0.44
193	-66.606	-27.185	18-03-08	3999	-0.63	34.653	0.37
193	-66.606	-27.185	18-03-08	2997	-0.46	34.658	0.38
193	-66.606	-27.185	18-03-08	2500	-0.36	34.661	0.35
193	-66.606	-27.185	18-03-08	2001	-0.24	34.664	0.35
193	-66.606	-27.185	18-03-08	1750	-0.16	34.667	0.24
193	-66.606	-27.185	18-03-08	1498	-0.06	34.67	0.25
193	-66.606	-27.185	18-03-08	1251	0.04	34.673	0.27
193	-66.606	-27.185	18-03-08	1000	0.16	34.678	0.26
193	-66.606	-27.185	18-03-08	753	0.29	34.682	0.24
193	-66.606	-27.185	18-03-08	501	0.45	34.687	0.38
193	-66.606	-27.185	18-03-08	400	0.47	34.685	0.36
193	-66.606	-27.185	18-03-08	301	0.40	34.676	0.25
193	-66.606	-27.185	18-03-08	201	-0.28	34.611	0.19
193	-66.606	-27.185	18-03-08	151	-1.52	34.507	0.24
193	-66.606	-27.185	18-03-08	102	-1.75	34.477	0.08
193	-66.606	-27.185	18-03-08	50	-1.65	34.133	0.06
193	-66.606	-27.185	21-03-08	24	-1.67	34.129	0.10
193	-66.606	-27.185	21-03-08	9	-1.68	34.129	0.17
198	-65.614	-36.398	21-03-08	4702	-0.86	34.642	0.30
198	-65.614	-36.398	21-03-08	4500	-0.79	34.647	0.27
198	-65.614	-36.398	21-03-08	4000	-0.65	34.652	0.28
198	-65.614	-36.398	21-03-08	3499	-0.57	34.655	0.29
198	-65.614	-36.398	21-03-08	2998	-0.48	34.657	0.32
198	-65.614	-36.398	21-03-08	2500	-0.39	34.66	0.31
198	-65.614	-36.398	21-03-08	2000	-0.26	34.664	0.16
198	-65.614	-36.398	21-03-08	1749	-0.18	34.666	0.18
198	-65.614	-36.398	21-03-08	1500	-0.08	34.669	0.15
198	-65.614	-36.398	21-03-08	1249	0.02	34.672	0.15
198	-65.614	-36.398	21-03-08	1000	0.14	34.677	0.16
198	-65.614	-36.398	21-03-08	749	0.27	34.682	(0.25)
198	-65.614	-36.398	21-03-08	500	0.40	34.685	0.11
198	-65.614	-36.398	21-03-08	401	0.38	34.68	0.06
198	-65.614	-36.398	21-03-08	300	0.23	34.666	0.04
198	-65.614	-36.398	21-03-08	200	0.24	34.667	0.10
198	-65.614	-36.398	21-03-08	149	-0.75	34.577	0.14
198	-65.614	-36.398	21-03-08	99	-1.73	34.505	0.04
198	-65.614	-36.398	21-03-08	74	-1.63	34.451	0.04
198	-65.614	-36.398	23-03-08	49	-1.42	34.167	0.04

DATA TABLE ANT XXIV/3 Continued

Station	Latitude [°N]	Longitude [°E]	Date	Depth [m]	θ (°C)	Salinity	dFe [nmol/l]
198	-65.614	-36.398	23-03-08	25	-1.45	34.161	0.06
204	-64.790	-42.858	23-03-08	3996	-0.66	34.652	0.61
204	-64.790	-42.858	23-03-08	3495	-0.58	34.654	0.27
204	-64.790	-42.858	23-03-08	2995	-0.49	34.657	0.38
204	-64.790	-42.858	23-03-08	2501	-0.39	34.66	0.29
204	-64.790	-42.858	23-03-08	2001	-0.27	34.663	0.2
204	-64.790	-42.858	23-03-08	1751	-0.19	34.665	0.2
204	-64.790	-42.858	23-03-08	1501	-0.10	34.668	0.13
204	-64.790	-42.858	23-03-08	1253	0.01	34.672	0.15
204	-64.790	-42.858	23-03-08	1004	0.12	34.676	0.12
204	-64.790	-42.858	23-03-08	756	0.25	34.68	0.16
204	-64.790	-42.858	23-03-08	502	0.36	34.682	0.2
204	-64.790	-42.858	23-03-08	401	0.26	34.672	0.12
204	-64.790	-42.858	23-03-08	301	0.17	34.663	0.14
204	-64.790	-42.858	23-03-08	250	0.18	34.663	0.11
204	-64.790	-42.858	23-03-08	199	0.00	34.647	0.14
204	-64.790	-42.858	23-03-08	151	-1.36	34.537	(1.30)
204	-64.790	-42.858	23-03-08	100	-1.79	34.504	0.06
204	-64.790	-42.858	23-03-08	75	-1.79	34.494	0.04
204	-64.790	-42.858	23-03-08	50	-1.72	34.469	0.10
204	-64.790	-42.858	25-03-08	30	-1.78	33.916	0.02
204	-64.790	-42.858	25-03-08	25	-1.78	33.916	0.03
210	-64.037	-48.278	25-03-08	3946	-0.82	34.633	0.69
210	-64.037	-48.278	25-03-08	3500	-0.50	34.656	0.45
210	-64.037	-48.278	25-03-08	2999	-0.41	34.659	0.44
210	-64.037	-48.278	25-03-08	2500	-0.32	34.661	0.33
210	-64.037	-48.278	25-03-08	2000	-0.17	34.666	0.27
210	-64.037	-48.278	25-03-08	1749	-0.08	34.669	0.33
210	-64.037	-48.278	25-03-08	1501	0.02	34.672	0.32
210	-64.037	-48.278	25-03-08	1000	0.26	34.681	0.33
210	-64.037	-48.278	25-03-08	750	0.40	34.686	0.25
210	-64.037	-48.278	25-03-08	500	0.38	34.674	0.23
210	-64.037	-48.278	25-03-08	350	0.39	34.671	0.19
210	-64.037	-48.278	25-03-08	249	0.47	34.674	(0.35)
210	-64.037	-48.278	25-03-08	200	0.19	34.649	0.18
210	-64.037	-48.278	25-03-08	150	-0.15	34.618	0.19
210	-64.037	-48.278	25-03-08	99	-1.14	34.533	0.08
210	-64.037	-48.278	25-03-08	49	-1.59	34.372	0.07
210	-64.037	-48.278	25-03-08	30	-1.71	34.022	0.12
210	-64.037	-48.278	26-03-08	25	-1.83	33.739	0.13
210	-64.037	-48.278	26-03-08	8	-1.81	33.738	0.16
212	-63.894	-49.079	26-03-08	400	0.48	34.671	0.34
212	-63.894	-49.079	26-03-08	201	-0.60	34.548	0.39
212	-63.894	-49.079	26-03-08	101	-1.82	34.434	0.26
212	-63.894	-49.079	27-03-08	50	-1.77	34.275	0.27
212	-63.894	-49.079	27-03-08	20	-1.77	34.173	0.33
216	-63.699	-50.845	27-03-08	2451	-1.26	34.607	0.30
216	-63.699	-50.845	27-03-08	2397	-1.18	34.61	0.29

DATA TABLE ANT XXIV/3 Continued

Station	Latitude [°N]	Longitude [°E]	Date	Depth [m]	θ (°C)	Salinity	dFe [nmol/l]
216	-63.699	-50.845	27-03-08	2397	-1.18	34.61	0.32
216	-63.699	-50.845	27-03-08	1999	-0.29	34.657	0.27
216	-63.699	-50.845	27-03-08	1750	-0.12	34.664	0.35
216	-63.699	-50.845	27-03-08	1500	0.03	34.669	0.23
216	-63.699	-50.845	27-03-08	1250	0.17	34.674	0.31
216	-63.699	-50.845	27-03-08	1000	0.33	34.679	0.29
216	-63.699	-50.845	27-03-08	749	0.48	34.682	0.21
216	-63.699	-50.845	27-03-08	500	0.47	34.669	0.15
216	-63.699	-50.845	27-03-08	399	0.42	34.653	0.14
216	-63.699	-50.845	27-03-08	300	-0.01	34.599	0.21
216	-63.699	-50.845	27-03-08	200	-1.48	34.458	0.09
216	-63.699	-50.845	27-03-08	150	-1.81	34.436	0.05
216	-63.699	-50.845	27-03-08	100	-1.81	34.427	0.10
216	-63.699	-50.845	27-03-08	74	-1.81	34.415	0.02
216	-63.699	-50.845	27-03-08	50	-1.81	34.27	0.11
216	-63.699	-50.845	27-03-08	40	-1.83	34.2	0.01
216	-63.699	-50.845	28-03-08	25	-1.85	34.135	0.01
216	-63.699	-50.845	28-03-08	10	-1.86	34.093	0.01
221	-63.401	-52.543	28-03-08	491	-0.75	34.591	0.87
221	-63.401	-52.543	28-03-08	479	-0.76	34.592	0.69
221	-63.401	-52.543	28-03-08	249	-1.23	34.507	0.99
221	-63.401	-52.543	29-03-08	99	-1.60	34.363	0.61
221	-63.401	-52.543	29-03-08	20	-1.83	34.138	1.48
222	-63.354	-52.847	29-03-08	425	-0.76	34.58	0.64
222	-63.354	-52.847	29-03-08	414	-0.76	34.58	0.69
222	-63.354	-52.847	29-03-08	404	-0.76	34.58	0.65
222	-63.354	-52.847	29-03-08	395	-0.76	34.58	0.69
222	-63.354	-52.847	29-03-08	385	-0.77	34.579	0.72
222	-63.354	-52.847	29-03-08	375	-0.78	34.577	0.77
222	-63.354	-52.847	29-03-08	365	-0.79	34.575	0.81
222	-63.354	-52.847	29-03-08	355	-0.80	34.573	0.66
222	-63.354	-52.847	29-03-08	345	-0.82	34.571	0.59
222	-63.354	-52.847	29-03-08	335	-0.84	34.568	0.62
222	-63.354	-52.847	29-03-08	300	-0.87	34.559	0.58
222	-63.354	-52.847	29-03-08	274	-0.86	34.547	0.60
222	-63.354	-52.847	29-03-08	250	-0.90	34.536	0.60
222	-63.354	-52.847	29-03-08	222	-1.01	34.522	0.56
222	-63.354	-52.847	29-03-08	200	-1.03	34.517	0.35
222	-63.354	-52.847	29-03-08	175	-1.22	34.489	0.12
222	-63.354	-52.847	29-03-08	150	-1.36	34.464	0.57
222	-63.354	-52.847	29-03-08	125	-1.51	34.424	0.74
222	-63.354	-52.847	29-03-08	100	-1.58	34.371	0.52
222	-63.354	-52.847	29-03-08	75	-1.51	34.316	0.24
222	-63.354	-52.847	29-03-08	50	-1.82	34.099	0.11
222	-63.354	-52.847	29-03-08	30	-1.81	34.08	0.08
223	-63.285	-53.237	29-03-08	416	-0.90	34.558	1.30
223	-63.285	-53.237	29-03-08	406	-0.90	34.559	1.35
223	-63.285	-53.237	29-03-08	394	-0.90	34.559	1.41

DATA TABLE ANT XXIV/3 Continued

Station	Latitude [°N]	Longitude [°E]	Date	Depth [m]	θ (°C)	Salinity	dFe [nmol/l]
223	-63.285	-53.237	01-04-08	384	-0.90	34.559	0.71
223	-63.285	-53.237	01-04-08	30	-1.82	34.18	0.89
226	-60.627	-53.830	01-04-08	898	0.80	34.687	1.04
226	-60.627	-53.830	01-04-08	750	0.78	34.674	0.87
226	-60.627	-53.830	01-04-08	582	0.58	34.626	1.36
226	-60.627	-53.830	01-04-08	551	0.71	34.631	0.91
226	-60.627	-53.830	01-04-08	501	0.77	34.621	0.91
226	-60.627	-53.830	01-04-08	447	0.79	34.612	(1.75)
226	-60.627	-53.830	01-04-08	401	0.69	34.57	1.40
226	-60.627	-53.830	01-04-08	354	0.64	34.546	1.63
226	-60.627	-53.830	01-04-08	300	0.46	34.499	1.49
226	-60.627	-53.830	01-04-08	275	0.42	34.476	1.35
226	-60.627	-53.830	01-04-08	250	0.35	34.459	1.47
226	-60.627	-53.830	01-04-08	223	0.32	34.442	1.78
226	-60.627	-53.830	01-04-08	200	0.35	34.422	1.57
226	-60.627	-53.830	01-04-08	175	0.38	34.4	1.25
226	-60.627	-53.830	01-04-08	148	0.46	34.369	0.95
226	-60.627	-53.830	01-04-08	127	0.49	34.361	1.43
226	-60.627	-53.830	01-04-08	99	0.56	34.336	1.15
226	-60.627	-53.830	01-04-08	80	0.62	34.323	0.98
226	-60.627	-53.830	01-04-08	60	0.63	34.322	1.12
226	-60.627	-53.830	01-04-08	53	0.63	34.321	1.09
226	-60.627	-53.830	01-04-08	40	0.63	34.321	1.19
226	-60.627	-53.830	01-04-08	28	0.63	34.32	1.12
226	-60.627	-53.830	03-04-08	20	0.63	34.321	1.84
226	-60.627	-53.830	03-04-08	9	0.63	34.321	1.28
230	-60.101	-55.275	03-04-08	3422	-0.26	34.658	0.65
230	-60.101	-55.275	03-04-08	3167	-0.16	34.662	0.6
230	-60.101	-55.275	03-04-08	2999	-0.11	34.664	0.75
230	-60.101	-55.275	03-04-08	2499	0.29	34.696	0.41
230	-60.101	-55.275	03-04-08	1998	0.62	34.708	0.35
230	-60.101	-55.275	03-04-08	1748	0.77	34.713	0.42
230	-60.101	-55.275	03-04-08	1501	0.95	34.718	0.44
230	-60.101	-55.275	03-04-08	1252	1.14	34.723	0.42
230	-60.101	-55.275	03-04-08	1000	1.36	34.727	(0.57)
230	-60.101	-55.275	03-04-08	750	1.55	34.722	0.41
230	-60.101	-55.275	03-04-08	600	1.74	34.715	0.40
230	-60.101	-55.275	03-04-08	498	1.79	34.692	0.41
230	-60.101	-55.275	03-04-08	399	1.91	34.674	0.39
230	-60.101	-55.275	03-04-08	353	1.93	34.654	0.58
230	-60.101	-55.275	03-04-08	300	1.55	34.592	0.64
230	-60.101	-55.275	03-04-08	249	0.26	34.44	1.03
230	-60.101	-55.275	03-04-08	199	0.33	34.405	1.32
230	-60.101	-55.275	03-04-08	148	0.48	34.349	1.86
230	-60.101	-55.275	03-04-08	96	0.60	34.309	2.22
230	-60.101	-55.275	03-04-08	75	0.61	34.301	1.94
230	-60.101	-55.275	03-04-08	49	0.83	34.133	1.13
230	-60.101	-55.275	05-04-08	23	1.29	33.923	0.21

DATA TABLE ANT XXIV/3 Continued

Station	Latitude [°N]	Longitude [°E]	Date	Depth [m]	θ (°C)	Salinity	dFe [nmol/l]
230	-60.101	-55.275	05-04-08	24	1.32	33.91	0.23
236	-58.970	-58.140	05-04-08	3500	-0.21	34.66	1.42
236	-58.970	-58.140	05-04-08	3198	-0.13	34.663	0.69
236	-58.970	-58.140	05-04-08	2797	0.04	34.672	0.57
236	-58.970	-58.140	05-04-08	2498	0.22	34.682	0.60
236	-58.970	-58.140	05-04-08	2251	0.39	34.691	0.49
236	-58.970	-58.140	05-04-08	1999	0.53	34.698	0.48
236	-58.970	-58.140	05-04-08	1748	0.68	34.701	0.46
236	-58.970	-58.140	05-04-08	1500	0.85	34.706	0.58
236	-58.970	-58.140	05-04-08	1251	1.07	34.712	0.43
236	-58.970	-58.140	05-04-08	1004	1.28	34.71	(0.67)
236	-58.970	-58.140	05-04-08	750	1.48	34.7	0.51
236	-58.970	-58.140	05-04-08	596	1.53	34.667	0.50
236	-58.970	-58.140	05-04-08	499	1.64	34.657	0.78
236	-58.970	-58.140	05-04-08	397	1.69	34.63	0.40
236	-58.970	-58.140	05-04-08	300	1.63	34.575	0.57
236	-58.970	-58.140	05-04-08	247	1.17	34.473	0.68
236	-58.970	-58.140	05-04-08	200	1.10	34.406	0.45
236	-58.970	-58.140	05-04-08	118	0.65	34.169	0.18
236	-58.970	-58.140	05-04-08	99	1.03	34.073	0.11
236	-58.970	-58.140	05-04-08	74	2.31	33.92	0.07
236	-58.970	-58.140	06-04-08	49	2.50	33.889	0.06
236	-58.970	-58.140	06-04-08	24	2.49	33.886	0.18
238	-58.300	-59.479	06-04-08	2953	0.37	34.697	0.59
238	-58.300	-59.479	06-04-08	2900	0.40	34.699	0.56
238	-58.300	-59.479	06-04-08	2748	0.45	34.7	0.53
238	-58.300	-59.479	06-04-08	2500	0.52	34.699	0.43
238	-58.300	-59.479	06-04-08	2249	0.64	34.705	0.53
238	-58.300	-59.479	06-04-08	1999	0.85	34.712	0.49
238	-58.300	-59.479	06-04-08	1749	0.51	34.65	(0.76)
238	-58.300	-59.479	06-04-08	1499	1.15	34.711	0.53
238	-58.300	-59.479	06-04-08	1248	1.38	34.723	0.42
238	-58.300	-59.479	06-04-08	1002	1.57	34.717	0.39
238	-58.300	-59.479	06-04-08	749	1.83	34.708	0.27
238	-58.300	-59.479	06-04-08	599	1.99	34.683	0.25
238	-58.300	-59.479	06-04-08	500	2.05	34.661	0.34
238	-58.300	-59.479	06-04-08	402	2.08	34.619	0.41
238	-58.300	-59.479	06-04-08	300	1.84	34.512	0.23
238	-58.300	-59.479	06-04-08	250	1.47	34.426	0.13
238	-58.300	-59.479	06-04-08	202	1.01	34.322	(0.52)
238	-58.300	-59.479	06-04-08	151	-0.12	34.163	0.04
238	-58.300	-59.479	06-04-08	102	1.36	33.861	0.01
238	-58.300	-59.479	06-04-08	77	2.17	33.774	0.01
238	-58.300	-59.479	06-04-08	49	2.20	33.773	0.02
238	-58.300	-59.479	06-04-08	40	2.22	33.771	0.02
238	-58.300	-59.479	07-04-08	26	2.23	33.769	0.29
238	-58.300	-59.479	07-04-08	9	2.26	33.768	1.32
241	-57.628	-60.898	07-04-08	3350	0.44	34.698	0.35

DATA TABLE ANT XXIV/3 Continued

Station	Latitude [°N]	Longitude [°E]	Date	Depth [m]	θ (°C)	Salinity	dFe [nmol/l]
241	-57.628	-60.898	07-04-08	3224	0.51	34.702	0.29
241	-57.628	-60.898	07-04-08	3002	0.51	34.702	0.30
241	-57.628	-60.898	07-04-08	2797	0.71	34.711	0.51
241	-57.628	-60.898	07-04-08	2500	0.90	34.716	0.72
241	-57.628	-60.898	07-04-08	2251	1.06	34.72	0.55
241	-57.628	-60.898	07-04-08	1999	1.26	34.724	0.52
241	-57.628	-60.898	07-04-08	1750	1.42	34.726	0.46
241	-57.628	-60.898	07-04-08	1499	1.63	34.725	0.30
241	-57.628	-60.898	07-04-08	1249	1.85	34.712	0.30
241	-57.628	-60.898	07-04-08	999	2.03	34.68	0.35
241	-57.628	-60.898	07-04-08	751	2.13	34.604	0.24
241	-57.628	-60.898	07-04-08	481	2.23	34.471	0.20
241	-57.628	-60.898	07-04-08	401	2.03	34.392	0.15
241	-57.628	-60.898	07-04-08	301	1.82	34.296	0.09
241	-57.628	-60.898	07-04-08	251	1.35	34.202	(0.24)
241	-57.628	-60.898	07-04-08	199	1.35	34.202	0.10
241	-57.628	-60.898	07-04-08	150	0.24	34.034	0.05
241	-57.628	-60.898	07-04-08	100	1.32	33.865	0.07
241	-57.628	-60.898	07-04-08	85	2.25	33.82	0.14
241	-57.628	-60.898	07-04-08	75	2.43	33.812	0.06
241	-57.628	-60.898	07-04-08	50	2.70	33.795	0.19
241	-57.628	-60.898	09-04-08	25	2.86	33.794	0.38
241	-57.628	-60.898	09-04-08	10	2.88	33.794	0.15
244	-56.919	-62.392	09-04-08	4002	0.48	34.699	0.33
244	-56.919	-62.392	09-04-08	3749	0.62	34.707	0.36
244	-56.919	-62.392	09-04-08	3501	0.69	34.71	0.39
244	-56.919	-62.392	09-04-08	2998	0.93	34.716	0.51
244	-56.919	-62.392	09-04-08	2497	1.30	34.725	0.41
244	-56.919	-62.392	09-04-08	1998	1.75	34.719	0.39
244	-56.919	-62.392	09-04-08	1749	1.75	34.719	0.45
244	-56.919	-62.392	09-04-08	1499	2.09	34.666	0.41
244	-56.919	-62.392	09-04-08	1250	2.26	34.617	0.52
244	-56.919	-62.392	09-04-08	1000	2.47	34.513	0.34
244	-56.919	-62.392	09-04-08	748	2.73	34.398	0.69
244	-56.919	-62.392	09-04-08	502	3.08	34.22	0.51
244	-56.919	-62.392	09-04-08	399	3.15	34.133	0.24
244	-56.919	-62.392	09-04-08	299	3.28	34.079	0.15
244	-56.919	-62.392	09-04-08	250	3.35	34.05	0.19
244	-56.919	-62.392	09-04-08	200	3.64	34.055	0.13
244	-56.919	-62.392	09-04-08	147	3.82	34.049	0.13
244	-56.919	-62.392	09-04-08	100	4.48	33.989	0.11
244	-56.919	-62.392	09-04-08	73	5.24	33.929	0.09
244	-56.919	-62.392	09-04-08	50	5.37	33.924	0.19
244	-56.919	-62.392	09-04-08	38	5.46	33.926	0.15
244	-56.919	-62.392	10-04-08	24	5.43	33.909	0.06
244	-56.919	-62.392	10-04-08	9	5.43	33.91	0.05
249	-56.119	-63.757	10-04-08	4253	0.35	34.692	1.00
249	-56.119	-63.757	10-04-08	4001	0.36	34.692	0.60

DATA TABLE ANT XXIV/3 Continued

Station	Latitude [°N]	Longitude [°E]	Date	Depth [m]	θ (°C)	Salinity	dFe [nmol/l]
249	-56.119	-63.757	10-04-08	3699	0.48	34.699	0.50
249	-56.119	-63.757	10-04-08	3497	0.57	34.703	0.43
249	-56.119	-63.757	10-04-08	2999	0.89	34.715	0.45
249	-56.119	-63.757	10-04-08	2498	1.30	34.725	0.91
249	-56.119	-63.757	10-04-08	1998	1.68	34.715	0.82
249	-56.119	-63.757	10-04-08	1749	1.79	34.708	0.61
249	-56.119	-63.757	10-04-08	1501	1.96	34.687	(0.93)
249	-56.119	-63.757	10-04-08	1250	2.18	34.639	0.27
249	-56.119	-63.757	10-04-08	1000	2.35	34.562	0.27
249	-56.119	-63.757	10-04-08	500	2.51	34.228	0.37
249	-56.119	-63.757	10-04-08	400	2.50	34.158	0.21
249	-56.119	-63.757	10-04-08	300	2.61	34.113	0.20
249	-56.119	-63.757	10-04-08	249	2.32	34.03	0.08
249	-56.119	-63.757	10-04-08	200	2.70	34.029	0.10
249	-56.119	-63.757	10-04-08	148	2.89	33.991	0.20
249	-56.119	-63.757	10-04-08	101	4.07	33.903	0.09
249	-56.119	-63.757	10-04-08	74	4.46	33.875	0.04
249	-56.119	-63.757	10-04-08	59	4.56	33.87	0.17
249	-56.119	-63.757	10-04-08	39	4.56	33.87	0.09
249	-56.119	-63.757	11-04-08	24	4.56	33.87	0.33
249	-56.119	-63.757	11-04-08	9	4.56	33.87	0.07
250	-55.702	-64.424	11-04-08	3725	0.43	34.696	0.70
250	-55.702	-64.424	11-04-08	3600	0.51	34.7	0.36
250	-55.702	-64.424	11-04-08	3299	0.71	34.709	0.34
250	-55.702	-64.424	11-04-08	3000	0.98	34.718	0.82
250	-55.702	-64.424	11-04-08	2749	1.16	34.721	0.86
250	-55.702	-64.424	11-04-08	2499	1.34	34.723	1.50
250	-55.702	-64.424	11-04-08	2200	1.57	34.718	1.94
250	-55.702	-64.424	11-04-08	2003	1.71	34.712	0.41
250	-55.702	-64.424	11-04-08	1601	2.03	34.682	0.37
250	-55.702	-64.424	11-04-08	1251	2.27	34.597	0.28
250	-55.702	-64.424	11-04-08	1000	2.51	34.505	(0.96)
250	-55.702	-64.424	11-04-08	901	2.57	34.456	0.41
250	-55.702	-64.424	11-04-08	701	2.81	34.346	0.50
250	-55.702	-64.424	11-04-08	500	2.98	34.191	0.63
250	-55.702	-64.424	11-04-08	400	2.90	34.116	0.52
250	-55.702	-64.424	11-04-08	302	3.22	34.063	0.21
250	-55.702	-64.424	11-04-08	200	3.42	34.039	0.08
250	-55.702	-64.424	11-04-08	150	3.63	34.017	0.10
250	-55.702	-64.424	11-04-08	100	4.74	33.92	0.04
250	-55.702	-64.424	11-04-08	74	5.07	33.896	(0.62)
250	-55.702	-64.424	11-04-08	59	5.08	33.896	0.14
250	-55.702	-64.424	11-04-08	39	5.10	33.896	(0.47)
250	-55.702	-64.424	12-04-08	26	5.10	33.896	0.16
250	-55.702	-64.424	12-04-08	10	5.10	33.896	(3.78)
251	-55.333	-65.176	12-04-08	1549	2.45	34.555	0.44
251	-55.333	-65.176	12-04-08	1476	2.45	34.556	0.38
251	-55.333	-65.176	12-04-08	1400	2.45	34.555	0.24

DATA TABLE ANT XXIV/3 Continued

Station	Latitude [°N]	Longitude [°E]	Date	Depth [m]	θ (°C)	Salinity	dFe [nmol/l]
251	-55.333	-65.176	12-04-08	1298	2.51	34.535	0.48
251	-55.333	-65.176	12-04-08	1199	2.62	34.501	0.24
251	-55.333	-65.176	12-04-08	1100	2.71	34.472	0.43
251	-55.333	-65.176	12-04-08	898	2.99	34.385	0.24
251	-55.333	-65.176	12-04-08	794	3.09	34.318	0.16
251	-55.333	-65.176	12-04-08	693	3.46	34.295	0.13
251	-55.333	-65.176	12-04-08	589	3.79	34.257	0.29
251	-55.333	-65.176	12-04-08	506	4.11	34.208	0.39
251	-55.333	-65.176	12-04-08	404	4.36	34.128	0.14
251	-55.333	-65.176	12-04-08	349	4.57	34.132	0.42
251	-55.333	-65.176	12-04-08	298	4.76	34.132	0.13
251	-55.333	-65.176	12-04-08	249	4.92	34.139	0.20
251	-55.333	-65.176	12-04-08	201	5.02	34.141	(0.04)
251	-55.333	-65.176	12-04-08	150	5.15	34.144	0.12
251	-55.333	-65.176	12-04-08	100	5.42	33.968	0.03
251	-55.333	-65.176	12-04-08	79	5.45	33.951	0.02
251	-55.333	-65.176	12-04-08	59	5.45	33.951	0.26
251	-55.333	-65.176	12-04-08	38	5.45	33.951	0.20
251	-55.333	-65.176	12-04-08	25	5.45	33.95	0.08
251	-55.333	-65.176	12-04-08	9	5.45	33.95	0.24
252	-55.128	-65.532	12-04-08	376	4.91	34.145	0.14
252	-55.128	-65.532	12-04-08	350	5.02	34.14	0.10
252	-55.128	-65.532	12-04-08	324	5.12	34.137	0.14
252	-55.128	-65.532	12-04-08	299	5.21	34.135	0.10
252	-55.128	-65.532	12-04-08	277	5.30	34.129	0.11
252	-55.128	-65.532	12-04-08	251	5.62	34.107	0.10
252	-55.128	-65.532	12-04-08	225	6.03	34.079	0.05
252	-55.128	-65.532	12-04-08	201	6.57	34.041	0.21
252	-55.128	-65.532	12-04-08	159	6.90	34.005	0.14
252	-55.128	-65.532	12-04-08	140	7.19	33.978	0.17
252	-55.128	-65.532	12-04-08	122	7.80	33.896	0.18
252	-55.128	-65.532	12-04-08	100	8.13	33.849	0.25
252	-55.128	-65.532	12-04-08	90	8.20	33.827	0.20
252	-55.128	-65.532	12-04-08	79	8.29	33.761	0.44
252	-55.128	-65.532	12-04-08	70	8.32	33.743	0.15
252	-55.128	-65.532	12-04-08	59	8.33	33.723	0.10
252	-55.128	-65.532	12-04-08	49	8.42	33.665	0.23
252	-55.128	-65.532	12-04-08	39	8.78	33.537	0.43
252	-55.128	-65.532	08-03-08	23	9.18	33.114	1.00
252	-55.128	-65.532	08-03-08	10	9.11	32.784	2.64
Surface-1	-66.055	0.0	08-03-08	1			0.22
Surface-2	-66.251	0.0	09-03-08	1			0.21
Surface-3	-66.409	0.0	09-03-08	1			0.12
Surface-4	-66.583	0.0	09-03-08	1			0.67
Surface-5	-66.720	0.0	09-03-08	1			0.10
Surface-6	-66.875	0.0	09-03-08	1			0.19
Surface-7	-67.025	0.0	09-03-08	1			0.11
Surface-8	-67.155	0.0	09-03-08	1			0.33

DATA TABLE ANT XXIV/3 *Continued*

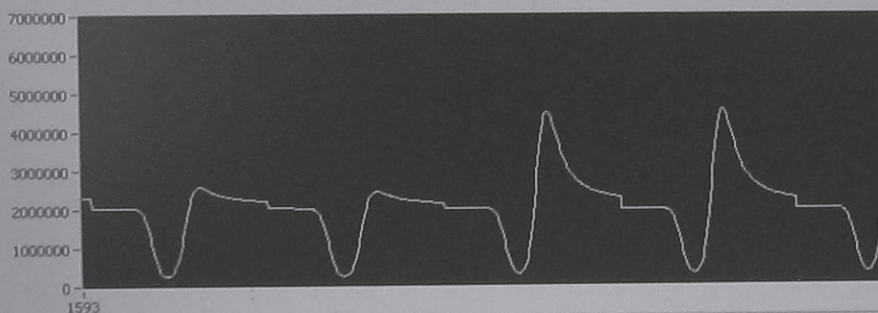
Station	Latitude [°N]	Longitude [°E]	Date	Depth [m]	θ (°C)	Salinity	dFe [nmol/l]
Surface-9	-67.272	0.0	10-03-08	1			0.12
Surface-10	-67.392	0.0	10-03-08	1			0.11
Surface-11	-67.597	0.0	10-03-08	1			0.15
Surface-12	-67.767	0.0	10-03-08	1			0.13
Surface-13	-67.914	0.0	10-03-08	1			0.25
Surface-14	-68.000	0.0	10-03-08	1			0.73
Surface-15	-68.250	0.0	10-03-08	1			0.28
Surface-16	-68.500	0.0	10-03-08	1			0.34
Surface-17	-68.514	0.0	10-03-08	1			0.13
Surface-18	-68.638	0.0	10-03-08	1			0.12
Surface-19	-69.258	0.0	10-03-08	1			0.15
Surface-20	-69.340	0.0	12-03-08	1			0.20
Surface-21	-69.507	0.0	12-03-08	1			0.21
Surface-22	-69.588	0.0	12-03-08	1			0.25
Surface-23	-69.586	0.0	12-03-08	1			0.15
Surface-24	-69.586	0.0	12-03-08	1			0.26

Trace-o-matic V2.02

Recipe

Insert Delete Save Load

	Monster	Load Time	Rinse Time	Inject Time	Sample name
1	1	10	60	150	0
2	1	10	60	150	0
3	1	10	60	150	0
4	1	120	60	150	0
5	1	120	60	150	0
6	2	120	60	150	0.15
7	2	120	60	150	0.15
8	3	120	60	150	0.30
9	3	120	60	150	0.30
10	4	120	60	150	0.30



Status

Load 105 sec Rinse 0 sec Inject 0 sec

Date: Tuesday, August 21, 2007 Selected sensor: Hamamatsu HC135 Integral: 70636739 Peak height: 5112144

Slide 7 of 15

Default Design

English (U.S.)

start

2 LabVIEW D...

Untitled - Note...

Microsoft Pow...

Desktop

DELL

Samenvatting



Samenvatting

Introductie

Fotosynthese, het proces waarbij koolstofdioxide en water met behulp van zonlicht worden omgezet in organische verbindingen is het belangrijkste proces voor fotoautotrofe organismen om te groeien. In de Oceaan bestaan fotoautotrofe, cellen die nutrienten omzetten met behulp van licht, organismen voor een groot deel uit eencelligen planten, fytoplankton (algen) genaamd. Deze algen staan aan de basis van de voedselketen in de oceaan, en zijn daarmee van wezenlijk belang voor het leven in de wereldzeeën. Dit proces van fotosynthese samen met andere essentiële processen in de cel, vereist verschillende chemische bouwstenen, waaronder koolstof. Tijdens de evolutie in de oceaan, zijn de destijds meest aanwezige en best beschikbare elementen het belangrijkste geworden voor groei; voor algen zijn dit met name stikstof (N) en fosfaat (P). Daarnaast zijn er nog elementen in kleinere hoeveelheden essentieel voor de groei van algen, de spoormetalen. Deze groep van zes metalen (mangaan (Mn), ijzer (Fe), cobalt (Co), nikkel (Ni), koper (Cu) en zink(Zn)) is onmisbaar voor omzettingprocessen in de cel. Met name ijzer is geschikt voor opslag, transport en het overbrengen van energie binnen de cel, het vastleggen van stikstof en een aantal andere belangrijke processen. Tijdens de evolutie van de aarde, 3.8-2.5 miljard jaar geleden was ijzer oplosbaar en er was een aanzienlijke hoeveelheid opgelost ijzer aanwezig als Fe^{2+} in de Oceanen. Echter, met het proces van fotosynthese kwam er meer en meer vrij zuurstof in de oceanen. Vanaf ongeveer 1 miljard jaar geleden reageerde dit vrije zuurstof op grote schaal met het ijzer (Fe(II)) en werden grote hoeveelheden ijzeroxiden gevormd en afgezet. Toen er geen Fe(II) meer beschikbaar was, leidde dat tot een toename van zuurstof in de atmosfeer en Oceaan. Daarnaast was het beschikbare ijzer in de oceaan veranderd van goed oplosbaar Fe(II) , dat in voldoende mate aanwezig was naar slecht oplosbaar Fe(III) , slechts aanwezig in hele lage (nanomolair) concentraties. Deze extreem lage concentratie van ijzer in de moderne oceaan is het onderwerp van dit proefschrift.

Al in 1934 viel het *Hart* op dat de fytoplankton concentraties rond South Georgia aanzienlijk hoger waren dan in andere delen van de Zuidelijke Ocean. Hij vermeldde: "...Een van de chemische elementen in zeewater...mogelijk limiterend voor fytoplanktongroei, zou zeker ijzer kunnen zijn (...) waarbij het land gezien kan worden als bron...". De extreem lage concentratie van ijzer in de oceaan maakte het echter moeilijk deze hypothese te testen. Het was pas in 1988 toen *John Martin* en collega's in experimenten groei van fytoplankton waarnamen na het toevoegen van ijzer aan SubArctisch Stille Oceaan water. In de vervolgens opgestelde "*ijzer hypothese*" werd gesteld dat ijzer depositie in de oceaan tijdens het laatste glaciële maximum (LGM) de ijzerstress van de algen wegnam, waardoor de algengroei enorm is toegenomen en veel koolstofdioxide uit de lucht in de Oceaan heeft vastgelegd, waardoor vervol-

gens de temperatuur afnam. In de jaren daarna, zorgden de ontwikkeling van schone monsternamen en analysetechnieken voor een veel beter begrip van de distributie en bronnen van ijzer in de oceanen.

In de oppervlakte wateren zijn de belangrijkste bronnen van ijzer depositie van stof door neerslag in de Oceaan, uitstromend rivier water en het vrijkomen van ijzer na gereduceerde condities op de suboxische oceaan bodem. Daarnaast is aanvoer vanaf de diepere oceaan erg belangrijk; door menging met en advectie van diepere wateren met hogere ijzerconcentraties wordt de concentratie in de oppervlakte wateren verhoogd. In de diepe wateren is er ook aanvoer van hydrothermale bronnen. IJzer wordt verwijderd uit de oceaan door biologische opname en vervolgens uitzinking, en ook door het invangen van ijzer door niet biologische deeltjes. De kringloop van biologische opname en export uit de oppervlakte wateren naar dieper water, en vervolgens weer de opwelling naar het oppervlaktewater speelt de grootste rol in de verdeling van ijzer in de oceanen.

De poolzeeën

De poolzeeën zijn een onmisbare schakel in de mondiale oceanstromingen, en daarmee, in het mondiale klimaat. Ondanks zijn relatief afgelegen locatie is de Noordelijke IJszee (Arctische Oceaan) een onmisbare schakel in de globale oceaan circulatie. De zware (koude) wateren uit de Arctische Oceaan, stromen in de Atlantische oceaan, alwaar ze de belangrijkste *driver* vormen voor de thermohaliene circulatie, en daarmee voor de golfstroom. Daarnaast speelt de Arctische Oceaan een belangrijke rol in de nutriënten huishouding; het fosfaat overschot in de wateren die vanuit de Arctische Oceaan in de Atlantische Oceaan stromen complementeert de binding van stikstof uit de lucht en reguleert daarmee de stikstof en fosfaat balans in de oceanen. Vanwege de moeilijke meetomstandigheden en het ontoegankelijke klimaat was er voor aanvang van onze expeditie vrijwel niets bekend over de cyclus van spoormetalen in de Arctische Oceaan, en over de ijzerconcentraties in de diepere wateren van de Centrale Arctische Oceaan was zelfs nog helemaal niets bekend.

De Arctische Oceaan wordt gekenmerkt door een grote invloed van rivierwater dat vanuit de grote Siberische en Noordamerikaanse rivieren in de ondiepe zeeën aan de randen van de oceaan stroomt, waardoor het aandeel zoet water erg groot is. Dit zoetwater reikt tot in het midden van de Arctische Oceaan, waardoor er een duidelijke halocliene, een scheiding van waterlagen door verschillende saliniteiten, ontstaat. Deze halocliene en de aanwezigheid van zeeijs, zorgen ervoor dat er nauwelijks menging plaatsvindt, waardoor een belangrijke route voor (spoormetalen) grotendeels geblokkeerd wordt. Deze grote hoeveelheid aan rivier water, de relatief grote rand-zeeën en het slechts mondjesmaat voorkomen van menging bepalen voor een groot deel de cyclus van spoormetalen in de Arctische Oceaan.

De Zuidelijke Oceaan speelt een belangrijke rol in de thermohaliene circulatie. Samengevat stromen de watermassa's op intermediaire diepte van de drie grote oceanen; de Atlantische, Pacifische en Indiase Oceaan, zuidwaarts richting de Zuidelijke Oceaan. Daar wordt het water meegenomen in een stroming rondom Antarctica; de Antarctic Circumpolar Current. In de Atlantische Oceaan is er zowel nabij het zeeoppervlak (Antarctic Intermediate Water; AAIW) als op grote diepte (Antarctic Bottom Water; AABW) een terugstroom vanuit de Zuidelijke Oceaan naar het noorden. Dit mechanisme is een belangrijke *driver* van de thermohaliene circulatie. Daarnaast is het van wezenlijk belang voor de biochemische kringloop van de Zuidelijke Oceaan. De sterke winden rond $\sim 40^\circ\text{S}$ zorgen ervoor dat het oppervlakte water naar het noorden stroomt (Ekman transport), waardoor het diepere water, dat rijk is aan nutriënten naar de oppervlakte kan komen. Omdat dit water naast fosfaat en nitraat ook veel silicaat bevat wordt de fytoplankton gemeenschap in de Zuidelijke Oceaan voor een groot deel gevormd door diatomeeën, die silicaat nodig hebben in hun groei. De hoge concentratie aan nutriënten wordt echter niet volledig opgenomen door het aanwezige fytoplankton. Er moet dus nog een limiterende (groei)factor zijn, en er is verondersteld dat dit (met name) ijzer is. Om deze hypothese te testen zijn er in de afgelopen decennia verschillende experimenten gedaan waarbij ijzer toegevoegd is aan water uit de Zuidelijke Oceaan (of andere gebieden waar water met een hoge nutriëntconcentratie maar relatief lage chlorofylconcentratie voorkomt). Uit deze experimenten blijkt dat inderdaad dat de groei gestimuleerd wordt door het toevoegen van ijzer. Daarnaast blijkt dat de soortensamenstelling van het water verandert; bij het toevoegen van ijzer komen er meer grote diatomeeën voor. Vanwege een ongunstige oppervlakte: volume verhouding kunnen deze grote diatomeeën weinig ijzer opnemen bij lage concentraties.

Hoewel er al gegevens bekend waren over de verdeling en beschikbaarheid van ijzer in de oceaan, is dit onderzoek (met de andere onderzoeken uitgevoerd in het kader van IPY, zie onder) het eerste waarbij systematisch ijzer in kaart gebracht is over de hele diepte van de oceaan over transecten in drie verschillende gebieden. Daarnaast bieden de simultaan genomen monsters van andere chemische, biologische parameters en de beschikbaarheid van fysisch oceanografische data de mogelijkheid de verdeling, herkomst en afname van ijzer in de context van het oceanografische en biologische systeem van de Zuidelijke Oceaan te plaatsen.

IPY GEOTRACES

Dit onderzoek is uitgevoerd in het kader van het "Internationaal Polar Year 2007-2008" (IPY), een internationaal gecoördineerd onderzoeksprogramma waarin de nadruk lag op onderzoek in de polaire gebieden. Daarnaast is dit werk uitgevoerd binnen de scope van het internationale GEOTRACES Programma; een internationaal onderzoeksprogramma binnen de oceanografie dat tot doel heeft;

“Het identificeren en kwantificeren van fluxen die bepalend zijn voor de verdeling van belangrijke spoorelementen en isotopen in de oceaan, en het onderzoeken van de gevoeligheid van deze elementen voor omgevingsveranderingen”

Doordat dit onderzoek is uitgevoerd in het kader van deze onderzoeksprogramma's is het goed mogelijk geweest de data te combineren met andere beschikbare data om tot conclusies te komen. Daarnaast heeft deze dataset van belang kunnen zijn bij het interpreteren van andere data beschikbaar binnen IPY:GEOTRACES.

Opzet van het proefschrift

Hoofdstuk 1 van dit proefschrift geeft een algemene introductie van het onderwerp.

Hoofdstuk 2 van dit proefschrift beschrijft de distributie van ijzer(Fe) in the Kara, Barentsz en Laptev zeeën en de oppervlaktewateren van de Noordelijke IJsee. In de Barentsz Zee en Kara Zee, is opname van ijzer door fytoplankton waargenomen in de laag net onder het oppervlak. Lagere concentraties in de Kara Zee duiden waarschijnlijk op het invangen van ijzer door biologisch materiaal en verwijdering door uitzinken. Uitzonderlijk hoge ijzerconcentraties in de Laptev Zee (2-10 nM) worden toegeschreven aan opwervelend sediment, het zinken van brijn en regeneratie van ijzer. Massabalansen van $\delta^{18}\text{O}$, saliniteit en nutriënten zijn gebruikt om onderscheid te maken tussen het zoetwater van verschillende herkomst; zee-ijs, rivierwater en het saliniteitsdeficiënt van Pacifisch water (wat kan worden gezien als relatief “zoet water” ten opzichte van het zoutere Atlantisch water). Het effect van smeltend zee-ijs is niet erg groot, en beperkt zich vooral tot het Nansen Bassin. De Trans Polar Drift (TDP) brengt rivierwater afkomstig van de Siberische rivieren naar de oppervlaktewateren in het midden van de Noordelijke IJsee (Amundsen en Makarov Basins) en veroorzaakt daarmee hoge (>2 nM) ijzerconcentraties. Twee stations waren duidelijk gelegen aan de Noord Amerikaanse zijde van de TPD ; dit is te zien in een relatief lage ijzer concentratie, die niet bepaald wordt door rivierwater, maar door de gecombineerde effecten van smelten van zee-ijs, biologische opname en remineralisatie processen.

De verdeling van ijzer in de diepe lagen van de Noordelijke IJsee wordt beschreven in **hoofdstuk 3**. Het zee-ijs en de sterke halocliene in de Noordelijke IJsee voorkomen een groot deel van de verticale menging met de bovenste wateren. Daarom speelt laterale aanvoer van ijzer een relatief belangrijke rol. De helling van het continentale plat en de stroom vanuit de Atlantische Oceaan zijn de belangrijkste bronnen van ijzer in het Nansen Bassin op tussenliggende diepte. Een sterk effect van hydrothermale bronnen op de aanvoer van ijzer ($\text{DFe} > 1.5 \text{ nM}$) is te zien in het grootste gedeelte van de Nansen en Amundsen Basins, waarbij concentraties oplopen met het naderen van eerder geïdentificeerde hydrothermale bronnen. Dit laat het belang

zien van hydrothermale bronnen voor de concentratie van ijzer in de diepe Noordelijke IJsee. De afwezigheid van aanvoerbronnen voor ijzer in de diepste (>3000m) Amundsen en Makarov Bassins kan niet volledig gecompenseerd worden door organische complexatie. Dit verklaart de gevonden lineaire relatie met opgelost mangaan, en de erg lage concentratie van ijzer in deze diepe laag.

Hoofdstuk 4 beschrijft de verdeling van opgelost ijzer over een traject langs de nulmeridiaan in de Zuidelijke Oceaan. De belangrijkste bronnen van ijzer naar het oppervlaktewater zijn verticale menging en het opwellen van dieper water. Plaatselijk kunnen ook atmosferische depositie (stof, neerslag) en smeltend zee-ijs belangrijke bronnen zijn. Inverse correlatie tussen ijzer en fluorescentie wijst op biologische opname van ijzer over het zuidelijkste deel van het transect, in de Weddell Zee. De concentratie in de diepere wateren wordt met name bepaald door intrusie van ijzerrijke noordelijke wateren (NADW), hydrothermale bronnen en verwijdering door het uitzinken van deeltjes. In de diepe Weddell Gyre, in de stroom in oostelijke richting, dichtbij het Antarctische continent, is aanzienlijk minder ijzer gevonden dan in de westelijke stroom, verder naar het noorden. Dit duidt op een aanvoer van ijzer vanaf het Antarctisch schiereiland en langs de Mid Ocean Ridge. De extreem lage ijzerconcentraties zo dichtbij het continent zijn uniek; de ijskap voorkomt de normale geobiochemische processen, die bij andere, niet ijsbedekte continentale randen, een toename van ijzer veroorzaken.

De verdeling van ijzer in de Westelijke Weddell Zee en de Drake Passage is het onderwerp van **hoofdstuk 5**. In de Weddell Sea worden zeer lage concentraties ijzer aangetroffen (0.01-0.1 nM). Deze kunnen deels worden verklaard door een hoge export van dood organisch materiaal (afgestorven algen) en primaire productie (zoals af te leiden uit de chlorophyll fluorescentie). De afname van de ratio stikstof:fosfor (N:P) in de Westelijke Weddell Zee is constant (~11) met toenemende ijzerconcentraties in het water, terwijl langs de nulmeridiaan een toename van deze ratio met toenemend ijzer was waargenomen. Dit is toe te schrijven aan het voorkomen van kleinere diatomeeën in de Westelijke Weddell Zee. Kleine diatomeeën ondervinden minder effect van ijzer limitatie vanwege een hoger oppervlakte:volume ratio en daarnaast is de diffuse laag van de cel kleiner, waardoor de concentratiegradient tussen de cel en daarbuiten relatief groot is. De aanvoer van opgelost ijzer van het continentaal plat van het Antarctisch Schiereiland heeft de grootste invloed in de Drake Passage, waar het water tot ver in de Passage, de lijnen van gelijke dichtheid volgt. Dit is consistent met de verspreiding van het opgelost mangaan, aluminium en radium. Een toename van ijzer (tot ~3 nM) en een lage saliniteit richting Tierra del Fuego duidt op aanvoer van rivieren of ijs uit Patagonië. In de diepe wateren van de Weddell Zee vormt zich water nabij de bodem ('Weddell Sea Bottom Water' (WSBW)) door convectie langs de continentale helling. Dit water heeft een relatief hoge ijzerconcentratie (0.6-0.8 nM), in vergelijking met de wateren daarboven (0.2-0.4 nM).

Een deel van de diepste wateren in de Weddell Zee passeert de Scotia Zee, waar het vervolgens ijzer opneemt, zoals te zien in de observatie van deze watermassa in de diepe zuidelijke Drake Passage, met een ijzerconcentratie van ~ 1 nM. Het Weddell Sea Deep Water (WSDW) verdeelt zich. Een deel stroomt door de Scotia Zee en gaat noordwaarts als Antarctic Bottom Water (AABW) over de diepe Atlantische Oceaan. Het grootste deel stroomt echter via de oostwaartse stroom van de Weddell Gyre terug naar de nulmeridiaan en wordt onderweg verrijkt met ijzer. Dichtbij de continentale helling van Zuid Amerika (Patagonië) bevindt zich een waterlaag met een uitzonderlijk hoge ijzerconcentratie (>1.5 nM), samenvallend met een maximum in mangaan en een $\delta^3\text{He}$ anomalie, welke wordt toegeschreven aan de hydrothermale bronnen in de Zuidelijke Stille Oceaan.

In **hoofdstuk 6** wordt de ijzer data zoals gemeten in het kader van dit proefschrift (van de ANT XXIV/3 cruise) gecombineerd met reeds bestaande data van ijzer binnen de Antarctic Circumpolar Current (ACC), Weddell Gyre (WG) en Ross Gyre (RG). Deze gecompileerde dataset is verdeeld over vier diepte lagen (de oppervlaktelaag (door de wind gemengd), vanaf de ondergrens van de oppervlaktelaag-300m, 300m-1000m, > 1000 m). De gemiddelde concentratie van opgelost ijzer neemt toe met de diepte, van gemiddeld 0.28 nM in de oppervlakte wateren tot gemiddeld 0.56 nM in de wateren dieper dan 1000 meter. Iets lagere concentraties ten zuiden van het Polaire Front worden verklaard door opwellend water, met name in de Atlantische Sector. Van Patagonië tot ongeveer 60°E worden relatief hoge ijzerconcentraties gerapporteerd in de bovenste 1000 m. Dit is zeer waarschijnlijk toe te schrijven aan een grote invloed van Patagonië (stofdepositie) en opwellend water. Binnen de Weddell Gyre is opgelost ijzer iets hoger in de oostelijke terugstroom dan in de westelijke stroom, die dicht bij het continent ligt. Nog hogere concentraties worden gevonden bij het Antarctisch schiereiland, dat waarschijnlijk als bron voor ijzer dient. Deze hoge concentratie nabij het schiereiland geeft de belangrijke rol van sedimentaire processen voor de aanvoer van ijzer in de Zuidelijke Oceaan weer. De compilatie van beschikbare ijzermetingen op vier verschillende dieptes, geeft inzicht in de hoeveelheid ijzer die beschikbaar is voor de groei van phytoplankton, en is van waarde voor modelstudies naar de biologie en chemie in de Zuidelijke Oceaan.

In **hoofdstuk 7** worden de bovenstaande hoofdstukken samengebracht en samengevat. Daarnaast worden er aanbevelingen gedaan voor verder onderzoek. Een van de belangrijkste conclusies die uit dit onderzoek naar voren komen is de grote hoeveelheid ijzer die uit hydrothermale bronnen komt en de afstand die dit ijzer aflegt. De cruises in het kader van dit onderzoek waren echter niet ontworpen om naar de invloed van hydrothermale bronnen te kijken. Daarom zou het goed zijn in een vervolgonderzoek te kijken naar de verspreiding van ijzer en andere metalen vanuit hydrothermale bronnen, door verschillende transecten vanaf geïdentificeerde bronnen, met monsternamen op de relevante dieptes. Daarnaast zou het van wezenlijk

belang zijn de seizoenscyclus van ijzer en andere elementen te kunnen inschatten. Tot zover is er slechts een studie in de –Antarctische- wintermaanden uitgevoerd. Toch is de hypothese dat in de winter er een aanvulling van ijzer plaatsvindt. De afwezigheid van ijzermetingen in de wintermaanden is een lacune in de beschrijving van de cyclus in de Poolzeeën en met name in de Zuidelijke Oceaan. Het zou erg relevant zijn hier in een vervolg onderzoek aandacht aan te besteden. Inmiddels zijn er enkele nieuwe ontwikkelingen gaande die komende expedities aanzienlijk waardevoller kunnen maken. De op het NIOZ ontwikkelde PRISTINE sampler maakt het mogelijk om ultraschoon 24 monsters van 27 liter te nemen. Verder is het met nieuwe ICP-MS technieken ook mogelijk meerdere metalen uit een monster te meten. Hierdoor zouden naast de chemische parameters uit het zelfde monster ook biologische parameters gemeten kunnen worden, waarvoor vaak een groter watervolume nodig is. Dit, samen met het verhogen van de resolutie van de metingen in de bovenste 300-500 m geeft een beter beeld van de wederzijdse invloed van ijzer op de biologie in de Oceaan.



Acknowledgements



Acknowledgements

First of all I would like to thank my supervisor, Hein De Baar. For giving me the opportunity to do this interesting research and thereby visit many interesting places around the globe. Thanks, Hein for the supervision, good advice, especially also in the last year, when I already left NIOZ. I also want to thank the reading committee, Prof. Ken Bruland, Prof. Eric Achterberg and Prof. Peter Sedwick, for the effort of thoroughly reading this thesis and giving useful comments.

Patrick, this thesis would not have been there without your experience and energetic effort. Thanks for explaining me how to measure iron, and more importantly, what can go wrong with a FIA system, and how it *may* be solved (if you're lucky). Also thanks for your nice company in the lab and in the lab container and for bringing a million different songs on board (amongst which Andre Hazes; "*die heeft 't pas echt zwaar*"). Also many thanks to my colleagues Rob and Charlie; we started this project together and, as more often I will leave last. Thanks for your help within the project and the good corporation. But more importantly, thanks for the nice times together, the good company and the nice holiday, the beer drunk and the (French) cheese eaten together. It's been a great time and I wish you both a great career in Brest, New Zealand or wherever science may bring you. Also Marie thank you for the good times and the hospitality in Brest and Charlotte thank you for your cooking and the good times spent! Many thanks also to Loes, who was a great colleague, always interested and helpful, during the ANT XXIV/3 cruise, and back on Texel of course. I am very pleased that you will be in my defence committee.

Dr. Dorothea Bauch from IfM GEOMar in Kiel is thanked for nice corporation on the results of ARK XXII/2 resulting in a publication (Chapter 2).

The success of oceanographic research largely depends on the organisation on board the ships used for expeditions. It is for this reason that I would like to thank Master John Ellen and his crew aboard Pelagia as well as chief scientist Klaas Timmermans and Marcel Bakker and Sven Ober for technical support during cruise 64PE267. I would like Master S. Scharze and his crew for excellent support during the ARK XXII/2 cruise in the Arctic Ocean. Also thanks to Prof. Ursula Schauer, chief scientist, and to Lorendz Boom and Sven Ober for their technical support during this cruise. Master S. Schwarze and his crew are also thanked for their support during the ANT XXIV/3 cruise. A special thanks also to the chief scientist of this difficult cruise, Professor Eberhard Fahrbach. In grateful memory also Willem Polman is thanked for the technical support during this cruise. Also many thanks to Michael Stimac for the technical assistance.

A special thanks also to doctor Eberhard Kohlberg and to Carsten Möllendorf, for your kind and professional assistance in one of the most remote places on our planet. I will not forget your help there and the luck I had with you both being present at that time and place.

For their nice company and some great parties I would like to thank all other participants of ARK XXII/2 and ANT XXIV/3, especially the Dutch Club (Lorendz, Karel, Patrick, Charlie, Rob, Sven, Anne-Carlijn, Babette, Cees, Claire, Erwin, Hans, Hein, Ika, Jan, Loes, Steven), the GEOTRACES team (Michiel, Pinghe, Lys, Sally, Kate, Lilith, Sabine, Patricia, Célia, Maya, Torben, Peter, Maya, Olivier, Katrin) and Célia Venchiarutti and Aurélie Spadone. Merci beaucoup! For the nice cruise and the good friendship afterwards! Also thanks to Florian Breier that I can use one of his pictures from the ARK XXII/2 for the cover of this thesis.

Also thanks to Henk Zemmeling, chief scientist and to Joost for helping me on measuring iron during the Pelagia cruise. Sorry I had to leave early, but you did a great job!

Also special thanks to Prof. H. Ridderinkhof for his support and efforts during and after cruises ANTXXIV/3 and 64PE294.

Of course, we did not spend all our time at sea. Back in the lab at Texel, I would like to thank the colleagues of BIO for their support and the good times in the lab. Klaas, Micha, Astrid, Lesley, Libby, Josje, Vero, Jeroen, Henk Z. and of course many other people did their contribution to make NIOZ a nice place to work; the guys from the 'werkplaats', the ladies from the reception, the financial department, (Joke Mulder) the cleaning ladies, and so many others I have come across, thanks guys!

Although Texel is a beautiful place it would have been half the fun without that many friends around. What I will remember most are the Thursday night football evenings. I have some great memories on Cees "we moeten over een kwartier spelen; we bakken nog even een pizza" van der Land, Allert "Pannekoek!" Bijleveld, Craig "Marking guys!" Grove, Pedro "Ah come on, ref!" Frade en Matthijs "Loop dan ook door!" van der Geest. And also on Bert, Santi, Ivo, Leon, Jan-Dirk, Rob, Luis and coach Peter. Thank you guys, for great times during the games, but definitely during the third half / "nabespreking". And for a great weekend in Edinburgh, next weekend coming up soon!

Coming home is double the fun with nice roommates, therefore I wanted to thank Allert (and sometimes Roos) and later Angela, Thorsten, Cindy and Claudia, for all the fun and for being nice roommate's and friends! Also the neighbours Andrea, Isla and Jenny thanks for the good times. Francien, Lukas, Thomas, Marcel, Lesley, Libby, Sabine, Darci, Tamar, Nicole, Furu, Lorendz, Karel, Janine, Roland, Aline, Arjen, Maarten B., Pieter, Rik, Cecile, Okka, Babette, Hauke, Cees v. S. and many others thanks, you

made (evenings) in Texel (whether it was in De Balcken, De Mans, the beach or somewhere else) much more enjoyable. Ulrike, it was nice to get to know you (watching the handball finale (mit Deutschland Fahne)) and I am happy to still be good friends.

Of course, when you live on Texel, people want to come and visit you (in summer at least). I would like to thank Fokko, Jop, Jan, Janne, Wietske, Bart, Annet, Karijn, Judith, Niels, Nine, Peter, Ellen and Klaas (and Jaap and Harm-Jan) and Maarten, Bram en Jaap for the nice weekends spend on Texel, for inviting me so I could still every now and then go out in a place with more than 14000 inhabitants (which is nice, for a change) and for good, relaxing holidays. But most of all, thanks for being good friends!

Fokko and Patrick, a special thanks because you want to be my paranymphs!

Mum, Renske and Harmke, thanks also for your help and support, in the sometimes difficult times over the last years. Thanks for nice visits to Texel and for always being there when needed. And for letting me stay in Wageningen of course!

Mam, bedankt voor alle goede zorgen, de bezoeken naar Texel en vooral ook voor je eeuwige interesse en steun voor wat ik aan het doen was/ben.

Carine, lief, zonder jou was het allemaal stukken moeilijker gegaan. Vooral de laatste jaren wist je precies op het juiste moment in te springen! En mij te overtuigen als het nodig was, bedankt lief! Mila, het leven bestaat niet alleen uit een proefschrift, en jij wist mij, soms luidruchtig, soms vrolijk, daarop te wijzen! Super! Ik ben blij bij jullie te zijn!

Twee mensen zullen deze woorden helaas nooit persoonlijk kunnen lezen.

Willem Polman is helaas niet meer teruggekeerd van ANT XXIV/3. Ik zal zijn inzet en vrolijkheid blijven herinneren en wens Dalea, Savannah en Brittany alle goeds.

Papa, bedankt voor alle steun en vertrouwen, ook toen ik naar Texel ging voor een promotie. Helaas heb je het eindresultaat niet meer mogen zien. "Doe je voorzichtig" was het standaard woordje als ik weer eens op reis of cruise ging. Dat heb ik gedaan, en zal ik blijven doen. Bedankt voor alles, pap.

Biography

Maarten Klunder was born on 19th August 1980 in Oss, The Netherlands. In 1999, after secondary education he started a BSc course on Environmental Science at Wageningen University. In 2000 he received his propedeuse. In 2001 he started a new BSc course on Water, Soil and Atmosphere, also in Wageningen. In 2005, he spent six months at NIOZ, Texel, The Netherlands, for a MSc thesis research project on the Silica fractionation of Antarctic diatoms with Dr. Klaas Timmermans. Here he also got his first experience in scientific research cruises as he participated in the 64PE241 cruise. November 2005, he joined a small group of TU Delft to Bangladesh for another MSc research project concerned with contamination of drinking water with arsenic. In June 2006 he did an internship at Rhine Main Research Institute/Hessenwasser in Biebesheim, Germany, with Dr. Sascha Wisser. The topic of this project was the filtering of radioactive (particles) from natural waters. In fall 2006 he received his MSc. in Water Quality and Hydrology and started the Phd project at NIOZ, Texel. Maarten Klunder is currently employed as environmental risk evaluator at the Dutch Board for the Authorisation of Plant Protection Products and Biocides (Ctgb) in Wageningen, The Netherlands. He lives in Utrecht with his girlfriend Carine and their daughter Mila.



Publications

Peer reviewed publications

- **Klunder, M. B.**, D. Bauch, P. Laan, H. J. W. de Baar, S. van Heuven, and S. Ober (2012), Dissolved iron in the Arctic shelf seas and surface waters of the central Arctic Ocean: Impact of Arctic river water and ice-melt, *Journal of Geophysical Research: Oceans*, 117, C01027, doi:10.1029/2011JC007133.
- **Klunder, M.B.**, P. Laan, R. Middag, H.J.W. de Baar, K. Bakker (2012): Dissolved iron in the Arctic Ocean: Important role of hydrothermal sources, shelf input and scavenging removal. *Journal of Geophysical Research: Oceans*, 117, C04014, doi:10.1029/2011JC007135.
- **Klunder, M.B.**, P. Laan, R. Middag, H.J.W. De Baar, J. v. Ooijen (2011). Dissolved Fe in the Southern Ocean (Atlantic Sector), *Deep-Sea Research II*, 58 (25-26), 2678-2694, doi:10.1016/j.dsr2.2010.10.042.
- **Klunder, M.B.**, P. Laan, I. Neven, R. Middag, H.J.W. De Baar and J. v. Ooijen (2012), Dissolved iron across the Weddell Sea and Drake Passage: impact of dissolved iron on nutrients uptake in the Weddell Sea. Submitted to *Biogeosciences*, September 2012.
- Tagliabue, A., T. Mtshali, O. Aumont, A. R. Bowie, **M. B. Klunder**, A.N. Roychoudhury, S. Swart, 2012. A global compilation of dissolved iron measurements: focus on distributions and processes in the Southern Ocean. *Biogeosciences*, 9, 2333-2349
- Rutgers van der Loeff, M., P. Cai, I. Stimac, A. Bracher, R. Middag, **M.B. Klunder**, S. van Heuven, 2011. ²³⁴Th in surface waters: distribution of particle export flux across the Antarctic Circumpolar Current and in the Weddell Sea during the GEOTRACES expedition ZERO and DRAKE. *Deep-Sea Research II*, 58 (25-26) , 2749-2766.
- Middag, R., H.J.W. de Baar, P. Laan, **M.B. Klunder**, 2011. Fluvial and hydrothermal input of manganese into the Arctic Ocean. *Geochimica et Cosmochimica Acta*, 75 (9), 2393-2408
- Thuróczy, C.E.T, L.J.A. Gerringa, **M.B. Klunder**, P. Laan, H.J.W. De Baar, 2011. Distinct trends in the iron speciation between the shallow shelf seas and the deep basins of the Arctic Ocean. *Journal of Geophysical Research – Oceans*, 116, C10009, doi:10.1029/2010JC006835.
- Thuróczy, C.E.T, L.J.A. Gerringa, **M.B. Klunder**, P. Laan, H.J.W. De Baar, 2011. Observation of consistent trends in the organic complexation of dissolved iron in the Atlantic Sector of the Southern Ocean. *Deep-Sea Research II*, 58 (25-26), 2678-2694.
- Thuróczy, C.E.T, L.J.A. Gerringa, **M.B. Klunder**, R. Middag, P. Laan, K.R. Timmermans, H.J.W. De Baar, 2010. Speciation of Fe in the Eastern North Atlantic Ocean. *Deep Sea Research I* 57, 1444-1453.
- De Baar, H.J.W., K.R. Timmermans, P. Laan, H.H. De Porto, S. Ober, J.J. Blom, M.C. Bakker, J. Schilling, G. Sarthou, M.G. Smit and **M.B. Klunder**, 2008. Titan: A new facility for ultraclean sampling of trace elements and isotopes in the deep oceans in the international Geotraces program. *Marine Chemistry* 111, 4–21.

Oral presentations

- **Klunder, M.B.**, R. Middag, C-E Thuróczy, L. Gerringa, H.J.W. De Baar. *Distribution and sources of dissolved iron in the Arctic Ocean*. SCAR-IASC IPY Conference, St Petersburg, Russia, July 2008.
- **Klunder, M.B.**, P. Laan, K. Bakker, S. Ober, H.J.W. De Baar. *IPY-GEOTRACES: sources and distribution of dissolved iron in the Arctic and Southern oceans*. ASLO Aquatic Sciences Meeting, Nice, France, January 2009.
- **Klunder, M.B.**, P. Laan, R. Middag, C-E Thuróczy, L. Gerringa, H.J.W. De Baar. *Trace Metals in the Polar Oceans*. IPY – Oslo Science Conference, Oslo, Norway, June 2010.

